THE JOURNAL OF

PHYSICAL CHEMISTRY

Volume 74, Number 8 April 16, 1970

The Kinetics of the Reaction between Neptunium(III) and Uranium(VI) in Aqueous Perchlorate Solutions . . . **T. W. Newton** 1655

The Kinetics of the Oxidation of Plutonium(III) by Neptunium(VI) . . . . . **R. B. Fulton and T. W. Newton** 1661

Reactions of Methylene with Dichloromethane in the Presence of Carbon Monoxide and the Collisional Deactivation of Vibrationally Excited 1,2-Dichloroethane by Carbon Monoxide and Perfluorocyclobutane . . . **W. G. Clark, D. W. Setser, and E. E. Siefert** 1670

Collisional Transition Probability Distributions for Deactivation of Vibrationally Excited Dimethylcyclopropane . . . **J. D. Rynbrandt and B. S. Rabinovitch** 1679

Photoisomerization of the Xylenes in Solution . . . . . **Duncan Anderson** 1686

Investigations on the Thermal and Radiolytic Decomposition of Anhydrous Crystalline Potassium Chlorite . . . **G. E. Boyd and L. C. Brown** 1691

The Flash Photolysis of Methyl Iodide . . . . . **Gilbert J. Mains and David Lewis** 1694

The Effects of Temperature and Additives in the Radiolysis of Potassium Nitrate . . . **H. Bernhard Pogge and F. T. Jones** 1700

Ionic Species Formed from Benzene during Radiolysis of Its Solutions in 3-Methylpentane at 77°K . . . **A. Ekstrom** 1705

Charge Scavenging in the Radiolysis at 20°K of Methylcyclohexane in the Glassy and Crystalline States . . . **A. Ekstrom and J. E. Willard** 1708

Vibrational Assignments and Potential Constants for *cis*- and *trans*-1-Chloro-2-fluoroethylenes and Their Deuterated Modifications . . . . **Norman C. Craig, Y.-S. Lo, Lawrence G. Piper, and John C. Wheeler** 1712

Nuclear Magnetic Resonance Isotropic Shifts in 4-Methylpyridine and 4-Methylpyridine N-Oxide Complexed with Copper(II) β-Diketonates . . . . . **C. H. Ke, R. J. Kurland, C. I. Lin, and N. C. Li** 1728

A Cryoscopic Study of the Association of Phenolic Compounds in Benzene . . . **Nicholas E. Vanderborgh, Neal R. Armstrong, and W. Dale Spall** 1734

Entropies of Transfer of Amino Acids from Water to Aqueous Ethanol Solutions . . . **Charles H. Spink and Michael Auker** 1742

Diffusion of Oxygen and Hydrogen in Aqueous Potassium Hydroxide Solutions . . . **M. K. Tham, R. D. Walker, and K. E. Gubbins** 1747

Normal Stress Effect of Dilute Polymer Solutions. III. Monodisperse Poly-α-methylstyrene in Chlorinated Biphenyl . . . . . **Kunihiro Osaki, Kuniaki Sakato, Masaaki Fukatsu, Michio Kurata, Kazumasa Matusita, and Mikio Tamura** 1752

Faradaic Admittance of the Bis(diethylenetriamine)cobalt(III)–Bis(diethylenetriamine)cobalt(II) System . . . **Peter J. Sherwood and H. A. Laitinen** 1757

Transport Properties of Borosilicate Glass Membranes in Molten Salts . . . . . **Harmon M. Garfinkel** 1764

Degrees of Freedom Effect and Internal Energy Partitioning upon Ion Decomposition . . . **Y. N. Lin and B. S. Rabinovitch** 1769

Salting Coefficients from Scaled Particle Theory . . . . . **W. L. Masterton and Tei Pei Lee** 1776

Thermodynamics of Molten Salt–Water Mixtures. I. Solubility of Water Vapor in a Potassium Nitrate–Sodium Nitrite Melt . . . . . **H. S. Hull and A. G. Turnbull** 1783

The Palladium-Catalyzed Carbon Monoxide Oxidation. Catalyst "Break-in" Phenomenon . . . **Raymond F. Baddour, Michael Modell, and Robert L. Goldsmith** 1787

Balancing act?

In the field of physical chemistry?

Of course.

The American Chemical Society's **Journal of Physical Chemistry** *does it all the time. It maintains an excellent balance between reporting on classical areas of chemistry and very modern structural quantum mechanical areas.*

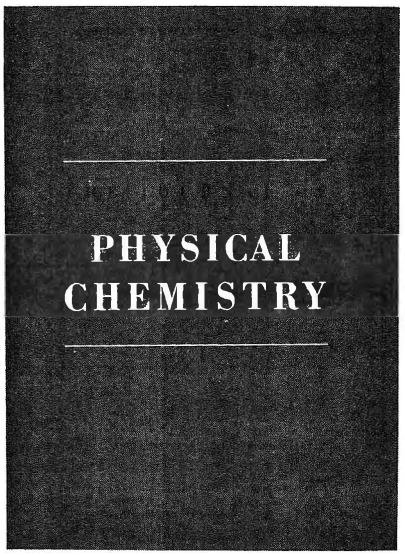

Preference is given to papers dealing with fundamental aspects of atomic and molecular phenomena. Emphasis is placed on reportage of work involving new concepts—new techniques—and new interpretations.

Now appearing biweekly, the JOURNAL OF PHYSICAL CHEMISTRY's forty or more articles per issue cover a wide range of subjects that are of interest to ALL physical chemists. You'll profit from the full articles, notes and communications published in the journal . . . since only those which represent distinct contributions to the literature are accepted.

For balanced reading, subscribe to the JOURNAL OF PHYSICAL CHEMISTRY now. Just complete and return the form below.

American Chemical Society / 1155 Sixteenth Street, N.W., Washington, D.C. 20036

Please enter my subscription to **The Journal of Physical Chemistry** at the rates checked below.

ACS Members: ☐ U.S. $20 ☐ Canada, PUAS $24 ☐ Other Nations $25
Nonmembers: ☐ U.S. $40 ☐ Canada, PUAS $44 ☐ Other Nations $45

☐ Bill me ☐ Bill employer ☐ Payment enclosed (Payable to American Chemical Society)

Name _____ Title _____

Employer _____

Address: ☐ Home ☐ Business _____

City _____ State/Country _____ Zip _____

Nature of employer's business? ☐ Manufacturing or processing ☐ Academic ☐ Government ☐ Other _____ (Please indicate)

Note: Subscriptions at ACS Member Rates are for personal use only.

☐ I am an ACS member ☐ I am not an ACS member

Payment must be made in U.S. currency, by international money order, UNESCO coupons, U.S. bank draft; or order through your book dealer.

HOA

Damping of Capillary Waves on Water by Monomolecular Films of Linear Polyorganosiloxanes . . . **W. D. Garrett and W. A. Zisman** 1796

The Vaporization Thermodynamics of Europium Dibromide . . . . . **John M. Haschke and Harry A. Eick** 1806

NOTES

Paramagnetic Relaxation of Hexacoordinated Chromium(III) Complexes with Anionic Ligands in Aqueous Solutions . . . . . **L. Burlamacchi, G. Martini, and E. Tiezzi** 1809

Evaluation of the Basic Ionization Constants of Water and Alcohols from Their Ionization Potentials . . . **L. S. Levitt and Barbara W. Levitt** 1812

Pure Nuclear Quadrupole Resonance in Hexachlorostannates of Hydrated Divalent Cations . . . **Jack D. Graybeal, Ruth J. McKown, and Shen D. Ing** 1814

Micelle Size of Barium Dinonylnaphthalenesulfonate in Low Polarity Solvents by Vapor Pressure Osmometry . . . **R. C. Little** 1817

On the Liquid Film Remaining in a Draining Circular Cylindrical Vessel . . . . . **Paul Concus** 1818

The Absolute Reactivity of the Oxide Radical Ion with Methanol and Ethanol in Water . . . **R. Wander, Bonnie L. Gall, and Leon M. Dorfman** 1819

Conductance of Dilute Aqueous Solutions of Hexafluorophosphoric Acid at 25° . . . **E. Baumgartner, Margarita Busch, and R. Fernández-Prini** 1821

COMMUNICATIONS TO THE EDITOR

Permittivity Measurements in the Time Domain . . . . . **T. A. Whittingham** 1824

AUTHOR INDEX

Anderson, D., 1686
Armstrong, N. R., 1734
Auker, M., 1742

Baddour, R. F., 1787
Baumgartner, E., 1821
Boyd, G. E., 1691
Brown, L. C., 1691
Burlamacchi, L., 1809
Busch, M., 1821

Clark, W. G., 1670
Concus, P., 1818
Craig, N. C., 1712

Dorfman, L. M., 1819

Eick, H. A., 1806
Ekstrom, A., 1705, 1708

Fernández-Prini, R., 1821
Fukatsu, M., 1752
Fulton, R. B., 1661

Gall, B. L., 1819
Garfinkel, H. M., 1764
Garrett, W. D., 1796
Goldsmith, R. L., 1787
Graybeal, J. D., 1814
Gubbins, K. E., 1747

Haschke, J. M., 1806
Hull, H. S., 1783

Ing, S. D., 1814

Jones, F. T., 1700

Ke, C. H., 1728
Kurata, M., 1752
Kurland, R. J., 1728

Laitinen, H. A., 1757
Lee, T. P., 1776
Levitt, B. W., 1812
Levitt, L. S., 1812
Lewis, D., 1694
Li, N. C., 1728
Lin, C. I., 1728
Lin, Y. N., 1769
Little, R. C., 1817
Lo, Y.-S., 1712

Mains, G. J., 1694
Martini, G., 1809
Masterton, W. L., 1776
Matusita, K., 1752
McKown, R. J., 1814
Modell, M., 1787

Newton, T. W., 1655, 1661

Osaki, K., 1752

Piper, L. G., 1712
Pogge, H. B., 1700

Rabinovitch, B. S., 1679, 1769
Rynbrandt, J. D., 1679

Sakato, K., 1752
Setser, D. W., 1670
Sherwood, P. J., 1757
Siefert, E. E., 1670
Spall, W. D., 1734
Spink, C. H., 1742

Tamura, M., 1752
Tham, M. K., 1747
Tiezzi, E., 1809
Turnbull, A. G., 1783

Vanderborgh, N. E., 1734

Walker, R. D., 1747
Wander, R., 1819
Wheeler, J. C., 1712
Whittingham, T. A., 1824
Willard, J. E., 1708

Zisman, W. A., 1796

THE JOURNAL OF
PHYSICAL CHEMISTRY

VOLUME 74, NUMBER 8 APRIL 16, 1970

The Kinetics of the Reaction between Neptunium(III) and Uranium(VI) in Aqueous Perchlorate Solutions[1]

by T. W. Newton

University of California, Los Alamos Scientific Laboratory, Los Alamos, New Mexico 87544
(Received September 29, 1969)

The overall reaction $2Np^{3+} + UO_2^{2+} + 4H^+ = 2Np^{4+} + U^{4+} + 2H_2O$ occurs by way of three separate reactions: (a) $Np^{3+} + UO_2^{2+} = Np^{4+} + UO_2^+$, (b) $Np^{3+} + UO_2^+ + 4H^+ = Np^{4+} + U^{4+} + 2H_2O$, and (c) $2UO_2^+ + 4H^+ = UO_2^{2+} + U^{4+} + 2H_2O$. The rate of the overall reaction was studied at $\mu = 1.0\ M$ in acid solutions from 0.11 to 0.99 M from 0.6° to 25.1°. The rate constants for the individual reactions (a) and (b) were determined; use was made of the previously determined values for (c). Activation parameters for the predominant net activation processes were determined from the temperature coefficients of the rates. For $Np^{3+} + UO_2^{2+} = [Np \cdot UO_2^{5+}]^*$, $\Delta F^* = 15.29$ kcal/mol ($k = 39\ M^{-1}\ sec^{-1}$ at 25°), $\Delta H^* = 2.60 \pm 0.16$ kcal/mol, and $\Delta S^* = -42.6 \pm 0.6$ cal/mol deg. For $Np^{3+} + UO_2^+ + H^+ = [Np \cdot UO_2 \cdot H^{5+}]^*$, $\Delta F^* = 15.29$ kcal/mol ($k = 38\ M^{-1}\ sec^{-1}$ at 25°), $\Delta H^* = 5.1 \pm 0.4$ kcal/mol, and $\Delta S^* = -34.1 \pm 1.2$ cal/mol deg. The equilibrium quotient for (a) was determined from the forward and reverse rates. For 1 M $HClO_4$, $\Delta F° = 2.06$ kcal/mol ($Q = 0.031$ at 25°), $\Delta H° = -8.67 \pm 0.16$ kcal/mol, and $\Delta S° = -36.0 \pm 0.6$ cal/mol deg. The results for (a) and (b) are compared with the similar Pu(III)–Pu(VI) and Np(III)–Np(V) reactions.

Introduction

The uranyl ion, UO_2^{2+}, is a very poor oxidizing agent in aqueous solutions and its rate of reduction has been studied for only a few reactions. Results have been published for the following reducing agents: Sn(II) in HCl solutions,[2] Fe(II) in H_3PO_4 solutions,[3] and Cr(II),[4] V(II),[5] and V(III)[6] in $HClO_4$ solutions. In this paper these studies are extended to include the actinide ion, Np^{3+}. An additional reason for interest in the Np^{3+}–UO_2^{2+} reaction is to compare the kinetic results with those for similar actinide(III)–actinide(VI) reactions.[7]

The published oxidation potentials[8] indicate that the equilibrium in reaction 1 will lie to the left; the calculated equilibrium quotient, $Q = [Np^{4+}][UO_2^+]/[Np^{3+}][UO_2^{2+}]$, is about 0.028 at 25°. Further reduction to U(IV) is thermodynamically favorable in 1 M acid; the equilibrium quotient for reaction 2 is about $4 \times 10^5\ M^{-4}$ at 25°.

$$Np^{3+} + UO_2^+ + 4H^+ = Np^{4+} + UO_2^{2+} \quad (1)$$

$$2Np^{3+} + UO_2^{2+} + 4H^+ = 2Np^{4+} + U^{4+} + 2H_2O \quad (2)$$

The expected mechanism for reaction 2 is reaction 1 followed by the parallel reactions 3 and 4.

$$Np^{3+} + UO_2^+ + 4H^+ = Np^{4+} + U^{4+} + 2H_2O \quad (3)$$

$$2UO_2^+ + 4H^+ = UO_2^{2+} + U^{4+} + 2H_2O \quad (4)$$

(1) Work done under the auspices of the U. S. Atomic Energy Commission.

(2) R. L. Moore, *J. Amer. Chem. Soc.*, **77**, 1504 (1955).

(3) C. F. Baes, Jr., *J. Phys. Chem.*, **60**, 805 (1956).

(4) T. W. Newton and F. B. Baker, *Inorg. Chem.*, **1**, 368 (1962).

(5) T. W. Newton and F. B. Baker, *J. Phys. Chem.*, **69**, 176 (1965).

(6) T. W. Newton and F. B. Baker, *ibid.*, **70**, 1943 (1966).

(7) R. B. Fulton and T. W. Newton, *J. Phys. Chem.*, **74**, 1661 (1970).

(8) J. J. Katz and G. T. Seaborg, "The Chemistry of the Actinide Elements," Methuen and Co., Ltd., London, 1957 (also John Wiley and Sons, Inc., New York, N. Y.), p 419.

In the present work it was found that this mechanism is adequate, reaction 1 comes essentially to equilibrium rather rapidly, and that both reactions 3 and 4 are important for the formation of U^{4+}. Spectrophotometric methods were used to determine the equilibrium quotient and the forward rate constant for reaction 1. The rates of formation of U(IV) were corrected for the known rates[9] of reaction 4 to obtain rate constants for reaction 3.

In addition it was found that UO_2^{2+} is a catalyst for the relatively slow[10] reaction 5. The most reasonable

$$Np^{3+} + Fe^{3+} = Np^{4+} + Fe^{2+} \quad (5)$$

mechanism for this catalysis is probably reaction 1 followed by the relatively rapid[11] re-oxidation of UO_2^+ according to reaction 6. This mechanism and the ob-

$$UO_2^+ + Fe^{3+} = UO_2^{2+} + Fe^{2+} \quad (6)$$

served rates lead to values for the forward rate constant for reaction 1 which are in good agreement with the directly determined ones.

Experimental Section

Reagents. The neptunium used was from a lot of NpO_2 for which spectrographic analysis showed the transition metals to be less than 0.1 ppm and the rare earths to be less than 0.5 ppm. Radio-assay showed the presence of about 200 ppm of ^{238}Pu-.[12] In addition, some thorium contamination was suspected so an ion-exchange method[13] was used for further purification. The NpO_2 was put into the form of a Np(VI) solution, reduced to Np(V) with $NaNO_2$, precipitated with NaOH, washed with water, and dissolved in $HClO_4$. This solution was placed on a column of Dowex-50 cation-exchange resin and eluted with 1 *M* $HClO_4$; only the middle fraction was retained. This solution was taken to strong fumes with $HClO_4$ to oxidize any organic contaminants and to produce Np(VI), then diluted and placed on a column similar to the first. The Np(VI) was eluted with 1.5 *M* HCl; again only the middle fraction was retained. Finally the solution was fumed with $HClO_4$ to remove organics and chloride. Solutions of $Np(ClO_4)_3$, $Fe(ClO_4)_3$, $UO_2(ClO_4)_2$, $HClO_4$, $LiClO_4$, and $NaClO_4$ were prepared and analyzed as previously described.[5,10] Further recrystallization of the lithium and sodium perchlorates was found to be without significant effect on the rates. The concentration units used in this paper are moles per liter, *M*, at 23°.

Zinc ions and possible impurities from the amalgam used in the preparation of Np(III) were found not to influence the reaction rates. Runs were made using Np(III) made from Np(VI) on zinc amalgam in the usual way. The unused Np(III) solution was then oxidized with air and re-reduced. This cycle was done a total of three times and further rate runs agreed with the first to within 1.3%.

Procedure. The reaction was run in stirred absorption cells and followed spectrophotometrically at 7230 Å where Np(IV) is the principal absorbing species. For this wavelength the Cary Model 14 recording spectrophotometer was operated in the ir mode in which the light from the tungsten source is focused directly through the cell. Tests showed that filtering out the light absorbed by U(VI), below 5300 Å, had no effect on the observed rates. The solutions were swept with purified argon for about 40 min to remove oxygen and were protected from air during the runs with a blanket of argon. After the runs the contents of the reaction cells were titrated with standard Ce(IV) sulfate to provide a check on the initial Np(III) concentrations. Other experimental details were essentially the same as those described for the Np(III)–Fe(III) reaction.[10]

Results and Calculations

The recordings of absorbance *vs.* time all show a relatively rapid increase in Np(IV) followed by a much slower increase to the final value. Typical results are shown in Figure 1. The approximate half-times for the

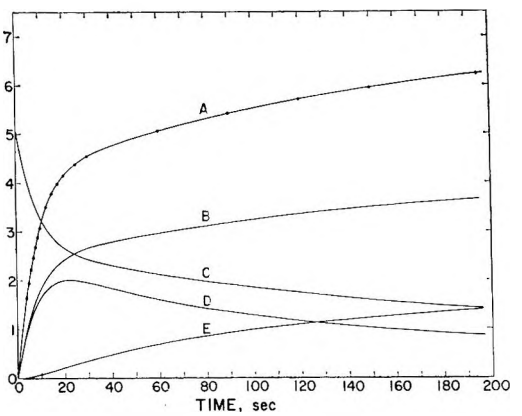

Figure 1. Typical rate run, 0.995 *M* $HClO_4$, 0.6°. Curve A: absorbance × 10; curve B: Np(IV), *M* × 10^4; curve C: Np(III), *M* × 10^4; curve D: U(V), *M* × 10^4; curve E: U(IV), *M* × 10^4.

initial increase range from about 5 to 10 sec for most of the experiments. The rates during the slower stage of reaction were found to depend directly on $[H^+]$. These results indicate the buildup of relatively high concentrations of an intermediate followed by its consumption in slower reactions. The most plausible mechanism of this sort is that suggested in the Intro-

(9) T. W. Newton and F. B. Baker, *Inorg. Chem.*, **4**, 1166 (1965).

(10) T. W. Newton and N. A. Daugherty, *J. Phys. Chem.*, **71**, 3768 (1967).

(11) R. H. Betts, *Can. J. Chem.*, **33**, 1780 (1955).

(12) These results were provided by the Analytical Chemistry Group of this laboratory.

(13) J. C. Sullivan, personal communication.

Table I: Effect of Reactant Concentrations[a]

10^4[Np(III)]$_0$, M	10^4[U(VI)]$_0$, M	No. of detns	k_1, M^{-1} sec^{-1}	Mean dev[b]	Q[c]	Mean dev	k_3, M^{-1} sec^{-1}	Mean dev
1.78	15.5	2	24.6	0.3	0.123	0.002	22.2	2.3
3.32	15.5	2	25.2	0.2	0.128	0.001	16.6	0.3
5.00	15.5	3	24.6	0.2	0.122	0.001	15.6	0.4
6.50	15.5	5	24.6	0.3	0.126	0.003	15.8	0.8
8.00	15.5	1	24.2	...	0.120	...	15.3	...
9.60	15.5	1	25.5	...	0.122	...	15.5	...
3.32	6.2	1	25.0	...	0.132	...	15.4	...
3.32	9.3	1	24.8	...	0.122	...	17.3	...
3.32	31.0	1	25.1	...	0.123	...	23.5	...
5.00	5.2	1	24.0	...	0.119	...	15.2	...
5.00	10.5	3	24.6	0.2	0.120	0.004	16.3	0.5
5.00	31.0	1	24.9	...	0.122	...	17.8	...
5.00	42.0	5	25.2	0.4	0.127	0.002	18.4	0.7
5.00	50.8	1	24.0	...	0.123	...	15.3	...
6.50	42.0	1	25.2	...	0.122	...	20.8	...
Sum or av[d]		29	24.8	0.3	0.124	0.003	17.3	1.8

[a] Conditions: 1.0 M $HClO_4$, 0.7°. k_4 was taken to be 15.9 M^{-1} sec^{-1}. [b] Mean deviation from the mean. [c] $Q = k_1/k_2$. [d] k_1, Q, and k_3 *vs.* concentration are given by the functions: $k_1 = (24.92 \pm 0.76) - (0.36 \pm 1.47)10^3[\text{Np(III)}]_0 - (0.32 \pm 3.95)10^2[\text{U(VI)}]_0 + (2.02 \pm 7.58)[\text{Np(III)}]_0[\text{U(VI)}]_0$. $Q = (0.121 \pm 0.006) + (3.6 \pm 11.7)[\text{Np(III)}]_0 + (2.29 \pm 3.15)[\text{U(VI)}]_0 - (3.49 \pm 6.04)\cdot 10^3[\text{Np(III)}]_0[\text{U(VI)}]_0$. $k_3 = (18.6 \pm 3.0) - (5.85 \pm 5.71)10^3[\text{Np(III)}]_0 + (1.09 \pm 1.53)10^3[\text{U(VI)}]_0 - (0.69 \pm 2.94)10^6[\text{Np(III)}]_0[\text{U(VI)}]_0$, where the uncertainties are the standard deviations.

duction: reaction 1 and its reverse, followed by the parallel reactions 3 and 4. The rate constants for these reactions are called k_1, k_2, k_3, and k_4, respectively. The equilibrium quotient $Q = k_1/k_2$. This scheme leads to the following rate equations

$$dx/dt = k_1(A - x - 2y)(B - x - y) - k_2(C + x + 2y)x - k_3(A - x - 2y)x - 2k_4x^2 \quad (7)$$

$$dy/dt = k_3(A - x - 2y)x + k_4x^2 \quad (8)$$

where $x = [\text{U(V)}]$, $y = [\text{U(IV)}]$, $A = [\text{Np(III)}]_0$, $B = [\text{U(VI)}]_0$, $C = [\text{Np(IV)}]_0$ and $[\text{U(V)}]_0 = 0$. When Np(III) is the limiting reactant, the absorbance is given by

$$D_t = D_0 + (x + 2y)(D_\infty - D_0)/A - xb\Delta\epsilon_4/2 \quad (9)$$

where D_t, D_0, and D_∞ are the absorbance values at times t, 0, and ∞, respectively, and b is the path length. The extinction coefficient change for reaction 4, $\Delta\epsilon_4$, was measured in separate experiments and found to be only about -1.8 M^{-1} cm^{-1} at 7230 Å.

Differential eq 7 and 8 cannot be solved in closed form, so numerical methods were used to test whether these equations are capable of reproducing the experimental data. A Fortran IV program based on the Runge-Kutta method[14] was written to solve the equations and to calculate the concentrations of the various species and the absorbance values *vs.* time for given values of k_1, k_2, k_3, k_4, A, B, C, D_0, D_∞, and $\Delta\epsilon_4$. This program was coupled to the Los Alamos nonlinear least-squares program[15] to determine values for k_1, k_2, and k_3 which best reproduce the observed absorbance *vs.* time data. Values for k_4 were taken from the previous work on reaction 4.[9] The fourth parameter set listed in Table V of ref 9 was used to calculate k_4 as a function of $[H^+]$, $[UO_2^{2+}]$, and temperature. These values apply to $\mu = 2$ M and were corrected to $\mu = 1$ M on the basis of the data in Table I of the reference. As an illustration of its effect, doubling k_4 caused an increase in k_1 of 2.8% and a decrease in k_2 and k_3 of 4.5% and 45%, in a typical example.

For all the rate runs values for k_1, k_2, and k_3 were found such that eq 9 and the solutions for eq 7 and 8 reproduced the observed absorbance *vs.* time curves within the experimental error. A typical example is shown by curve A in Figure 1. The root-mean-square deviation between the observed and calculated absorbance values is less than 0.001 for this and for almost all the other runs. Figure 1 also shows the calculated concentrations of the various species as a function of time. The validity of the rate equations was further tested in a set of runs at 0.7° in 1 M $HClO_4$ in which the initial concentration ranges were (1.78–9.6) $\times 10^{-4}$ M Np(III) and (6.2–50.8) $\times 10^{-4}$ M U(VI). Values for k_1, k_2, and k_3, determined as described above, showed no trend with the reactant concentrations. The results are summarized in Table I. The equilibrium quotient, Q, for reaction 1 has been tabulated rather than k_2.

(14) (a) H. Margenau and G. M. Murphy, "The Mathematics of Physics and Chemistry," Van Nostrand-Reinhold Co., Inc., Princeton, N. J., 1943, p 469; (b) H. R. Siewert, P. N. Tenney, and T. Vermeulen, University of California Radiation Laboratory Report UCRL-10575, 1962.

(15) This program was written by R. H. Moore and R. K. Ziegler and is described in Los Alamos Scientific Laboratory Report LA-2367, 1959, and Addenda.

Table II: Runs with Excess U(V)[a]

10^4Initial concn, M			k_1,		k_3,
U(VI)	Np(IV)	U(V)	M^{-1} sec^{-1}	Q	M^{-1} sec^{-1}
2.72	3.06	3.51	26.1	0.129	14.9
2.67	4.62	3.56	27.3	0.138	14.0
2.88	4.06	3.41	24.5	0.114	18.0
2.71	4.06	3.52	24.5	0.121	16.2
9.06	4.06	3.40	24.1	0.112	18.9

[a] Conditions: 1.0 M $HClO_4$, 0.7°.

The values for k_1, Q, and k_3 were fit to functions of the form $a + b[\text{Np(III)}]_0 + c[\text{U(VI)}]_0 + d[\text{Np(III)}]_0[\text{U(VI)}]_0$ by a least-squares procedure. The parameters and their standard deviations are shown in footnote *d* of Table I. The standard deviations of *b*, *c*, and *d* are large enough to indicate that the apparent trends with concentration are very probably accidental.

The effect of the reaction products was studied in three runs in which the average initial concentrations of Np(IV) and U(IV) were 3.7×10^{-4} M and 1.85×10^{-4} M, respectively. These runs started close to equilibrium so k_1 was determined with less accuracy than usual. The average value for k_1 for the three runs was only 4.5% lower than for a set of comparable runs without initial concentrations of products.

A set of rate runs was made in which equilibrium in reaction 1 was approached from the right. A solution of Eu(II) was prepared on zinc amalgam and injected into the appropriate U(VI)–Np(IV) mixture in the reaction cell. The reduction of U(VI) by Eu(II) is much faster than that of Np(IV), so the required U(V)–Np(VI) mixtures are readily prepared in this way. The results are summarized in Table II. The average values for k_1, Q, and k_3 are in reasonably good agreement with those in Table I.

Uranium(VI) has been found to catalyze the reaction between Np(III) and Fe(III). The proposed mechanism, reactions 1 and 5, leads to rate law 10. It is very likely that k_6 is greater than k_2 and indeed the integrated form of (10), under the assumption that $k_2[\text{Np(IV)}]/k_6[\text{Fe(III)}] \ll 1$, was found to be in good agreement with the data. This is shown for a typical run in Table III. The results for the set of these runs are summarized in Table IV. The values for k_1 were calculated using a nonlinear least-squares method applied to the integrated rate law; the value used for k_5 is the average determined in separate experiments without U(VI).

$$\frac{d[\text{Np(IV)}]}{dt} = \frac{k_1[\text{Np(III)}][\text{U(VI)}]}{1 + k_2[\text{Np(IV)}]/k_6[\text{Fe(III)}]} + k_5[\text{Np(III)}][\text{Fe(III)}] \quad (10)$$

Table III: Absorbance *vs.* Time, U(VI)-Catalyzed Np(III)–Fe(III) Reaction[a]

Time,	Absorbance		Time,	Absorbance		Time,	Absorbance	
sec	Obsd	Calcd[b]	sec	Obsd	Calcd[b]	sec	Obsd	Calcd[b]
0	0.010	...	17.5	0.628	0.629	40	0.844	0.845
5	0.270	0.270	20	0.669	0.670	55	0.895	0.894
6	0.313	0.313	22.5	0.706	0.705	70	0.916	0.916
8	0.389	0.389	25	0.734	0.734	80	0.924	0.924
10.0	0.454	0.454	30	0.782	0.782	95	0.931	0.930
12.5	0.524	0.523	35	0.817	0.818	110	0.933	0.933
						∞	...	0.936

[a] Conditions: 0.8°, 1.0 M $HClO_4$, 5.52×10^{-4} M Np(III), 7.44×10^{-4} M Fe(III), and 16.0×10^{-4} M U(VI). [b] Calculated using $k_1 = 25.16$ M^{-1} sec^{-1} and $k_5 = 46.45$ M^{-1} sec^{-1}.

Table IV: Effect of U(VI) on the Np(III)–Fe(III) Reaction[a]

10^4Initial concn, M			k_5,	k_1,
U(VI)	Np(III)	Fe(III)	M^{-1} sec^{-1}	M^{-1} sec^{-1}
0.0	3.69	4.96	46.9	...
0.0	3.73	14.9	47.1	...
0.0	4.05	14.9	45.2	...
0.0	5.55	14.9	46.6	...
10.4	4.10	4.89	46.45[b]	25.0
10.4	3.92	4.89	46.45[b]	28.9
10.7	4.07	4.96	46.45[b]	24.7
16.0	5.52	7.44	46.45[b]	25.2
26.7	4.05	4.96	46.45[b]	24.4

[a] Conditions: 0.8°, 1.0 M $HClO_4$. Rate law: $d[\text{Np(IV)}]/dt = k_1[\text{Np(III)}][\text{U(VI)}] + k_5[\text{Np(III)}][\text{Fe(III)}]$. [b] Av of first four, uncatalyzed runs.

The effect of hydrogen ion concentration and temperature was studied in a series of runs at unit ionic strength, held constant with $LiClO_4$. The results are summarized in Table V. It is seen that k_1 decreases slightly with increasing $[H^+]$, Q is nearly independent of $[H^+]$, and k_3 is essentially proportional to $[H^+]$.

The effect of varying the ionic strength was studied in a short series of runs at 0.6° in 0.109 M $HClO_4$. $LiClO_4$ was added to give ionic strengths in the range 0.12 to 2.57 M. The results of these experiments are summarized in Table VI. Values for k_4 were required for the calculation of k_1, Q, and k_3 and were estimated

Table V: Hydrogen Ion and Temperature Dependence[a]

Temp, °C	[H⁺], M	k_4,[b] M^{-1} sec^{-1}	k_1, M^{-1} sec^{-1}		$Q \times 10^2$		k_3, M^{-1} sec^{-1}	
			Obsd	Calcd[c]	Obsd	Calcd[d]	Obsd	Calcd[e]
0.6	0.106[f]	2.4	26.1	26.3	10.8	11.3	1.90	1.73
	0.140	3.2	25.9	25.8	11.1	11.4	2.39	2.28
	0.186[f]	4.2	25.6	25.3	11.5	11.4	3.30	3.03
	0.510	9.8	24.5	24.6	11.2	11.4	8.36	8.31
	0.994[f]	16.0	24.6	24.3	11.9	11.4	14.7	16.2
12.7	0.106[f]	5.9	35.6	36.2	5.60	5.70	2.72	2.69
	0.140	7.5	36.8	34.9	5.62	5.73	3.74	3.55
	0.186[f]	9.8	35.0	33.9	5.59	5.75	4.92	4.72
	0.510	21.5	32.8	31.9	5.93	5.80	12.9	12.9
	0.994[f]	32.6	31.9	31.3	6.18	5.81	23.7	25.2
17.7	0.106[f]	8.2	40.7	41.8	4.57	4.35	3.10	3.19
	0.186[f]	13.5	38.6	38.3	4.58	4.41	5.43	5.60
	0.510[f]	28.7	35.9	35.5	4.50	4.45	15.2	15.4
	0.994[f]	42.2	34.9	34.7	4.75	4.47	28.1	29.9
25.1	0.106[f]	13.3	52.0	52.0	2.84	2.95	4.21	4.08
	0.186[f]	21.2	47.4	46.3	2.74	3.01	7.96	7.16
	0.510	43.3	41.8	41.5	3.14	3.06	20.7	19.6
	0.994[f]	60.3	39.0	40.2	3.10	3.07	38.2	38.3

[a] Conditions: μ = 1.00 M ($LiClO_4$). [b] From previous work, ref 9. [c] Calculated using eq 13 and $\Delta H_a^* = 2.58$ kcal/mol, $\Delta S_a^* = -42.6$ cal/mol deg, $\Delta H_b^* = 11.3$ kcal/mol, and $\Delta S_b^* = -20$ cal/mol deg. [d] Calculated using $\Delta H^\circ = -8.67$ kcal/mol, $\Delta S^\circ = -36.0$ cal/mol deg, and a correction for the small amount of hydrolysis of Np(IV). [e] Calculated using eq 12 and $\Delta H^* = 5.12$ kcal/mol and $\Delta S^* = -34.1$ cal/mol deg. [f] Average of duplicate determinations at this [H⁺].

as follows. The Debye–Hückel expression, eq 11, was

$$\log k = \log k_0 + \frac{\Delta z^2 A \mu^{1/2}}{1 + B\mathring{a}\mu^{1/2}} + C\mu \qquad (11)$$

assumed to be applicable to the data for k_1 at 25° and μ = 0.5 and 2.1 M.[9] The "distance of closest approach" term, $\mathring{a}$, was taken to lie in the range 7 to 8.7 Å and corresponding values for C were found to range from 0.176 to 0.22 M^{-1}. These values were used to estimate the plausible ranges for k_4 given in Table VI. It is seen that the values for k_3 depend significantly on k_4 but it was found that those for k_1 and Q do not. The observed values of k_1 fit eq 11 quite well with k_0 = 0.600 M^{-1} sec^{-1}, Δz^2 = 12, $\mathring{a}$ = 8.94 Å, and $C = 0.148\ M^{-1}$.

A few hydrogen ion dependence runs were made in which $NaClO_4$ rather than $LiClO_4$ was used to maintain the ionic strength. In contrast to the results using $LiClO_4$, essentially no hydrogen ion dependence was observed. The results are summarized in Table VII.

Table VI: Effect of Ionic Strength[a]

Ionic strength,[b] M	k_1, M^{-1} sec^{-1}		$Q \times 10^2$	k_3, M^{-1} sec^{-1} (range)	k_4,[c] M^{-1} sec^{-1} (range)
	Obsd	Calcd[d]			
0.120	6.48	6.45	10.6	0.11–0.14	0.86–0.90
0.565	17.4	17.7	12.1	0.87–0.92	1.79–1.85
1.23	32.5	31.9	11.6	2.48–2.56	3.07–3.18
2.57	66.0	66.3	7.46	9.8–9.9	6.76–7.01

[a] Conditions: 0.6°, 5.1 × 10^{-4} M Np(III), 20.6 × 10^{-4} M U(VI), 0.109 M $HClO_4$. [b] Made up with $LiClO_4$. [c] Estimated as described in text. [d] Calculated using $\log k_1 = \log (0.600) + (5.865\mu^{1/2})/(1 + 2.90\mu^{1/2}) + 0.148\mu$.

Table VII: Effect of $NaClO_4$

Temp, °C	$HClO_4$, M	$NaClO_4$, M	$k_1(Na^+)$, M^{-1} sec^{-1}	$k_1(Li^+)$,[a] M^{-1} sec^{-1}
12.7[b]	0.143	1.851	50.7 ± 0.8[c]	
	0.228	1.736	49.3 ± 0.7	59.3
	1.111	0.833	53.2 ± 0.9	
	1.993	0.00	52.1 ± 0.6	
17.7[d]	0.106	0.836	35.6 ± 0.4	40.8[e]
	0.186	0.806	34.5 ± 0.3	38.6[e]
	0.508	0.433	33.4 ± 0.5	35.9[e]
	0.992	0.00	34.9[e]	

[a] Value obtained under comparable conditions using $LiClO_4$. [b] Other conditions: 5.1 × 10^{-4} M Np(III), 15.5 × 10^{-4} M U(VI), μ = 2.00 M. [c] Uncertainty is the standard deviation determined by the least-squares program; it is essentially the same as the mean deviation from the mean for replicates. [d] Other conditions: 4.9 × 10^{-4} M Np(III), 10.4 × 10^{-4} M U(VI), μ = 1.00 M. [e] Value from Table V.

Discussion

The proposed mechanism for reaction 2 is in good agreement with the observed absorbance *vs.* time data over wide concentration ranges. However, the system is complicated enough so that additional independent evidence supporting the correctness of the mechanism is essential.

Such evidence is provided by the rates of the U(VI)-catalyzed Np(III)–Fe(III) reaction. The average value for k_1 from these rates (Table IV) is only 3% higher than for k_1 determined from the overall reaction under comparable conditions (Table I).

Additional support comes from a consideration of the values found for Q, the equilibrium quotient for reaction 1. A least-squares procedure was used to determine the values of ΔH° and ΔS° which best reproduce the observations. The results are -8.67 ± 0.16 kcal/mol and -36.0 ± 0.6 cal/mol deg, respectively. These values reproduce the experimental values with a mean deviation of 4% and a maximum deviation of 11%. The uncertainties are the standard deviations determined by the least-squares program. The slight trend in Q with $[H^+]$ was assumed to be due to the hydrolysis of Np(IV).[16] Correction for hydrolysis was made assuming $\Delta H_h^\circ = 10$ kcal/mol and $\Delta S_h^\circ = 23$ cal/mol. The thermodynamic quantities for Q are very insensitive to these estimates.

These results for Q may be compared with other work. Published values[17] of the appropriate thermodynamic quantities lead to $\Delta H^\circ = -8.8$ kcal/mol and $\Delta S^\circ = -37$ cal/mol deg for 1 M $HClO_4$ at 25°. The good agreement here shows at least that the kinetically determined equilibrium quotients are consistent with Katz and Seaborg's plausible estimates of the thermodynamic quantities for UO_2^+.

The results for reaction 3, shown in Table V, suggest

$$d[Np(IV)]/dt = k[H^+][Np(III)][U(V)] \quad (12)$$

rate law 12 which has the same form as that found for the formally similar Np(III)–Np(V) reaction.[18] Assuming the applicability of eq 12 and the Eyring equation, values of ΔH^* and ΔS^* were determined by a least-squares procedure which minimized the per cent deviations between the observed and calculated rate constants. The results are $\Delta H^* = 5.1 \pm 0.2$ kcal/mol and $\Delta S^* = -34.1 \pm 0.8$ cal/mol deg. These activation parameters reproduce the data with a mean deviation of 5% and a maximum deviation of 19%. The uncertainties are the standard deviations computed by the least-squares program; the actual uncertainties are somewhat higher because k_4 was measured at $\mu = 2$ M and corrected to $\mu = 1$ M, as described above. The results for the analogous Np(III)–Np(V) reaction are $\Delta H^* = 5.93 \pm 0.53$ kcal/mol and $\Delta S^* = -33.3 \pm 1.6$ cal/mol deg.[19] Thus the proposed mechanism for reaction 2 leads to activation parameters for reaction 3 which are remarkably close to those for a similar reaction.

The above discussion makes it appear very likely that the mechanism for reaction 2 is indeed reaction 1 and its reverse followed by the parallel reactions 3 and 4.

The effect of $[H^+]$ on k_1 in $LiClO_4$ solutions studied in the absence of Fe(III) suggests a rate law of the form of (13). This rate law is satisfactory in that,

$$d[Np(IV)]/dt = (k_a + k_b/[H^+])[Np(III)][U(VI)] \quad (13)$$

together with the Eyring equation, values for ΔH_a^*, ΔS_a^*, ΔH_b^*, and ΔS_b^* can be found which reproduce the k_1 values at all the experimental $[H^+]$ and T values simultaneously with a mean deviation of 2.2% and a maximum deviation of 8.8%. The least-squares best values for these four activation parameters are 2.58 ± 0.16 kcal/mol, -42.6 ± 0.6 cal/mol deg, 11.3 ± 1.9 kcal/mol, and -20 ± 6.5 cal/mol deg, respectively. The uncertainties are the standard deviations calculated by the least-squares program. The calculated values given in Table V were obtained using the parameters listed above.

The fact that the $[H^+]$ dependence is much smaller in $NaClO_4$ than in $LiClO_4$ solutions suggests that the minor, inverse $[H^+]$, term in rate law 13 might be due at least partially to a medium effect. Accordingly, the alternative rate law 14 was examined. The temperature dependence of α was assumed to be linear and a least-squares treatment gave $\Delta H^* = 2.62 \pm 0.20$ kcal/mol, $\Delta S^* = -42.5 \pm 0.7$ cal/mol deg, $\alpha = 0.0756$ at 0° and 0.246 at 25°. These parameters reproduce

$$d[Np(IV)]/dt = k_a' \exp(\alpha[Li^+])[Np(III)][U(VI)] \quad (14)$$

Table VIII: Comparison of Reactions[a]

Reaction	Np(III) + U(VI) = Np(IV) + U(V)	Pu(III) + Pu(VI) = Pu(IV) + Pu(V)
ΔF°, kcal/mol	2.06	1.51
ΔH°, kcal/mol	−8.7	−9.3
ΔS°, cal/mol/deg	−36	−36
k, M^{-1} sec^{-1}	39	2.66
ΔF^*, kcal/mol	15.29	16.86
ΔH^*, kcal/mol	2.60 ± 0.16	4.83 ± 0.09
ΔS^*, cal/mol/deg	−42.6 ± 0.6	−40.4 ± 0.3

[a] Conditions: 25° and 1.0 M $HClO_4$.

(16) J. C. Sullivan and J. C. Hindman, *J. Phys. Chem.*, **63**, 1332 (1959).

(17) Reference 8, pp 172 and 221.

(18) J. C. Hindman, J. C. Sullivan, and D. Cohen, *J. Amer. Chem. Soc.*, **80**, 1812 (1958).

(19) Calculated for $\mu = 1.0$ M from the data in ref 18 under the assumption that the ionic strength dependence is the same as that for k_3 as shown in Table VI. For $\mu = 2.0$ M, where the measurements were made, $\Delta S^* = -31.2 \pm 1.6$ cal/mol deg.

the data nearly as well as those given above; the mean and maximum deviations are 2.4% and 10.8%, respectively. It is important to note that the activation parameters for the predominant path for reaction are essentially independent of the form assumed for the minor term in the rate law.

The activation parameters for reaction 1 are compared with those for similar actinide(III)–actinide(VI) reactions in Table VIII of ref 7.

Acknowledgments. I gratefully acknowledge many helpful discussions with Dr. R. B. Fulton and with Dr. C. E. Holley, Jr., under whose general direction this work was done.

The Kinetics of the Oxidation of Plutonium(III) by Neptunium(VI)[1]

by R. B. Fulton[2] and T. W. Newton

University of California, Los Alamos Scientific Laboratory, Los Alamos, New Mexico 87544
(Received September 29, 1969)

The reaction Pu(III) + Np(VI) = Pu(IV) + Np(V) has been studied at unit ionic strength in acid perchlorate solutions from 0.06 to 1.00 M $HClO_4$ and temperatures from 0.8 to 53.2°. At low acid concentrations and high temperatures the rate constants were corrected for the effects of disproportionation and further oxidation of Pu(IV). Two net activation processes are important: (1) $Pu^{3+} + NpO_2^{2+} = [Pu \cdot NpO_2^{5+}]^*$ for which $\Delta F^* = 15.34$ kcal/mol ($k_{25°} = 35.5\ M^{-1}\ sec^{-1}$), $\Delta H^* = 3.49 \pm 0.05$ kcal/mol, and $\Delta S^* = -39.73 \pm 0.16$ cal/mol deg; (2) $Pu^{3+} + NpO_2^{2+} + H_2O = [Pu \cdot OH \cdot NpO_2^{4+}]^* + H^+$ for which $\Delta F^* = 16.78$ kcal/mol ($k_{25°} = 3.1\ M^{-1}\ sec^{-1}$), $\Delta H^* = 12.82 \pm 0.12$ kcal/mol, and $\Delta S^* = -13.28 \pm 0.39$ cal/mol deg. Chloride ion was found to cause a moderate increase in rate. The effect of ionic strength was studied from 0.24 to 3.7 M and is found to be in agreement with the extended Debye–Hückel theory. The results are compared with other analogous actinide(III)–actinide(VI) reactions.

Introduction

The importance of studying the kinetics of the oxidation of Pu(III) by Np(VI) is twofold. First, it extends the chemistry of actinide–actinide reactions; none of the possible plutonium–neptunium reactions has been examined quantitatively and only a few other reactions in which Pu(III) is oxidized have been studied.[3] Second, this reaction is of interest for comparing the kinetic results with those for analogous actinide(III)–actinide(VI) reactions.[4,5]

The published heat and entropy data[6] indicate that the equilibrium quotient, Q_1, for reaction 1 at 25° and

$$Pu^{3+} + NpO_2^{2+} = Pu^{4+} + NpO_2^{+} \qquad (1)$$

1 M $HClO_4$ is approximately 350. However, at higher temperatures Q_1 is much smaller, about 75 at 45°, and the effects of the back-reaction, reaction 2, must be considered.

$$Pu^{4+} + NpO_2^{+} = Pu^{3+} + NpO_2^{2+} \qquad (2)$$

In addition to the back-reaction, two other reactions become significant at high temperatures and low hydrogen ion concentrations. They are the disproportionation of Pu(IV), reaction 3, and the further oxidation of Pu(IV) by Np(VI), reaction 4.

$$Pu^{4+} + Pu^{4+} + 2H_2O = PuO_2^{+} + Pu^{3+} + 4H^+ \qquad (3)$$

$$Pu^{4+} + NpO_2^{2+} + 2H_2O = PuO_2^{+} + NpO_2^{+} + 4H^+ \qquad (4)$$

Rabideau[7] found that the rate constant for reaction 3 has an inverse third power dependence on the $[H^+]$ and therefore its effects in low acid and high temperatures should be considered. Reaction 4 has not been previously studied, but separate experiments showed that at low $[H^+]$ and high temperature its rate was large enough to be significant. Finally, reactions 5 and

(1) Work done under the auspices of the U. S. Atomic Energy Commission.

(2) Los Alamos Scientific Laboratory Post-Doctoral Fellow.

(3) T. W. Newton and F. B. Baker, Advances in Chemistry Series, No. 71, American Chemical Society, Washington, D. C., 1967, p 278.

(4) T. W. Newton, *J. Phys. Chem.*, **74**, 1655 (1970).

(5) S. W. Rabideau and R. J. Kline, *ibid.*, **62**, 617 (1958).

(6) J. J. Katz and G. T. Seaborg, "The Chemistry of the Actinide Elements," Methuen and Co., Ltd., London, 1957 (also John Wiley and Sons, New York, N. Y.), pp 429–430.

(7) S. W. Rabideau, *J. Amer. Chem. Soc.*, **75**, 798 (1953).

6, which determine the fate of the relatively unstable

$$Pu^{4+} + PuO_2^{+} = Pu^{3+} + PuO_2^{2+} \quad (5)$$

$$NpO_2^{2+} + PuO_2^{+} = NpO_2^{+} + PuO_2^{2+} \quad (6)$$

Pu(V) produced in reactions 3 and 4, are included to complete the mechanism.

In the present study, the mechanism represented by reactions 1 through 6 was found to be adequate. The reaction of primary interest was reaction 1, and therefore, the observed rates were corrected, when necessary, for the combined effects of reactions 2 through 6.

Experimental Section

Reagents. The neptunium used was from a lot of NpO_2 for which spectrographic analysis showed the transition metals to be less than 0.1 ppm and the rare earths to be less than 0.5 ppm. Radio assay showed the presence of about 200 ppm of ^{238}Pu.[8] In addition, some thorium contamination was suspected so an ion-exchange method[9] was used for further purification. The NpO_2 was put into the form of a Np(VI) solution, reduced to Np(V) with $NaNO_2$, precipitated with NaOH, washed with water, and dissolved in $HClO_4$. This solution was placed on a column of Dowex-50 cation-exchange resin and eluted with 1 *M* $HClO_4$; only the middle fraction was retained. This solution was taken to strong fumes with $HClO_4$ to oxidize any organic contaminants and to produce Np(VI), then diluted and placed on a column similar to the first. The Np(VI) was eluted with 1.5 *M* HCl; again only the middle fraction was retained. Finally, the solution was fumed with $HClO_4$ to remove organics and chloride.

The Np(VI) solutions were prepared from the above neptunium stock as described below. A portion of the stock solution was taken nearly to dryness and weighed. The 71% $HClO_4$ remaining was determined by subtracting the weight of the $NpO_2(ClO_4)_2$. The solution was diluted with the appropriate amount of standardized $HClO_4$ to give Np(VI) in the desired acid concentration. Separate experiments showed that fuming $HClO_4$ oxidizes neptunium quantitatively to the (VI) state and that no substance capable of oxidizing Pu(III), other than the Np(VI) itself, was found in the resulting solutions. A portion of the Np(VI) solution was reduced to Np(III) with zinc amalgam and the total neptunium content of ths completely reduced solution was determined by a spectrophotometric titration using standard Ce(IV).[10]

Stock solutions of plutonium were prepared by dissolving high-purity plutonium wire in concentrated $HClO_4$. The resulting solutions were filtered and then fumed with $HClO_4$ to remove any chloride formed in the dissolution process. A portion of this plutonium stock solution was taken nearly to dryness and weighed to determine the 71% $HClO_4$ remaining. It was diluted with the appropriate amount of standardized $HClO_4$ to give the desired acid concentration. The resulting solution was completely reduced to Pu(III) with zinc amalgam just prior to use. The Pu(III) content of this solution was determined by a spectrophotometric titration using standard Ce(IV). In 0.5 *M* H_2SO_4, the oxidation of Pu(III) to Pu(IV) by Ce(IV) is quantitative. Separate experiments, using solutions prepared from ultrahigh-purity electrolytic plutonium metal[11] and plutonium wire solutions that had been purified by an ion-exchange procedure similar to that used for the neptunium, gave the same results as the solutions of plutonium described above.

Table I: Reactant Dependences, 0.8° and 0.98 *M* $HClO_4$

$10^3[Np]_0$, *M*	$10^3[Pu]_0$, *M*	No. of detns	k_1, M^{-1} sec^{-1}	Mean dev
1.05	2.58	1	19.9	...
1.05	5.15	1	19.5	...
1.05	0.86	2	20.1	0.5
1.05	8.59	2	19.1	0.1
1.08	5.76	2	19.9	0.2
1.08	5.55	2	19.7	0.0
1.08	5.54	2	20.4	0.2
0.95	0.96	2	19.7	0.1
1.51	0.96	1	20.2	...
3.15	0.96	1	20.4	...
4.71	0.96	1	20.8	...
6.25	0.96	1	20.8	...
4.79	0.99	1	20.7	...
6.70	1.29	3	19.7	0.1
8.12	1.29	3	19.7	0.1
1.02	1.29	2	19.7	0.0
1.23	1.29	2	19.7	0.1
1.11	1.41	2	19.6	0.1
6.68	1.41	2	19.6	0.0
3.34	1.41	1	19.8	...
4.46	1.41	1	19.6	...
5.57	1.41	1	19.4	...
1.33	1.36	2	19.8	0.0
1.34	1.18	2	19.4	0.1
6.57	1.19	2	19.6	0.2
Total or av		42	19.8	0.3

Stock solutions of $HClO_4$ (~4 *M*) were prepared by diluting commercial 71% acid which had been boiled and cooled in a stream of argon. The diluted solutions were boiled again and analyzed by titration with standard NaOH before use. Solutions of $LiClO_4$, $NaClO_4$, and $La(ClO_4)_3$ were prepared by neutralizing analytical reagent grade carbonates (or oxide for La) with $HClO_4$. These were purified by two or three recrystallizations from water. The concentrations of the stock solutions were determined by passing aliquots through ion-exchange columns filled with Dowex-50

(8) These results were provided by the Analytical Chemistry Group of this Laboratory.

(9) J. C. Sullivan, personal communication.

(10) T. W. Newton and N. A. Daugherty, *J. Phys. Chem.*, 71, 3768 (1967).

(11) We thank Dr. L. J. Mullins of this laboratory for providing this sample. Reported analyses showed 99.99% Pu with the greatest impurities being 11 ppm U, 6 ppm Am, and 2 ppm Fe.

Table II: Effect of Initial Reactant Ratio and Wavelength on k_1, 44.7° and Unit Ionic Strength

$[H^+]$, M	$[Pu]_0$, $M \times 10^3$	$[Np]_0$, $M \times 10^3$	Wavelength	No. of detns	k_1, M^{-1} sec^{-1}	Mean deviation
0.060	1.66	1.15	6005	2	264.1	6.3
0.060	1.66	1.15	4696	2	248.8	1.1
0.060	1.11	1.73	4696	2	279.4	9.6
0.071	1.86	1.20	6005	2	246.6	2.5
0.071	1.86	1.20	4696	2	247.5	1.1
0.071	1.25	1.80	4696	2	250.5	0.1
0.100	1.66	1.15	6005	1	181.8	...
0.100	1.66	1.15	4696	3	183.3	2.9
0.100	1.11	1.73	4696	2	185.7	6.2

in the acid form and titrating the eluents with standardized NaOH. The HCl stock solutions were prepared by diluting analytical reagent HCl to about 6 M and distilling it in an all-glass still. The distillate was diluted and analyzed by titrating with standard NaOH. The LiCl stock was prepared by recrystallizing LiCl from water and was analyzed gravimetrically by evaporating portions of the solution to dryness.

Doubly distilled water was used for preparing all solutions; the second distillation was made from alkaline permanganate in all-Pyrex still. All concentration units employed in this paper are moles per liter, M, at 23°.

Procedure. The reaction rates were determined spectrophotometrically in rapidly stirred 10-cm absorption cells which have been described previously.[12] The reactions were followed at either 4696 Å, where Pu(IV) is the principal absorbing species, or at 6005 Å, which is an absorption peak for Pu(III). In a rate run the initial reactant, usually Pu(III), was added to a cell containing the appropriate amounts of acid and/or salt. The cell was then positioned in a thermostated water bath in the cell compartment of a Cary 14 recording spectrophotometer and the temperature was allowed to equilibrate for 20 min. Since the oxidation of Pu(III) by oxygen in $HClO_4$ solutions is extremely slow,[13,14] no attempts were made to protect the solution from air during this period. The reaction was started by injecting the final reactant, usually Np(VI), into the stirred cell from a calibrated hypodermic syringe with a Teflon needle. No significant effects were observed when the order of addition of the reactants was reversed.

Results and Calculations

For rate runs carried out under conditions of high hydrogen ion concentration and low temperature, the observed absorbance *vs.* time data can be described by the following rate equation

$$d[Pu(IV)]/dt = k_1[Pu(III)][Np(VI)] \quad (7)$$

A typical example is shown by curve A in Figure 1. The validity of this rate equation was further established by experiments at 0.8° in 1 M $HClO_4$ in which

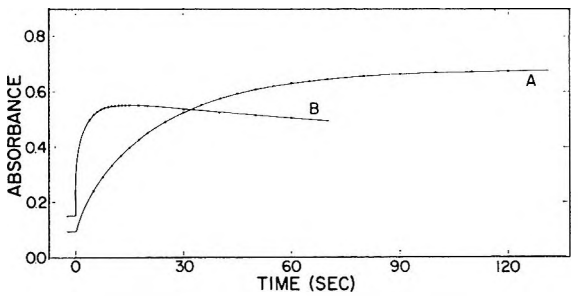

Figure 1. Typical rate recorded at 4696 Å in a 10-cm cell. Curve A, $[Pu(III)]_0 = 2.6 \times 10^{-3}$ M, $[Np(VI)]_0 = 1.0 \times 10^{-3}$ M, $[H^+] = 0.98$ M, $\mu = 1.00$ M, and $T = 0.8°$. Curve B, $[Pu(III)]_0 = 1.1 \times 10^{-3}$ M, $[Np(VI)]_0 = 1.7 \times 10^{-3}$ M, $[H^+] = 0.06$ M, $\mu = 1.00$ M, and $T = 44.7°$.

the initial concentrations of Pu(III) and Np(VI) were varied by factors of 10 and 8.5, respectively. The results are shown in Table I. The values of k_1 were fitted to the function $k_1 = a + b[Pu(III)]_0 + c[Np(VI)]_0$ by a least-squares procedure and the parameters were found to be: $a = 19.9 \pm 0.1$, $b = 44 \pm 30$, and $c = 7 \pm 25$. The values of b and c are small enough and their uncertainties are large enough to indicate no significant effect of concentration on k_1.

When the disproportionation or further oxidation of Pu(IV) is appreciable, the absorbance *vs.* time data, illustrated by curve B in Figure 1, are more complex. However, these observations are consistent with reactions 1 through 6, which yield the following rate equations

$$dx/dt = k_1(A - x - y)(B - x - 3y) - (Q_1/k_1)(x)(x + 3y) - 2k_3(x)(B - x - 3y) - [k_3(x)^2 + k_4(x)(B - x - 3y)]/[1 + k_6(B - x - 3y)/k_5(x)] \quad (8)$$

$$dy/dt = k_3(x)^2 + k_4(x)(B - x - 3y) \quad (9)$$

(12) T. W. Newton and F. B. Baker, **67**, *J. Phys. Chem.*, 1425 (1963).

(13) T. W. Newton and F. B. Baker, *ibid.*, **60**, 1417 (1956).

(14) R. E. Connick and W. H. McVey, Paper 3.9, and K. A. Kraus and J. R. Dam, Paper, 4.14, in "The Transuranium Elements," G. T. Seaborg, J. J. Katz, and W. M. Manning, Ed., National Nuclear Energy Series, Division IV, Vol. 14B, McGraw-Hill Book Co., Inc., New York, N. Y., 1949.

where Q_1 and k_1 are the equilibrium and rate constants for reaction 1 and k_3 through k_6 are the forward rate constants corresponding to reactions 3 through 6, x = [Pu(IV)], y = [Pu(VI)], A = [Pu(III)]$_0$, B = [Np(VI)]$_0$, and [Pu(IV)]$_0$ = [Np(V)]$_0$ = [Pu(VI)]$_0$ = 0.

Table III: Hydrogen Ion Concentration and Temperature Dependences at Unit Ionic Strength

Temp	[H$^+$], M	No. of detns	k_1 (obsd), M^{-1} sec^{-1}	k_1 (calcd),[a] M^{-1} sec^{-1}
0.8	0.029	2	33.8	34.2
	0.032	1	32.4	32.8
	0.037	1	30.1	31.0
	0.053	1	26.2	27.5
	0.061	1	26.1	26.4
	0.077	1	24.6	24.9
	0.110	1	23.3	23.3
	0.174	1	21.8	21.8
	0.980	42	19.8	19.8
15.2	0.059	1	53.0	52.9
	0.071	1	48.9	48.7
	0.083	1	47.2	45.7
	0.100	1	42.4	42.7
	0.125	1	40.1	39.8
	0.167	1	36.8	36.9
	0.250	1	34.6	33.9
	0.980	1	29.4	29.6
24.8	0.034	1	129.5	126.7
	0.051	2	97.6	96.2
	0.059	4	88.8	88.0
	0.071	5	77.0	79.1
	0.084	2	72.9	72.3
	0.101	4	66.9	66.1
	0.117	3	63.4	61.9
	0.184	2	52.2	52.2
	0.250	3	48.8	47.8
	0.544	1	40.0	41.1
	0.985	11	37.9	38.5
36.2	0.059	2	163.0	166.7
	0.065	2	156.0	155.5
	0.071	2	142.6	146.2
	0.083	2	133.8	131.7
	0.100	5	115.9	117.1
	0.125	2	108.7	102.8
	0.146	1	95.9	94.6
	0.167	2	96.5	88.4
	0.250	2	80.5	74.2
	0.362	1	66.0	65.4
	0.980	5	55.1	53.0
40.3	0.973	2	58.5	59.7
44.7	0.060	6	264.1	267.7
	0.071	6	248.2	234.7
	0.085	2	183.3	205.1
	0.100	6	183.9	182.5
	0.125	6	155.1	156.9
	0.167	3	131.2	131.2
	0.250	3	102.2	105.8
	0.500	3	77.1	80.3
	0.977	7	67.1	67.8
48.5	0.973	2	76.1	76.0
53.2	0.973	2	88.9	87.8

[a] Calculated using the values of ΔH_d^*, ΔH_e^*, ΔS_d^*, and ΔS_e^* given in the text.

The absorbance at any time during the reaction, D_t, is given by

$$D_t = D_0 + l(\sum_i \epsilon_i C_{i_t}) \qquad (10)$$

where D_0 is the absorbance reading at time = 0, l is the cell path length, the C_{i_t}'s are the concentrations of the various species in solution [Pu(III), Pu(IV), Pu(VI), Np(V), and Np(VI)] at time = t, and the ϵ_i's are their respective extinction coefficients at the wavelength employed.

Since eq 8 and 9 cannot readily be solved in closed form, numerical methods employing a computer program based on the Runge-Kutta method[15] were used. This program solved the equations and calculated the concentrations of the various species, as well as the absorbance readings, as a function of time for given values of k_1, Q_1, k_3–k_6, A, B, D_0, l, and the extinction coefficients of the species in solution. The values of k_1, $\epsilon_{Pu(IV)}$, and $\epsilon_{Pu(VI)}$ which best reproduced the observed absorbance *vs.* time data were determined by coupling this program to the Los Alamos nonlinear least-squares program.[16] For all these calculations the root-mean-square deviations were 0.0025 or less.

The values of $\epsilon_{Pu(IV)}$ and $\epsilon_{Pu(VI)}$ determined by the program were found to be in satisfactory agreement with the values determined directly in separate experiments. Values for Q_1 and the other rate constants and extinction coefficient were either determined in separate experiments or taken from previously published works. A detailed summary of these values, as well as their [H$^+$] and temperature dependences, is presented in the Appendix.

It is important to note that although reactions 2 through 6 play an important part in the overall reaction, they are relatively unimportant in the initial stages where reaction 1 predominates. It is in this region that k_1 is determined, so the effects of the complicating reactions amount only to small corrections. The calculated k_1 values are relatively insensitive to the values for the rate constants for reactions 2 through 6, as shown in the Appendix.

The adequacy of the proposed reaction scheme was further checked by showing that the value calculated for k_1 was independent of which reactant was in excess. Further, rates determined at 6005 Å, where the reactant Pu(III) absorbs, were not significantly different from those at 4696 Å, where the product Pu(IV) is the principal absorbing species. These results are summarized in Table II.

(15) (a) H. Margenau and G. M. Murphy, "The Mathematics of Physics and Chemistry," Van Nostrand-Reinhold Co., Inc., Princeton, N. J., 1943, p 469; (b) H. R. Siewert, P. N. Tenney, and T. Vermeulen, University of California Radiation Laboratory Report UCRL-10575, 1962.

(16) This program was written by R. H. Moore and R. K. Zeigler and is described in Los Alamos Scientific Laboratory Report LA-2367, 1959, and Addenda.

Table IV: Chloride Dependence, 24.8° and Unit Ionic Strength

$[H^+]$, M	$[Cl^-]$,[a] M	k (obsd), M^{-1} sec^{-1}	k (calcd),[b] M^{-1} sec^{-1}
1.00[c]	0.000	38.35	38.1
	0.047	51.4	52.1
	0.094	67.15	67.3
	0.156	89.0	88.6
	0.234	118.2	116.3
	0.391	169.9	171.7
0.100[d]	0.000	70.2	69.8
	0.040	81.8	82.9
	0.121	113.1	111.4
	0.161	126.2	126.3
	0.241	155.5	156.6
	0.322	187.15	186.9

[a] The $[Cl^-]$ was varied using either LiCl or HCl. [b] Calculated using eq 18 and the values on line 1 of Table VII for 1 M $HClO_4$ and on line 6 for 0.10 M $HClO_4$. [c] Sets of runs with excess Np(VI) agreed with those with excess Pu(III) with an average deviation of 0.9%. Average reactant concentrations were 1.28×10^{-3} M Np(VI) and 1.24×10^{-3} M Pu(III). [d] Reactant concentrations were 1.42×10^{-3} M Np(VI) and 1.08×10^{-3} M Pu(III).

The effect of the hydrogen ion concentration and temperature on k_1 was studied over a wide range in solutions in which the ionic strength was maintained at unity with $LiClO_4$. The results, which are summarized in Table III, indicate that k_1 has a pronounced inverse first-power dependence on the $[H^*]$. Thus, the apparent second-order rate constant for reaction 1 can be represented by the relationship $k_1 = k_d + k_e[H^+]^{-1}$.

The effect of chloride on k_1 was studied in solutions of 0.1 and 1.0 M $HClO_4$ at unit ionic strength and 24.8°. The results, presented in Table IV, indicate a moderate, nearly linear increase in rate with chloride ion.

The ionic strength dependence was studied at 0.8° in solutions of $LiClO_4$, $NaClO_4$, and $La(ClO_4)_3$ that were 0.22 M in $HClO_4$. Also, a short series was done at 25.1° in solutions of $LiClO_4$ that were 1 M in $HClO_4$. Table V summarizes the results for k_1, as well as for the d term of k_1. The ionic strength dependence of k_1 can be described in terms of the extended Debye–Hückel eq 11. The least-squares best values for the

$$\log k = \log k^0 + \frac{A\Delta Z^2\mu^{1/2}}{1 + B\mu^{1/2}} + C\mu \qquad (11)$$

parameters k^0, A ΔZ^2, B, and C are summarized in Table VI. The ionic strength dependence of the k_d term was obtained by subtracting the $k_e[H^+]^{-1}$ term from k_1 at each ionic strength. The ionic strength dependence of k_e was estimated from eq 11 by assuming that the values of B and C are the same as those determined for k_1. The k_d values determined in this way are also in accord with eq 11, as shown by the calculated values in Table V. The values of the various Debye–Hückel parameters are presented in Table VI.

The data for the three salts agree fairly well; at unit ionic strength, 0.22 M $HClO_4$ and 0.8 the values of k_1 vary from 16.2 M^{-1} sec^{-1} for La to 21.6 M^{-1} sec^{-1} for Li with Na being in between at 19.1 M^{-1} sec^{-1}. The data for $La(ClO_4)_3$ also indicate that changing the overall $[ClO_4^-]$ has little effect on the rate constant. Finally, the divergent values obtained for k^0 indicate the unreliability of extrapolating to zero ionic strength from a value as high as 0.22 M.

Table V: Ionic Strength Dependence

Salt	Temp, °C	Ionic strength, M	k_1 (obsd), M^{-1} sec^{-1}	k_d,[a] M^{-1} sec^{-1}	k_d (calcd),[b] M^{-1} sec^{-1}
$LiClO_4$	0.8	0.236	8.1[c]	6.9	6.9
		0.473	12.5	11.0	11.2
		0.889	19.6	17.7	18.0
		1.422	29.4[c]	27.0	26.7
		1.956	39.2	36.3	36.4
		3.201	70.2[c]	65.4	65.6
$NaClO_4$	0.8	0.237	8.25[c]	7.1	7.1
		0.508	12.5	11.1	11.2
		0.870	17.3	15.7	15.8
		1.412	24.6[c]	22.6	22.3
		1.955	31.5	29.1	29.3
		2.678	41.8	38.7	40.0
		3.582	61.5[c]	57.2	56.6
$La(ClO_4)_3$	0.8	0.237	8.35[c]	7.4	7.3
		0.412	10.1	9.0	9.3
		0.937	15.5	14.1	14.2
		1.463	20.8[c]	19.0	18.9
		1.988	26.7	24.6	24.2
		3.741	53.5[c]	49.5	49.7
$LiClO_4$	25.1	1.000	37.2[c]	34.0	34.0
		2.000	71.0[c]	66.2	66.1
		3.000	112.4[c]	105.8	105.7

[a] $k_d = k_1(\text{obsd}) - k_e[H^+]^{-1}$ as described in text. [b] Calculated on the basis of the Debye-Hückel parameters in Table VI. [c] Average of two determinations.

Discussion

The data in Table III were obtained under conditions where the hydrolysis constants for Pu(III) and Np(VI) are much smaller than the $[H^+]$. They lead to the following rate law

$$d[Pu(IV)]/dt = [Pu^{3+}][NpO_2^{2+}](k_d + k_e[H^+]^{-1}) \qquad (12)$$

This rate law implies two net activation processes: (13), which does not involve hydrogen ions, and (14), which

$$Pu^{3+} + NpO_2^{2+} = [Pu \cdot NpO_2^{5+}]^{*}\,^{17} \qquad (13)$$

(17) The composition, but not the structure of the activated complex is indicated.

Table VI: Debye-Hückel Parameters

Salt[a]	Temp, °C	Constant	k^0, M^{-1} sec^{-1}	B, $M^{-1/2}$	C, M^{-1}	$A\Delta Z^2$, $M^{-1/2}$
$LiClO_4$	0.8	k_1 (obsd)	0.491	2.91	0.145	5.864
		k_d	0.376	2.71	0.140	5.864
		k_e	0.096	(2.91)	(0.145)	1.955
	25.1	k_1 (obsd)	0.489	2.47	0.118	6.113
		k_d	0.394	2.36	0.116	6.113
		k_e	0.610	(2.47)	(0.118)	2.038
$NaClO_4$	0.8	k_1 (obsd)	0.628	3.34	0.132	5.864
		k_d	0.494	3.14	0.129	5.864
		k_e	0.096	(3.34)	(0.132)	1.955
$La(ClO_4)_3$	0.8	k_1 (obsd)	0.943	4.42	0.152	5.864
		k_d	0.774	4.20	0.151	5.864
		k_e	0.096	(4.42)	(0.152)	1.955

[a] At 0.8° the $[H^+] = 0.218\ M$, at 25.1° the $[H^+] = 0.968\ M$.

shows the formation of the activated complex with the

$$Pu^{3+} + NpO_2^{2+} + H_2O = [Pu\cdot OH\cdot NpO_2^{4+}]^* + H^+ \quad (14)$$

prior loss of one hydrogen ion.

An interpretation of the chloride dependence requires the formulation of a rate law in terms of the species actually present in the solution

$$d[Pu(IV)]/dt = [Pu^{3+}][NpO_2^{2+}](k_a + k_b[Cl^-] + k_c[Cl^-]^2) \quad (15)$$

The concentrations of the species indicated here can be estimated by considering the chloride complexing of Pu(III) and Np(VI).

Studies of the chloride complexing of Pu(III)[18] indicate that only the 1:1 complex, $PuCl^{2+}$, is important in solutions less than 1 M in chloride. However, studies of Np(VI)[19] and its analog Pu(VI)[20] indicate that two chloride complexes of Np(VI), NpO_2Cl^+ and NpO_2Cl_2, are probably important. In terms of the formation constants for the three complexes, the following relationships hold

$$[Pu(III)] = [Pu^{3+}](1 + \beta_1[Cl^-]) \quad (16)$$

and

$$[Np(VI)] = [NpO_2^{2+}](1 + \beta_2[Cl^-] + \beta_3[Cl^-]^2) \quad (17)$$

where β_1, β_2, and β_3 are the formation constants for the $PuCl^{2+}$, NpO_2Cl^+, and NpO_2Cl_2 complexes, respectively.

In view of the above, the rate law in terms of the stoichiometric concentrations becomes

$$d[Pu(IV)]/dt = [Pu(III)][Np(VI)] \times \frac{(k_a + k_b[Cl^-] + k_c[Cl^-]^2)}{(1 + \beta_1[Cl^-])(1 + \beta_2[Cl^-] + \beta_3[Cl^-]^2)} \quad (18)$$

It should be noted that $k_a = k_d + k_e[H^+]^{-1}$.

Ward and Welch[18] have found the value of the formation constant for $PuCl^{2+}$ to be 1.1 M^{-1}. However, this value has been criticized[21] as having been measured on solutions contaminated by Pu(IV), in which case the true value of $\beta_{PuCl^{2+}}$ would be smaller than 1.1 M^{-1}. The chloride complexing of Np(VI) has been studied in connection with work on the kinetics of isotopic exchange reactions,[19] but the interpretation of the results may be questioned since the $\Delta H°$ reported for the NpO_2Cl^+ complex is negative, whereas the data for UO_2Cl^+ [22] and PuO_2Cl^+ [20] indicate the $\Delta H°$'s to be positive. In the case of U(VI), Day and Powers[22] reported that only the 1:1 complex, UO_2Cl^+, seemed important and found its formation constant, $\beta_{UO_2Cl^+}$, to be 0.88 M^{-1} at 25°. Newton and Baker[20] studied the chloride complexes of Pu(VI) and found that at 25° the formation constants for PuO_2Cl^+ and PuO_2Cl_2 were 1.25 M^{-1} and 0.35 M^{-2}, respectively.

Since the values of the formation constants for the three complexes involved appear to be somewhat uncertain, the values of k_a, k_b, and k_c were calculated by a least-squares method using a range of values for β_1, β_2, and β_3. These values, summarized in Table VII, indicate that the values of k_a and k_b are not significantly affected by uncertainties in the formation constants, whereas the values obtained for k_c are quite dependent on the values chosen for β_1, β_2, and β_3.

The uncertainties associated with each calculation shown in Table VII are the standard deviations calculated by the least-squares program. In the cases of k_a and k_b these statistical uncertainties are larger than those resulting from the different assumptions about

(18) M. Ward and G. A. Welch, *J. Inorg. Nucl. Chem.*, 2, 395 (1956).

(19) D. Cohen, J. C. Sullivan, and J. C. Hindman, *J. Amer. Chem. Soc.*, **77**, 4964 (1955).

(20) T. W. Newton and F. B. Baker, *J. Phys. Chem.*, **61**, 934 (1957).

(21) See ref 6, p 305.

(22) R. A. Day, Jr. and R. M. Powers, *J. Amer. Chem. Soc.*, **76**, 3895 (1954).

Table VII: Values of k_a, k_b, and k_c at 25° and Unit Ionic Strength

$[H^+]$, M	β_1, M^{-1}	β_2, M^{-1}	β_3, M^{-2}		k_a, M^{-1} sec^{-1}	k_b, M^{-1} sec^{-1}	k_c, M^{-1} sec^{-1}
1.0	1.10	0.80	0.00		38.1 ± 0.3	355 ± 9	953 ± 34
	1.10	1.25	0.35		38.2 ± 0.2	353 ± 6	1314 ± 26
	0.82	0.88	0.00		38.1 ± 0.4	351 ± 9	849 ± 35
	0.82	1.25	0.35		38.2 ± 0.3	350 ± 7	1137 ± 28
				Av	38.2 ± 0.3	352 ± 9	1063 ± 251
0.1	1.10	0.80	0.00		69.8 ± 1.0	447 ± 25	1010 ± 90
	1.10	1.25	0.35		69.9 ± 1.2	460 ± 65	1402 ± 62
	0.82	0.88	0.00		69.8 ± 1.0	436 ± 25	898 ± 88
	0.82	1.25	0.35		69.9 ± 1.0	447 ± 25	1213 ± 92
				Av	69.8 ± 1.0	447 ± 25	1131 ± 271

Table VIII: Thermodynamic and Activation Parameters for Similar Reactions[a]

Reaction	$\Delta F°$	$\Delta H°$	$\Delta S°$	k(25°)	ΔF^*	ΔH^*	ΔS^*	Ref
Np(III) + U(VI)	2.06	−8.7	−36.0	39	15.39	2.60 ± 0.16	−42.6 ± 0.6	4
Pu(III) + Pu(VI)	1.51	−9.3	−36.1	2.7	16.86	4.83 ± 0.09	−40.4 ± 0.3	5
Pu(III) + Np(VI)	−3.59	−14.5	−36.6	35.5	15.34	3.49 ± 0.05	−39.73 ± 0.16	This work
U(III) + U(VI)	−16.0	−26.8	−36	5.5×10^4	11.0	4.33 ± 0.18	−22.3 ± 0.6	*c*
				1.14×10^4	11.92	4.15 ± 0.07	−26.1 ± 0.25 (at μ = 0.1)	
Np(III) + Np(VI)	−22.6	−33.8	−38	1.05×10^5	10.6	1.0	−32[b]	*c*
				2.18×10^4	11.54	0.90 ± 0.11	−35.7 ± 0.4 (at μ = 0.1 M)	

[a] Conditions: 25° and 1.0 M $HClO_4$, unless otherwise indicated. Heats and free energies are in kcal/mol, entropies are in cal/mol deg, and rate constants are in M^{-1} sec^{-1}. [b] The values were estimated for 1 M $HClO_4$ from those observed in 0.1 M $HClO_4$ under the assumption that the ionic strength dependence is the same as for the U(III)–U(VI) reaction. [c] T. W. Newton and R. B. Fulton, *J. Phys. Chem.*, in press.

the formation constants. However, the lack of precise values for β_1, β_2, and β_3 causes an uncertainty in k_c much larger than the calculated standard deviations. The uncertainties listed with the average values in Table VII are our estimates of the actual ones.

The values of k_b at 0.1 M and 1.0 M $HClO_4$ indicate that it, like k_a, has an inverse $[H^+]$ dependence. This dependence can be described by $k_b = (k_b)_0 + (k_b)_{-1} \cdot [H^+]^{-1}$ with $(k_b)_0 = 342\ M^{-2}$ sec^{-1} and $(k_b)_{-1} = 10.5\ M^{-1}$ sec^{-1}. The small apparent $[H^+]$ dependence shown for k_c is probably not significant because of its large uncertainty.

At 25° and 1 M $HClO_4$, the ratio k_b/k_a is about 9.2. The corresponding ratio for the known chloride bridged Cr(II)–Fe(III) reaction is about 10^4.[23] Therefore, it is reasonable to assume that the Pu(III)–Np(VI) reaction takes place by either an outer-sphere mechanism or an inner-sphere mechanism in which the chloride does not occupy a bridging position.

Assuming that the Eyring equation is applicable to the rate constants in eq 12, the data in Table III were treated by least squares to extract values of the activation parameters which best reproduce the observed values of k_1. The results are $\Delta H_d^* = 3.49 \pm 0.05$ kcal/mol and $\Delta S_d^* = 39.73 \pm 0.16$ cal/mol deg for the hydrogen ion independent path and $\Delta H_e^* = 12.82 \pm 0.12$ kcal/mol and $\Delta S_e^* = -13.3 \pm 0.4$ cal/mol deg for the other path; the uncertainties are the standard deviations computed by the least-squares program. The calculated values in Table III are based on these values of ΔH_d^*, ΔH_e^*, ΔS_d^*, and ΔS_e^*.

The definite but relatively small $[H^+]$ dependence found in the Pu(III)–Np(VI) reaction is interesting for two reasons: first, no hydrogen ions are involved in the overall reaction, and second, no $[H^+]$ dependence was observed for the Pu(III)–Pu(VI) reaction, while that observed for the Np(III)–U(VI) reaction was small enough to be explained in terms of medium effects.

Since both the Pu(III)–Pu(IV) and Np(V)–Np(VI) exchange reactions have been studied, it is of interest to see whether k_d is consistent with eq 19, the Marcus cross relation.[24] At 0° the rate constant for the hydrogen ion independent part of the Pu(III)–Pu(IV) ex-

$$k_{12} = (k_{11}k_{22}K_{12}f)^{1/2};$$

$$\log f = (\log K_{12})^2/[4 \log (k_{11}k_{22}/Z^2)] \quad (19)$$

(23) G. Dulz and N. Sutin, *J. Amer. Chem. Soc.*, 86, 829 (1964).
(24) R. A. Marcus, *J. Phys. Chem.*, 67, 853 (1963).

Table IX: Equilibrium and Rate Constants Used

Reaction	Constant	Values of constants 25°	45°	n^a	Reference
$Pu^{4+} + H_2O = PuOH^{3+} + H^+$	K_h	3.1×10^{-2}	6.9×10^{-2}	...	*b, h, i*
$Pu^{3+} + NpO_2^{2+} = Pu^{4+} + NpO_2^+$	Q_1	3.5×10^{2}	7.5×10^{1}	...	*c*
$2Pu^{4+} + 2H_2O = PuO_2^+ + Pu^{3+} + 4H^+$	k_3	3.8×10^{-5}	2.4×10^{-3}	−3	*d*
$Pu^{4+} + NpO_2^{2+} + 2H_2O = PuO_2^+ + NpO_2^+ + 4H^+$	k_4	3.2×10^{-3}	3.4×10^{-2}	−2	*e*
$Pu^{4+} + PuO_2^+ = Pu^{3+} + PuO_2^{2+}$	k_5	4.0×10^{1}	1.7×10^{2}	0	*f*
$PuO_2^+ + NpO_2^{2+} = PuO_2^{2+} + NpO_2^+$	k_6	2.4×10^{3}	4.7×10^{3}	0	*g*

[a] Hydrogen ion dependence, $[H^+]^n$. [b] References *h* and *i*, $\Delta H°$ at $\mu = 1$ *M* taken to be the same as that determined at $\mu = 2$ *M*. [c] Reference 4. [d] 25° value and *n* from ref 5, 45° value from this work. [e] This work. [f] Reference 3. [g] k_6 found to be 1.05×10^3 M^{-1} sec^{-1} at 2°, ΔS^* and *n* assumed to be the same as for the analogous Np(V)–Np(VI) exchange reaction, ref 24. [h] S. W. Rabideau and J. F. Lemons, *J. Amer. Chem. Soc.*, **73**, 2895 (1951). [i] S. W. Rabideau, *ibid.*, **79**, 3675 (1957).

change reaction was found to be 183 M^{-1} sec^{-1},[25] and that for the Np(V)–Np(VI) exchange reaction is 30 M^{-1} sec^{-1}.[26] Since these exchange reactions may occur at least in part by inner-sphere mechanisms the rate constants are upper limits for the outer-sphere constants required in (19). The equilibrium quotient for the Pu(III)–Np(VI) reaction at 0° was calculated from the heat and entropy data,[6] to be 3250. Substituting these values into (19) leads to a value of $\leq$ 3400 M^{-1} sec^{-1} for the outer-sphere rate constant. This is not inconsistent with the observed value of 19.4 M^{-1} sec^{-1}, and indicates that one or both of the exchange reactions is predominantly inner sphere.

The results for the five actinide(III)–actinide(VI) reactions which have been studied are summarized in Table VIII. The overall reactions are formally identical and are similar in the sense that the $\Delta S°$ values are the same within 2 cal/mol deg. Except for the Np(III)–U(VI) reaction, the ΔF^* values increase smoothly with $\Delta F°$. This is qualitatively in accord with the Marcus cross relation with the additional assumption that the rates of the actinide M^{3+}–M^{4+} and the MO_2^+–MO_2^{2+} exchange reactions do not depend strongly on the atomic number. The agreement is not quantitative, however, since the average slope of observed ΔF^* *vs.* $\Delta F°$ is about 0.29 compared with the value of 0.4 from the Marcus relation, corrected for *f*.

Quantitative agreement with (19) can be obtained only by accepting unreasonably large values for the ratios of the rate constants for similar exchange reactions. For example, the observed rate constants for the Pu(III)–Np(VI) and the Np(III)–Np(VI) reactions lead to a rate constant for the Pu(III)–Pu(IV) exchange which is about 3×10^4 times as large as for the Np(III)–Np(IV) exchange.

When the other activation parameters, ΔH^* and ΔS^*, are examined, however, the regular dependence of ΔF^* on $\Delta F°$ appears to be largely fortuitous. Thus the ΔS^* values range from −22 to −42.6 cal/mol deg and the ΔH^* values vary irregularly from 1 to 4.8 kcal/mol. It appears that the ions involved show individual characteristics probably based on their electronic configurations.

Acknowledgment. The authors gratefully acknowledge many helpful discussions with Dr. C. E. Holley, Jr., under whose general direction this work was done.

Appendix

Under some conditions reactions 2–6 contributed appreciably to the observed absorbance changes. For these conditions the calculation of k_1 required values for Q_1, k_3–k_6, and the appropriate extinction coefficients,

Table X: Extinction Coefficients at 45°

Ion	ϵ_{4896}	ϵ_{6005}
Pu^{3+}	2.70	35.35
NpO_2^{2+}	6.00	2.47
NpO_2^+	3.15	3.41
Pu^{4+} (ϵ_0)	59.50	0.50
$Pu(OH)^{3+}$ (ϵ_1)	12.05	6.89
PuO_2^{2+}	$10.8 + 0.03/[H^+]$	1.28

as previously described. In all cases the effect was relatively small, so highly accurate values were not needed. Where the necessary rate constants could not be found in the literature they were determined spectrophotometrically with sufficient precision for these calculations. The hydrogen ion dependences for the reactions involving Pu(IV) were corrected for its hydrolysis, which is particularly important in solutions at low acid and higher temperatures. Values and sources of these various constants are listed in Table IX. Values for other temperatures were obtained by interpolation or extrapolation.

Values for the various extinction coefficients were determined at 45° and found to be in good agreement

(25) T. K. Keenan, *J. Phys. Chem.*, **61**, 1117 (1957).

(26) D. Cohen, J. C. Sullivan, and J. C. Hindman, *J. Amer. Chem. Soc.*, **76**, 352 (1954).

Table XI: Effect of Changing the Values of the Parameters, 44.7° and 0.06 M $HClO_4$

Parameter changed	% Change in parameter	% Change in k_1
$[Pu(III)]_0$	−0.5	1.0
$[Np(VI)]_0$	−0.6	0.4
$\epsilon_{Pu(III)}^{4696}$	−5.9	0.2
$\epsilon_{Pu(III)}^{6005}$	−0.5	0.2
$\epsilon_{Np(VI)}^{4696}$	−1.5	0.2
$\epsilon_{Np(VI)}^{6005}$	−3.8	0.1
Q	−33.0	1.1
k_3	−13.6	0.6
k_4	−7.3	0.4
k_6/k_5	200	1.3

with published values for 25°.[27,28] This agreement indicates that the temperature dependences of the extinction coefficients are quite small. The values chosen are shown in Table X.

Calculations were made which show that the parameters involved in the corrections for reactions 2–6 need not be known with high accuracy. The data from a typical run at low acid and high temperature were recalculated after changing each parameter in turn. The size of the change was chosen to represent the uncertainty in the parameter. The results, summarized in Table XI, show that reasonable uncertainties in the parameters introduce negligible uncertainties in the values for k_1.

All of the calculations discussed above were made under the simplifying assumption that the occurrence of reactions 3 through 6 in the reverse directions could be ignored. However, these back-reactions were included in recalculations of eight runs representing several temperatures and $[H^+]$'s. The effects of these back-reactions were found to be insignificant; in the least favorable case, low $[H^+]$ and high temperature, the recalculated rate constants differed from the originals by less than 2%.

(27) R. Sjoblom and J. C. Hindman, *J. Amer. Chem. Soc.*, **73**, 1744 (1951).

(28) D. Cohen, *J. Inorg. Nucl. Chem.*, **18**, 211 (1961).

Reactions of Methylene with Dichloromethane in the Presence of Carbon Monoxide and the Collisional Deactivation of Vibrationally Excited 1,2-Dichloroethane by Carbon Monoxide and Perfluorocyclobutane[1]

by W. G. Clark,[2] D. W. Setser,[3] and E. E. Siefert

Chemistry Department, Kansas State University, Manhattan, Kansas 66502 *(Received November 21, 1969)*

The reactions of CH_2, produced by ketene photolysis, with CH_2Cl_2 in the presence of variable quantities of CO was investigated. The addition of small quantities of CO to mixtures of ketene and dichloromethane reduced yields of products associated with triplet CH_2 reactions; however, large amounts of CO ($CO:CH_2Cl_2$ = 30:1) were required to decrease the triplet level to below 5%. The results indicate that singlet CH_2 abstracts only chlorine and triplet CH_2 abstracts only hydrogen from CH_2Cl_2; the rate constants are of comparable magnitude. Singlet methylene reacts with the double bond of butene-2 and with CH_2Cl_2 at the same rates. The ratio of reaction rate constants for $CH_2(^3\Sigma_g^-)$ with CO and CH_2Cl_2 was estimated at ~3. The collisional deactivation of chemically activated 1,2-$C_2H_4Cl_2$ by carbon monoxide and perfluorocyclobutane was studied, and the average amount of vibrational energy lost per collision was measured as 6 ± 2 and ~12 kcal mol^{-1} for CO and C_4F_8, respectively.

Introduction

Methylene, when produced by photolysis of ketene or diazomethane, reacts with chloro- and bromomethanes by H and Cl or Br abstraction but not to an appreciable extent by insertion.[4,5] Since both singlet ($^1A_1$) and triplet ($^3\Sigma_g^-$) methylene are produced from photolysis of ketene[6] or diazomethane,[7] it has not been possible to unambiguously assign elementary reactions to the singlet or triplet methylene with the halomethanes. Carbon monoxide preferentially removes triplet methylene,[8] and the addition of CO to a ketene photolysis system enhances the singlet CH_2 reactions. Bamford and coworkers[9] used the CO technique to study the reactions of singlet methylene with chloroethane; they concluded that $CH_2(^1A_1)$ reacted at least 16 times faster by Cl abstraction than by H abstraction while the $CH_2(^3\Sigma_g^-)$ mainly reacted by H abstraction.

We wish to report photolysis experiments of ketene with CH_2Cl_2 using CO to remove selectively $CH_2(^3\Sigma_g^-)$. The ratio of singlet to triplet methylene was directly monitored by adding *cis*-2-butene to the reaction mixture and measuring the ratio of *cis*- to *trans*-1,2-dimethylcyclopropane.[10] Results will be presented which generally agree with the conclusions of previous workers[8,9] who used CO to remove $CH_2(^3\Sigma_g^-)$. However, even for large ratios of $CO:CH_2Cl_2$, up to 30:1, a small amount of $CH_2(^3\Sigma_g^-)$ was still present, and some care must be used in deducing singlet *vs.* triplet methylene reaction mechanisms and rate constant ratios by the CO addition technique. For example, it seems likely that the C–H abstraction measured by Bamford[9] was due to residual triplet methylene, and that the rate constant ratio for H *vs.* Cl abstraction by $CH_2(^1A_1)$ is less than 1:50.

In spite of the slight complication mentioned in the above paragraph, the addition of convenient amounts of CO can greatly simplify CH_2 plus chloroalkane reaction systems because secondary radical–radical processes associated with the H abstraction reaction are reduced. Thus, ketene plus chloro- or bromoalkane photolysis systems with added CO provide a way for studying nonequilibrium unimolecular reactions of chemically activated chloro- and bromoalkanes. For suchs tudies with haloalkanes or other CH_2-initiated

(1) Abstracted from the M.S. thesis of W. G. Clark, submitted in partial fulfillment of requirement of the Master of Science Degree, Kansas State University, Manhattan, Kansas, 1969.

(2) NASA Predoctoral Fellow.

(3) Alfred P. Sloan Foundation Fellow.

(4) (a) J. C. Hassler and D. W. Setser, *J. Chem. Phys.*, **45**, 3237 (1966); (b) J. C. Hassler, D. W. Setser, and R. L. Johnson, *ibid.*, **45**, 3231 (1966); (c) C. H. Bamford, I. E. Casson, and R. P. Wayne, *Proc. Roy. Soc.*, **A289**, 287 (1965); (d) K. Dees and D. W. Setser, *J. Chem. Phys.*, **49**, 1193 (1968).

(5) R. L. Johnson and D. W. Setser, *J. Phys. Chem.*, **71**, 4366 (1967).

(6) (a) R. W. Carr, Jr., and G. B. Kistiakowsky, *ibid.*, **70**, 118, 1970 (1966); (b) S. Y. Ho and W. A. Noyes, Jr., *J. Amer. Chem. Soc.*, **89**, 5091 (1967); (c) A. N. Strachan and D. E. Thornton, *Can. J. Chem.*, **46**, 2353 (1968); (d) P. G. Bowers, *J. Chem. Soc., A*, 466 (1967).

(7) (a) B. M. Herzog and R. W. Carr, Jr., *J. Phys. Chem.*, **71**, 2688 (1967); (b) F. H. Dorer and B. S. Rabinovitch, *ibid.*, **69**, 1952 (1965).

(8) (a) B. A. DeGraff and G. B. Kistiakowsky, *ibid.*, **71**, 3984 (1967); (b) R. A. Cox and R. J. Cvetanović, *ibid.*, **72**, 2236 (1968).

(9) C. H. Bamford, J. E. Casson, and A. N. Hughes, *Proc. Roy. Soc.*, **A306**, 135 (1968).

(10) T. W. Eder and R. W. Carr, Jr., *J. Phys. Chem.*, **73**, 2074 (1969). This reference summarizes the problems and controversies of the CH_2 *cis*- or *trans*-butene technique of measuring singlet and triplet CH_2 ratios.

chemical activation systems, the deactivating efficiency of CO for the vibrationally excited molecules is required so that the rate constants observed with CO as the deactivating gas can be related to the intrinsic unimolecular reaction rate constants, which are the rate constants obtained with gases having near unit deactivation efficiency.[11] The nonequilibrium HCl elimination rate constant for 1,2-$C_2H_4Cl_2$* formed by combination of CH_2Cl radicals served as a prototype, and the collisional deactivation efficiency of CO was measured and compared to an efficient gas, perfluorocyclobutane.

Experimental Section

Photolysis samples used to study the effects of variable $CO:CH_2Cl_2$ ratios were prepared by transferring the CH_2CO and CH_2Cl_2 into vessels of desired sizes using standard vacuum techniques. For some experiments *cis*-2-butene was added to the CH_2Cl_2–CH_2CO mixtures; in other cases *cis*-2-butene replaced CH_2Cl_2. The noncondensable CO was then metered into the vessel, which was immersed in liquid nitrogen, until the desired pressure of CO was obtained. The experiments were done at constant pressure, usually 350 Torr, with a nearly constant amount of CH_2Cl_2 (2.1 cc) and constant $CH_2CO:CH_2Cl_2$ ratio of 1:7. Thus the vessel size increased as $CO:CH_2Cl_2$ was increased.

Dichloromethane was Fisher Certified Reagent Grade; the *cis*-2-butene was Phillips Research Grade and contained no detectable *trans*-2-butene; carbon monoxide was Matheson CP grade. Mass spectral analysis shows the CO to contain less than 1 part per thousand O_2. Ketene was prepared and purified as described previously.[4] Photolyses were done in Pyrex vessels at room temperature with the unfiltered light of a General Electric A-H6 high-pressure mercury lamp. A rough calculation, using the lamp output, molar absorbancy of ketene, quantum yields of ketene,[12] and transmittance curves of Pyrex, showed that ~75% of the methylene originated from photolysis at 3000–3200 Å and ~25% at 3200–3400 Å.

The condensable products were recovered by pumping the photolyzed sample through a glass wool packed trap at 77°K. These products were then transferred to a gas chromatograph inlet and injected onto the columns described below, which were followed by a thermal conductivity detector. For the products from the $CH_2 + CH_2Cl_2$ reaction, the column consisted of 3 ft of Porapak S and 6 ft of Porapak T. For the products from the reaction of CH_2 with CH_2Cl_2 and *cis*-C_4H_8 mixtures a double-pass analysis scheme was necessary. The entire sample was first passed through the Porapak columns for analysis of chloroethanes. The C_5H_{10} products along with CH_2Cl_2 were trapped from the glpc effluent and *cis* and *trans*-dimethylcyclopropane were analyzed on a column consisting of 15 ft of 12% diisodecyl phthalate on Chromosorb P in series with 15 ft of 40% of $AgNO_3$-saturated ethylene glycol on Chromosorb P. Gas chromatographic peaks were identified from retention times of pure samples and from mass spectra cracking patterns of samples trapped from the glpc effluent. Empirical calibrations were made with prepared standard samples which were near replicas of the photolyzed samples. Also the prepared calibration samples were subjected to the same recovery procedure that was used for the photolyzed samples as a check for possible handling losses.

Series of experiments were done with constant $CO:CH_2Cl_2:CH_2CO$ ratios (10:1:0.2), but at variable total pressure, in order to measure the rate constant for HCl elimination from vibrationally excited $C_2H_4Cl_2$*. Some experiments were also done using $CH_2 + CH_3Cl$ rather than $CH_2 + CH_2Cl_2$ as the source of CH_2Cl radicals. The samples were photolyzed as described above. Since low-pressure experiments are needed to obtain collisional deactivation efficiencies, vessels ranging from 10 to 10,000 cm^3 in volume were used. Constant quantities of CH_2Cl_2 (2.0 cm^3 of gas) were used to improve reliability of analyses, which consisted of Porapak columns in a gas chromatograph unit equipped with hydrogen flame detectors and a temperature programmer. Careful empirical calibrations of the sensitivity of the gas chromatograph unit for 1,2-$C_2H_4Cl_2$ and C_2H_3Cl were made. A double-pass analysis was necessary for the *c*-C_4F_8 experiments. The C_4F_8 was removed by putting the samples through a Porapak column (thermal conductivity detector); the other components were trapped from the He effluent and were subsequently run back through the glpc with the H_2-flame detector.

Results

Methylene Reactions with Dichloromethane in the Presence of Carbon Monoxide. The photochemical processes (eq 1 and 2) are the formation of singlet and triplet methylene, which may react by either H or Cl abstraction (eq 3–6).[4] The photodissociation of CH_2CO is undoubtedly not as simple as implied by (1) and (2). Triplet ketene is involved in the mechanism and ϕ_1 and ϕ_3 are wavelength dependent.[6] On the basis of previous data, it was not possible to eliminate any of the four following reactions although reactions 4 and 5 were thought to be the most important. The methyl and chloromethyl radicals subsequently combine in all possible binary combinations, but the relevant reactions for our present purposes are

$$CH_2CO + h\nu \xrightarrow{\phi_3} {}^3CH_2 + CO \quad (1)$$

$$\xrightarrow{\phi_1} {}^1CH_2 + CO \quad (2)$$

(11) (a) D. W. Setser and J. C. Hassler, *J. Phys. Chem.*, **71**, 1364 (1967); (b) H. W. Chang and D. W. Setser, *J. Amer. Chem. Soc.*, **91**, 7648 (1969).

(12) G. A. Taylor and G. B. Porter, *J. Chem. Phys.*, **36**, 1353 (1962).

$$^3CH_2 + CH_2Cl_2 \xrightarrow{^3k_{Cl}} 2CH_2Cl \quad (3)$$

$$\xrightarrow{^3k_H} CH_3 + CHCl_2 \quad (4)$$

$$^1CH_2 + CH_2Cl_2 \xrightarrow{^1k_{Cl}} 2CH_2Cl \quad (5)$$

$$\xrightarrow{^1k_H} CH_3 + CHCl_2 \quad (6)$$

$$2CH_2Cl \longrightarrow CH_2ClCH_2Cl^* \quad (7)$$

$$CH_3 + CH_2Cl \longrightarrow CH_3CH_2Cl^* \quad (8)$$

$$2CH_3 \longrightarrow C_2H_6^* \quad (9)$$

At high pressure the C_2H_6 to 1,2-$C_2H_4Cl_2$ ratio gives $k_9[CH_3]^2/k_7[CH_2Cl]^2$ and the C_2H_5Cl to 1,2-$C_2H_4Cl_2$ ratio gives $k_8[CH_3]/k_7[CH_2Cl]$. From previous work it is known that $k_7 = k_9 = {}^1/_2k_8$, as would be expected for simple radical combination reactions.[13] Thus these two product ratios can be used to obtain relative steady-state radical concentrations; this technique only gives an approximation to the true instantaneous relative radical concentration, since integration of the ratios of reaction rates to give product ratios assumes that the relative radical concentrations do not vary with time.

The molecules formed in steps 7–9 are highly vibrationally excited, ~90 kcal mol^{-1}, but at the pressure used in these experiments, 350 ± 50 Torr, the vibrationally excited 1,2-dichloroethane formed in step 7 is completely stabilized;[4d] 350 Torr also is sufficient to quench the ethane dissociation reaction.[14] Since the half-quenching pressure of the $C_2H_5Cl^*$ formed by reaction 8 is 350 Torr[5d] in an efficient quenching gas, about half of these molecules will decompose to form HCl and ethene at the pressure used in these experiments. If the yields of chloroethane were used to estimate methyl radical yields, the C_2H_5Cl measured at 350 Torr was corrected (see a later section for details) to give the infinite high-pressure yield.

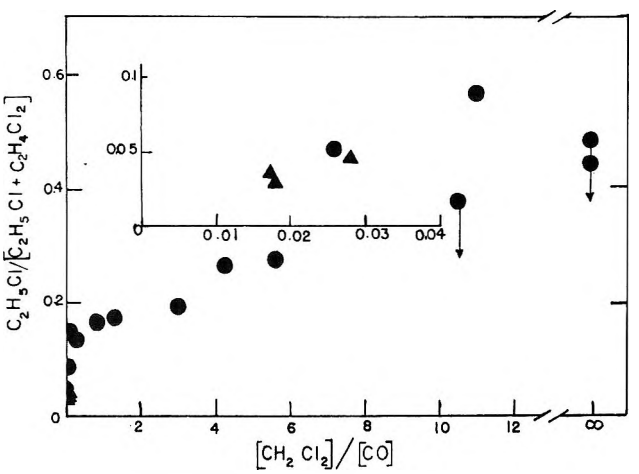

Figure 1. The ratio of the C_2H_5Cl yield (corrected to high pressure) to the sum of the C_2H_5Cl plus 1,2-$C_2H_4Cl_2$ yields from photolysis of ketene with CO and CH_2Cl_2 mixtures. The insert shows the data for high values of $[CO]/[CH_2Cl_2]$: ●, P = 350 Torr; ▲, P = 1600 Torr:

The results from the experiments in which the ratio $CO:CH_2Cl_2$ was varied and the C_2H_5Cl and 1,2-$C_2H_4Cl_2$ product yields were measured are shown in Figure 1; the C_2H_5Cl yield has been corrected for the unimolecular reaction of $C_2H_5Cl^*$. The $C_2H_5Cl/1,2\text{-}C_2H_4Cl_2$ ratio with no added CO was 0.9 and agrees with previously measured values.[4a] The addition of two parts of CO relative to CH_2Cl_2 reduced the yield of C_2H_5Cl from ~50% to ~15%. Further addition of CO reduced the C_2H_5Cl but not to the same degree. The detailed interpretation of this curve is delayed until the Discussion. However, it is clear from Figure 1 that CO drastically reduced the yield of C_2H_5Cl, which is equivalent to reducing the concentration of CH_3 radicals. Since small amounts of CO apparently reduce $[CH_3]$ and since CO is known to remove $CH_2(^3\Sigma_g^-)$, it is obvious, on a qualitative basis, that reaction 4 is favored over reaction 3. The experiments with large amounts of CO, *i.e.*, small $[CH_2(^3\Sigma_g^-)]$, show that CH_3 radicals are not present; hence, reaction 5 is greatly favored over reaction 6.

Some experiments were done to measure the ratio of C_2H_6 to $C_2H_4Cl_2$ yields as a function of $[CO]/[CH_2Cl]$. The results[15] are very similar to Figure 1 and show that the concentration of CH_3 radicals is drastically reduced by small quantities of CO. With no added CO, the CH_2Cl and $CHCl_2$ radicals combine to give $C_2H_3Cl_3$;[4a] this product was absent from experiments with ten parts of added CO.

Reactions of Methylene with Mixtures of CH_2Cl_2 and cis-2-C_4H_8 and CO. To confirm that singlet CH_2 only abstracted chlorine from CH_2Cl_2, it was desirable to measure $[^3CH_2]/[^1CH_2]$ at high concentrations of CO and see whether the residual $[CH_3]$ was due to small concentrations of $CH_2(^3\Sigma_g^-)$ or to a slow C–H abstraction reaction by $CH_2(^1A_1)$. The stereospecific reactions with singlet CH_2 with *cis*- and *trans*-2-butene have been used by many investigators[10] to measure $[^3CH_2]/[^1CH_2]$. We used *cis*-butene because it provides the most sensitive measurement of the triplet component. Most investigators agree that the singlet CH_2 addition is stereospecific providing the pressure is sufficiently high to quench the unimolecular *cis–trans* isomerization of the chemically activated 1,2-dimethylcyclopropanes (DMC).[16] In contrast there is little agreement for the

(13) J. M. Tedder and J. C. Walton, *Progr. React. Kinet.*, **4**, 37 (1967).

(14) M. L. Halberstadt and J. R. McNesby, *J. Amer. Chem. Soc.*, **89**, 3417 (1967).

(15) W. G. Clark, Master's Thesis, Kansas State University, 1969. Some of the conclusions reached in this reference differ from the ones in the text of the paper; the latter takes precedence.

(16) (a) J. W. Simons and G. W. Taylor, *J. Phys. Chem.*, **73**, 1274 (1969); (b) D. W. Setser and B. S. Rabinovitch, *Can. J. Chem.*, **40**, 1425 (1962); (c) J. W. Simons and B. S. Rabinovitch, *J. Phys. Chem.*, **78**, 1322 (1964).

ratio of *cis*- and *trans*-DMC resulting from addition of $CH_2(^3\Sigma_g^-)$ to *cis*- or *trans*-2-butene.[10] Although the suggestion that $CH_2(^3\Sigma_g^-)$ plus either *cis*- or *trans*-2-butene gives the same ratio (2.9) of *trans*- to *cis*-DMC is attractive,[17] most investigations have found different ratios. We will use the recent value[10] of 1.8 for the ratio of *trans*- to *cis*-DMC from reaction of $CH_2(^3\Sigma_g^-)$ with *cis*-butene; this ratio is 2.7 for $CH_2(^3\Sigma_g^-)$ plus *trans*-2-butene.

Experiments were done at 350 and 800 Torr total pressure with various combinations of CO, CH_2Cl_2, and *cis*-C_4H_8. The *trans*-DMC/(*trans*-DMC + *cis*-DMC) was measured as 0.18 in the absence of CO or CH_2Cl_2. This ratio indicated a 28% triplet methylene reaction system. Such a calculation assumes ${}^1k_{C_4H_8}/{}^3k_{C_4H_8} = 1.0$, a view which, although widely held, does not seem to have been proven. Our 28% value agrees with conclusions from other photolysis studies of CH_2CO.[6-8] The *trans*-DMC/(*trans*-DMC + *cis*-DMC) ratio was unchanged by the addition of CH_2Cl_2, and it follows that $[CH_2(^1A_1)]/[CH_2(^3\Sigma_g^-)]$ also was unchanged. This has several ramifications. (1) The chloromethanes apparently do not induce fast collisional crossing of $CH_2(^1A_1) \rightarrow CH_2(^3\Sigma_g^-)$. (2) Since reaction of $CH_2(^1A_1)$ and $CH_2(^3\Sigma_g^-)$ with CH_2Cl_2 did not affect $[CH_2(^1A_1)]/[CH_2(^3\Sigma_g^-)]$, it seems that ${}^3k_H/{}^1k_{Cl} \approx {}^3k_{C_4H_8}/{}^1k_{C_4H_8}$. However, it is always possible that this overall result may be the fortuitous combination of several effects.

Adding CO to mixtures of CH_2Cl_2 and *cis*-C_4H_8 affects the yield of *trans*-DMC as shown in Figure 2. Ten parts CO reduced *trans*-DMC to a value which corresponds to 15% triplet methylene; further addition of CO, up to 50 parts, reduced the triplet level to $\lesssim 7\%$. This residual triplet CH_2 presumably also will be present in the CO–CH_2Cl_2 system. Our results differ from DeGraff and Kistiakowsky in that 10 parts CO was not entirely sufficient to remove $CH_2(^3\Sigma_g^-)$.

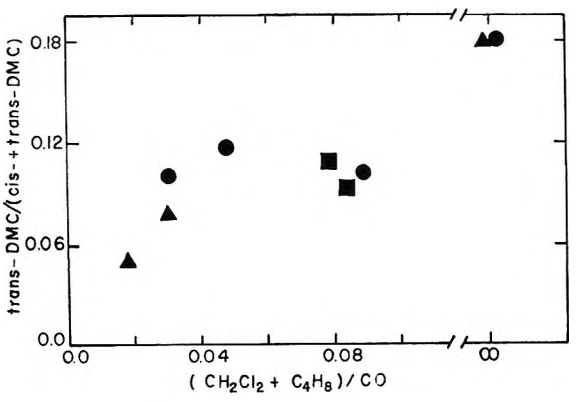

Figure 2. Ratio of [*trans*-DMC]/[*trans*- + *cis*-DMC] yields *vs.* amount of CO added to mixtures of CH_2Cl_2 and *cis*-butene: ●, $[CH_2Cl_2]/[cis\text{-}C_4H_8] = 1$, $P = 350$ Torr; ■, $[CH_2Cl_2]/[cis\text{-}C_4H_8]$ was either 3 or 0.3, $P = 350$ Torr; ▲, $[CH_2Cl_2] = 0$, $P = 800$ Torr.

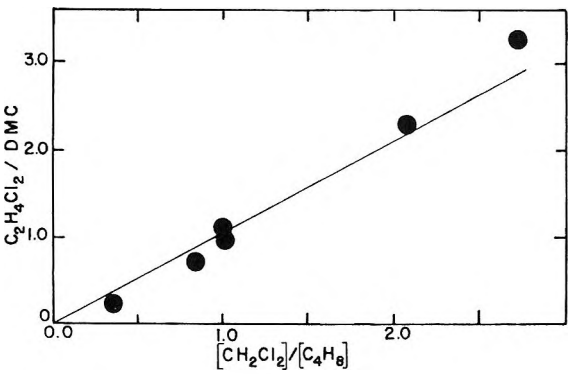

Figure 3. Ratio of $C_2H_4Cl_2$/*cis*-dimethylcyclopropane yields *vs.* the composition of the CH_2Cl_2 and C_4H_8 mixture, the [CO] was 10–20 times the sum of $[CH_2Cl_2]$ and $[C_4H_8]$ and the total pressure was 350 Torr.

This difference may arise from slightly different experimental conditions (different light intensity or spread in wavelength) or because DeGraff and Kistiakowsky used *trans*-C_4H_8 to measure $CH_2(^3\Sigma_g^-)$. Ten per cent $CH_2(^3\Sigma_g^-)$ would give [*cis*-DMC]/[*cis*- + *trans*-DMC] = 0.02 (using [*trans*-DMC]/[*cis*-DMC] = 3.6 from the $CH_2(^3\Sigma_g^-)$ + *trans*-C_4H_8 reaction), and this small quantity could have been overlooked. DeGraff and Kistiakowsky also found a more rapid removal of the nonstereospecific component of the reaction at intermediate [CO] than shown in Figure 2.

The ratio of reaction rates of $CH_2(^1A_1)$ with *cis*-C_4H_8 (double-bond addition only) and CH_2Cl_2 is proportional to the ratio of *cis*-DMC and 1,2-$C_2H_4Cl_2$ products. Photolyses were done for various $[CH_2Cl_2]/[cis\text{-}C_4H_8]$ with 10–20 parts of added CO. The results, corrected for a small contribution to *cis*-DMC from $CH_2(^3\Sigma_g^-)$, are shown in Figure 3. The slope of the line gives ${}^1k_{Cl}/{}^1k_{C_4H_8} = 1.0 \pm 0.1$. Loss of CH_2Cl radicals by H abstraction from CH_2Cl_2 was monitored by observing the formation of CH_3Cl. Under most conditions the CH_3Cl yield was negligible relative to the $C_2H_4Cl_2$ yield.

The two points denoted by the squares of Figure 2 have quite different ratios of CH_2Cl_2 to *cis*-C_4H_8, but the [*trans*-DMC]/[*trans*- + *cis*-DMC] ratio was unchanged. The same observation was made when no CO was present, *i.e.*, the addition of CH_2Cl_2 does not alter the steady-state ratio, $[CH_2(^1A_1)]/[CH_2(^3\Sigma_g^-)]$, in a ketene–butene-2 photolysis mixture. The information from Figures 1–3 will be integrated with published information in the Discussion to obtain rate constant ratios for $CH_2(^3\Sigma_g^-)$ with CH_2Cl_2 relative to CO.

Collisional Deactivation Efficiency of CO and C_4F_8 with 1,2-$C_2H_4Cl_2$.* Since CO was not expected to be a highly efficient deactivating gas, the competition be-

(17) (a) C. McKnight, P. S. T. Lee, and F. S. Rowland, *J. Amer. Chem. Soc.*, **89**, 6802 (1967); (b) D. C. Montague and F. S. Rowland, *J. Phys. Chem.*, **72**, 3705 (1968).

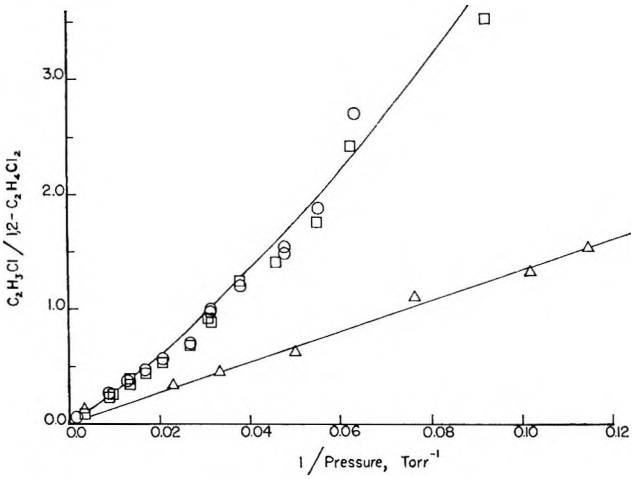

Figure 4. Ratio of the product yields of vinyl chloride-1,2-dichloroethane *vs.* $1/P$ for photolysis of (a) ○, CH_3Cl or □, CH_2Cl_2, CH_2CO, and CO mixtures in the ratio of 10:1.5:105; (b) △, CH_3Cl, CH_2CO, and *c*-C_4H_8 in the ratio of 10:1.5:82. The curve through the CO bath gas points was calculated from a stepladder deactivation model with ΔE = 5.7 kcal and adjusted to the experimental k_a^∞ of 27 Torr. The curve through the *c*-C_4F_8 points is just a straight line through the data points and is not related to a model.

tween collisional deactivation and unimolecular reaction of the chemically activated 1,2-$C_2H_4Cl_2$* was studied and compared to a more efficient gas, perfluorocyclobutane. Figure 4 is a plot of the ratio of the C_2H_3Cl decomposition product, D, to the $C_2H_4Cl_2$ stabilized product, S, *vs.* $1/P$. The analysis of these plots has been previously discussed;[11] the specific rate constant for the unimolecular reaction may be expressed as $k_a = \omega D/S$, where ω is the collisional frequency of $C_2H_4Cl_2$* with bath gas molecules. The two deactivating gases illustrate the difference between an efficient, *c*-C_4F_8, and a less efficient, CO, deactivator. The cascade deactivation by CO is evident from the curvature of the plot. In the region for $D/S \leq 0.5$, both sets of data are essentially linear and the slopes of the lines in this pressure region are a measure of the overall relative deactivating efficiencies. These slopes are 27 Torr and 13.5 Torr for CO and *c*-C_4F_8; CH_2Cl_2 had a value of 17.2 Torr.[4a,18] Converting these values to units of sec^{-1} by using Lennard-Jones collision diameters[19] ($\sigma(C_2H_4Cl_2)$ = 5.5 Å, $\sigma(CO)$ = 3.69 Å, $\sigma(CH_2Cl_2)$ = 4.90 Å, $\sigma(C_4F_8)$ = 7.03 Å) gives k_a = 3.09 × 10^8, 1.63 × 10^8, and 1.76 × 10^8 sec^{-1} for CO, C_4F_8, and CH_2Cl_2. A more detailed analysis based upon the curvature of the CO plot, which gives the average energy transferred per collision, is presented in the Discussion.

It should be noted that experiments using both CH_3Cl–CO and CH_2Cl_2–CO mixtures were done and the results, Figure 4, were identical, which increases our confidence in the data. Also it shows the usefulness of CO in simplifying the chemistry of systems involving CH_2 and chloroalkanes; our earlier studies[4a,11a] of CH_2 + CH_2Cl_2 always showed excess vinyl chloride yields due to complicating secondary radical reactions. These complications were removed by addition of CO because the product yields associated with the hydrogen abstraction reaction of $CH_2(^3\Sigma_g^-)$ were diminished.

Assuming that CO has the same deactivating efficiency toward C_2H_5Cl* as it does for 1,2-$C_2H_4Cl_2$*, the measured yield of C_2H_5Cl can be corrected for decomposition in mixtures of CH_2Cl_2 and CO. This was done by using $D/S = (\alpha\chi_{CO} + \chi_{CH_2Cl_2})k_a/P$ with $[C_2H_5Cl]_\infty$ given by $(D/S)S + S$. The deactivation efficiency on a pressure for pressure basis of CO relative to CH_2Cl_2 is α = 1.55; χ denotes the respective mole fraction of bath gas, S is the measured yield of C_2H_5Cl, k_a is the specific rate constant for chloroethane decomposition (35 cm in pressure units),[4d] and $[C_2H_5Cl]_\infty$ is the yield of chloroethane at infinitely high pressure.

Discussion

General Reactions of Methylene with Dichloromethane. The curve in Figure 1 has an intercept, $[CO] \rightarrow \infty$, that is very small. Since CO removes $CH_2(^3\Sigma_g^-)$, it is apparent that $CH_2(^1A_1)$ reacts with dichloromethane by abstracting a chlorine atom. We attribute the small amount of C_2H_5Cl remaining at high concentrations of CO to residual $CH_2(^3\Sigma_g^-)$ and *not* to a small amount of H abstraction by $CH_2(^1A_1)$. Insertion reactions, either C–H or C–Cl, were not observed in this study or in previous work[4,5] which sets a limit to these reactions of less than 3% of the main chlorine abstraction reaction.

It is more difficult to show directly that $CH_2(^3\Sigma_g^-)$ only abstracts hydrogen. However, mass balance arguments require all of the $CH_2(^3\Sigma_g^-)$ for generation of CH_3 in order to properly account for the methyl products. Triplet CH_2 has some properties that are similar to conventional radicals,[2c] and abstraction of H rather than Cl is similar to the behavior of CF_3 with halomethanes. In fact the abstraction of Cl by CF_3 has a 5 kcal mol^{-1} higher activation energy than abstraction of H.[21] Triplet CH_2 also abstracts secondary H more readily than primary H which is consistent with normal radical behavior.[20]

There are two studies which must be considered before our interpretation that $CH_2(^1A_1)$ abstracts only Cl and $CH_2(^3\Sigma_g^-)$ abstracts only H can be taken as entirely correct. DeGraff and Kistiakowsky[8a] found that only 10 parts CO was needed to reduce the triplet

(18) D. W. Setser, *J. Amer. Chem. Soc.*, **90**, 582 (1968).

(19) J. O. Hirschfelder, C. F. Curtis, and R. B. Bird, "Molecular Theory of Gases and Liquids," John Wiley and Sons, New York, N. Y., 1964, pp 1210–1214.

(20) S. Krzyzanowski and R. J. Cvetanović, *Can. J. Chem.*, **45**, 665 (1967).

(21) (a) W. G. Alcock and E. Whittle, *Trans. Faraday Soc.*, **62**, 664 (1966); (b) J. I. G. Cadogan, D. H. Hey, and P. G. Hibbert, *J. Chem. Soc.*, 3939 (1965).

methylene to zero in their reaction system of methylene with *trans*-2-butene. We have already pointed out that their analytical technique was less sensitive than the one used here; they could easily have overlooked the small yield of *cis*-DMC associated with the residual triplet CH_2. Bamford, *et al.*,[9] have reported that singlet methylene abstracted chlorine at least 16 times faster than hydrogen, and triplet methylene abstracted hydrogen seven times faster than chlorine. However, their conclusions were based on data obtained with only six parts of added CO, instead of using very large amounts of CO as was done in this study. It seems likely that Bamford, *et al.*, had insufficient CO to remove all of the triplet CH_2; hence, the results were obtained from a mixture of singlet and a small amount of triplet methylene. We feel that the room temperature reactions 4 and 5 are faster than 3 and 6 by factors of nearly 50.

Explaining the fast Cl abstraction reaction of $CH_2(^1A_1)$, even on a qualitative basis, presents a challenge. The discrimination for Cl abstraction *vs.* H abstraction cannot be explained on the basis of the heats of reactions, since both reactions would have about the same values. We suggest that $CH_2(^1A_1)$ initiates the Cl abstraction reaction by accepting an electron pair from chlorine into its vacant orbital. This is followed by bond cleavage of $Cl–CH_2Cl$ and internal electronic rearrangement of the newly formed $CH_2–Cl$. In this sense the $CH_2(^1A_1)$ is behaving as a Lewis acid and should show electrophilic character for *this type* of reaction. This is consistent with the observed[5] greater reaction rate with CH_3Br[6] relative to CH_3Cl. Singlet methylene does not exhibit electrophilic character in the reaction with olefins.[20] However, the double bond addition reaction involves attack by the pair of nonbonded electrons. In contrast, we propose, as did Bamford and coworkers, that the vacant orbital is important for reaction with the Cl or Br in chloro- and bromomethanes.

Reactions of Methylene in Mixtures of CO, CH_2Cl_2, and CH_2CO. The effect of small amounts of CO upon the product yields is quite dramatic and is explained by the more rapid reaction of CO with $CH_2(^3\Sigma_g^-)$ than with $CH_2(^1A_1)$. We shall try to formulate a mechanism which matches the observed variation of the $C_2H_5Cl/C_2H_4Cl_2$ product yield ratio with $[CO]/[CH_2Cl_2]$. Ignoring possible collisional effects of the CH_2CO^* formed by reaction of CH_2 and CO, the following equations may be written

$$CH_2(^1A_1) + CO \xrightarrow{^1k_{CO}} CH_2CO \quad (10)$$

$$CH_2(^3\Sigma_g^-) + CO \xrightarrow{^3k_{CO}} CH_2CO \quad (11)$$

Collisional induced intersystem crossing is a way of preparing $CH_2(^3\Sigma_g^-)$, and quantitative data have been published for rate constants with various third bodies.[22]

$$CH_2(^1A_1) + M \xrightarrow{^1k_3} CH_2(^3\Sigma_g^-) + M \quad (12)$$

We include reaction 12 with carbon monoxide, although it is not demanded by our data. The main reactions[20] of $CH_2(^1A_1)$ and $CH_2(^3\Sigma_g^-)$ with CH_2CO also are needed

$$CH_2(^1A_1) + CH_2CO \xrightarrow{k_{CH_2CO}} C_2H_4 + CO \quad (13)$$

$$CH_2(^3\Sigma_g^-) + CH_2CO \xrightarrow{^3k_{CH_2CO}} C_2H_4 + CO \quad (14)$$

(eq 13 and 14). Removal of CH_2Cl and CH_3 by abstraction reactions is slow under our photolysis conditions and such reactions will be neglected. Steady-state expressions for $[^1CH_2]$ and $[^3CH_2]$ may be obtained from reactions 1, 2, 4, 5, and 10–14. Substitution for $[^1CH_2]$ in the $[^3CH_2]$ expression and taking the ratio indicated below leads to eq I. The second

$$\frac{^3k_H[^3CH_2]}{^1k_{Cl}[^1CH_2]} = \frac{\phi_3}{\phi_1}\left[\frac{1 + \dfrac{(^1k_{CO} + {}^1k_3)[CO]}{^1k_{Cl}[CH_2Cl_2]} + \dfrac{^1k_{CH_2CO}[CH_2CO]}{^1k_{Cl}[CH_2Cl_2]}}{1 + \dfrac{^3k_{CO}[CO]}{^3k_H[CH_2Cl_2]} + \dfrac{^3k_{CH_2CO}[CH_2CO]}{^3k_H[CH_2Cl_2]}}\right] + \frac{\dfrac{^1k_3[CO]}{^1k_{Cl}[CH_2Cl_2]}}{1 + \dfrac{^3k_{CO}[CO]}{^3k_H[CH_2Cl_2]} + \dfrac{^3k_{CH_2CO}[CH_2CO]}{^3k_H[CH_2Cl_2]}} \quad (I)$$

term arises from reaction 12 as a source of $CH_2(^3\Sigma_g^-)$. Only rate constant ratios are involved and it is possible to assign values to most of them; Table I gives a summary. Setting $[CO]/[CH_2Cl_2] = 0$ in eq I gives eq II.

$$\frac{^3k_H[^3CH_2]}{^1k_{Cl}[^1CH_2]} = \frac{\phi_3}{\phi_1}\left[1 + \frac{^1k_{CH_2CO}[CH_2CO]}{^1k_{Cl}[CH_2Cl_2]}\right] \Big/ \left[1 + \frac{^3k_{CH_2CO}[CH_2CO]}{^3k_H[CH_2Cl_2]}\right] \quad (II)$$

The right-hand side of (II) is the ratio of triplet to singlet quantum yields modified by various rate constant ratios, and if $^3k_H = {}^1k_{Cl}$, the right-hand side of (II) gives the steady-state ratio of singlet–triplet methylene.

If the rate constants for CH_2Cl_2 are changed to those for C_4H_8, eq II applies to the butene–ketene experiments. The rate constant ratios are available from Table I, the experimental value, Figure 2, of $^3k_{C_4H_8}[^3CH_2]/{}^1k_{C_4H_8}[^1CH_2]$ is 0.39, and $\phi_3/\phi_1 = 0.37$ or 0.38 depending upon which $^3k_{CO}/{}^3k_{C_4H_8}$ value is used to determine $^3k_{CH_2CO}/{}^3k_{C_4H_8}$. It is clear that for small ratios of

(22) (a) T. W. Eder, R. W. Carr, Jr., and J. W. Loenst, *Chem. Phys. Lett.*, **3**, 520 (1969); (b) R. A. Cox and K. F. Preston, *Can. J. Chem.*, **47**, 3345 (1969); (c) R. D. Koob, *J. Phys. Chem.*, **73**, 3169 (1969).

Table I: Rate Constant Ratios at 300°K for Methylene Radicals

Rate constant ratios	Value	Reference
$^3k_{CO}/^3k_{CH_2CO}$	3.6	See ref 8a
$^1k_{CO}/^1k_{CH_2CO}$	0.14 ± 0.02	See ref 8a
	0.121 ± 0.5	See ref 22b
$^3k_{CO}/^3k_{C_4H_8}$	1.3 ± 0.3	See ref 8a
	2.08	See ref 8b
$^1k_{CO}/^1k_{C_4H_8}$	0.10 ± 0.02	See ref 8a
$^1k_{Cl}/^1k_{C_4H_8}$	1.0 ± 0.1	This work, Figure 3
$^1k_{CO}/^1k_{Cl}$	0.10	$^1k_{Cl} = {}^1k_{C_4H_8}$
$^1k_{CH_2CO}/^1k_{Cl}$	0.71	$\frac{^1k_{CO}}{^1k_{Cl}} \cdot \frac{^1k_{CH_2CO}}{^1k_{CO}}$
$^1k_3/^1k_{CH_2CO}$	0.01	See ref 8a
$^3k_H/^3k_{C_4H_8}$	1.0	See *a*
$^3k_{CH_2CO}/^3k_H$	0.36 or 0.58	$\frac{^3k_{C_4H_8}}{^3k_H} \cdot \frac{^3k_{CO}}{^3k_{C_4H_8}} \cdot \frac{^3k_{CH_2CO}}{^3k_{CO}}$; also see *b*

[a] This ratio was derived from $^1k_{Cl}/^1k_{C_4H_8} = 1.0$ and $^3k_H/^1k_{Cl} = {}^3k_{C_4H_8}/^1k_{C_4H_8}$; the error limits are probably no better than 30%. (See text for further discussion.) [b] The two values correspond to the two values for $^3k_{CO}/^3k_{C_4H_8}$. This ratio also can be obtained from the relationship $(^3k_{CO}/^3k_H)(^3k_{CH_2CO}/^3k_{CO})$. (See text for further discussion.)

$[CH_2CO]/[C_4H_8]$ the quantum yields are hardly altered by the rate constant ratio expression of eq II.

The value of ϕ_3/ϕ_1 determined above also was used for the CH_2Cl_2 experiments. Since the yield of [*trans*-DMC]/[*cis*-DMC] was independent of the ratio of $[CH_2Cl_2]/[cis\text{-}C_4H_8]$, we can use the data points with no added CO with the relationship that $^3k_H[^3CH_2]/{}^1k_{Cl}[^1CH_2] = {}^3k_{C_4H_8}[^3CH_2]/{}^1k_{C_4H_8}[^1CH_2]$ to evaluate the proportionality factor between the $C_2H_5Cl/C_2H_4Cl_2$ yield ratio and $^3k_H[^3CH_2]/{}^1k_{Cl}[^1CH_2]$. The factor was 0.89. This factor was assumed to be independent of the amount of CO added to the reaction mixture, and the data from Figure 1 were used to construct the experimental points of Figure 5. It would have been desirable to obtain values of $^3k_H[^3CH_2]/k_{Cl}[^1CH_2]$ more directly from experimental measurements of *total product* yields from the CH_3, CH_2Cl, and $CHCl_2$ radicals. Without careful and simultaneous control of light intensity, pressure, radical concentrations, etc., which are very difficult to do while adding large quantities of inert gas, such experiments would not be worthwhile. These problems emphasize the need for development of methods for *direct* monitoring of both $[^3CH_2]$ and $[^1CH_2]$ as a function of all experimental variables.

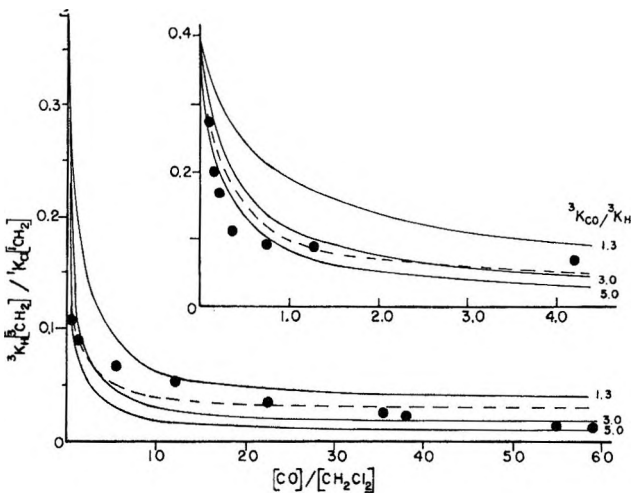

Figure 5. Comparison of calculated, eq II, and experimental values of $^3k_H[^3CH_2]/{}^1k_{Cl}[^1CH_2]$ *vs.* $[CO]/[CH_2Cl_2]$. The points represent the experimental data; the lines are calculated for values of rate constant ratios appearing on the right side of the graph. The dashed curve shows the effect of increasing $^1k_3/{}^1k_{Cl}$ from 0.01 to 0.1 with $^3k_{CO}/^3k_H = 5.0$.

Equation I was used to assign values of $^3k_{CO}/^3k_H$ by comparing the calculated and experimental values of $^3k_H[^3CH_2]/{}^1k_{Cl}[^1CH_2]$ at various $[CO]/[CH_2Cl_2]$. The comparisons are summarized in Figure 5. The ratios of rate constants for $^1CH_2$ reactions are listed in Table I. The value of $^3k_{CH_2CO}/^3k_H$ can be estimated as indicated in Table I or it can be expressed as $(^3k_{CO}/{}^3k_H)(^3k_{CH_2CO}/^3k_{CO})$. The only unknown remaining in eq I is $^3k_{CO}/^3k_H$, and a series of curves were calculated with this ratio varying from 1.3–9.0; the best fit obtained for $^3k_{CO}/^3k_H$ = 3–5. The effect of changing $^1k_3/^1k_{Cl}$ from 0.01 to 0.1 is indicated by comparison to the dotted line of Figure 5. Our data do not set a clearly defined limit to this rate constant ratio; however, best agreement seems to be for $^3k_{CO}/^3k_H$ of ~5 and $^1k_3/^1k_{Cl}$ of ~0.1. This value is a little higher than the $^1k_3/^1k_{CH_2CO}$ value of 0.01 suggested by Kistiakowsky but is not inconsistent with the rate constants for similar third bodies.[22] The initial rapid drop in the curves of Figure 5 is due to the importance of the term, $^3k_{CO}/^3k_H$, in the denominator of eq I. For very large $[CO]/[CH_2Cl_2]$, eq I reduces to

$$\frac{^3k_H[^3CH_2]}{^1k_{Cl}[^1CH_2]} = \frac{\phi_3}{\phi_1}\left[\frac{^1k_{CO} + {}^1k_3}{^1k_{Cl}}\right]\frac{^3k_H}{^3k_{CO}} + \frac{^1k_3}{^1k_{Cl}}\frac{^3k_H}{^3k_{CO}} \quad \text{(III)}$$

For $^3k_H/^3k_{CO}$ = 5.0 and $^1k_3/^1k_{Cl}$ = 0.1, the limiting ratio is 0.04; this is reduced to 0.01 for $^1k_3/^1k_{Cl}$ = 0.01. It is interesting to note that even if $^1k_3/^1k_{Cl}$ = 0, eq III has a finite intercept of ~0.01. Therefore, the CO addition technique could never give more than a 99% singlet methylene reaction system.

We concluded that, within our experimental error, $CH_2(^1A_1)$ added to the double bond of *cis*-C_4H_8 at the same rate as Cl was abstracted from CH_2Cl_2. Qualitative arguments also indicated that $^1k_{Cl}/^3k_H = {}^1k_{C_4H_8}/^3k_{C_4H_8}$, and since $^1k_{Cl} = {}^1k_{C_4H_8}$, we should find $^3k_{C_4H_8} = {}^3k_H$. A more direct comparison can be obtained from the rate constants for C_4H_8 and CH_2Cl_2 relative to CO. We obtained $^3k_{CO}/^3k_H$ values of 3–5 which are similar to the higher value for $^3k_{CO}/^3{}_{C_4H_8}$ of 2.08 measured by Cox and Cvetanović. It is usually assumed that $^3k_{C_4H_8} = {}^1k_{C_4H_8}$ and that the quantum

yield ratios of eq II are equivalent to $[^3CH_2]/[^1CH_2]$. Since the same value for $^3k_{C_4H_8}[^3CH_2]/^1k_{C_4H_8}[^1CH_2]$ is obtained under a wide variety of reaction conditions in several different laboratories, we agree that $^3k_{C_4H_8} \simeq {}^1k_{C_4H_8}$, which in turn forces the conclusion that $^3k_H \simeq {}^1k_{Cl}$. Cox and Preston[22b] found that $CH_2(^3\Sigma_g^-)$ reacts much faster with O_2 than with CO. Thus these H and Cl abstraction reactions may be relatively fast but reaction certainly does not occur on every collision and may be as slow as $1/10^2$–10^3 collisions.[23]

Other Reaction Systems. We have made some preliminary investigations of the reactions of CH_2 with 1,2-$C_2H_4Cl_2$ in the presence of ten parts carbon monoxide. At pressure above 5 Torr the system behaves as expected and the only products found were from radicals formed by chlorine abstraction by singlet CH_2. However, at lower pressures complications were encountered which can be attributed to inefficient removal of CH_2 $(^3\Sigma_g^-)$ by reaction 11. This suggests that collisional stabilization and reverse dissociation of triplet CH_2CO^* formed in reaction 11 may be competitive in this pressure range. Another problem which can arise in the CH_2CO–CO–chloroalkane systems is secondary abstraction processes. These also tend to be more important at low pressure because the radical concentrations decline since vessels become very large in order to hold reactant proportions constant. We also encountered problems with secondary radical reactions in the CH_2CO–CD_3Cl–CO reaction system at high pressures for unknown reasons.

Collisional Deactivation of $C_2H_4Cl_2^*$ by CO, CH_2Cl_2, and C_4F_8. The exothermic reactions of singlet CH_2 provide numerous chemical activation systems. The addition of CO as a bath gas can serve to simplify the chemistry of such studies, and we have measured the relative efficiencies of CO, CH_2Cl_2, and *c*-C_4F_8 which are 0.50:0.77 and 1.0 on a pressure for pressure basis. The use of conventional collision diameters converts this to a collision for collision basis of 0.53:0.93:1.0. These efficiencies were measured for $D/S \leq 0.5$ and are sufficient to give an estimate of the unit deactivation nonequilibrium rate constant for chemically activated molecules in a CO bath gas.

The methods used to analyze the D/S plots in order to obtain detailed vibrational energy transfer information from the high- and low-pressure regions have been presented elsewhere.[11,24] If the experimental rate constant for some gas, A, is defined as $k_a(A) = \omega_A D/S$, the high-pressure rate constant ratio for gases A and B according to simple cascade deactivation model with initially formed monoenergetic $C_2H_4Cl_2^*$ has the form

$$\frac{k_a^\infty(A)}{k_a^\infty(B)} = \frac{\beta_B}{\beta_A} \sum_{t=1}^{T_A} k_{et} / \sum_{t=1}^{T_B} k_{et} \qquad \text{(IV)}$$

The β term allows for uncertainties in the values chosen for the collision diameters needed to calculate ω_A and ω_B; T_A and T_B are the number of steps, of size ΔE, in the cascade. If the gas used for comparison has nearly a unit deactivation efficiency (a ΔE of ~14 kcal mol^{-1} is equivalent to unit deactivation) and if the cross sections are known, the high-pressure ratio can be used to assign values of ΔE. These ΔE values correspond to the average energy, $\langle \Delta E \rangle$, removed from the *active* degrees of freedom of $C_2H_4Cl_2^*$ per collision (according to a symmetric model of collision transition probabilities). A calculated plot of eq IV *vs.* $\langle \Delta E \rangle$ for simple stepladder cascade of $C_2H_4Cl_2^*$ with the β ratio equal to unity is shown in Figure 6. The full 300°K distribution function of the activated $C_2H_4Cl_2^*$ was used in the calculations. This curve may be used to obtain an estimate for $\langle \Delta E \rangle$; for example $k_a^\infty(CO)/k_a^\infty(C_4H_8)$ gives $\langle \Delta E \rangle$ = ~5 kcal mol^{-1}. The analysis just described for finding $\langle \Delta E \rangle$ is an approximate procedure, at best, because of the uncertainties associated with the collision diameters. Analysis of the curvature of the low pressure data, *i.e.*, variation of k_a with pressure, is a more reliable way of finding $\langle \Delta E \rangle$,[11,24] and it is independent of the values chosen for the collision diameter or of the specific rate constants, k_ϵ. This was done for the CO data, and the calculated results from a simple cascade model with $\langle \Delta E \rangle = 5.7$ kcal mol^{-1} are shown as the solid line in Figure 4. Since high- and low-pressure data gave the same answer, the average energy removed from $C_2H_4Cl_2^*$ per collision with CO can be placed with confidence[25a] as 6 ± 2 kcal mol^{-1}. Problems of analysis made the low-pressure data for C_4F_8 difficult to obtain. However, no evidence for an increase in k_a with pressure (or any corresponding[25b,c] curvature in the D/S plot) was found for $D/S \leq 2.0$. This can be interpreted as $\langle \Delta E \rangle \sim 12$–14 kcal mol^{-1}.

We previously found that CH_2Cl_2 and CH_3Cl removed 11 ± 2 kcal mol^{-1} from $C_2H_4Cl_2^*$. Furthermore, the rather uncertain data previously obtained

(23) W. Braun, A. M. Bass, and M. Pilling, Fifth International Conference on Photochemistry, 1969. This flash photolysis study suggests that C–H abstraction by $CH_2(^3\Sigma_g^-)$ is a relatively slow reaction.

(24) (a) G. H. Kohlmaier and B. S. Rabinovitch, *J. Chem. Phys.*, **38**, 1709, 1692 (1963); (b) D. W. Setser, B. S. Rabinovitch, and J. W. Simons, *ibid.*, **40**, 1751 (1964); (c) D. C. Tardy and B. S. Rabinovitch, *ibid.*, **48**, 5194 (1968).

(25) (a) This ΔE is from a simple cascade model, which is equivalent to the average energy, $\langle \Delta E \rangle$, transferred per collision for a *symmetric* distribution of energy transfer probabilities. For values of $\langle \Delta E \rangle$ near 6 kcal mol^{-1}, the curvature of the D/S *vs.* $1/P$ plot is very similar for even the two extreme types of energy transfer probabilities, *i.e.*, the exponential or the symmetric distribution models. Our data, at the present time, are not capable of distinguishing between these two types of models; (b) N. L. Craig and D. W. Setser, unpublished data. Preliminary work with chemically activated CH_3CF_3 in a C_4F_8 bath shows $\langle \Delta E \rangle$ = 14 kcal. This conclusion is based upon the actual curvature of low-pressure data, such as shown in Figure 4 for CO. Reinvestigation of the deactivation of chemically activated dimethylcyclopropane by *cis*-butene-2 (J. D. Rynbrandt and B. S. Rabinovitch, *J. Phys. Chem.*, **74**, 1679 (1970) has confirmed[24b] the previously measured $\langle \Delta E \rangle$ of 11–12 kcal mol^{-1}. These data suggest that the large deactivating molecules, such as C_4F_8 and C_4H_8, may reach an upper limit of perhaps 12–14 kcal mol^{-1} for the amount of energy removed per collision; (c) large values of $\langle \Delta E \rangle$, such as 12 kcal, are only compatible with a symmetric distribution of energy transfer probabilities.[24,27]

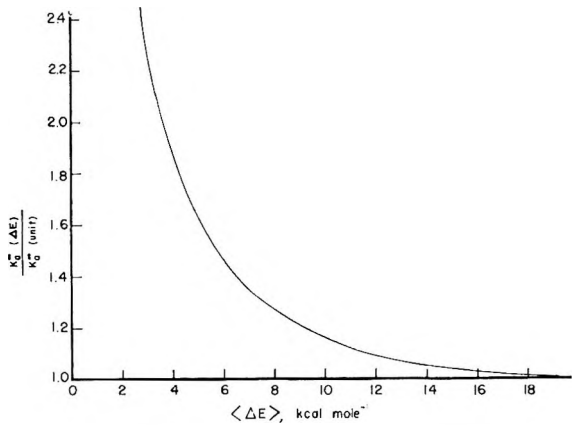

Figure 6. The calculated values of $k_a^{\infty}(\Delta E)/k_a^{\infty}$ (unit), *vs.* $\langle\Delta E\rangle$ for chemically activated $C_2H_4Cl_2$* according to a stepladder deactivation model.

for N_2, $\langle\Delta E\rangle \simeq 6$ kcal mol^{-1}, are in agreement with the present result with CO. We conclude that the change from an optically inactive vibration in N_2 to an optically active vibration in CO had no effect upon the amount of energy removed from 1,2-$C_2H_4Cl_2$* by collisions at 300°K. This must mean that the long-range dipole–dipole interactions[26] are not very important for this type of energy transfer. This was anticipated since Ar was only slightly less effective than N_2 in removing energy from $C_2H_4Cl_2$* or C_3H_6*,[24b] which implies that vibrational–vibrational transfer is not a significant mechanism for N_2 or CO colliding with molecules such as $C_2H_4Cl_2$* or C_3H_6.[27]

The conclusions regarding efficient collisional vibrational energy transfer with polyatomic molecules recently have been challenged by Thrush and Atkinson.[28] They interpret their data from the photoexcitation of cycloheptatriene in terms of removal of small quantities of energy rather than the large values derived from studies of chemically activated chloroethanes, hydrocarbon radicals, or cyclopropanes. The work reported here and elsewhere for 1,2-$C_2H_4Cl_2$*[29] and 1,2-$C_2H_4F_2$*,[11b] new work[30] with 3,3-dimethylhexyl-2* and 3-methylhexyl-2* radicals, and studies[31] with NO_2* all favor efficient collisional energy transfer with collision diameters near gas kinetic values and large values of $\langle\Delta E\rangle$ per collision. At present the evidence is overwhelmingly in favor of the conclusions drawn from chemical activation studies. It should be emphasized that the curvature of the D/S *vs.* (pressure)$^{-1}$ plots provides information regarding $\langle\Delta E\rangle$ which is independent[24] of the values for k_e and of collision diameters. The same type of information from the cycloheptatriene study should be interesting.[32]

Acknowledgment. Acknowledgment is made to the donors of the Petroleum Research Fund, administered by the American Chemical Society, for support of this research.

(26) (a) B. H. Mahan, *J. Chem. Phys.*, **46**, 98 (1967); (b) J. T. Yardley, *ibid.*, **50**, 2464 (1969).

(27) D. C. Tardy and B. S. Rabinovitch, *ibid.*, **48**, 1282 (1968). These authors analyzed the collisional efficiency of several gases from thermal activation experiments with CH_3NC; N_2 transferred somewhat more energy than Ar in this case which involves excitation of CH_3NC to about 40 kcal mol^{-1}.

(28) R. Atkinson and B. A. Thrush, *Chem. Phys. Lett.*, **3**, 684 (1969).

(29) E. E. Siefert and D. W. Setser, unpublished data for Ne with $C_2H_4Cl_2$* presented at the Gordon Conference on Molecular Energy Transfer, 1969.

(30) C. W. Larson and B. Rabinovitch, *J. Chem. Phys.*, **61**, 2293 (1969).

(31) S. E. Schwartz and H. S. Johnston, *ibid.*, **51**, 1286 (1969).

(32) Note Added in Proof. Recent studies of the reactions of CH_2 with chloropropanes [C. H. Bamford and J. E. Casson, *Proc. Roy. Soc.*, **A312**, 141, 163 (1969)] are in accord with the main conclusions of this paper. Additional evidence[23] for slow abstraction reactions ($>10^9$ collisions with CD_4) by $CH_2(^3\Sigma_g^-)$ has been reported [P. S. T. Lee, R. L. Russel, and F. S. Rowland, *Chem. Comm.*, 18 (1970)].

Collisional Transition Probability Distributions for Deactivation of Vibrationally Excited Dimethylcyclopropane[1a]

by J. D. Rynbrandt[1b] and B. S. Rabinovitch

Department of Chemistry, University of Washington, Seattle, Washington 98105 *(Received November 3, 1969)*

The collisional deactivation efficiencies of *cis*-butene-2 and carbon monoxide with singlet dimethylcyclopropane, chemically activated to ~113.6 kcal mol^{-1}, have been determined. *cis*-Butene was found to remove 4000 cm^{-1} (11.4 kcal mol^{-1}) on each collision on the basis of a stepladder or gaussian form for the collisional transition probability distribution function. An exponential distribution of transition probabilities cannot fit the data. The carbon monoxide transition probabilities are poorly described by a 1500 cm^{-1} (4.3 kcal mol^{-1}) stepladder model and well-described by an exponential model with an average down step of 1600 cm^{-1} (4.6 kcal mol^{-1}). These energy magnitudes agree with earlier findings on this system from studies of this type but are considerably more reliable by virtue of improved experimental and calculational procedures which were employed. The findings with regard to preferred transition probability models, for weaker and stronger colliders, support earlier and similar conclusions from other systems.

Introduction

Reactions between methylene radicals and hydrocarbons produce molecules at high levels of vibrational excitation.[2] These chemically activated molecules may either react (isomerize) or be stabilized by collisional deactivation below the reaction threshold by heat bath molecules.[3] The pressure dependence of the ratio of stabilization to isomerization amounts can be used to provide information about the nature of the collisional energy transfer transition probabilities.[4]

Studies of this type have been carried out earlier with vibrationally excited dimethyl-,[3a,b] methyl-,[5] and unsubstituted[3c] cyclopropane. Previous energy transfer studies used methylene radicals produced by photolyzing ketene[3b] at 3200 Å and diazomethane[3a] at 4350,[3c] or by pyrolyzing diazomethane.[3a] Several chemical complications which were not recognized at the time are now known. It has been shown that photolysis of ketene[6] and of diazomethane[7] leads to triplet $^3CH_2$ as well as singlet $^1CH_2$ species. Also, the percentage of triplet methylene formed in ketene photolysis is least, and minor in amount, when radiation at 2700 Å is used, by contrast with light of longer wavelengths.[6b,c,8] Still another difficulty that complicated the early data is the recent discovery that the proportions of products derived from $^3CH_2$–butene-2 reaction is pressure dependent in a manner quite different from that in singlet radical systems.[9] Finally, it has been shown that the measurement of the olefin decomposition products at low pressures is complicated by the consecutive decomposition of these products;[10] this confuses an already cumbersome problem of analysis for some four or five C_5 decomposition products.

In the present work we have undertaken a reinvestigation of the *cis*-dimethylcyclopropane (CDMC) system. The importance of this system which involves energy cascade from levels at ~110 kcal mol^{-1} down to 60 kcal mol^{-1} warrants the renewed attention. Triplet complications have been reduced by use of higher energy ketene photolysis systems and by addition of triplet getters—O_2 and, especially, CO which has been shown by DeGraff and Kistiakowsky[6c] to inhibit triplet radical product formation. In addition to improved analytical accuracy relative to the older work, the internal standard technique of Dorer and Rabinovitch[11] has also been adopted. This technique eliminates complications due to pentene product decomposition at

(1) (a) This work was supported by the U. S. Air Force Office of Scientific Research, Contract No. AF49(638)-1633; (b) Standard Oil Predoctoral Fellow.

(2) H. M. Frey and G. B. Kistiakowsky, *J. Amer. Chem. Soc.*, **79**, 6373 (1957).

(3) (a) D. W. Setser and B. S. Rabinovitch, *Can. J. Chem.*, **40**, 1425 (1962); (b) D. W. Setser, B. S. Rabinovitch, and J. W. Simons, *J. Chem. Phys.*, **40**, 1751 (1964); (c) J. W. Simons, B. S. Rabinovitch, and D. W. Setser, *ibid.*, **41**, 800 (1964).

(4) G. H. Kohlmaier and B. S. Rabinovitch, *ibid.*, **38**, 1692, 1709 (1963).

(5) (a) J. N. Butler and G. B. Kistiakowsky, *J. Amer. Chem. Soc.*, **82**, 759 (1960); (b) **83**, 1324 (1961).

(6) (a) J. W. Simons and B. S. Rabinovitch, *J. Phys. Chem.*, **68**, 1322 (1964); (b) R. W. Carr, Jr. and G. B. Kistiakowsky, *ibid.*, **70**, 118 (1966); (c) B. A. DeGraff and G. B. Kistiakowsky, *J. Amer. Chem. Soc.*, **71**, 1553 (1967); **71**, 3984 (1967); (d) T. W. Eder and R. W. Carr, Jr., *J. Phys. Chem.*, **73**, 2074 (1969).

(7) F. H. Dorer and B. S. Rabinovitch, *ibid.*, **69**, 1952, 1964 (1965); (b) B. S. Rabinovitch, K. W. Watkins, and D. F. Ring, *J. Amer. Chem. Soc.*, **87**, 4960 (1965).

(8) (a) S. Ho, I. Unger, and W. A. Noyes, Jr., *ibid.*, **87**, 2297 (1965); (b) S. Ho and W. A. Noyes, Jr., *ibid.*, **89**, 5091 (1967).

(9) (a) F. J. Duncan and R. J. Cvetanović, *ibid.*, **84**, 3593 (1962); (b) D. F. Ring and B. S. Rabinovitch, *Can. J. Chem.*, **46**, 2435 (1968).

(10) J. W. Simons and G. W. Taylor, *J. Phys. Chem.*, **73**, 1274 (1969).

(11) F. H. Dorer and B. S. Rabinovitch, *ibid.*, **69**, 1973 (1965).

low pressures; use of a standard directly provides a measure of the amount of $^1CH_2$ produced and makes analysis for and measurement of the several pentene products less critical. Finally, the initial hot *cis* species isomerizes geometrically to the *trans* isomer and both isomerize structurally to pentenes; this complication has been explicitly treated in detail in the present calculations.

Experimental Section

Materials. Ketene was prepared by pyrolysis of acetic anhydride and was purified by repeated trap-to-trap distillation. Phillips research grade (99.9%) *cis*-butene-2 (CB2) was used without further purification. Chemical Samples' 2,4-dimethylpentane (99%) was degassed and purified by vacuum distillation. Tank grade oxygen, Airco analyzed reagent carbon monoxide (99.9%), and Airco prepurified nitrogen were used.

Apparatus and Procedure. All gas handling was performed on a greaseless vacuum system. The filtered radiation of a G.E. AH-6 high-pressure mercury arc lamp was used for all photolyses. The filter consisted of a 2-cm quartz tube containing ~2 atm of chlorine gas,[12] followed by an aqueous solution of $NiSO_4$ and $CoSO_4$[13] which was circulated through a quartz envelope having a light path of 2 cm. The transmission of the filter was measured. From the known lamp output, from the dependence of ketene extinction coefficient on wavelength,[14] and from the known ketene decomposition quantum yields,[15] the average wavelength for ketene decomposition was determined to be ~2800 Å.

Mixtures of *cis*-butene and 2,4-dimethylpentane (either 4:1 or 8:1) were prepared. All reactions were carried out at room temperature in quartz reactors fitted with Teflon valves and previously seasoned by photolysis of ketene. The photolysis reaction times varied between 2 and 6 hr. The ratio of ketene to butene plus 2,4-dimethyl pentane used was ~1:20 over the pressure range of this study, 0.1–600 mm.

Analysis. Gas chromatography was used for all quantitative analysis. The gas chromatographic injection system accepted the sample directly from the reactor with sharp injections at carrier gas flows as low as 8 cm^3/min. One hundred feet of a Perkin-Elmer support coated open tubular squalane column cooled to 0° adequately separated the C_5 isomers. Following the detection of the C_5 compounds, the column temperature was raised to speed the passage of C_8 compounds.

Results

Low-Pressure CDMC Formation. It is well-established that the initially formed hot CDMC* isomerizes to its geometric isomer TDMC* at a considerably faster rate than the structural isomerization[6a,16]

$$\text{CDMC}^* \underset{k_g'}{\overset{k_g}{\rightleftharpoons}} \text{TDMC}^* \qquad (1)$$

$$\text{CDMC}^* \xrightarrow{k_s} \text{pentenes} \begin{cases} \text{2-methylbutene-1} \\ \text{2-methylbutene-2} \end{cases} \qquad (2)$$

$$\text{TDMC} \xrightarrow{k_s'} \text{pentenes} \begin{cases} \textit{cis}\text{-pentene-2} \\ \textit{trans}\text{-pentene-2} \end{cases} \qquad (3)$$

As the pressure is lowered, the proportions of TDMC:CDMC approach closer to the equilibrium value.[6a] Unfortunately, some disagreement exists regarding the equilibrium value of this ratio for chemically activated singlet systems. Frey reported an extrapolated value of 3 for $K = k_g/k'_g$,[17] while Simons and Rabinovitch report intercepts of 1.5 and 2.0 for TDMC:CDMC product amounts in pure and 10% oxygen systems, respectively. Setser, Rabinovitch, and Simons[3b] have reported a lower value of the ratio, 1.4. Recently, Simons and Taylor[10] observed TDMC:CDMC ratios as high as 2 at 0.5 mm total pressure in a 10% O_2–diazomethane system. In the work reported here, the extrapolated zero pressure ratio was 2.6 in the systems with CB2 as the principal collider and 2.4 in the CO and N_2 systems. These extrapolated ratios enter into the calculation of corrections to the data that arise at lowest pressures, as will now be described.

It has been noted earlier,[3] and was found to be the case here also, that the observed ratio TDMC:CDMC passed through a maximum value with decrease of reaction pressure. In both the pure and oxygen-added systems, in which *cis*-butene-2 was the principal heat bath molecule, the maximum occurred near 0.3 mm. For the systems with diatomic deactivators the maximum occurred near 1.0 mm. This phenomenon has been attributed to wall (or some other) reaction, possibly of an ionic character, which gives rise to stereospecific production of nonactivated CDMC.

The amount of CDMC product at lower pressures was obtained as an average of corrected amounts found by two procedures which were usually in good agreement. In the first, the observed TDMC product amounts were multiplied by a ratio (CDMC:TDMC), found by extrapolating a higher-pressure plot of observed (CDMC:TDMC) ratios *vs.* collision number through the minimum values of (CDMC:TDMC) to the low-pressure region. The second procedure used the extrapolated low-pressure ratio of (CDMC:TDMC)

(12) J. G. Calvert and J. N. Pitts, Jr., "Photochemistry," John Wiley and Sons, New York, N. Y., 1966.

(13) W. A. Noyes and P. A. Leighton, "Photochemistry of Gases," Van Nostrand-Reinhold Co., Inc., Princeton, N. J., 1941.

(14) J. Knox, R. G. W. Norrish, and G. Porter, *J. Chem. Soc.*, 1477 (1952).

(15) B. T. Connelly and G. B. Porter, *Can. J. Chem.*, **36**, 1640 (1958); *J. Chem. Phys.*, **33**, 81 (1960).

(16) M. C. Flowers and H. M. Frey, *Proc. Roy. Soc.*, **A257**, 122 (1960); **A260**, 424 (1961).

(17) H. M. Frey, *ibid.*, **A251**, 575 (1959).

for a given system to estimate the fraction of extraneous CDMC. A smooth curve was calculated through the square roots of these fractions plotted against the percentage of wall collisions. The squared smooth curve values gave the amount which was subtracted from the observed amount to give the collisionally stabilized CDMC.

Since CDMC is a minor component of the stabilization yield S at these pressures, the maximum possible uncertainty in S, for the worst possible misassignment of K, is 20%; the actual effective error, even in this case, would be not more than 10% because of relative cancellation of errors.

Evidence for $^3CH_2$. The proportion of $^3CH_2$ resulting from ketene photolysis and problems resulting therefrom are reduced at lower wavelengths.[6b,c,8] The percentage of triplet produced at 2800 Å is still uncertain.[6bc,8] Our data provide evidence regarding this matter and are pertinent to the evaluation of the present work.

3-Methylbutene-1 (3MB1) is a characteristic product of the reaction of $^3CH_2$ with CB2.[7b,18] Two other products, TDMC and *trans*-pentene-2 (TP2), are also indicative of $^3CH_2$ when they are present at high pressures where their formation is not due to isomerization of singlet products.[7b,18] The average high-pressure product yields are shown in Table I for the several sets of conditions.

3MB1 was not detected at any pressures in the O_2 runs. Trace peaks were observed in the CO runs amounting to 0.2% of the high-pressure C_5 products.[19] TP2 was found in negligible amounts in both the O_2 and CO systems at highest pressures. TDMC was observed in both sets of runs.

These results indicate that $^3CH_2$ products are effectively absent from the CO and O_2 systems. Based on the product composition of the CB2 triplet systems studied previously,[6d,9] the amount of $^3CH_2$ in the O_2 system is zero and is 1.5% in the CO system based on 3MB1, and 3% and 2%, respectively, based on TP2. These amounts are almost halved if a very recent triplet product composition determination[6d] is used.

The high-pressure amounts of TDMC are more ambiguous indicators of triplet proportion; for whatever they are worth, they suggest triplet percentages of ~15% in the O_2 system and ~25% in the CO system; these values are halved on the basis of ref 6d.

Table I: Triplet Products (% C_5) at Highest Pressures (300–600 mm)

	System			
Product	Pure	N_2	O_2	CO
3MB1	2.7	4.2	0.0	0.2
TDMC	7.7	10.9	2.2	3.9
TP2	3.2	5.6	0.3	0.2

The corresponding triplet proportion in the pure system is 30% based on 3MB1, 35% based on TP2 and 30–50% based on TDMC. Since the latter value especially is higher than any previous estimates,[6,8] we believe that the triplet percentage was overestimated on this basis for the O_2 and CO systems. We shall therefore treat them as substantially free of triplet effects in the later discussion. There is no doubt that a substantial percentage of $^3CH_2$ ($\lesssim$50%) is present in the N_2 system.

Use of an Internal Standard. The standard reagent 2,4-dimethylpentane reacts as follows

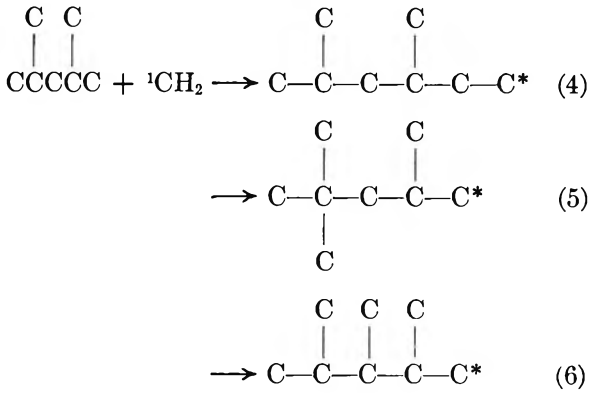

The statistical probability of these reactions is (4):(5):(6) = 6:1:1, so that the excited product 2,4-dimethylhexane (24DMH*) is the principal standard product. The decomposition of 24DMH* standard at the lowest pressures (0.1 mm) was shown to be small or zero, by product formation. Also, ketene was photolyzed in a 2,4-dimethylpentane–cyclooctane mixture over a series of pressures. Methyloctane is even more stable to decomposition than 24DMH* and no change in the ratio of stabilized 24DMH to methylcyclooctane attributable to decomposition was observed at pressures extending below the range of this study.

It has been observed that the various proportions of C_5 products in a $^3CH_2$–CB2 reaction system vary with pressure.[9b] Also, the structural isomerization rates of the C_5 triplet diradical formed from triplet methylene reaction with CB2 are almost two orders of magnitude larger than[20] those of the vibrationally excited singlet dimethylcyclopropane. These two phenomena increase the problem of assigning the limiting high-pressure ratio of (CDMC + TDMC):24DMH in the pure and N_2 systems where some $^3CH_2$ is present. Fortunately, a ratio could be assigned for the O_2 and CO series where this difficulty was virtually absent. The values were 0.40 and 0.35, respectively, in good agreement. The

(18) H. M. Frey, *J. Amer. Chem. Soc.*, 82, 5947 (1960).

(19) In this system and others where 3MB1 was observed, the ratio 3MB1:24DMH (standard product) remained remarkably constant with pressure. For further details see the Ph.D. thesis of J. D. Rynbrandt.

(20) D. F. Ring and B. S. Rabinovitch, *Int. J. Chem. Kinet.*, 1, 11 (1969).

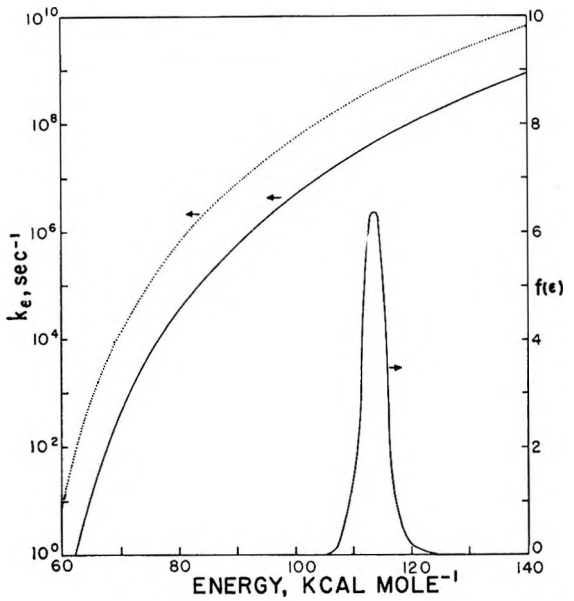

Figure 1. Plots of f(E) and of k_E for CDMC geometric isomerization, ——; and total structural isomerization, ...; (note k_E (pentenes) $\simeq$ k_E (butenes)).

values derived for the pure and N_2 systems are 0.41 and 0.48, respectively, so that the former system, particularly, is not much disturbed in this respect.

Energy Distribution of Reacting CH_2. The energy distribution of the reacting ketene was found by multiplying the known lamp power output, as a function of wavelength, by the measured transmittance of the filters and the extinction coefficient of ketene.[14] At these energies the quantum yield was taken to be 1.0.[15] The excess energy of the photolyzed ketene was assumed to be equally divided between its CH_2 and CO products.[3a] The vibrational energy distribution of CDMC is shown on Figure 1. Because of the high average CH_2 energy, ~10 kcal, the form of the product CDMC energy would not be significantly altered by considering the thermal energy distributions of ketene and/or CB2.

Once the CH_2 energy distribution was determined, its form was retained and the energies in the stochastic calculation were adjusted by shifting the entire distribution to the level which best fitted the data.

Presentation of the Data. The experimental dimethycyclopropane structural isomerization total rate constant k_a, for the 10% O_2, pure, and 10-fold excess CO systems are shown as a function of S/D in Figures 2 and 3, respectively. All sets of data exhibit "turn-up" (*i.e.*, enhanced decomposition amounts) of the experimental rates, due to a decrease in the collisional efficiency. A pragmatic measure of collisional inefficiency is given by

$$\beta = k_a^{wc}/k_a^{sc}$$

where the superscripts wc and sc represent the weak and strong inert bath collider conditions, respectively, for a given system. The onset and steepness of turn-up are related to the reach and form of the collisional transition probabilities described later.

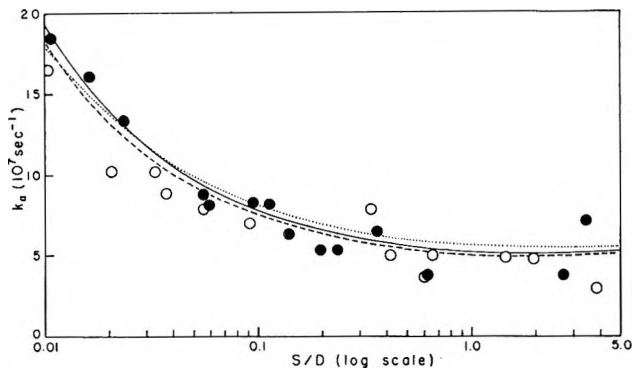

Figure 2. CDMC corrected experimental data: 10% O_2 systems, ●; pure system, O; calculated stochastic curves for various transition models and mixture proportions ($\langle E \rangle$ = 113.6 kcal mol^{-1}): (a) 4000-cm^{-1} stepladder model (SL) (0.89) with 2200-cm^{-1} SL (0.11), ——; (b) 4000-cm^{-1} poisson (0.89) with 2200-cm^{-1} SL (0.11), ...; (c) 4000-cm^{-1} SL with 3000-cm^{-1} SL (0.05), - - -.

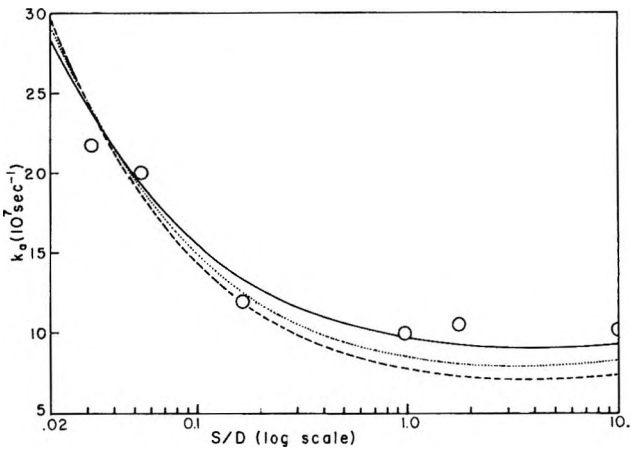

Figure 3. CDMC corrected experimental data for the CO system, O, with various calculated curves ($\langle E \rangle$ = 112.7 kcal mol^{-1}): (a) 1600 exponential model (0.89), ——; (b) 1500-cm^{-1} poisson (0.89), ...; (c) 1500-cm^{-1} SL (0.89), - - -. All with 4000-cm^{-1} SL (0.11).

The k_a values were found from the expression

$$k_a = \omega D/S \qquad (7)$$

where

$$S = \left(\frac{\text{CDMC} + \text{TDMC}}{24\ \text{DMH}}\right)_{obsd} \Big/ \left(\frac{\text{CDMC} + \text{TDMC}}{24\ \text{DMH}}\right)_{p=\infty}$$

and $D = 1 - S$. Here D is the total structural isomerization to methylbutenes and pentenes from CDMC and TDMC and S is stabilized CDMC plus TDMC. At highest pressures, D is found from the difference of two comparable magnitudes so that some scatter results.

Discussion

Stochastic Calculations. The computational procedures followed the earlier descriptions,[21] with some improvements. As before,[21] an initial CDMC population vector, $f(E)$ (Figure 1), was simultaneously operated upon by the normalized matrices of the collisional transition probabilities and the energy-dependent structural and geometric isomerization rate constants, k_E^s and k_E^g. The operation was repeated on the new CDMC and TDMC population vectors and was iterated to completion. The constant k_a was calculated from eq 1.

The correct form of the collisional transition probability distribution for vibrational deactivation is presently unknown; two extreme models, the stepladder and the exponential, were used to bracket the behavior of the system.[4,21] An improved method is used here for generating the transition probability matrix **P** for the exponential model (Appendix), and calculational error[21] caused by coarse graining of energy levels is reduced (such graining being desirable to reduce the computation time). The envelopes of the present transition probabilities are, nonetheless, fairly similar to those used in the earlier work and result in specification of mean down-step sizes which would differ by $\sim$20 cm^{-1} for equivalent **P**.

A change of notation has also been made. The exponential models are here designated by specification of the average step down, $\langle\Delta E\rangle^{\text{Exp}}$, at the mean energy of the chemically activated species; this convention characterizes the model at the energy of greatest relevance. Previously, $\langle\Delta E\rangle^{\text{Exp}}$ had been specified at the highest level in **P**. For an arbitrary illustrative case, the pentyl radical system,[22] an exponential model which in the older notation was called a "450"-cm^{-1} model is now called a "410"-cm^{-1} model; in addition, a present "390"-cm^{-1} model would be equivalent. In other cases, only slight variation in nominal equivalence of models will occur.

In the CDMC reaction system the geometric isomerization to TDMC is approximately ten times faster than subsequent reaction.[6a,10] Previously, the structural isomerization of CDMC had been treated as though it occurred from a single average *cis–trans* species.[6b] Here, the geometric isomerization is handled explicitly (Appendix), and the structural isomerization from each of CDMC and TDMC treated. The geometric and structural rate constants required in the stochastic calculations were calculated from the RRKM expression; the requisite sums and densities of active vibrational–rotational states were calculated by methods described previously.[21] Some changes in the models and frequency assignments previously used by Simons and Rabinovitch were made on the basis of a new assignment given by Sverdlov.[23] Values of k_E are graphed in Figure 1.

Finally, the earlier calculations employed, at least on some occasions, a δ-function approximation for the input energy distribution $f(E)$. The present work used a more realistic distribution (Figure 1).

Energetics and Vibration Frequencies. The CDMC–TDMC equilibrium has been studied in a thermal system.[16] At 431°, a TDMD:CDMC ratio, K = 2.25, and a heat of reaction of 1.07 kcal mol^{-1} were measured.[16] The recent vibrational assignment for CDMC and TDMC by Sverdlov[23] does not give good agreement with the experimental K value, nor with some recently observed spectra.[24] However, both the assigned[23] and observed[24] frequencies indicate that several frequencies used in the model of SR[6a] should be lowered. The following changes have been made in the SR model. The CH_3–C bending frequencies were changed from 700 (2), 400 (2) to 425 (2) and 250 (2) in CDMC and to 425 (2) and 237 (2) in TDMC.

An average activated complex was constructed to describe the two methylbutene products. The grouped complex frequencies are 2985 (9), 1350 (10), 946 (10), 685 (3), 430 (2), 250 (2) for the methylbutene complex, with E_0 = 60.5 kcal mol^{-1} for the *cis* precursor; and 2985 (9), 1327 (11), 957 (8), 700 (4), 450 (2), 250 (2) for an average pentene-2 complex, with E_0 = 60.0 kcal for the *cis* precursor; and 2982 (10), 1350 (10), 952 (9), 490 (3), 233 (2), 175, 150 for the geometric complex, with E_0 = 57.2 kcal for the *cis* precursor. These frequencies and energetics gave a good fit to the Arrhenius parameters and absolute rates observed in the thermal system for CDMC:[16] for average methylbutene parameters, log A = 14.00, E_a = 62.03 kcal; for pentenes, log A = 13.96, E_a = 61.43 kcal; and for CDMC → TDMC, log A = 15.25, E_a = 59.41 kcal.

The new TDMC frequencies were used with the same geometric complex. When coupled with a decrease in ΔH_f of 1.1 kcal, a calculated K equal to that observed[16] at 430.9° was obtained. The structural isomerization rates for TDMC were calculated using the same butene and pentene complex frequencies and with the E_0 values raised by 1.1 kcal mol^{-1}.

CB2–O_2 Collider System. Figure 2 shows the calculated plots of k_a *vs.* S/D and experimental points for the 10% oxygen system. For the former system, the best fit is obtained for a value of $\langle\Delta E\rangle$ = 4000 ± 300 cm^{-1} (11 ± 1 kcal) based on a stepladder model of the transition probabilities for CB2 bath molecule collisions (at an average input energy of 39,750 cm^{-1} (113.6 kcal) for

(21) D. C. Tardy and B. S. Rabinovitch, *J. Chem. Phys.*, **45**, 3720 (1966); **48**, 1282 (1968).

(22) J. H. Georgakakos, B. S. Rabinovitch, and E. J. McAlduff, *ibid.*, **52**, 2143 (1970).

(23) E. P. Krainov and L. M. Sverdlov, *Izv. Vysshikh Uchebn. Zavedenii, Fiz.*, **10**, 31 (1967).

(24) V. T. Aleksanyan, M. R. Aliev, M. Yu. Lukina, O. A. Nesmeyanova, and G. A. Khotimskaya, *Izv. Akad. Nauk SSSR, Ser. Khim.*, 807 (1968).

CDMC); both the high-pressure absolute rate value as well as the low-pressure turn-up are simultaneously satisfied.

Account was taken of the fact that 11% of the gas collisions occurred with O_2 or ketene by assigning an average (see CO discussion below) step size of 2200 cm^{-1} to these components; this is a minor correction. Wall collisions were considered to be strong; the fraction of wall collisions increased at lower pressures but never reached more than 0.015 of the total collisions and it was demonstrated by trial calculations that their inclusion in the calculations was unnecessary here.

A change in the average energy assigned to the formed CDMC of 1 kcal would result in a 300-cm^{-1} change in $\langle \Delta E \rangle$ calculated for *cis*-butene-2 collider.

An exponential collision transition probability model gave a distinctly poorer fit to the CB2 system data than was obtained using the stepladder model. The relative inefficiency of the exponential model at higher pressures forces either the assumption of an impossibly low initial CDMC energy or an implausibly large average down step in excess of 10,000 cm^{-1} in order to match the observed rates in this region. In either case, these changes virtually eliminated turn-up for the calculated system in the region where it was observed experimentally, due to the increasing efficiency of the exponential model relative to a stepladder model at low pressures. Such a distribution, which emphasizes the importance of small steps, may be ruled out and this conclusion is independent of any uncertainty in the energy of CDMC.

For this large average step size (4000 cm^{-1}), a gaussian or a poisson model of transition probabilities gives calculated behavior which differs only a little from those obtained on the basis of the stepladder model (Figure 2).

The high-pressure structural isomerization rate reported by SR[6a] was recalculated for a 4000-cm^{-1} stepladder model with use of the new molecule and complex frequency assignments and consideration of *cis–trans* isomerization. We confirm their magnitude of ~106 kcal for chemically activated CDMC formed in the 3200 Å ketene photolysis system. A comparison of this energy with that found in the present system implies that methylene formed by photolyzing ketene at 2800 Å carries 7.8 kcal more excess vibrational energy into CDMC than does methylene from 3200-Å ketene photolysis; this is roughly 60% of the energy difference between the two wavelengths.

CO Diatomic Collider System. The k_a *vs.* S/D plots for the CO study are shown in Figure 3. Stochastic fits to the data were calculated. The CB2 and internal standard (24DMP) components were represented by a 4000-cm^{-1} stepladder model for 0.11 of the gas collisions; wall collisions never amounted to more than 0.004 of the total. An exponential model with a down step of 1600 cm^{-1} (net step of 1420 cm^{-1}) fitted the data at an average CDMC input energy of 39430 cm^{-1} (112.7 kcal).

The agreement with experiment of calculated curves for poisson and stepladder-gaussian models is optimized by a choice of $\langle \Delta E \rangle$ = 1500 cm^{-1} at the same CDMC input energy. These are, respectively, poorer descriptions of the data (Figure 3). The better fit of the exponential model is indicative of changes in the form of the appropriate collisional transition probability distribution that applies for weaker colliders. This conclusion is only weakly dependent on uncertainty in the initial energy of CDMC.

The optimum average input energy in this system is 1 kcal less than required in the CB2 systems. The hot methylene makes an average of ten gas (CO) collisions before it collides with the CB2; this implies that CO is an inefficient deactivator of $^1CH_2$, but the *apparent* inefficiency of CO is accentuated because repeated collisions of $^1CH_2$ with inert gas lead to intersystem crossing with subsequent removal of $^3CH_2$ by CO.

Pure and N_2 Triplet Containing Systems. Both the pure and N_2 systems contain more $^3CH_2$, the latter system more than the former. Fortunately, the presence of triplet does not seem to alter markedly the low-pressure turn-up so that the energy transfer conclusions drawn from triplet containing systems, here and in previous work, retain their qualitative validity but should be considered less accurate than the studies in triplet-free systems.

The low-pressure turn-up and high-presure rate were fitted with a 4000-cm^{-1} (11.4 kcal) stepladder model CB2 at a CDMC input energy of 113.6 kcal (Figure 2). These numbers agree with those for the O_2 system within the experimental error, particularly when allowance is made for the absence of the weaker O_2 collider (10% in the CB2–O_2 system).

The N_2 system was plagued with excessive amounts of $^3CH_2$ which made it difficult to assign a high-pressure limiting ratio of dimethylcyclopropane to standard product and led to subsequent inaccuracies in assignments of the absolute rates. The data may be found in ref 19. However, the turn-up was found to occur in the same region (below $S:D$ = 1.0) as the CO system. This behavior suggests that the collisional efficiency of N_2 is similar to that of CO and is in agreement with earlier work.

It is of interest to note that the average amount of energy transferred per collision to weaker colliders in this system[3] is approximately double that transferred from molecules of comparable complexity[4] excited to only 45 kcal $mol.^{-1}$

Transition Probability Distributions. The present and earlier cyclopropane[3c] data suggest that for the weaker collider CO, the preferred form of the collisional transition probability distribution function is one in which smaller down steps are more probable than larger steps. These are typified by an exponential distribu-

tion. Similar conclusions from other chemical activation systems have previously been reached for other inefficient deactivators such as He, H_2, *etc.*[4] Results from dilution studies with He in thermal activation systems also led to the same interpretation.[25]

More efficient bath gases show a distinctly different form for the applicable distribution function. As seen here, larger transitions are more probable than very small ones. Unfortunately, the data cannot yet distinguish between alternative forms such as gaussian distribution of down transitions or skewed forms. The conclusion is unequivocal that an exponential-type model cannot possibly apply. These findings reinforce the conclusions from the earliest chemical activation work[26] as well as from later studies.[3b,4,22]

Appendix

Calculation of Transition Probability Matrix. The transition probabilities of the last column representing transitions from the highest energy level of the matrix were generated by multiplying the quantity $(g_i \exp(-E_i/RT))^{1/2}$ by a symmetrical attentuating factor and then normalizing the column to obey completeness; the accumulated probability for the (negligible) up-transitions were put into the diagonal element. Here g_i is the density of states in the active species. The relative weights of the diagonal and down-transition elements for lower energy levels were determined in a similar manner; all up-transition probabilities excluded by finite matrix size were lumped into the highest row. The absolute value of the up-transition probabilities were determined by applying the detailed balance condition to the known down-transition elements of higher columns.

The attenuating terms were chosen so as to give the nominal model with regard to form and average down-step size at the average input energy of the system.[19]

All matrices were truncated at an energy that was 70% of E_0 and the elements below E_0 were lumped into a single row. Of course, when the down- and net-step sizes were determined, the probabilities and ΔE values below E_0 were calculated with their original weights and positions.

The graining effect on the elastic level of the matrix was reduced by using attenuating terms whose relative values were determined by taking a crude integral over the energy span represented by that matrix element. This procedure gives a down-step size which is relatively free of grain effects.

Treatment of Isomerization. The geometric isomerization reaction between CDMC and TDMC was treated as follows. Instead of being counted as a decomposition product, the isomerized molecule was shuffled into the appropriate level of the column vector representing the active populations of the new isomer.

Table II: Collision Diameter Parameters

Molecule	σ, Å
DMC	6.92
CB2	6.66
CO	3.80
N_2	3.80
O_2	3.60
Ketene	5.45
24DMP	8.6

Other details of the calculations, particularly concerning the approach to equilibrium without excessive cycling of isomers, may be found elsewhere.[19]

Molecular Diameters. The molecular collision diameters which were used in these calculations are listed in Table II. They were calculated by multiplying the Lennard-Jones constants[27] by the square root of the collision integral $\Omega^{2,2*}(kT/\epsilon)$. Errors in the collision frequency due to incorrect cross sections have little effect on the energy transfer aspects of this study.[4]

(25) Y. N. Lin and B. S. Rabinovitch, *J. Phys. Chem.*, **72**, 1726 (1968).

(26) R. E. Harrington, B. S. Rabinovitch, and M. R. Hoare, *J. Chem. Phys.*, **33**, 744 (1960).

(27) J. O. Hirschfelder, C. F. Curtiss, and R. B. Bird, "Molecular Theory of Gases and Liquids," John Wiley and Sons, New York, N. Y., 1954, p 209.

Photoisomerization of the Xylenes in Solution[1]

by Duncan Anderson

Department of Chemistry, The University of Texas at Austin, Austin, Texas 78712 *(Received October 10, 1969)*

The photolyses of the xylenes (mainly *m*-xylene) have been studied at 248 and 275 nm in *n*-hexane, EPA (a 5:5:2 mixture of diethyl ether, isopentane, and ethanol), and perfluorohexane solution. The quantum yields of isomerization are independent of exciting wavelength, and independent of solvent, but increase with temperature. For the isomerization of *m*-xylene, $\Phi_p = 0.0032$ and $\Phi_o = 0.00075$. Both yields have an activation energy of approximately 4.7 kcal mol^{-1}, so that the *p*/*o* ratio is independent of all conditions studied. It is not possible to say whether benzvalene or prismane type molecules are precursors of the isomerization products.

Introduction

The photochemistry of benzene and its derivatives has been the subject of considerable interest in recent years.[2] Much of the work has centered on the determination of fluorescence and triplet-state yields, but it is also well established that certain reactions, most notably isomerization,[3,4] also occur. Gas-phase studies on benzene,[5,6] on toluene,[7] and on the xylenes,[8] have shown that the quantum yields of fluorescence depend strongly on exciting wavelength. The yields decrease to zero at wavelengths shorter than 240 nm, and increase to a constant value, less than unity, for wavelengths in the region of the 0,0 bands. An increase in pressure generally causes an increase in the quantum yields of fluorescence, but the values never exceed those obtained at the longest wavelengths. The isomerization yields behave in a complementary fashion and are largest for short wavelengths and decrease with an increase in pressure.

In the liquid phase, the study of wavelength effects has been largely limited to measurements of fluorescence. In contrast to the gas phase, it has been observed that the fluorescence quantum yields are generally independent of exciting wavelength.[9] Where exceptions to this rule have occurred, absorption to a mixture of states was involved.[10] A study of the isomerization of the xylenes in solution affords an opportunity to examine whether fluorescence and isomerization are truly complementary processes. In particular, it is important to determine whether a wavelength effect exists for isomerization quantum yields.

Experimental Section

Materials. Phillips research grade *o*-, *m*-, and *p*-xylene were used without further purification. Analysis by capillary gas chromatography showed the level of impurities other than xylene isomers to be less than 0.01%. The isomeric purity was better than 99.9%. The solvents, also used without further purification, were *n*-hexane (Matheson Coleman and Bell Spectrograde), EPA (also Matheson Coleman and Bell), and perfluorohexane (Pierce Chemical Co.).

Analyses. All analyses were performed by use of capillary gas chromatography. The instrument was a Perkin-Elmer F-11 chromatograph, with a 17 m × 0.05 cm MBMA[11] support coated open tubular column. An internal standard, *n*-nonane, was used to determine the concentrations of the various isomers in the product mixture. The relative sensitivities of the detector to the xylenes and to nonane were calibrated over a range of xylene concentrations, for a fixed concentration of nonane. These varied smoothly with concentration, although the sensitivities for all three xylenes at any particular concentration were identical within experimental error.

Photolyses. The photolyses of the xylenes were studied by use of light isolated by a monochromator, and also light isolated by a set of filters. The optical system for the monochromator experiments is shown in Figure 1. Samples of xylene solution were first degassed on a vacuum line by several freeze–thaw cycles, sealed off, and placed in the optical path. The light source was an Osram HBO 500 lamp, and the monochro-

(1) This work was supported by a grant to W. Albert Noyes, Jr., from the Office of Aerospace Research, Air Force Office of Research and Development, United States Air Force, Grant AF-AFOSR-69-1682. The author wishes to thank Dr. Noyes for many helpful discussions.

(2) W. A. Noyes, Jr., and C. S. Burton, *Ber. Bunsenges. Phys. Chem.*, 72, 146 (1968), and references therein.

(3) K. E. Wilzbach and L. Kaplan, *J. Amer. Chem. Soc.*, 86, 2307 (1964).

(4) K. E. Wilzbach, A. L. Harkness, and L. Kaplan, *ibid.*, 90, 1116 (1968).

(5) J. A. Poole, *J. Phys. Chem.*, 69, 1343 (1965).

(6) W. A. Noyes, Jr., W. A. Mulac, and D. A. Harter, *J. Chem. Phys.*, 44, 2100 (1966).

(7) W. A. Noyes, Jr., and C. S. Burton, *ibid.*, 49, 1705 (1968).

(8) W. A. Noyes, Jr., and D. A. Harter, private communication, to be published.

(9) G. Weber and F. W. J. Teale, *Trans. Faraday Soc.*, 53, 640 (1957).

(10) J. B. Birks, J. C. Conte, and G. Walker, *J. Phys. B, Ser 2*, 1, 934 (1968).

(11) MBMA is a mixture of *m*-bis(*m*-phenoxyphenoxy) benzene and Apiezon L grease.

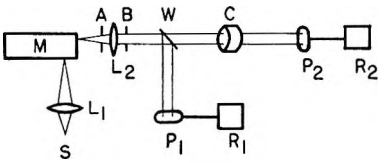

Figure 1. Apparatus for absolute quantum yield: S, light source (Osram HBO 450); L_1, L_2, lenses; M, monochromator; A, B, light stops; W, Suprasil window at 45° to light beam; P_1, P_2, phototubes; R_1, R_2, chart recorders; C, cell.

mator was a Bausch and Lomb 0.5-m grating instrument, with a reciprocal dispersion of 1.6 nm mm^{-1}. The slits were set at 2 mm and the wavelength at 248 or 275 nm, since these are the wavelengths at which maximum absorption by the xylenes occurs. The window W served as a beam splitter, so that both incident and transmitted intensity could be monitored continuously. Such monitoring was necessary because of the relatively low intensities and low quantum yields. A typical photolysis required two to three days to produce an amount of isomer sufficient for analysis. During this time the intensity of the lamp dropped appreciably. The responses of the phototubes were calibrated against the ferrioxalate actinometer,[12] and found to remain invariant over a period of several months.

A series of experiments was also performed using light isolated by two chemical filters. The first filter contained a mixture of nickel and cobalt sulfates at concentrations of 2 mol $l.^{-1}$ and 0.6 mol $l.^{-1}$, respectively. The path length was 1 cm. The second filter was a 5-cm path length of chlorine gas at 1 atm pressure. This combination had a high transmission for light in the 250-nm region and greatly reduced the intensity of all other wavelengths emitted by the lamp. Attempts to produce further monochromaticity with a potassium iodide–iodine filter[13] were unsuccessful due to the drastic drop in transmission at 250 nm. In any case the amount of light absorbed by the xylene could be readily calculated. The input to the cell was two orders of magnitude greater than in the experiments with a monochromator, so that the time span of a photolysis was much shorter. The lamp intensity did not vary greatly, and continuous monitoring was unnecessary. More recently, the chemical filters have been replaced by an interference filter (Oriel G-521-2537) whose maximum transmission is at 250 nm. The available intensity is equal to that obtained by use of the chemical filters, and all wavelengths outside the 210–290-nm region are totally blocked. The same system was used for the temperature studies, with the inclusion of a simple box with Suprasil windows. The temperature was adjusted by passing either heated or cooled air through the box, and could be regulated to ±1°.

Results

Wavelength Effect. Most of the work was performed with *n*-hexane as the solvent, and an approximate concentration of xylene of 7.8×10^{-3} mol $l.^{-1}$. The exact composition of the mixture was determined by weight. The quantum yields of isomerization for 248 nm, 275 nm, and filtered radiation are collected in Table I.

Table I: Quantum Yields for Isomerization of Xylenes[a]

Reaction	Wavelength, nm 248	275	230–280
$\Phi_{\Delta o}$	0.00755	0.00680	0.00775
$\Phi_{o\rightarrow m}$	0.00210	0.00202	0.00222
$\Phi_{o\rightarrow p}$	0.000232	0.000240	0.000252
$\Phi_{\Delta m}$	0.00570	0.00520	0.0111
$\Phi_{m\rightarrow o}$	0.00071	0.00067	0.00083
$\Phi_{m\rightarrow p}$	0.00326	0.00313	0.00340
$\Phi_{\Delta p}$			0.00274

[a] Solvent, *n*-hexane; concentration, 7.8×10^{-3} mol $l.^{-1}$; temperature 27°.

Due to the higher conversions involved in the experiments where filtered light was used, it was possible to estimate a quantum yield for the loss of parent xylene. The error in estimating these yields is larger, due to the inherent difficulty of accurately determining a small difference between two large values. However, the following points are noticeable.

(1) Isomerization quantum yields are independent of exciting wavelength or whether non-monochromatic light is used.

(2) Isomerization accounts for only a fraction of the parent compound lost. No products other than xylene isomers were detected by gas chromatography, although there was a slight difference in the uv spectrum of the product mixture as compared to that of the starting sample. It is probable, as suggested by Wilzbach and Kaplan,[3] that the lost starting material results in formation of polymer.

(3) Compounds such as hydrogen, methane, and ethyl toluene, which would normally be derived from free radical reactions, were absent from the products.

The quantum yields presented here have not been corrected for back reaction. However, a simple check on the effect of conversion showed that serious reduction of the uncorrected quantum yield did not occur until over 10% conversion. In the present work the conversion was always between 2 and 5%, so that no correction was necessary.

Solvent Effect. The photoisomerization of *m*-xylene was further examined in different solvents by use of the system with filters. The results are collected in Table II and show that isomerization quantum yields are essentially independent of solvent. On the other

(12) C. G. Hatchard and C. A. Parker, *Proc. Roy. Soc.*, A235, 518 (1956).

(13) J. G. Calvert and J. N. Pitts, Jr., "Photochemistry," John Wiley and Sons, New York, N. Y., 1966, p 729.

Table II: Quantum Yields for Isomerization of *m*-Xylene in Solution[a]

Reaction	Solvent: *n*-Hexane	*n*-Perfluorohexane	EPA
$\Phi_{\Delta m}$	0.0111	0.00945	0.0205
$\Phi_{m\rightarrow o}$	0.00083	0.00084	0.00074
$\Phi_{m\rightarrow p}$	0.00340	0.00310	0.00315

[a] Exciting wavelength 230–280 nm; concentration 7.8×10^{-3} mol $l.^{-1}$; temperature 27°.

hand, the loss of *m*-xylene is considerably greater in EPA than in the other two solvents. This is possibly due to the presence of ethanol, which is known to undergo a photoaddition reaction with benzene and some of its derivatives.[14] No new products were detected by gas chromatography, but the uv spectrum of the irradiated sample did indicate the presence of a new absorbing species.

Temperature Effect. The effect of temperature on the isomerization of *m*-xylene was studied with the filtered light system in the temperature range −10 to +80°. Arrhenius plots for Φ_p, $\Phi_{\Delta m}$, and Φ_o were straight lines. Within experimental error, the activation energy derived from each line was 4.7 ± 1 kcal mol^{-1}. The results are shown in Figure 2.

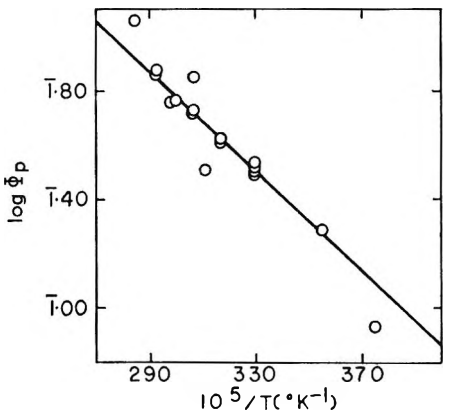

Figure 2. Temperature dependence of $\Phi_{m\rightarrow p}$. Exciting wavelength 230–280 nm; concentration 7.8×10^{-3} mol $l.^{-1}$.

Discussion

The gas-phase fluorescence behavior of benzene,[5,6] toluene,[7] and the xylenes[8] suggested the desirability of extending the investigations to much higher pressures. In this respect the liquid phase with a theoretical internal pressure of several hundred atmospheres was considered to be an extension of the gas phase. Dexter and Fowler[15] have calculated that solvent effects may result in very large changes in the rates of radiationless processes without observable change in spectral behavior. There may, however, be no effect. Such seems to be the case in the present work. The uv spectrum of *m*-xylene was identical in each of the three solvents used, and the quantum yield of isomerization is independent of the surrounding medium. It must be concluded, therefore, that the solvents act only as vibrational energy sinks.

It is evident from Table I, since there is no effect of varying the initial vibrational energy, *i.e.*, the excitation wavelength, that the liquid phase is extremely effective in removing energy from the excited molecules. Since the fluorescent yields for benzenoid compounds are also independent of exciting wavelength in solution,[9,10,16] it is concluded that vibrational relaxation occurs before any other processes on excitation of the first singlet. Wavelength effects can, however, occur on excitation to a higher singlet,[16] to a mixture of states,[10] or to different chromophores of the same molecule.[17]

The isomerization quantum yields of the xylenes in the gas phase for long wavelength excitation are comparable[8] to the yields obtained in solution at room temperature, and the activation energies for $m \rightarrow p$ isomerization are probably equal in both phases. At the longest exciting wavelengths, the gas-phase fluorescent yields increase slightly with decrease of pressure in the range of 1–400 Torr, although they never approach unity at 1 Torr, the lowest pressure studied. The liquid-phase quantum yields are peculiarly independent of exciting wavelength. The explanation is straightforward if one can assume that isomerization occurs from the singlet, in competition with fluorescence; that increased vibrational energy of the singlet results in more efficient isomerization; and that no isomerization at all occurs from the vibrationally cold singlet. For toluene[7] at least, the sum of fluorescent and triplet-state yields from the vibrationally cold singlet appears to be unity within experimental error. Ermolaev[18] has also shown that the sum of fluorescence and triplet-state yields in solution is, for several molecules, unity within experimental error. Wilzbach and Kaplan[19] have shown that photoisomerization of the xylenes proceeds intramolecularly, and probably through a benzvalene intermediate. Indeed, the same authors[20] have shown that a stable benzvalene can be isolated from benzene irradiated at 254 nm in solution. A simplified

(14) L. Kaplan, J. S. Ritscher, and K. E. Wilzbach, *J. Amer. Chem. Soc.*, 88, 2881 (1966).

(15) D. L. Dexter and W. B. Fowler, *J. Chem. Phys.*, 47, 5444 (1967).

(16) C. L. Braun, S. Kato, and S. Lipsky, *ibid.*, 39, 1645 (1963).

(17) N. Baumann and E. F. Ullman, *J. Amer. Chem. Soc.*, 90, 4157 (1968).

(18) V. L. Ermolaev, *Izv. Akad. Nauk S.S.S.R., Ser. Fiz.*, 32 (8), 1287 (1968).

(19) L. Kaplan, K. E. Wilzbach, W. G. Brown, and S. S. Yang, *J. Amer. Chem. Soc.*, 87, 675 (1965).

(20) K. E. Wilzbach, J. S. Ritscher, and L. Kaplan, *ibid.*, 89, 1031 (1967).

mechanism for the isomerization of *m*- to *p*-xylene would be as follows

$$M + h\nu \longrightarrow {}^1M_v \quad (1)$$

$${}^1M_v \longrightarrow M + h\nu_v \quad (2)$$

$$\longrightarrow X \quad (3)$$

$$\longrightarrow p\text{-}Bv_v \quad (4)$$

$${}^1M_v + N \longrightarrow {}^1M_e + N \quad (5)$$

$${}^1M_e \longrightarrow M + h\nu_e \quad (6)$$

$$\longrightarrow X \quad (7)$$

$$\longrightarrow p\text{-}Bv_v \quad (8)$$

$$\longrightarrow M \quad (9)$$

$$p\text{-}Bv_v \longrightarrow P \quad (10)$$

$$+ N \longrightarrow p\text{-}Bv_e + N \quad (11)$$

$$p\text{-}Bv_e \longrightarrow M \quad (12)$$

$$\longrightarrow P \quad (13)$$

The subscripts v and e refer to vibrationally excited and vibrationally equilibrated species, respectively. X represents the triplet state, N is an inert molecule whose only function is to induce vibrational relaxation, and *p*-Bv is the supposed benzvalene intermediate. Based on the numbering system shown below, *p*-Bv is named as 1,3-dimethyltricyclo[3.1.0.0^{2,6}]hex-3-ene.

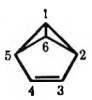

The mechanism admits of the possibility that vibrational relaxation of the benzvalene intermediate, as distinct from vibrational relaxation of the singlet xylene, may also be a factor in determining the quantum yield of isomerization. However, in the limit of high pressure, as appears to be true for solution

$$\Phi_p = \frac{k_8 k_{13}}{(k_6 + k_7 + k_8)(k_{12} + k_{13})}$$

and also

$$\Phi_f = \frac{k_6}{k_6 + k_7 + k_8}$$

Thus both isomerization and fluorescent yields are independent of v, whether v is initially greater or less than e. For 248-nm excitation, v is undoubtedly greater than e, but for excitation at 275 nm, which lies below the 0,0 band in energy, v may be zero, or close to zero. In solution, however, thermal equilibration is so fast that the original vibrational energy of the singlet is irrelevant. In the gas phase the most interesting results concern the increase of fluorescent quantum yield at low pressures, for long-wavelength excitation. Here indeed, the excited singlet is formed in a situation where v is less than e, but where the pressure is too low for collisional equilibration to occur before fluorescence.

The mechanism given above accounts for the overall details of isomerization and fluorescence, but is certainly not complete. If benzvalenes are the intermediates responsible for isomerization, two new intermediates should be introduced into the scheme for *m*-xylene photolysis. One of these, 1,2-dimethyltricyclo[3.1.0.0^{2,6}]hex-3-ene (*o*-Bv), could theoretically give *o*-xylene or revert to *m*-xylene, while the other, 2,4-dimethyltricyclo[3.1.0.0^{2,6}]hex-3-ene (*m*-Bv), could only revert to *m*-xylene. In addition, since $\Phi_{\Delta m}$ is greater than $(\Phi_p + \Phi_o)$, decomposition reactions of either the xylene singlet or more probably the benzvalene intermediates must occur. An examination of the dimethylbenzvalenes which may be derived from *m*-xylene shows that, on a purely statistical basis, one would expect the ratio Φ_p/Φ_o to be 1/1. That the experimental ratio is close to 4/1 indicates that some benzvalenes are formed in preference to others and probably also that the isomerization reactions from the benzvalenes proceed with differing probabilities. Qualitatively one may say that the probabilities of formation are in the order *p*-Bv > *m*-Bv > *o*-Bv. Wilzbach and Kaplan[19] also point out that prismanes are possible intermediates in isomerization of xylenes, and in this case also, the statistical probability for the ratio Φ_p/Φ_o would be 1/1.

There is no firm evidence at present, therefore, to distinguish between benzvalenes and prismanes as intermediates, or even whether both species occur. Since no products other than xylene isomers were detected by capillary gas chromatography, any intermediates must be short-lived and may only be transition complexes. As Wilzbach and Kaplan[19] have pointed out, *o*-xylene can isomerize to *p*-xylene and *vice versa* through a prismane intermediate, though not through a benzvalene intermediate. The data of Table I show that $\Phi_{o\rightarrow p}$ is small but finite, but that $\Phi_{p\rightarrow o}$ is zero within experimental error. The relatively small value of $\Phi_{\Delta p}$ is in agreement with the idea that *p*-Bv reverts to *p*-xylene in preference to forming *m*-xylene.

The effect of temperature is difficult to interpret at present because of the complexity of the expressions for isomerization quantum yields. In the expression for Φ_p one might suppose that k_{12} and k_{13} have similar activation energies and that k_8 is small compared to k_6 and k_7. The expression then reduces to

$$\Phi_p = \frac{\alpha k_8}{k_6 + k_7}$$

where α is a constant, less than unity. Thus the activation energy obtained approximately reflects the activation energy difference between reaction 8 (formation of the benzvalene intermediate), and reactions 6 and 7

(fluorescence and intersystem crossing from the singlet). It is possible, though not necessary, that E_6 and E_7 are close to zero, so that E_8 is approximately 4 kcal mol^{-1}, but further experiments will be necessary to prove the point.

Appendix

The calculation of absolute quantum yields of isomerization is not straightforward and should be given here. In computing the number of quanta of light absorbed, the following corrections should be considered. (1) Some light is reflected back into the cell from the exit window. (2) The intensity of the lamp generally decreases during a photolysis. (3) The concentration of starting xylene decreases, and strongly absorbing polymeric species may be formed, so that the fraction of incident light absorbed by the xylene decreases during the reaction. (4) Back reaction may occur at sufficiently high conversions.

In the system shown in Figure 1, the response of phototube 2 at zero time is defined as follows: $R_{1,0}$ = reading with no cell in position; $R_{2,0}$ = reading with hexane filled cell in position; $R_{3,0}$ = reading with sample filled cell in position.

The following definitions are also made: f = fraction of light reflected by each window of the cell; x = fraction of light absorbed by the sample for one traverse of the cell; S_t = response of phototube 1 at time t. It follows that

$$\frac{R_{2,0}}{R_{1,0}} = (1 - f)^2$$

and

$$\frac{R_{3,0}}{R_{2,0}} = (1 - x)$$

If the intensity of the lamp decreases with time, we make the definition $I = I_0 (1 - at + bt^2 - \ldots)$ but in practice approximate $I = I_0 (1 - at)$ so that $S_t/S_0 = 1 - at$.

It was assumed in this work that any decrease in the ratio transmitted intensity:incident intensity is due to the deposition of polymer on the front window of the cell. The intensity of light incident on the sample solution then becomes: $(1 - f)I(1 - bt)$ and $R_{3,t}/R_{1,t} = (1 - f)^2(1 - x)(1 - bt)$.

Finally, since light is reflected back into the cell from the exit window, the instantaneous rate of light absorption will be given by

$$\frac{dI_a}{dt} = (1 - f)I_0(1 - at)(1 - bt)x + f(1 - f)I_0(1 - at)(1 - bt)(1 - x)x$$

and the total light absorbed during the photolysis is

$$I_{abs} = [(1 - f)xI_0 + f(1 - f)x(1 - x)] \times \int_0^t [1 - (a + b)t + abt^2]dt =$$
$$[(1 - f)xI_0 + f(1 - f)x(1 - x)I_0] \times [t - (1/2)(a + b)t^2 + (1/3)abt^3$$

Investigations on the Thermal and Radiolytic Decomposition of Anhydrous Crystalline Potassium Chlorite

by G. E. Boyd and L. C. Brown

Oak Ridge National Laboratory, Oak Ridge, Tennessee 37830 *(Received October 23, 1969)*

Measurements of the radiolysis at *ca.* 38° of anhydrous crystalline $KClO_2$ by ^{60}Co γ rays showed that chlorite ion decomposed in the solid *via* the overall reaction: $3ClO_2^- \rightsquigarrow Cl^- + 2ClO_3^-$. Radiolytic yields for a dose of 1.0×10^{23} eV/mol $KClO_2$ were: $G(-ClO_2^-) = 33.5 \pm 1.7$; $G(Cl^-) = 10.7 \pm 0.2$; $G(ClO^-) = 0.0$; $G(ClO_3^-) = 22.5 \pm 0.8$; and $G(ClO_4^-) = 0.0$ molecules per 100 eV absorbed. The energy absorbed (3.3 eV/molecule) in the decomposition of ClO_2^- was nearly the same as that required to break a Cl–O bond. The thermal decomposition of $KClO_2$ was strongly exothermic between 135 and 165°, and the stoichiometry of the reaction was identical with that observed in the radiolysis. A reaction mechanism based on the production of O atoms and their addition to ClO_2^- ions in the crystal lattice is suggested.

Chlorite ion, ClO_2^-, is a major chlorine-containing product in the room temperature decomposition of the crystalline alkali metal and alkaline earth chlorates by small doses of energetic ionizing radiations.[1-3] The concentration of this species produced in crystalline $KClO_3$ by ^{60}Co γ rays or X-rays has been shown to increase linearly with increasing dose up to *ca.* 4.4×10^{23} eV/mol $KClO_3$, but, when the dose exceeds *ca.* 12×10^{23}, the concentration of ClO_2^- ion becomes and remains nearly constant. The drop in the net rate of chlorite ion formation has been attributed[1] to its radiolysis in the chlorate lattice according to the reaction

$$ClO_2^- \rightsquigarrow Cl^- + O_2(g) \qquad (1)$$

Heating irradiated alkali metal chlorates at temperatures above 100° reduces the concentration of ClO_2^- ion and removes all the ClO^- present. However, approximately half of the ClO_2^- ion remains even when the crystal is heated almost to its melting point.

Observations on the thermal decomposition of the anhydrous alkali metal chlorites have indicated that the predominant reaction is disproportionation according to

$$ClO_2^- \longrightarrow {}^1/_3Cl^- + {}^2/_3ClO_3^- \qquad (2)$$

For example, sodium chlorite which is stable at room temperatures is reported[4] to decompose less than 5% with the evolution of $O_2(g)$. Investigations on the chemical behavior of recoil 37.3 *m* ^{38}Cl activity formed in crystalline $NaClO_2$[5] or $KClO_2$[6] by thermal neutron irradiation lend support to the view that reaction 2 rather than 1 occurs on heating these salts. The fraction of chlorine activity retained as $^{38}ClO_2^-$ ion decreased on annealing the crystals above 120°, and the increases in the yields of $^{38}Cl^-$ and $^{38}ClO_3^-$ ions after heating[6] were consistent with reaction 2.

There are no published accounts of investigations on the radiolysis of any of the anhydrous crystalline alkali metal chlorites, and their thermal decomposition has not been studied with modern analytical techniques. The observations reported below indicate that ^{60}Co γ rays cause an efficient disproportionation of ClO_2^- ion in solid $KClO_2$ to give Cl^- and ClO_3^- ions. Thermoanalytical measurements with the same compound showed that disproportionation can also be initiated at 135° and is complete at *ca.* 165°.

Experimental Section

Sample Preparation. Pure potassium chlorite was prepared from $ClO_2(g)$ by an adaptation of the method of Ito[7] for the separation of alkali metal chlorites from aqueous solutions. Chlorine dioxide, diluted with CO_2 for safety, was prepared from $KClO_3$, oxalic acid, and sulfuric acid as described by Brauer.[8] A stream of $ClO_2 + CO_2$ was bubbled into 200 ml of cold 0.5% H_2O_2. The solution was adjusted to neutrality with 0.5 *M* KOH, boiled to decompose the excess H_2O_2, and treated with sufficient $Pb(NO_3)_2$ solution to precipitate *ca.* 95% of the chlorite as $Pb(ClO_2)_2$. The precipitate was separated, thoroughly washed with water, and treated with K_2CO_3 solution to convert *ca.* 90% of the $Pb(ClO_2)_2$ to $PbCO_3$. The aqueous supernatant solution was separated from the insoluble lead

(1) H. G. Heal, *Can. J. Chem.*, **37**, 979 (1959).

(2) C. E. Burchill, P. F. Patrick, and K. J. McCallum, *J. Phys. Chem.*, **71**, 4560 (1967).

(3) L. C. Brown and G. E. Boyd, *ibid.*, **73**, 396 (1969).

(4) M. C. Taylor, J. F. White, G. P. Vincent, and G. L. Cunningham, *Ind. Eng. Chem.*, **32**, 899 (1940).

(5) M. Vlatković and A. H. W. Aten, Jr., *J. Inorg. Nucl. Chem.*, **24**, 139 (1962).

(6) G. E. Boyd and Q. V. Larson, *J. Amer. Chem. Soc.*, **90**, 5092 (1968).

(7) T. Ito, *Chem. Abstr.*, **52**, 10519c (1958).

(8) "Handbook of Preparative Inorganic Chemistry," G. Brauer, Ed., Vol. 1, 2nd ed, Academic Press Inc., New York, N. Y., 1963, p 312.

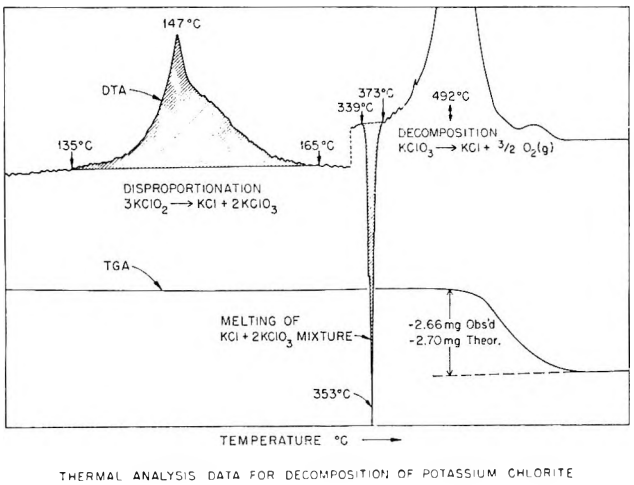

Figure 1. Thermal analysis data for the decomposition of $KClO_2$(c) (9.0 mg sample heated in Ar gas at 6°/min to 120°, then 0.5°/min to 175°, and at 6°/min to 600°). DTA = differential thermal analysis trace of ΔT *vs.* sample temperature; TGA = thermo-gravimetric analysis trace of weight loss *vs.* sample temperature.

salts and passed through a column of Dowex 50W-X8 cation exchanger in the potassium form to remove all Pb^{2+} ion. The eluent was collected and evaporated, and crystalline $KClO_2$ was isolated by freeze-drying. Analysis of the product showed it to contain less than 1% Cl^- and less than 0.3% ClO_3^- ion.

Irradiations. The irradiations were conducted at constant geometry in a 10-kCi ^{60}Co γ ray source where the equilibrium temperature was *ca.* 38° and the dose rate, as measured with a Fricke dosimeter ($G(Fe^{3+})$ = 15.6), was 1.03×10^{18} eV g^{-1} min^{-1}. The ratio of the numbers of electrons per gram in $KClO_2$ and in H_2O was employed to estimate the dose absorbed. Thus, dose($KClO_2$) = 0.879 dose(H_2O). The irradiated $KClO_2$ was stored in solid CO_2 until analysis.

Chemical Analyses. Aqueous solutions of irradiated or unirradiated salt were analyzed for chloride ion by dissolving weighed portions in 0.01 *M* borax solution[1] and titrating potentiometrically with 0.100 *M* Ag^+. Analyses for hypochlorite and chlorite were performed[3] by dissolving weighed aliquots of $KClO_2$ in 0.3 *M* $NaHCO_3$ and titrating potentiometrically with 0.0100 *N* arsenous acid. Osmium tetroxide catalyst was added to assist in the titration for ClO_2^- ion. Chlorate ion was determined by the difference in the Cl^- ion titres of aliquots of solution reduced by H_2SO_3 and by AsO_2^- + OsO_4, respectively.

Spectral Measurements. Irradiated $KClO_2$ also was examined by infrared methods with a Perkin-Elmer Model 521 double-beam spectrophotometer operated in the double-beam mode with dry air in the reference beam. Measurements at 25° on the finely divided crystalline solid were performed with KBr pressed pellet techniques (0.20 wt % in 400 mg KBr). Dry Nujol mulls were examined to establish that absorption bands from water were absent in the salt. The frequencies of the absorptions by unirradiated $KClO_2$ were: $\nu_1(A_1)$ = 788, $\nu_2(A_1)$ = 426, and $\nu_3(B_1)$ = 822 cm^{-1}, respectively. These values are close to, but not identical with, the values observed in the Raman spectrum of solid $NaClO_2$.[9]

Thermal Decomposition Measurements. The thermolysis in air of unirradiated $KClO_2$ was studied in preliminary investigations with thermal gravimetric methods utilizing a Stanton TGA recording balance. A detailed examination of the decomposition on heating was performed in Ar gas with DTA and TGA techniques in a Mettler Thermoanalyzer.[10] Scan rates of 6° and 0.5° per min were employed, and temperatures were estimated to ±1° with platinum—platinum–10% rhodium thermocouples. A typical thermogram is shown in Figure 1. Thermal analyses performed in O_2(g) at one atmosphere did not differ within experimental error from those conducted in argon. Mass spectrometric analyses of the Ar showed no oxygen gas until the sample temperature reached 340°.

Experimental Results

Substantial radiolytic decompositions (5.7 and 21.3%) were observed with samples of $KClO_2$ exposed to doses of $1.0_1 \times 10^{23}$ and $3.5_6 \times 10^{23}$ eV/mol $KClO_2$, respectively. The yield for the decomposition of chlorite ion at the lower dose was $G(-ClO_2^-)$ = 33.5 ± 1.7 molecules/100 eV. Yields for chloride and chlorate ion were: $G(Cl^-)$ = 10.7 ± 0.2 and $G(ClO_3^-)$ = 22.5 ± 0.8, respectively. No hypochlorite nor perchlorate ion could be detected. The errors quoted above are standard deviations and represent the precision of the chemical analyses only.

The relative magnitudes of $G(Cl^-)$, $G(ClO_3^-)$, and $G(-ClO_2^-)$ stand approximately in the ratio 1:2:3. This stoichiometry and the absence of other chlorine oxidation states suggested that the decomposition effected by ^{60}Co γ rays followed the overall reaction

$$ClO_2^- \rightsquigarrow {}^1/_3Cl^- + {}^2/_3ClO_3^- \qquad (2')$$

The large absolute magnitudes of the yields indicate that the radiolytic disproportionation was exceptionally efficient. The dissipation of γ energy in $KClO_2$ was *ca.* 3.3 eV/molecule [*i.e.*, $1/G(-ClO_2^-)$], an amount of energy which is close to that required to break a Cl–O bond in ClO_2.[11] Thus, the stability of ClO_2^- ion is such that virtually all the energy deposited leads to bond rupture.

The infrared absorption measurements (Figure 2) with radiolyzed $KClO_2$ served to establish that ClO_3^-

(9) J. P. Mathieu, *Compt. Rend.*, **234**, 2272 (1952).

(10) Performed by E. T. Creech, Y-12 Analytical Chemistry Section, Union Carbide Nuclear Co., Oak Ridge, Tenn. 37830.

(11) V. I. Vedeneev, *et al.*, "Bond Dissociation Energies, Ionization Potentials and Electron Affinities," Moscow Academy of Sciences, 1962, p 78.

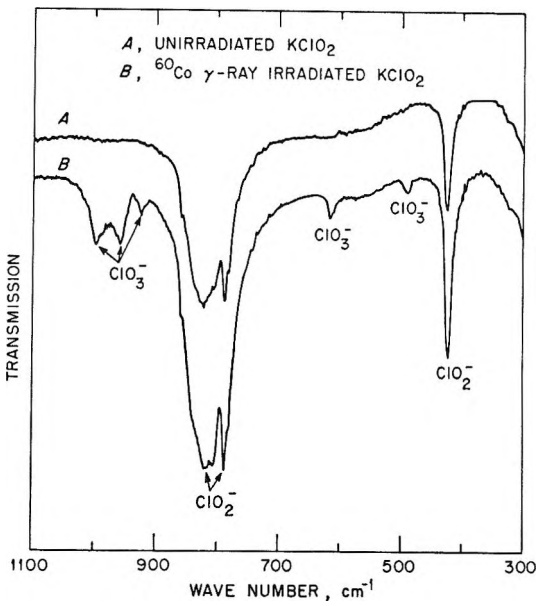

Figure 2. Infrared absorption spectrum of $KClO_2$ (c) at room temperature (KBr pellet technique: concentration of $KClO_2$ *ca.* 0.2% by weight; dose to irradiated $KClO_2$: 1.0×10^{23} eV mol^{-1}).

ion was produced in the crystal lattice and hence was not formed in aqueous solutions by disproportionation of ClO_2, or, possibly by reaction of a trapped, unstable intermediate. The frequencies of the bands assigned to ClO_3^- ion, $\nu_1(A_1) = 932$, $\nu_2(A_1) = 613$, $\nu_3(E) = 982$, and $\nu_4(E) = 479$ cm^{-1}, respectively, are in agreement with accepted values[12] for the ion in aqueous solutions.

The thermal decomposition of $KClO_2$ occurred with a stoichiometry which was identical with that for the radiolytic disproportionation reaction. Decomposition began at 135°, was strongly exothermic, and was complete at *ca.* 165°. There was no weight loss in this temperature interval, nor was oxygen gas detected above the heated $KClO_2$. The resulting mixture of KCl–$2KClO_3$ melted at 353° or approximately 10° below the melting point of pure $KClO_3$ (364°) observed in the same experimental arrangement. Exothermic decomposition to oxygen gas plus KCl began at *ca.* 375° and weight losses were detectable at *ca.* 480°.

Discussion

The mechanism whereby the disproportionation reaction proceeds in the crystalline alkali metal chlorites is of interest. The decomposing entities cannot be identified positively, but probably they are not ClO_2 molecules or radicals in the ground state which are stable. Molecular oxygen is not observed as a decomposition product; hence, ClO_2^- does not undergo internal recombination to form Cl^- ion and $O_2(g)$ according to reaction 1 above. Because of the large electron affinities of ClO and ClO_2 relative to oxygen atoms,[11] the thermal and radiolytic decompositions therefore are assumed to involve a free radical type of dissociation

$$ClO_2^- \rightsquigarrow {}^*ClO_2^- \longrightarrow ClO^- + O \quad (3a)$$
$$\hookrightarrow Cl^- + 2O \quad (3b)$$

or

$$ClO_2^- \rightsquigarrow {}^*ClO^- + O \quad (4a)$$
$$\hookrightarrow Cl^- + O \quad (4b)$$

Chlorate ion then may be formed *via* an efficient scavenging of O atoms by unexcited ClO_2^- ions

$$ClO_2^- + O \longrightarrow ClO_3^- \quad (5)$$

Reaction 5 may occur without extensive O atom migration in a lattice of predominantly undamaged ClO_2^- ions. However, long-range migration must occur if this reaction is responsible for the consumption of chlorite present in low concentrations in radiolyzed $KClO_3$. It seems more likely, however, that the O atoms produced in (3) and (4) are scavenged by neighboring ClO_3^- ion *via* addition and abstraction reactions 6 and 7, respectively.

$$ClO_3^- + O \longrightarrow ClO_4^- \quad (6)$$

$$ClO_3^- + O \longrightarrow ClO_2^- + O_2(g) \quad (7)$$

Comparisons of the radiolysis of the crystalline alkali metal chlorites and nitrites would be of interest, but, unfortunately, there appear to be no published reports of the stable products formed in the latter at room temperatures. Investigations[13] on dilute mixtures of KNO_2 in KBr have given some evidence that radiolytic oxygen atoms may exhibit long-range diffusion. Nitrate ion but not oxygen gas was observed. However, other unidentified products must be formed as the number of NO_3^- ions found was but $^1/_5$ the number of NO_2^- ions decomposed.

Chlorite is not observed in the thermal decomposition of chlorates because of the lower decomposition temperature of the former species. Interestingly, the free energy decrease at 298.2°K for the decomposition of $NaClO_2$ by internal recombination, reaction 1, is greater than by disproportionation, reaction 2 (*i.e.*, -37.3 *vs.* -17.1 kcal mol^{-1}); however, the decomposition in the solid both thermally and radiolytically occurs exclusively *via* reaction 2. A similar behavior is exhibited in the decomposition of the alkali metal chlorates where the free energy decrease for the reaction

$$NaClO_3 \longrightarrow NaCl + {}^3/_2O_2(g) \quad (8)$$

(12) H. Siebert, "Anwendungen der Schwingungsspektroscopie in der Anorganischen Chemie," Springer-Verlag, New York, N. Y., 1966, p 57.

(13) A. R. Jones and R. L. Durfee, *Radiat. Res.*, **15**, 546 (1961).

is -32.7 kcal mol^{-1} while the decrease for

$$NaClO_3 \longrightarrow {}^3/_4NaClO_4 + {}^1/_4NaCl \qquad (9)$$

is but -9.9 kcal mol^{-1}. Yet, at 542° in the molten state more than two-thirds of the $NaClO_3$ decomposes *via* reaction 9 and the remainder *via* reaction 8.[14]

Tentatively it is concluded that chlorite ion is decomposed thermally and by ^{60}Co γ rays to give oxygen atoms when the ion is present either in an alkali metal chlorite lattice or in an alkali metal chlorate crystal at relatively low concentration. In a chlorite lattice, the addition reaction 5 is of dominant importance and the abstraction reaction

$$ClO_2^- + O \longrightarrow ClO^- + O_2(g) \qquad (10)$$

is either absent or is greatly suppressed; in a chlorate lattice the O atoms releasedin ClO_2^- ion decomposition may react either by reaction 6 or 7.

Acknowledgment. The research was sponsored by the United States Atomic Energy Commission under contract with Union Carbide Corp.

(14) M. M. Markowitz, D. A. Boryta, and H. Stewart, Jr., *J. Phys. Chem.*, **68**, 2282 (1964).

The Flash Photolysis of Methyl Iodide[1]

by Gilbert J. Mains[2] and David Lewis

Department of Chemistry, Carnegie-Mellon University, Pittsburgh, Pennsylvania *(Received June 4, 1969)*

The flash photolysis of methyl iodide in the gas phase produces methane, ethane, ethylene, acetylene, and iodine as products. Methylene iodide which has been reported as a product in the low-intensity photolysis was not detected among the products of the high-intensity photolysis. The quantum yield of methane was found to be a function of pressure and ranged from 0.10 to 0.001 in high-intensity experiments and from 0.020 to 0.005 in the low-intensity experiments. It is suggested that the activation energy for the reaction $CH_3 + CH_3I \rightarrow CH_4 + CH_2I$ is supplied by the methyl radicals in the low-intensity photolysis while in the high-intensity photolysis the energy is provided by both methyl radical and methyl iodide molecule.

Introduction

Although the low-intensity photolysis of methyl iodide has been reported by a number of authors,[3-7] the high-intensity photolysis has been only partially studied.[8] A more detailed study of the high-intensity photolysis has been performed as part of a program investigating the reactions of "hot" radicals.

Methyl iodide shows a strong absorption at 2580 Å, an excitation which has been attributed to an $n \rightarrow \sigma^*$ transition leading to the unbound state[9,10] from which the dissociation products share energy of some 36 kcal mol^{-1}.

$$CH_3I + h\nu \longrightarrow CH_3^* + I(^2P_{1/2}) \qquad (1)$$

Calculations by Bass and Pimentel[11] suggest that the methyl radical obtains 9.5 kcal mol^{-1} of this energy as vibrational energy and that the remainder is divided between the iodine atom and the methyl radical according to the laws of the conservation of energy and of momentum. The methyl radical is formed with up to 9.5 kcal mol^{-1} vibrational energy and about 23 kcal mol^{-1} translational energy. Ausloos[12] has suggested that the translational energy of the product methyl radical is only slightly above the activation energy for the hydrogen abstraction reaction (2). Since the quantum yield for the formation of methane is low, Φ_{CH_4} is approximately 3×10^{-3}, it has been concluded that

$$CH_3^* + CH_3I \longrightarrow CH_4 + CH_2I \qquad (2)$$

(1) Supported by the Air Force Office of Scientific Research.

(2) Department of Chemistry, University of Detroit, Detroit, Mich. 48221.

(3) R. D. Shultz and H. D. Taylor, *J. Chem. Phys.*, **18**, 194 (1950).

(4) R. B. Martin and W. A. Noyes, *J. Amer. Chem. Soc.*, **75**, 4183 (1953).

(5) R. D. Souffie, R. R. Williams, Jr., and W. H. Hamill, *ibid.*, **78**, 917 (1956).

(6) F. P. Hudson, R. R. Williams, and W. H. Hamill, *J. Chem. Phys.*, **21**, 1894 (1953).

(7) G. M. Harris and J. E. Willard, *J. Amer. Chem. Soc.*, **76**, 4678 (1954).

(8) N. R. Davidson and T. Carrington, *ibid.*, **74**, 6277 (1952).

(9) D. Porrett and C. F. Goodeve, *Proc. Roy. Soc.*, **31**, A165 (1938).

(10) M. Ito, P. C. Huang, and E. M. Kosower, *Trans. Faraday Soc.*, **57**, 1662 (1961).

(11) C. D. Bass and G. C. Pimentel, *J. Amer. Chem. Soc.*, **83**, 3754 (1961).

(12) R. D. Doepker and P. Ausloos, *J. Chem. Phys.*, **41**, 1865 (1964).

reaction 2 is much less efficient than the thermalization reaction 3. The thermal methyl radicals produced by

$$CH_3^* + (M) \longrightarrow CH_3 + (M) \quad (3)$$

the nonreactive collision 3 do not possess enough energy to undergo reaction 2 and are removed from the system by several routes

$$CH_3 + I_2 \longrightarrow CH_3I + I \quad (4)$$

$$CH_3 + I \longrightarrow CH_3I \quad (5)$$

$$2CH_3 \longrightarrow C_2H_6 \quad (6)$$

The present studies of both high- and low-intensity photolysis show that the above mechanism is inadequate and must be modified.

Experimental Section

Materials. Analytical grade methyl iodide obtained from Baker Chemical Company was dried over Drierite and distilled *in vacuo* from copper wire. The sample was degassed using a standard freeze–pump–thaw cycle at −112° and stored as liquid in a darkened Pyrex bulb. The 70-V mass spectrum and the gas chromatogram, obtained using a 12-ft Apiezon column in conjunction with a flame ionization detector, indicated the absence of ethyl and diiodo compounds. The perfluorodimethylcyclobutane used in the inert gas studies was obtained from du Pont. It was dried over Drierite, distilled *in vacuo* and degassed at −120°. The 70-V mass spectrum indicated the absence of any hydrogen containing impurities. Analytical grade iodine obtained from Baker Chemical Co. was dried over phosphorus pentoxide, distilled *in vacuo*, and stored in Pyrex reaction ampoules. Methyl iodide-*d*-3, obtained from Stohler Chemical Co., was distilled *in vacuo* from copper wire and was degassed using a standard freeze–pump–thaw cycle at −112°. The methyl iodide-*d*-3 was stored as liquid in a darkened Pyrex bulb. The 70-V mass spectrum showed the hydrogen impurities, measured as methyl iodide-*d*-2, to be 4%.

Apparatus. High Intensity. A General Electric FT 524 xenon-filled flash tube was connected across a condenser bank of 62.5 μF charged to 4 kV and was discharged by means of a Tesla coil. The lifetime of the flash was measured by means of a 931A phototube oscilloscope combination and was found to be 150 microseconds. The spectral characteristics of the FT 524 flash tube have been reported by Kuebler and Nelson.[13] Uranyl oxalate actinometry was performed for the same conditions and geometries employed in the experiments. Estimating an average value of 0.57 for the quantum yield, the light absorbed by the actinometer solution was found to be 25 μEinsteins flash^{-1} corresponding to a flux of 15 mEinsteins sec^{-1} cm^{-3}.

The quartz vessels used in the flash photolysis had a surface to volume ratio of 3.1 cm^{-1}, volume 25 cm^3, and were equipped with a graded-seal and a Pyrex break-seal.

Table I: Effect of Perfluorodimethylcyclobutane and *n*-Hexane on Methane and Ethane Yields per Flash

CH_3I, Torr	*n*-C_6H_{12}, Torr	P.F.C., Torr	CH_4, μmol	C_2H_6, μmol
50	...	...	2.04	0.175
50	20	...	0.035	0.200
50	...	20	0.031	0.195
50	20	30	0.013	0.097
50	...	51	0.007	0.091

Low Intensity. Low-intensity photolysis experiments were carried out using a Hanovia SC-2537 low-pressure mercury lamp coiled into a helix form. Using uranyl oxalate actinometry the flux in the center of the lamp was found to be 0.224 μEinsteins min^{-1} cm^{-3} for the same geometry as that used in the experiments.

The quartz cells used in these experiments were Cell A, volume 410 cm^3, which has a surface to volume ratio of 0.702 cm^{-1}, and Cell B, volume 50 cm^3, which had a surface to volume ratio of 1.33 cm^{-1}.

Procedure. The usual high-vacuum techniques were used in the preparation of all samples. During the preparation of samples for both high- and low-intensity photolysis, mercury was excluded from the reaction vessel by the use of a granulated zinc trap. The volatile products were separated from the methyl iodide and iodine at −156° (isopentane slush).

Analysis. Mass spectra of the volatile products were obtained using a modified Consolidated Electrodynamics Corp. Model 21-103C mass spectrometer. The residue after removal of the gaseous products at −156° was also analyzed using the same instrument.

Results. The products observed in the flash photolysis of methyl iodide are methane, ethane, ethylene, acetylene, and iodine. Methylene iodide which is produced in high yield in the low-intensity experiments was not detected among the products of the flash photolysis. The ethylene and acetylene were observed in much larger quantities relative to the ethane yield than had been observed in low-intensity photolysis.

Experiments were performed to determine the effects of substrate pressure, surface to volume ratio, temperature, and the addition of inert gas to the system. The results of these series of experiments are shown in Figures 1–7. As may be seen from Figure 1 an unusual relationship exists between the methane yield and the substrate pressure. As there was no previous report of any pressure effect in low-intensity photolysis, the pressure effect at low intensities was studied and the results are presented in Figure 8. It may be pointed out here that earlier workers used methyl iodide pressures

(13) N. A. Kuebler and L. S. Nelson, *J. Opt. Soc. Amer.*, **51**, 1411 (1961).

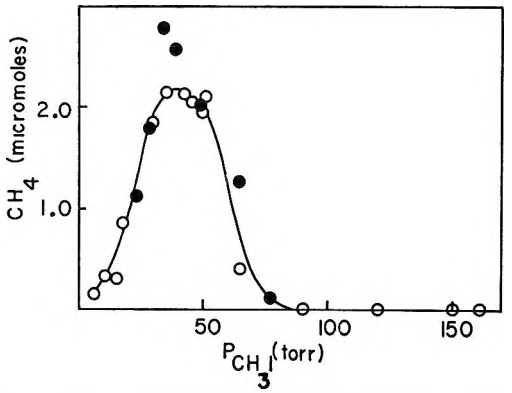

Figure 1. Flash photolysis methane yield (moles per flash) *vs.* methyl iodide pressure; ●, iodine added to the system.

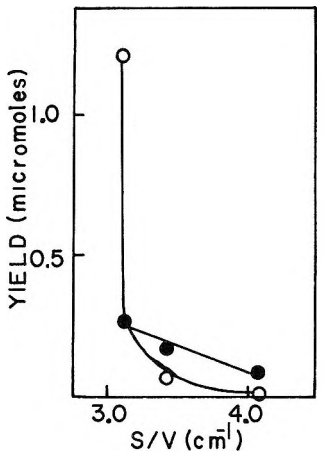

Figure 2. ○, Methane; and ●, ethane; yields per flash as a function of surface to volume ratio (pressure of methyl iodide 50 Torr).

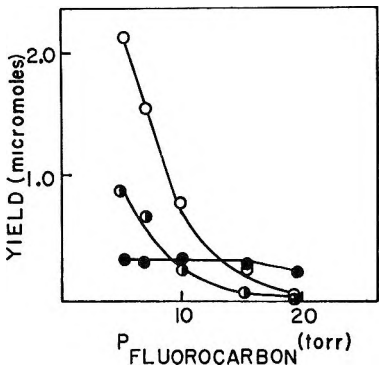

Figure 3. Dependence of product yields per flash upon the addition of perfluorodimethyl cyclobutane; methyl iodide pressure 50 Torr; ○, methane; ●, ethane; ◑, ethylene.

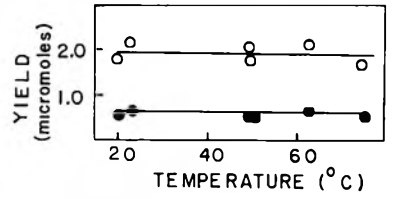

Figure 4. Product yields (moles per flash) as a function of temperature; ○, methane; ●, ethane; (pressure of methyl iodide 50 Torr).

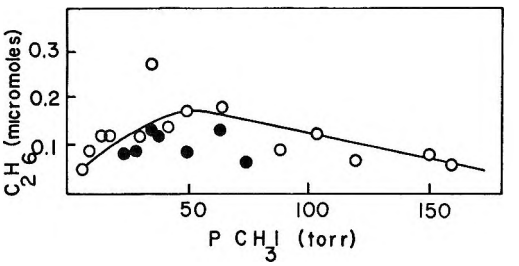

Figure 5. Ethane yield per flash as a function of methyl iodide pressure; ●, iodine added.

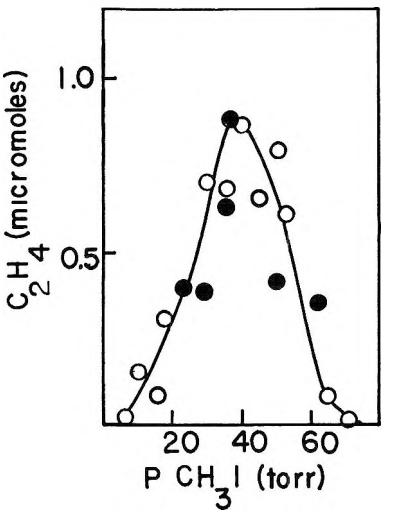

Figure 6. Ethylene yield per flash as a function of methyl iodide pressure; ●, iodine added.

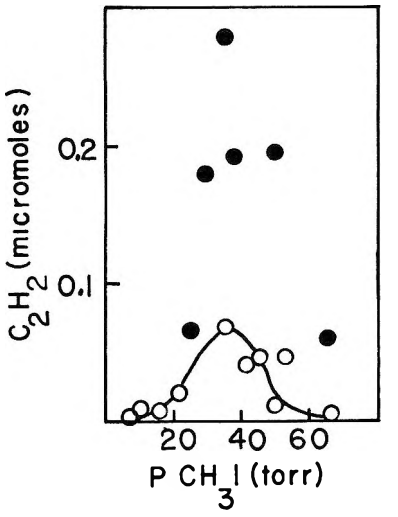

Figure 7. Acetylene yield per flash as a function of methyl iodide pressure; ●, iodine added.

of 6–7 Torr and 60–331 Torr. The quantum yields obtained in the two regions are essentially the same. The dependence of the methane yield upon the surface to volume ratio was also studied and the results are shown in Figure 9. High-intensity photolysis experiments in

which *n*-hexane was added to methyl iodide were performed and the results are to be found in Table I. Mixtures of methyl iodide and methyl iodide-*d*-3 were photolyzed at high intensity and the distributions of the methane determined. The results are recorded in Table II.

Table II: Distribution of Deuterated Methanes

CH_3I: CD_3I	Methanes (as percentages of total) d_4	d_3	d_2	d_1	d_0
0.67	29.0	29.9	...	18.2	23.0
1.00	19.3	28.6	1.7	19.4	30.5
1.00	19.9	28.9	2.0	21.0	28.1

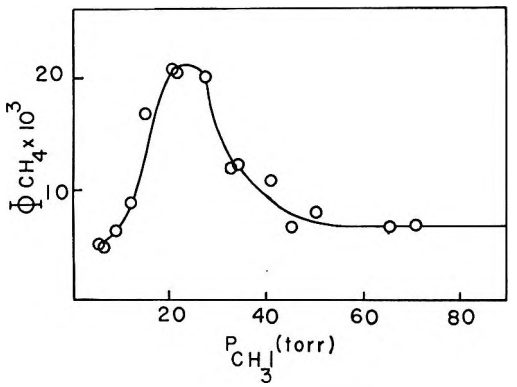

Figure 8. Quantum yield of methane as a function of methyl iodide, pressure at 2537 Å.

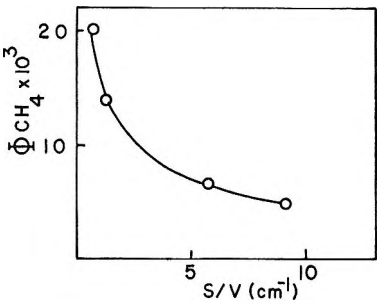

Figure 9. Low-intensity methane quantum yield as a function of surface to volume ratio, methyl iodide pressure 20 Torr.

Discussion

Methane Production. As may be seen from Figures 1 and 8, the pressure dependence of the methane yield is qualitatively similar for both high- and low-intensity photolyses. In both cases the maximum methane yield occurs at about 90% light absorption so that the increase is almost certainly due to an increase in the absorbed intensity. The decrease in methane yield as the pressure of methyl iodide is increased further may be attributed to several factors and will be discussed later.

The determination of a quantum yield for flash photolysis is necessarily difficult but we may define a lower limit by the use of uranyl oxalate actinometry to determine the maximum number of quanta incident upon the reaction cell. The average quantum yield of methane, over the wavelengths absorbed by the actinometer (as a lower limit), is 1.10 at the maximum and falls to 0.001 at higher pressures. At low light intensities the quantum yield for methane production is 0.021 at the maximum falling to 0.005 at higher pressures. The effects of changing the surface to volume ratio upon methane yield is similar for both high and low light intensities (Figures 2 and 9, respectively). As the surface to volume ratio is increased the methane yield is decreased. In comparing the quantum yields for the low- and high-intensity studies we should note that equalization of the surface to volume ratios for the two systems would increase the quantum yield for the high-intensity studies with respect to the quantum yield at low intensities. At maximum in both cases the ratio is as follows

$$\frac{\Phi_{CH_4}^{max} \text{ (high intensity)}}{\Phi_{CH_4}^{max} \text{ (low intensity)}} \geq 5$$

Since we have shown that the high-intensity quantum yield is low due to the definition used and that equalization of the surface to volume ratios would increase the above ratio, the value obtained above must be regarded as minimal. We therefore conclude that at high light intensities there is at least one more reaction leading to methane formation than at low light intensities. The high-pressure limit

$$\frac{\Phi_{CH_4} \text{ (high pressure, high intensity)}}{\Phi_{CH_4} \text{ (high pressure, low intensity)}} \geq 0.2$$

is apparently less than unity but we may use the same arguments as above to show that this is a minimal value so that the same reaction could be responsible for the methane formation in both high-pressure cases. The temperature dependence of the methane yield is shown in Figure 4. Over the temperature range 20–70° the methane yield is independent of starting temperature. Since the activation energy[14] for the abstraction of a hydrogen atom by a methyl radical is about 10 kcal mol^{-1}, we must assume that either the methyl radical or the methyl iodide molecule is taking the major portion of this energy into the reaction. In order to establish which of the reactants was the principal energy donor, experiments were performed in which perfluorodimethylcyclobutane was added to methyl iodide: the results are shown in Figure 3. As the pressure of inert gas is increased, the methane yield is decreased, showing that the perfluorocarbon acts as a thermalizing agent. Flash photolysis of methyl iodide–*n*-hexane mixtures,

(14) A. F. Trotman-Dickenson, J. R. Birchard, and E. W. R. Steacie, *J. Chem. Phys.*, 19, 163 (1951).

Table I, show that the *n*-hexane also acts as a thermalizing agent. If the methyl radicals produced in the primary process are responsible for the methane production, *i.e.*, the methyl radicals supply the necessary activation energy for reaction 2, then we might reasonably expect that the addition of *n*-hexane would increase the methane yield or at least maintain the yield at the same level through reaction 7. As may be seen

$$CH_3^* + n\text{-}C_6H_{14} \longrightarrow CH_4 + C_6H_{13} \qquad (7)$$

from Table I, the methane yield is reduced, demonstrating that the methyl radicals are not the means by which the energy is brought into the reaction. Majer and Simons[15] have proposed a mechanism by which energy is transferred from the "hot" methyl radical, formed in the primary process, to a methyl iodide molecule by an iodine abstraction process.

$$CH_3^* + CH_3I \longrightarrow CH_3I^* + CH_3 \qquad (8)$$

Whittle[16] and Fox[17] have shown that for thermal methyl radicals the ratio of the rate constants k_{8a}/k_{2a} is about 10^3.

$$CH_3 + CH_3I \longrightarrow CH_3I + CH_3 \qquad (8a)$$

$$CH_3 + CH_3I \longrightarrow CH_4 + CH_2I \qquad (2a)$$

Methyl iodide molecules formed in reaction 8 may have up to 9.5 kcal mol^{-1} excess vibrational energy, as calculated from the extension of the methyl iodide spectrum observed in flash photolysis.[18,19] The value of the excess vibrational energy is in surprisingly good agreement with the theoretical value[12] of 9.5 kcal mol^{-1} for the methyl radical formed in the primary process. Since a large portion of the energy could be vibrational energy in the C–H bond, the ratio of the rate constants k_{8b}/k_{2b}

$$CH_3 + CH_3I^* \longrightarrow CH_3I + CH_3 \qquad (8b)$$

$$CH_3 + CH_3I^* \longrightarrow CH_4 + CH_2I \qquad (2b)$$

may well be decreased leading to high yields of methane. The above effect would not be observed in the low-intensity photolysis as the excited methyl iodide molecules would have to survive 10^5–10^6 collisions before encountering a methyl radical, by which time the excess vibrational energy would certainly have been lost. However, in high-intensity photolysis the concentrations of such radicals and excited intermediates would be increased by about 10^5 making measurable reactions between two excited molecules or an excited molecule and a radical. As the methyl iodide pressure is increased, the effective surface to volume ratio is increased. Since both "hot" methyl radicals and excited methyl iodide molecules will become deactivated upon wall collision the methane yield is lowered. The addition of iodine to the system does not lower the methane yield since neither "hot" methyl radicals nor excited methyl iodide molecules are scavengable.

Isotope Effect. The distribution of methanes produced in the flash photolysis of methyl iodide and methyl iodide-d_3 are given in Table II. The methane-d_2 produced arises from methyl iodide-d_2 and lies within the impurity limits. The ratios of CD_4:CD_3H and CH_3D:CH_4 indicate that an isotope effect is present. The ratios π_H/π_D, where π_H and π_D are the probabilities for hydrogen and deuterium abstraction respectively, are 1.45 ± 0.11. This is in good agreement with the value 1.3 reported by Ausloos and Doepker in their experiments at 2537 Å using an equimolar mixture of CH_3I and CD_3I. Since the contribution of the methyl iodide molecules to the relative probabilities of abstraction would be expected to cancel regardless of whether reaction 2a or 2b was responsible for the methane production, the intensity independence of π_H/π_D is not surprising.

Ethane Production. The ethane yield as a function of substrate pressure is shown in Figure 5. There is a small pressure effect, probably due to the increase in absorbed intensity, reaching a poorly defined maximum and then slowly declining. The addition of iodine to the system reduces the yield to about 60% of the original yield. Ethane formation probably occurs solely *via* reaction 6, $2CH_3 \rightarrow C_2H_6$. Reaction 6 is in competition with reactions 9 and 10. The 60%

$$CH_3 + I_2 \longrightarrow CH_3I + I \qquad (9)$$

$$CH_3 + I \longrightarrow CH_3I \qquad (10)$$

yield of ethane in the presence of iodine does not mean that 60% of the ethane is unscavengable but that the initial concentration of methyl radicals is so high that reaction 6 is able to compete with reactions 9 and 10. The addition of inert gas to the system (Figure 3) does not affect the ethane yield until relatively high pressures of perfluorocarbon are added. While the perfluorocarbon will increase the concentration of thermal methyl radicals and thus increase the rate of reaction 6, the perfluorocarbon also acts as a third body for the recombination of iodine and for reaction 10.

Souffie[5] has proposed reaction 11 on the basis that

$$CH_3^* + CH_3I \longrightarrow C_2H_6 + I \qquad (11)$$

7.5% of the ethane is not scavengable at low intensities. Doepker and Ausloos[12] also support reaction 11 in their low intensity experiments. However, recent work by Meyer[20,21] using time-of-flight mass spectroscopy has

(15) J. R. Majer and J. P. Simons, *Advan. Photochem.*, Vol. II, (1964).

(16) W. G. Alcock and E. Whittle, *Trans. Faraday Soc.*, 61, 244 (1965).

(17) R. J. Fox, F. W. Evans, and M. Swarz, *ibid.*, 57, 1915 (1961).

(18) J. C. Biordi and G. J. Mains, private communication.

(19) J. F. McKellar and R. G. W. Norrish, *Proc. Roy. Soc.*, A263, 51 (1961).

(20) R. T. Meyer, *J. Chem. Phys.*, 46, 4146 (1967).

(21) R. T. Meyer, *J. Phys. Chem.*, 72, 1583 (1968).

suggested an alternate reaction to reaction 11 as a source of iodine atoms. Meyer noted that upon flash photolysis of methyl iodide, iodine was formed at two different rates. The fast reaction was assigned to the reaction

$$I(^2P_{1/2}) + CH_3I \longrightarrow CH_3 + I_2 \qquad (12)$$

and the slow rate assigned to a number of other reactions including

$$2I \longrightarrow I_2 \qquad (13)$$

Willard[22] has since shown that reaction 12 does not occur in the room temperature photolysis of iodine–methyl iodide mixtures where the excited iodine atoms are produced by the photolysis of iodine molecules. The apparent discrepancy between the work of Willard and of Meyer may be resolved if a small activation energy is required for reaction 12, and it is assumed in the methyl iodide photolysis this activation energy is provided by the excited methyl iodide molecules produced by reaction 8. The findings of Meyer have been substantiated by Donovan, *et al.*[23], in their studies of methyl iodide–perfluoromethyl iodide photolysis where the excited iodine atom concentration was monitored by kinetic spectroscopy. Thus, reaction 11 can be ruled out as the major source of ethane at flash intensities even though it is probably the source of unscavengable ethane at low intensities.

Ethylene. The ethylene yield in all experiments using flash photolysis is about 50% of the methane yield (Figure 6) and since methylene iodide is not detected as a product in these experiments, the reaction

$$2CH_2I \longrightarrow C_2H_4 + I_2 \qquad (14)$$

is probably responsible for the ethylene yield. A two-step reaction may be written

$$2CH_2I \longrightarrow (CH_2ICH_2I)^* \qquad (15)$$

$$(CH_2ICH_2I)^* \longrightarrow C_2H_4 + I_2 \qquad (16)$$

If the two-step mechanism is responsible for the ethylene formation, we should expect to observe 1,2-diiodoethane in the products as a percentage of the excited intermediate would be deactivated by collision. In view of the absence of diiodoethane in the products, the one-step mechanism is preferred. Methylene iodide is formed in the low-intensity photolysis by the reaction

$$CH_2I + I_2 \longrightarrow CH_2I_2 + I \qquad (17)$$

which competes with reaction 14 in flash photolysis. Of the methylene iodide produced, the larger part will probably be photolyzed to yield methylene and iodine, *i.e.*

$$CH_2I_2 + h\nu \longrightarrow CH_2 + I_2 \qquad (18)$$

However, the absence of detectable quantities of methylene iodide and ethyl iodide in the product mixture suggests that the larger part of the methyl iodide radicals react according to reaction 14.

Acetylene. The acetylene yield as a function of substrate pressure (Figure 7) shows the same pressure dependence as the methane yield. The acetylene yield, unlike the methane yield, is strongly dependent upon the addition of iodine, which increases its yield fourfold. As in the case of ethylene formation, the acetylene probably arises from the reaction between two methyl iodide radicals.

$$2CH_2I \longrightarrow C_2H_2 + 2HI \qquad (19)$$

The reaction is likely to be a two-stage process involving reaction of a methyl iodide radical with iodine in the first stage.

$$CH_2I + I_2 \longrightarrow CH_2I\text{–}I_2 \qquad (20)$$

$$CH_2I + CH_2I\text{–}I_2 \longrightarrow C_2H_2 + 2HI + I_2 \qquad (21)$$

While no hydrogen iodide was detected in the products of the photolysis, it is entirely possible that the small quantities formed in reaction 21 could be absorbed on the walls of the glass inlet system of the mass spectrometer and not be detected.

Acknowledgment. Financial support of this research was provided by the U. S. Air Force Office of Scientific Research and is gratefully acknowledged here. Also, the authors wish to thank Mr. S. Wrbican for determining the mass spectra used in product analyses.

(22) S. Aditya and J. E. Willard, *J. Chem. Phys.*, **44**, 418 (1966).
(23) R. J. Donovan, F. G. M. Hawthorn, and D. Husain, *ibid.*, **49**, 953 (1968).

The Effects of Temperature and Additives in the Radiolysis of Potassium Nitrate[1]

by H. Bernhard Pogge and F. T. Jones

Department of Chemistry and Chemical Engineering, Stevens Institute of Technology, Hoboken, New Jersey 07030
(Received December 4, 1969)

The γ radiolysis of KNO_3 was studied as a function of radiation dose and temperature, and with added NO_2^-, ClO_4^-, and ($N^{18}O_3$) incorporated in the KNO_3 lattice. O_2 and NO_2^- are formed as products by at least two mechanisms, one of which involves O atoms. Both the $KNO_3 \cdot KNO_2$ and $KNO_3 \cdot KClO_4$ systems indicate an O-atom yield of $G_O = 0.45$. O_2 and NO_2^- are also produced by processes not involving O atoms at yields $G_{O_2} = 0.30$ and $G_{NO_2} = 1.15$. The isotopic distribution of O_2 formed in $KN^{16}O_3 \cdot KN^{18}O_3$ crystals can be interpreted on the basis of $G_O = 0.50$ and $G_{O_2} = 0.25$. After correcting for thermal decomposition, $G(O_2)$ and $G(NO_2^-)$ in KNO_3 are independent of temperature between 24° and 128°, but more than double at 128° and continue to increase with temperature up to the melting point.

Introduction

The mechanism by which molecules decompose under radiation is usually derived not from studies with pure compounds, but from mixtures containing additives capable of reacting with the intermediates. This technique has been used extensively in the radiation and photochemistry of gases, liquids, and rigid glasses, but has rarely been used for crystalline solids.

KNO_3 is an example of a solid which has been studied extensively in the pure state, but the mechanism by which the ultimate products are formed is still not understood. It has been postulated[2,3] that NO_2^- and O_2 are formed by reactions I–III at room temperature

$$NO_3^- \rightsquigarrow NO_2^- + O \qquad \text{(I)}$$

$$O + NO_2^- \longrightarrow NO_3^- \qquad \text{(II)}$$

$$O + NO_3^- \longrightarrow NO_2^- + O_2 \qquad \text{(III)}$$

Esr[4] and X-ray diffraction[5] techniques have shown that small amounts of NO_2^- can be incorporated into KNO_3 without significantly changing the lattice parameters of the host crystal. It should also be possible to incorporate other molecules into KNO_3 if the cell dimensions of both crystals are almost the same.

If additional NO_2^- is incorporated into the KNO_3 lattice, reaction II should be favored over (III) and the O_2 yield should decrease. Alternatively, in the presence of ClO_4^-, the NO_2^- yield should decrease because of the competition between (III) and (IV), and the O_2 yield should remain unchanged

$$O + ClO_4^- \longrightarrow ClO_3^- + O_2 \qquad \text{(IV)}$$

O_2 and NO_2^- may also be formed by reactions not involving the oxygen atom. The present work is an attempt to determine the mechanism for O_2 and NO_2^- formation in KNO_3 by incorporating KNO_2, $KClO_4$, and ^{18}O-labeled KNO_3 into the KNO_3 crystalline lattice to act as O-atom scavengers.

Experimental Section

Materials. Baker Reagent Grade KNO_3, $KClO_4$, and KNO_2 were recrystallized three times from warm solution of KNO_3 and $KClO_4$ from triply distilled water, and KNO_2 from anhydrous methanol, since KNO_2 forms a stable hydrate with water. The crystals were then dried, crushed to an average size of less than 0.7 mm, and stored over P_2O_5 in desiccators. To check for the effect of impurities in the radiolysis, a portion of the KNO_3 was further purified by zone refining using the technique of Sue, *et al.*,[6] passing the zone over the sample twenty times at a pass rate of 0.5 cm/hr. KNO_3 with high ^{18}O enrichment was obtained from the Weizmann Institute, Israel (84% ^{18}O enrichment) and Isomet Corp. (70% ^{18}O). The crystals with 84% enrichment were zone refined, but the 70% ^{18}O enriched crystals were used without further purification.

Doped crystals ($KNO_3 \cdot KNO_2$, $KNO_3 \cdot KClO_4$, and $KN^{16}O_3 \cdot KN^{18}O_3$) were prepared by mixing appropriate amounts of the respective salts in the melt. The mixtures were then quenched to −195° and crushed. Chemical analysis of small random samples always agreed with the stoichiometric composition of the original mixture.

(1) Submitted in partial fulfillment of the degree Doctor of Philosophy in Chemistry at Stevens Institute of Technology, September 1967.

(2) A. O. Allen and J. Ghormley, *J. Chem. Phys.*, **15**, 208 (1947).

(3) E. R. Johnson and J. Forten, *Discuss. Faraday Soc.*, **31**, 238 (1961).

(4) H. Zeldes, "Paramagnetic Resonance," Vol. II, Academic Press, Inc., New York, N. Y., 1963, p 764.

(5) J. Forten and E. R. Johnson, *J. Phys. Chem. Solids*, **15**, 218 (1960).

(6) P. Sue, J. Pauly, and A. Nouaille, *Compt. Rend.*, **244**, 1212 (1957).

Apparatus. Two cobalt-60 γ sources, of nominal strengths 1000 Ci and 300 Ci, were used in this work. An electrical furnace for irradiations at elevated temperatures could be accommodated in the 300-Ci source. The furnace consisted of a solid aluminum cylinder with a small cavity for the irradiation cells and was wrapped with Nichrome heating wire. Temperature was monitored remotely with thermocouples placed at various positions in the furnace.

Most of the irradiations were carried out in 4-cm^3 Pyrex break-seal vials or, when gas analyses were not required, 2-cm^3 screw-cap vials. Energy absorption was determined by the Fricke dosimeter, using the mass absorption coefficients of Hochanadel and Davis.[7]

Analyses. The crystalline samples were degassed before irradiation by pumping at 1×10^{-7} Torr for 10 hr at 110° before sealing the vials. After irradiation the seal was broken under vacuum, deaerated water was distilled into the sample container, and volatile products were removed on refluxing the solution with mild heat. The gases were analyzed by combustion with hydrogen or by mass spectrometry. The residual solution was analyzed for nitrite ion by the colorimetric method of Shinn.[8] Similar results were obtained using the method of Rider and Mellon.[9] The extinction coefficient was determined in this laboratory to be 48,800 M^{-1} cm^{-1} at 538 nm.

ClO_3^- and other oxidizing ions formed from $KClO_4$ were determined by the oxidation of ferrous ion in 0.8 N H_2SO_4. NO_3^-, ClO_4^-, and Cl^- do not interfere, but NO_2^- undergoes a slow reaction with Fe^{2+} to form Fe^{3+} and $Fe(NO)^{2+}$, making it necessary to correct the results for NO_2^- formed in the radiolysis. ClO_3^- was determined by dissolving the irradiated samples of $KNO_3 \cdot KClO_4$ in 10^{-3} M Fe^{2+} and following the optical density of Fe^{3+} as a function of time at 305 nm; the contribution due to NO_2^- was subtracted by extrapolating to zero time. The reliability of this method of analysis was verified with solutions containing known amounts of ClO_3^-, NO_2^-, and NO_3^-.

Results

Irradiation of KNO_3 at 24°. Yields of nitrite ion and oxygen gas were measured as a function of radiation dose up to a total dose of 6×10^{21} eV/gm. NO_2^- formation is linear with dose up to *ca.* 1×10^{21} eV/g, but a gradual decrease in the rate occurs at higher doses. Figure 1 shows that the yield–dose relationship is a smooth curve and cannot realistically be broken into linear segments, as has been done by several previous authors.

The initial yield corresponds to $G(NO_2^-) = 1.60 \pm 0.02$, in good agreement with 1.57 obtained by Hochanadel and Davis[7] and 1.65 by Forten and Johnson[5] at similar doses but somewhat lower than 1.70 recently reported by Cunningham.[10] Yields were independent of radiation intensity, at least over the range 0.18–1.8 $\times 10^{17}$ eV/gm min. Crystals purified by zone refining gave the same results as those purified by recrystallization from aqueous solution.

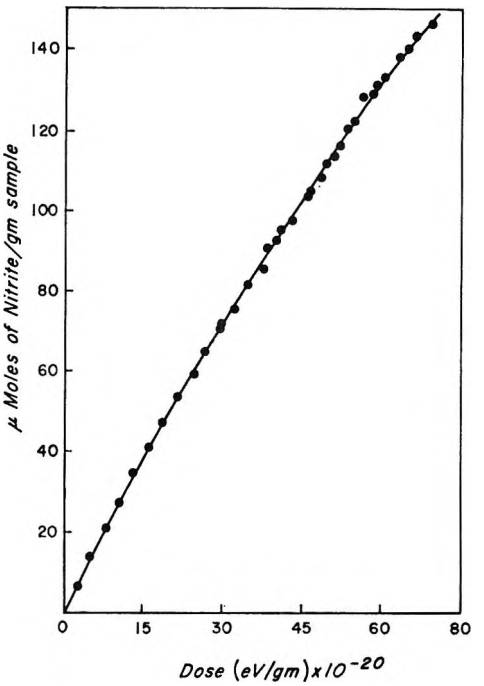

Figure 1. Dose dependence in radiolysis of KNO_3 at 24°. Dose rate = 1.8×10^{17} eV g^{-1} min^{-1}.

Over the entire dose range the $NO_2^-:O_2$ product ratio was found to be 2.2 ± 0.1 instead of 2.0 expected from stoichiometry if these are the only products. The same $NO_2^-:O_2$ ratio was obtained when O_2 was removed from the irradiated sample by briefly heating to the melting point instead of the usual H_2O dissolution technique. A deviation from stoichiometry of similar magnitude has also been reported by Chen and Johnson.[11] These authors attributed the discrepancy to a loss of O_2 by diffusion out of the crystal, but the results described in the next two sections suggest a reaction with surface impurities to form CO or CO_2.

Thermal and Radiation Decomposition of KNO_3 at Elevated Temperatures. In the absence of radiation KNO_3 is stable below 150° but significant thermal decomposition was observed at higher temperatures. At 340°, the highest temperature used in this work, NO_2^- is produced in the thermal reaction at an initial rate of 1.9×10^{-2} μmol/(g of KNO_3 min), corresponding to a first-order rate constant of $k = 2 \times 10^{-6}$ min^{-1}. Between 195 and 340° the data conform to an Arrhenius equation, with an activation energy of 8 kcal/mol. O_2 was not observed as a product under these conditions,

(7) C. Hochanadel and T. Davis, *J. Chem. Phys.*, **27**, 333 (1957).
(8) M. Shinn, *Ind. Eng. Chem., Anal. Ed.*, **13**, 33 (1941).
(9) B. F. Rider and M. G. Mellon, *ibid.*, **18**, 96 (1946).
(10) J. Cunningham, *J. Phys. Chem.*, **65**, 628 (1961).
(11) T. H. Chen and E. R. Johnson, *ibid.*, **66**, 2249 (1962).

but mass spectrometric analysis of the gas showed CO_2 present in molar amounts equal to that expected for O_2, *i.e.*, $NO_2^-:CO_2 \sim 2$. Similar results were obtained for both zone refined and recrystallized KNO_3, and using either Pyrex or Vycor vessels. Neither baking nor etching the cells had any effect on the thermal reaction. In blank runs with an empty Pyrex cell any gas released by heating was below the limits of detection. Bartholomew[12] found $k = 5 \times 10^5 \exp(-31{,}000/RT)$ for the extensive thermal decomposition of molten KNO_3 between 550 and 750°, which corresponds to $k \sim 8 \times 10^{-6}$ min^{-1} when extrapolated to 340°. The smaller activation energy observed in the present work may be ascribed to either the greater mobility in the crystalline phase than in the liquid phase, or to a reaction with impurities on the surface or leached from the glass. But the fact that $E_a = 8$ kcal/mol for the present work is less than ΔH for the decomposition of KNO_3, and that a platinum vessel was found to accelerate the reaction, argues in favor of a surface reaction.

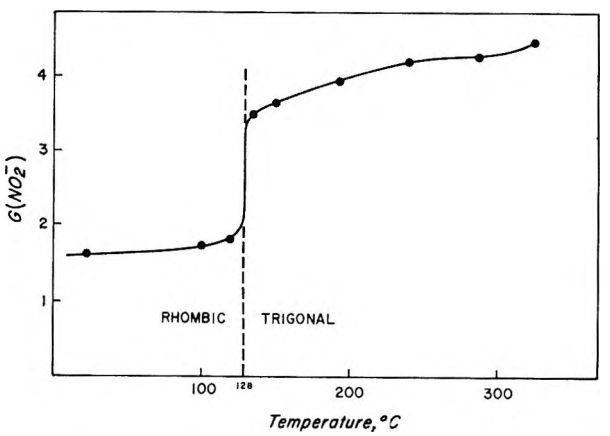

Figure 2. Temperature dependence of $G(NO_2^-)$ after correcting for thermal decomposition.

Both NO_2^- and O_2 are produced in the radiolysis at elevated temperatures. If no correction is made for the thermal decomposition, the results are essentially in agreement with those of Cunningham,[10] showing a gradual increase in nitrite yield with temperature and reaching a value of 5.9 NO_2^- ions/100 eV at 325° (compared with Cunningham's value of 5.8 at 330°). But after correcting for thermal decomposition, $G(NO_2^-)$ is practically independent of temperature up to 128°, the temperature at which a rhombic → trigonal transition occurs in KNO_3,[13] and then suddenly increases to $G(NO_2^-) = 3.4$ at 134° as shown in Figure 2. The corrected yield at 325° is $G(NO_2^-) = 4.6$. Over the entire temperature range $G(NO_2^-)_{cor}/G(O_2) = 2.2$.

Irradiation of ^{18}O-Labeled KNO_3 at 24°. KNO_3 with 84% ^{18}O enrichment was irradiated at various doses from 7×10^{20} eV/g up to 4×10^{21} eV/g. $G(NO_2^-)$ was consistently 13% lower than the yields from unlabeled samples, at least over this dose range.

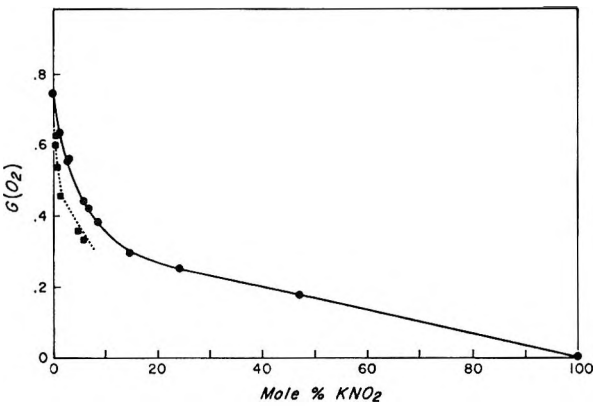

Figure 3. Dependence of $G(O_2)$ on KNO_2 concentration in $KNO_3 \cdot KNO_2$ mixtures. (Broken line: NO_2^- formed by radiolysis).

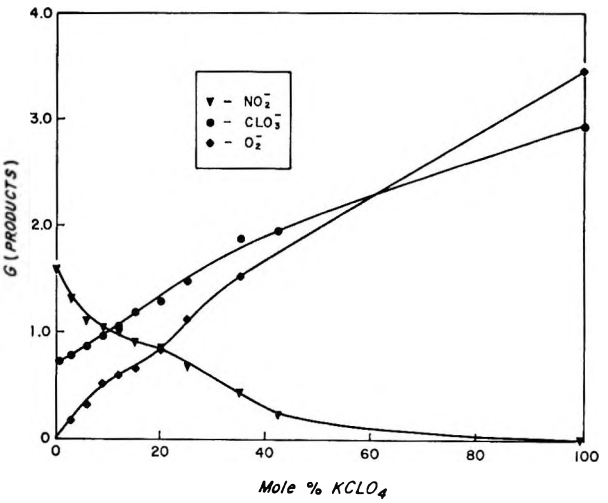

Figure 4. Dependence of product yields on $KClO_4$ concentration in $KNO_3 \cdot KClO_4$ mixtures.

In various mixtures of $KN^{16}O_3$ and $KN^{18}O_3$, $G(NO_2^-)$ also showed an isotope effect although less than that for $KN^{18}O_3$ alone. The sum of the O_2 yields, $G(^{16,16}O_2) + G(^{16,18}O_2) + G(O_2{}^{18,18})$, determined mass spectrometrically showed the same isotope effect as $G(NO_2^-)$.

In addition to peaks at *m/e* 32, 34, and 36, trace amounts of *m/e* 28 and, for samples containing $KN^{18}O_3$, *m/e* 30 were also observed in the mass spectra. These peaks could be due to CO, or $C^{18}O$, formed in a thermal reaction during degassing, as described in the previous section. Peaks at *m/e* 46, 48, and 50 (corresponding to the various isotopic modifications of NO_2) were conspicuously absent, even when the gas had been removed from the irradiated crystals by melting instead of the usual H_2O dissolution technique.

Radiolysis of KNO_3 Containing Additives. a. $KNO_3 \cdot KNO_2$. Oxygen yields were measured at 24° in

(12) R. Bartholomew, *J. Phys. Chem.*, **70**, 3442 (1966).

(13) A. G. Maddock and S. R. Mohanty, *Discuss. Faraday Soc.*, **31**, 193 (1961).

the radiolysis of KNO_3 containing various amounts of added KNO_2. $G(O_2)$ is independent of dose up to at least 12×10^{20} eV/g. Figure 3 shows that the yield of O_2 depends on the concentration of added NO_2^-, decreasing nonlinearly with $[KNO_2]$. Oxygen is not produced in the radiolysis of pure KNO_2.

b. $KNO_3 \cdot KClO_4$. O_2, NO_2^-, and ClO_3^- or other oxidizing species of chlorine are produced in the radiolysis of KNO_3 containing added $KClO_4$. Prince and Johnson[14] have shown that ClO_3^- is the major product in the radiolysis of $KClO_4$, with ClO_2^- and ClO^- being formed in only minor amounts. Therefore no attempt was made in the present work to evaluate the individual contributions of these other species and the total oxidizing yield is expressed as equivalents of "ClO_3^-." Figure 4 shows that NO_2^- decreases and O_2 and "ClO_3^-" increase with increasing $KClO_4$ concentration. The values $G(O_2) = 2.9$ and $G(\text{"}ClO_3^-\text{"}) = 3.5$ for 100% $KClO_4$ can be compared with those of Prince and Johnson, where $G(O_2) = 2.7$ and $G(\text{"}ClO_3^-\text{"}) = 3.2$ can be calculated.

Discussion

Radiolysis of $KNO_3 \cdot KNO_2$ Mixtures. The amount of energy deposited by ionizing radiation in a pure compound depends primarily on the electron density of the material. If the energy absorbed in a mixture of two compounds depends only on the total averaged electron density, the measured yield of a product due to energy absorbed in each component separately can be expressed by eq 1

$$G(P) = G(P)_A(e.f.)_A + G(P)_B(e.f.)_B \qquad (1)$$

where $G(P)_A$, $G(P)_B$ are the yields due to energy absorbed in components A and B, respectively, and $(e.f.)_A$, $(e.f.)_B$ are the corresponding electron fractions. This assumes that energy is not preferentially absorbed by one of the components and that energy is not transferred from one component to the other. Dividing eq 1 by $(e.f.)_A$ and noting that $(e.f.)_B/(e.f.)_A = \sigma_B{}^{(B)}/\sigma_A{}^{(A)}$, where σ_A, σ_B are the mass absorption coefficients and

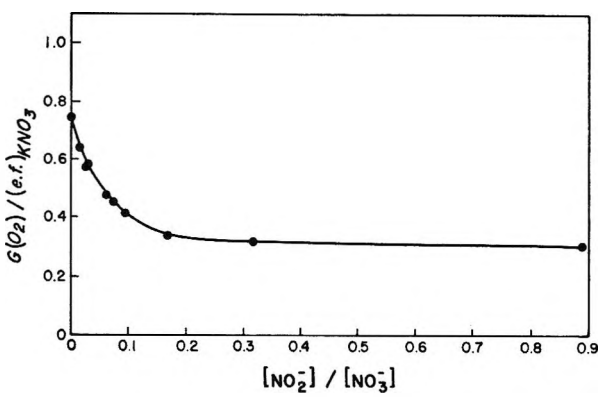

Figure 5. Dependence of O_2 yields on $[NO_2^-]/[NO_3^-]$. Test of eq 3.

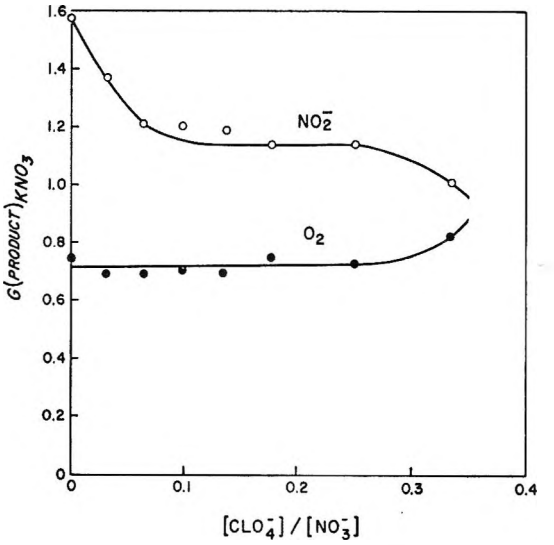

Figure 6. Dependence of NO_2^- and O_2 yields on $[ClO_4^-]/[NO_3^-]$. Test of eq 2.

(A), (B) are the corresponding concentrations in grams of A and B, respectively, gives eq 2

$$\frac{G(P)}{(e.f.)_A} = G(P)_A + G(P)_B \frac{\sigma_B(B)}{\sigma_A(A)} \qquad (2)$$

Thus, $G(P)_A$ and $G(P)_B$ can be determined from the slope and intercept when the left-hand side of eq 2 is plotted as a function of (B)/(A).

The O_2 yields in the radiolysis of $KNO_3 \cdot KNO_2$ mixtures should therefore be given by

$$\frac{G(O_2)}{(e.f.)_{KNO_3}} = G(O_2)_{KNO_3} + G(C_2)_{KNO_2} \frac{(0.0264)(KNO_2)}{(0.0263)(KNO_3)} \qquad (3)$$

Figure 5 shows that above 15% KNO_2 the slope is zero, indicating that $G(O_2)_{KNO_2} = 0$ which is consistent with the fact that O_2 is not produced in the radiolysis of KNO_2. Nitrite ion causes $G(O_2)_{KNO_3}$ to decrease from 0.75 to 0.30 molecule/100 eV, and not to zero as would be expected if reaction III were the only source of O_2. These results suggest that O_2 resulting from energy absorbed in KNO_3 is formed by at least two processes: a "molecular" process which is not affected by added NO_2^- and yielding $G_{O_2} = 0.30$, and a process involving intermediates such as oxygen atoms which is suppressed by the presence of NO_2^-, contributing 0.45 molecule of O_2/100 eV in pure KNO_3.

The reduction in yields caused by intentionally adding NO_2^- to KNO_3 is not the same as that observed in undoped KNO_3 at high doses where NO_2^- is formed radiolytically. In the latter case O_2 is also a product at room temperature and may undergo back-reaction to further reduce the decomposition yield, or O_2 itself

(14) L. Prince and E. R. Johnson, *J. Phys. Chem.*, 69, 359 (1965).

Table I: Isotopic Distribution of Oxygen Yields

	Isotope	Mol mechanism (M)	Atomic mechanism	Obsd distribution	% M
50% $KN^{16}O_3$ 50% $KN^{18}O_3$	$^{32}O_2$	50.00%	44.04%	45.75%	28.7
	$^{34}O_2$	30.62	44.65	40.15	32.1
	$^{36}O_2$	19.30	11.32	14.09	34.6
80% $KN^{16}O_3$ 20% $KN^{18}O_3$	$^{32}O_2$	80.00%	75.19%	76.63%	30.0
	$^{34}O_2$	12.25	23.04	19.79	33.2
	$^{36}O_2$	7.75	1.76	3.82	34.3
				Av	32.2

may act as a free-radical or electron scavenger when allowed to build up in the crystal under prolonged irradiation. This is seen in Figure 3 where O_2 yields are also shown as a function of the concentration of NO_2^- formed radiolytically in undoped KNO_3 (broken curve). The effect of O_2 buildup is similar to the very efficient scavenging effect of $AgNO_3$ in $KNO_3 \cdot AgNO_3$ crystals[15] which has been ascribed to electron trapping by Ag^+.

Radiolysis of $KNO_3 \cdot KClO_4$ Mixtures. In the presence of $KClO_4$, when reactions II and III are replaced by IV, the decrease in the NO_2^- yield should be a measure of the O-atom yield in KNO_3. Applying an equation analogous to eq 3, it is found that $G(NO_2^-)_{KClO_4} = 0$ implying NO_2^- is not formed from energy absorbed in $KClO_4$, and therefore $G(NO_2^-)/(\text{e.f.})_{KNO_3} = G(NO_2^-)_{KNO_3}$. Figure 6 shows that $G(NO_2^-)_{KNO_3}$ drops from 1.60 to 1.15 NO_2^- ions/100 eV at $[ClO_4^-]/[NO_3^-] = 0.1$. It must therefore be concluded that (a) 0.45 oxygen atom/100 eV which would have reacted with NO_3^- to form NO_2^- is now reacting with ClO_4^-, and (b) NO_2^- is also produced at a yield of 1.15 ions/100 eV by processes which do not involve O atoms.

O_2 is a product from both KNO_3 and $KClO_4$, and treating the data for $KNO_3 \cdot KClO_4$ mixtures by eq 2 gives $G(O_2)_{KClO_4} = 2.90$, in excellent agreement with the O_2 yield of 2.95 molecules O_2/100 eV measured in pure $KClO_4$. Figure 6 shows that $G(O_2)_{KNO_3}$ is essentially independent of ClO_4^- concentration, as is to be expected since O_2 is a product in both (III) and (IV).

Above 20% $KClO_4$ the NO_2^- yield begins to decrease and O_2 increases. In this region, either the samples may be no longer homogeneous, because separation into regions of KNO_3 and $KClO_4$ occurs when melts of these compositions are cooled, or KNO_3 may be assuming the role of an impurity in a $KClO_4$ lattice.

Radiolysis of Isotopically Labeled KNO_3. If KNO_3 decomposes by a molecular mechanism, the distribution of $^{16,16}O_2$, $^{16,18}O_2$, and $^{18,18}O_2$ should be different from that expected for the O-atom mechanism, and the observed distribution should represent a combination of the two mechanisms. The distribution expected for each mechanism can be calculated if judicious assumptions are made about (a) the initial distribution of ^{18}O in KNO_3, and (b) the origin of the overall isotope effect of 13% in $KN^{18}O_3$.

^{18}O is incorporated in KNO_3 by an exchange reaction with ^{18}O-enriched water in the presence of a small amount of fuming nitric acid. At 70° about three days is required[16] to yield 84% ^{18}O enrichment in KNO_3; without nitric acid no exchange occurs up to 100°. If a stepwise exchange occurs ($KN^{16}O_3$ becomes $KN^{16}O_2{}^{18}O$, etc.) the isotopic distribution for 70% enrichment should be: 10% $KN^{18}O_3$, 90% $KN^{16}O\text{-}^{18}O_2$.

An isotope effect of at most 6%, calculated from the mass ratio $\sqrt{18/16}$, is expected for each step in the mechanism. For a two-step mechanism, therefore, an overall isotope effect of 12% is indicated, which compares favorably with the 13% effect observed. Thus, assuming an isotope effect of 6% for each oxygen bond broken, the expected distribution for the atomic and molecular mechanisms are compared in columns 3 and 4 of Table I. Column 6 shows the contribution of the molecular mechanism (% M) necessary to explain the observed results. It is therefore concluded that 32% of the O_2 formed in KNO_3 arises from reactions which are not affected by O-atom scavengers, yielding the value $G_{O_2} = 0.25$, which is consistent with the value 0.30 obtained from $KNO_3 \cdot KNO_2$ and $KNO_3 \cdot KClO_4$ mixed crystals.

Possible Precursors. Several species are observed in the low-temperature esr spectra of irradiated KNO_3 which are logical precursors of O_2 and the O atom.

NO_3 is found in the esr spectrum[17] at 4°K and may be responsible for the residual O_2 yield which is unaffected by O-atom scavengers

$$NO_3 \longrightarrow NO + O_2 \qquad (V)$$

NO_3 is also an intermediate in the pyrolysis[18] of N_2O_5 and has been shown to decompose by reaction V rather than by the alternative reaction $NO_3 \rightarrow NO_2 + O$. If NO_3 is responsible for the molecular oxygen yield

(15) J. Cunningham, *J. Chem. Phys.*, **41**, 3522 (1964).

(16) M. Anbar, M. Halmann, and S. Pinchas, *J. Chem. Soc.*, 1242 (1960).

(17) J. Cunningham, *J. Phys. Chem.*, **66**, 779 (1962).

(18) M. Clyne and B. Thrush, *J. Chem. Phys.*, **38**, 1252 (1963).

$G_{O_2} = 0.30$, then (V) implies the formation of NO in equivalent amounts, $G_{NO} = 0.30$. NO has also been detected in the esr spectrum of KNO_3 at low temperatures[16] but disappears on warming, possibly by reacting with electrons trapped at a lattice site $NO + (NO_3^-)^- \rightarrow 2\,NO_2^-$. Although NO is not found in the gaseous products at room temperature, Cunningham[19] has recently found evidence for NO or some other reducing species when NO_2^- is analyzed by the reduction of ceric ion.

O atoms may be formed in the dissociation of excited nitrate ions

$$(NO_3^-)^* \longrightarrow NO_2^- + O \qquad \text{(VI)}$$

The dissociation of $(NO_3^-)^-$ has also been suggested as a source of O atoms $(NO_3^-)^- \rightarrow NO_2^{2-} + O$. However, the value $G_O = 0.45$ must be considered only as a lower limit for the primary yield of O atoms at room temperature. If NO_2^- and O atoms are formed in pairs as suggested by (VI), then the reverse of (VI), or reaction (II), may ensue even in the absence of added KNO_2 unless the O atom has been able to migrate away from its sibling NO_2^-. The difference between the O_2 yields in pure KNO_3 and in the presence of scavengers, therefore, may not be a true measure of the primary O-atom yield. The sudden increase in yields at the crystal transition temperature, 128°, is evidence of the important role mobility plays in determining the reactions in crystalline solids.

Acknowledgment. The authors are indebted to the donors of the Petroleum Research Fund, administered by the American Chemical Society, the donors of the Robert Crooks Stanley Fellowship, and to the NASA for providing a Training Grant.

(19) J. Cunningham, *J. Phys. Chem.*, **67**, 1772 (1963).

Ionic Species Formed from Benzene during Radiolysis of Its Solutions in 3-Methylpentane at 77°K[1a]

by A. Ekstrom[1b]

Department of Chemistry, University of Wisconsin, Madison, Wisconsin *(Received September 17, 1969)*

Benzene as a solute in γ-irradiated 3-methylpentane glass at 77°K captures both electrons and positive charge to form anions and cations with distinctive optical absorption spectra. At concentrations below 0.3 mol % these ions appear to be monomeric with absorption maxima at 525 nm and 320 nm, respectively, while above 1 mol % they appear to be dimeric (or polymeric) with absorption maxima at 930 and 1030 nm.

Introduction

γ Irradiation of hydrocarbon glasses produces physically trapped electrons and positive ions, which in the presence of appropriate solutes can be chemically trapped as anions and cations.[2] Well known charge scavengers include such aromatic compounds as biphenyl,[3] naphthalene,[4] and toluene,[5] but relatively little is known about the charge scavenging ability of benzene. When 2 mol % benzene in 3-methylpentane (3MP) glass is γ irradiated at 77°K, a species with an absorption maximum at 930 nm is formed. This absorption has been attributed to the benzene cation.[6] Exploratory experiments in our laboratory showed quite different absorption spectra at lower concentrations of benzene. This has led us to make a systematic investigation of the effect of benzene concentration on the optical spectra of γ-irradiated C_6H_6–3MP glasses, with and without CCl_4 present as an electron scavenger. The

(1) (a) This work has been supported in part by U. S. Atomic Energy Commission Contract AT(11-1)-1715 and by the W. F. Vilas Trust of the University of Wisconsin. (b) Chemistry Division, Australian Atomic Energy Commission, Private Mail Bag, Post Office Sutherland, Sydney, Australia.

(2) Recent reviews of such investigations include: (a) J. E. Willard, "Radiation Chemistry of Organic Solids," a chapter in "Fundamentals of Radiation Chemistry," P. Ausloos, Ed., John Wiley and Sons, New York, N. Y., 1969; (b) W. H. Hamill, "Ionic Processes in Irradiated Organic Solids," a chapter in "Radical Ions," E. T. Kaiser and L. Kevan, Ed., John Wiley and Sons, New York, N. Y., 1968; (c) D. S. Whelan, *Chem. Rev.*, **69**, 179 (1969).

(3) J. B. Gallivan and W. H. Hamill, *J. Chem. Phys.*, **44**, 1279 (1966).

(4) M. R. Ronayne, J. P. Guarino, and W. H. Hamill, *J. Amer. Chem. Soc.*, **84**, 4230 (1962).

(5) D. W. Skelly and W. H. Hamill, *J. Phys. Chem.*, **70**, 1630 (1966).

(6) J. P. Guarino and W. H. Hamill, *J. Amer. Chem. Soc.*, **86**, 777 (1964).

results are revealing as to the effect of concentration on the state of aggregation of benzene in the 3MP glass and as to its charge scavenging ability and the absorption spectra of its positive and negative ions. The results also raise the question as to whether charge scavenging studies with other aromatic molecules, in which the concentration has been varied, may have been complicated by dimerization effects.

Experimental Methods

Baker Analyzed benzene was further purified by fractional crystallization and was dried by storage over sodium. The samples were made up volumetrically. They were dried on the vacuum line with P_2O_5 and were degassed by freeze–pump–thaw cycles and by pumping on the liquid sample. The techniques of 3MP purification irradiation and spectrophotometric measurements have been described previously.[7]

Results and Discussion

Evidence for Electron Scavenging and Formation of Monomer and Dimer Anions. Figure 1 shows that solutions of 0.1 mol % and 2 mol % benzene in irradiated 3MP glass have dramatically different optical absorption spectra with maxima at 525 nm and 930 nm, respectively, the latter species apparently being identical with that previously described.[6] A study of the benzene concentration dependency of the yields of the 525- and 930-nm species shows that as the benzene concentration in the 3MP matrix is increased, the yield of the 525-nm species at first increases, passes through a plateau and then, above 0.3 mol %, decreases while the 930-nm band appears and grows (Figure 2). Samples containing more than 2 mol % C_6H_6 in 3MP in-

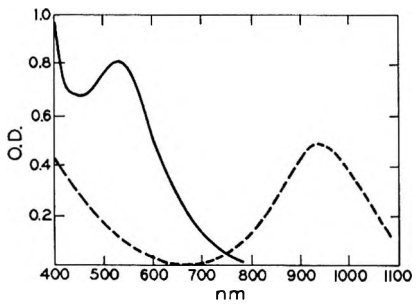

Figure 1. Effect of C_6H_6 concentration on the spectra of γ-irradiated solutions of C_6H_6 in 3MP glass: ———, 0.10 mol % benzene; – – –, 2.0 mol% benzene; dose, 2.4×10^{19} eV g^{-1} at 77°K.

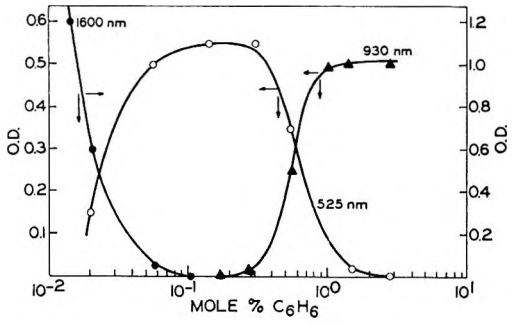

Figure 2. Effect of C_6H_6 concentration in 3MP glass on the radiolysis yields of trapped electrons (1600 nm), the 525-nm species, and the 930-nm species. Dose, 7×10^{18} eV g^{-1} at 77°K.

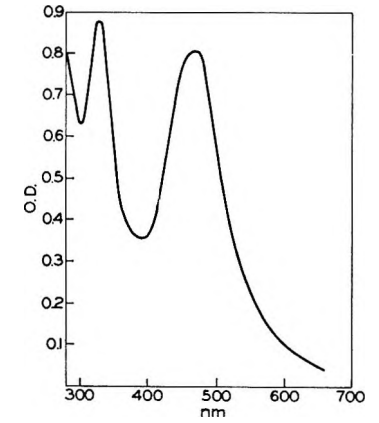

Figure 3. Spectrum of γ-irradiated solution of 2.8 mol % CCl_4 and 0.54 mol % benzene in 3MP glass. Dose, 7×10^{18} eV g^{-1} at 77°K.

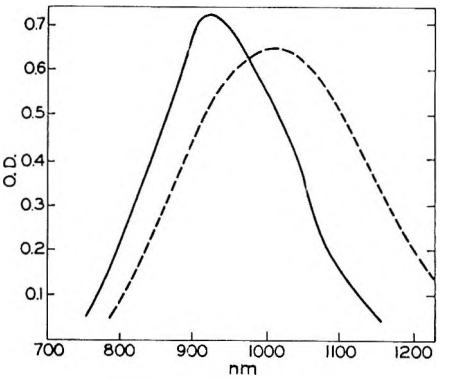

Figure 4. Effect of CCl_4 on spectrum of γ-irradiated 3MP glass containing 2.8 mol % benzene: ———, 2.8 mol % benzene, 1.5×10^{19} eV g^{-1}; – – –, 2.8 mol % benzene + 5.0 % CCl_4, 0.4×10^{19} eV g^{-1}; at 77°K (note difference in dose).

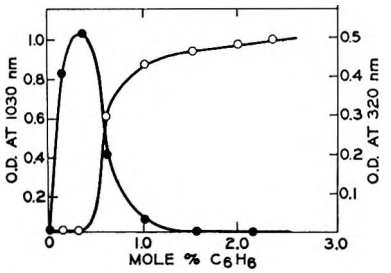

Figure 5. Effect of benzene concentration on the yield of the 320-nm and 1030-nm species in 3MP samples containing 5 mol % CCl_4. Dose, 7×10^{18} eV g ●, 320 nm; ○, 1030 nm.

(7) M. Shirom and J. E. Willard, *J. Phys. Chem.*, 72, 1702 (1968).

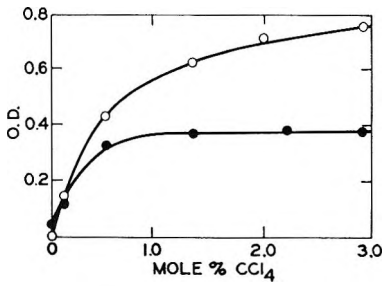

Figure 6. Effect of CCl_4 concentration on the intensity of the 320-nm and 475-nm bands of γ-irradiated solutions of 0.13 mol % C_6H_6 in 3MP glass. Dose, 1.1×10^{19} eV g $^{-1}$; 77°K; O, 475-nm band; ●, 320-nm band.

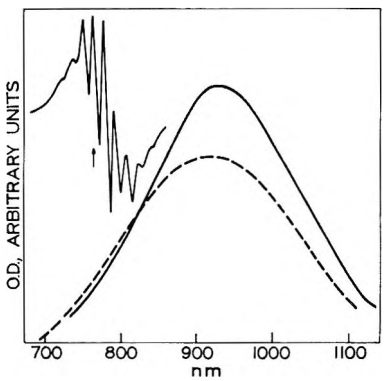

Figure 7. Comparison of the absorption spectra obtained from (a) benzene on silica gel and (b) benzene in 3MP matrix. ———, 2.8 mol % benzene, in 3MP at 77°K, 8×10^{18} eV g^{-1}; ------, 0.2 mole fraction benzene on SiO_2 at 77°K, 2.4×10^{19} eV g^{-1}; (insert, esr spectrum from silica gel sample).

variably freeze to a milky white glass, indicating the precipitation of the benzene in the 3MP during the freezing process.

The formation of the 525- and 930-nm species is accompanied by the elimination of the trapped electron, as indicated by the disappearance of its absorption at 1600 nm (Figure 2). Both the 525- and 930-nm spectra can be bleached by exposure to a tungsten light, and their formation is prevented by the presence of CCl_4 in the 3MP matrix. These properties suggest that both species are anionic. We suggest that the 525-nm absorption may be attributed to the benzene monomer anion, and the 930-nm species to a benzene dimer or polymer anion, $(C_6H_6)_2^-$ or $(C_6H_6)_n^-$.

Evidence for Formation of Monomer and Dimer Cations. The addition of CCl_4, which is an effective electron scavenger, to a sample of benzene in 3MP causes the following changes in the optical spectra relative to those in the absence of CCl_4. (a) At low concentrations of benzene, a weak peak at 320 nm is greatly enhanced, and the 525-nm peak is replaced by one with a maximum at 475 nm (Figure 3). The 475 peak is also observed in γ-irradiated samples of CCl_4 in 3MP in the absence of benzene. As evidence on the system has increased, it has been assigned in turn to CCl_4^-,[4] CCl_4^+,[6] and $CCl_4 \cdot Cl$.[8] (b) At high benzene concentrations, the 930-nm absorption spectrum is replaced by a peak with a maximum at 1030 nm (Figure 4), and the 475-nm species referred to above is also formed.

The dependence of the intensity of the 320- and 1030-nm peaks on the benzene concentration at a constant CCl_4 concentration (Figure 5) is analogous to that of the 525-nm species and the 930-nm species formed in the absence of CCl_4. Since CCl_4 is a highly efficient electron scavenger, and as such inhibits anion formation by other additives while enhancing cation formation, we attribute the 320-nm peak to the benzene monomer cation and the 1030-nm species to the benzene dimer or polymer cation. Since it has been reported[6] that irradiation of 2 mol % of C_6H_6 in 3MP glass produces an absorption with a maximum at 930 nm both in the absence and presence of CCl_4, we have examined the spectra of such systems with care and conclude that, as shown in Figure 4, the best values of λ_{max} of the peak in the presence of 5 mol % CCl_4 or higher is 1030 nm while that of the peak in the absence of CCl_4 is 930 nm.

The 475-nm peak produced in 3MP glass containing 0.13 mol % C_6H_6 continues to increase in intensity with increasing concentration of CCl_4 at concentrations much higher than required to achieve a plateau in the intensity of the 320-nm peak (Figure 6). If the assignment of the 320-nm peak to a cation is correct, this result indicates that the CCl_4 is not competing with the C_6H_6 for positive charge. If the species which originates from the CCl_4 and which is responsible for the 475-nm species is cationic,[6] the CCl_4 must be scavenging a type of positive charge (excited holes)[5,8] which cannot be scavenged by the C_6H_6.

Comparison of Spectra of Dimeric Benzene Ions Produced by Radiolysis in 3MP Glass and on Silica Gel. γ-Irradiation at 77°K of silica gel containing low concentrations of benzene produces a species having a 7-line esr spectrum with a splitting of 4.2 G.[9,10] At higher concentrations of benzene, this is replaced by a 9-line spectrum with a splitting of 2 G. These spectra have been attributed to the benzene monomer and dimer anion, respectively. We have compared the optical spectrum of an irradiated sample of a high concentration of C_6H_6 on silica gel[11] with the spectrum of irradiated 2.8 mol % C_6H_6 in 3MP at 77°K (Figure 7). The similarity of the spectra strongly suggests that the same species is produced in each system, and is thus

(8) P. W. F. Louwrier and W. H. Hamill, *J. Phys. Chem.*, **72**, 1702 (1969).

(9) O. Edlund, P. O. Kinell, A. Lund, and A. Shimizu, *J. Chem. Phys.*, **46**, 3679 (1967).

(10) T. Tanei, *Bull. Chem. Soc. Jap.*, **41**, 833 (1968).

(11) We are indebted to P. K. Wong for the samples which were prepared and examined by techniques described by P. K. Wong and J. E. Willard in *J. Phys. Chem.*, **72**, 2623 (1968).

Table I: Absorption Maxima of Biphenyl Anions and Cations Compared to Monomeric, Dimeric Benzene Anions and Cations

Biphenyl anion[a]	408 nm	650 nm
Biphenyl cation[a]	388 nm	700 nm
	Monomer	Dimer
Benzene anion	515 nm	930 nm
Benzene cation	320 nm	1030 nm

[a] See ref 3 and 12.

consistent with the conclusion that the species produced in the 3MP matrix is a dimeric benzene ion.

Comparison of Spectra from Benzene with Those from Biphenyl. Table I compares the absorption maxima of the benzene monomer and dimer anion and cation[12] with the absorption maxima of the biphenyl anion and cation. The biphenyl anion and cation each exhibit two absorption bands, one in the uv and the other in the visible and near-infrared. Comparing the uv bands, the biphenyl cation absorption at 388 nm shows a blue shift with respect to that of the anion at 408 nm, a similar shift being observed for the benzene cation and anion monomers. The biphenyl cation peak at 700 nm is red shifted with respect to the anion at 650 nm, a similar shift being observed for the benzene anion and cation dimers. This similarity raises the question as to whether the biphenyl anion and cation peaks at 650 and 700 nm may be due to biphenyl anion and cation dimers. If, in fact, monomers and dimers with different absorption spectra exist in solutions in the concentration range normally used for electron scavenging studies, serious error could be introduced into quantitative determinations of electron yields by measuring only the absorption in the monomer band while ignoring that in the dimer band or vice versa.

Acknowledgment. The author wishes to thank Professor John E. Willard for his helpful suggestions and encouragement during the course of this research.

(12) S. Arai, H. Veda, R. F. Firestone, and L. M. Dorfman, *J. Chem. Phys.*, **50**, 1072 (1969).

Charge Scavenging in the Radiolysis at 20°K of Methylcyclohexane in the Glassy and Crystalline States[1]

by A. Ekstrom and J. E. Willard

Department of Chemistry, University of Wisconsin, Madison, Wisconsin *(Received October 27, 1969)*

The γ radiolysis of polycrystalline methylcyclohexane containing CCl_4, at 20°K or 77°K, produces an intense absorption band with a maximum at 425 nm. This is not formed in glassy samples. Competition studies using positive ion scavengers indicate that the species is cationic and that the mobility of positive charge is considerably greater in the crystalline state of methylcyclohexane at 20°K than in the glassy state.

Introduction

The radiolysis of glassy hydrocarbons at 77[2] and 4°K[3] produces physically trapped electrons, readily identifiable by their esr and optical spectra. There is evidence that many electrons and positive ions migrate some distance through the matrix before being trapped and can react with charge scavengers present as solutes.[4] Electrons stabilized in glassy matrices in the absence of scavengers appear to be trapped in preexisting cavities[2c,5] by the polarization of the molecules surrounding cavities of propitious geometry. Absence of electron trapping in polycrystalline matrices of low molecular weight[2c,6] has been attributed to the absence of suitable cavities in the crystalline matrix.[5-7] Alternatively, however, the absence of observable trapping in poly-

(1) This work has been supported in part by the U. S. Atomic Energy Commission under Contract AT(11-1)-1715 and by the W. F. Vilas Trust of the University of Wisconsin.

(2) (a) D. W. Skelly and W. H. Hamill, *J. Chem. Phys.*, **44**, 2891 (1966); (b) J. Lin, K. Tsuji, and F. Williams, *J. Amer. Chem. Soc.*, **90**, 2766 (1968); (c) A. Ekstrom and J. E. Willard, *J. Phys. Chem.*, **72**, 4599 (1968).

(3) D. R. Smith and J. J. Pieroni, *Can. J. Chem.*, **45**, 2723 (1967).

(4) Recent review of such investigations include: (a) J. E. Willard, "Radiation Chemistry of Organic Solids," a chapter in "Fundamentals of Radiation Chemistry," P. Ausloos, Ed., John Wiley and Sons, 1969; (b) W. H. Hamill, "Ionic Processes in Irradiated Organic Solids," a chapter in "Radical Ions," E. T. Kaiser and L. Kevan, Ed., John Wiley and Sons, New York, N. Y., 1968.

crystalline matrices might result from a high probability of rapid electron neutralization. Such neutralization would be favored, for example, if the ability of positive charge to migrate is greater in the polycrystalline state than in the glassy state.

Investigation of charge migration with the aid of charge scavengers in polycrystalline matrices is limited by the fact that scavengers tend to precipitate out of the solvent when the solution is frozen. We have found, however, that low concentrations of biphenyl and of carbon tetrachloride can be used as scavengers in polycrystalline methylcyclohexane (MCHx). Furthermore, small samples of MCHx can be frozen to either the glassy or polycrystalline state,[8] and larger samples can be frozen to the glassy state if they contain 1 mol % or more of 3-methylpentane, or certain other additives. This paper reports investigations with polycrystalline and glassy MCHx matrices designed to obtain information on the charge trapping and the charge conduction properties of polycrystals.

Experimental Section

Reagent purification, sample preparation, and irradiation procedures were similar to those described previously.[8,9] A Cryotip unit was used to achieve temperatures of 20°K. The reaction cells and application of the Cryotip to maintaining their temperature during γ irradiation and subsequent spectrophotometric analysis have been described.[10] The cooling of samples with this equipment was inevitably slow compared to that achieved by rapid immersion in a liquid coolant. Glassy samples were water white, although cracked. Crystalline samples were opaque white. Good spectra could be obtained for both types of samples with 1–2-mm optical paths, using a high-intensity light source with a Cary 14R spectrophotometer.

Results

Absorption spectra obtained after radiolysis at 20°K of pure crystalline CCl_4, 1 mol % CCl_4 in glassy 3MP, and 2.15 mol % CCl_4 in crystalline MCHx are shown in Figure 1. The features of the spectra of the pure CCl_4[11] and CCl_4 in 3MP[10,12] have been discussed earlier. The

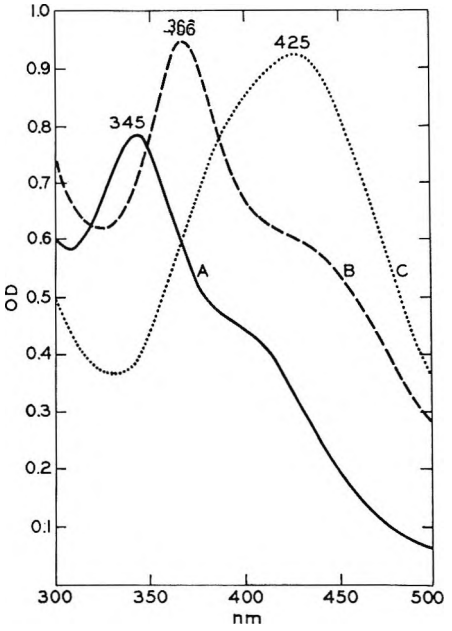

Figure 1. Absorption spectra at 20°K from: (A) polycrystalline pure CCl_4, 0.5-mm cell, 1.5×10^{18} eV g^{-1}; (B) glassy 3MP containing 1 mol % CCl_4, 1.8-mm cell, 9.9×10^{18} eV g^{-1}; (C) polycrystalline MCHx containing 1.25 mol % CCl_4, 1.8-mm cell, 3.3×10^{18} eV g^{-1}.

425-nm absorption in the crystalline MCHx matrix is unique in a number of respects. It has the following properties. (a) The band is unusually intense. The optical density is *ca.* 30 times as intense, for the same dose and path length, as the 475-nm absorption in glassy 3MP–CCl_4 samples irradiated at 77°K.[13] (b) The absorbing species does not decay significantly at temperatures below *ca.* 125°K. (c) The band is easily bleached with 425-nm light (Figure 2) revealing a weaker underlying band, which may result from the same species as observed at 366 nm in 3MP–CCl_4 glasses[10] and (Figure 3) in MCHx–CCl_4 glasses. (d) Formation of the 425-nm species is critically dependent on the crystallinity of the matrix. A sample of 2.15 mol % CCl_4 in MCHx containing 5% 3MP or 4% 2MP-1 yields a glass upon freezing to 20°K, and production of the 425 nm species is essentially eliminated (Figure 3).

Table I: Effect of Initial Carbon Tetrachloride Concentration on the 425-nm Band Formed in Crystalline MCHx Samples[a]

Initial CCl_4 concn, mol %	Od (425 nm)
0 (cryst)	0
0.07 (cryst)	0.30
0.15 (cryst)	0.90
1.0 (cryst)	0.95
5.0 (glassy)	<0.10

[a] Dose: 3.3×10^{18} eV g^{-1}, nominal 1.8-mm path length.

(5) B. G. Ershov, J. E. Makarov, and A. K. Pikaev, *High Energy Chem.*, *I*, 414 (1967).

(6) N. A. Bonin, J. Lin, K. Tsuji, and F. Williams, Advances in Chemistry Series, No. 82, American Chemical Society, Washington, D. C., 1968, Vol. II, p 269.

(7) J. Teply, *Radiat. Res. Rev.*, **I**, 361 (1969).

(8) A. C. Ling and J. E. Willard, *J. Phys. Chem.*, **73**, 2408 (1969).

(9) M. Shirom and J. E. Willard, *ibid.*, **72**, 1702 (1968).

(10) R. F. C. Claridge, R. M. Iyer, and J. E. Willard, *ibid.*, **71**, 3527 (1967).

(11) T. Shida and W. H. Hamill, *J. Chem. Phys.*, **44**, 2369 (1966).

(12) (a) D. W. Skelly and W. H. Hamill, *J. Phys. Chem.*, **70**, 1630 (1966); (b) W. F. Louwrier and W. H. Hamill, *ibid.*, **73**, 1702 (1969).

(13) J. P. Guarino and W. H. Hamill, *J. Amer. Chem. Soc.*, **86**, 777 (1964).

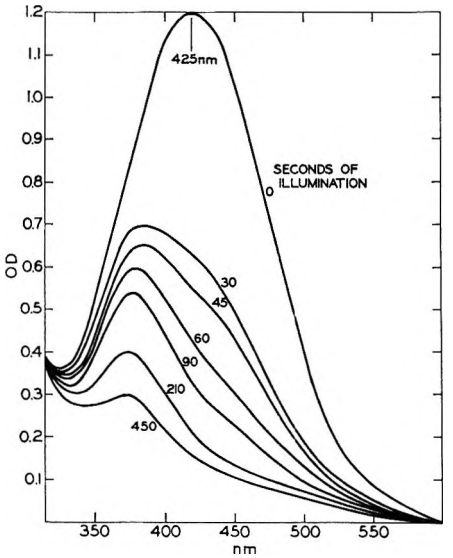

Figure 2. Effect of bleaching with 425-nm light on the absorption spectra from crystalline MCHx–CCl_4 samples, 1.8-mm cell, 4.15×10^{18} eV g^{-1}.

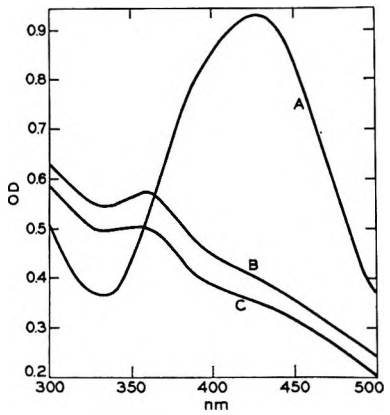

Figure 3. Absorption spectra from: (A) crystalline MCHx containing 1.25 mol % CCl_4; (B) glassy MCHx containing 1.25 mol % CCl_4 and 5 mol % 3MP; (C) glassy MCHx containing 10% CCl_4. All samples irradiated to a dose of 3.3×10^{18} eV g^{-1} in a 1.8-mm cell at 20°K.

The 680-nm band of the 2MP-1 cation[14] is not observed in such a sample. MCHx containing 10% CCl_4 yields a glassy sample, which shows only the 366-nm species upon radiolysis.

The effect of CCl_4 concentration on the intensity of the 425-nm band is shown in Table I. The band intensity appears to reach its maximum in the range of *ca.* 1% CCl_4 and then decreases nearly to zero at 5 mol %, reflecting the crystal–glass transition which occurs in this CCl_4 concentration region. This result contrasts with the 475-nm band in 3MP–CCl_4 glasses at 77°K which rises toward a plateau value of the intensity at CCl_4 concentrations above 5 mol %.[13]

With 0.4 mol % TMPD in a sample of 1.25 mol % CCl_4 in MCHx, a crystalline sample was obtained at 20°K. Irradiation of the sample yielded a spectrum

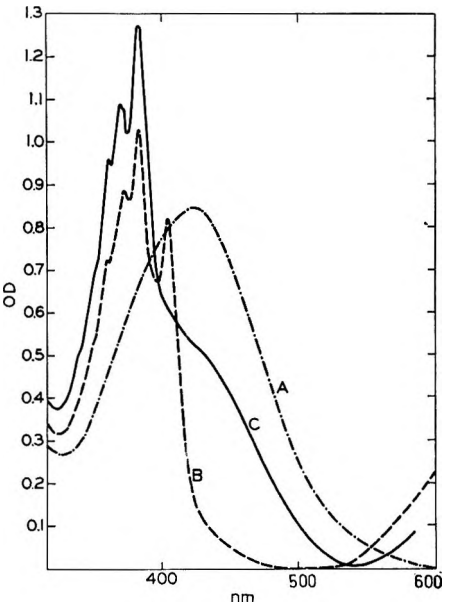

Figure 4. Absorption spectra from polycrystalline MCHx matrices containing: (A) 0.15 mol % CCl_4; (B) 0.15 mol % biphenyl; (C) 0.15 mol % CCl_4 and 0.15 mol % biphenyl. All samples irradiated to a dose of 3.3×10^{-18} eV g^{-1} at 20°K in a 1.8-mm cell.

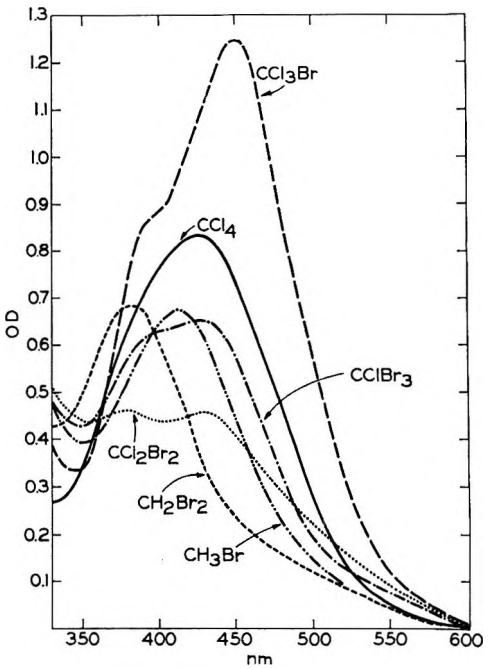

Figure 5. Spectra produced by γ radiolysis of polyhalomethanes in polycrystalline MCHx at 20°K. Concentration 0.1 mol %, 1.8-mm cell, 3.4×10^{18} eV g^{-1}.

which was that of the TMPD cation,[11] while the 425-nm species appeared to be completely eliminated.

Figure 4 allows comparison of the absorption spectra of crystalline MCHx matrices containing (a) 0.15 mol % CCl_4, (b) 0.15 mol % biphenyl, and (c) 0.15 mol %

(14) J. P. Gallivan and W. H. Hamill, *J. Chem. Phys.*, **44**, 2378 (1966).

CCl_4 and 0.15 mol % biphenyl. The absorption spectrum of the sample containing only biphenyl is characterized by a peak at 408 nm, generally associated with the biphenyl anion[14] and by a peak at 388 nm, which has been attributed to the biphenyl cation.[14] In the presence of 0.15 mol % CCl_4 the intensity of the biphenyl anion peak is greatly reduced while that of the cation peak is considerably increased. The intense band at 425 nm associated with CCl_4 in MCHx was greatly reduced by the presence of the biphenyl, suggesting either that the band is due to a cationic CCl_4 species, or that its precursor is cationic.

Spectra similar to those obtained from γ-irradiated solutions of CCl_4 in polycrystalline MCHx at 20°K are produced by other polyhalomethane solutes under the same conditions (Figure 5). The absorption maxima of the species produced by the various additives are at quite different values from those obtained by γ radiolysis of solutions of these additives in glassy 3MP at 77°K,[13] and are also different from the species produced by 254-nm photolysis of these additives in glassy 3MP.[15]

Discussion

Evidence for Greater Positive Charge Migration in Crystals than Glasses. The facts that the intense 425-nm band produced by the radiolysis of 1 mol % CCl_4 in polycrystalline MCHx at 20°K or 77°K is not produced from CCl_4 in matrices of quite similar composition which are glassy (*e.g.*, CCl_4 in glassy 3MP; glassy 5% CCl_4 in MCHx, glassy 4% 2MP-1 in MCHx), and that it is greatly reduced by as little as 1% 3MP in the CCl_4–MCHx matrix, strongly suggest that its formation requires a crystalline matrix. The fact that the peak is removed by 0.4% TMPD in polycrystalline MCHx containing 1.25 mol % CCl_4, while the $TMPD^+$ cation is formed, argues that it is due to a cationic species. This is further indicated by the fact that when the polycrystalline MCHx matrix contains biphenyl as well as CCl_4 the peak is absent, while the biphenyl cation peak is enhanced relative to that in the absence of CCl_4.

If the 425 peak is due to a cation, the fact that it achieves the maximum optical density with as little as 0.15 mol % CCl_4 (Table I) indicates that positive charge is much more readily scavenged in the polycrystalline matrix than in typical glassy matrices. The maximum scavenging effectiveness is achieved at concentrations even lower than observed for electron scavenging by good electron scavengers in 3MP and MTHF glasses.[4]

Polycrystalline hydrocarbons of low molecular weight are much less efficient in trapping electrons than glassy hydrocarbons.[2c,6] In view of the data presented above, the possibility must be considered that this difference is due to greater migration of the positive charge in the crystalline media, rather than to fewer or less favorable electron trapping sites. Presumably such migration occurs by a chain of electron hopping steps, rather than by proton transfer or hydride ion transfer, since the latter would require movement of an atomic entity in the lattice.

The fact that 0.4 mol % TMPD eliminates the 425-nm peak from CCl_4 in polycrystalline MCHx even when 1.25 mol % CCl_4 is present indicates that the probability that migrating positive charge will be immobilized on an encounter with CCl_4 is less than 10%. Since nearly maximum possible charge capture is accomplished by 0.15% CCl_4 in MCHx (Table I), and the encounters must be less than 10% efficient, it appears that the migration distances must be such as to provide 10^3 molecular encounters, or more.

Identity of the 425-nm Species. The experimental data indicate that the species responsible for the 425-nm absorption must be cationic, must be of a nature such that it can be formed by positive charge which has migrated hundreds of molecular diameters from its site of formation, and must be readily destroyed by light in its absorption band. Since the gas-phase ionization potential of CCl_4 is 1.6 eV[16] greater than that of MCHx, electron transfer from CCl_4 to ground state $MCHx^+$ ions cannot occur in the matrix unless the relative ionization potentials are much different in the solid than the gas. The energy deficiency for transfer of charge from $MCHx^+$ to CCl_4 could be overcome if transfer of electronic excitation together with positive charge (*i.e.*, transfer of "excited holes")[12a,12b] can occur. Although such transfer over hundreds of molecular diameters cannot be excluded as a possibility, it seems unlikely. We therefore suggest the hypothesis that the 425-nm species is a charge-transfer complex between a CCl_4 molecule and an $MCHx^+$ ion. Since the ionization potential of the CCl_4 exceeds that of the matrix molecules, the transfer of an electron does not occur spontaneously but may occur with the aid of energy supplied by the analyzing beam. The energy of the absorption maximum of the 425-nm band is 2.6 eV, and is thus somewhat larger than the difference in gas-phase ionization potentials between CCl_4 and MCHx. The ion CCl_4^+ is reported to be unstable.[13] It is plausible that dissociation may follow charge transfer, quite possibly accompanied by attack of Cl on the matrix to form HCl, thus precluding the reverse of the charge transfer process.

$$MCHx^+ \cdot CCl_4 \xrightarrow{h\nu} MCHx + CCl_4^+$$

$$(CCl_4^+ \rightarrow CCl_3^+ + Cl)$$

This mechanism appears to account satisfactorily for the bleaching properties of the 425-nm species.

(15) J. P. Simons and P. E. R. Tatham, *J. Chem. Soc., A*, 854 (1966).

(16) (a) W. C. Price, L. Bralsford, P. V. Harris, and R. G. Riley, *Spectrochim. Acta*, **14**, 45 (1959); (b) K. Watanabe, T. Nakayama, and J. Mottl, *J. Quant. Spectrosc. Radiat. Transfer*, **2**, 369 (1962).

Vibrational Assignments and Potential Constants for *cis*- and *trans*-1-Chloro-2-fluoroethylenes and Their Deuterated Modifications[1]

by Norman C. Craig,[2] Y.-S. Lo, Lawrence G. Piper, and John C. Wheeler

Department of Chemistry, Oberlin College, Oberlin, Ohio 44074 *(Received October 29, 1969)*

From infrared and Raman spectra a complete assignment of vibrational fundamentals has been obtained for *cis*- and *trans*-CClHCFH, CClDCFH, CClHCFD, and CClDCFD. For *cis*-CClHCFH the a' modes are 3114, 3102, 1661, 1335, 1231, 1062, 812, 656, and 205 cm^{-1}, and the a'' modes are 857, 735, and 442 cm^{-1}. For *trans*-CClHCFH the a' modes are 3103, 3094, 1647, 1296, 1218, 1127, 876, 447, and 270 cm^{-1}, and the a'' modes are 888, 784, and 270 cm^{-1}. $\Delta E_0°$ (electronic) is then found to be 867 ± 90 cal/mol with the *cis* isomer having the *lower* energy. Urey–Bradley force constants for the in-plane vibrations have been calculated by fitting the frequencies of all eight species at once. General valence force (GVF) constants for the out-of-plane modes have been calculated for the *cis* and *trans* species separately. The GVF constants for the two isomers are consistent with each other and with those obtained previously for the *cis*- and *trans*-1,2-difluoroethylenes.

The *cis* isomers of the symmetrically substituted species 1,2-difluoroethylene,[3] 1,2-dichloroethylene,[4] and 1,2-difluorodiazene, NF=NF,[5] are known to be of lower energy than the corresponding *trans* isomers. This energy difference is believed to be due to a nonbonded attractive force between the halogen atoms in the *cis* configuration. In an exploratory study Viehe also found the *cis* isomers of ethylenes containing a fluorine atom and a chlorine, bromine, or iodine atom to be more stable than the corresponding *trans* isomers.[6] As representatives of these mixed halogen systems the 1-chloro-2-fluoroethylenes appear to be the best choice for a thorough thermodynamic and spectroscopic investigation. For the *cis–trans* isomerization of the chlorofluoroethylenes we have confirmed Viehe's observation of *cis* stability and have found $\Delta H°_{615}$ = 782 ± 22 cal/mol and $\Delta S°_{615}$ = 0.21 ± 0.04 cal/mol°K.[7]

The present paper is concerned, however, principally with obtaining complete assignments of the vibrational fundamentals of *cis*- and *trans*-CClHCFH as a step toward understanding *cis* stability in this system. From infrared spectra alone Viehe and coworkers assigned ten of the twelve fundamentals of the *cis* isomer and eight of the fundamentals of the *trans*.[8] With the aid of Raman spectra we have completed the assignments of the vibrational fundamentals for these two species and have also obtained assignments for the three deuterated modifications of each isomer. The frequencies of the deuterated species are of interest not only as support for the assignments of the undeuterated molecules but as a basis for exploring the force fields in *cis* stable isomer pairs. The present paper includes preliminary results of such normal coordinate calculations.

Experimental Section

Syntheses. A mixture of *cis*-CClHCFH (bp 15.2°)[6] and *trans*-CClHCFH (bp −3.8°)[6] was prepared in 70% yield by dehalogenating $CCl_2HCClFH$[9] with zinc dust in refluxing ethanol. The product, which was continuously distilled out of the reaction mixture and trapped at Dry Ice temperature, was about two-thirds *cis* isomer.

cis- and *trans*-CClDCFH were obtained by dehalogenating CClBrDCClFH. This ethane mixed with its isomer CCFBrCClHD was prepared by irradiating equimolar gaseous mixtures of hydrogen bromide and CClFCClD[10] in a fused-silica flask with ultraviolet light from a mercury arc. The product of the dehalogenation consisted of about 2 parts of *cis*- and *trans*-

(1) Presented, in part, at the 22nd Symposium on Molecular Structure and Spectroscopy, Columbus, Ohio, Sept 1967.

(2) Author to whom inquiries should be addressed.

(3) (a) N. C. Craig and E. A. Entemann, *J. Amer. Chem. Soc.*, **83**, 3047 (1961); (b) N. C. Craig and J. Overend, *J. Chem. Phys.*, **51**, 1127 (1969).

(4) (a) K. S. Pitzer and L. J. Hollenberg, *J. Amer. Chem. Soc.*, **76**, 1493 (1954); (b) R. E. Wood and R. G. Dickinson, *ibid.*, **61**, 3259 (1939).

(5) G. T. Armstrong and S. Marantz, *J. Chem. Phys.*, **38**, 169 (1963).

(6) H. G. Viehe, *Ber. Deut. Chem. Ges.*, **93**, 1697 (1960).

(7) To be published. Temperatures in °K.

(8) H. G. Viehe, J. Dale, and E. Franchimont, *Ber. Deut. Chem. Ges.*, **97**, 244 (1964).

(9) N. C. Craig and Y.-S. Lo, *J. Mol. Spectrosc.*, **23**, 307 (1967).

(10) N. C. Craig, G. Y.-S. Lo, C. D. Needham, and J. Overend. *J. Amer. Chem. Soc.*, **86**, 3232 (1964).

CClDCFH and about 1 part of CClFCHD. Small amounts of *cis*- and *trans*-CFClCFH were also found in the product mixture and were believed to have been derived from CClFCClF, present as a contaminant in the starting ethylene.

cis- and *trans*-CClHCFD were prepared by dehalogenating $CCl_2HCFBrD$. This ethane was made photochemically from gaseous hydrogen bromide and CCl_2-CFD.[9]

cis- and *trans*-CClDCFD were synthesized by re-

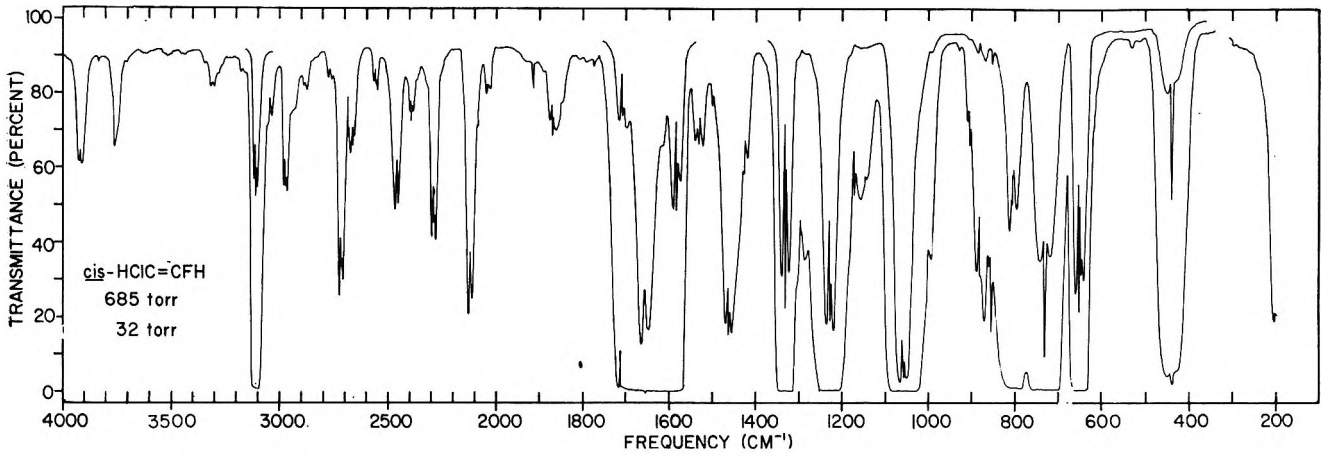

Figure 1. Gas-phase infrared spectrum of *cis*-1-chloro-2-fluoroethylene.

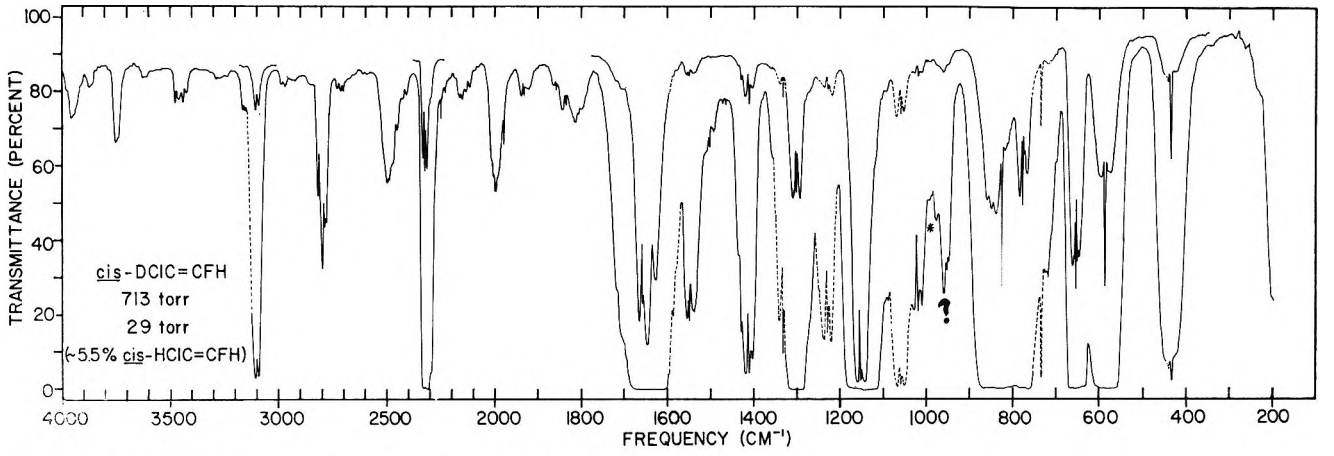

Figure 2. Gas-phase infrared spectrum of *cis*-1-chloro-2-fluoroethylene-1-d_1.

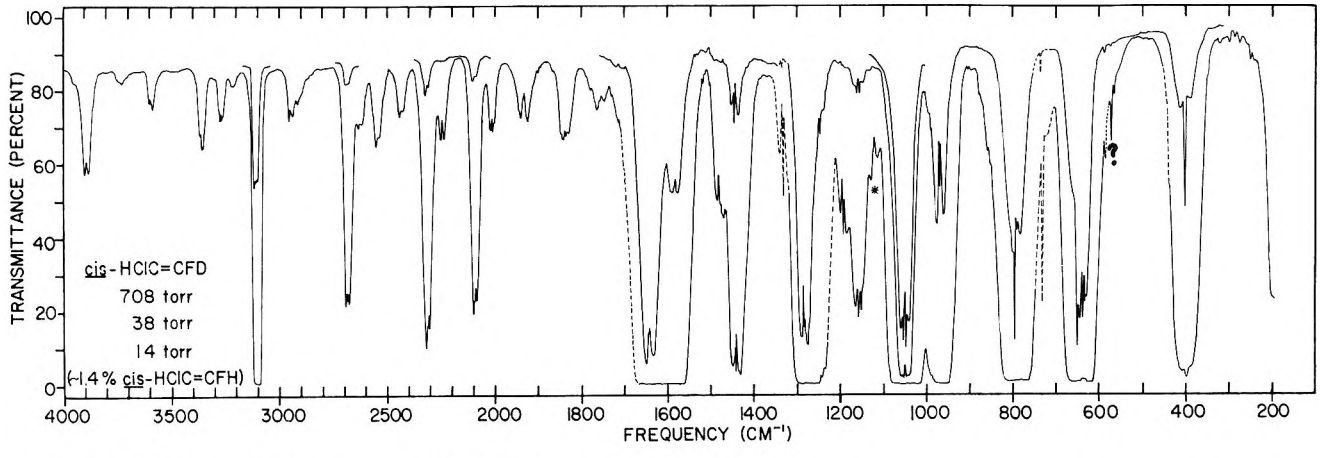

Figure 3. Gas-phase infrared spectrum of *cis*-1-chloro-2-fluoroethylene-2-d_1.

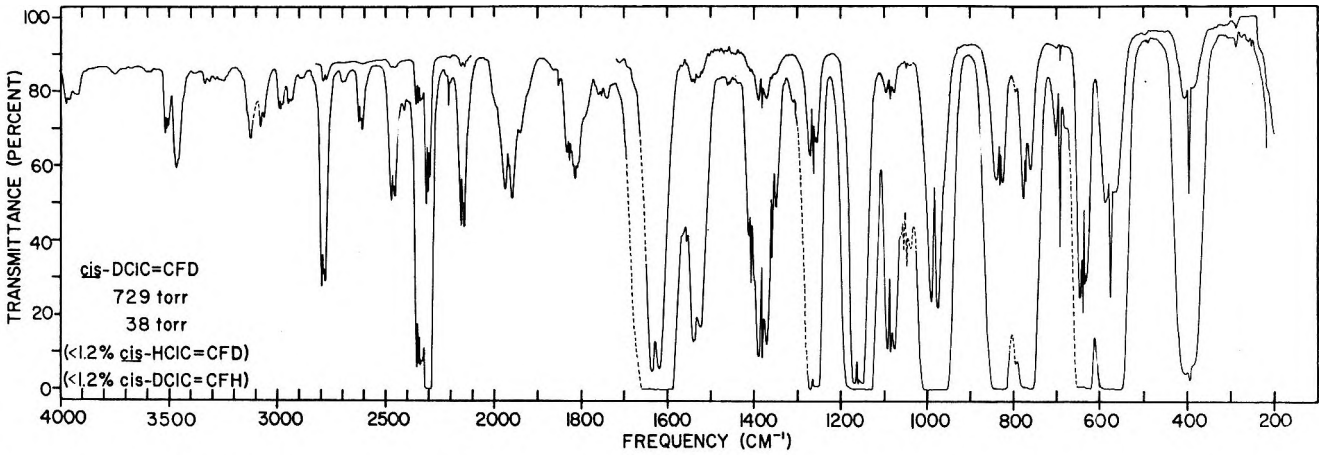

Figure 4. Gas-phase infrared spectrum of *cis*-1-chloro-2-fluoroethylene-1,2-d_2.

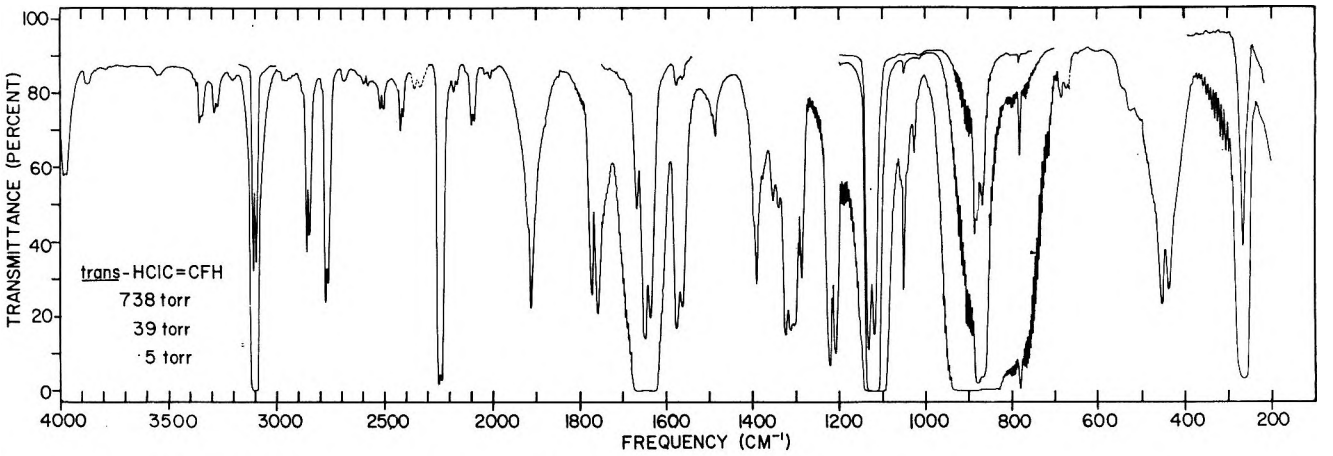

Figure 5. Gas-phase infrared spectrum of *trans*-1-chloro-2-fluoroethylene.

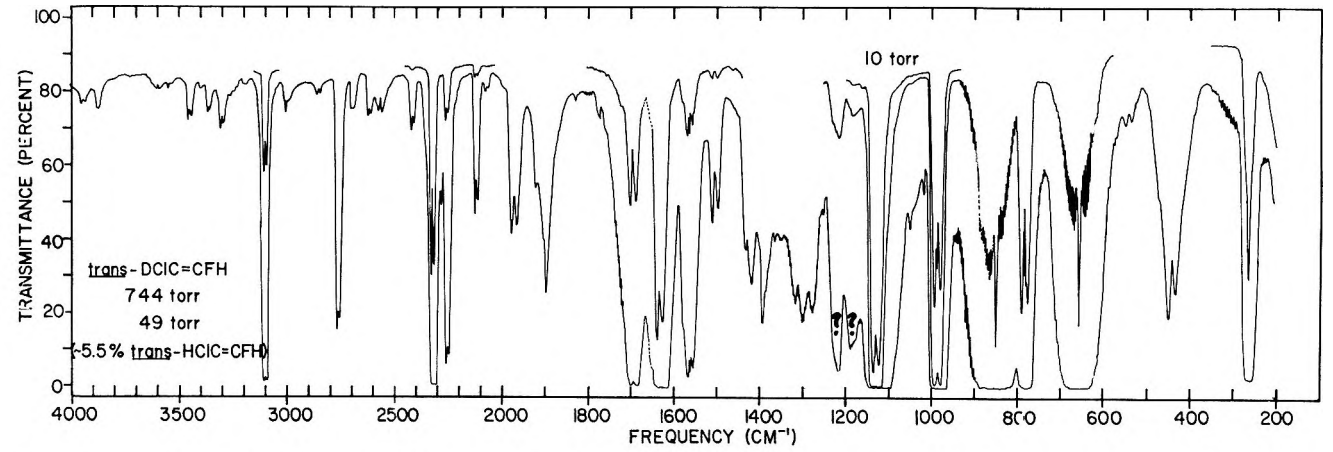

Figure 6. Gas-phase infrared spectrum of *trans*-1-chloro-2-fluoroethylene-1-d_1.

peated exchange of a *cis–trans* mixture of CClHCFH with 99.7% deuterium oxide saturated with dried calcium oxide. These reactions were performed in sealed standard-wall Pyrex tubes pressurized externally to 225 psi in a rocking bomb. The temperature was about 125° and exchanges were run about 1 day.[11]

In each case purified samples of the isomers were obtained by gas chromatographic fractionation at room temperature on 6-ft or 12-ft columns packed with

(11) The exchange reaction was stereospecific and proceeded much more rapidly on the chlorinated end of the molecule, a temperature of about 90° being sufficient to effect exchange in 1 day in this case.

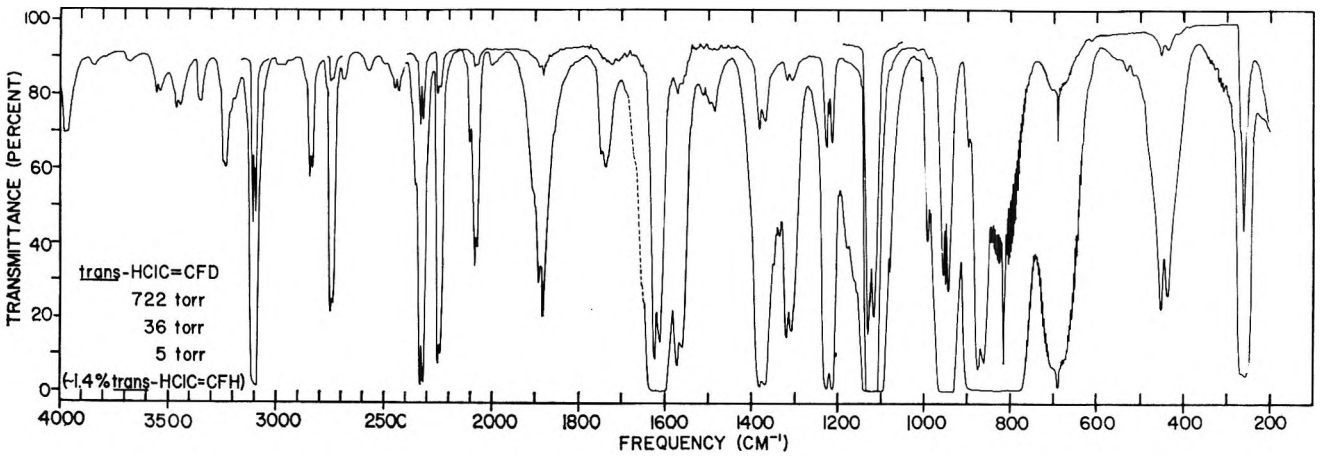

Figure 7. Gas-phase infrared spectrum of *trans*-1-chloro-2-fluoroethylene-2-d_1.

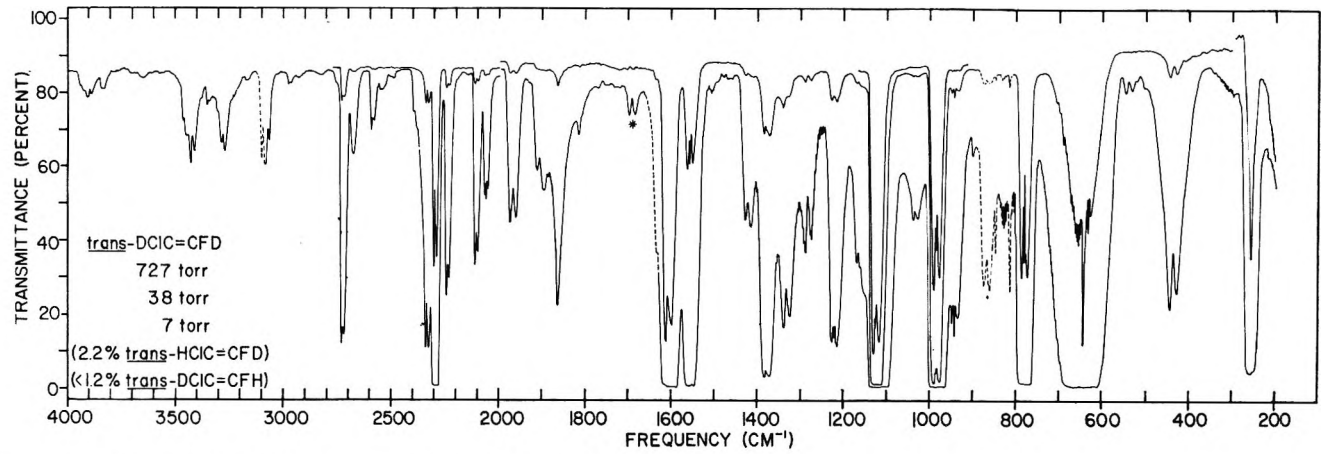

Figure 8. Gas-phase infrared spectrum of *trans*-1-chloro-2-fluoroethylene-1,2-d_2.

dibutyl phthalate on firebrick. These samples were dried by passing them over phosphorus pentoxide. An attempt to remove impurity carbon dioxide with Ascarite led to a small amount of exchange at the chlorinated end of *trans*-CClDCFD. Thereafter, Ascarite treatment was confined to the undeuturated species. In all cases final purities were greater than 99.5% based on gas chromatographic analysis. In the infrared spectra (Figures 1–8) of *cis*- and *trans*-CClDCFH unidentified weak bands were taken as evidence of somewhat lower purity. Isotopic purities given in Figures 2–4 and 6–8 were estimated from infrared intensities. In these figures bands due to isotopic impurities are shown with dashed lines. Other known impurity bands are marked with asterisks.

Spectroscopy. Gas-phase infrared spectra, Figures 1–8, were obtained on a Perkin-Elmer 621 filter-grating spectrometer with samples held in a 10-cm cell fitted with cesium iodide windows. Frequencies, Tables I–VIII, were measured to ± 1 cm^{-1} for well defined bands under expanded-scale, high-resolution conditions.

Liquid-phase Raman spectra, Tables I–VIII, were recorded photographically on a Hilger E612 spectrograph with mercury 4358-Å excitation. Capillary cells were used, and some samples were as small as 8 mmol. Qualitative depolarizations were obtained by the Edsall–Wilson method.

Results and Discussion

Configurational Assignments. Viehe[6] assigned the isomeric configurations of the 1-chloro-2-fluoroethylenes on the basis of a higher boiling point for the more polar *cis* isomer and the strong infrared band for the out-of-plane CH motion of the *trans* isomer at about 880 cm^{-1}. This assignment of configuration is confirmed, as Viehe also noted for his low resolution spectra, by the abundant rotational structure evident in the gas-phase infrared spectra (see Figures 5–8) of the four *trans* species. The assignment is also consistent with the observed coupling constants from the nuclear magnetic spectra of the *cis* and *trans* isomers. We find $J_{HF(trans)}$ = 27.3 Hz for the *cis* isomer (AMX spectrum) and $J_{HF(cis)}$ = 8.9 Hz for the *trans* isomer (ABX spectrum) in consonance with the relative magnitudes of HF coupling constants for similar olefins.[10,12]

(12) G. W. Flynn, M. Matsushima, J. D. Baldeschwieler, and N. C. Craig, *J. Chem. Phys.*, **38**, 2295 (1963).

Vibrational Assignments. General. All of the chlorofluoroethylene molecules under consideration have C_s symmetry and consequently have nine a′ in-plane and three a″ out-of-plane fundamentals. The a′ fundamentals should have gas-phase infrared band shapes ranging between type A and type B and have polarized Raman bands. The a″ fundamentals should have type C band shapes in the gas-phase infrared and depolarized Raman bands. The *trans* isomer is a prolate near-symmetric top, $\kappa = -0.996$, with a moment of inertia of 9 amu Å^2 around the unique axis. As a consequence, vibrations which produce dipole

Table I: Infrared and Raman Spectra and Assignments for *cis*-CClH=CFH

Raman (liquid)			Ir (gas)			Assignment		
Freq, cm^{-1}	I	Polarization	Freq, cm^{-1} [a]	α[b]	Band shape[c]	Freq, cm^{-1}		Sym species
			3919 (16)	0.018	B	3926	$\nu_1 + \nu_7$	A′
			3755 (16)	0.015	A/B	3770	$\nu_1 + \nu_8$	A′
			3114 (15)	0.52	A	ν_1	Fund.	a′
			3115[d]					
3105	wm	p	3102	?	?	ν_2	Fund.	a′
			2977 (16)	0.017	A/B	2996	$\nu_3 + \nu_4$	A′
			2717 (15)	0.056	A/B	2733	$\nu_3 + \nu_6$	A′
			2663 (16)	0.016	A/B	2670	$2\nu_4$	A′
			2462 (16)	0.029	B	2473	$\nu_3 + \nu_7$	A′
						2462	$2\nu_5$	A′
			2287 (16)	0.039	A/B	2317	$\nu_3 + \nu_8$	A′
			2119 (16)	0.067	B	2124	$2\nu_6$	A′
			1872 (15)	0.012	A	1874	$\nu_6 + \nu_7$	A′
			1714 (17)	0.29	A/B	1718	$\nu_6 + \nu_8$	A′
						1714	$2\nu_{10}$	A′
						Fermi resonance with ν_3?		
1660	s	p	1661 (17)	1.9	B	ν_3	Fund.	a′
			1664[d]					
			1588 (16)	0.60	A	1624	$2\nu_7$	A′
						Fermi resonance with ν_3?		
						1592	$\nu_{10} + \nu_{11}$	A′
			1534 (15)	0.014	A	1540	$\nu_4 + \nu_9$	A′
			1466 (16)[e]	0.092	A	1470	$2\nu_{11}$	A′
						1468	$\nu_2 + \nu_8$	A′
			1459	?	?	~1456	$\nu_3 - \nu_9$	A′
			1430	0.02	A/B	1436	$\nu_5 + \nu_9$	A′
			1335 (16)	1.1	A	ν_4	Fund.	a′
			1339[d]					
			1298	0.044	A/B	1312	$2\nu_8$	A′
						1299	$\nu_{10} + \nu_{12}$	A′
1214	m	dp	1231 (16)	1.8	A	ν_5	Fund.	a′
			1232[d]					
			1176 (15)	0.03	A/B	1177	$\nu_{11} + \nu_{12}$	A′
1049	m	p	1062 (16)[e]	3.6	A/B	ν_6	Fund.	a′
			1063[d]					
			1008	0.05	A/B	1017	$\nu_7 + \nu_9$	A′
			908	0.01	A	?		A′
			884 (17)	0.05	A/B	884	$2\nu_{12}$	A′
~863	wm	dp	857	0.05	C	ν_{10}	Fund.	a″
			~875[d]					
803	m	p	812 (16)[e]	0.71	B	ν_7	Fund.	a′
			809[d]					
~737	vw		735[e,f]	1.0	C	ν_{11}	Fund.	a″
			735[d]					
648	m	p	656 (17)[e]	1.3	A	ν_8	Fund.	a′
			657[d]					
444	m	dp	442	0.18	C	ν_{12}	Fund.	a″
			443[d]					
205	w	dp	~200	0.08	A/B	ν_9	Fund.	a′

[a] Spacing of P–R branches in parentheses. [b] Absorption coefficient in cm^{-1} atm^{-1}. [c] A and B band shapes are approximate for this molecule of C_s symmetry. [d] Reference 8. [e] Structure present due to chlorine isotope shifts or hot bands. [f] Rotational structure in P and R branches with spacing of 0.8–0.9 cm^{-1}.

moment changes perpendicular to this rotation axis should lead to nearly perpendicular-type bands with readily resolved rotational structure. The out-of-plane modes necessarily have this structure since the unique axis lies in the plane of the molecule. Rotational structure may also be evident for some in-plane modes in the wings of bands when the vibration has a large component of dipole moment change perpendicular to the unique axis, which passes nearly through the two halogen atoms. The *cis* isomer is a less good approximation to a prolate symmetric top since $\kappa = -0.895$. The least moment of inertia of about 31 amu Å^2 is,

Table II: Infrared and Raman Spectra and Assignments for *cis*-CClD=CFH

Raman (liquid)			Ir (gas)			Assignment		
Freq, cm^{-1}	I	Polarization	Freq, cm^{-1} [a]	α[b]	Band shape[c]	Freq, cm^{-1}		Sym species
			3751(18)	0.013	A/B	3753	$\nu_1 + \nu_8$	A′
			3114	?			*cis*-CClHCFH impurity	
3103	m	p	3098 (17)	0.16	B	ν_1	Fund.	a′
			2807 (15)	0.025	B	2807	$\nu_5 + 2\nu_{10}$	A′
			2786 (16)	0.032	A/B	2792	$\nu_3 + \nu_6$	A′
			2486	0.02	A/B	2524	$\nu_2 + \nu_9$	A′
						2488	$\nu_3 + \nu_5$	A′
			2457	0.01	B	2459	$\nu_4 + \nu_6$	A′
2327	s	p	2322 (17)	0.44	A	ν_2	Fund.	a′
			2250		C	2240	$2\nu_{10} + \nu_{11}$	A″
			2220		C	2225	$\nu_3 + \nu_{11}$	A″
			2000	0.02	?	2006	$\nu_5 + \nu_6$	A′
			1980	0.01	C	1981	$\nu_5 + \nu_{10}$	A″
1663	w	p	1659 (17)[e]	1.8	A/B	1652	$2\nu_{10}$	A′
						Fermi resonance with ν_3		
1642	vs	p	1637 (19)	1.2	B	ν_3	Fund.	a′
			1588				*cis*-CClHCFH impurity	
			1552 (16)	0.067	A/B	1556	$2\nu_7$	A′
			1434[e]	0.05	C	1439	$\nu_6 + \nu_{11}$	A″
			1414 (16)	0.13	A	1414	$\nu_{10} + \nu_{11}$	A′
			1353		C	1366	$\nu_7 + \nu_{11}$	A″
			1335 (16)	1.3	A		*cis*-CClHCFH impurity	
1298	sm	p	1304 (17)[e]	0.62	A	ν_4	Fund.	a′
			1231 (16)	1.6	A		*cis*-CClHCFH impurity	
1135	w	p	1155 (16)	~5	A/B	ν_5	Fund.	a′
~1050	vw		1062 (17)	3.9	A		*cis*-CClHCFH impurity	
			1021 (18)[e]	0.066	A	1022	$\nu_{11} + \nu_{12}$	A′
			989		A/B	989	*trans*-CClD=CFH impurity	
			955		A/B		Impurity?	
~870	w	p				868	$2\nu_{12}$	A′
848	s	p	851 (18)	0.64	A/B	ν_6	Fund.	a′
830	w	dp	826[d]	0.38	C	ν_{10}	Fund.	a″
~800	vw					803	*cis*-CClHCFH impurity	
772	s	p	778 (16)[e]	0.56	A	ν_7	Fund.	a′
			735		C		*cis*-CClHCFH impurity	
649	s	p	655 (16)[e]	1.1	A/B	ν_8	Fund.	a′
592	vw	dp?	588[e]	0.54	C	ν_{11}	Fund.	a″
			442		C	442	*cis*-CClHCFH impurity	
434	s	dp	434	0.15	C	ν_{12}	Fund.	a″
202	s	p?	~200	0.07	?	ν_9	Fund.	a′

[a–c] See Table I. [d] Rotational structure in P and R branches with 0.8 cm^{-1} spacing. [e] See Table I.

however, small enough to lead to rotational structure which can be resolved in favorable regions of the spectrum.

cis-1-Chloro-2-fluoroethylene. In the infrared spectrum of *cis*-CClHCFH in Figure 1 seven prominent type A/B bands for in-plane fundamentals are located at 3114, 1661, 1335, 1231, 1062, 812, and 656 cm^{-1}. Each of these bands with the exception of the 3114-cm^{-1} band has a counterpart in the Raman spectrum (Table I). All but the 1231-cm^{-1} band are definitely polarized. Well defined type C bands in the infrared spectrum at 735 and 442 cm^{-1} account for two of the out-of-plane fundamentals. The Raman spectrum has a very weak band corresponding to the higher frequency out-of-plane fundamental and a depolarized band of medium intensity corresponding to the lower frequency one. Though not apparent in the survey scan in Figure 1, rotational spacing of about 0.8 cm^{-1} was resolved in the 735-cm^{-1} band. Only the spike of the Q branch of the third out-of-plane fundamental (ν_{10}) appears at 857 cm^{-1} in the infrared, but this assignment is well supported by a depolarized Raman band. The low infrared intensity of ν_{10} is attributable to a CH torsion with a_2-like symmetry. The shoulder of a band seen at the low-frequency edge of the infrared spectrum must be due to an in-plane fundamental even though

Table III: Infrared and Raman Spectra and Assignments for *cis*-CClH=CFD

Raman (liquid)			Ir (gas)			Assignment		
Freq, cm^{-1}	I	Polarization	Freq, cm^{-1} [a]	α [b]	Band shape [c]	Freq, cm^{-1}		Sym species
			3899 (18)	0.018	B	3903	$\nu_1 + \nu_7$	A′
			3365 (16)	0.014	A/B	3369	$\nu_2 + \nu_5$	A′
						3287	$\nu_2 + \nu_6$	A′
3110	wm	p	3112 (15)	0.40	A/B	ν_1	Fund.	a′
			2691 (15)	0.064	A/B	2695	$\nu_3 + \nu_5$	A′
			2549 (15)	0.013	B	2566	$2\nu_4$	A′
2325	s	p	2318 (16)	0.091	A/B	ν_2	Fund.	a′
			2249 (16)	0.014	B	2252	$\nu_4 + \nu_6$	A′
			2100 (15)	0.067	A/B	2102	$2\nu_5$	A′
			2022 (16)	0.012	B	2020	$\nu_5 + \nu_6$	A′
			1934 (15)	0.010	B	1938	$2\nu_6$	A′
			1840 (17)	0.013	A/B	1842	$\nu_6 + \nu_7$	A′
1641	vs	p	1644 (16)	2.7	B	ν_3	Fund.	a′
			1584 (14)	0.48	B	1606	$\nu_3 + \nu_8$	A′
						Fermi resonance with ν_8		
						1592	$2\nu_{10}$	A′
			1482 (16)	0.027	B	1488	$\nu_4 + \nu_9$	A′
			1446 (17)	0.16	A	1446	$\nu_{10} + \nu_{11}$	A′
			1335	1.2	A		*cis*-CClHCFH impurity	
1268	vw	dp	1283 (15) [e]	2.3	B	ν_4	Fund.	a′
			1245		C?	~1244	$\nu_3 - \nu_{12}$	A″
			1196 (15)	0.030	A	1196	$\nu_{11} + \nu_{12}$	A′
			1162 (16)	0.066	A/B	1174	$\nu_6 + \nu_9$	A′
			1127 (15)	0.016	A/B		*trans*-CClHCFD impurity	
1038	sm	p	1051 (17)	4.1	B	ν_5	Fund.	a′
			990		A?	996	$\nu_7 + \nu_9$	A′
965	m	p?	969 (16) [d,e]	0.80	A	ν_6	Fund.	a′
804	w	dp?	796 [d]	~0.6	C	ν_{10}	Fund.	a″
789	s	p	791 (16)	0.72	A	ν_7	Fund.	a′
			735	1.3	C		*cis*-CClHCFH impurity	
652	wm	dp	650 [d]	~0.5	C	ν_{11}	Fund.	a″
632	s	p	637 [e]	1.2	A	ν_8	Fund.	a′
			588		C		*cis*-CClDCFH impurity	
			575 [e]		C		*cis*-CClDCFD impurity	
			567		C	~569	$\nu_6 - \nu_{12}$?	A″
404	m	dp	400	0.20	C	ν_{12}	Fund.	a″
205	sm	p?	200	~0.07	?	ν_9	Fund.	a′

[a–c] See Table I. [d] Rotational structure in P and/or R branches with 0.85–0.95 cm^{-1} spacing. [e] See Table I.

its Raman counterpart is depolarized. Only the second CH-stretching mode remains to be assigned. It appears an an indistinct shoulder on the low-frequency side of the 3114-cm^{-1} infrared band and as a polarized Raman band at 3105 cm^{-1}. Table I also includes the ten assignments of Viehe, *et al.*[8] Agreement is within a few cm^{-1} for all but ν_{10}.

cis-1-Chloro-2-fluoroethylene-1-d_1. Bands for all twelve fundamentals of *cis*-CClDCFH are clearly apparent in the gas-phase infrared in Figure 2. Each of the nine with a type A/B shape corresponds to a polarized Raman band (Table II), and each of the three with a type C shape corresponds to a depolarized Raman band. Although ν_6 and ν_{10} overlap in the gas-phase infrared, the characteristic shapes are evident, and 0.8 cm^{-1} rotational spacing is present in the P branch of the ν_{10} band.

cis-1-Chloro-2-fluoroethylene-2-d_1. At first glance the gas-phase infrared spectrum of *cis*-CClHCFD in Figure 3 appears to have only eight type A/B bands, even if the shoulder at about 200 cm^{-1} is included, and only two type C bands. Closer inspection reveals overlap between bands for in-plane and out-of-plane fundamentals at both 800 and 650 cm^{-1}. This interpretation is confirmed by the Raman spectrum (Table III) in which a pair of polarized and depolarized bands is present in each of these regions. The assignment of bands due to out-of-plane fundamentals to these two regions is also supported by the 0.9 cm^{-1} rotational spacing in R branches of the type C parts of the bands.

Table IV: Infrared and Raman Spectra and Assignments of *cis*-CClD=CFD

Raman (liquid)			Ir (gas)			Assignment		
Freq, cm^{-1}	I	Polarization	Freq, cm^{-1} [a]	α[b]	Band shape[c]	Freq, cm^{-1}		Sym species
			3505 (15)	0.010	A	3504	$\nu_1 + \nu_4$	A′
			3460	0.017	?	3459	$\nu_2 + \nu_4$	A′
			3120	0.011	?	3128	$\nu_2 + \nu_6$	A′
			2782 (15)	0.050	B	2791	$\nu_3 + \nu_6$	A′
			2459 (16)	0.023	B	2460	$\nu_3 + \nu_6$	A′
2342	s	p	2342 (17)	0.13	A	ν_1	Fund.	a′
2305	m	dp	2297 (16)	0.44	A	ν_2	Fund.	a′
			2138 (16)	0.031	B	2146	$\nu_4 + \nu_6$	A′
			1964 (17)	0.023	B	1993	$\nu_4 + \nu_6$	A′
			1825 (15)	0.016	A	1832	$\nu_3 + \nu_9$	A′
			1810	?	?	1815	$\nu_5 + \nu_6$	A′
1624	vs	p	1629 (16)	2.9	B	ν_3	Fund.	a′
			1537 (16)	0.079	B	1540	$2\nu_7$	A′
			1406	0.034	C	1406	$\nu_6 + \nu_{11}$	A″
			1381 (17)	0.095	A	1408	$\nu_7 + \nu_8$	A′
						1382	$2\nu_{10}$	A′
			1356	0.037	C	1378	$\nu_5 + \nu_{12}$	A″
						1345	$\nu_2 + \nu_{11}$	A″
			1303	?	?		*cis*-CClDCFH impurity	
			1263 (15)[e]	0.28	A	1276	$2\nu_8$	A′
						1266	$\nu_{10} + \nu_{11}$	A′
						1187	$\nu_5 + \nu_9$	A′
						Fermi resonance with ν_4		
1142	vw	p	1162 (17)	5.2	A	ν_4	Fund.	a′
			1085 (16)	0.095	A	1085	$\nu_{10} + \nu_{12}$	A′
			1051	~3.3	A/B		*cis*-CClHCFD impurity	
977	m	p	984 (15)[d]	1.2	B	ν_5	Fund.	a′
830	s	p	831 (16)[e,f]	0.42	A	ν_6	Fund.	a′
			745[e]		C?		*cis*-CClHCFD impurity?	
764	s	p	770 (16)	0.42	A	ν_7	Fund.	a′
690	s	dp	691[f]	0.012	C	ν_{10}	Fund.	a″
632	s	p	638 (15)[e]	1.1	A	ν_8	Fund.	a′
578	vw	p?	575[e]	0.52	C	ν_{11}	Fund.	a″
395	m	dp	394	0.16	C	ν_{12}	Fund.	a″
203	s	p	<200	?	?	ν_9	Fund.	a′

[a–c] See Table I. [d] Rotational spacing of 0.71 cm^{-1} in R branch; poorly resolved structure in *P*. [e] See Table I. [f] Poorly resolved rotational structure.

Of the nine bands assigned to in-plane modes only the one at 1283 cm^{-1} corresponds to a depolarized Raman band, but there can be no doubt about this assignment.

cis-1-Chloro-2-fluoroethylene-1,2-d_2. In contrast to the spectra of the other three *cis* species, the infrared spectrum of *cis*-CClDCFD does not have any overlapping bands due to fundamentals. In Figure 4 eight prominent type A/B bands and a wing of a band

Table V: Infrared and Raman Spectra and Assignments for *trans*-CClH=CFH

Raman (liquid)			Ir (gas)			Assignment		
Freq, cm^{-1}	I	Polarization	Freq, cm^{-1} [a]	α [b]	Band shape [c]	Freq, cm^{-1}		Sym species
			3977 (13)	0.02	B	3979	$\nu_1 + \nu_7$	A′
			3350	0.008	B	3364	$\nu_2 + \nu_9$	A′
							$\nu_2 + \nu_{12}$	A″
			3103 (12) [f]	0.82	A/B	ν_1	Fund.	a′
			3115 [d]					
3094	m	p				ν_2	Fund.	a′
			2854 (12)	0.035	B	2865	$\nu_3 + \nu_5$	A′
			2769 (11)	0.044	A/B	2774	$\nu_3 + \nu_6$	A′
			2247 (12)	0.20	A/B	2254	$2\nu_6$	A′
			2090	0.01	B	2094	$\nu_3 + \nu_8$	A′
							$\nu_5 + \nu_7$	A′
			1914 [f]	0.062	~C	1917	$\nu_5 + \nu_9$	A′
							$\nu_3 + \nu_{12}$	A″
			1768 (13) [f]	0.060	B	1776	$2\nu_{10}$	A′
						1764	$\nu_7 + \nu_{10}$	A″
			1666 (14)	0.51	B	1672	$\nu_{10} + \nu_{11}$	A′
						1665	$\nu_5 + \nu_8$	A′
						Fermi resonance with ν_3		
1643	s	p	1647 (12)	1.5	B	ν_3	Fund.	a′
			1647 [d]					
			1572 (14)	0.061	B	1574	$\nu_6 + \nu_8$	A′
						Fermi resonance with ν_3		
						1568	$2\nu_{11}$	A′
			1489	0.011	~C	1488	$\nu_6 + \nu_9$	A′
							$\nu_5 + \nu_{12}$	A″
			1395	0.051	~C	1397	$\nu_3 + \nu_9$	A′
							$\nu_6 + \nu_{12}$	A″
			1375	0.02	C	1377	$\nu_3 - \nu_9$	A′
							$\nu_3 - \nu_{12}$	A″
			1349 (14)	0.025	B		?	
			1321 (11)	0.079	B	1323	$\nu_7 + \nu_8$	A′
			1317 [d]					
1294	s	p	1296 (15)	0.047	A/B	ν_4	Fund.	a′
1218	m	p	1218 (13) [f]	0.11	B	ν_5	Fund.	a′
			1217 [d]					
1112	m	p	1127 (13)	12	A/B	ν_6	Fund.	a′
			1127 [d]					
			1054 [e]	0.052	~C	1054	$\nu_9 + \nu_{11}$	A′
							$\nu_{11} + \nu_{12}$	A″
			1028 [e]	0.014	~C	1026	$\nu_4 - \nu_8$	A′
							$\nu_4 - \nu_{12}$	A″
~896	vw	dp?	888 [f]	1.3	C	ν_{10}	Fund.	a″
			~885 [d]					
871	m	p	876 (13)	2.8	A/B	ν_7	Fund.	a′
			875 [d]					
785	m	dp	784 [f]	0.12	C	ν_{11}	Fund.	a″
			784 [d]					
			678 (13)	0.005	B	679	$\nu_6 - \nu_8$	A′
			525	0.007	?	540	$2\nu_9$	A′
							$\nu_9 + \nu_{12}$	A″
							$2\nu_{12}$	A′
447	s	p	447 (15)	0.060	B	ν_8	Fund.	a′
274	m	dp	270 [g]	0.82	~C	ν_9	Fund.	a′
						ν_{12}	Fund.	a″

[a–e] See Table I. [f] Rotational structure with spacing of 3.0–3.6 cm^{-1} in wings of band. [g] 6.4 cm^{-1} spacing in R branch.

near 200 cm^{-1} account for the nine in-plane fundamentals, and three type-C bands account for the three out-of-plane fundamentals. All but the 2305-cm^{-1} in-plane fundamental have definitely polarized bands in the Raman spectrum (Table IV). Depolarized bands in the Raman spectrum correspond to two of the out-of-plane modes, and the polarization of the third band, which is of very low intensity, is in doubt. As in the case of *cis*-CClHCFH, the weakest band in the infrared for an out-of-plane fundamental corresponds to a well defined, depolarized Raman band and thus to a CD torsion with a_2-like symmetry.

trans-1-Chloro-2-fluoroethylene. The infrared spectrum of *trans*-CClHCFH in Figure 5 has five prominent type-A/B bands located at 3103, 1647, 1112, 876, and 447 cm^{-1}, which are undoubtedly due to in-plane fundamentals. The corresponding Raman bands (Table V) are polarized. A partly overlapped band at 1296 cm^{-1}, supported by a strong, polarized counterpart in the Raman, is the sixth in-plane fundamental. A stronger band at 1218 cm^{-1}, also supported by a polarized Raman band, is the seventh. The second CH-stretching frequency is observed only in the Raman spectrum as a polarized band at 3094 cm^{-1}. Without a more detailed analysis of the spectra there is no evidence for the ninth in-plane fundamental.

Three type C bands attributable to out-of-plane fundamentals seem to be present in the gas-phase infrared

Table VI: Infrared and Raman Spectra and Assignments for *trans*-CClD=CFH

Raman (liquid)			Ir (gas)			Assignment		
Freq, cm^{-1}	*I*	Polarization	Freq, cm^{-1} [a]	α[b]	Band shape[c]	Freq, cm^{-1}		Sym species
			3360	0.005	~C	3365	$\nu_1 + \nu_9$	A′
							$\nu_1 + \nu_{12}$	A″
3093	wm	p	3099 (12)	0.25	B	ν_1	Fund.	a′
			2757 (12)	0.072	B	2762	$\nu_2 + \nu_8$	A′
							$\nu_3 + \nu_5$	A′
2313	m	p	2318 (12)[d]	0.71	B	ν_2	Fund.	a′
			2280	0.02	C	2287	$\nu_3 + \nu_{11}$	A″
			2253 (12)	0.11	B	2264	$2\nu_5$	A′
			2120 (13)	0.025	B	2121	$\nu_5 + \nu_6$	A′
			1973 (13)	0.030	B	1978	$2\nu_6$	A′
			1915	<0.02	B?	1914	$\nu_5 + \nu_7$	A′
			1896	0.053	~C	1896	$\nu_3 + \nu_9$	A′
							$\nu_3 + \nu_{12}$	A″
			1695 (13)	0.37	B	1702	$2\nu_{10}$	A′
1626	vs	p	1630 (12)	1.1	B	ν_3	Fund.	a′
~1550	vw		1563 (11)	0.14	A	1564	$2\nu_7$	A′
			1506 (12)	0.026	B	1508	$\nu_{10} + \nu_{11}$	A′
			1429 (13)	0.036	A/B	1439	$\nu_7 + \nu_{11}$	A′
						1433	$\nu_6 + \nu_9$	A′
			1395	0.064	~C	1398	$\nu_5 + \nu_9$	A′
							$\nu_5 + \nu_{12}$	A″
			1309 (13)[d]	0.06	B	1314	$2\nu_{11}$	A′
1283	s	p	1284 (14)	0.074	B	ν_4	Fund.	a′
			1218	0.28	?	1226	$\nu_7 + \nu_8$ Impurity?	A′
			1183	0.15	?	1186	$\nu_3 - \nu_8$ Impurity?	A′
1115	m	p	1132 (13)	8.9	B	ν_5	Fund.	a′
			1046 (12)	0.037	A	1048	$\nu_7 + \nu_9$	A′
							$\nu_7 + \nu_{12}$	A″
			1016	0.021	C	1018	$\nu_4 - \nu_{12}$	A″
980	sm	p	989	4.0	B	ν_8	Fund.	a′
			~875				*trans*-CClHCFH impurity	
853	m	dp	851[d,e]	0.40	C	ν_{10}	Fund.	a″
782	sm	p	782 (13)	0.88	B	ν_7	Fund.	a′
654	m	dp	657[d,e]	0.38	C	ν_{11}	Fund.	a″
			546 (12)	0.006	B	545	$\nu_8 - \nu_8$	A′
442	vs	p	444 (14)[d]	0.058	B	ν_8	Fund.	a′
270	s	dp?	266[f]	0.79	~C	ν_9	Fund.	a′
						ν_{12}	Fund.	a″

[a–c] See Table I. [d] Rotational spacing of 2.5–2.9 cm^{-1} in P and R branches. [e] See Table I. [f] Rotational spacing of 5.1 cm^{-1} in R branch.

spectrum. The assignment of one at 888 cm^{-1}, which overlaps the ν_7 band, is supported by the well developed rotational structure in the R branch and an apparently depolarized Raman band. Rotational structure also supports the assignment of the second type C band at 784 cm^{-1} to ν_{11} and apparently also the third one at 274 cm^{-1}. The ν_{11} fundamental, which has a prominent, depolarized Raman band and a relatively weak infrared band, must be the CH motion which correlates with b_g symmetry in a symmetrically substituted dihaloethylene. The 6.4-cm^{-1} spacing of the rotational structure of the R branch of the 274-cm^{-1} band is nearly twice the normal spacing of 3.3 cm^{-1}. Furthermore, the general appearance of this lowest frequency band is almost identical with that of the corresponding band in the spectrum of *trans*-CFHCFH. For the difluoroethylene

Table VII: Infrared and Raman Spectra and Assignments for *trans*-CClH=CFD

Raman (liquid)			Ir (gas)			Assignment		
Freq, cm^{-1}	I	Polarization	Freq, cm^{-1} [a]	α [b]	Band shape [c]	Freq, cm^{-1}		Sym species
			3968 (16)	0.012	A/B	3971	$\nu_1 + \nu_7$	A′
			3348	0.006	?	3361	$\nu_1 + \nu_9$	A′
							$\nu_1 + \nu_{12}$	A″
			3233 (11)	0.018	B	3240	$2\nu_3$	A′
3095	m	p	3099 (13)	0.54	A	ν_1	Fund.	a′
			2835 (12)	0.021	B	2841	$\nu_3 + \nu_4$	A′
			2740 (11)	0.062	A/B	2745	$\nu_3 + \nu_5$	A′
			2570	0.003	?	2585	$\nu_2 + \nu_9$	A′
							$\nu_2 + \nu_{12}$	A″
						2571	$\nu_3 + \nu_6$	A′
			2340	<0.02	?	2346	$\nu_4 + \nu_5$	A′
2330	m	p	2323 (12) [d]	0.21	B	ν_2	Fund.	a′
			2242 (12)	0.10	A/B	2250	$2\nu_6$	A′
			2093 (12)	<0.15	B	2093	$\nu_4 + \nu_7$	A′
			2072 (12)	0.042	A	2076	$\nu_5 + \nu_8$	A′
			1900	<0.024	?	1902	$2\nu_6$	A′
			1892	0.069	~C	1882	$\nu_3 + \nu_9$	A′
			1882				$\nu_3 + \nu_{12}$	A″
			1742 (11)	0.019	?	1744	$2\nu_7$	A′
1619	vs	p	1620 (12)	1.8	B	ν_3	Fund.	a′
			1567 (12)	0.12	A/B	1569	$\nu_5 + \nu_8$	A′
			1480	0.007	~C	1483	$\nu_3 + \nu_9$	A′
							$\nu_3 + \nu_{12}$	A″
			1378 (12) [d]	0.21	B	1395	$\nu_6 + \nu_8$	A′
						1382	$2\nu_{11}$	A′
			1341	<0.04			?	
			1315	0.10	B	1316	$\nu_7 + \nu_8$	A′
1213	s	p	1221 (13) [d,e]	0.31	A	ν_4	Fund.	a′
			<1140			1133	$\nu_7 + \nu_9$	A′
							$\nu_7 + \nu_{12}$	A″
1112	m	p	1125 (13) [d,e]	11	B	ν_5	Fund.	a′
			1080	<0.04	~C	1079	$\nu_{10} + \nu_{12}$	A′
							$\nu_9 + \nu_{10}$	A″
			988 (10) [e]	<0.04	A/B	953	$\nu_{11} + \nu_{12}$	A′
						Fermi resonance with ν_6		
~945	vw	dp	951 (12) [e]	1.0	A	ν_6	Fund.	a′
			894 (10)	<0.3	A/B	888	$2\nu_8$	A′
869	m	p	872 (13) [e]	2.3	B	ν_7	Fund.	a′
813	vw	dp	817 [d]	0.75	C	ν_{10}	Fund.	a″
~775	vw	dp				785	*trans*-CClHCFH impurity	
689	m	dp	691 [d]	0.15	C	ν_{11}	Fund.	a″
			523	0.003	B	524	$2\nu_9$	A′
							$2\nu_{12}$	A′
446	s	p	444 (14)	0.062	B	ν_8	Fund.	a′
266	m	dp?	262 [f]	0.75	~C	ν_9	Fund.	a′
						ν_{12}	Fund.	a″

[a–c] See Table I. [d] Rotational structure in P and R branches with 2.4–2.9 cm^{-1} spacing. [e] See Table I. [f] Rotational structure in P and R branch with 5.2-cm^{-1} spacing.

Table VIII: Infrared and Raman Spectra and Assignments for *trans*-CClD=CFD

Raman (liquid)			Ir (gas)			Assignment		
Freq, cm^{-1}	I	Polarization	Freq, cm^{-1} [a]	α [b]	Band shape [c]	Freq, cm^{-1}		Sym species
			3424 (15)	0.013	B	3425	$\nu_2 + \nu_4$	A′
			3284 (12)	0.012	B	3286	$\nu_2 + \nu_5$	A′
						3284	$\nu_1 + \nu_6$	A′
			3099 (13)	0.008	B	3099	*trans*-CClDCFH impurity	
							trans-CClHCFD impurity	
			3078 (13)	0.012	B	3081	$\nu_2 + \nu_7$	A′
			2730 (11)	0.084	A/B	2738	$\nu_2 + \nu_8$	A′
						2737	$\nu_3 + \nu_4$	A′
			2680	0.013	?	2690	$\nu_4 + 2\nu_7$	A′
			2598	0.012	~C	2598	$\nu_1 + \nu_9$	A′
							$\nu_1 + \nu_{12}$	A″
			~2390	0.01	A/B	2393	$\nu_3 + \nu_7$	A′
2345	s	p	2339 (14) [d]	0.20	B	ν_1	Fund.	a′
~2304	vw	dp	2299 (12)	1.0	B	ν_2	Fund.	a′
			2244 (12)	0.052	B	2252	$2\nu_4$	A′
			2111 (12)	0.040	B	2113	$\nu_4 + \nu_5$	A′
			2066 (11)	0.021	A	2071	$\nu_4 + \nu_6$	A′
			1975 (13)	0.030	B	1974	$2\nu_5$	A′
			1911 (14)	0.018	B	1908	$\nu_4 + \nu_7$	A′
			1866 (14)	0.06	~C	1870	$\nu_3 + \nu_9$	A′
							$\nu_3 + \nu_{12}$	A″
			1695	w	B		*cis*-CClFCFD impurity	
			~1630				*trans*-CClDCFH impurity	
1609	vs	p	1611 (13)	1.8	B	ν_3	Fund.	a′
			1560 (12)	0.41	A	1565	$\nu_4 + \nu_8$	A′
						1564	$2\nu_7$	A′
			1427 (12)	0.028	B	1426	$\nu_5 + \nu_8$	A′
			1382 (11) [d]	0.25	A/B	1384	$\nu_6 + \nu_8$	A′
							$2\nu_{10}$	A′
			1336 (12)	0.070	B	1338	$\nu_{10} + \nu_{11}$	A′
			1287 (12) [d]	0.033	B	1292	$2\nu_{11}$	A′
			1224 (12)	0.13	~B	1221	$\nu_7 + \nu_8$	A′
			1166	0.06	B	1172	$\nu_3 - \nu_8$	A′
1113	s	p	1126 (13) [e]	8.7	B	ν_4	Fund.	a′
			1038 (10)	0.029	B	1041	$\nu_7 + \nu_9$	A′
							$\nu_7 + \nu_{12}$	A″
984	s	p	987 (13) [e]	4.7	B	ν_5	Fund.	a′
~944	vw	dp	945 (14)	0.065	A	ν_6	Fund.	a′
						951	$\nu_{10} + \nu_{12}$	A′
							$\nu_9 + \nu_{10}$	A″
			904	0.01	~C	905	$\nu_{11} + \nu_{12}$	A′
							$\nu_9 + \nu_{11}$	A″
			871 (12)		A/B		*trans*-CClHCFD impurity	
						878	$2\nu_8$	A′
			850		C		*trans*-CClDCFH impurity	
			817 [f]		C		*trans*-CClHCFD impurity	
782	s	p	782 (12)	1.1	B	ν_7	Fund.	a′
691	s	dp	692	<0.05	C	ν_{10}	Fund.	a″
~642	vw	dp?	646 [d]	0.78	C	ν_{11}	Fund.	a″
			546 (13)	0.004	B	548	$\nu_8 - \nu_5$	A′
442	vs	p	441 (14) [d]	0.061	B	ν_8	Fund.	a′
262	s	dp?	259 [g]	1.0	~C	ν_9	Fund.	a′
						ν_{12}	Fund.	a″

[a–c] See Table I. [d] Rotational spacing of 1.7–2.4 cm^{-1} in P and R branches. [e] See Table I. [f] Rotational spacing of 2.5 cm^{-1} in R branch, 2.9 cm^{-1} in P branch. [g] Rotational spacing of 4.3 cm^{-1} in R branch.

Table IX: Vibrational Fundamentals of *cis*-1-Chloro-2-fluoroethylene and Deuterated Modifications (Frequencies in cm^{-1})

	Obsd				Calcd			
	CClHCFH	CClDCFH	CClHCFD	CClDCFD	CClHCFH	CClDCFH	CClHCFD	CClDCFD
a′								
ν_1	3114	3098	3112	2342	3136	3135	3113	2311
ν_2	3102	2322	2318	2297	3112	2289	2310	2289
ν_3	1661[a]	1637[a]	1644[a]	1629	1649	1638	1621	1609
ν_4	1335	1304	1283	1162[a]	1351	1322	1273	1171
ν_5	1231	1155	1051	984	1209	1144	1075	974
ν_6	1062	851	969	831	1086	854	962	837
ν_7	812	778	791	770	795	778	793	775
ν_8	656	655	637	638	650	643	627	623
ν_9	205[b]	202[b]	205[b]	203[b]	204	203	203	203
a″								
ν_{10}	857	826	796	691	857	826	797	691
ν_{11}	735	588	650	575	737	587	650	573
ν_{12}	442	434	400	394	442	434	400	395

[a] Uncorrected for probable shift due to Fermi resonance with a combination tone. [b] From liquid-phase Raman spectra; all others from gas-phase infrared.

case much evidence has been found in support of this band being due to two almost degenerate fundamentals distorted by a strong Coriolis perturbation.[3b] We therefore confidently assign both ν_9 and ν_{12} to the 274-cm^{-1} band. Table V also includes the eight frequencies which Viehe, *et al.*, assigned to fundamentals.[8] Agreement with our assignments is within a few cm^{-1} in every case.

trans-1-Chloro-2-fluoroethylene-1-d_1. Given the interpretation that the band in the 270-cm^{-1} region is due to overlap of the ν_9 and ν_{12} fundamentals as in *trans*-CClHCFH, one finds the vibrational assignment for *trans*-CClDCFH to be straightforward. Seven type A/B bands are quickly found in the gas-phase infrared spectrum in Figure 6 and are assigned to in-plane fundamentals. The eighth band, 1284 cm^{-1}, is sufficiently weak in the infrared that the strong, polarized Raman band (Table VI) at this frequency becomes the basis for the assignment. Two type C bands stand out clearly with well defined rotational structure in the gas-phase infrared and have depolarized counterparts in the Raman. In the low-frequency region, where ν_9 and ν_{12} overlap, exaggerated rotational spacing of 5.1 cm^{-1}, compared with a normal value of about 2.7 cm^{-1}, is again present.

trans-1-Chloro-2-fluoroethylene-2-d_1. The gas-phase infrared spectrum in Figure 7 of *trans*-CClHCFD contains seven prominent type A/B bands which we have assigned to fundamentals. All but the 951-cm^{-1} band are supported by polarized bands in the Raman spectrum (Table VII). The 951-cm^{-1} mode causes a weak, apparently depolarized Raman band. The eighth in-plane fundamental must correspond to the type A/B band at 1221 cm^{-1} and not to the band of comparable intensity at 1378 cm^{-1}. A frequency of 1378 cm^{-1} is too high for this fundamental, and the 1221-cm^{-1} assignment is supported by a strong, polarized Raman band. Well defined type C bands with obvious rotational structure are at 813 and 689 cm^{-1} in the infrared spectrum. These fundamentals also produce medium intensity, depolarized Raman bands. With eight of the in-plane and two of the out-of-plane fundamentals assigned we turn, as in the *trans*-CClHCFH and *trans*-CClDCFH cases, to the distorted band at the low-frequency end of the spectrum. We assign this band with its 5.2-cm^{-1} rotational spacing to both the ν_9 and ν_{12} fundamentals. The spectrum of this molecule provides, however, further support for this interpretation beyond that found for *trans*-CClHCFH and CClDCFH. Although the band for the overlapped fundamentals looks like the corresponding bands for the other two species, but with more poorly defined rotational structure in the R branch, the combination band at 1885 cm^{-1} has two distinct features. This band is assigned as $\nu_3 + \nu_9$ and $\nu_3 + \nu_{12}$ and has a shape strongly suggestive of overlapped type A/B and type C bands.

trans-1-Chloro-2-fluoroethylene-1,2-d_2. Six prominent type A/B bands seen at 2339, 1611, 1126, 987, 782, and 441 cm^{-1} in the gas-phase infrared spectrum of *trans*-CClDCFD in Figure 8 correspond to polarized Raman bands (Table VIII) and are confidently assigned as in-plane fundamentals. The unusual intensity of the band for the CD-bending mode at 987 cm^{-1} is due to considerable CF-stretching character in this vibration. Although the type A/B band at 2304 cm^{-1} corresponds to a very weak, depolarized Raman band, it must certainly be the second CD stretch. The location of the second CD-bending mode is less certain. Compared with the values of the CD-bending frequencies in the *trans*-CClDCFH and CClHCFD the low-intensity infrared band at 945 cm^{-1} seems to be the correct assignment, even though the corresponding

Table X: Vibrational Fundamentals of *trans*-1-Chloro-2-fluoroethylenes and Deuterated Modifications (Frequencies in cm^{-1}).

	Obsd				Calcd			
	CClHCFH	CClDCFH	CClHCFD	CClDCFD	CClHCFH	CClDCFH	CClHCFD	CClDCFD
a′								
ν_1	3103	3099	3099	2339	3120	3118	3111	2301
ν_2	3094[a]	2318	2323	2299	3110	2288	2298	2284
ν_3	1647[b]	1630	1620	1611	1666	1652	1635	1619
ν_4	1296	1284	1221	1126	1287	1279	1210	1124
ν_5	1218	1132	1125	987	1214	1128	1123	995
ν_6	1127	989	951[b]	945	1117	986	952	931
ν_7	876	782	872	782	886	781	877	781
ν_8	447	444	444	439	452	449	450	448
ν_9	270	265	262	259	277	271	268	263
a″								
ν_{10}	888	851	817	692	888	851	817	692
ν_{11}	784	657	691	646	784	657	691	646
ν_{12}	270	266	262	259	268	266	262	259

[a] From liquid-phase Raman spectra; all others from gas-phase infrared. [b] Uncorrected for probable Fermi resonance with a combination tone.

Raman band is very weak and apparently depolarized. The corresponding fundamental in *trans*-CClHCFD also has a weak, apparently depolarized Raman band. Further, there is no other candidate in the infrared spectrum of reasonable intensity and shape in this region. For the out-of-plane fundamentals only the type C band at 646 cm^{-1} stands out clearly in the infrared. This band has rich rotational structure and an apparently depolarized version in the Raman spectrum. Close examination of the infrared spectrum reveals the Q branch of a weak type C band at 691 cm^{-1}, which is confirmed by a strong depolarized Raman band. As in the three other *trans* species we assign the spike-like band in the low-frequency region to a near degeneracy in ν_9 and ν_{12}. Rotational spacing of 4.3 cm^{-1} in the R branch and two features for the combination band, $\nu_1 + \nu_9$ and $\nu_1 + \nu_{12}$ at 2598 cm^{-1}, provide further support for this assignment.

Table XI: Product Rule Check of Assignments and Principal Moments of Inertia in amu $Å^2$ [a]

		cis-Isomer		*trans*-Isomer	
		Calcd	Obsd	Calcd	Obsd
CClDCFH	a′	0.512	0.508	0.509	0.523
CClHCFH	a″	0.754	0.757	0.798	0.791
CClHCFD	a′	0.515	0.523	0.510	0.520
CClHCFH	a″	0.742	0.743	0.793	0.787
CClDCFD	a′	0.264	0.271	0.260	0.272
CClHCFH	a″	0.557	0.562	0.622	0.616

	I_a	I_b	I_c	I_a	I_b	I_c
CClHCFH	31.22	136.1	167.3	8.99	210.6	219.6
CClDCFH	34.97	136.2	171.2	11.30	210.7	222.0
CClHCFD	32.91	140.3	173.2	11.12	211.5	222.6
CClDCFD	36.63	140.4	177.0	13.48	211.5	225.0

[a] Geometric parameters: r_{CC} = 1.333 Å, r_{CCl} = 1.726 Å, r_{CF} = 1.348 Å, r_{CH} = 1.079 Å, α_{CCCl} = 123.6°, α_{CCH} = 123.2°, and α_{CCF} = 121.0°. J. A. Howe, *J. Chem. Phys.*, **34**, 1247 (1961).

Summary. For the four *cis* species we are confident of the assignments of the vibrational fundamentals, which are summarized in Table IX. Although some of the evidence is less direct, we believe that we have also obtained complete assignments of the fundamentals of the *trans* species, Table X. All of the assignments are consistent with the isotope product rule (Table XI) and with the Rayleigh rule. As shown in Tables I–IV for the *cis* species and Tables V–VIII for the *trans*, it is possible in almost every case to assign the weaker bands as binary combinations. This agreement was also found for very weak bands with absorption coefficients less than 0.01 cm^{-1} atm^{-1}. These very weak bands were omitted from the tables except where they were of special interest such as combinations involving the entangled ν_9 and ν_{12} fundamentals of the *trans* species.

Thermodynamic Functions. With a complete vibrational assignment of the fundamentals in hand one may check the $\Delta S°$ obtained from the thermodynamic measurements and extract $\Delta E_0°$ (electronic), the electronic energy difference between the two isomers, from $\Delta H°$. A rigid-rotor, harmonic-oscillator treatment of *cis*- and *trans*-CClHCFH gives $\Delta S°_{615}$ = 0.24 ± 0.04 cal/mol °K and $\Delta H°_{615}$ (thermal) = 184 cal/mol for the *cis*-to-*trans* reaction. The calculated value of $\Delta S°_{615}$ is in satisfactory agreement with the experimental value of 0.21 cal/mol °K. From the calculated value of $\Delta H°_{615}$(thermal), the experimental value of $\Delta H°_{615}$ = 782 ± 22 cal/mol, and $\Delta E_0°$(vibration) = −269 ± 70 cal/mol, one obtains $\Delta E_0°$(electronic) = 867 ± 90 cal/mol. This value for $\Delta E_0°$(electronic) is very nearly

Table XII: Potential Constants for Vibrations of 1-Chloro-2-fluoroethylenes

A. In-Plane Modes; Modified Urey–Bradley Field [K, F, and C in mdyn/Å; H in mdyn Å/radian^2]

	Zero-order[a]	Overlay	Dispersion
K_{CC}	7.48	7.50	0.14
K_{CH}	4.83	4.82	0.051
K_{CF}	5.20	4.67	0.22
K_{CCl}	2.66	2.75	0.32
H_{CCH}	0.335	0.187	0.065
H_{HCF}	0.500[b]	0.491	0.074
H_{CCF}	0.172	1.14	0.21
H_{HCCl}	0.383	0.273	0.079
H_{CCCl}	0.207		
F_{CH}	0.450	0.394	0.086
F_{CF}	1.37	0.754	0.21
F_{HF}	0.34[b]	0.557	0.089
F_{CCl}	0.92	0.769	0.10
F_{HCl}	0.30	0.524	0.087
C_{HH}	0.0	−0.009	0.022
C_{FCl}	0.080	−0.004	0.028
C_{HF}	−0.045	−0.043	0.038
C_{HCl}	0.030	−0.077	0.040
T_δ	0.0	0.097	0.031

B. Out-of-plane Modes; General Valence Field [mdyn Å/radian^2]

	cis		*trans*	
	Refined[c]	Dispersion	Refined[c]	Dispersion
F_γH(Cl)	0.356	0.0006	0.345	0.0004
F_γH (F)	0.353	0.0007	0.363	0.0005
F_τ	0.529	0.0017	0.468	0.0029
$F_{\gamma\gamma}$	0.064	0.0005	0.143	0.0004
$F_{\tau\gamma}$H(Cl)	−0.267	0.0016	−0.220	0.0028
$F_{\tau\gamma}$H(F)	−0.211	0.0010	−0.195	0.0023

[a] Reference 11. [b] Reference 16. [c] Zero-order force constants: $F_\delta = 0.30$ and $F_\tau = 0.30$; all others 0.0.

the mean of the values for CFHCFH, 1086 cal/mol,[3b] and CClHCClH, 642 cal/mol.[4a]

Normal Coordinate Calculations. In-Plane Modes. For the in-plane normal coordinate calculations five valence bond stretching coordinates and six unscaled valence angle bending coordinates were used. Two rocking and two scissors coordinates and two angle redundancy relationships were then defined as before for halogenated ethylenes.[10,13] The geometric parameters (Table XI) were based in part on microwave results for the *cis* isomer. The calculations were performed with the Minnesota normal coordinate programs, which employ a modified GF formalism.[14] These programs were adapted for use on an IBM 360/44 computer.

The four *cis* species and the four *trans* species were treated together in an overlay calculation with a modified Urey–Bradley force field (MUBFF). All force constants except those for the *cis* interaction were considered to be the same for the two isomers. In addition, the same stretching (K_{CH}), bending (H_{CCH}), and *gem* interaction (F_{CH}) constants were used for the hydrogen atoms on the two ends of the molecule. A *trans* CH-bend interaction force constant (T_δ), which had proved useful before for *trans* haloethylenes,[3b,15] was added to improve the frequency fit and reduce the force constant dispersions. This interaction constant compensated in part for the constraint imposed by using only one H_{CCH} constant. Even though this normal coordinate problem with 22 force constants seemed well determined by the 72 observed frequencies, it proved necessary to hold the H_{CCCl} constant at its zero-order value. Of course, frequency changes due to deuteration provide little new information about the force constants for carbon–halogen-rich modes, and the MUBFF is a questionable approximation.

The zero-order force constants (Table XII) are the same as those used in our earlier CClFCClH calculations,[10] except where supplemented with force constants from the CFHCFH calculations.[3b] The average differences between calculated and observed frequencies (Tables X and XI) are 1%. With the exception of the CH-stretching frequencies, where neglect of anharmonicity corrections is most serious, almost all of the calculated frequencies are within 15 cm^{-1} of the observed ones. The refined force constants (Table XII) compare favorably with the zero-order values except in the case of H_{CCF}. Attempts to hold this force constant to a smaller value were unsuccessful. Dispersions of refined force constants are of reasonable magnitude except for those of the *cis* interaction constants. The satisfactory overlay calculation is added evidence in support of the assignments of the vibrational fundamentals.

Exploratory calculations with the MUBFF for the *cis* and *trans* species separately were unrewarding as the calculations either diverged or refined to unacceptable force constants. We expect, however, to make a more thorough study of the normal coordinates with several force field approximations for separate isomers.

One of the goals of this study of *cis–trans* isomerism in haloethylenes is to find evidence for *cis* stability in the force constants. In contrast to the CFHCFH case the *cis*-type interaction constants are apparently too poorly defined to permit any, even tentative, deductions. We do find, however, the same pattern in the fit of the CC-stretching frequencies. The overlay values for the *cis* isomers are, on the average, 14 cm^{-1} too low and those for the *trans* isomers are 15 cm^{-1} too high. This result may imply a larger K_{CC} force constant for the *cis* isomer, which correlates with its lower electronic energy.

Out-of-Plane Modes. As in our previous haloethylene calculations two wagging coordinates and one torsion

(13) J. R. Scherer and J. Overend, *J. Chem. Phys.*, **32**, 1720 (1960).
(14) (a) J. R. Scherer and J. Overend, *ibid.*, **32**, 1289 (1960); (b) C. D. Needham, Ph.D. Thesis, University of Minnesota, 1965.
(15) J. R. Scherer and J. Overend, *J. Chem. Phys.*, **33**, 1681 (1960).

coordinate were defined for out-of-plane vibrations.[3b,16] One wagging coordinate, R_γFH, was the change in angle between a CH bond and the plane defined by the CCF atoms, and the other was the change in angle between the second CH bond and the plane defined by the CCCl atoms. The change in the dihedral angle between the CCF and CCCl planes was the torsion coordinate. The *cis* and *trans* isomers were treated separately with six-parameter general valence force fields.

As shown in Tables X and XI, calculated frequencies fit the experimental ones within 1 cm^{-1} in all but three instances, and all of the calculated force constants, Table XII, have convincingly low dispersions. The diagonal force constants are in good agreement with the ones obtained in the separate calculations for the *cis* and *trans* isomers of CFHCFH.[3b] For *cis*-CFHCFH, $F_\gamma = 0.362$, $F_\tau = 0.551$, $F_{\gamma\gamma} = 0.0534$, and $F_{\gamma\tau} = -0.246$; for *trans*-CFHCFH, $F_\gamma = 0.347$, $F_\tau = 0.460$, $F_{\gamma\gamma} = 0.141$, and $F_{\gamma\tau} = -0.190$. The pattern of a wagging force constant that is nearly independent of configuration and a torsion force constant that is significantly larger for the *cis* isomer is repeated. The off-diagonal force constants are also in good agreement with those for the difluoroethylenes. The difference in torsion force constants correlates with the lower electronic energy of the *cis* isomer. Furthermore, the 13% difference in the F_τ force constants for the chlorofluoroethylenes is less than the 20% difference for the difluoroethylenes in parallel with the order of the difference in the electronic energies of the *cis* and *trans* isomers.

Acknowledgments. This research was supported by the Petroleum Research Fund (Grant 2422-B). J. C. W. and L. G. P. were National Science Foundation undergraduate research participants. We are indebted to John K. Piraino and David D. Sherertz for adapting the Minnesota normal coordinate programs for use on the IBM 360/44 computer.

(16) E. B. Wilson, J. C. Decius, and P. C. Cross, "Molecular Vibrations," McGraw-Hill Publications, New York, N. Y., 1955, pp 58–62.

Nuclear Magnetic Resonance Isotropic Shifts in 4-Methylpyridine and 4-Methylpyridine N-Oxide Complexed with Copper(II) β-Diketonates[1]

by C. H. Ke,[2a] R. J. Kurland,[2a] C. I. Lin,[2b] and N. C. Li[2b]

Departments of Chemistry, Duquesne University, Pittsburgh, Pennsylvania 15219 and State University of New York at Buffalo, Buffalo, New York 14214 *(Received October 27, 1969)*

Isotropic nuclear magnetic resonance shifts have been measured for 4-methylpyridine and 4-methylpyridine N-oxide complexed with $Cu(\beta\text{-dik})_2$ in $CDCl_3$ (β-dik = β-diketonate). The β-diketonates chosen are acetylacetonate (AA), trifluoroacetylacetonate (TFA), and hexafluoroacetylacetonate (HFA). In both 4-methylpyridine and 4-methylpyridine N-oxide complexes, the magnitude of the contact shifts lie in the order $Cu(HFA)_2 > Cu(TFA)_2 > Cu(AA)_2$. This order is the same as that for the stability constants for the adduct formation found from spectrophotometric studies. For a given $Cu(\beta\text{-dik})_2$, 4-methylpyridine (4-MePy) forms a stronger adduct than 4-methylpyridine N-oxide (4-MePyO). The isotropic shifts vary linearly with the reciprocal of the absolute temperature for $Cu(HFA)_2 \cdot 2(4\text{-MePy})$ and $Cu(HFA)_2 \cdot 2(4\text{-MePyO})$ throughout the temperature range of -50 to $+50°$. However, anomalous temperature variation was found for $Cu(AA)_2 \cdot 4\text{-MePy}$, $Cu(TFA)_2 \cdot 4\text{-MePyO}$, and $Cu(TFA)_2 \cdot 4\text{-MePy}$.

Nuclear magnetic resonance isotropic shift studies of paramagnetic transition metal complexes can provide useful information on the electronic structure.[3] Relatively small isotropic shifts are found in studies reported for copper(II) complexes,[4-7] compared to those for analogous nickel(II) and cobalt(II) complexes.[3] Moreover, in copper(II) compounds the isotropic shifts in some cases do not follow a Curie law temperature dependence.[4,5]

Copper(II) β-diketonates are known to form 1:1 and 1:2 adducts with pyridine and pyridine N-oxide type ligands.[5,8-11] Such adduct formation through axial coordination has a dramatic influence on the electronic spectra,[12-14] esr parameters,[15,16] and solvent extraction properties.[17] Stoichiometric and equilibrium studies have shown that fluorine substitution in the acetylacetone moiety markedly enhances adduct formation.[11,18] Thus, in a benzene solution containing 4-methylpyridine, copper(II) bisacetylacetonate, $Cu(AA)_2$, forms only a 1:1 adduct, whereas copper(II) bis(hexafluoroacetylacetonate), $Cu(HFA)_2$, and copper(II) bis(trifluoroacetylacetonate), $Cu(TFA)_2$, form both 1:1 and 1:2 adducts.

The present study was undertaken to investigate the effect of fluorine substitution in acetylacetone on the nuclear magnetic resonance isotropic shifts of 4-methylpyridine (4-MePy), and 4-methylpyridine N-oxide (4-MePyO) coordinated to copper(II) β-diketonates. The temperature variation of the isotropic shifts was examined for all systems and the results were compared with the stoichiometry of the adduct species in the solution. The pyridine nitrogen group in the ligand also serves as a useful model for the corresponding group in the biologically important compounds.

Experimental Section

Materials. 4-Methylpyridine was obtained from Eastman Organic Co. and was purified by distillation.

(1) This investigation was supported by National Science Foundation Grant No. GB 8237 and by Atomic Energy Commission Contract No. AT(30-1)-1922 at DU, and by National Science Foundation Grant No. GP 10463 at SUNYAB.

(2) (a) State University of New York at Buffalo; (b) Duquesne University.

(3) D. R. Eaton and W. D. Phillips, *Advan. Magn. Resonance*, I, 103 (1965).

(4) Z. Luz and R. G. Shulman, *J. Chem. Phys.*, **43**, 3750 (1965).

(5) R. W. Kluiber and W. D. Horrocks, Jr., *Inorg. Chem.*, **6**, 1427 (1967).

(6) C. C. Hinckley, *ibid.*, **7**, 396 (1968).

(7) A. F. Garito and B. B. Wayland, *J. Amer. Chem. Soc.*, **91**, 866 (1969).

(8) D. P. Graddon and E. C. Watton, *J. Inorg. Nucl. Chem.*, **21**, 49 (1961).

(9) R. D. Gillard and G. Wilkinson, *J. Chem. Soc.*, 5885 (1963).

(10) W. R. May and M. M. Jones, *J. Inorg. Nucl. Chem.*, **25**, 507 (1963).

(11) W. R. Walker and N. C. Li, *ibid.*, **27**, 2255 (1965).

(12) R. L. Belford, A. E. Martell, and M. Calvin, *J. Chem. Phys.*, **26**, 1165 (1957).

(13) D. P. Graddon, *J. Inorg. Nucl. Chem.*, **14**, 161 (1960).

(14) L. L. Funk and T. R. Ortolando, *Inorg. Chem.*, **7**, 567 (1968).

(15) B. R. McGarvey, *J. Phys. Chem.*, **60**, 71 (1956).

(16) (a) H. A. Kuska, M. T. Rogers, and R. F. Drullinger, *ibid.*, **71**, 109 (1967); (b) H. A. Kuska and M. T. Rogers, *J. Chem. Phys.*, **43**, 1744 (1965).

(17) H. Irving and D. E. Edginton, *J. Inorg. Nucl. Chem.*, **27**, 1359 (1965).

(18) C. H. Ke and N. C. Li, *ibid.*, **28**, 2255 (1966).

4-Methylpyridine N-oxide was purchased from K and K Laboratories and was recrystallized twice from benzene and dried in a vacuum desiccator over P_2O_5. $Cu(AA)_2$, $Cu(TFA)_2$, and $Cu(HFA)_2$ were prepared and analyzed as previously described.[18] All the copper chelates were dried in a vacuum desiccator over P_2O_5. Chloroform was purified as previously described.[15]

Nmr Measurements. Proton nmr spectra were obtained at 60 MHz *via* Varian A-60 and HA-60 nmr spectrometers. Deuteriochloroform was used as a solvent and TMS as an internal reference. The chemical shifts were obtained by side band interpolation techniques. For line width and variable temperature experiments, the Varian HA-60 nmr spectrometer was used in the field-frequency controlled mode. Temperature measurements were calibrated by a thermistor[19] and should be accurate to $\pm 1°$. The line widths, measured as the full width at the half maximum peak intensity, and the isotropic shifts, defined as the difference between the observed chemical shifts in the presence of copper chelate and the chemical shifts of the free ligand, are accurate to 0.2 Hz or 2%, whichever is greater. Upfield shifts are defined as positive and downfield shifts as negative.

Optical Spectra and Stoichiometry. Optical spectra were recorded with a Cary 14 recording spectrophotometer at room temperature. Purified chloroform was used as solvent. The stoichiometry of the adduct species in solution was deduced from the spectral change as a function of the molar ratios of ligand to copper chelate.

Electron Spin Resonance. Esr spectra of chloroform solutions of $Cu(TFA)_2$, $Cu(HFA)_2$, and 4-methylpyridine or 4-methylpyridine N-oxide were obtained using a Varian V4500-10A spectrometer operating at about 9.2 kMHz.

Results and Discussion

Adduct formation of $Cu(TFA)_2$ and $Cu(HFA)_2$ with 4-MePy and 4-MePyO in chloroform solution was observed spectrophotometrically. $Cu(AA)_2$ had been reported to form only a 1:1 adduct with 4-MePy in chloroform.[8] No adduct formation of $Cu(AA)_2$ with 4-MePyO in chloroform was detected. The stoichiometry of the adduct species in solution was deduced from the spectral change as a function of the molar ratio of ligand to copper chelate. Thus, $Cu(TFA)_2$ forms mainly 1:1 adducts with 4-MePy and 4-MePyO up to a ligand to $Cu(TFA)_2$ ratio of 100:1, and $Cu(HFA)_2$ forms mainly 1:2 adducts with 4-MePy and 4-MePyO when the ligand to $Cu(HFA)_2$ ratio exceeds 5:1 and 20:1, respectively. These results are consistent with other spectrophotometric results.[5,8,11]

Electron spin resonance spectra of the 1:1 adducts of $Cu(TFA)_2$ with 4-MePy and 4-MePyO and the 1:2 adducts of $Cu(HFA)_2$ with 4-MePy and 4-MePyO were obtained for chloroform solutions at 20° and for frozen, glassy "solutions" at about −180°. Isotropic and anisotropic g values were calculated directly from the observed spectra. The g values obtained are essentially the same for all the complexes. Thus $g_{\parallel}$ and $g_{\perp}$ are: 2.32 and 2.07 for $Cu(TFA)_2 \cdot 4$-MePy, 2.34 and 2.06 for $Cu(TFA)_2 \cdot 4$-MePyO, 2.36 and 2.07 for $Cu(HFA)_2 \cdot 2(4\text{-MePy})$, 2.39 and 2.05 for $Cu(HFA)_2 \cdot 2(4\text{-MePyO})$. These results compare well with the values 2.30 and 2.07 for $Cu(AA)_2$ in pyridine,[16a] and 2.28 and 2.08 for $Cu(TFA)_2 \cdot 4$-MePyO.[5]

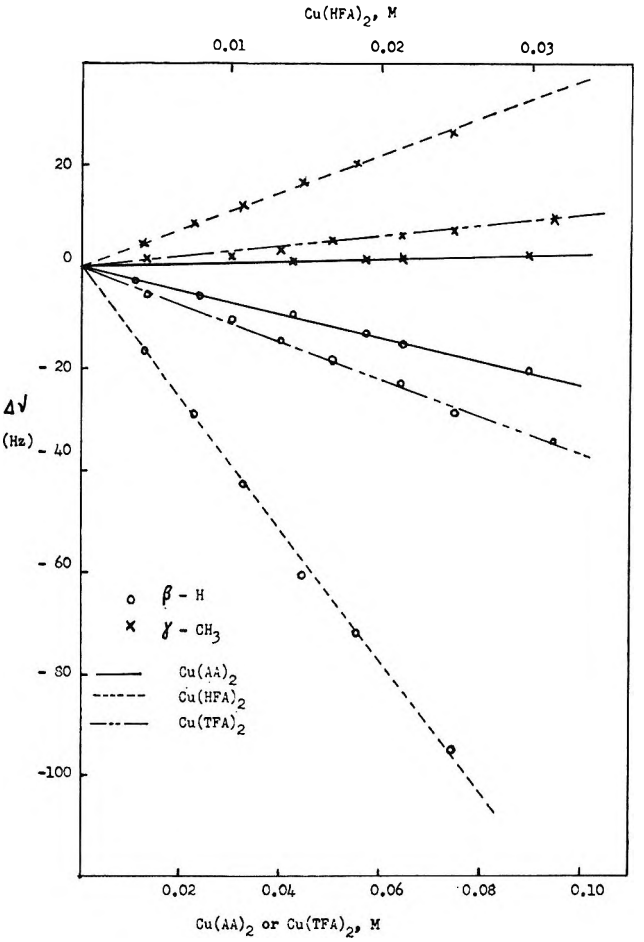

Figure 1. Variation of isotropic shifts of 4-methylpyridine in $CDCl_3$ with $Cu(chelate)_2$ concentration; (a) upper scale for $Cu(HFA)_2$ in 3 *M* 4-methylpyridine; (b) lower scale for $Cu(AA)_2$ and $Cu(TFA)_2$ in 2 *M* 4-methylpyridine at 36°.

Isotropic proton magnetic resonance shifts of (a) 4-MePy coordinated with $Cu(AA)_2$, $Cu(TFA)_2$, and $Cu(HFA)_2$ and (b) 4-MePyO coordinated with $Cu(TFA)_2$ and $Cu(HFA)_2$ were obtained in $CDCl_3$ solution samples. The lines of 4-MePyO did not shift upon addition of $Cu(AA)_2$; this result is consistent with the optical results which showed that $Cu(AA)_2$ does not form an adduct with 4-MePyO in chloroform solution. Typical nmr data are shown in Figures 1 and 2.

In all cases studied the ligand concentration was kept in excess. The fast-exchange limit prevailed in the

(19) A. L. Van Geet, *Anal. Chem.*, **40**, 2227 (1968).

temperature range of −40° to +50°, as shown by the linear plot of the log of the line width (the γ-CH_3 peak of the ligand) *vs.* the reciprocal of the absolute temperature, as shown in Figure 3, and by the fact that the observed shifts depended only on the ratio of metal ion-to-adduct concentrations. The temperature variation of the nmr shifts is illustrated in Figures 4 and 5.

The isotropic shifts are found to vary linearly, under the experimental conditions chosen, with increasing copper chelate concentration as shown in Figures 1 and

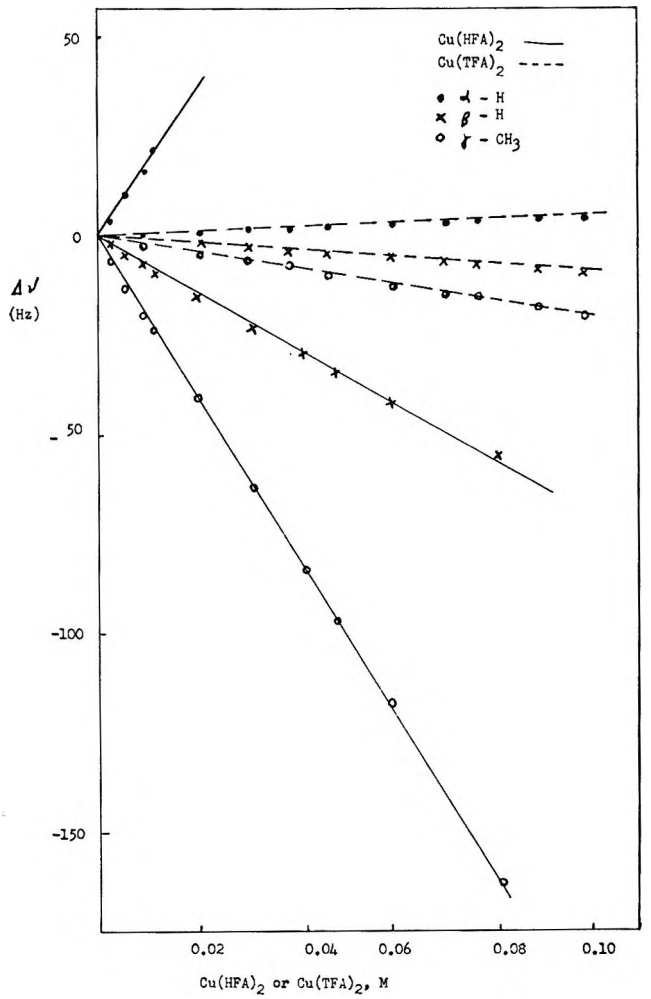

Figure 2. Variation of isotropic shifts of 1 *M* 4-methylpyridine N-oxide in $CDCl_3$ with Cu(chelate)$_2$ concentration at 36°.

2. Furthermore, from room temperature measurements, the slope of such a plot is reduced to one-half if the total ligand concentration is doubled; the slope was calculated from the portions where the ligand to copper chelate ratio is high. These results suggest that under the experimental conditions used, one adduct species predominates in the solution. However, the presence of a small amount of other species cannot be ruled out. The spectrophotometric results indicate that the following species are responsible for the observed isotropic shifts in $CDCl_3$ solution: Cu(AA)$_2$·4-MePy, Cu-

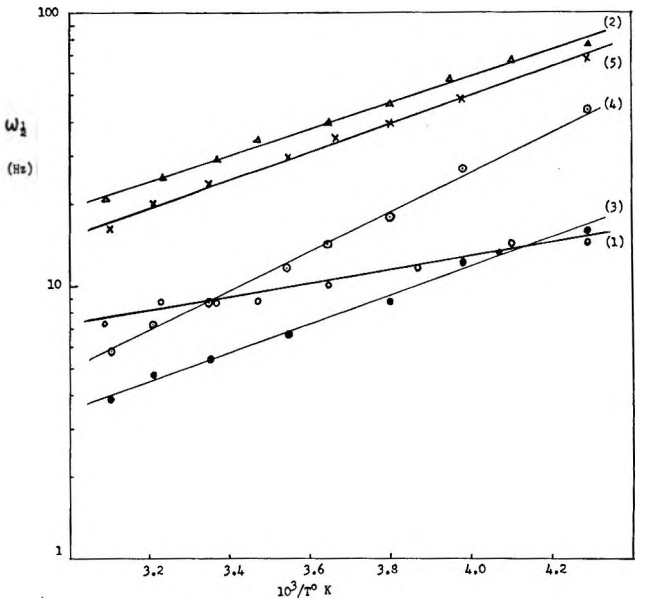

Figure 3. Plots of log $\omega_{1/2}$ ($\omega_{1/2}$ is the full line width of the γ-CH_3 peak measured at half-maximum peak intensity) *vs.* $10^3/T$°K in $CDCl_3$ for: (1) 0.03814 *M* Cu(TFA)$_2$ in 1 *M* 4-methylpyridine N-oxide, (2) 0.01131 *M* Cu(HFA)$_2$ in 1 *M* 4-methylpyridine N-oxide, (3) 0.0871 *M* Cu(AA)$_2$ in 2 *M* 4-methylpyridine, (4) 0.0782 *M* Cu(TFA)$_2$ in 2 *M* 4-methylpyridine, (5) 0.0331 *M* Cu(HFA)$_2$ in 2 *M* 4-methylpyridine.

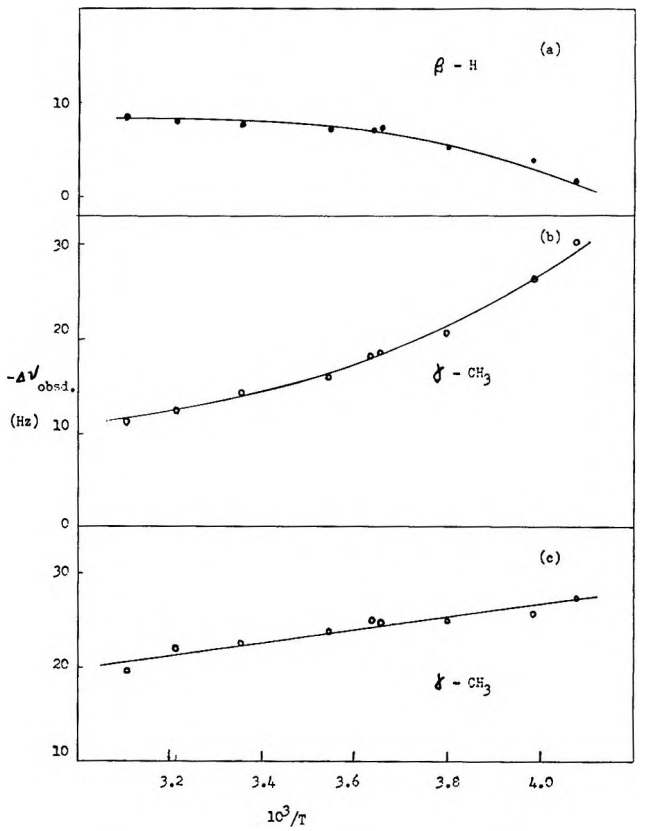

Figure 4. Temperature effect on isotropic shifts of 2 *M* 4-methylpyridine in $CDCl_3$: (a) 0.0870 *M* Cu(AA)$_2$; (b) 0.0782 *M* Cu(TFA)$_2$, (c) 0.0436 *M* Cu(HFA)$_2$.

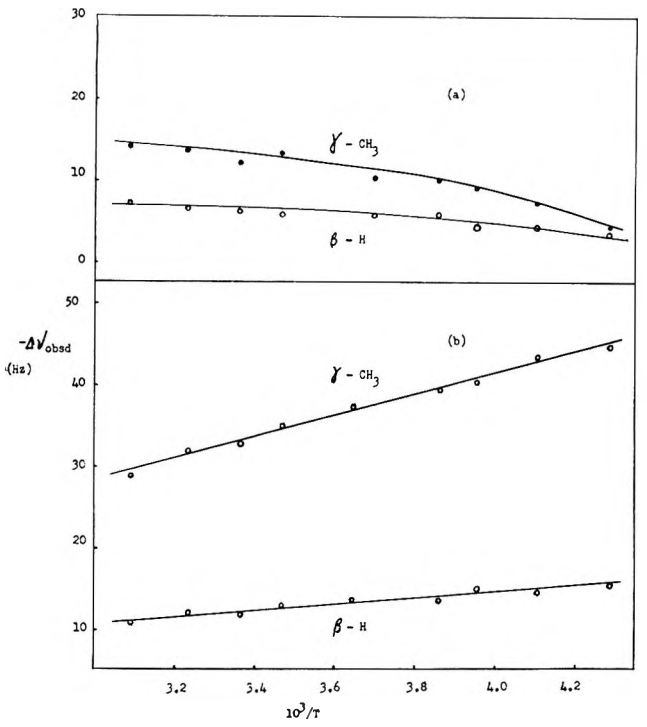

Figure 5. Temperature effect on isotropic shifts of 1 *M* 4-methylpyridine N-oxide in $CDCl_3$: (a) 0.09413 *M* $Cu(TFA)_2$; (b) 0.0165 *M* $Cu(HFA)_2$.

$(TFA)_2 \cdot$4-MePy, $Cu(HFA)_2 \cdot 2$(4-MePy), $Cu(TFA)_2 \cdot$4-MePyO, and $Cu(HFA)_2 \cdot 2$(4-MePyO).

The isotropic nmr shift may be decomposed into the Fermi contact and pseudocontact contributions.[3] In the fast-exchange limit, if (1) the rotational correlation time is short compared to the g-tensor anisotropy, (2) no more than one Kramers multiplet is populated, and (3) there is no orbital contribution to the paramagnetism from unpaired electron spin in orbitals centered at the nucleus in question, then the Fermi contact contribution is given by eq 1.[20,21] In eq 1, $(\Delta\nu_i)_F$ is the

$$(\Delta\nu_i)_F = -A_i \frac{\gamma_e}{\gamma_n} \frac{S(S+1)}{3kT} \bar{g}\beta\nu P_c \qquad (1)$$

Fermi contact contribution to the paramagnetic nmr shift for nucleus i; A_i is the Fermi contact constant for this proton; γ_e and γ_n are the gyromagnetic ratios for electron and nuclear spins, respectively; S is the spin quantum number for the complex; $\bar{g}$ is the rotationally averaged value of the g tensor; β is the value of the Bohr magneton (in ergs/G); ν is the nuclear Larmor frequency; and P_c is the fraction of ligand coordinated to the metal ion.

Under the conditions listed above, the pseudocontact shift is given by eq 2.[21] In eq 2, $(\Delta\nu_i)_D$ is the pseudocontact contribution to the isotropic paramagnetic shift; χ_{xx}, χ_{yy}, χ_{zz} are the principal axis components of the molecular susceptibility tensor; R_i is the length of a vector from the metal ion center to nucleus i; Ω is the polar angle and ψ is the azimuthal angle between this vector and the principal axes of the susceptibility tensor; and $\bar{\chi}$ is the rotationally averaged susceptibility [$\bar{\chi} = 1/3(\chi_{xx} + \chi_{yy} + \chi_{zz})$]. The low-temperature esr results indicate that the g tensor and, thus, the susceptibility tensor are axially symmetric, so that the pseudocontact shift can be put in terms of $g_{||}$, the g tensor component along the symmetry axis and $g_\perp$, the component perpendicular to the symmetry axis, $\bar{g} = 1/3\,(g_{||} + 2g_\perp)$, as in eq 3.

$$(\Delta\nu_i)_D = \frac{\nu\beta^2 S(S+1)}{9kT} \bar{g}(g_{||} - g_\perp)\left(\frac{1 - 3\cos^2\Omega}{R_i^3}\right)P_c \qquad (3)$$

$$(\Delta\nu_i)_D = \frac{\nu}{2R_i^3}[(1 - 3\cos^2\Omega)(\chi_{zz} - \bar{\chi}) + \sin^2\Omega\cos 2\psi(\chi_{yy} - \chi_{xx})]P_c \qquad (2)$$

The observed isotropic shifts for the copper complexes are given in Tables I and II. They are relatively small compared to the analogous nickel(II) and cobalt(II) bisacetylacetonates.[22,23] In the 4-methylpyridine systems the α-H and β-H are shifted downfield whereas the γ-CH_3 is shifted upfield. The isotropic shifts attenuate regularly as the number of bonds between the proton and the metal increases, as can be seen in Table I. The γ-H in pyridine is shifted downfield in contrast to the upfield shift of the γ-CH_3 in 4-MePy. All the proton lines are broadened to at least some extent by the paramagnetic copper chelate. The broadening increases with the isotropic shift. Thus, the α-H of the 4-MePy in the $Cu(TFA)_2$ and $Cu(HFA)_2$ systems can be observed only at low concentrations of copper chelate and high concentrations of 4-MePy. In the 4-methylpyridine N-oxide systems the α-H line is shifted upfield whereas the β-H and γ-CH_3 lines are shifted downfield. Again, the γ-H line in pyridine N-oxide is shifted in a direction opposite to that of the γ-CH_3 line in 4-MePyO. Although the broadening of the proton lines in the 4-MePyO systems is less than in the 4-MePy systems, the α-H line in the $Cu(HFA)_2$ system is broadened so much that it can be observed only at low concentrations of $Cu(HFA)_2$. The magnitude of the isotropic shifts of the $Cu(HFA)_2 \cdot$4-MePyO adduct decreases in the order γ-CH_3 > α-H > β-H, while with $Cu(TFA)_2 \cdot$4-MePyO the order is γ-CH_3 > β-H > α-H. The fact that the isotropic shift for the α-H line is smaller than for β-H in this system cannot be rationalized in terms of a pseudocontact contribution.

(20) H. M. McConnell and D. B. Chesnut, *J. Chem. Phys.*, **28**, 107 (1958).

(21) R. J. Kurland and B. R. McGarvey, *Advan. Magn. Resonance*, in press.

(22) J. A. Happe and R. L. Ward, *J. Chem. Phys.*, **39**, 1211 (1963).

(23) R. W. Kluiber and W. D. Horrocks, Jr., *J. Amer. Chem. Soc.*, **87**, 5350 (1965).

Table I: Isotropic Shifts of 4-Methylpyridine Systems in $CDCl_3$ at 36°

M(chelate)$_2$	Ligand proton	Concn, M: Ligand	Concn, M: M(chelate)$_2$	$\Delta\nu_{obsd}$, Hz	Pseudocontact shift, Hz[c]	$\Delta\nu_{cor}$[d]	β ratio[e]
Cu(AA)$_2$	α-H	1.000	0.0241	−9.0	−2.3	−6.7	0.37
	β-H			−3.8	−1.3	−2.5	1.00
	γ-CH_3			−0.3	−0.8	0.5	−5.0
Cu(AA)$_2$	α-H	2.000	0.0244	−5.7	−1.4	−4.3	0.28
	β-H			−2.0	−0.8	−1.2	1.00
	γ-CH_3			−0.4	−0.6	0.2	−6.0
Cu(TFA)$_2$	α-H[b]	1.000	0.0130		−1.5		
	β-H			−16.8	−0.8	−16.0	1.00
	γ-CH_3			4.6	−0.5	5.1	−3.14
Cu(TFA)$_2$	α-H	2.000	0.0094	−18.2	−0.6	−17.6	0.31
	β-H			−5.7	−0.3	−5.4	1.00
	γ-CH_3			1.8	−0.1	1.9	−2.84
Cu(HFA)$_2$	α-H[b]	3.000	0.0134		−1.1		
	β-H			−13.6	−0.6	−13.0	1.00
	γ-CH_3			3.7	−0.3	4.0	−3.25
Cu(HFA)$_2$	α-H[b]	3.000	0.0316		−2.6		
	β-H			−34.3	−1.5	−32.8	1.00
	γ-CH_3			9.5	−0.8	10.3	−3.18
Ni(AA)$_2$[a]	α-H			−10.00			0.28
	β-H			−2.78			1.00
	γ-CH_3			0.90			−3.09
Co(AA)$_2$[a]	α-H			−10.00		−10.00	0.30
	β-H			−0.88		−2.97	1.00
	γ-CH_3			4.61		1.17	−2.54

[a] Taken from ref 22. The isotropic shifts are expressed in relative magnitude giving the isotropic shift of the α proton equal to 10.00. [b] The α-proton signals in these concentrations are not observed. They can be observed at much lower M(chelate)$_2$ concentrations. [c] Pseudocontact shifts are estimated from eq 3, using the geometric factor found for Ni(AA)$_2$ (ref 22) and the experimentally found g anisotropy for Cu(AA)$_2$·4MePy, Cu(TFA)$_2$·4-MePy, and Cu(HFA)$_2$·(4-MePy)$_2$. The g anisotropy for Cu(AA)$_2$·4-MePy is taken from ref 14a. Furthermore, a formation constant of 2.0 (estimated from ref 6 and 8) for the reaction Cu(AA)$_2$ + 4-MePy = Cu(AA)$_2$·4-MePy in chloroform and 36° is used to calculate the P_c value of this system. [d] Isotropic shift corrected for pseudocontact shift to give contact shift. [e] The ratio of β-proton contact shift to that of the given proton contact shift.

Table II: Isotropic Shifts of 4-Methylpyridine N-Oxide Systems in $CDCl_3$ at 36°

M(chelate)$_2$	Ligand proton	Concn, M: Ligand	Concn, M: M(chelate)$_2$	$\Delta\nu_{obsd}$, Hz	Pseudocontact shift,[b] Hz	$\Delta\nu_{cor}$[c]	β ratio[d]
Cu(TFA)$_2$	α-H	1.00	0.0390	1.9	−0.2	2.1	−1.71
	β-H			−3.8	−0.2	−3.6	1.00
	γ-CH_3			−7.9	−0.1	−7.8	0.46
Cu(TFA)$_2$	α-H	2.00	0.0920	1.0	−0.3	1.3	−2.54
	β-H			−3.6	−0.3	−3.3	1.00
	γ-CH_3			−7.4	−0.1	−7.3	0.45
Cu(HFA)$_2$	α-H	1.00	0.0118	20.9	−0.1	21.0	−0.43
	β-H			−9.2	−0.1	−9.1	1.00
	γ-CH_3			−23.9	−0.1	−23.0	0.40
Cu(HFA)$_2$	α-H	2.00	0.0103	10.8	−0.1	10.9	−0.43
	β-H			−4.8	−0.1	−4.7	1.00
	γ-CH_3			−11.3	−0.1	−11.2	0.42
Ni(AA)$_2$[a]	α-H	2.33	0.097	95		95	−0.53
	β-H			−50		−50	1.00
	γ-CH_3			−119		−119	0.42
Co(AA)$_2$[a]	α-H	2.33	0.097	113	20	93	−0.52
	β-H			−28	20	−48	1.00
	α-CH_3			−100	11	−111	0.43

[a] Taken from ref 23. [b] Pseudocontact shifts are estimated from eq 3 using the geometric factor found in ref 23 and the experimentally obtained g anisotropy for Cu(TFA)$_2$·4-MePyO and Cu(HFA)$_2$·2(4-MePyO). [c] Isotropic shift corrected for pseudocontact shift to give contact shift. [d] The ratio of β-proton contact shift to that of the given proton contact shift.

Table III: Estimated Pseudocontact Shifts in Hz (for $P_c = 1$)

Complex	α-H	β-H	γ-CH_3
$Cu(AA)_2 \cdot 4\text{-MePy}$	−145	−81	−47
$Cu(TFA)_2 \cdot 4\text{-MePy}$	−113	−63	−36
$Cu(HFA)_2 \cdot 2(4\text{-MePy})$	−126	−71	−41
$Cu(TFA)_2 \cdot 4\text{-MePyO}$	−5	−6	−3
$Cu(HFA)_2 \cdot 2(4\text{-MePyO})$	−6	−7	−4

The fact that the isotropic shift changes sign when a methyl group is substituted at the γ position in pyridine or pyridine N-oxide suggests that the major contribution to the observed isotropic shifts in these copper complexes is the Fermi contact interaction. According to eq 3, if the pseudocontact interaction is dominant, then lines of protons with approximately the same geometric factor, $(1 - 3\cos^2 \Omega/R_i^3)$, would be shifted in the same direction. Furthermore, esr measurements of these copper chelates[16] and their 4-MePy and 4-MePyO adducts in chloroform have shown that the g anisotropy $(g_{||} - g_\perp)$ is about 0.3, so that one would not expect a large pseudocontact interaction in these copper complexes. However, as shown in Tables I and II, the relative contribution of the pseudocontact interaction is more important in those systems where the total isotropic shift is small.

Without knowing the exact geometry of these copper complexes, one cannot calculate exactly the correction for the pseudocontact shift. If one uses the geometric factors of the corresponding nickel(II) bisacetylacetonate complexes,[22,23] one can estimate the pseudocontact shifts of the copper complexes with the results listed in Table III. In Tables I and II, corrections for the pseudocontact interaction are included. It is clear that for the 4-MePyO adducts of $Cu(TFA)_2$ and $Cu(HFA)_2$, the pseudocontact contribution to the observed isotropic shifts may be neglected. However, in the 4-MePy adducts the pseudocontact contribution is appreciable, especially in the $Cu(AA)_2 \cdot 4\text{-MePy}$ complex.

The downfield shifts of α-H and β-H and the regular attenuation of the β-H and γ-CH_3 shifts in the 4-methylpyridine systems clearly indicate that unpaired electron spin density has been delocalized to the ligand *via* the σ-molecular orbitals of the 4-methylpyridine molecules. The upfield shift of the γ-CH_3 in this ligand indicates that there is negative spin density at this position, and the Fermi contact interaction reflects probably a σ–π correlation mechanism.[7] Delocalization of unpaired spin into the 4-methylpyridine ligand occurs *via* a σ mechanism, consistent with the fact that pyridine type ligands are poor recipients of π-electron density from transition metal ions, as found by infrared studies.[24] The pattern of the isotropic shifts, both in magnitude and sign, found in the 4-methylpyridine N-oxide systems is that of a typical conjugated aromatic system. This suggests that unpaired spin is delocalized into the ligand *via* the π-molecular orbitals of the 4-methylpyridine N-oxide molecule. Recently, Byers, *et al.*,[25] have reported that the lowest energy M → L charge transfer band of the essentially octahedral copper–pyridine N-oxide complex arises from an $e_g \rightarrow \pi^*$ transition. In tetragonally distorted octahedral adducts of $Cu(TFA)_2 \cdot 4\text{-MePyO}$ and $Cu(HFA)_2 \cdot (4\text{-MePyO})_2$, the unpaired electron resides in the e_g orbital; thus, the $e_g \rightarrow \pi^*$ charge-transfer process may well account for the observed isotropic shifts.

A qualitative comparison can be drawn between the magnitude of the isotropic shifts and the tendency for adduct formation in these copper chelates. Thus, from the equation $\Delta\nu_{obsd} = \Delta\nu_c P_c$[26] (where $\Delta\nu_{obsd}$ is the observed contact shift, after correction of pseudocontact shift, and $\Delta\nu_c$ is a "unit" contact shift), the contact shifts of the 4-methylpyridine complexes at 36° are found to be (for the β-H of 4-MePy): −101 Hz, −1190 Hz, and −1506 Hz for $Cu(AA)_2 \cdot 4\text{-MePy}$, $Cu(TFA)_2 \cdot 4\text{-MePy}$, and $Cu(HFA)_2 \cdot 2(4\text{-MePy})$ respectively. Similarly, unit contact shifts obtained for the γ-CH_3 proton of the 4-methylpyridine N-oxide complexes at 36° are −180 Hz for $Cu(TFA)_2 \cdot 4\text{-MePyO}$ and −1036 Hz for $Cu(HFA)_2 \cdot (4\text{-MePyO})_2$. In both 4-methylpyridine and 4-methylpyridine N-oxide complexes the magnitudes of the contact shifts lie in the order $Cu(HFA)_2 > Cu(TFA)_2 > Cu(AA)_2$. This order is the same as that for the stability constants for adduct formation found from spectrophotometric studies.[11,18] It is interesting to note that Garito and Wayland[7] have recently reported that in copper *t*-butylacetoacetate–pyridine type ligand complexes, the isotropic shifts increase as the basicity of the ligand is increased.

For a system in which the Fermi contact interaction is dominant, the isotropic shifts should vary linearly with the reciprocal of the absolute temperature, $1/T$, *i.e.*, shows a Curie law dependence. However, the temperature effects in these copper complexes are not all linear, as can be seen from Figures 4 and 5. We have found a correlation between the temperature effect and the stoichiometry of these copper complexes, although such a correlation is not obvious from *a priori* considerations. We have found (a) a normal temperature effect with six-coordinated bis adducts of $Cu(HFA)_2 \cdot 2(4\text{-MePy})$ and $Cu(HFA)_2 \cdot 2(4\text{-MePyO})$ throughout the temperature range of −50 to +50°, (b) an abnormal temperature effect, *i.e.*, the isotropic shifts increase as the temperature is increased, with five-coordinated mono adducts of $Cu(AA)_2 \cdot 4\text{-MePy}$ and $Cu(TFA)_2 \cdot 4\text{-MePyO}$, and (c) a nonlinear temperature effect, the isotropic shifts decreasing with in-

(24) W. D. Horrocks, Jr., and R. C. Taylor, *Inorg. Chem.*, 2, 723 (1963).

(25) W. Byers, B. Fa-chun Chou, A. B. P. Lever, and R. V. Parish, *J. Amer. Chem. Soc.*, 91, 1329 (1969).

(26) B. B. Wayland and R. S. Drago, *ibid.*, 87, 2372 (1965).

creasing temperature, but not varying linearly with $1/T$, in the system of $Cu(TFA)_2 \cdot 4\text{-MePy}$. As eq 1 implies, the hyperfine coupling constant, A, can be obtained from the linear plot of contact shift *vs.* $1/T$.

For the $Cu(HFA)_2 \cdot 2(4\text{-MePy})$ and $Cu(HFA)_2 \cdot 2(4\text{-MePyO})$ complexes, the calculated hyperfine coupling constants for γ-CH_3 are, respectively, $+3.0 \times 10^5$ Hz and $+7.7 \times 10^5$ Hz.

Kluiber and Horrocks[5] have reported a similar abnormal temperature effect for $Cu(TFA)_2 \cdot 4\text{-MePyO}$ complex. They have proposed that a five-coordinated complex of low symmetry or a tetrahedral four-coordinated complex (with the opening of one TFA ring) accounts for the observed temperature variation at elevated temperature (above 30°) for this complex. However, this model of Kluiber and Horrocks is not consistent with our results on the $Cu(HFA)_2$ complexes. $Cu(HFA)_2$ forms tetragonally distorted octahedral bis adducts with 4-methylpyridine and 4-methylpyridine N-oxide in chloroform solution. Since $Cu(HFA)_2$ is less stable than $Cu(TFA)_2$,[27] one would expect ring opening to be easier for $Cu(HFA)_2$ than $Cu(TFA)_2$ at elevated temperatures. The fact that $Cu(HFA)_2 \cdot 2(4\text{-MePy})$ and $Cu(HFA)_2 \cdot 2(4\text{-MePyO})$ show appreciable spin delocalization and a normal temperature effect is not consistent, then, with a tetrahedral species being present for $Cu(HFA)_2$ complexes. Thus, since this tetrahedrally coordinated complex does not occur for the $Cu(HFA)_2$ complexes, we think it even less likely to occur for the $Cu(TFA)_2$ complexes.

Acknowledgment. The authors thank Dr. A. Allendoerfer of the State University of New York at Buffalo for his assistance in obtaining the esr g values.

(27) L. G. Van Uitert, W. C. Fernelius, and B. E. Douglas, *J. Amer. Chem. Soc.*, **75**, 457 (1953).

A Cryoscopic Study of the Association of Phenolic Compounds in Benzene

by Nicholas E. Vanderborgh, Neal R. Armstrong, and W. Dale Spall

Department of Chemistry, University of New Mexico, Albuquerque, New Mexico 87106 *(Received June 12, 1969)*

The cryoscopic behavior of phenol, positional isomers of chlorophenol and cresol, and 2,5-, 2,6-, 3,4-, and 3,5-dimethyl phenol were studied in benzene, and equilibrium constants describing this behavior in terms of association were determined for the concentration range 0–0.8 *m*. The results indicate that substitution of a ring hydrogen of phenol by either chlorine or methyl decreases the amount of association of the parent phenol, chloro isomers having less association than methyl isomers. The degree of association is qualitatively related to the effects of the substituents on the π electron cloud of the phenyl ring.

The measurement of colligative properties of liquid solutions, those properties which depend upon the number and not the type of dissolved species, has long been recognized as an important method for the study of molecular association. Of the several colligative property techniques, one of the most accurate and experimentally simple is the depression of the freezing point, cryoscopy. Early workers studying this technique discovered that many organic solutes, when used to depress the freezing points of aprotic solvents, showed smaller freezing point depressions than would be predicted on the basis of their formula weights. The most commonly used explanations for this observed nonideal behavior are the formation of solid solutions, changes in activity coefficients with concentration, and molecular association.

Solid solution formation greatly complicates the interpretation of cryoscopic data. The existence of solid solutions may be detected either by chemical analysis of the frozen solid or by the method of Van Bijlert.[1] Compounds suspected of forming solid solutions or mixed crystals in benzene solutions include acetic acid[2-4] and phenol.[2,5,6] However, in these previous studies, the existence of solid solutions was not verified by chemical analysis. The usual method for correcting cryoscopic data for the effects of solid solu-

(1) A. Van Bijlert, *Z. Phys. Chem.* (Leipzig), **8**, 343 (1891).
(2) C. R. Bury and H. O. Jenkins, *J. Chem. Soc.*, 688 (1934).
(3) A. G. Milligan, *J. Phys. Chem.*, **33**, 1363 (1929).
(4) R. Marc and W. Wenk, *Z. Phys. Chem.* (Leipzig), **68**, 104 (1910).
(5) F. Garelli, *ibid.*, **21**, 122 (1896).
(6) J. A. Davison, *J. Amer. Chem. Soc.*, **67**, 222 (1945).

Table I: Reagents

Reagent	Symbol	Method of purification	Anal. of purity[d,e] Rel wt % major	Anal. of purity[d,e] H_2O wt %
Benzene	B	*a*	99.6	0.025
Naphthalene	N	*b*	99.9+	Not detectable
Biphenyl	BP	*c*	99.9+	Not detectable
Phenol	P	*a*	99.7	0.055
o-Cresol	OC	*a*	99.3	0.030
m-Cresol	MC	*a*	99.3	0.030
p-Cresol	PC	*b*	99.4	0.030
o-Chlorophenol	OCP	*a*	99.6	0.029
m-Chlorophenol	MCP	*a*	99.6	0.033
p-Chlorophenol	PCP	*c* and *b*	99.8	0.019
2,5-Dimethylphenol	25DMP	*b*	99.1	0.041
2,6-Dimethylphenol	26DMP	*b*	99.1	0.048
3,4-Dimethylphenol	34DMP	*b*	99.3	0.043
3,5-Dimethylphenol	35DMP	*b*	99.2	0.047

[a] Fractional distillation from Linde 4A molecular sieves; system flushed with dried and purified argon. [b] Fractional crystallization from benzene, vacuum dried. [c] Sublimation. [d] Glpc: 2-m Silicone Oil DE-710 on firebrick; T = 190° for phenols, T = 80° for benzene. [e] Error in major component analysis is ±0.5 wt %.

tion formation is the use of an expression of the form[7,8]

$$\Delta T = K_f C_0(1 - k)$$

where ΔT is the observed temperature lowering, K_f the freezing depression constant, C_0 the "observed concentration," and k is the distribution coefficient for the solute between the solid and liquid phases. Using an expression this form, Bury and Jenkins[2] report a value of 0.47 for k while Davidson[6] reports a value of 0.41 for solutions of phenol in benzene.

Even though the existence of solid solutions is suspected, it is not reasonable to interpret cryoscopic data solely on this basis for systems which might show other causes for nonideal behavior. Phenolic solutions in benzene show infrared spectra characteristic of hydrogen bonded systems and the nonideal cryoscopic behavior should be, in part, attributed to association. Deviation from ideal solution behavior for these systems may also be due to activity effects. Several theories for the determination of activity coefficients of nonelectrolytes in nonaqueous media have been put forth; the one derived from the normal theory of liquids[9] is perhaps the most used. These theories are generally unsatisfactory in explaining the data since quite large activity corrections are necessary. For example, phenol has been reported to have an activity coefficient of less than 0.3 at 0.5 *m* benzene solution.[10]

Another cause for nonideal behavior may be loosely classified as molecular association. The solute may associate with itself, the solvent, or with impurities present. In this investigation, equilibrium constants for the self-association of phenol (P), orthocresol (OC), metacresol (MC), paracresol (PC), orthochlorophenol (OCP), metachlorophenol (MCP), parachlorophenol (PCP), 2,5-dimethylphenol (25DMP), 2,6-dimethylphenol (26DMP), 3,4-dimethylphenol (34DMP), and 3,5-dimethylphenol (35DMP) are reported in the solvent benzene. Infrared spectra of these compounds in benzene solution are accepted as showing hydrogen bonding;[10] it is assumed that self-association of the phenols is the cause of this spectral behavior.

The formation of solid solutions of phenol in benzene has also been investigated. In this investigation we shall assume that the cryoscopic data can be explained solely on the basis of molecular association after the effects of possible solid solution formation have been explored.

Experimental Section

Reagents. The chemicals used for this study as well as the method of purification and analyzed purity are shown in Table I.

Apparatus. The apparatus used for these investigations was designed to measure the freezing points of solutions at millimolal and higher concentrations using a procedure to maximize accuracy and to minimize time spent in data collection. The test solution was maintained under an atmosphere of dried argon at all times. Stirring was accomplished by a Teflon disk stirrer driven at 600 rpm by a synchronous motor. The apparatus was sealed except when solution concentrations were changed. (See Figure 1.)

A Veco 51A1 100,000-ohm thermistor was used as

(7) S. Glasstone, "Textbook of Physical Chemistry," 2nd ed, Van Nostrand–Reinhold Co., Inc., Princeton, N. J., 1949, p 649.

(8) See ref 7, p 650.

(9) G. N. Lewis and M. Randal, revised by Pitzer and Brewer, "Thermodynamics," 2nd ed, McGraw-Hill Publications, New York, N. Y., 1961, chapter 20.

(10) G. C. Pimentel and A. L. McClellan, "The Hydrogen Bond," W. H. Freeman and Co., San Francisco, Calif., 1960.

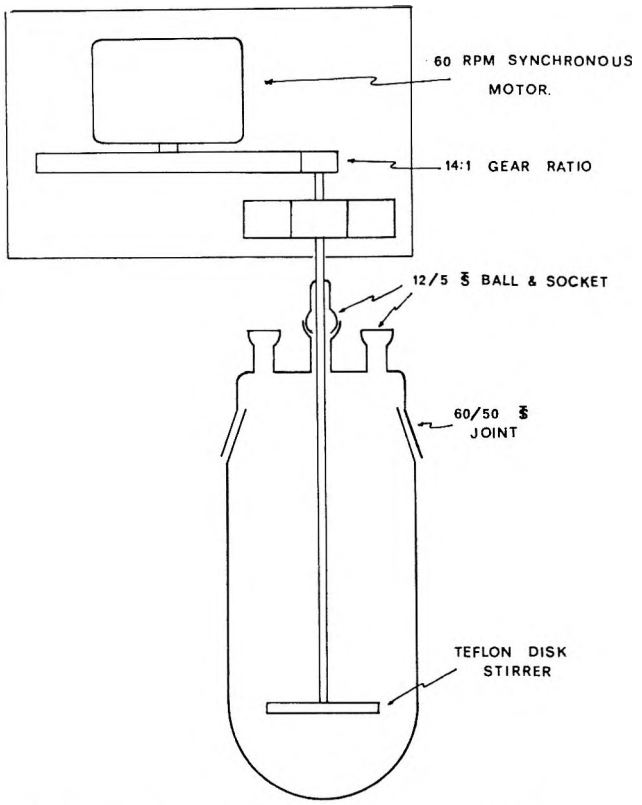

Figure 1. Cryoscopic cell assembly, constructed from Pyrex, described in text.

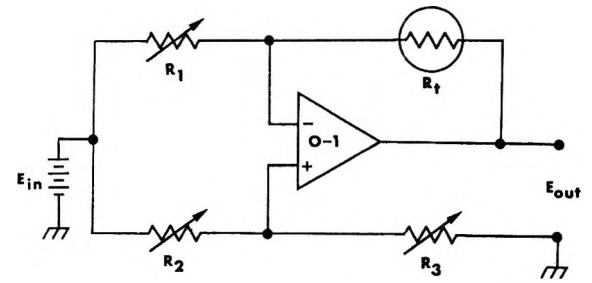

Figure 2. Temperature measuring circuit; E_{in} = 1.35 V Mallory mercury battery; $R_1 = R_2 = R_3$ = 500,000-ohm cermet trimpot, R_f = 100,000 ohm Veco 51A1 thermistor; O-1, Fairchild ADO-44, operational amplifier.

the temperature sensing device with the measuring circuit shown in Figure 2. The apparatus shown is capable of an output sensitivity of approximately 150 mV/deg C and can detect 0.001° changes in temperature under the conditions used in this study. Use of the full sensitivity of this circuit would allow investigation of 2.5×10^{-4} *m* solutions. Operating conditions were such that approximately a 2° change in the temperature corresponded to maximum response. Discussion of the measuring circuit may be found elsewhere.[11]

Experimental Procedure

The apparatus was carefully cleaned and dried in a vacuum oven (110°) before use. A weighed charge of pure solvent was placed in the cell, a blanket of argon introduced, and the solvent benzene frozen by raising a constant temperature bath (0°) into position. The cooling curve was recorded on a recorder. After melting the benzene frozen during the initial determination, a known volume of a solution of known composition of the solute in benzene was introduced and the freezing curve for this solution determined. Repeated additions allowed the measurement of the cryoscopic solution behavior throughout the desired concentration range.

Solid Solution Studies. Benzene solutions of phenol, *o*-chlorophenol, and *p*-cresol were prepared by weight, maintained under dry argon, and while vigorously stirred partially frozen by emersion of the flask containing the solution into a bath maintained at 2°. The partially frozen solution was then transferred under an argon layer into a refrigerated Hirsch funnel and the liquid fraction separated. The remaining solid was washed with 5.0 ml of 6° benzene; these washings were added to the liquid fraction and the total volume noted. The collection vessel was then changed, the solid allowed to melt, and collected. Analyses of the resulting solutions were made on a Varian Auto-Prep gas chromatograph. The analytical results were compared to results obtained with standard solutions of the same compounds. From these measurements, the value for the distribution coefficient for each solute was determined. Concentration values for the liquid fraction were corrected for dilution by the 5.0-ml wash fraction of benzene.

Experimental Error

An error analysis showed the average error in the analytical solution concentrations was ±0.5% and 1.0% in the cryoscopically observed concentration. Maximum error occurred in the lowest analytical concentrations studied, below 100 m*m*, where the error in CA was from ±0.8 to 1.0% and the corresponding error in CO was from ±2.0 to 3.0%. The measuring circuit was calibrated by comparison with thermometers traceable to the National Bureau of Standards.

Results

Determination of the Cryoscopic Constant of Benzene. Cryoscopic techniques require a known relationship between the observed freezing point lowering and the concentration of a species known to behave ideally in the solvent under study. If such ideal behavior has not been reported, a "reference compound" may be selected and all concentrations can be related to this standard. In this study, naphthalene and biphenyl were chosen as the nonassociated standards. Biphenyl is known to be nearly ideal in benzene solu-

(11) "Handbook of Operational Amplifiers," Burr-Brown Research Corp., Tucson, Ariz., 1960, p 30.

tions;[12] positive deviations from Raoult's law for the liquid-vapor equilibrium are less than 2% at relatively low concentrations. The freezing points of a series of solutions of naphthalene and biphenyl were determined; the value of K_f determined with either compound was 5.112°C/m, in good agreement with 5.070 reported by Barton and Kraus,[13] 5.122 by Bury and Jenkins,[2] 5.10 by Peterson and Rodebush,[14] 5.12 from latent heat of fusion by Huffman, Parks and Daniels,[15] and 5.11 by Auwers,[16] but differing with the value of 5.492 reported by White and Kilpatrick.[17] When using the apparatus shown, the output of the temperature measuring circuit was linear with concentration of the standard species to within 0.0091 σ unit with an intercept of 6×10^{-3}°, less than experimentally observable. The apparent linearity of data is attributed to a fortuitous cancellation of the nonlinear response of the temperature-measuring device with the change of K_f with temperature.

Interpretation of Experimental Data

The experimental data determined must be examined in terms of association since reliable theories of nonelectrolyte activity are nonexistent. As has been pointed out succinctly by Rossotti and Rossotti,[18] association data of this sort result in essentially two equations with n unknowns, a problem which may in theory be solved; however, experimental error usually makes the set of equations ill-conditioned. Attempts to increase the number of equations available for data analysis results in fixing some arbitrary relationship between successive equilibrium constants for the associative reaction. Notable contributions on this line have been made by Lassettre,[19-21] Dunken,[22,23] and Bejerrum,[24] modified by Fronaeus.[25] A second approach is based on the minimization of undetermined thermodynamic functions and on statistical curve fitting.[26,27]

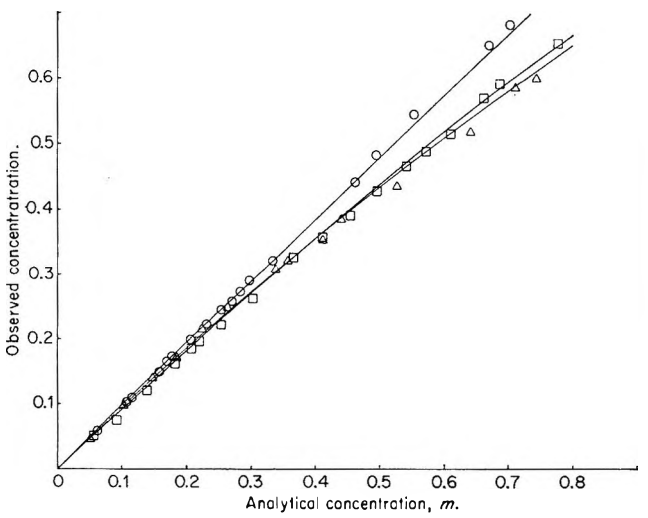

Figure 3. Cryoscopic behavior of the chlorophenols. Observed concentration (m) *vs.* analytical concentration; line calculated from equilibrium constants shown in Table II; O, OCP; □, MCP; △, PCP.

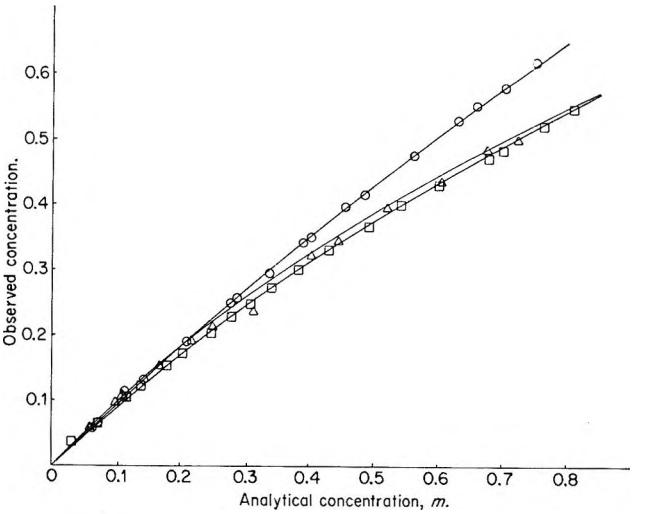

Figure 4. Cryoscopic behavior of cresols and phenols. Observed concentration (m) *vs.* analytical concentration; line calculated from equilibrium constants shown in Table II; O, OC; □ MC; △, PC.

The relationship of CO, the "observed concentration" determined from the apparent freezing point depression, to CA, the "analytical concentration," for the compounds used in this investigation is shown in Figures 3–6. Figures 3 and 6 include the data of Davison and those of Bury and Jenkins for purposes of comparison. Table II lists equilibrium constants determined by curve fitting, those determined by Lassettre's method, as well as those previously reported.

(12) Laszlo and Szabados, *Kozp. Fiz. Kut. Intez., Kozlem*, **15**, 283 (1967).

(13) B. C. Barton and C. A. Kraus, *J. Amer. Chem. Soc.*, **56**, 2017 (1934).

(14) J. M. Peterson and W. H. Rodebush, *J. Phys. Chem.*, **32**, 709 (1928).

(15) H. M. Huffman, G. S. Parks, A. C. Daniels, *J. Amer. Chem. Soc.*, **52**, 1547 (1930).

(16) K. Auwers, *Z. Phys. Chem.*, **42**, 513 (1902).

(17) N. E. White and M. Kilpatrick, *J. Phys. Chem.*, **59**, 1044 (1955).

(18) (a) F. J. C. Rossotti and H. Rossotti, "The Determination of Stability Constants," McGraw-Hill Publications, New York, N. Y., 1961; (b) F. J. C. Rossotti and H. Rossotti, *J. Phys. Chem.*, **65**, 926 (1961).

(19) E. N. Lassettre, *Chem. Rev.*, **20**, 259 (1937).

(20) E. N. Lassettre, *J. Amer. Chem. Soc.*, **59**, 1383 (1937).

(21) E. N. Lassettre and R. G. Dickinson, *ibid.*, **61**, 54 (1939).

(22) H. Dunken, *Z. Phys. Chem.*, **45B**, 201 (1940).

(23) K. L. Wolf, H. Dunken, and K. Merkel, *Z. Phys. Chem.* (Leipzig), **46B**, 287 (1940).

(24) J. Bjerrum, *Kem Maanedsbl. Nord. Handelsblad Kem. Ind.*, **24**, 21 (1943).

(25) S. Fronaeus, "Komplexsystem hos Koppar," Dissertation, University of Lund, 1948.

(26) F. J. Zlesnik and S. Gordon, *Ind. Eng. Chem.*, **60**, 27 (1968).

(27) A. Pullman and H. Berthod, *Theor. Chim. Acta*, **10**, 461 (1968).

Table II: Summary of Cryoscopically Determined Equilibrium Constants for the Association of Phenolic Compounds in Benzene

		Equil const for assocn					
		This investigation					
		By curve fitting		By method of Lassettre		Previously repd	
Compd	∇ % assocd[a]	K_{12}	K_{13}	K_{12}	K_{13}	K_{12}	Ref
PB	84.75	125	450	0.556	0.190	61	32
34DMP	21.81	0.30	2.1	0.653	0.640		
35DMP	19.35	0.20	2.0	0.556	0.464		
25DMP	31.95	0.47	*b*	0.309	0.143		
26DMP	14.51	0.17	*b*	...	...		
OC	16.27	0.58	*b*	0.18	0.14	1.1	3
						0.28	19
MC	23.18	0.50	1.80	0.578	0.955		
PC	18.96	0.30	1.60	0.675	0.595	1.1	3
						0.42	19
OCP	9.09	0.10	*b*	0.006	0.004		
MCP	31.51	0.46	*b*	0.168	0.04		
PCP	35.49	0.55	*b*	0.242	0.09		

[a] ∇ = % associated, defined in text. [b] $K_{13} < 0.01$.

The equilibrium constants shown in Table II were determined by a curve-fitting technique. A series of CA *vs.* CO curves were generated using incremented values of monomer concentration and overall equilibrium constants. The experimental data were then displayed graphically and the resulting curves overlayed on the various calculated curves to achieve a "best fit." Criteria for "best fit" were that the deviations of the experimental points from the calculated curves were a minimum, the same order of magnitude as the experimental error, and that the least number of equilibrium constants necessary to describe the data were used. This leads to the simplest model to adequately explain the experimental data. To obtain a reasonable value of the initial dimerization constant, the data obtained for low analytical concentrations were used since the contribution of higher order polymers to CO, the observed concentration, should be small; the initial part of the CO–CA curve, then, was used to evaluate the dimerization association equilibrium constant. Once this was done, this constant was used to evaluate the trimerization constant. In no cases were association constants higher than the trimerization necessary. This approach is generally similar to that often used for the determination of successive formation constants of complex ions.[18]

Also shown in Table II is the function ∇, the per cent of association, evaluated at an analytical concentration of 0.5 *m*. ∇ = concentration of all associated species × 100 divided by the concentration of all species; ∇ = (CO − $C_{monomer}$)100)/(CO). The monomer concentration was obtained from solution of the equation relating

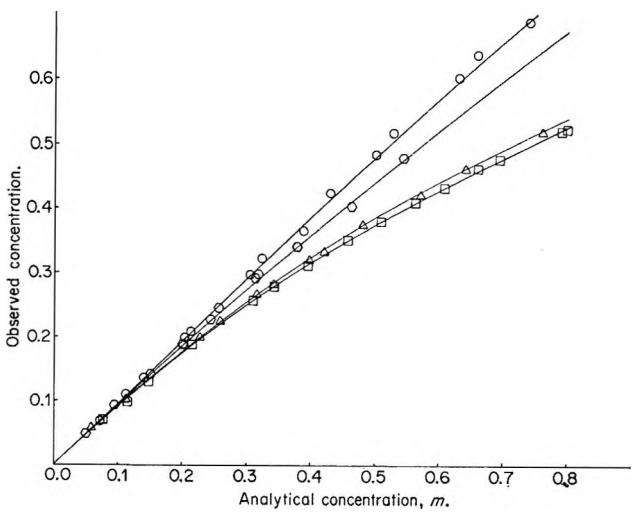

Figure 5. Cryoscopic behavior of dimethylphenols. Observed concentration (*m*) *vs.* analytical concentration; line calculated from equilibrium constants shown in Table II. ○, 2,6-; ○, 2,5-; □, 3,4-; △, 3,6-.

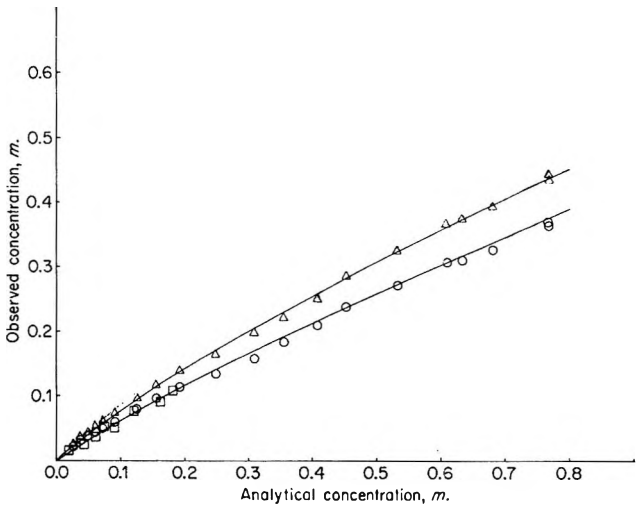

Figure 6. Cryoscopic behavior of benzene solutions of phenol. Observed concentration (*m*) *vs.* analytical concentration; ○, this investigation; □, Bury and Jenkins: △, corrected for solid solution formation.

CO to the monomer concentration through the equilibrium constants.

If a large concentration range is studied and the resulting data are used to determine equilibrium constants, corrections for the temperature dependence of these constants may be necessary since the measurements are not isothermal. In theory, this effect may be used to predict thermodynamic parameters[9] derived from the van't Hoff equation. For phenolic systems in benzene, these deviations of the equilibrium constants with temperature are limited by values of ΔH for the associative reaction.[10] Calculations based on an average value of ΔH for OH··O hydrogen bonds indicate that for observed concentrations of 0.5 *m*, only 5% change in the equilibrium constants results from these effects. Since the highest observed concentrations found in this investigation were of this magnitude, the temperature dependence effects should introduce error of no greater than 5%.

Table II also includes the results obtained by analysis of our data using the method described by Lassettre.[19-21] This approach assumes three possible functional forms for the relationship between CO and CA; two of these describe a hyperbole and one a quadratic. When the proper relationship has been selected, the maximum number of equilibrium constants is determined by the degree of experimental error. Using the equilibrium constants obtained from this method, we attempted to reconstruct our experimental data. It was found that the reconstruction required a greater number of equilibrium constants than the experimental error indicated were significant. Sillén[28] and Rossotti and Rossotti[18] have pointed out that the precision of measurements as well as computational errors introduced by smoothing of experimental error seldom justifies more than three independent parameters. The errors introduced by forcing the data to conform to a predetermined function may actually increase the overall error. In a similar data analysis, Sillén[28] introduced a graphical curve-fitting procedure which has been expanded in an attempt to reduce the error. We feel that the curve for fitting technique which we have described allows more latitude in suggesting a model than does an explicit solution.

It has been reported previously[2,5,6] that phenol forms solid solutions with benzene. It was therefore necessary to investigate the extent of this solid solution formation. The results of these studies are shown in Table III. Ir data indicate that OCP is slightly associated,[10] in agreement with our cryoscopic studies. It is therefore reasonable to assume that the partition coefficient determined for OCP is one which results from a residual absorption and occlusion with the solid phase and not from solid solution formation. Due to the observed partition coefficient for PC, a similar conclusion results even though the cryoscopic behavior of PC is indicative of considerably increased association. OCP and PC were chosen as reference compounds due to their structural similarity to phenol. Both show partition coefficients of 0.19 ± 0.08; this value is taken as representative of absorption and occlusion effects.

No attempt to utilize the Van Biljert method was made since it was felt that addition of a third component to the cryoscopic solution could alter the solvent properties, or, more importantly, alter the extent of solid solution formation. The average value of the partition coefficient of OCP and PC was subtracted from the observed value for phenol, 0.36, to yield a partition coefficient of 0.17 for phenol corrected for surface absorption and occlusion inherent in this procedure. Using this corrected value, the cryoscopic data were then corrected for the effects of solid solutions. These data are shown in Figure 6 and equilibrium constants are included in Table II.

Table III: Solid Solution Analysis of Benzene Solutions

Solute	Concn			
	Original[a]	Liquid phase[b,c]	Solid phase[b]	k[d]
o-Chlorophenol	0.257	2.99	0.57	0.189
p-Cresol	0.263	2.99	0.54	0.179
	0.258	2.88	0.58	0.200
Phenol	0.267	2.64	0.92	0.349
	0.481	6.00	2.04	0.340
	0.797	7.59	2.93	0.386

[a] *m*. [b] Wt %. [c] Corrected for dilution. [d] Apparent distribution coefficient, solid:liquid.

Discussion

Phenolic compounds are thought to self-associate in solution because of the favorable difference in energy between the associated and monomeric forms. This energy difference is termed the delocalization energy; a significant fraction of this difference is due to the hydrogen bond. Theories of hydrogen bonding predict that several factors contribute to the total energy of the bond. The differences in magnitude of these factors in different systems have made the complete description of the hydrogen bond difficult. Hydrogen bonding has been extensively studied using various spectral techniques. Ultraviolet methods indicate varying degrees of π cloud interactions while infrared methods indicate varying amounts of hydroxyl interactions in the phenolic compounds under study.[10] Recent theoretical studies[27,29-31] show π interactions may arise in several ways and may contribute to the stability of the asso-

(28) L. G. Sillén, *Acta Chem. Scand.*, **10**, 186 (1956).

(29) S. Bratoz, *Advan. Quantum Chem.*, **3**, 207 (1967).

(30) K. Morokumo, H. Kato, T. Yonezawa, and K. Fukui, *Bull. Chem. Soc. Jap.*, **38**, 1263 (1965).

(31) A. Ocvirk, H. A. Zuman, and D. Hadji, *Theor. Chem. Acta* (Berl), **10**, 187 (1968).

Table IV: Selected CA and CO Values: Cryoscopic Data; CA, Analytical Concentration, *m*; CO, Cryoscopically Observed Concentration, *m*

Phenol		CO′ cor for solid soln	*o*-Chlorophenol		*m*-Chlorophenol		*p*-Cresol		2,6-Xylenol		2,5-Xylenol	
CA	CO		CA	CO	CA	CO	CA	CO	CA	CO	CA	CO
0.0261	0.0216	0.0260	0.0616	0.0593	0.0552	0.0510	0.0587	0.0570	0.0724	0.0683	0.0941	0.0907
0.0382	0.0305	0.0367	0.1073	0.1021	0.0932	0.0748	0.0993	0.0961	0.1124	0.1088	0.1058	0.1004
0.0498	0.0368	0.0443	0.1207	0.1151	0.1082	0.0973	0.1157	0.1104	0.1407	0.1353	0.1518	0.1395
0.0608	0.0432	0.0520	0.1578	0.1495	0.1390	0.1199	0.1682	0.1519	0.2053	0.1981	0.1710	0.1646
0.0714	0.0495	0.0596	0.1697	0.1650	0.1591	0.1424	0.2193	0.1899	0.2137	0.2079	0.2011	0.1842
0.0912	0.0584	0.0704	0.1773	0.1685	0.1822	0.1602	0.2503	0.2101	0.3056	0.2958	0.2439	0.2233
0.1262	0.0800	0.0964	0.2062	0.1994	0.2081	0.1840	0.3152	0.2635	0.3244	0.3210	0.2566	0.2400
0.1562	0.0953	0.1148	0.2317	0.2231	0.2218	0.1958	0.4033	0.3228	0.3891	0.3642	0.3135	0.2889
0.1927	0.1143	0.1377	0.2528	0.2434	0.2552	0.2219	0.4467	0.3442	0.4317	0.4228	0.3179	0.2930
0.2494	0.1329	0.1601	0.2715	0.2587	0.3030	0.2635	0.5230	0.3964	0.5013	0.4843	0.3780	0.3377
0.3091	0.1567	0.1888	0.2839	0.2730	0.3662	0.3264	0.6050	0.4379	0.5289	0.5164		
0.3545	0.1828	0.2202	0.2977	0.2908	0.4107	0.3572	0.6763	0.4866	0.6306	0.6015		
0.4077	0.2089	0.2517	0.3340	0.3216	0.4535	0.3928	0.7234	0.5020	0.6588	0.6378		
0.4508	0.2374	0.2860	0.4614	0.4439	0.4948	0.4273			0.7413	0.6880		
0.5326	0.2706	0.3260	0.4937	0.4842	0.5412	0.4652			0.7725	0.7466		
0.6091	0.3062	0.3689	0.5538	0.5459	0.5730	0.4902						
0.6317	0.3098	0.3733	0.6037	0.5815	0.6111	0.5175						
0.6809	0.3264	0.3933	0.6681	0.6527	0.6615	0.5720						
0.7672	0.3610	0.4349	0.7022	0.6836	0.6870	0.5934						
0.7661	0.3691	0.4447			0.7779	0.6551						

p-Chlorophenol		*o*-Cresol		*m*-Cresol		3,4-Xylenol		3,6-Xylenol	
CA	CO	CA	CO	CA	CO	CA	CO	CA	CO
0.0480	0.0463	0.0635	0.0570	0.0315	0.0368	0.0754	0.0697	0.0438	0.0418
0.0958	0.0950	0.0735	0.0635	0.0711	0.0653	0.1142	0.0963	0.0581	0.0558
0.1485	0.1389	0.1239	0.1128	0.1391	0.1222	0.1470	0.1284	0.0851	0.0809
0.1835	0.1721	0.1437	0.1306	0.1796	0.1531	0.2150	0.1842	0.1128	0.0990
0.2247	0.2160	0.2109	0.1899	0.2041	0.1721	0.3100	0.2540	0.1644	0.1437
0.2642	0.2492	0.2776	0.2469	0.2463	0.2018	0.3415	0.2749	0.2283	0.1967
0.3386	0.3086	0.2883	0.2587	0.2800	0.2279	0.3946	0.3098	0.2593	0.2233
0.3567	0.3204	0.3381	0.2955	0.3104	0.2492	0.4566	0.3489	0.3171	0.2651
0.4123	0.3537	0.3910	0.3442	0.3428	0.2730	0.5079	0.3768	0.3445	0.2791
0.4400	0.3869	0.4557	0.3988	0.3836	0.3026	0.5617	0.4061	0.3937	0.3182
0.5273	0.4356	0.4853	0.4178	0.4310	0.3323	0.6077	0.4312	0.4215	0.3307
0.6431	0.5222	0.5627	0.4795	0.4932	0.3679	0.6582	0.4605	0.4808	0.3726
0.7100	0.5887	0.6330	0.5329	0.5427	0.4023	0.6963	0.4745	0.5238	0.3935
0.7443	0.6005	0.6591	0.5554	0.6012	0.4320	0.7888	0.5191	0.5711	0.4187
		0.7031	0.5839	0.6708	0.4724	0.7998	0.5219	0.6405	0.4605
		0.7512	0.6231	0.7014	0.4866	0.9410	0.5861	0.7616	0.5164
				0.7646	0.5246				
				0.8120	0.5519				

ciated phenolic species much more than was originally believed.

Initial theories to explain the hydrogen bond used a purely electrostatic approach; these have been shown to be less than completely adequate.[10] However, an electrostatic parameter might be quite successful to predict trends of associative behavior within a group of chemically similar compounds, especially if one particular compound can be selected as an arbitrary reference. A logical choice for such a reference compound among the compounds reported in this work might be the unsubstituted basis compound, phenol. Phenol is the most associated of all the compounds investigated, exhibiting a cryoscopic behavior quite similar to that of the carboxylic acids. Properties of phenol such as the dielectric constant, dipole moment, aqueous pK_a, and absorption spectra are not dissimilar to that of the substituted phenols. This study indicates that addition of a substituent to phenol lowers the degree of association, analogous to the cryoscopic behavior of benzoic acid and its substituted analogs; benzoic acid is also the most highly associated.[10] For these reasons, phenol cannot be taken as a reference point.

For the compounds investigated in this study, the methyl derivatives are more highly associated than the corresponding chloro compounds. From the extent of association of the cresols, as well as that of the chloro substituted compounds, one is led to the conclusion that

charge density of the carbon atoms *ortho* to the hydroxyl group is qualitatively related to the extent of association; increasing this charge density leads to the increasing association while decreasing the charge density leads to the opposite effect, on a relative basis. The order of decreasing association for an *ortho–para* directing substituent would then be *meta, para, ortho*. For a substituent that directs *meta*, the order would be *para, ortho, meta*. The low extent of association of the *ortho* isomers has been attributed to steric effects;[31–34] recent work, however, indicates the effect may be primarily a resonance or electrical one.[35] In either case, the degree of association for *ortho*-substituted phenols is less than would be predicted on the basis of association exhibited by *meta* and *para* isomers.

Greater complexity is observed with the dimethyl phenols. If the above assumption is correct and the effects are additive, a dimeta (3,4-) substitution should show the highest extent of association followed in order of decreasing association by *meta–para* (3,4-), *ortho–meta* (2,5-, then 2,3-), *ortho–para* (2,4-) and the least associated should be the *ortho–ortho* compound (2,6-). Furthermore, one would expect the 3,5-isomer to be slightly more associated than the *meta* compound, the 3,4-isomer slightly more than the *para* compound, and the 2,3- and 2,5-isomers to both be more associated than the *ortho* compound. The 2,6-isomer should show a small extent of association. On this basis, one would expect phenol to exhibit an association intermediate to the chloro and methyl substituted phenols. Clearly, phenol is more highly associated than either. The effects of solid solution formation upon observed cryoscopic data are large and thus a relatively small error in the determination of the distribution coefficient, k, can markedly influence the data. However, a distribution coefficient considerably greater than that reported here would be necessary to yield the expected behavior.

The general trends predicted above are shown by the data in Table IV with the sole exception of the reversal of the expected behavior of the *meta* and *para* isomers of chlorophenol. Calculations are now in progress to evaluate the net charge densities of the carbon atoms *ortho* to the hydroxyl group; these might help to place the above observations on a more quantitative basis and, hopefully, help explain the anomaly noted in the two isomers of chlorophenol.

Acknowledgment. This work was supported by the United States Atomic Energy Commission.

(32) M. Davies, *Trans. Faraday Soc.*, **36**, 333 (1940).
(33) M. Davies, *ibid.*, **34**, 410 (1938).
(34) M. Davies, *ibid.*, **34**, 1427 (1938).
(35) M. Charton and B. I. Charton, *J. Org. Chem.*, **33**, 3872 (1968).

Entropies of Transfer of Amino Acids from Water to Aqueous Ethanol Solutions

by Charles H. Spink and Michael Auker

Department of Chemistry, State University College—Cortland, Cortland, New York 13045 *(Received August 21, 1969)*

Heats of solution of the amino acids, glycine, DL-alanine, DL-α-aminobutyric acid, and L-valine, have been measured in water and in aqueous ethanol solutions. The results have been combined with published free energy data to obtain the entropies of transfer of the amino acids from water to the alcohol–water mixtures. The transfer entropies suggest that the amino acids cause a breakdown of structure in the mixed ethanol–water solvent, largely a result of perturbation by the highly polar zwitterion portion of the molecule. The effect of the side chains is to produce order in proportion to the size of the side chain, and the ordering effect is greater in water than in the mixed-solvent systems.

Introduction

There is considerable interest in aqueous solutions of the lower aliphatic alcohols because of their unique structural relationship to pure water.[1] As a solvent system, aqueous alcohol solutions have remarkable effects on the behavior of solute molecules, causing specific changes as solvent composition is changed in equilibrium properties and the rates of reactions involving the solute.[2] Biochemical interest in aqueous alcohol solutions has centered around the denaturing effects on proteins of the highly aqueous mixtures.[3]

Franks[1] has reviewed studies of the thermodynamic behavior of solutes in aqueous alcohol solvents. The data have led to suggestions regarding the structure of the solvent systems as well as the effect of solute on the properties of the solutions. For instance, the free energy of transfer of electrolytes from water to aqueous alcohol solutions generally shows an increase with increasing alcohol concentration, which is largely determined by progressively decreasing entropy term. The entropy decrease has been explained as a result of the ordering effect that the ionic fields of the electrolyte have in the mixed solvent.[4] However, the situation is complicated in the dilute alcohol region since the transfer enthalpy shows an endothermic maximum at about 0.1 mole fraction alcohol.

For the transfer of nonelectrolytes from water to aqueous alcohol the situation is somewhat different.[1,2,5] The transfer free energy usually decreases (though rather slightly) with increasing alcohol concentration. The decrease is a result of an increasing entropy contribution and corresponding enthalpy increase. Again the dilute alcohol region is more complex with most nonelectrolyte solutes showing endothermic maxima in the transfer enthalpies in the vicinity of 0.1–0.2 mole fraction alcohol.[2] The complexities in dilute alcohol solutions (0–0.2 mole fraction alcohol) have been explained as due to solution structure breaking that the solute imposes on the rather highly structured alcohol–water mixtures.[2] Both electrolytes and nonelectrolytes cause the structure breaking to occur, but electrolytes generally cause less change due to the compensating ordering of structure by the ionic fields.[1] For example, the entropy of transfer of KCl from water to aqueous methanol solutions is negative, even in the more dilute region,[1] while the transfer entropies for argon from water to aqueous ethanol are rather large and positive in this region.[5]

An interesting class of solutes is the amino acids, which are highly polar, but structurally contain differing nonpolar side chains. It would thus be of interest to know for this group of solutes whether the polar character of the zwitterion is dominating or whether the nonpolar side chain predominates in determining the thermodynamic transfer properties. Although transfer free energy data are available for the amino acids from solubility measurements,[6] there are no enthalpy data to allow a complete description of the basic transfer properties. Measurements of the heats of solution of several amino acid solutes in aqueous ethanol solutions are reported below in the region from pure water to 0.25 mole fraction ethanol. The results are discussed in terms of the competing effects of solute polarity and the general structure-breaking consequences of introduction of the solute into aqueous alcohol mixtures.

Experimental Section

The calorimeter used in making the thermochemical measurements was a 250-ml dewar flask fitted with a

(1) F. Franks and D. J. G. Ives, *Quart. Rev.*, **20**, 1 (1966).

(2) E. M. Arnett, *et al.*, *J. Amer. Chem. Soc.*, **87**, 1541 (1965).

(3) J. F. Brandts and L. Hunt, *ibid.*, **89**, 4826 (1967).

(4) R. W. Gurney, "Ionic Processes in Solution," McGraw-Hill Publications, New York, N. Y., 1953.

(5) A. Ben Naim and S. Baer, *Trans. Faraday Soc.*, **60**, 1736 (1964).

(6) J. P. Greenstein and M. Winitz, "Chemistry of the Amino Acids," John Wiley and Sons, New York, N. Y., 1961, p 547.

Table I: Heats of Solution of Amino Acids in Ethanol–Water Mixtures[a]

X_{EtOH}	Glycine	DL-Alanine	DL-α-Amino-butyric acid	L-Valine
0.000	3390 ± 50 (6)	2210 ± 40 (4)	1350 ± 30 (4)	740 ± 40 (5)
0.013	3560 ± 10 (2)	2450 ± 90 (5)	1630 ± 20 (2)	950 ± 30 (3)
0.034	4160 ± 160 (2)[b]	2830 ± 10 (2)	1980 ± 70 (4)	1310 ± 40 (3)
0.067	4310 ± 30 (3)	3300 ± 20 (3)	2670 ± 30 (2)	2260 ± 50 (3)
0.100	4790 ± 60 (3)	3870 ± 30 (3)	3190 ± 40 (4)	2970 ± 40 (3)
0.150	5050 ± 20 (2)	...	3840 ± 40 (2)	...
0.200	5090 ± 30 (5)	...	4020 ± 90 (4)	...
0.250	...	...	4150 ± 170 (3)	...
0.300	4860 ± 10 (3)	...	...	...

[a] Values are in cal/mol. Uncertainties are the standard deviation, and the number in parentheses is the number of measurements. [b] Mole fraction ethanol for this value is 0.050.

Teflon top that extended into the dewar to reduce dead space above the solution. A stirrer, thermistor sensor, calibration heater, and sample injection system were positioned in the Teflon cap. The thermistor probe formed one arm of a Sargent dc Wheatstone bridge (Model S81601), the output of which was fed to a Varian 1-mV recorder. Power for the calibration heater was provided by a Harrison Labs power supply (Model 6203A). Voltages across the 1-ohm standard resistor and the heater were measured with a Hewlett-Packard Model 741A differential voltmeter. The injection system was a polyethylene syringe, cut off at the bottom, holding a glass cup containing the sample, and a rubber plug to isolate the sample cup from the solution prior to injection.[2] To ensure control of the environmental temperature, the dewar flask was placed in a 25.00 ± 0.02° temperature bath.

Two electrical calibrations were made before and after each sample injection. Precision of the calibrations was on the average about ±0.6% relative standard deviation. The thermistor probe was calibrated so that the temperature in the dewar flask could be monitored. In this way injections could be made at 25.00°, usually within ±0.02°. The heat of injection of the syringe system was negligible for the levels of heat changes involved in the solution measurements. The calorimeter accuracy was determined by measuring the heat of solution of KCl in the dilution range from 2800 to 5200 mol of water per mol of solute. After correcting the measured values to infinite dilution, the average value was 4.14 ± 0.03 kcal/mol. This value compares well with 4.12 kcal/mol obtained by Gunn.[7]

The amino acid experiments were run by injecting from 1 to 5 mmol of amino acid into about 210 g of solvent. These relative amounts gave final concentrations of about 0.01 *m* amino acid in the solvent systems. The heats of solution of the amino acids are considered the values at infinite dilution because of the low concentrations involved. Repeat measurements in at least triplicate into the same solvent were not different from the first injection value within the experimental error.

The aqueous ethanol solvent mixtures were made up by volume from fractionally distilled, 95.6% water–ethanol azeotrope and from doubly distilled, CO_2-free water. Compositions were calculated from known density data for the mixtures. The amino acids were from Mann Research Labs (MA grade), and were dried at 45° *in vacuo* for at least 12 hr.

Results

Table I is a summary of the data for the heats of solution of glycine, DL-α-alanine, DL-α-aminobutyric acid, and L-valine in several aqueous ethanol solutions. The precision of the numbers is generally from 1 to 2% relative standard deviation and is limited to about ±40 cal/mol by the readability of the recorder deflections. Precision at mole fractions ethanol above 0.2 is not as good, especially with α-aminobutyric acid, because smaller samples and higher bridge sensitivities had to be used to compensate for slower rates of solution. The values for the heat of solution of glycine and DL-alanine in water agree well with previous work. Scheraga, *et al.*,[8] report 3410 and 2200 cal/mol for glycine and DL-alanine, respectively. His value of 1520 cal/mol for DL-α-aminobutyric acid was based on only one measurement.

Figure 1 shows explicitly the behavior of the enthalpy of transfer of the amino acids from water to the aqueous ethanol solutions. To about 0.1 mole fraction ethanol the transfer enthalpies increase linearly, the amino acids with larger nonpolar side chains showing steeper slopes. Above 0.1 mole fraction ethanol the glycine values level off, and at 0.2 mole fraction the enthalpies are decreasing. Although for α-aminobutyric acid the transfer enthalpy increases less sharply above 0.1 mole fraction ethanol, it does not reach a maximum value in the composition range studied.

In order to obtain transfer entropies, free energy data are required. Nozaki and Tanford have calculated

(7) S. R. Gunn, *J. Phys. Chem.*, 69, 2902 (1965).

(8) G. C. Kresheck, H. Schneider, and H. A. Scheraga, *J. Phys. Chem.*, 69, 3132 (1965).

transfer free energies for amino acids from water to urea solutions,[9] and from water to ethylene glycol solutions[10] from solubility data in these solvent systems. In the calculation of the free energy activity coefficient, data were required for the solutes in the mixed solvent systems. Since these data were not available, Nozaki and Tanford assumed that the activity coefficients of the amino acids in the mixed solvent were the same as in water at the same molality of solute. It was found that the activity coefficient term contributed only slightly to the overall transfer free energy, being almost at the expected experimental error in the measurements. Because of the lack of data on the activity coefficients, and because the magnitude of the activity coefficient correction seems small, we have calculated the free energy from the solubility, $\Delta G_t = RT \ln (N_{aq}/N_{alc})$, where the N's are the solubilities in water and in aqueous ethanol solutions, using the mole fraction concentration scale.[6] These data are plotted in Figure 2. From the smoothed curve of the free energy data and from the transfer enthalpies obtained above, it is possible to calculate the transfer entropies. Figure 3 shows values of $T\Delta S_t$ as a function of mole fraction ethanol in the solvent for the amino acids studied.

Summarizing the free energy data, the transfer values all increase steadily in the solvent composition range

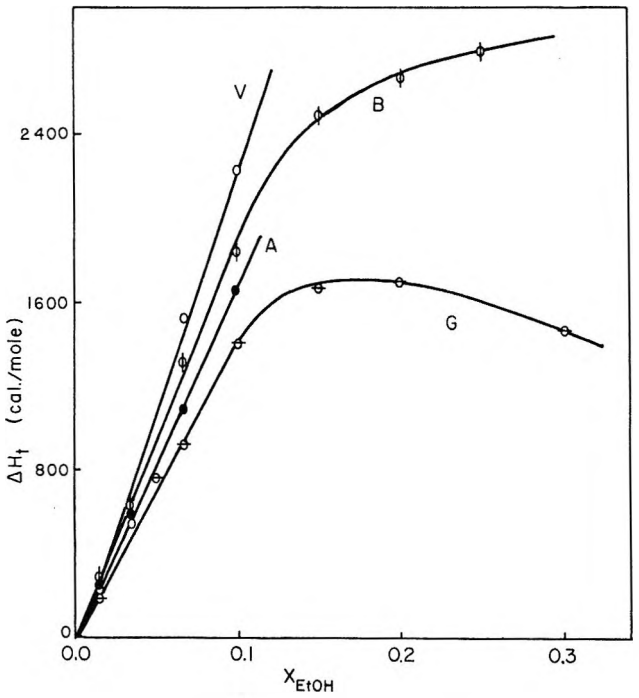

Figure 1. Enthalpy of transfer of glycine (G), DL-alanine (A), DL-α-aminobutyric acid (B), and L-valine (V) from water to aqueous ethanol solutions at 25°.

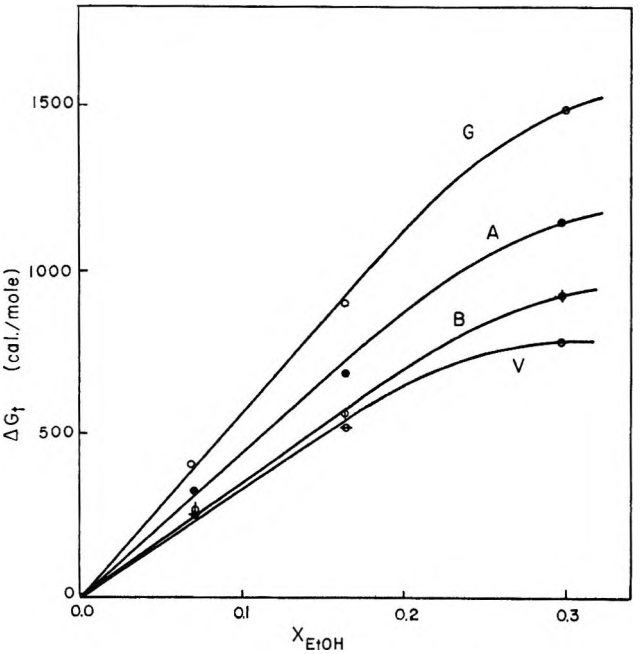

Figure 2. Free energy of transfer of glycine (G); DL-alanine (A), DL-α-aminobutyric acid (B), and L-valine (V) from water to aqueous ethanol solutions at 25°, calculated from data in ref 6.

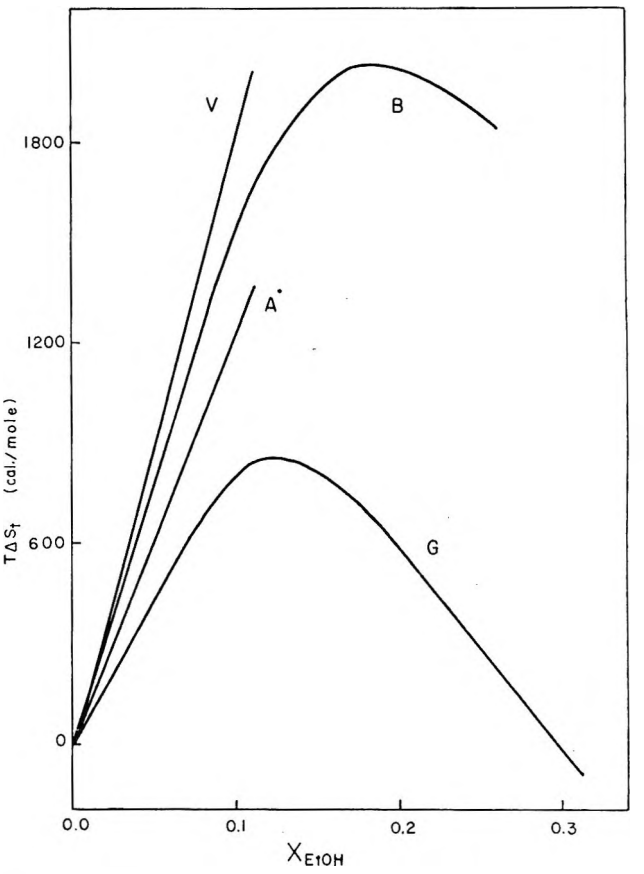

Figure 3. Entropy of transfer of glycine (G), DL-alanine (A), DL-α-aminobutyric acid, and L-valine (V) from water to aqueous ethanol solutions at 25°.

(9) Y. Nozaki and C. Tanford, *J. Biol. Chem.*, 238, 4074 (1963).
(10) Y. Nozaki and C. Tanford, *ibid.*, 240, 3568 (1965).

studied, with glycine showing the sharpest increase with increasing ethanol in the solvent. On the other hand, the transfer entropies show marked changes in the vicinity of 0.1–0.2 mole fraction ethanol. In particular, the transfer entropies for glycine, the unsubstituted amino acid, start to decrease sharply above 0.1 mole fraction ethanol and eventually become negative at about 0.3 mole fraction. The importance of the size of the side chain in the amino acid is indicated by comparing the relative magnitudes of the transfer entropies at 0.1 mole fraction ethanol. The largest amino acid, L-valine, shows the largest entropy increase in transferring from water to the aqueous ethanol mixture, and there is a progressive decrease in the transfer entropy in the series valine, α-aminobutyric acid, alanine, and glycine. The behavior of the larger amino acids at higher ethanol concentrations is indicated by the values for α-aminobutyric acid. Again there is a break in the curve, as with glycine, in the vicinity of 0.15 mole fraction ethanol, but the subsequent decrease is not as sharp.

It should be noted that the relatively small monotonic increases in the transfer free energies of the solutes are a result of compensating changes in the enthalpy and entropy contributions. In the dilute ethanol region the increasing transfer enthalpy is compensated by an increasing transfer entropy, keeping the free energy values relatively small. When the enthalpy change is beginning to level off in the region of 0.2 mole fraction, there is a corresponding decrease in the entropy term. These compensating factors tend to cause the free energy to increase in an almost linear fashion.

Table II: Thermodynamic Transfer Properties of Glycine and Nonpolar Groups from Water to Various Solvents

	$T\Delta S_t$	ΔH_t	ΔG_t
Transfer from water to 0.1 mole fraction ethanol[a]			
Glycine	850	1400	540
CH_3–	1200	1080	−120
CH_3CH_2–	1510	1300	−210
$(CH_3)_2CH$–	1850	1620	−230
Transfer from water to nonpolar medium[b]			
CH_3–	2840	1500	−1300
$(CH_3)_2CH$–	4100	2200	−1900
Transfer from water to 7 *M* urea[c]			
Glycine	−1044	−1011	33
CH_4	1230	1300	70
CH_3CH_3	1950	1910	−40
$CH_3CH_2CH_3$	1850	1760	−130

[a] Data from this work. [b] Data were calculated by Nemethy and Scheraga in ref 18. [c] Data from D. B. Wetlaufer, *et al.*, *J. Amer. Chem. Soc.*, **86**, 508 (1964).

Discussion

Before discussing the behavior of the transfer properties it is necessary to show that changes in the thermodynamic quantities as solvent is changed are not a result of changes in acid or base dissociation of the amphiprotic zwitterion. That these reactions are not responsible for the observed changes in transfer properties can be rationalized by consideration of the magnitudes of the equilibrium constants for acidic and basic dissociation of the amino acids. For glycine the effective acid dissociation constant is $10^{-9.72}$, and the basic dissociation constant is $10^{-11.65}$.[11] These values lead to the conclusion that glycine is 99.99% in the nondissociated form in aqueous solution. Almost identical values are observed for the other amino acids studied. Changes in the ionization reactions as ethanol is added to the solvent have been shown to produce small effects on the equilibrium constants, thus changing the degree of ionization only slightly.[12] We conclude that the observed changes in the thermodynamic transfer properties are not a result of changes in heats or free energies of ionization reactions which can occur with the amino acids.

The interpretation of the transfer entropies must be approached with regard for the structure of the infinitely dilute solutions of solute in the various solvent systems. There is considerable evidence that ethanol causes a net increase in the structure in aqueous solutions as compared with pure water. This evidence comes from the behavior of the heats of mixing, partial molal volumes, ultrasound absorption, and the effect of ethanol on the temperature of maximum density of water when aqueous solutions are formed in the highly aqueous region.[1,2] In the following discussions it will be assumed that up to 0.1 mole fraction ethanol there is enhanced structure in the solvent mixtures, and that the transfer properties can be interpreted in terms of structure-making and structure-breaking effects that the solute has in the solutions, as has been postulated by Frank and Evans.[13]

Longsworth[14] has studied the diffusion of amino acids in water and has concluded that glycine is a structure breaker in water. Kay and Evans[15] draw similar conclusions from interpretation of the temperature dependence of the Walden products of the amino acids in aqueous solution. In addition, Robinson[16] has interpreted the behavior of the partial molal entropy of water in aqueous solutions of the amino acids that glycine is a net structure breaker, while the higher aliphatic homologs are structure makers. Using the above descriptions of glycine in water, the positive transfer entropies support the interpretation that gly-

(11) Reference 6, p 447.
(12) Reference 6, p 511.
(13) H. S. Frank and M. W. Evans, *J. Chem. Phys.*, **13**, 507 (1945).
(14) L. G. Longsworth, *J. Amer. Chem. Soc.*, **75**, 5707 (1953).
(15) R. L. Kay and D. F. Evans, *J. Phys. Chem.*, **70**, 2325 (1966).
(16) A. L. Robinson, *J. Chem. Phys.*, **14**, 588 (1946).

cine is even more effective as a structure breaker in alcohol–water mixtures than in water, at least up to 0.1 mole fraction ethanol. (See Figure 3.) The increased structure breaking by glycine in the mixed solvent is likely due to the already enhanced structure in the original solvent mixtures. Thus, the unfavorable free energy of transfer of glycine from water to aqueous ethanol mixtures is a result of a structure breaking effect that causes the entropy and enthalpy terms to be positive with the enthalpy contribution dominating.

It appears that the amino acids with larger side chains show a greater loss of order in transferring from water to the alcohol–water mixtures. This effect can be seen in Table II, in which the values of the transfer properties of glycine have been subtracted from the values of the other amino acids to obtain the side chain contributions at 0.1 mole fraction ethanol. The side chains produce a negative free energy contribution, the result of an increased entropic term for the larger side chains.

There are a number of studies in the literature which support the idea that hydrocarbon groups promote structure in aqueous solutions.[8,13,17,18] Robinson's study[16] suggests that amino acids with hydrocarbon side chains increase structure in water in proportion to the size of the group. Using that interpretation, the positive transfer entropies for the hydrocarbon side chains thus mean that these groups are less effective in promoting structure in the alcohol–water mixtures than in water. Otherwise, the transfer entropies would be zero or negative for the side chains. Arnett has reached a similar conclusion about nonpolar solutes in his studies of the enthalpy of solution of a number of different types of solutes.[2]

Thus, summarizing, up to about 0.1 mole fraction ethanol the entropy data suggest that the amino acids are causing a breakdown in structure in the mixed ethanol–water solvent, largely a result of perturbation by the highly polar zwitterion portion of the molecule. Assuming that the side chains promote structure in water, then the entropy data imply that the side chains promote less structure in the mixed solvent system.

Beyond 0.1 mole fraction ethanol the transfer entropy for glycine decreases rather sharply. This effect must be a result of dipolar and hydrogen bonding interactions of the zwitterion with solvent molecules, producing a competing ordering effect similar to that which is observed for simple ions.[4] Similar behavior above 0.1 mole fraction ethanol is observed for α-aminobutyric acid, except that the magnitudes of the $T\Delta S_t$ values are larger, and the maximum is shifted to slightly higher mole fraction ethanol. The larger ordering effect in water as compared to the mixed solvent produced by the ethyl side chain must make the transfer entropies larger for α-aminobutyric acid as compared to glycine.

Arnett has suggested that there is a significant structural change in the ethanol–water mixtures at about 0.1 mole fraction ethanol.[2] The addition of ethanol up to a mole fraction of about 0.1 causes enhancement of structure in the solutions, but at that composition the maximum order has been obtained. Additional ethanol can no longer build structure without interfering with the established order in the system. Thus, many properties of the mixtures, such as partial molal volumes, activity coefficients, sound velocity, and temperature of maximum density of water, all show maxima at this composition. The effect of the structural change on the amino acid transfer entropies is that above 0.1 mole fraction ethanol the structure breaking effect is less in the mixtures. Beyond the maximum the competing solvation of the zwitterion produces ordering effects that become increasingly significant in the transfer entropy, and the values decrease as a result.

It is of interest to compare the transfer properties of solutes from water to other solvent systems. Shown in Table II are values for the transfer of several hydrocarbon side chains from water to a "nonpolar" medium. The side chain values were calculated by Nemethy and Scheraga,[17,18] based on the solubility of hydrocarbons in water. In addition, values of the transfer properties are given for 7 *M* urea solutions for glycine and several hydrocarbons.[19,20]

Nemethy and Scheraga's calculation for the transfer of methyl and isopropyl groups from water to a nonpolar medium shows a considerable gain in entropy for the process, presumably a result of the lack of order in the nonpolar medium as compared with water. These entropy increases are much larger than the transfer values into 0.1 mole fraction ethanol or into 7 *M* urea. This comparison adds support to the idea that the nonpolar hydrocarbon groups have a tendency to promote structure in the mixed aqueous solvents, but not so much as is obtained in pure water.

A comparison of the glycine transfer properties for aqueous ethanol solutions with those for 7 *M* urea solutions shows rather striking differences. Both the entropy and enthalpy of transfer are negative for the 7 *M* urea solvent system. The negative entropy and enthalpy values have been interpreted as due to a direct hydrogen bonding interaction between urea and the polar zwitterion.[19] Thus, the structure breaking effect produced by the polar zwitterion in transferring to aqueous ethanol, and the structure making effect due to the direct interaction of urea with the zwitterion in 7 *M* urea solutions, account for the general stability of amino acids in 7 *M* urea solutions and the instability of the amino acid solutes in aqueous ethanol mixtures.

(17) G. Nemethy, *Angew. Chem. Int. Ed., Engl.*, **6**, 195 (1967).

(18) G. Nemethy and H. A. Scheraga, *J. Chem. Phys.*, **36**, 3382 (1962).

(19) G. C. Kresheck and L. Benjamin, *J. Phys. Chem.*, **68**, 2476 (1964).

(20) D. B. Wetlaufer, S. K. Malik, L. Stoller, and R. L. Coffin, *J. Amer. Chem. Soc.*, **86**, 508 (1964).

In conclusion, the expected intermediate behavior of the amino acids between nonelectrolyte and electrolyte is manifested in the thermodynamic transfer properties for aqueous ethanol solutions. The highly polar zwitterion, glycine, is perhaps more like an electrolyte than the other solutes studied, causing the transfer entropy to decrease rather sharply with increasing ethanol in the solvent. The behavior of the zwitterion points out the importance of ionic fields in disrupting structure in highly ordered aqueous solutions. The larger amino acid solutes produce greater endothermic enthalpy changes and larger positive entropy changes in transferring to dilute solutions of ethanol in water. The increased endothermicity in the enthalpy change compensates the relatively higher entropy contribution, causing the free energies of transfer to remain small and nearly constant. The data show that the free energies do not reflect the complicating structural changes that occur as the solvent composition is changed. The hydrocarbon side chains in the amino acid solutes have the effect of increasing order both in water and in the ethanol–water mixtures. The promotion of structure in the mixtures by the side chains up to 0.1 mole fraction ethanol has not been previously recognized and points out the rather complex nature of the effects of added alcohol on the thermodynamic properties of solutes in mixed solvent systems.

Acknowledgments. This work was supported by the National Institutes of Health of the Public Health Service (Grant No. GM-12987), and by the Research Foundation of the State of New York.

Diffusion of Oxygen and Hydrogen in Aqueous Potassium Hydroxide Solutions[1]

by M. K. Tham, R. D. Walker, and K. E. Gubbins

Department of Chemical Engineering, University of Florida, Gainesville, Florida 32601 *(Received August 12, 1969)*

Diffusion coefficient measurements made by the stagnant microelectrode method are reported for oxygen and hydrogen in KOH solutions. The temperature and KOH concentration ranges covered are 25–100° and 0–14 *M*, respectively. Results agree with behavior expected from the Eyring theory at lower KOH concentrations, but deviations occur for concentrated solutions. The results are also discussed in relation to the theory of Cohen and Turnbull.

Introduction

The rate of diffusion of dissolved gases in electrolytic solution is an important consideration in determining the performance of porous gas electrodes. The theoretical analysis of Srinivasan, *et al.*,[2] has shown that concentration polarization is a serious limitation for such electrodes. Diffusion coefficients of oxygen and hydrogen in potassium hydroxide solutions have been previously reported in the literature.[3-5] In this work diffusion coefficient measurements are reported for a wider range of temperature (25–100°) and KOH concentration (zero to saturation). Shoor, Walker, and Gubbins[6] have recently reported solubilities and thermodynamic data for the O_2–KOH and H_2–KOH systems. The concentration of these dissolved gases is so low that for the purposes of discussing the diffusion the system may be regarded as a pseudo-binary one composed of gas and electrolyte solution. The measured diffusion coefficients are those for infinite dilution of the gas.

As both oxygen and hydrogen react at a platinum electrode, electrochemical methods of measurement offer some advantages. However, the dropping mercury electrode method[3] involves the use of an uncertainly known empirical constant in the Ilkovic equation,

(1) These studies were supported by the National Aeronautics and Space Administration and by the National Science Foundation.

(2) S. Srinivasan, H. D. Hurwitz, and J. O'M. Bockris, *J. Chem. Phys.*, **46**, 3108 (1967).

(3) K. E. Gubbins and R. D. Walker, *J. Electrochem. Soc.*, **112**, 469 (1965).

(4) R. E. Davis, G. L. Horvath, and C. W. Tobias, *Electrochim. Acta*, **12**, 287 (1967).

(5) P. Ruetschi, *J. Electrochem. Soc.*, **114**, 301 (1967).

(6) S. K. Shoor, R. D. Walker, and K. E. Gubbins, *J. Phys. Chem.*, **73**, 312 (1969).

while Davis, *et al.*[4], showed that the rotating disk electrode was not diffusion controlled under all conditions. We have therefore used a modification of the stagnant microelectrode method of Laitinen and Kolthoff.[7,8] With this procedure it is possible to set up the necessary boundary conditions more easily than with a rotating disk, and diffusion control is more readily assured because of the long diffusion path.

Experimental Section

Materials. Potassium hydroxide pellets (meet ACS specification) containing a maximum of 1% K_2CO_3 were used. Solutions were prepared with doubly distilled water and stored in polyethylene bottles fitted with glass bulbs containing ascarite to minimize carbon dioxide absorption. Potassium ferrocyanide solutions were prepared from analyzed reagent grade standard volumetric solutions.

Apparatus. The method used was that of Laitinen and Kolthoff.[7] Figure 1 shows the diffusion cell. The platinum microelectrode A was connected through a pool of mercury in tube B to the voltage source. Fritted disk C was used to disperse the gas under study during the saturation process. D was a silver counterelectrode (5.2 × 4.5 cm), and E and F were a vent and a port used for flushing and filling the microelectrode, respectively. The solution under study was contained in the glass vessel G; the two parts were held together tightly by means of springs (not shown). For experiments on diffusion of dissolved gases the diffusion was in a downward direction, as shown in Figure 1. Calibration experiments (using potassium ferrocyanide) were carried out in a similar diffusion vessel, but with upward diffusion; in this way convective mixing due to density changes was avoided.

The microelectrode consisted of a bright platinum disk cemented (fluorocarbon epoxy cement) between two sections of precision bore capillary. Capillary diameters ranged from 1.75 ± 0.02 to 2.75 ± 0.035 mm depending on the viscosity of the solutions. A platinum wire spot-welded to the disk was immersed in the mercury column in tube B. Voltage supply and current measurement were provided by a Sargent Model XV polarograph equipped with a microrange extender.

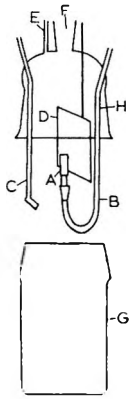

Figure 1. Experimental apparatus.

Procedure. Gas supplied to the dispersion disk C was presaturated by first passing it through two gas-washing bottles filled with potassium hydroxide of the same concentration as that under study. The presaturators and the diffusion vessel were immersed in an oil bath controlled to within ±0.01°. The partial pressure of the dissolved gas was taken to be atmospheric minus the vapor pressure of the KOH solution. Equilibration of the solution with the gas took about 30 min. The procedure used to ensure attainment of equilibrium was the same as that described by Shoor, *et al.*[6] The microelectrode was filled by drawing the gas-saturated solution into it by means of a syringe. After stopping the gas flow, the solution was allowed to equilibrate under an atmosphere of presaturated solute gas for 10 min. A fixed potential was then applied to the microelectrode and the current measured as a function of time for about 20 min. The diffusion limiting potentials used were −0.4 to −0.65 V for oxygen and 0.1 to 0.25 V for hydrogen, both referred to the saturated calomel electrode; the exact voltage required depended on the KOH concentration. Residual currents were measured in a similar way after first stripping off dissolved solute gas with nitrogen.

Diffusion coefficients were calculated from the equation[8]

$$D = \left(\frac{i_t}{nFAS}\right)^2 \pi t \qquad (1)$$

where i_t is net diffusion current in amperes (after deduction of residual current), n is number of electrons transferred, F is the Faraday, A is microelectrode area in cm^2 (obtained from calibration), S is concentration of dissolved gas in g mol/ml, and t is time in seconds. Values of S were obtained from the solubility measurements of Shoor.[6]

The constancy of $i_t\sqrt{t}$ was tested for each run. Such constancy was satisfactory provided diffusion occurred in the upward direction, and the microelectrode was carefully cleaned. The microelectrode was pretreated by the method suggested by Bockris, *et al.*[9] To clean the electrode surface further, cathodic evolution of hydrogen or anodic evolution of oxygen was applied periodically. After such gas evolution, care was taken to ensure that any gas bubbles near the electrode surface had been removed by mechanical circulation and reaction before carrying out a run. The constancy of $i_t\sqrt{t}$ indicated the absence of such errors.

(7) H. A. Laitinen and I. M. Kolthoff, *J. Amer. Chem. Soc.*, **61**, 3344 (1939).

(8) I. M. Kolthoff and J. J. Lingane, "Polarography," Vol. 1, Interscience Publishers, New York, N. Y., 1952, pp 19–29.

(9) J. O'M. Bockris, A. Damjanovic, and M. A. Genshaw, *J. Electrochem. Soc.*, **114**, 1107 (1967).

Calibration of the Microelectrode. The electrode area was determined by measuring the diffusion current *vs.* time for the diffusion of 0.0004 *m* potassium ferrocyanide in a supporting electrolyte of 0.1 *N* KCl. The applied potential was +0.7 V. Diffusion was in the upward direction in these experiments. For this system the *D* value has been determined by Von Stackelberg, *et al.*,[10] as 0.768 × 10^{-5} cm²/sec. This value was used in eq 1 to determine *A*.

Results

Figures 2 and 3 show the experimental data for oxygen and hydrogen in potassium hydroxide at 25, 40, 60, 80, and 100°. Each experimental point in these figures is the arithmetic mean of five or six replicate measurements. The standard deviation was about ±0.07 for oxygen and ±0.13 for hydrogen. The estimated accuracy of the measurements is ±10%; the main uncertainty arises from the concentration value which appears squared in eq 1.

Also included in Figures 2 and 3 are data of other workers. For oxygen diffusion at 25° the previous values of Gubbins and Walker[3] are in good agreement except at the highest KOH concentrations, where the present values are significantly larger; this discrepancy may reflect the poor accuracy of the polarographic method for such low diffusion rates. The data of Davis, *et al.*,[4] are also in excellent agreement with the present data for the most part, though some deviation occurs at 60°. It is worthwhile to note that the solubility values used by Davis, *et al.*, to calculate their diffusion coefficients differed slightly from those used here. For hydrogen the only data in the literature appear to be those of Ruetschi.[5] From Figure 3 it is seen that his values agree well with those reported here at low KOH concentrations, but show a stronger KOH concentration dependence.

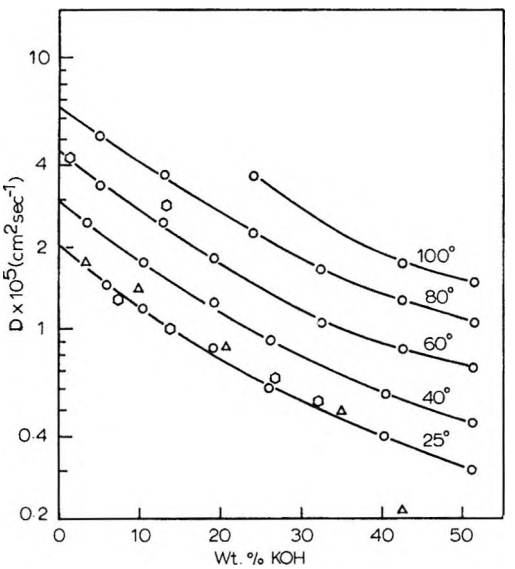

Figure 2. Diffusion coefficients for oxygen in KOH solutions; △, Gubbins and Walker,[3] 25°; ○, Davis, *et al.*,[4] 25° and 60°; ○, this work.

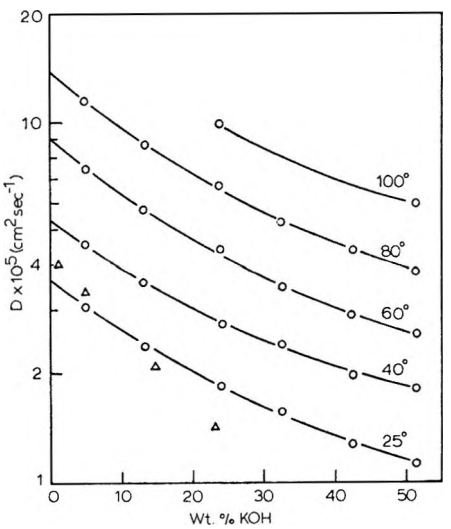

Figure 3. Diffusion coefficients for hydrogen in KOH solutions; △, Ruetschi,[5] 30°; ○, this work.

Table I: Diffusion Coefficients (cm²/sec) of Oxygen and Hydrogen in Water at 25°

Oxygen		Hydrogen	
10^5D	Method	10^5D	Method
2.55	Dissolution of bubble[a]	7.07	Wetted sphere[b]
2.42	Wetted sphere[b]	5.8	Dissolution of bubble[a]
2.41	Diaphragm cell[c]	4.8	Diaphragm cell[c]
2.20	Laminar dispersion[d]	4.27	Laminar jet[f]
2.12	Polarography[e]	4.2	Rotating electrode[i]
2.03	Laminar jet[f]	4.1	Diaphragm cell[j]
1.95	Microelectrode[g]	4.08	Gas absorption[k]
1.90	Polarography[h]	3.49	Gas absorption[l]
2.00	This work	3.7	This work

[a] D. L. Wise and G. Houghton, *Chem. Eng. Sci.*, **21**, 999 (1966). [b] J. F. Davidson and E. J. Cullen, *Trans. Inst. Chem. Eng.*, **35**, 51 (1957). [c] J. E. Vivian and C. J. King, *A.I.Ch.E. J.*, **10**, 220 (1964). [d] R. T. Ferrell and D. M. Himmelblau, *J. Chem. Eng. Data*, **12**, 111 (1967). [e] J. Jordan, E. Ackerman, and R. L. Berger, *J. Amer. Chem. Soc.*, **78**, 2979 (1956). [f] M. H. I. Baird and J. F. Davidson, *Chem. Eng. Sci.*, **17**, 473 (1962). [g] See ref 4. [h] See ref 3. [i] See ref 5. [j] K. E. Gubbins, K. K. Bhatia, and R. D. Walker, *A.I.Ch.E. J.*, **12**, 548 (1966). [k] G. Tammann and V. Jessen, *Z. Anorg. Allgem. Chem.*, **179**, 125 (1929). [l] W. W. Ipatieff, W. P. Teodorovitsch, and S. I. Drushina-Artemovich, *ibid.*, **216**, 66 (1933).

Diffusion coefficients of oxygen and hydrogen in pure water were obtained by extrapolation. Values at 25° are seen from Table I to compare favorably with those reported in the literature. Similar agreement is found for the other temperatures.

(10) H. Von Stackelberg, M. Pilgrim, and V. Toome, *Z. Electrochem.*, **57**, 342 (1953).

Discussion

There is no satisfactory theory available to describe the effect of ionic concentration on the diffusion coefficient of dissolved gases. Indeed, the statistical mechanical theory of liquid diffusion is as yet incomplete even for molecularly simple systems.[11]

An approximate description of the variation of D with ionic concentration is obtained from a modification of the Eyring absolute reaction rate theory, proposed by Ratcliff and Holdcroft.[12] In addition to the approximations implicit in the Eyring theory, it is assumed that the molecules and ions are randomly distributed and that the principal effect of ionic concentration is on the activation free energy term. The resulting equation is

$$\frac{D}{D_0} = \exp\left\{-\frac{1}{RT}\left[\frac{18Cz(\nu_+\delta_+ + \nu_-\delta_-)}{1000\rho - CM + 18C(\nu_+ + \nu_-)}\right]\right\} \quad (2)$$

where D and D_0 are the diffusion coefficient in the electrolyte solution and pure water, respectively, ν_+ and ν_- are the number of positive and negative ions per mole of electrolyte, C is molarity of electrolyte, M is electrolyte molecular weight, ρ is density, z is the number of particles with which a gas molecule interacts, and δ_+ and δ_- are free energy perturbation parameters characteristic of the ions and the dissolved gas. Equation 2 shows that a plot of ln (D/D_0) *vs.* $C/[1000\rho - CM + 18C(\nu_+ + \nu_-)]$ should be linear, with a slope $-18z(\nu_+\delta_+ + \nu_-\delta_-)/RT$. Such plots have been found to be approximately linear for several simple gas–electrolyte systems.[12,13]

A plot of this type is shown in Figure 4 for the systems studied here. The curves are approximately

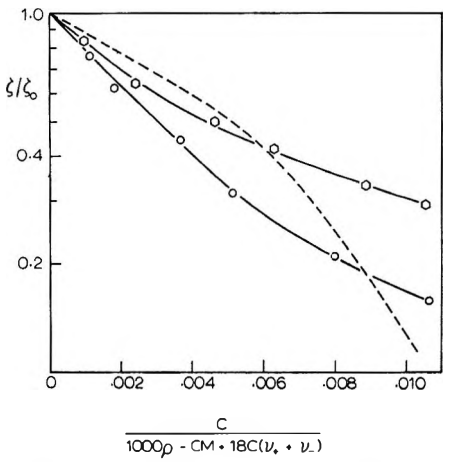

Figure 4. Test of absolute rate theory for diffusion, with ζ = transport property in electrolyte, ζ_0 = transport property in pure water, both at 25°. —○—, diffusion coefficient for oxygen; —○—, diffusion coefficient for hydrogen; ---, fluidity of KOH solutions.

linear at low concentrations, but the theory fails at high molarities. It may be noted that assumptions in the theory are more closely obeyed for dilute electrolytes, so that deviations are to be expected at higher electrolyte concentrations. Similar theories have been presented for fluidity (ϕ),[14] electrolyte mutual diffusion coefficient (D_m),[15] and self-diffusion of water (D^w).[14] Thus the equation for fluidity is[14]

$$\frac{\phi}{\phi_0} = \exp\left\{-\frac{1}{RT}\left[\frac{18(1 + r')C(\nu_+z_+\delta_+' + \nu_-z_-\delta_-')}{1000\rho - CM + 18C(\nu_+ + \nu_-)}\right]\right\} \quad (3)$$

where r' is a constant equal to 0.055, and z_+ and z_- are the number of neighboring particles with which positive and negative ions interact. The perturbation parameters δ_+' and δ_-' are in general different from δ_+ and δ_- since the former arise from ion–water interactions and the latter from ion–solute gas interactions.

These theories predict linear plots of ϕ/ϕ_0, D^w/D_0^w and $x_wD_m^{id}/D_{mo}$, respectively, against $C/[1000\rho - CM + 18C(\nu_+ + \nu_-)]$; here x_w is mole fraction of water, D_m^{id} is the electrolyte mutual diffusion coefficient divided by the thermodynamic factor, and D_{mo} and D_0^w are mutual diffusion coefficient and self-diffusion coefficient of water at infinite dilution of electrolyte, respectively. Such a plot for $x_wD_m^{id}/D_{mo}$ for KOH has been found to be closely linear up to high electrolyte concentrations.[15] The plot for self-diffusion coefficient of water is linear at low concentrations.[15] For fluidity a plot is included in Figure 4; approximate linearity is observed at low electrolyte concentrations, but the theory again fails for concentrated solutions. It may be noted that eq 2 and 3 predict that the product $D\mu$, where $\mu = 1/\phi$ is viscosity, will not be a constant for various electrolyte concentrations. From Figure 4 it is clear that this product is found experimentally to depend on C.

An alternative framework for the discussion of diffusion in these systems is given by the free-volume theory of Cohen and Turnbull.[16] According to this theory the molecules may be thought of as hard spheres, and a diffusive jump will only occur if an adjacent hole (or "free volume") is available for the molecule to move into. Then

$$D = BP(r_c \geq \sigma) \quad (4)$$

(11) S. A. Rice and P. Gray, "The Statistical Mechanics of Simple Liquids," Interscience Publishers, New York, N. Y., 1965.

(12) G. A. Ratcliff and J. G. Holdcroft, *Trans. Inst. Chem. Eng.*, **41**, 315 (1963).

(13) K. E. Gubbins, K. K. Bhatia, and R. D. Walker, *A.I.Ch.E. J.*, **12**, 548 (1966).

(14) R. J. Podolsky, *J. Amer. Chem. Soc.*, **80**, 4442 (1958).

(15) R. N. Bhatia, K. E. Gubbins, and R. D. Walker, *Trans. Faraday Soc.*, **64**, 2091 (1968).

(16) M. H. Cohen and D. Turnbull, *J. Chem. Phys.*, **31**, 1164 (1959).

Table II: Gibbs Free Energy for Cavity Formation at 25° and Activation Energy of Diffusion (cal/g mol) for Oxygen and Hydrogen in KOH Solutions

C^a	$-(G_c - G_c^0)/RT^b$	$\ln (D/D_0)^c$	E
	O_2 Solute		
0	0	0	4700
2	−1.12	−0.541	4680
5	−2.82	−1.069	4740
10	−5.70	−1.627	4560
14	−8.10	−1.902	4580
	H_2 Solute		
0	0	0	5240
2	−0.84	−0.352	5010
5	−2.06	−0.655	4850
10	−4.13	−1.024	4810
14	−5.82	−1.197	4500

[a] Molarity of KOH at 25°. [b] Calculated from scaled particle theory (eq 12 of Shoor and Gubbins,[18] using the following σ values for the various particles present: $\sigma_{H_2O} = 2.75$; $\sigma_{K^+} = 2.60$; $\sigma_{OH^-} = 3.30$; $\sigma_{O_2} = 3.46$; $\sigma_{H_2} = 2.87$ Å. Here G_c is the Gibbs free energy to form a mole of cavities in the electrolyte solution; G_c^0 is the corresponding quantity for pure water. [c] At 25°.

where $P(r_c \geq \sigma)$ is the probability that a cavity of radius greater than or equal to σ is available for the diffusing molecule to move into, σ being an appropriate measure of the solute molecular diameter. Cohen and Turnbull give an equation for the preexponential constant B for pure liquids, but not for mixtures.

According to the Einstein theory of fluctuations, the probability $P(r_c \geq \sigma)$ for a system at constant temperature and pressure is related to the Gibbs free energy change needed to form a cavity, g_c, by[17]

$$P(r_c \geq \sigma) = \exp[-g_c/kT] \tag{5}$$

so that from (4) and (5)

$$D = B \exp[-G_c/RT] \tag{6}$$

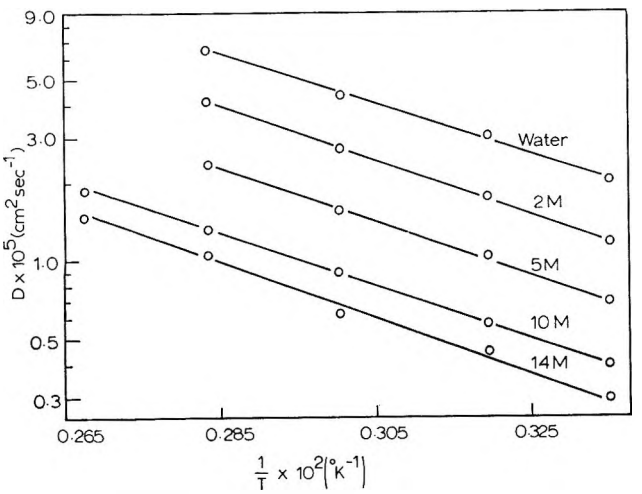

Figure 5. Temperature dependence of D for oxygen in KOH solution.

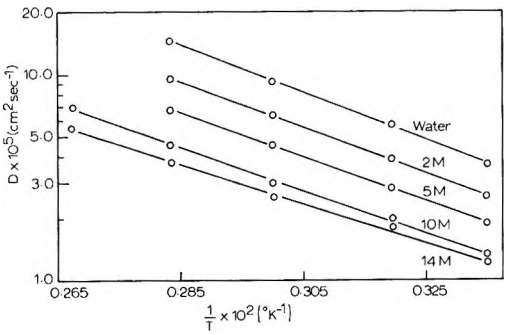

Figure 6. Temperature dependence of D for hydrogen in KOH solution.

where G_c is the Gibbs free energy change per mole of cavities. The latter can be calculated from the scaled particle theory of Reiss, *et al.*[17,18] Table II compares values of $-(G_c - G_c^0)/RT$ with $\ln(D/D_0)$ for the systems studied here. The results lend qualitative support to the ideas of the Cohen–Turnbull theory. Thus the number of cavities of suitable size decreases as the KOH concentration increases. This effect is common to most electrolytes, and evidence for this trend is also available from partial molal entropy measurements.[19,20] It is also seen from Table II that the decrease in the number of cavities when electrolyte is added is more pronounced for oxygen than for hydrogen (because of the larger σ value for oxygen), and this trend parallels the greater decrease in D/D_0 for oxygen. A more quantitative test of the Cohen–Turnbull theory is difficult because of the unknown concentration dependence of the term B.

The temperature dependence of the experimental D values is well represented by the usual equation of Arrhenius type

$$\ln D = A - \frac{E}{RT} \tag{7}$$

This equation fitted the data within about 3% at all KOH concentrations. Plots are shown in Figures 5 and 6. Experimental values of the activation energy obtained by a least-squares fit to eq 7 are included in Table II. For oxygen and hydrogen in water, values for E found here are somewhat higher than those found by Wise and Houghton,[21] who obtained 4390 and 3960 cal/g mol, respectively; our values for water are tentative, however, since they are based on extrapolated D values. The KOH concentration seems to have little effect on E; such effect as there is seems to consist of a decrease in E with rising concentration.

(17) H. Reiss, H. L. Frisch, and J. L. Lebowitz, *J. Chem. Phys.*, **31**, 369 (1959).

(18) S. K. Shoor and K. E. Gubbins, *J. Phys. Chem.*, **73**, 498 (1969).

(19) D. D. Eley, *Trans. Faraday Soc.*, **35**, 1281 (1939).

(20) A. Ben-Naim and M. Egel-Thal, *J. Phys. Chem.*, **69**, 3250 (1965).

(21) Reference *a* of Table I.

Normal Stress Effect of Dilute Polymer Solutions. III. Monodisperse Poly-α-methylstyrene in Chlorinated Biphenyl

by Kunihiro Osaki, Kuniaki Sakato, Masaaki Fukatsu,[1a]
Michio Kurata, Kazumasa Matusita,[1b] and Mikio Tamura[1b]

Institute for Chemical Research, Kyoto University, Uji, Japan, and Department of Industrial Chemistry, Kyoto University, Kyoto, Japan *(Received September 22, 1969)*

The normal and shear stresses in steady shear flow were measured on dilute solutions of monodisperse poly-α-methylstyrene in two chlorinated biphenyls. The zero-shear viscosity η and the reduced steady shear compliance γ were evaluated from these measurements as functions of concentration and molecular weight. The intrinsic viscosity of the polymer in the chlorinated biphenyls was found to be very close to that in benzene, a good solvent. In the limit of zero concentration, the γ value was about 0.20 irrespective of the molecular weight. The quantity increased with concentration and attained to a value as high as 0.7 which exceeds the value 0.40 corresponding to the so-called free-draining limit. It is concluded from this evidence that the polymer chain behaves as a nondraining coil at infinite dilution and that the increase in γ with concentration does not arise from a decrease in the hydrodynamic interaction of the segments.

Introduction

In previous publications[2] we have reported the results of the measurements of the normal and the shear stresses in steady shear flow of dilute solutions of polystyrene in dioctylphthalate and in chlorinated biphenyl. It was found that the secondary normal stress, if any, is negligibly small compared to the principal normal stress and that the shear and the normal stresses are proportional to the first and the second power of the rate of shear κ, respectively, if κ is sufficiently small. Thus the stress measurement in steady shear flow was found to be a most convenient method for evaluation of the steady shear compliance J_e which, together with the viscosity η, represents the mechanical properties of liquids in slow deformation. These parameters were obtained for dilute polystyrene solutions but the broad distribution of the molecular weight of the polystyrene samples restricted further discussion of the data on the basis of molecular theories.

In the present study we measured the normal and the shear stresses in steady shear flow of dilute solutions of monodisperse poly-α-methylstyrene in chlorinated biphenyl. The effect of the molecular weight, the concentration, and the viscosity of the solvent on the parameters, J_e and η, were investigated for elucidation of the nature of the interaction between polymer segments in slow deformation of dilute polymer solutions.

In the course of preparing this paper, Holmes, *et al.*,[3-5] published analogous results for dilute polystyrene solutions obtained through dynamic mechanical measurements. Some of their results, especially the concentration dependence of the steady shear compliance, are different from the present results.

Experimental Section

Samples. Poly-α-methylstyrene samples were a part of the samples synthesized anionically and fractionated by Sakato, *et al.* Details of the synthesis and the characterization of the samples are found in another publication.[6,7] The ratio of the weight average molecular weight to the number average is below 1.01 for each sample, so that the molecular weight distribution of the sample is very sharp. The weight average molecular weight of the samples as determined from light scattering are shown in Table I.

As solvents, we used two kinds of chlorinated biphenyl, Aroclor 1248 from Monsanto Chemicals Company and Kaneclor 500 from Kanegafuchi Chemical Industry Company. Both of the solvents are mixtures of chlorinated biphenyl but the former is chlorinated to a lesser degree. Viscosities of Aroclor and Kaneclor are 1.25 and 37.0 P, respectively, at 30°. These solvents do not show non-Newtonian effect, Weissenberg effect, or viscoelastic dispersion in the range of the time scale of our measurements.

For preparation of the polymer solutions, weighed

(1) (a) Deceased. (b) K. Matusita and M. Tamura did research in the Department of Industrial Chemistry at Kyoto, Japan.

(2) (a) M. Tamura, M. Kurata, K. Osaki, and K. Tanaka, *J. Phys. Chem.*, **70**, 516 (1966); (b) K. Osaki, K. Tanaka, M. Kurata, and M. Tamura, *ibid.*, **70**, 2271 (1966).

(3) L. A. Holmes, K. Ninomiya, and J. D. Ferry, *ibid.*, **70**, 2714 (1966).

(4) L. A. Holmes and J. D. Ferry, *J. Polym. Sci., Part C*, **23**, 291 (1968).

(5) S. Kusamizu, L. A. Holmes, A. A. Moore, and J. D. Ferry, *Trans. Soc. Rheol.*, **12**, 559 (1968).

(6) M. Abe, K. Sakato, T. Kageyama, M. Fukatsu, and M. Kurata, *Bull. Chem. Soc. Jap.*, **41**, 2330 (1968).

(7) K. Sakato and M. Kurata, to be published.

Table I: Parameters for Steady Shear Flow of Dilute Poly-α-methylstyrene Solutions at 30°

PMS code	$10^{-5}M_w$	Solvent	10^2c, g/ml	η, P	10^3J_e, cm²/dyn	$[\eta]$, ml/g	γ
BB7	16.8	Aroclor	1.72	25.4	1.40	315	0.402
			1.27	13.5	1.60		0.373
			0.983	9.1	1.70		0.349
			0.412	3.85[a]			
			0.275	2.73[a]			
			0.205	2.25[a]			
		Kaneclor	0.765	172	2.60	265	0.485
			0.574	125	2.30		0.402
			0.423	95	2.00		0.341
			0.255	68	1.30		0.216
BB5	14.3	Aroclor	2.15	37.0	1.63	250	0.665
			1.82	25.0	1.75		0.626
			1.45	15.5	1.60		0.480
			1.16	10.6	1.65		0.435
			0.874	7.3	1.45		0.326
			0.724	5.7	1.45		0.304
			0.568	4.04[a]			
			0.374	2.82[a]			
			0.258	2.35[a]			
		Kaneclor	0.794	155	2.43	225	0.587
			0.633	127	2.05		0.456
			0.445	94	1.60		0.332
			0.304	68	1.15		0.297
			0.234	59	1.20		0.352
			0.151	51	0.70		0.248
BB10	6.40	Aroclor	5.56	155	0.310	150–210	0.693
			3.92	53	0.330		0.538
			3.16	33.0	0.375		0.504
			2.29	17.0	0.400		0.422
			1.92	11.9	0.410		0.388
		Kaneclor	2.24	560	0.470	165	0.477
			1.70	310	0.450		0.392
			1.22	186	0.470		0.353
			0.803	118	0.450		0.304
			0.604	89	0.400		0.280
			0.393	67	0.320		0.248
BB9	3.55	Aroclor	6.02	60	0.105	100	0.470
			4.45	26.0	0.130		0.452
			1.15	3.30[a]			
			0.781	2.48[a]			
			0.572	2.09[a]			
		Kaneclor	2.61	285	0.230	110	0.564
			1.91	185	0.200		0.425
			1.43	120	0.180		0.384
			0.780	80	0.155		0.298
			0.619	70	0.140		0.277

[a] Measured with Ostwald viscometer.

amounts of freeze-dried polymer and the solvent were kept at 50° with occasional stirring for three weeks. No change in viscosity was observed if the solution was kept at 50° for longer times. The solution was filtered with a glass filter before the measurement.

Apparatus and Method. Normal stress measurement was carried out with an apparatus of a parallel disk type.[8] The polymer solution is placed between a pair of parallel disks. The lower disk is rotated at an angular velocity Ω and the pressure P exerted by the solution to the upper disk is measured at several points with various distances r from the center of rotation. The gradient of this pressure is related to the normal stress components as with $\kappa = r\Omega/l$. Here σ_{11}, σ_{22},

$$-\partial P/\partial \ln r = \sigma_{11} - \sigma_{33} + \partial(\sigma_{22} - \sigma_{33})/\partial \ln \kappa$$

and σ_{33} are the normal stress components in the flow direction, in the shear plane, and in the plane perpendicular to both of the flow direction and the shear plane,

(8) M. Tamura, M. Kurata, and T. Kotaka, *Bull. Chem. Soc. Jap.*, **32**, 471 (1959); T. Kotaka, M. Kurata, and M. Tamura, *J. Appl. Phys.*, **30**, 1705 (1959).

respectively, κ is the rate of shear, and l is the distance between two disks.

The measurement of the shear stress σ_{12} was performed with a rheometer of a coaxial cylinder type. Because the degree of non-Newtonian effect was not very large in our experiment, the correction for the non-Newtonian effect was not necessary in the estimation of the rate of shear. Precise description of the apparatus used for normal stress and shear stress measurements is found elsewhere.[8]

Two parameters to describe the slow deformation, the zero-shear viscosity η, and the steady shear compliance J_e, were evaluated with

$$\eta = \lim_{\kappa \to 0} \sigma_{12}/\kappa \quad (1)$$

$$J_e = {}^1/_2 \lim_{\kappa \to 0} (-\partial P/\partial \ln r)/\kappa^2 \quad (2)$$

respectively. The validity of applying the latter formula to polymer solutions was shown in previous publications.[1,2,9]

For measurement of the viscosity of very dilute solutions, viscometers of the Ostwald type were used. Flow time for the solvent in each viscometer was longer than 100 sec/ml and the correction for the kinetic energy, and the effect of the rate of shear were negligible.

Results

On Figure 1 are shown results of normal stress and shear stress measurements for solutions of poly-α-methylstyrene BB5 in Aroclor. Circles and thick lines represent the normal stress $(-\partial P/\partial \ln r)$ and thin lines represent the shear stress σ_{12} plotted against the rate of shear κ. Obviously $(-\partial P/\partial \ln r)$ and σ_{12} are proportional to κ^2 and κ, respectively, through a wide range of κ. This proportionality is a characteristic property of slow flow of viscoelastic fluids and makes it easy to evaluate the parameters, η and J_e, with eq 1 and 2, respectively. Only at very high rate of shear a slight deviation from the proportionality appears; $(-\partial P/\partial \ln r)/\kappa^2$ and σ_{12}/κ decrease slightly with increasing κ. The raw results of normal stress and shear stress measurements for other samples of poly-α-methylstyrene will not be shown here because they are not much different from those shown in Figure 1.

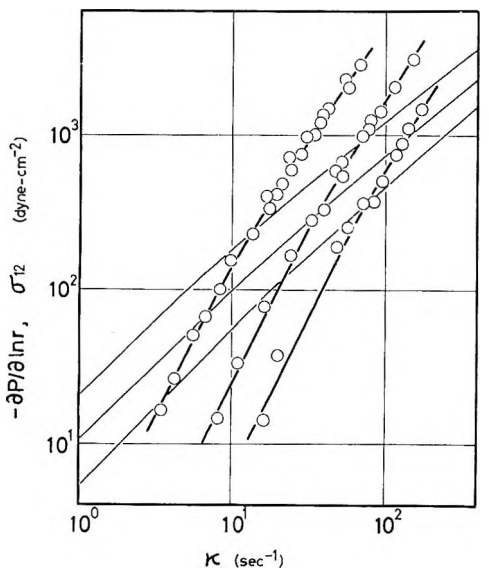

Figure 1. The normal stress $(-\partial P/\partial \ln r)$ and the shear stress σ_{12} plotted against the rate of shear κ for dilute poly-α-methylstyrene solutions in Aroclor at 30°. Circles and thick lines represent $(-\partial P/\partial \ln r)$ and thin lines, σ_{12}. The concentrations of the solutions are 1.82, 1.16, and 0.724 g/dl from left to right.

The values of the zero shear viscosity, η, and of the steady shear compliance, J_e, calculated from eq 1 and 2, respectively, are listed in Table I. The zero shear viscosities of very dilute solutions as measured with Ostwald viscometers are also included in the table.

Discussion

Intrinsic Viscosity. The intrinsic viscosity $[\eta]$ was evaluated from the data of viscosity in Table I. Three types of plot were employed to extrapolate the result to zero concentration; η_{sp}/c *vs.* c, $\ln \eta_r/c$ *vs.* c, and η_{sp}/c *vs.* η_{sp}, where η_{sp}, η_r and c are specific viscosity, relative viscosity, and concentration in g/ml, respectively.

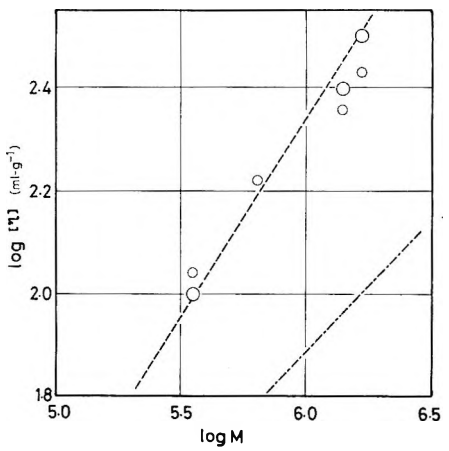

Figure 2. The intrinsic viscosity $[\eta]$ plotted against the molecular weight M in double logarithmic scale for poly-α-methylstyrene in chlorinated biphenyl at 30°. Small circles represent the results in Kaneclor and large circles in Aroclor. The dashed line and the chain line represent the results in benzene at 30° and in cyclohexane at 39°, respectively.

The Huggins constants evaluated from the plot of η_{sp}/c *vs.* c and of $\ln \eta_r/c$ *vs.* c lie between 0.35 and 0.45 while those obtained from the plot of η_{sp}/c *vs.* η_{sp} lie between 0.20 and 0.30. This discrepancy may probably imply that the concentration was not low enough to allow very accurate estimation of the intrinsic viscos-

(9) K. Osaki, M. Tamura, T. Kotaka, and M. Kurata, *J. Phys Chem.*, 69, 3642 (1965).

ity. Nevertheless, the extrapolation to zero concentration was not very difficult and the three types of plot gave the same value for the intrinsic viscosity except for the case of the sample BB10 in Aroclor. The results were shown in the 7th column of Table I and in Figure 2. In Figure 2 is plotted the intrinsic viscosity $[\eta]$ of poly-α-methylstyrene in Aroclor and in Kaneclor against the molecular weight M. The relations between $[\eta]$ and M for solutions in benzene (good solvent) and in cyclohexane (Θ solvent) are also shown in the figure. Obviously, no significant difference is observed between $[\eta]$ in Aroclor and that in Kaneclor. It falls very near to that in benzene, a good solvent. Therefore chlorinated diphenyl, irrespective of the degree of chlorination, is as good a solvent as benzene is for poly-α-methylstyrene.

Steady Shear Compliance. As seen in Table I, the steady shear compliance increases with increasing molecular weight if compared at the same concentration. It simply increases with concentration for solutions in Kaneclor but varies in a complicated manner in Aroclor. This difference may be due to the difference in the range of concentration investigated. It may be easily seen that J_e is zero for the solvent and it increases with increasing concentration of the polymer at low concentration. In the range of high concentration it is well known that J_e decreases with increasing concentration. Thus J_e assumes a maximum value at some concentration which depends probably on the molecular weight of the polymer and on the viscosity of the solvent.

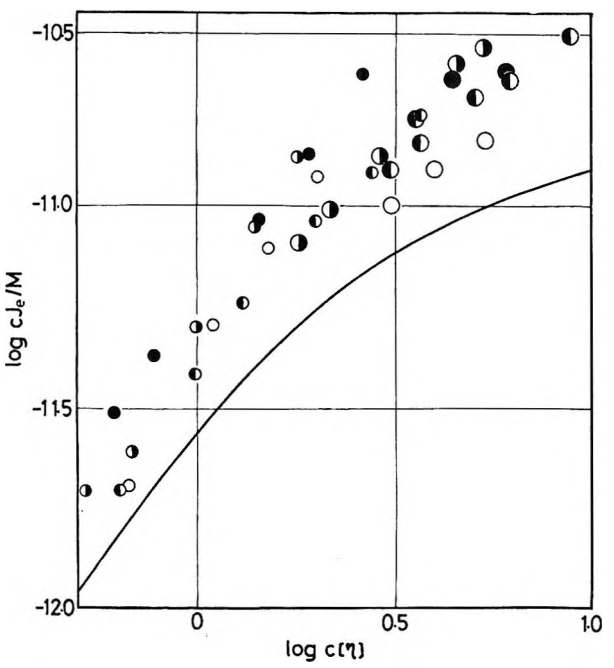

Figure 3. Reduced steady shear compliance cJ_e/M plotted against reduced concentration c $[\eta]$ for dilute poly-α-methylstyrene solutions in chlorinated biphenyl. Large circles represent the results in Aroclor and small circles in Kaneclor. Different types of circles represent different molecular weight; white circles, 1.68×10^6; right black, 1.43×10^6; left black, 6.40×10^5; and black, 3.55×10^5. The curve represents the relation given by eq 3 of the text.

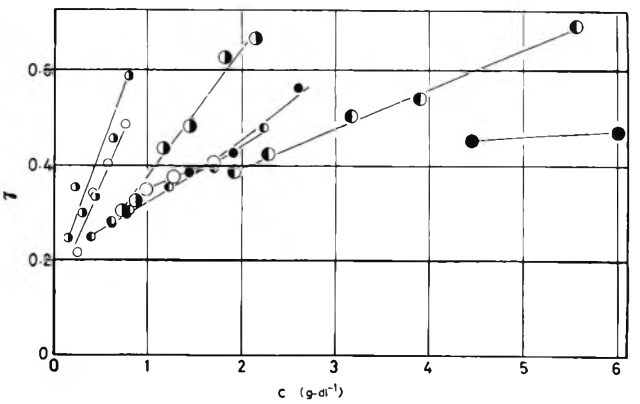

Figure 4. The parameter γ plotted against the concentration c for dilute poly-α-methylstyrene solutions in chlorinated biphenyl. The meaning of the marks is the same as shown in Figure 3.

On this problem, Holmes, *et al.*,[3] proposed from a phenomenological consideration an equation

$$J_e = (M/5RT)c[\eta]^2/(1 + c[\eta]/2)^2 \qquad (3)$$

where R and T are the gas constant and the temperature, respectively. In order to see the validity of this equation for the present data, J_ec/M is plotted against $c[\eta]$ in Figure 3. The curve corresponding to eq 3 is also written in the figure. Several observations can be made on the figure. First the quantity J_ec/M for a given solvent seems to be determined solely by the reduced concentration $c[\eta]$. That is to say, J_ec/M when plotted against $c[\eta]$, falls very near to a single curve which is independent of the molecular weight of each solution, although the data are fairly scattered. Secondly, the relation between cJ_e/M and $c[\eta]$ is affected by the viscosity of the solvent at least at high values of $c[\eta]$. Thus cJ_e/M is a little larger in Kaneclor solutions than in Aroclor solutions compared at the same value of $c[\eta]$. Thirdly, the observed values for J_ec/M are much larger than predicted from Holmes' equation. The discrepancy is about 50% at low $c[\eta]$, increases monotonously with increasing $c[\eta]$, and the maximum discrepancy observed is about 300%. This discrepancy is quite large even if the experimental error is considered. Therefore eq 3 may not be applied to poly-α-methylstyrene solutions. However, we are tempted to conclude that this discrepancy is not due to the difference in material. It is most probable that the discrepancy is due to the difference in the range of molecular weight studied by Holmes, *et al.*, and by us. The study of Holmes, *et al.*, covers the range of molecular weight lower than ours does. In fact, some values of J_e reported for high molecular weight samples in their paper are in good agreement with the present data, showing deviation from the prediction of eq 3, though the original authors attributed it to the

effect of molecular weight distribution. In this connection, we note that the maximum of J_e as function of concentration often attains to a value several times larger than the prediction of eq 3.[10,11]

Comparison with Molecular Theories. It was pointed out in previous publications that a parameter γ, a kind of reduced steady shear compliance, is convenient for molecular theoretical discussion of slow deformation of dilute polymer solutions. The parameter γ is defined as

$$\gamma = (cRT/M)(\eta/\eta - \eta_s)^2 J_e \qquad (4)$$

This quantity is written as S'/S^2 in Holmes' paper.[3] In theories based on spring-bead models, this quantity assumes a value 0.40 if the flow line of the solvent is assumed not to be disturbed by the polymer segment (free draining case)[12] and a value 0.206 if it is assumed to be perturbed extremely (nonfree draining case).[13]

The parameters γ for poly-α-methylstyrene solutions were calculated from the viscosity and the steady shear compliance in Table I and added to the last column of the table. They are plotted against the concentration in Figure 4. It is seen at once that the parameter γ is an increasing function of the molecular weight, the concentration, and the viscosity of the solvent except for sample BB7 where the value of γ is lower than that of BB5 with a lower molecular weight. T he parameter seems to increase almost linearly with eincreasing concentration. Therefore the result may be extrapolated to zero concentration although without much accuracy. The extrapolated values of γ at zero concentration lie between 0.15 and 0.25 except for the solution of the sample BB9 in Aroclor for which the experiment was restricted to a narrow range of rather high concentration. From this result it is concluded that the γ value of infinitely dilute polymer solutions is very close to 0.2 even in a good solvent. The theory based on the spring-bead models can be applied to slow deformation of extremely dilute polymer solutions with the assumption that the flow line of the solvent is highly perturbed by existence of the polymer segments. This result is in agreement with the current interpretation of the intrinsic viscosity of polymers.[14]

Effect of Finite Concentration. In the range of finite concentration the value of γ increases almost linearly with increasing concentration and attains a value as high as 0.7. In the experimental relation of the parameter γ and the concentration, the value 0.40 for γ does not seem to have a special significance; no inflection point or no tendency to saturation is observed at the value 0.40 for γ. This result is in contrast with the result of Holmes, *et al.*, who found that the γ value increases monotonously from 0.2 with increasing concentration and does not much exceed 0.4 even if the concentration is increased to the range of so-called concentrated solution. The present data for poly-α-methylstyrene does not show any tendency to saturation at least if $\gamma < 0.6$. This discrepancy may be due to the difference in the range of molecular weight studied by these two groups. The same reason as stated in the last part of the discussion of J_e leads to the conclusion that γ for high molecular weight increases from 0.2 with increasing concentration, takes on a maximum value much higher than 0.4 at moderate concentration, and then decreases in the range of higher concentration.[10,11] This result may imply that the free draining limit does not have special significance in the actual flow of dilute polymer solutions and that the increase of γ with increasing concentration should be attributed to other mechanism than the decrease of hydrodynamic interaction.

(10) M. Kurata, K. Osaki, and M. Tamura, *Bull. Inst. Chem. Res., Kyoto Univ.*, **46**, 87 (1968); K. Osaki, Y. Einaga, T. Sugie, M. Kurata, and M. Tamura, to be published.

(11) H. Janeschitz-Kriegl, *Advan. Polym. Sci.*, **6**, 170 (1969).

(12) P. E. Rouse, *J. Chem. Phys.*, **21**, 1272 (1953).

(13) B. H. Zimm, *ibid.*, **24**, 266 (1956).

(14) P. J. Flory, "Principles of Polymer Chemistry," Cornell University Press, Ithaca, N. Y., 1953, Chapter 14.

Faradaic Admittance of the Bis(diethylenetriamine)cobalt(III)-Bis(diethylenetriamine)cobalt(II) System

by Peter J. Sherwood and H. A. Laitinen

Department of Chemistry and Chemical Engineering, University of Illinois, Urbana, Illinois 61801
(Received January 17, 1969)

The impedance behavior of the bis(diethylenetriamine)cobalt(III)-bis(diethylenetriamine)cobalt(II) system at the dropping mercury electrode has been measured over the range 200 Hz to 20 KHz. The results could not be interpreted in terms of the classical model in which specific adsorption is ignored and separability of faradaic and nonfaradaic currents is assumed. The Senda-Delahay model was found inapplicable; the Sluyters-Rehbach-Delahay model yields results consistent with the adsorption of the single species (the oxidant), a large charge-separation capacitance, and a rapid charge-transfer reaction. Limits of error in the evaluation of the adjustable parameters are discussed.

Introduction

The faradaic admittance of the tris(ethylenediamine)-cobalt(III)-tris(ethylenediamine)cobalt(II) system has been found[1] to be anomalous, and has been interpreted in terms of specific adsorption of the reactants at a mercury surface. In the present study, another cobalt(III)-cobalt(II) system was chosen to see whether analogous behavior would be found and whether the electrode impedance could be interpreted in the light of recent theories.[2-4]

The amine chosen for this study was diethylenetriamine (dn), a tridentate ligand. High formation constants ($\log K_f^{II} = 14$; $\log K_f^{III} \sim 48$) assured the metal would be essentially entirely coordinated, even without added dn, or in the compact double layer, where the dn concentration could be considerably less than in bulk solution.

Theoretical Section

The experiment considered is the determination of the equivalent impedance or admittance of an electrochemical cell at a given frequency, ω, of sinusoidal potential variation. The sine wave alternating voltage is superposed onto a constant dc potential, not necessarily the equilibrium potential of the redox couple. The electrode reaction is ox + $ne \rightarrow$ red.

The *a priori* inseparability of faradaic and nonfaradaic currents has been suggested by Delahay;[2] based on his three fundamental equations, he later treated the problem of faradaic impedance.[3]

Sluyters and coworkers[4] have questioned Delahay's expansions of $d\Gamma_i/dt$'s, Γ_i's being surface excesses; $\Gamma = \Gamma_{ox} + \Gamma_{red}$. According to Timmer,[4] Γ may be expressed as a function of three independent variables, c_{ox}, c_{red}, and E, with the c's representing concentrations at the electrode surface, and E the instantaneous potential of the indicator electrode

$$\Gamma = \Gamma(c_{ox}, c_{red}, E)$$

For systems with large rate constants, use of the Nernst equation reduces the number of independent variables by one, and we may write

$$\frac{d\Gamma}{dt} = \left(\frac{\partial\Gamma}{\partial c_{ox}}\right)_E \frac{dc_{ox}}{dt} + \left(\frac{d\Gamma}{\partial E}\right)_{c_{ox}} \frac{dE}{dt} \quad (1a)$$

or

$$\frac{d\Gamma}{dt} = \left(\frac{\partial\Gamma}{\partial c_{red}}\right)_E \frac{dc_{red}}{dt} + \left(\frac{\partial\Gamma}{\partial E}\right)_{c_{red}} \frac{dE}{dt} \quad (1b)$$

depending on our choice of variables.

If either ox or red is only weakly adsorbed at the electrode, eq 1 can be approximated by (as pointed out by a referee, these approximations are also valid at saturation coverage, where $(\partial\Gamma/\partial c_i)_{j\neq i}$ is also small)

$$\frac{d\Gamma}{dt} \simeq \left(\frac{\partial\Gamma}{dE}\right)_{c_{ox}} \frac{dE}{dt} \quad (2a)$$

or

$$\frac{d\Gamma}{dt} \simeq \left(\frac{d\Gamma}{\partial E}\right)_{c_{red}} \frac{dE}{dt} \quad (2b)$$

Equation 2a corresponds to eq 1a with $(\partial\Gamma/\partial c_{ox})_E$ small and eq 1b and 2b with $(\partial\Gamma/\partial c_{red})_E$ small. In Delahay's original treatment of the faradaic impedance, and

(1) H. A. Laitinen and J. E. B. Randles, *Trans. Faraday Soc.*, **51**, 54 (1955).

(2) P. Delahay, *J. Phys. Chem.*, **70**, 2373 (1966).

(3) P. Delahay and G. Susbielles, *ibid.*, **70**, 3150 (1966).

(4) B. Timmer, M. Sluyters-Rehbach, and J. H. Sluyters, *J. Electroanal. Chem.*, **15**, 343 (1967).

also in a paper by Sluyters-Rehbach,[5] an assumption mathematically equivalent to eq 2 was made, namely

$$\frac{d\Gamma}{dt} = \frac{d\Gamma}{dE}\left(\frac{dE}{dt}\right) \tag{3}$$

In neither of these papers was only one species assumed adsorbed; however, in a later paper by Timmer,[4] impedance data for In(III) in 1 *M* KCNS were found to fit a model in which the reduced form was not adsorbed ($\Gamma_{red} = 0$). It was also found in their analysis that the same results were obtained whether eq 3 or the more rigorous eq 1 was used in the derivation. From eq 2 that result is explicable by assuming, as did Timmer, that only one species is specifically adsorbed, so that the first term in eq 1 may be neglected.

Assuming eq 3 is valid, it may be shown that

$$Y' = \frac{\omega^{1/2}}{\sigma}\frac{p+1}{p^2+2p+2} + \omega K\frac{p}{p^2+2p+2} \tag{4}$$

and

$$Y'' = \frac{\omega^{1/2}}{\sigma}\frac{1}{p^2+2p+2} + \omega K\frac{p+2}{p^2+2p+2} + \omega C_d$$

wherein Y' and Y'' are the real and imaginary components of the cell admittance after correction for the solution resistance. The parameters p and K are defined according to Sluyters-Rehbach[5] by

$$p = p'\omega^{1/2} = \frac{\theta}{\sigma\omega^{-1/2}}$$

$$K = \frac{\sigma_{ox}}{\sigma}nF\frac{d\Gamma_{ox}}{dE} + \frac{\sigma_{red}}{\sigma}\left(nF\frac{d\Gamma_{red}}{dE}\right)$$

with θ, the charge-transfer resistance, and σ, the Warburg coefficient, given by

$$\theta = RT/nF_{i_0}$$

and

$$\sigma_{ox} = \frac{RT[1+\exp(-\phi)]}{n^2F^2\sqrt{2D_{ox}}(c^b_{ox} + d^{1/2}c^b_{red})}$$

$$\sigma_{red} = \frac{RT[1+\exp(\phi)]}{n^2F^2\sqrt{2D_{ox}}(c^b_{ox} + d^{1/2}c^b_{red})}$$

$$\sigma = \sigma_{ox} = \sigma_{red} = \frac{4RT}{n^2F^2\sqrt{2D_{ox}}(c^b_{ox} + d^{1/2}c^b_{red})}\cosh^2\left(\frac{\phi}{2}\right)$$

$$\phi = \frac{nF}{RT}(E_{DC} - E_{1/2})$$

The charge-transfer resistance and the Warburg coefficient are as defined by Randles;[6] D is the diffusion coefficient, $E_{1/2}$ is the polarographic half-wave potential, c^b is the bulk concentration, i_0 is the exchange current density at E_{DC}, and the other symbols have their usual significance.

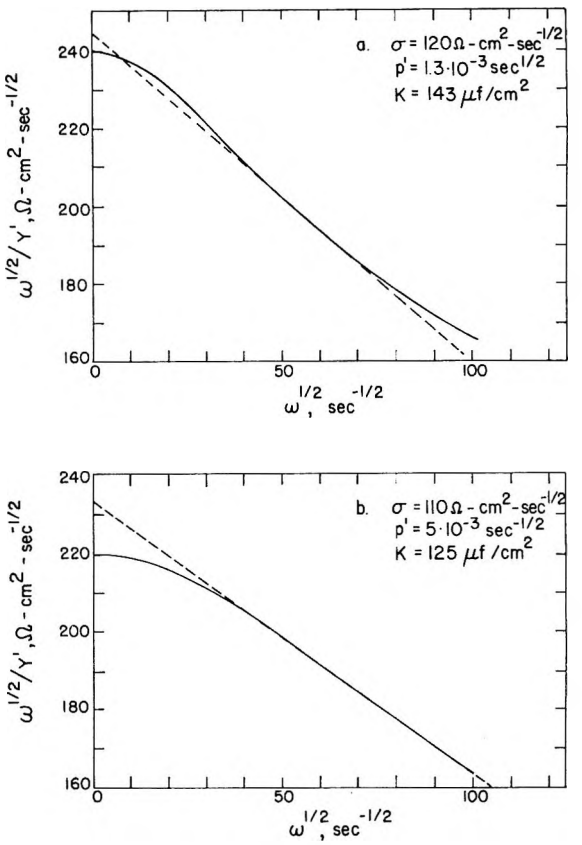

Figure 1. Calculated $\omega^{1/2}/Y'$ *vs.* $\omega^{1/2}$ curves.

The function $\omega^{1/2}/Y'$ may be written from eq 4 as

$$\frac{\omega^{1/2}}{Y'} = \frac{p^2+2p+2}{\frac{p+1}{\sigma} + \omega^{1/2}Kp} \tag{5}$$

The limiting value of p at zero frequency is zero, since $p = p'\omega^{1/2}$. Proceeding from eq 5

$$\lim_{\omega^{1/2}\to 0}\left(\frac{\omega^{1/2}}{Y'}\right) = \frac{2}{1/\sigma} = 2\sigma \tag{6}$$

From eq 6 it is evident that a plot of $\omega^{1/2}/Y'$ *vs.* $\omega^{1/}$ should have an intercept of 2σ. Taking the derivative of eq 5 with respect to $\omega^{1/2}$ gives

$$\frac{d}{d\omega^{1/2}}\left(\frac{\omega^{1/2}}{Y'}\right) = \frac{\omega^{1/2}p'(p'/\sigma - 2K)(p'\omega^{1/2}+2)}{\left[\frac{p'\omega^{1/2}}{\sigma} + \frac{1}{\sigma} + Kp'\omega\right]^2}$$

as $\omega^{1/2}$ becomes small

$$\lim_{\omega^{1/2}\to 0}\left[\frac{d}{d\omega^{1/2}}\left(\frac{\omega^{1/2}}{Y'}\right)\right] = \frac{0}{1/\sigma^2} = 0$$

so the limiting slope is zero, and $\omega^{1/2}/Y'$ cannot be linear with $\omega^{1/2}$, as implied by Sluyters-Rehbach[5] even in the case where $K = 0$. To illustrate this point,

(5) M. Sluyters-Rehbach, B. Timmer, and J. H. Sluyters, *J. Electroanal. Chem.*, 15, 151 (1967).

(6) J. E. B. Randles, *Discuss. Faraday Soc.*, 1, 11 (1947).

Figure 1 shows plots of $\omega^{1/2}/Y'$ *vs.* $\omega^{1/2}$ for $p' = 1.3 \times 10^{-2}$, $\sigma = 120$ ohm cm^2/sec$^{-1/2}$, $K = 143$ μF/cm^2 (Figure 1a), and for $p' = 0.5 \times 10^{-2}$, $\sigma = 110$ ohm cm^2/sec$^{-1/2}$, $K = 125$ μF/cm^2 (Figure 1b). These values for p', σ, and K are taken from Table II of Sluyters-Rehbach's data for 0.5 m*M* Pb(II) in 0.01 *M* HCl and 1 *M* KCl. Equation 4 was used to calculate $\omega^{1/2}/Y'$. The experimental data in ref 3 were obtained over the frequency range 320–4500 Hz; thus the smallest value of $\omega^{1/2}$ was 45. In Figure 1a, a straight-line extrapolation to $\omega^{1/2} = 0$ using only points with $\omega^{1/2} \geq 45$ gives $2\sigma = 233$, while the actual function $\omega^{1/2}/Y'$, a sigmoid curve, has an intercept of 240, as predicted by eq 6. Here the error of +1.7% is hardly enough to detect by comparison of half the intercept with a σ calculated from polarographic data. However, Figure 1b shows a much worse case: the straight-line intercept is 234, compared to the correct value of 220. This error of +6% is enough to cause quite a variation in the calculated charge separation parameters. Such a variation is evident from Sluyters-Rehbach's calculations of p', θ, K, and C_d from a single set of impedance data, but using different values for σ; thus, choosing $\sigma = 115$, they calculated $p' = 0.008$, $\theta = 0.9$, $K = 124$, $C_d = 27$, but choosing $\sigma = 120$, they obtained $p' = 0.013$, $\theta = 1.6$, $K = 143$, $C_d = 41$.

To calculate σ accurately from polarographic data requires precise evaluation of at least one of the diffusion coefficients; in this work D_{ox} and D_{red} were determined from single drop current–time curves, to a precision of about 1%. The accuracy of these measurements is not directly verifiable, however.

An alternative not used in this work is to treat σ as unknown and find the best fit of the experimental data to a model with C_{dl}, K, p', and σ as parameters to be found.

In this connection it should be mentioned that as long as no present model completely accounts for observed faradaic impedance behavior, the Sluyters-Delahay model with three parameters is to be preferred to the Senda–Delahay model[7] which has six.

Experimental Section

Impedance measurements were made on solutions consisting of 0.98 *M* $NaClO_4$ + 0.0932 *M* dn as supporting electrolyte and various concentrations of Co(II) and Co(III). Co(III) was added as a stock solution of $Co(dn)_2(ClO_4)_3$, while Co(II) was generated by partial reduction of the Co(III). A conventional cell was used; the temperature was held constant at 25° by a water jacket. A large platinum gauze served as counter electrode, and a saturated sodium chloride calomel electrode (ssce) was connected by two salt bridges to the cell solution. The dropping mercury electrode used was all-Pyrex glass.

A transformer bridge, the Wayne-Kerr B221 Universal Bridge (Wayne-Kerr Corp., Montclair, N. J.) was employed for impedance measurements, using an external HP 241A oscillator (Hewlett-Packard, Palo Alto, Calif.) as source and a GR1232-A tuned amplifier (General Radio Co., West Concord, Mass.) as detector. The advantages of this transformer bridge over conventional ac Wheatstone bridges as previously used in this laboratory were lower noise pickup, due to the low impedance of the bridge transformers, and simpler grounding arrangements, obviating the need for Wagner earthing. Dc potentials were applied to the cell as shown in Figure 2; the dc blocking capacitors, C, were 250-μF electrolytic condensers, placed with opposite polarity to cancel any parasitic voltages. The inductor L was wound on a 2-cm toroidal ferrite core and consisted of 21 turns of no. 18 wire; its function was to keep the 4.5-mHz oscillator in the birth detector from being shorted out by the bridge. Because of the low resistance of the bridge transformers—typically 0.06 ohm—it was unnecessary to correct for iR drop in the bridge circuit. The components shown in the dotted outline contributed a small but significant impedance, Z_{corr}, to the total measured by the bridge; correction was effected by measuring Z_{corr} alone with the Wayne-Kerr Q221 low impedance adapter. Graphs of $Z_{corr} = R_{corr} + jX_{corr}$ were made *vs.* frequency, f (at high frequencies), and $1/f$ (at low frequencies) over the range used, 200 Hz to 20 kHz, and the smoothed curves used to obtain the appropriate corrections. At 1 kHz, $Z_{corr} = 0.250 - 1.09j$ ohms ($j = \sqrt{-1}$).

The time interval between drop birth and bridge balance was measured on the oscilloscope which was used as a null detector. The oscilloscope time base was calibrated immediately following each experiment. Drop birth was indicated by an overdamped 4.5-MHz oscillator circuit connected between the DME and counterelectrode, a large platinum gauze. The transformer bridge used measured parallel conductance, G_p, and capacitance, C_p. These were converted to series impedances through the relations

real

$$Z_s = \frac{1}{G_p\left[1 + \left(\frac{\omega C_p}{G_p}\right)^2\right]}$$

imaginary

$$Z_s = \frac{1}{\omega C_p\left[1 + \left(\frac{G_p}{\omega C_p}\right)^2\right]}$$

From the real part of Z_s the solution resistance was subtracted; real and imaginary components of Z_{corr} were also subtracted and both parts of Z multiplied by drop area to obtain Z' (real) and Z'' (imaginary), both in

(7) M. Senda and P. Delahay, *J. Phys. Chem.*, **65**, 1580 (1961).

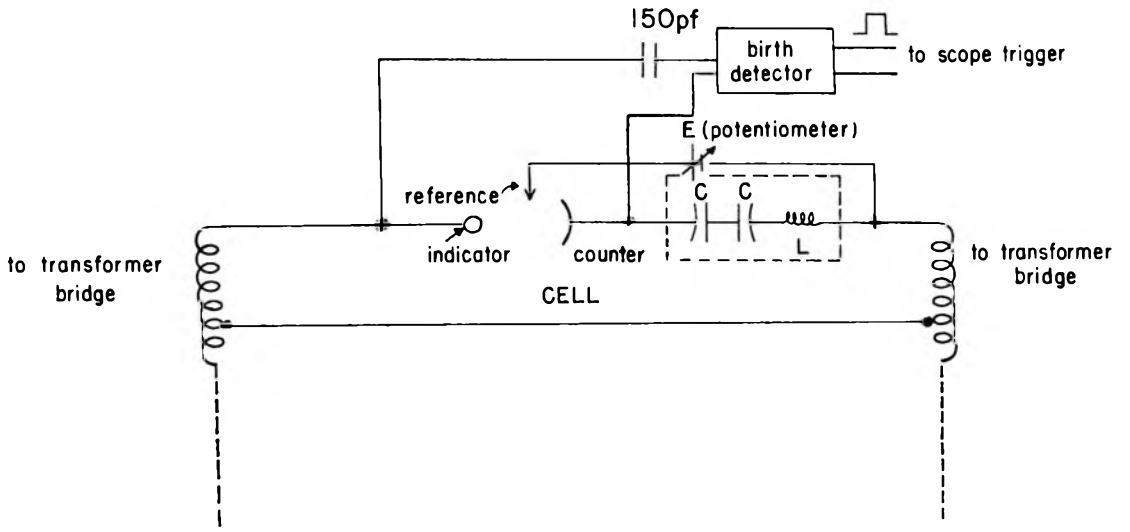

Figure 2. Cell connection.

ohm cm². These were converted to parallel admittances by the relations

$$Y' = \frac{z'}{(z')^2 + (z'')^2}; \qquad Y'' = \frac{z''}{(z')^2 + (z'')^2}$$

in which ′ indicates the real and ″ the imaginary components.

The area of the drop at balance was calculated by the procedure described by Nancollas and Vincent.[8] The Warburg coefficient, σ, was calculated from the polarographic data $D_{ox}^{1/2} = 2.33 \times 10^{-3}$, $D_{ox}^{1/2}/D_{red}^{1/2} = 1.010$ ($D_{ox}^{1/2}$, as calculated from Koutecky's eq for instantaneous current,[9] was found to increase about 2.5% between 3 and 5 sec after drop birth. The value given is for 2.5 sec after drop birth, the time at which the impedance was measured.) and $E_{1/2} = -431.5$ mV *vs.* ssce.

The parameter p in eq 4 was obtained by writing that equation for any two frequencies and solving simultaneously for $p' = p\omega^{-1/2}$ and K. In this way p', K values were computed for each of the $n(n-1)/2$ pairs of the n points in a set of data. The values of p' were then put into numerical order and divided into classes by the first two significant figures of its value. A histogram was made of the frequency of occurrence of each class. If the distribution of frequencies was anywhere near Gaussian looking, the median value was chosen. In cases where an abnormal looking histogram was found, an attempt was made to choose a value which was the median of a smaller subgroup within the histogram; *i.e.*, if there were two clumps of recurring values, the median of the group with the most points was chosen.

Sluyters-Rehbach[5] describes straight-line plots for evaluation of θ, K, and C_d, using equations derived from eq 5 and 6. Thus

$$Y'\left(\frac{p^2 + 2p + 2}{p}\right) - \frac{\omega^{1/2}}{\sigma} = \frac{1}{\theta} + \omega K \qquad (7)$$

$$Y'\left(\frac{p+2}{p}\right) = Y'' = \frac{1}{\theta} - \omega C_d \qquad (8)$$

$$\frac{1}{\omega}\left(Y'' - \frac{Y'}{p+1}\right) = \frac{K}{p+1} - C_d \qquad (9)$$

Plots of the left-hand side of eq 7 and 8 *vs.* ω, and of eq 9 *vs.* $1/(p+1)$ gave two values each for θ, K, and C_d.

Results and Discussions

Table I shows the electrode parameters calculated from experimental data such as those given in Table II for one set of conditions; additional data for other experimental conditions are available.[10] The subscripts 0, 1, and 2 refer to plots of eq 7, 8, and 9, respectively. It may be seen that there is good agreement between θ_0, θ_1, and p'_σ ($= \theta$); C_{d_1} and C_{d_2}; and K_0, K_2, and K, the last being the best value calculated from eq 4 by the procedure described in the Experimental Section. Plotting Z_f' and Z_f'' *vs.* $\omega^{-1/2}$ (Randles' model[6] for the faradaic impedance) did not give the predicted parallel straight lines; Z_f' was curved, and Z_f'' had a negative intercept. The Randles equivalent circuit is inapplicable in case of specific adsorption.

Figure 3 shows the double-layer capacitance as a function of potential. The lower graph gives the capacitance for the supporting electrolyte, C_{d_1}, as measured in the conventional manner. The sharp rise in capacitance at potentials anodic of −350 mV is due to the pseudocapacitance associated with the oxidation of Hg to $Hg_2(dn)_2^{2+}$. This rise unfortunately obscures the usual hump near the electrocapillary maximum

(8) G. H. Nancollas and C. A. Vincent, *Electrochim. Acta*, 10, 97 (1965).

(9) J. Koutecky, quoted in J. Heyrovsky and J. Kuta, "Principles of Polarography," Academic Press Inc., New York, N. Y., 1966, p 137.

(10) P. Sherwood, Ph.D. thesis, University of Illinois, 1968.

Table I: Calculated Electrode Parameters for the Sluyters-Delahay Model

Bulk, Co(III), mM	Bulk, Co(II), mM	$-E$, mV ssce	$10^2p'$, sec$^{1/2}$	σ, ohm cm^2 sec$^{1/2}$	$p'\sigma$, ohm cm^2	K, μF/cm^2	θ_0, ohm cm^2	θ_1, ohm cm^2	C_{d1}, μF/cm^2	C_{d2}, μF/cm^2	K_0, μF/cm^2	K_2, μF/cm^2
0.500	0	425	0.54	666.9	3.60	17.3	3.69	3.57	23.6	21.7	17.6	15.0
0.500	0	430	0.55	656.4	3.61	17.9	3.70	3.68	22.6	22.1	17.8	18.8
0.500	0	435	0.61	659.0	4.02	17.9	4.16	4.02	23.2	22.4	18.0	18.9
0.500	0	440	0.67	676.0	4.53	18.0	4.62	4.54	23.4	22.2	17.6	19.3
0.500	0	445	0.74	704.2	5.21	16.7	5.26	5.26	23.9	23.7	15.9	16.7
1.061	0	446	1.9	361.7	6.86	51.5	7.70	6.99	23.5	23.0	51.5	61.0
1.061	0	446	1.9	335.3	6.37	59.0	6.25	5.65	17.7	22.6	53.8	76.0
1.283	2.467	448	3.2	96.68	3.10	170	3.03	3.03	40.2	37.5	222	228
3.701	0	325	4.3	89.02	3.04	310	3.84	4.34	39.9	40.0	327	343
3.765	0	440	1.6	89.81	1.44	170	1.45	1.45	13.6	17.8	175	175

(ecm): an inflection point is barely present, at about -520 mV.

The upper graph in Figure 3 shows C_d, the double-layer capacitance in the presence of 0.5 mM $Co(dn)_2^{3+}$ in the immediate vicinity of $E_{1/2}$. There is a significant lowering of the capacitance in the presence of the redox couple, with the minimum occurring at -430 mV, very close to $E_{1/2}$. Furthermore, the increase cathodic of -430 mV is in opposition to a decrease in the capacitance of the supporting electrolyte. As the reduction in all probability involves adsorption of a transition state activated complex, it is not surprising that the minimum double-layer capacitance occurs near $E_{1/2}$.

From the theory of semi-infinite linear diffusion to a planar electrode one may calculate the concentrations of the $Co(dn)_2^{2+}$ and $Co(dn)_2^{3+}$ at the electrode surface and compare them to the change in C_d, taken as $C_d - C_{d_1} = \Delta C$. Figure 4 shows such a comparison. If only one form, oxidant or reductant, were adsorbed, a plot of the surface concentration should be directly related to the adsorption isotherm for the species adsorbed, while ΔC should vary randomly with the surface concentration of the other species. It is assumed that adsorption of either species changes C_d in the same direction. Figure 4 indicates that ox is adsorbed much more strongly than red, as the c_{ox} *vs.* ΔC plot is a smooth curve, and the c_{red} *vs.* ΔC graph is not. The same set of data is being plotted in both graphs, so that the points are not independent. The evidence of this plot is not really conclusive; a better set of experiments would be a series with constant c_{ox} and varying c_{red} and vice versa. From Figure 4, lim $\Delta C \simeq -15$ μF/cm^2, corre-

Table II: Data for 0.500 mM Co(III) at -440 mV

Freq, Hz	Z', ohm cm^2	Z'', ohm cm^2	Y', (ohm cm^2)$^{-1}$	Y'', (ohm cm^2)$^{-1}$
10,000	0.0727	0.4915	0.2946	1.9908
8,000	0.1072	0.5955	0.2929	1.6264
6,000	0.1529	0.7608	0.2537	1.2632
4,000	0.2160	1.0861	0.1760	0.8856
2,000	0.4541	1.9665	0.1114	0.4827
1,000	0.9439	3.5244	0.0709	0.2647
900	1.0673	3.8230	0.0677	0.2426
800	1.1770	4.2388	0.0608	0.2190
700	1.3493	4.7166	0.0560	0.1959
600	1.6068	5.3529	0.0514	0.1713
500	1.9942	6.1734	0.0473	0.1466
400	2.4538	7.3497	0.0408	0.1224
335	2.9898	8.5158	0.0367	0.1045
235	4.2953	11.1326	0.0301	0.0781

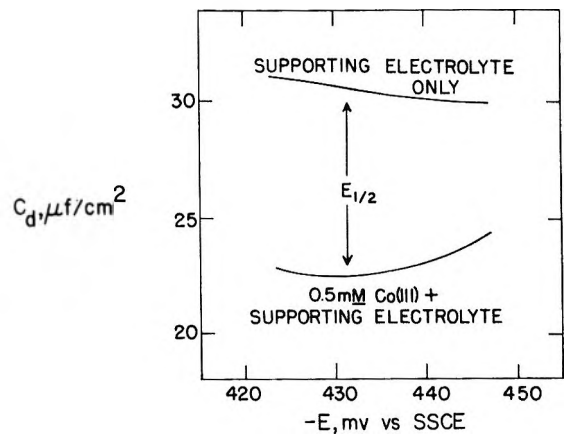

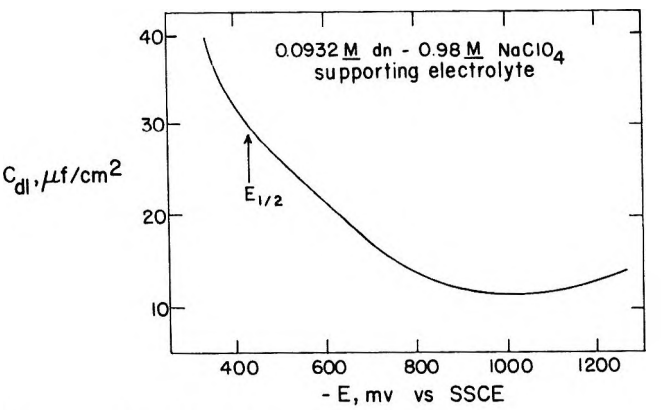

Figure 3. Double-layer capacitance.

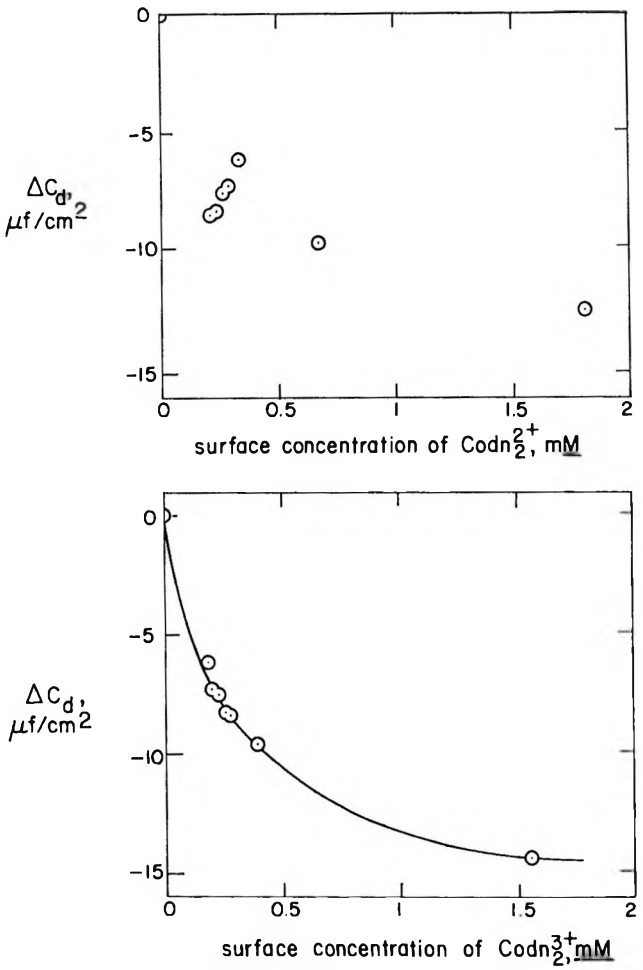

Figure 4. Changes in C_d.

sponding to high concentrations of Co in solution (not necessarily full coverage of the electrode surface). In theory, it would be possible to find the adsorption isotherm by rfist assuming a dependence of the free energy of adsorption on potential and then attempting to fit the data to isotherm models;[11] however, in view of the limited number of data, and Parsons' arguments that charge is a more suitable electrical variable than potential, such a correlation will not be attempted here. A less sophisticated approach is discussed later in connection with the discussion on K.

The ecm for the supporting electrolyte (0.0932 M dn and 0.98 M $NaClO_4$) was at −450 mV *vs.* ssce, as determined from drop-time measurements. In the presence of 4.11 mM Co(III), the ecm shifts anodically to −405 mV, indicating predominantly cation specific adsorption. These electrocapillary curves are shown in Figure 5; the two curves are displaced from each other along the ordinate, so the drop times are not comparable as to absolute value. The reason for this shift is that it was not possible to obtain reproducible drop times between replicate experiments, although curve shape was relatively invariant. Thus $\partial^2\gamma/\partial E^2$ but not γ was calculated from electrocapillary curves.

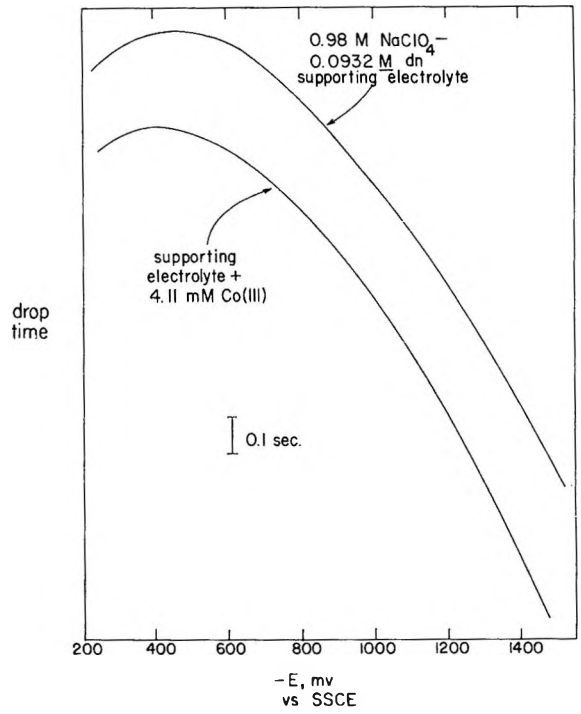

Figure 5. Electrocapillary curves.

A derivation analogous to that of Mohilner's thermodynamic derivation for double-layer properties in the presence of a faradaic reaction[12] was used by Timmer, Sluyters-Rehbach, and Sluyters[4] to derive the following relation between the interfacial tension γ and the double-layer parameters for the Sluyters–Delahay model

$$-\left(\frac{\partial^2\gamma}{\partial E^2}\right) = \frac{dq}{dE} + K - \frac{n^2F^2}{RT}\left(\frac{\sigma_{ox}\sigma_{red}}{\sigma^2}\Gamma\right) \qquad (10)$$

This equation was applied to a solution of 1.061 mM Co(III) at −446 mV. The measurements were made at 20°. From a plot of $d\gamma/dE$ *vs.* E, the slope $= (d^2\gamma/dE^2)$ at −446 mV was found to be −13.87 μF/cm². From Table I, $C_d = dq/dE = 23.25$ μF/cm², and K is 51.5 μF/cm². From eq 10, with $\sigma_{ox}/\sigma = 0.6443$ and $\sigma_{red}/\sigma = 0.3555$, Γ was calculated to be 0.697×10^{-10} mol/cm².

As Timmer points out,[4] if a low total concentration of the electroactive species is used, it is reasonable to approximate the adsorption of said species by a linear isotherm, *i.e.*

$$\Gamma_i = k_i c_i \qquad (11)$$

From the behavior of ΔC it was deduced that the oxidized species was more strongly adsorbed than the reduced; if Γ_{red} is assumed to be negligible, and if

$$\frac{1}{k_{ox}}\frac{dk_{ox}}{dk} \ll \frac{1}{c_{ox}}\frac{dc_{ox}}{dE} \qquad (12)$$

(11) R. Parsons, *J. Electroanal. Chem.*, **5**, 397 (1963).
(12) D. M. Mohilner, *J. Phys. Chem.*, **66**, 724 (1962).

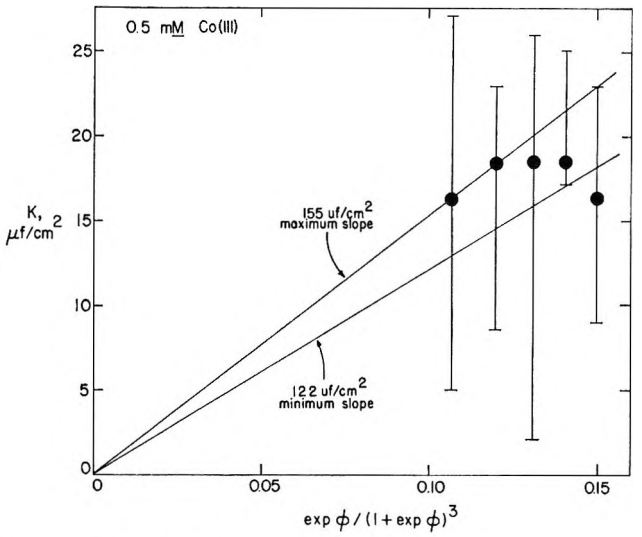

Figure 6. Variation of K.

it may be shown[13] that

$$K = k_{ox}c^{b}_{ox}\frac{n^2F^2}{RT}\frac{\exp\phi}{(1+\exp\phi)^3} \qquad (13)$$

with $\theta = (nF/RT)(E_{dc} - E_{1/2})$. From our data we can show either eq 11 or eq 12 is applicable: according to eq 13, a plot of K against $(\exp\theta)/(1+\exp\theta)^3$ should be linear, with zero intercept and a slope of $k_{ox}c^{b}_{ox}(n^2F^2/RT)$. Figure 6 shows this plot for $c^{b}_{ox} = 0.5$ mM, $c^{b}_{red} = 0$. It is evident that not all the points fall on a line passing through the origin, a consequence of the large error inherent in the calculation of K from the impedance data. Errors shown are 1% limits of error calculated from a standard propagation-of-errors treatment, using the following limits of error, λ, estimated for the experimental variables from replicate measurements: $\lambda(E) = 2$ mV, $\lambda(E_{1/2}) = 0.5$ mV, $\lambda(D_{ox}^{1/2})/D_{ox}^{1/2} = 1\%$, $\lambda(D_{red}^{1/2})/D_{red}^{1/2} = 1.5\%$, $\lambda(t)/t = 1.5\%$, $\lambda(G_p)/G_p = 0.5\%$, $\lambda(C_p)/C_p = 0.5\%$, $\lambda(R_{soln})/R_{soln} = 1\%$, $\lambda(R_{corr})/R_{corr} = 3\%$, $\lambda(X_{corr})/X_{corr} = 3\%$. From the slope of 151 $(+4, -29)$ μF/cm^2, (based on lines passing through the origin), k_{ox} is estimated as 8.04 $(+0.21, -1.5) \times 10^{-5}$ cm, or the area "covered" by a single molecule is 414 Å^2. At a surface concentration of 0.5 mM, then, $\Gamma_{ox} = 0.4 \times 10^{-10}$ mol/cm^2, and $0.33 \times 10^{-10} \leq \Gamma_{ox} \leq 0.41 \times 10^{-10}$. This value may be compared with $\Gamma_{ox} = 1.0 \times 10^{-10}$ mol/cm found by Timmer[4] for 0.4 mM In(III) 1 M KCNS. It should be noted that for the indium, as here for the cobalt, no abnormality was evident from the shape of the electrocapillary curve.

According to the above assumptions, at a surface concentration of 0.380 mM, corresponding to that existing at the electrode for 1.061 mM Co(III) at -446 mv, the value of Γ_{ox} would be 0.304×10^{-10} mol/cm^2. That at least one of the assumptions inherent in eq 11 and 12 is invalid for this higher surface concentration is easily shown: if the assumptions are allowed, it can be demonstrated[4] from eq 10, 11, and 12, expressions for σ_{ox} and σ_{red}

$$\sigma_{ox} = \frac{\sigma}{1+\exp(\phi)}; \qquad \sigma_{red} = \frac{\sigma}{1+\exp(-\phi)}$$

and

$$\frac{c^{b}_{ox}}{c_{ox}} = 1 + \exp(\phi)$$

that

$$-\left(\frac{\partial^2\gamma}{\partial E^2}\right) = \frac{dq}{dE} + K(1 - \exp(\phi)) \qquad (14)$$

but with $K = 51.5$ μF/cm^2, $\exp\phi = 0.552$, and $C_d = 23.3$ μF/cm^2, the right-hand side of eq 14 becomes 46.4 μF/cm^2, while $-d^2\gamma/dE^2$ is 13.9 μF/cm. It is likely that neither the linear isotherm (eq 11) nor the potential independence of k_{ox} (eq 12) is true for the higher Co concentration.

An estimate of the kinetic parameters is possible in principle from the variation of θ, the charge-transfer resistance, with E_{DC}. From the well-known equation

$$\theta = \frac{RT}{n^2F^2k_{sh}c_{ox}^{1-\alpha}c_{red}^{\alpha}} \qquad (15)$$

a plot of $\log\{n^2F^2/RT\theta c_{ox}\}$ *vs.* ϕ has a slope $\alpha/2.303$ and an intercept of $-\log k_{sh}$ at E^0. Because of the large errors in θ and a moderate error in ϕ, the plot of $\log\{n^2F^2/RT\theta c_{ox}\}$ proved unworkable. From eq 15, if $c_{ox} = c_{red}$, the unknown α vanishes. The data taken at -429.8 mV are closest to E^0 ($E^0 = E_{1/2} + RT/nF \ln d^{1/2} = -431.8$ mV, with $d^{1/2} = D_{red}^{1/2}/D_{ox}^{1/2} = 0.99$). Allowing for $\lambda(\phi) = 0.097$, $0.249 \leq c_{ox} \leq 0.273$ and $0.229 \leq c_{red} \leq 0.254$. Considering the function $\xi_x(\alpha, c_{ox}, c_{red})$ defined by

$$\xi = 10^6c_{ox}^{1-\alpha}c_{red}^{\alpha}$$

we may say that $0.229 \leq \xi \leq 0.273$ (assuming $0 \leq \alpha \leq 1$). An analysis of the error involved gives $2.71 \leq \theta \leq 6.64$. Use of eq 15 permits calculation of the limits of error for k_{sh}, the heterogeneous first-order rate constant at E°: $0.147 \leq k_{sh} \leq 0.429$ cm/sec. The large lower limit of k_{sh} ensures that the redox process is reversible, justifying the use of the Nernst equation in writing eq 1.

Some of the data were also analyzed according to the theory of Senda and Delahay.[7] In view of the objections of Sluyters *et al.*[14] to the high- and low-frequency extrapolation method used by Baticle and Perdu,[15] the analysis was treated as a problem in nonlinear least-squares fitting with R_t, R_{ao}, R_{ar}, C_{ao}, C_{ar}, and C_d as six parameters to be determined. The fitting procedure

(13) G. S. Smith, *Trans. Faraday Soc.*, **47**, 63 (1951).

(14) M. Sluyters-Rehbach, B. Timmer, and J. A. Sluyters, *J. Electroanal. Chem.*, **19**, 302 (1968).

(15) A. M. Baticle and F. Perdu, *ibid.*, **13**, 364 (1967).

used was that outlined by Wolberg.[16] In many cases, the best-fit values for these parameters were inconclusive, because of large standard deviations in their estimated values. The large uncertainties are attributable to two features of the Senda–Delahay model which make it unsuitable for meaningful analysis of faradaic impedance data: too many adjustable parameters and a lack of physical justification.

For 0.5 mM Co(III) over the potential range −425 to −445 mV, R_t was found roughly constant at 2.6 ohm cm², and C_d remained around 30 μF/cm². Since R_t is expected to vary exponentially with E, the Senda–Delahay model is inapplicable. The other four parameters varied irregularly with potential.

(16) J. R. Wolberg, "Prediction Analysis," Van Nostrand-Reinhold Co., Inc., Princeton, N. J., 1967.

Transport Properties of Borosilicate Glass Membranes in Molten Salts

by Harmon M. Garfinkel

Research and Development Laboratories, Corning Glass Works, Corning, New York 14830 *(Received October 27, 1969)*

The transference numbers of potassium and sodium into Code 7740 borosilicate glass were determined as a function of bath composition and temperature. The mobility ratio $u_{Na}:u_K$ is essentially independent of salt-bath composition at 354°; the temperature coefficient of the mobility ratio was found to be 10.9 ± 0.5 kcal/mol. These results are in good agreement with those determined from emf studies and reported previously. The enthalpy change for potassium for sodium exchange in the borosilicate glass was estimated to be 3.2 ± 0.9 kcal/mol; the change in entropy at 354° was estimated to be 4.4 ± 0.9 eu. The effect of the two-phase nature of the borosilicate glass is discussed with respect to potassium for sodium and silver for sodium ion exchange.

Introduction

In terms of the ion-exchange model for membrane potentials, the mobility ratio plays an important role in determining the electrode selectivity of a glass electrode.[1] Although equilibrium–sorption measurements indicated that Corning Code 7740 borosilicate glass is a two-phase system, the electrode behavior of the glass in fused sodium nitrate–potassium nitrate was fitted quite satisfactorily by the ion-exchange model without explicitly taking the two-phase nature of the glass into account.[2] It was assumed that only the minor borosilicate phase was potential determining, and this assumption allowed calculation of the mobility ratio $u_{Na}:u_K$ as a function of temperature.

In this work the transport numbers of sodium and potassium are determined from sodium nitrate–potassium nitrate melts into the borosilicate glass as a function of composition and temperature. The mobility ratios $u_{Na}:u_K$ were then calculated from these results and found to be independent of composition and in good agreement with those values reported in ref 2. The significance of these results is discussed with respect to those reported by Keenan and Duewer[3] on the transport numbers of silver and sodium into the borosilicate glass from binary melts.

Experimental Section

The technique used was similar to that reported by Keenan and Duewer.[3] The transport numbers were determined by measuring the change in composition of a borosilicate glass bulb filled with a silver nitrate–sodium nitrate melt and immersed in a sodium nitrate–potassium nitrate melt, after the passage of a known amount of current for a known amount of time.

The transference cell consisted of a Vycor brand beaker fitted with a transite top, which had four holes drilled into it to position the borosilicate glass bulb, a 96% silica glass stirring rod, a 96% silica glass thermocouple well, and a large platinum electrode. The glass bulbs, which were blown at the end of borosilicate tubing 5 mm o.d. × 3 mm i.d. × 12 cm long, were 30 mm in diameter with a wall thickness of 0.2–0.3 mm. The dc resistances of these bulbs varied from 5 to 7 kilohms at 354°. The internal solution was a mixture of silver nitrate–sodium nitrate (7 to 80 mol % silver nitrate depending on the temperature) into which was immersed a silver-wire cathode. The external solution

(1) G. Eisenman, "Glass Electrodes for Hydrogen and Other Cations," Marcel Dekker, Inc., New York, N. Y., 1967, pp 133–173.

(2) H. M. Garfinkel, *J. Phys. Chem.*, **73**, 1766 (1969).

(3) A. G. Keenan and W. H. Duewer, *ibid.*, **73**, 212 (1969).

was a 745 g sodium nitrate–potassium nitrate mixture into which was immersed a large platinum anode of several square centimeters in surface area. This whole assembly was heated in a Marshall tube furnace and maintained at constant temperature within ±1°.

The power supply for the electrolysis was an E/M Model C638 constant current source. The total charge passed through the cell was determined with an Analytical Instruments current integrator. Input currents ranged from 1 to 20 mA. The instrument was calibrated frequently with a GR-Type 631-BL strobotac operated from an American Time Products frequency standard at 10,000 cps. A 1-ohm L and N standard resistor was put in series with the current integrator and power supply. The current was adjusted so that the potential drop across the resistor measured with an L and N Type K-2 potentiometer was 60.30 mV; and then the 0.1 A input resistor of the current integrator was trimmed so that the bar of the stroboscope disk attached to the shaft of the control motor appeared stationary when viewed with the strobotac.

The borosilicate bulb along with the salt and electrode was weighed before and after electrolysis. In addition, the bulb alone was weighed before and after electrolysis. The salt was removed by repeated washings with distilled water in an ultrasonic cleaner. In several runs after removal of the salt, the electrolyzed bulb was dissolved in an $HF–H_2SO_4$ solution and analyzed for sodium and potassium with a flame photometer. Blank determinations were made on the unelectrolyzed borosilicate glass bulbs. It was assumed that sodium and potassium carried all the current through the borosilicate glass, since it is well known that only cations are mobile in silicate glass.

Charles,[4] in studies of phase separation in sodium borosilicate glasses, concluded that Code 7740 glass is a two-phase system. He suggested that one phase is borate rich and contains virtually all the sodium in the glass, while the other phase is almost all silica. The volume fraction of the conductive borosilicate phase can be estimated from Charles' data to be about 0.14. Charles suggested further that phase separation in the borosilicate glass is essentially complete and that the minor phase is continuous. Our results on ion-exchange equilibrium between the borosilicate glass and potassium nitrate–sodium nitrate melts as well as Doremus' results with silver nitrate–sodium nitrate are consistent with the two-phase model.[2,5] It was concluded from our work and Charles' results that the major phase was high in silica and contained about 0.08 of the sodium originally in the glass, while the minor phase is essentially a borosilicate glass with 0.92 of the sodium originally in the glass. Doremus and Turkalo[6] reported that they could see phase separation with the electron microscope on a 30-Å scale after heightening the contrast by silver exchange. Since the borosilicate glass contains some chloride, we believe Doremus and Turkalo actually saw silver chloride nucleated by the borate-rich phase.[7] However, this does not alter the conclusion that the borosilicate glass is phase separated.

In calculating the transference numbers it was assumed from the ion-exchange equilibrium studies that potassium would exchange and carry current only through the borosilicate phase. Sodium would exchange and carry current through both phases. We seek the mobility of potassium relative to sodium in the borosilicate phase, which, we suggested in our emf studies, determined the membrane potential.[2] Therefore, it was assumed that the fraction of sodium transported through phase I, the major phase (*i.e.*, high in silica), is equal to N_I, the mole fraction of exchange sites in phase I. The amount of potassium taken up by thermal exchange, *i.e.*, in the absence of an applied field, which never exceeded 5% of the potassium introduced into the glass by electrolysis, was subtracted from the total potassium in the glass. Independent data on the amount of uptake of potassium as a function of temperature were used for the correction.[8] It was assumed that the equilibrium-sorption isotherm is ideal in applying this correction.

Thus, from the weight change of the bulb, salt, and electrode, the transference number of potassium in the borosilicate phase is given by

$$t_{K,II} = \frac{\Delta W_T^* - \phi M_{Na}}{\phi(M_K N_{II} - M_{Na}) + N_I \Delta W_T^*}$$

where ΔW_T^* is the total weight change corrected for thermal exchange, ϕ is the number of Faradays passed through the cell, and M is the gram-atomic weight. The transference number of potassium is calculated from the weight change of the bulb alone by

$$t_{K,II} = \frac{\Delta W_b^*}{\phi N_{II}(M_K - M_{Na}) + N_I \Delta W_b^*}$$

where ΔW_b^* is the weight change of the bulb corrected for any thermal exchange. Finally, the transference number of potassium is determined from the results of the chemical analyses by

$$t_{K,II} = \frac{2\Delta f_{K_2O} W_s - M_{K_2O} Q A}{M_{K_2O}(\phi N_{II} - N_I Q A) + 2 N_I \Delta f_{K_2O} W_s}$$

where Δf_{K_2O} is the difference in the weight fraction of potassium oxide before and after electrolysis, W_s is the weight of glass sample analyzed, M is the gram-molecular weight as indicated, Q is the number of moles of potassium taken up by thermal exchange, and A is the superficial area of the bulb exposed to

(4) R. J. Charles, *J. Amer. Ceram. Soc.*, **47**, 559 (1964).
(5) R. H. Doremus, *J. Phys. Chem.*, **72**, 2665 (1968).
(6) R. H. Doremus and A. M. Turkalo, *Science*, **164**, 418 (1969).
(7) H. M. Garfinkel, *Appl. Opt.*, **7**, 789 (1968).
(8) H. M. Garfinkel, *Phys. Chem. Glasses*, in press.

the molten salt. Since the bulb was not filled completely, A was estimated from the expression for the area of a curved surface of a spherical segment. Once $t_{K,II}$ is determined, $t_{Na,II}$ is obtained from $t_{K,II} + t_{Na,II} = 1$.

Results and Discussion

The transference numbers of potassium and sodium into the minor phase of the borosilicate glass were determined as a function of external bath composition at 354°. The transference number of potassium $t_{K,II}$ is given in Table I as a function of the mole fraction of potassium in the molten salt at 354°. Thus, the transference number is a strong function of bath composition, and any junction model for membrane potentials of the borosilicate glass electrode would have to be consistent with this concentration dependence.

Table I: Transport Data for a KNO_3–$NaNO_3$ Melt into the Borosilicate Glass at 354°

N_{KNO_3}	ϕ, mfara-days	$t_{K,II}$	ΔW_T,[a] mg	Method[b]
0.400	7.9432	0.0165	185.3	Av T and b
0.500	6.0456	0.0278	141.9	Av T and b
0.600	6.1485	0.0455	145.9	Av T and b
0.700	6.0541	0.0672	145.0	Av T and b
0.800	3.6965	0.166	94.79	T
0.800	1.4750	0.140	37.47	Av T and b
0.900	1.1727	0.303	32.77	T
0.942	1.2170	0.457	36.97	T
0.950	2.3970	0.514	74.99	T
0.990	0.5854	0.791	20.96	T
0.990	0.6356	0.812	23.23	T

[a] Not corrected for thermal exchange. [b] T = total weight change, b = weight change of bulb.

In a previous report,[2] it was suggested that the electrode selectivity constant k of the borosilicate glass is given by

$$k = \beta K_{II} \tag{1}$$

where $\beta = u_{Na,II}/u_{K,II}$, the mobility ratio of sodium and potassium in the borosilicate phase, and K_{II} is the ion-exchange selectivity constant for the borosilicate phase. Since it was assumed that the borosilicate phase is thermodynamically ideal[2]

$$k = \beta \frac{a_{Na}\bar{N}_{K,II}}{a_K\bar{N}_{Na,II}} \tag{2}$$

where a refers to activity in the melt and $\bar{N}$ refers to mole fraction in the glass. The transport number of sodium in phase II is

$$t_{Na,II} = \frac{\bar{N}_{Na,II}u_{Na,II}}{\bar{N}_{Na,II}u_{Na,II} + \bar{N}_{K,II}u_{K,II}} \tag{3}$$

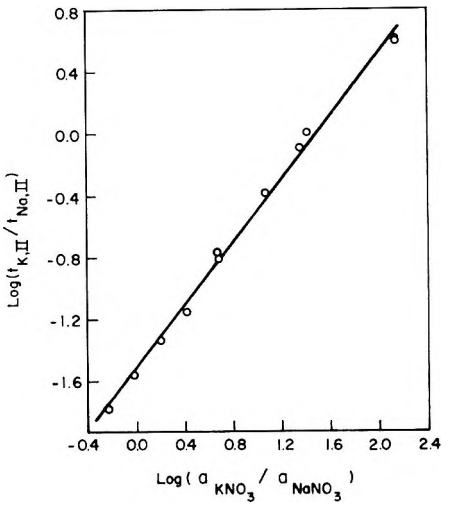

Figure 1. Dependence of the transference numbers of potassium and sodium in the borosilicate phase on bath composition.

Combining eq 2 and 3 yields the transference number of sodium in the borosilicate phase as

$$t_{Na,II} = \frac{\beta^2\omega N_{Na}}{k + N_{Na}(\beta^2\omega - k)} \tag{4}$$

where N refers to the mole fraction in the molten salt and $\omega = \gamma_{Na}/\gamma_K$, the ratio of activity coefficients of the two salts in the melt. Since it was assumed that the molten sodium nitrate–potassium nitrate mixture is a regular solution,[2] ω is obtained from

$$\log \omega = -\frac{442}{2.303RT}(1 - 2N_{Na}) \tag{5}$$

The electrode selectivity k was determined previously[2] and is given experimentally by

$$\log k = 6.063 - \frac{2.0531 \times 10^3}{T} \tag{6}$$

Rearranging eq 4, one finds that the mobility ratio β is given by

$$\beta^2 = \frac{t_{Na,II}N_K k}{t_{K,II}N_{Na}\omega} \tag{7}$$

Thus, from eq 7 a plot of log $(t_{K,II}/t_{Na,II})$ against log (a_K/a_{Na}) should have a slope of unity if β^2/k is independent of composition. Such a graph is shown in Figure 1. The slope of the curve is 1.02, indicating that β^2/k and hence β are indeed independent of composition. Since the intercept of the graph in Figure 1 is log (k/β^2), the mobility ratio β was found to be 22.5 ± 1.2 with $k = 15.6$ from eq 6. In view of eq 1, K_{II} was determined as 0.692 ± 0.064 at 354°. Thus, while the transference number is a function of composition, the mobility ratio is not, and it is the latter quantity that is more useful in any model for membrane potentials.

The transference numbers of potassium and sodium into the borosilicate glass were determined over the temperature range 235–401° in an equimolar potassium nitrate–sodium nitrate bath. The results are summarized in Table II. Although there is some scatter, the general trend is for $t_{K,II}$ to decrease with increasing temperature. The mobility ratio which was calculated from the data in Table II and eq 6, is plotted in Figure 2 against the reciprocal of the absolute temperature on semilogarithmic paper. The points (squares) calculated from emf and ion exchange equilibrium data and reported previously[2] are included for comparison. The line in Figure 2 was obtained by a least-squares analysis of the points obtained from the transference-number data. The temperature coefficient of the mobility ratio was found to be 10.9 ± 0.5 kcal/mol. From eq 1, the ion-exchange selectivity constant K_{II} was found to be given by

$$\log K_{II} = 0.9581 - \frac{0.6967 \times 10^3}{T} \qquad (8)$$

Thus, $\Delta H°$ for potassium for sodium exchange in the borosilicate phase is 3.21 ± 0.87 kcal/mol; at 354°, $\Delta S°$ = 4.39 ± 0.87 eu. The calculated value of K_{II} from eq 8 is 0.702, which is in good agreement with the value obtained from the data in Figure 1. At 454°, K_{II} = 1, in fair agreement with the values of K_{II} obtained by ion-exchange equilibrium studies described in ref 2. The value of the enthalpy change is reasonably close to the value obtained in a soda–alumina–titania–silica glass.[9] Thus, it is shown that emf, equilibrium sorption, and transference studies can be used to characterize the ion-exchange properties of glass. Furthermore, these results show that in a fixed-site membrane, such as the borosilicate glass, the electrode selectivity is determined mainly by the difference in mobility of the two exchanging species.

Table II: Transference Numbers of Potassium as a Function of Temperature in the Equimolar Potassium Nitrate–Sodium Nitrate Melt

Temp, °C	$t_{K,II}$	Method[a]
235	0.187	c
237	0.175	Av T and b
237	0.109	b
248	0.142	c
250	0.0881	T
258	0.0823	Av T and b
269	0.0450	Av T and b
269	0.0375	T
286	0.0549	Av T and b
303	0.0436	T
304	0.0529	Av T, b, and c
311	0.0375	T
345	0.0275	b
353	0.0278	Av T and b
378	0.0372	c
381	0.0259	c
381	0.0328	b
401	0.0208	b

[a] T = total weight change, b = weight change of the bulb, c = chemical analysis.

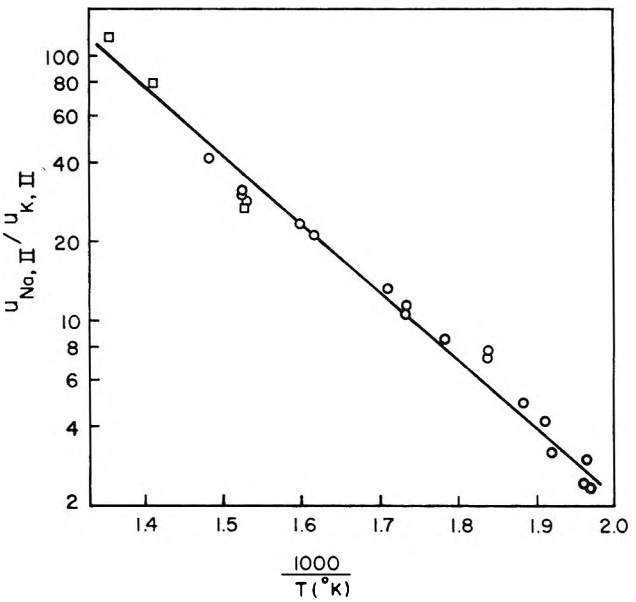

Figure 2. Temperature dependence of the mobility ratio in the borosilicate phase: □, ref 2; ○, this study.

Tracer-diffusion studies of sodium (22) in the borosilicate glass gave an activation energy for self-diffusion of sodium of about 22 kcal/mol.[8] From the temperature coefficient of the mobility ratio, the activation energy for self-diffusion of potassium in the glass is estimated to be 11 kcal/mol. Thus, the slower ion, which is also the larger ion, has a smaller activation energy than the faster ion. However, studies of the electrical conductivity in the end members prepared by melting would be expected to indicate that the ions have about the same activation energies for self diffusion, although the absolute rates would be different.[10] This emphasizes the fact that the structure of the glass is determined by its composition during melting at high temperatures. Once the glass is cooled below the glass transition temperature, the structure remains the same, even if ion exchange occurs. Data on the density variation in an ion-exchanged glass indicates that some relaxation does take place during the course of ion exchange. de Waal[11] has suggested that there is some relaxation process that occurs in ion-exchanged glass upon reheating at temperatures well below the transformation range. This is most likely related to the relaxation phenomenon discussed recently with respect to strengthening.[12]

(9) H. M. Garfinkel, *J. Phys. Chem.*, **72**, 4175 (1968).

(10) R. H. Doremus in "Ion Exchange," J. A. Marinsky, Ed., Marcel Dekker Inc., New York, N. Y., 1969, pp 1–42.

(11) H. de Waal, *Phys. Chem. Glasses*, **10**, 108 (1969).

(12) H. M. Garfinkel, *Glass Ind.*, **50**, 28, 74 (1969).

The good agreement between mobility ratios determined by emf-equilibrium studies and emf-transference studies represents a satisfactory test of the ion-exchange model for membrane potentials and justifies the assumption that the borosilicate phase is potential determining.

Keenan and Duewer[3] found that the transference numbers of sodium and silver ions at 318° into the borosilicate glass are equal to their respective mole fractions in the binary nitrate melt. They explained this result in terms of a junction model without surface

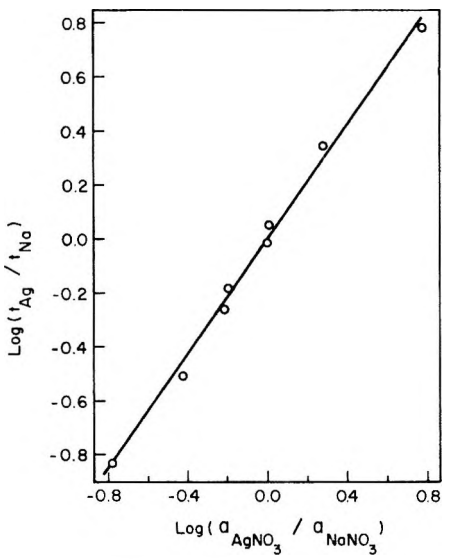

Figure 3. Dependence of the transference numbers of silver and sodium on bath composition from data in ref 3.

exchange in contrast to their earlier membrane potential studies, which required an ion-exchange model.[13,14] However, one does not necessarily need to use a junction model to explain their results. Doremus[5] showed that the ion-exchange selectivity coefficient for Ag^+–Na^+ exchange in the borosilicate glass at 335° is essentially constant ($K_{NaAg} \approx 2$) from about 0.05–0.40 mole fraction silver nitrate in the melt; below 0.05 mole fraction silver nitrate the selectivity coefficient depended on concentration. With the assumption that the selectivity coefficient is constant over the range 0.1–0.9 mole fraction silver nitrate, Keenan's and Duewer's results can be plotted according to eq 7 in the same way that the potassium nitrate–sodium nitrate results for the borosilicate glass were treated. This is shown in Figure 3; the quantity ω was obtained from[9]

$$\log \omega = \frac{590}{2.303RT}(1 - 2N_{Na}) \qquad (9)$$

The line drawn through the points was obtained by the least-squares method, which yielded a slope of 1.06 and a value of 1.01 ± 0.03 for β^2/k. Since the electrode selectivity k_{NaAg} was reported to be about unity with little temperature variation,[15] the average mobility ratio $u_{Na}:u_{Ag}$ through the borosilicate glass is also unity. Inspection of eq 4 shows that when k and β are unity, the transference number of sodium is equal to its mole fraction, and similarly for the transference number of potassium. This is the result found by Keenan and Duewer. Thus, the ion-exchange selectivity coefficient over the range 0.1–0.9 mole fraction silver nitrate in the bath is also unity.

This analysis for Ag^-–Na^+ exchange neglects the two-phase nature of the borosilicate glass. Doremus[16] reported from the results of a study of diffusion of sodium and silver ions into the borosilicate glass at 335° that although the tracer-diffusion coefficient of sodium is essentially independent of concentration in the glass, the tracer-diffusion coefficient of silver decreases when $\bar{N}_{Ag}$ in the glass is less than about 0.3. It was suggested that this behavior is related to the two-phase nature of the borosilicate glass. Although the high-silica phase rejects potassium, it has a very high affinity for silver. At low silver concentrations most of the silver is in the major phase. Tighter binding of the silver ions in this phase leads to lower diffusion coefficients of the silver. At high concentrations of silver most of the silver is in the borosilicate phase in which it has the same diffusion coefficient as sodium. Thus, it is evident from the different behavior of silver and potassium how the two-phase nature of the borosilicate glass affects the overall exchange process.

Acknowledgment. The author is grateful to G. Eisenman and B. R. Sundheim for helpful discussions and R. J. Kerr for technical assistance.

(13) K. Notz and A. G. Keenan, *J. Phys. Chem.*, **70**, 662 (1966).
(14) A. G. Keenan, K. Notz, and F. L. Wilcox, *ibid.*, **72**, 1085 (1968).
(15) R. H. Doremus, *J. Electrochem. Soc.*, **115**, 924 (1968).
(16) R. H. Doremus, *Phys. Chem. Glasses*, **9**, 131 (1968).

Degrees of Freedom Effect and Internal Energy Partitioning upon Ion Decomposition

by Y. N. Lin and B. S. Rabinovitch

Department of Chemistry, University of Washington, Seattle, Washington 98105 *(Received October 21, 1969)*

A random statistical theory has been applied to the internal energy partitioning that accompanies parent ion decomposition for a homologous series of primary alcohols from propanol to heptanol. The metastable ion abundances upon decomposition of the common product ion $C_2H_5O^+$ were calculated on this basis and found to be in reasonable agreement with the data of McLafferty and Pike which demonstrated the dependence of the metastable ion abundances on the number of internal degrees of freedom of the parent alcohol.

Introduction

Fragmentation of vibrationally excited molecular ions has recently been examined from the point of view of energy partitioning among the fragments produced. McLafferty and Pike[1] studied the fragmentation of homologous alcohol series. They found that the log of the relative abundance of the metastables produced from the intermediate $C_2H_5O^+$ ion was inversely proportional to the number of vibrational degrees of freedom in the parent molecular alcohol ion. This experimental demonstration is novel and important.

A degrees of freedom effect was also later examined by Cooks and Williams[2] in the study of the relative rates of fragmentation of benzoyl ions generated by electron impact upon different precursors.

This phenomenon has not heretofore been the subject of quantitative theoretical examination. By assuming the randomization of the *excess* energy of the molecule ion above the critical threshold for reaction, *i.e.*, $E^{\dagger M} = E^M - E_0^M$, among the active degrees of freedom of the activated complex of concern, as is appropriate in the RRKM formulation, it should, in principle, be a straightforward matter to calculate the distribution of excess energy among the fragment species in the case of endothermic reactions involving no reorganization energy of the products. This model is applicable whenever the initially formed electronic states relax quickly to the lowest level.

In this paper the model has been applied to the calculation of the energy distribution in the fragmentation of normal primary alcohols which give rise to $C_2H_5O^+$ and alkyl radicals. As a practical matter, it is necessary to introduce several assumptions concerning specifics of energetics, critical threshold, molecule-ion structure, etc., which together may mean that the present results may not precisely represent the alcohol system. This is not too important, however, since we are primarily interested in exploring the expected behavior for what should be a typical illustrative system. It can then readily be seen whether the model reasonably encompasses observed behavior.

For exothermic reactions, or for endothermic processes which involve a reorganization energy of the products relative to the activated complex, *i.e.*, $E_0^M - E_0^{pr} > 0$, where E_0^{pr} is the zero point level of the products, it should be clear that RRK or RRKM unimolecular reaction theories offer no generalization concerning the distribution of the reorganization energy among products of decomposition: the latter aspect depends on the details of the potential surface.

Reaction Scheme

The general alcohol decomposition scheme is

$$RC_2H_4OH^+(M^+) \longrightarrow \begin{cases} C_2H_5O^+(P^+) + R & (a) \\ \xrightarrow{m^*(8.0)} H_3O^+(D^+) + C_2H_2 & (b) \\ \xrightarrow{m^{*\prime}(18.7)} CHO^+(D'^+) + CH_4 & (c) \end{cases} \quad (1)$$

where M^+ is the molecular ion produced by electron impact; the intermediate ion $C_2H_5O^+(P^+)$ formed from M^+ can undergo (metastable) decomposition to daughter ions D^+ and D'^+, corresponding to $m^* = 8.0$ and $m^{*\prime} = 18.7$, respectively; R is an alkyl radical.

Model for Energy Partitioning. The model for energy partitioning has the following features. (1) The total excess energy of M^+ is assumed available for energy partitioning and is completely randomized through all internal modes before decomposition. (2) For the homologous series, the excess energy of M^+ is assumed constant, and the only variable parameter is the chain length. (3) During the decomposition, one stretching mode disappears and becomes the relative translation, and the other five modes (if both fragments are

(1) F. W. McLafferty and W. T. Pike, *J. Amer. Chem. Soc.*, 89, 5951 (1967).

(2) R. G. Cooks and D. H. Williams, *Chem. Commun.*, 627 (1968).

polyatomic) go to the rotations and perpendicular relative translations; these are termed the transition modes. (4) The probability of the energy, ΔE, being found in P^+ is proportional to the product of the degeneracy, D, of the internal degrees of freedom of P^+, at energy ΔE, and the sum of the degeneracies of all permitted energy eigenstates of the active degrees of freedom of the rest of the molecule ion, *i.e.*, (alkyl radical plus transition modes) at energy $E^{\dagger M} - \Delta E$.

The probability of ΔE in $C_2H_5O^+$ is

$$Pr(\Delta E)_{P^+} = \frac{[D(\Delta E)_{P^+}]\left[\sum_{E^\dagger=0}^{E^{\dagger M}-\Delta E} P(E^\dagger)_{rest}\right]}{\sum_{E^{\dagger M}=0}^{E^{\dagger M}} P(E^{\dagger M})} \quad (2)$$

The total specific rate of decomposition of M^+ is (with neglect of centrifugal effects)

$$k(E^M) = \frac{C \cdot \sum_{E^{\dagger M}=0}^{E^{\dagger M}} P(E^{\dagger M})}{hN^*(E_0{}^M + E^{\dagger M})} \quad (3)$$

where $\Sigma P(E^{\dagger M})$ is the sum of the degeneracies of all permitted energy eigenstates of the activated complex of M^+, $N^*(E^M)$ is the density of eigenstates of the active degrees of freedom of M^+ at energy E, and C is a constant. No restrictions were placed on the small fraction of complexions which placed an energy greater than a bond dissociation energy in stretching modes. This ostensibly resulted in a slight overcount of states but helps to compensate for neglect of anharmonicity effects on the density of vibrational levels;[3] no consideration need be given these complications here.

Calculated Energy Distribution of $C_2H_5O^+$

Energy Distribution of M^+. It was assumed that the internal energy of M^+ has a "conventional" parabolic distribution[4] (Figure 1) which ranges from 0 to 13 eV (0–299 kcal mol^{-1}). If the critical threshold energy $E_0{}^M$ for alcohol ion decomposition is somewhere in the region of a C–C bond energy, say 69 kcal (3 eV),[5] the excess energy of M^+ ions which decompose is 0 to 230 kcal mol^{-1} (0 to 10 eV), with a truncated parabolic distribution. No account was taken of alteration of this shape due to competitive processes and their change in relative importance with energy.

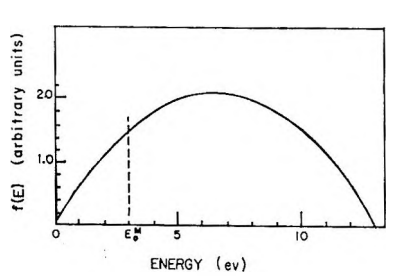

Figure 1. Internal energy distribution assumed for parent ions. The vertical line is at $E_0{}^M$ and the area to the right represents the excess energy distribution.

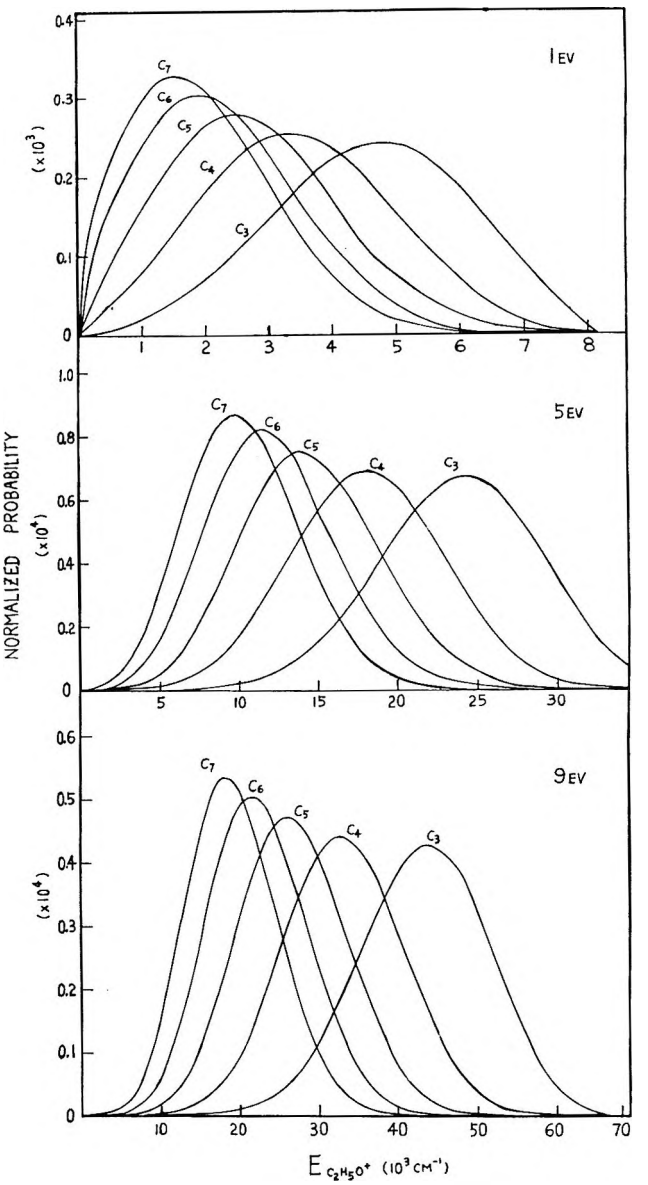

Figure 2. Curves showing random statistical distribution of excess energy of M^+ in $C_2H_5O^+$ product. Illustrative values of $E\dagger^M$ are 1, 5, and 9 eV.

Vibrational Models of the Molecular Ion and Activated Complex. Two vibrational models were considered for the activated complex for M^+ decomposition, a rigid model and a loose model. These correspond roughly to preexponential factors of $\sim 10^{13-14}$ and $\sim 10^{16-17}$ sec^{-1}, respectively, in the Arrhenius equation. In the former model, the complex retains the frequencies of the par-

(3) F. W. Schneider and B. S. Rabinovitch, *J. Amer. Chem. Soc.*, **84**, 4215 (1962).

(4) (a) I. Howe and D. H. Williams, *ibid.*, **90**, 5461 (1968); (b) R. G. Cooks, R. S. Ward, I. Howe, and D. H. Williams, *Chem. Commun.*, 837 (1968).

(5) A referee suggests that 1 eV is a better estimate; little change would result in the calculations and virtually none if the energy distribution of M^+ assumed ranges from 0 to 11 eV.

Table I: Some Energy Quantities for $C_2H_5O^+$

$E^{\dagger M}$, eV	Compd	E_{mp}, kcal (eV)	$\langle E \rangle$, kcal (eV)	$\langle E \rangle / E^{\dagger M}$	Fraction of DF[a]
1	C_3	13.7 (0.60)	12.9 (0.56)	0.56	0.60
	C_4	9.60 (0.42)	9.68 (0.42)	0.42	0.46
	C_5	7.20 (0.31)	7.65 (0.33)	0.33	0.38
	C_6	5.40 (0.23)	6.23 (0.27)	0.27	0.32
	C_7	4.40 (0.19)	5.32 (0.23)	0.23	0.27
3	C_3	39.0 (1.70)	39.2 (1.70)	0.57	
	C_4	30.4 (1.32)	29.4 (1.28)	0.43	
	C_5	23.3 (1.01)	23.4 (1.02)	0.34	
	C_6	19.0 (0.83)	19.2 (0.84)	0.28	
	C_7	16.1 (0.70)	16.4 (0.71)	0.24	
5	C_3	69.4 (3.02)	67.0 (2.91)	0.58	
	C_4	52.2 (2.27)	50.6 (2.20)	0.44	
	C_5	39.3 (1.71)	40.5 (1.76)	0.35	
	C_6	33.6 (1.46)	33.5 (1.46)	0.29	
	C_7	27.8 (1.21)	28.6 (1.24)	0.25	
7	C_3	98.1 (4.26)	94.5 (4.11)	0.59	
	C_4	72.5 (3.15)	72.0 (3.13)	0.45	
	C_5	58.1 (2.52)	57.8 (2.51)	0.36	
	C_6	48.1 (2.09)	48.0 (2.09)	0.30	
	C_7	39.6 (1.72)	41.2 (1.79)	0.26	
9	C_3	126.0 (5.48)	122.0 (5.31)	0.59	
	C_4	94.2 (4.10)	93.3 (4.06)	0.45	
	C_5	75.5 (3.28)	75.1 (3.26)	0.36	
	C_6	61.3 (2.67)	62.7 (2.72)	0.30	
	C_7	52.2 (2.27)	53.9 (2.34)	0.26	

[a] DF (degrees of freedom) in $C_2H_5O^+$: DF in M^+.

ent ion except for a C–C bond stretch assigned as the reaction coordinate. In the loose model, several frequencies are reduced relative to the parent. The assignments are given in the Appendix.

Computational Results. Calculations were made at integral values of $E^{\dagger M}$ for primary alcohols from C_3 to C_7. The two models for the activated complex gave similar distribution curves, the loose complex being shifted a little to lower energies; only the behavior for one of these models need be described in detail in the remainder of this paper.

Some illustrative distributions of the internal energy of the $C_2H_5O^+$ ion for the rigid complex case are shown in Figure 2 at three values of $E^{\dagger M}$. The distribution curves at other energies may be readily inferred; details of the distributions for all other energy states and for both complex models can be found in ref 6. It is seen that for a given value of $E^{\dagger M}$, the maximum probability shifts to lower energies with increase of molecular size. The separation of the maxima of the distribution curves also increases somewhat as $E^{\dagger M}$ increases.

Table I gives the most probable and the average energies of P^+ at some representative values of $E^{\dagger M}$. The fractions of the average energy carried by P^+ relative to the total excess energy are also given. As $E^{\dagger M}$ increases, the fraction of the average energy carried by P^+ approaches the fraction of the total degrees of internal freedom of M^+ associated with P^+.

Table II: The Standard Deviation and Coefficient of Dispersion for the Energy Distribution of P^+

$E^{\dagger M}$, eV	σ, kcal (eV)		K_σ	
	C_3	C_7	C_3	C_7
1	4.29 (0.19)	3.11 (0.14)	0.327	0.507
3	9.63 (0.42)	7.19 (0.31)	0.238	0.404
5	14.3 (0.62)	10.4 (0.45)	0.209	0.348
7	18.6 (0.81)	13.3 (0.58)	0.194	0.315
9	22.6 (0.98)	16.3 (0.71)	0.193	0.294

Because of the fluctuations about the average value,[7] the minimum value of $E^{\dagger M}$ required in order to produce a (small percentage of) daughter ion P^+ with sufficient energy to decompose further is simply the critical threshold value for the latter process. The standard deviation σ of the energy distribution in P^+ produced from various ROH^+ precursors has been calculated at five values of $E^{\dagger M}$. The coefficient of dispersion is defined as $K_\sigma = \sigma/a$, where a is the arithmetic mean. Illustrative calculational results are given in Table II. It is evident that σ increases as the molecular ion energy increases and decreases as the molecular ion size increases. The coefficient of dispersion decreases as the molecular ion energy increases and increases as the molecular ion size increases.

Relative Abundances of Parent $C_2H_5O^+$ and Metastable Ions

Thermochemistry and Structure of $C_2H_5O^+$. Several isomers of $C_2H_5O^+$ have been proposed;[8] heats of formation are listed under the structure number in kcal mol^{-1} (eV). From deuterium labeling and energetic studies of reaction 1b in 2-alkanols, Van Raalte and Harrison[12] proposed that the fragmenting ions had structure I

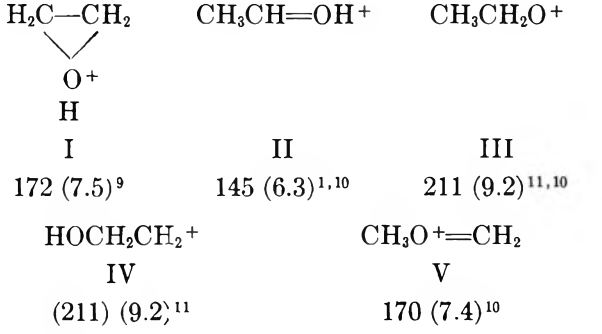

(6) Y. N. Lin, Ph.D. Thesis, University of Washington, 1970.

(7) H. M. Rosenstock and M. Krauss, "Mass Spectrometry of Organic Ions," F. W. McLafferty, Ed., Academic Press, New York, N. Y., Chapter 1.

(8) A. G. Harrison and B. G. Keyes, *J. Amer. Chem. Soc.*, **90**, 5046 (1968).

(9) J. L. Beauchamp and R. C. Dunbar, *ibid.*, **92**, 1477 (1970).

(10) A. G. Harrison, A. Ivko, and D. Van Raalte, *Can. J. Chem.*, **44** 1625 (1966).

(11) F. W. McLafferty, private communication.

(12) D. Van Raalte and A. G. Harrison, *Can. J. Chem.*, **41**, 3118 (1963).

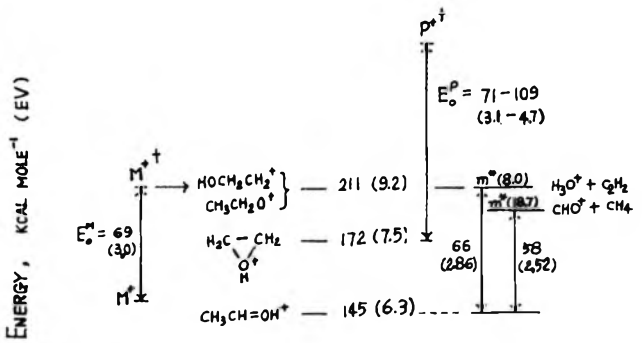

Figure 3. Schematic reaction path energy diagram.

rather than II; support was advanced by Shannon and McLafferty.[13] Recently, Harrison and Keyes[8] reported studies of 2-propanol-2-^{13}C; ^{13}C retention in CHO^+ (reaction 1c) indicates that 64% (using 20-eV electrons) or 52% (using 70-eV electrons) of the $C_2H_5O^+$ ions are structure I; support for II has been given recently.[9]

Since I apparently contributes most among isomers giving rise to the metastable decomposition, we have assumed for simplicity that we may specialize our considerations to the symmetrical oxirane ion structure for P^+. It is plausible that in the 1-alkanol decomposition, $C_2H_5O^+$ is formed with structure IV[13] and rearranges to I (and other isomers). Figure 3 is an energy diagram for reaction scheme 1. The constant increment 39 kcal (*i.e.*, 211–172) is to be superimposed on the distribution of P^+ in Figure 2.

Model for $C_2H_5O^+$ Decomposition. In order to calculate the mass spectrometric ion abundances, the critical threshold E_0^P for $C_2H_5O^+$ decomposition and vibrational models for the precursor and the activated complexes are required. No literature value for E_0^P is available and the consequences of several assumed values were examined, namely, 71, 78, 87, and 109 kcal mol^{-1} (3.08, 3.39, 3.78, and 4.74 eV), called cases a, b, c, and d, respectively. McLafferty, *et al.*,[1] have noted that the activation energies for the two paths in scheme 1 are closely the same, and that the specific rates differ by a factor of 1.8–2.8,[13,14] with m* (8.0) being larger. The activated complexes for the two decomposition paths were chosen to account for these facts (Appendix). The exact choice of frequencies is in no way crucial for our purpose here.

Relative Abundances. Metastables are observed in the conventional mass spectrometer if the rate constant $k(E^P)$ for decomposition is 10^5–10^6 sec^{-1}: for $k(E^P) > 10^6$ sec^{-1}, daughter ions are mainly observed and for $k(E^P) < 10^5$ sec^{-1}, most P^+ ions reach the collector. To find the yields of m* (8.0) and P^+ once E_0^P was assigned, the total energy E^P of I required to give a specific rate of decomposition of 3.3×10^5 sec^{-1} was computed. For the four E_0^P values of 71, 78, 87, and 109 kcal, E^P (3.3×10^5) is 76.2, 84.7, 96.2, and 124.8 kcal mol^{-1} (3.31, 3.68, 4.18, and 5.42 eV), respectively. By defining a practical energy width for metastable ion detection, the abundance can be found. An energy width was arbitrarily assigned to $k(E^P)$ values corresponding to one-tenth of the range from 10^5 to 10^6 sec^{-1}.[15] This range of $k(E^P)$ corresponds to 5.56 kcal (0.24 eV) for E_0^P = 71 kcal mol^{-1} (3.08 eV) and 6.86 kcal (0.30 eV) for E_0^P = 109 kcal mol^{-1} (4.74 eV), for the m* = 8.0 process. For simplicity, 5.71 kcal (0.25 eV) was taken for all cases in the calculation of the metastable ion abundances. This procedure is justified in the Appendix.

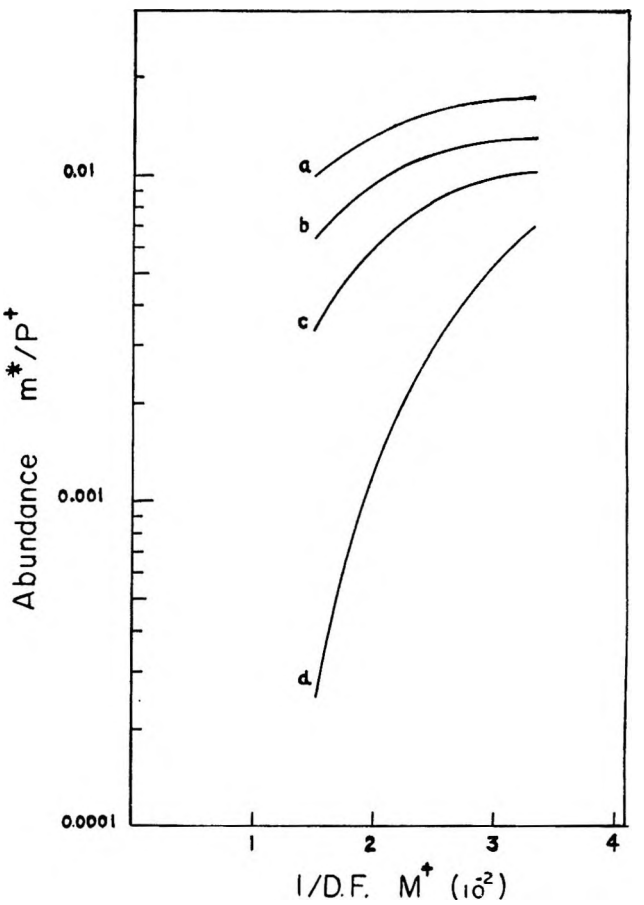

Figure 4. Illustration of variation of relative abundance of m* (8.0) *vs.* inverse degrees of freedom of M^+ for several assumed values of E_0^P ranging from 71 (case a) to 109 (case d) kcal mol^{-1}.

The relative abundance of the metastable and the parent ion was calculated for the energy distributions of P^+ (Figure 2), each evaluated at integral energy increment between 0 and 10 eV for $E^{\dagger M}$. The parabolic weighting of Figure 1 was applied to each energy state of the molecular ion. Table III gives the details of the calculational results.

(13) T. W. Shannon and F. W. McLafferty, *J. Amer. Chem. Soc.*, 88, 5021 (1966).

(14) F. W. McLafferty and H. D. R. Schuddemage, *ibid.*, 91, 1866 (1969).

(15) W. A. Chupka, private communication.

Table III: The Abundance[a,b] of $m^*_{8.0}$ and P^+

$E^{\dagger M}$, eV	M^+ C_2 m*	C_2 P^+	C_3 m*	C_3 P^+	C_6 m*	C_6 P^+	C_6 m*	C_6 P^+	C_7 m*	C_7 P^+
					Case a: E_0^P = 71 kcal (3.08 eV)					
0	0.0	1.0	0.0	1.0	0.0	1.0	0.0	1.0	0.0	1.0
1	0.0	1.0	0.0	1.0	0.0	1.0	0.0	1.0	0.0	1.0
2	0.0101	0.930	0.0011	0.994	0.0	1.0	0.0	1.0	0.0	1.0
3	0.0220	0.354	0.0176	0.744	0.0074	0.923	0.0023	0.978	0.0011	0.985
4	0.0090	0.075	0.0196	0.366	0.0184	0.665	0.0119	0.836	0.0066	0.921
5	0.0021	0.020	0.0106	0.138	0.0182	0.368	0.0178	0.602	0.0140	0.765
6	0.0006	0.003	0.0047	0.050	0.0121	0.165	0.0177	0.374	0.0176	0.538
7	0.0002	0.001	0.0019	0.015	0.0068	0.078	0.0129	0.208	0.0172	0.374
8	0.0	0.0	0.0007	0.006	0.0034	0.036	0.0084	0.108	0.0132	0.225
9	0.0	0.0	0.0003	0.002	0.0017	0.014	0.0049	0.056	0.0092	0.138
10	0.0	0.0	0.0001	0.0001	0.0008	0.005	0.0020	0.027	0.0050	0.070
Tot abund	0.0896	5.39	0.116	7.33	0.130	9.16	0.132	10.83	0.126	12.00
m* (8.0)/P^+	0.017		0.016		0.014		0.012		0.010	
D^+/P^+	1.95		1.15		0.735		0.547		0.298	
					Case b: E_0^P = 78 kcal (3.39 eV)					
0	0.0	1.0	0.0	1.0	0.0	1.0	0.0	1.0	0.0	1.0
1	0.0	1.0	0.0	1.0	0.0	1.0	0.0	1.0	0.0	1.0
2	0.0	1.0	0.0	1.0	0.0	1.0	0.0	1.0	0.0	1.0
3	0.0174	0.685	0.0054	0.941	0.0012	0.993	0.0001	0.998	0.0	1.0
4	0.0150	0.236	0.0170	0.657	0.0089	0.880	0.0036	0.963	0.0012	0.990
5	0.0053	0.060	0.0156	0.326	0.0158	0.632	0.0103	0.831	0.0055	0.930
6	0.0018	0.015	0.0092	0.137	0.0159	0.383	0.0153	0.633	0.0113	0.783
7	0.0005	0.004	0.0044	0.049	0.0114	0.211	0.0157	0.426	0.0154	0.622
8	0.0	0.0	0.0020	0.022	0.0070	0.101	0.0126	0.247	0.0152	0.447
9	0.0	0.0	0.0008	0.009	0.0040	0.043	0.0089	0.140	0.0131	0.294
10	0.0	0.0	0.0003	0.003	0.0020	0.020	0.0050	0.070	0.0110	0.160
Tot abund	0.088	6.68	0.106	8.99	0.111	11.01	0.103	12.42	0.088	13.84
m* (8.0)/P^+	0.013		0.012		0.010		0.0083		0.0064	
D^+/P^+	1.38		0.760		0.432		0.255		0.148	
					Case c: E_0^P = 87 kcal (3.78 eV)					
0	0.0	1.0	0.0	1.0	0.0	1.0	0.0	1.0	0.0	1.0
1	0.0	1.0	0.0	1.0	0.0	1.0	0.0	1.0	0.0	1.0
2	0.0	1.0	0.0	1.0	0.0	1.0	0.0	1.0	0.0	1.0
3	0.0042	0.965	0.0002	0.995	0.0	1.0	0.0	1.0	0.0	1.0
4	0.0182	0.573	0.0068	0.916	0.0015	0.985	0.0003	0.998	0.0	1.0
5	0.0120	0.213	0.0146	0.648	0.0072	0.893	0.0026	0.973	0.0008	0.990
6	0.0050	0.061	0.0141	0.364	0.0132	0.690	0.0075	0.882	0.0037	0.945
7	0.0018	0.023	0.0093	0.176	0.0142	0.460	0.0180	0.707	0.0076	0.875
8	0.0006	0.006	0.0052	0.081	0.0117	0.280	0.0140	0.525	0.0112	0.718
9	0.0002	0.0005	0.0026	0.030	0.0084	0.155	0.0124	0.360	0.0132	0.565
10	0.0001	0.0	0.0012	0.007	0.0050	0.071	0.0110	0.200	0.0130	0.410
Tot abund	0.085	8.22	0.093	10.98	0.085	13.02	0.075	14.42	0.048	15.23
m* (8.0)/P^+	0.010		0.0085		0.0065		0.0052		0.0032	
D^+/P^+	0.908		0.443		0.221		0.107		0.057	
					Case d: E_0^P = 109 kcal (4.74 eV)					
0	0.0	1.0	0.0	1.0	0.0	1.0	0.0	1.0	0.0	1.0
1	0.0	1.0	0.0	1.0	0.0	1.0	0.0	1.0	0.0	1.0
2	0.0	1.0	0.0	1.0	0.0	1.0	0.0	1.0	0.0	1.0
3	0.0	1.0	0.0	1.0	0.0	1.0	0.0	1.0	0.0	1.0
4	0.0003	0.998	0.0	1.0	0.0	1.0	0.0	1.0	0.0	1.0
5	0.0187	0.885	0.0017	0.985	0.0	1.0	0.0	1.0	0.0	1.0
6	0.0134	0.578	0.0044	0.924	0.0008	0.990	0.0	1.0	0.0	1.0
7	0.0106	0.291	0.0096	0.765	0.0032	0.955	0.0007	0.990	0.0	1.0
8	0.0059	0.123	0.0116	0.533	0.0070	0.836	0.0025	0.963	0.0007	0.990
9	0.0030	0.056	0.0101	0.338	0.0097	0.682	0.0054	0.875	0.0023	0.960
10	0.0015	0.020	0.0050	0.170	0.0110	0.500	0.0100	0.760	0.0046	0.870
Tot abund	0.088	12.30	0.048	14.57	0.024	15.78	0.010	16.19	0.004	16.32
m* (8.0)/P^+	0.0072		0.0033		0.0015		0.00062		0.00025	
D^+/P^+	0.290		0.103		0.0319		0.00970		0.00328	

[a] Weighted by the parabolic function $y = ax^2$ and weights 0.72, 1.81, 2.04, 2.12, 2.12, 2.04, 1.81, 1.54, 1.17, 0.74, 0.20 at the excess energy values $E^{\dagger M}$ of 0, 1, 2, 3, 4, 5, 6, 7, 8, 9, 10 eV, respectively. [b] The abundance of m*′ (18.7) is one-half that for m* (8.0) and no further description is necessary.

Table IV: Comparison of Methods of Calculating Metastable Abundances

	$E^{\dagger M}$, eV	1	2	3	4	5	6	7	8	9
C_3	Practical	0.0	0.0	0.0194	0.0150	0.0053	0.0018	0.0005	0.0	0.0
	Correct	0.0	0.0	0.0210	0.0141	0.0048	0.0015	0.0003	0.0	0.0
C_7	Practical	0.0	0.0	0.0	0.0012	0.0055	0.0113	0.0154	0.0152	0.0131
	Correct	0.0	0.0	0.0001	0.0018	0.0069	0.0126	0.0161	0.0155	0.0129

Some trends may be noted. The relative abundance of P^+ is appropriately higher at lower energies. The metastable abundance is a maximum at lower energy for C_3, moving to higher energy as n increases. For a given E_0^P, m* (8.0)/P^+ decreases from C_3 to C_7.

The reason for this decrease is, of course, the fact that as R increases in size, the curves in Figure 2 which give the energy distribution of P^+ ions formed from M^+ shift to lower energies. Thus, for example, if an abscissa mark is placed on the 5 eV diagram of Figure 2 at 24,800 cm^{-1}, corresponding to E_0^P = 71 kcal mol^{-1}, a larger fraction of the distribution for C_7 lies to the left of this mark, and corresponds to P^+ product, than is the case for the distribution for C_3; the decomposition of P^+ to yield detectable metastable arises mainly from a narrow region to the right of this abscissa mark; and most of the area to the right of this narrow region corresponds to production of daughter ions.

The log of the relative abundances of the metastables are plotted in Figure 4 against the reciprocal of the degrees of freedom of the molecular ion. The parameter m* (8.0)/P^+ ranges from 0.017 for C_3 precursor to 0.010 for C_7 precursor in case a, and 0.013 to 0.0064 in case b and in case d, the corresponding values are reduced to 0.0072 for C_3 precursor and 0.00025 for C_7 precursor. Experimentally, McLafferty and Pike[1] found the value of the quantity m*/P^+ to be 0.0032 for C_3 precursor and 0.0014 for C_7 precursor, with a ratio of roughly 2, for the m* (8.0) process. Cases a and b in our calculation give the correct ratios but have larger absolute abundances for m*/P^+; however, the experimental absolute abundance is instrumentally dependent, and is frequently less than the theoretical prediction; hence cases a and b may be considered to be good representations of the n-primary alcohol molecule ion decomposition.

Other systems with much greater spread in m*/P^+ than the alcohols were also observed by McLafferty and Pike.[1] The calculations show that one way this can be realized is by going to higher values of E_0^P.

Discussion

The quasi-linearity of the plot of log m*/P^+ *vs.* $(DF)^{-1}$ observed by McLafferty and Pike was not explained by them. From our calculational result, a slight curvature was found for this relationship. The agreement with the experimental data is quite satisfactory.

Since there is an equilibrium between structure I and others,[8] the energetics used for the metastable decomposition (39 kcal released by IV → I as used above to calculate the total excess energy of I) are somewhat arbitrary. Nevertheless, the calculated characteristic properties are still valid. The quantity of the energy released will only affect the choice of the $C_2H_5O^+$ energy in counting the abundance of m*.

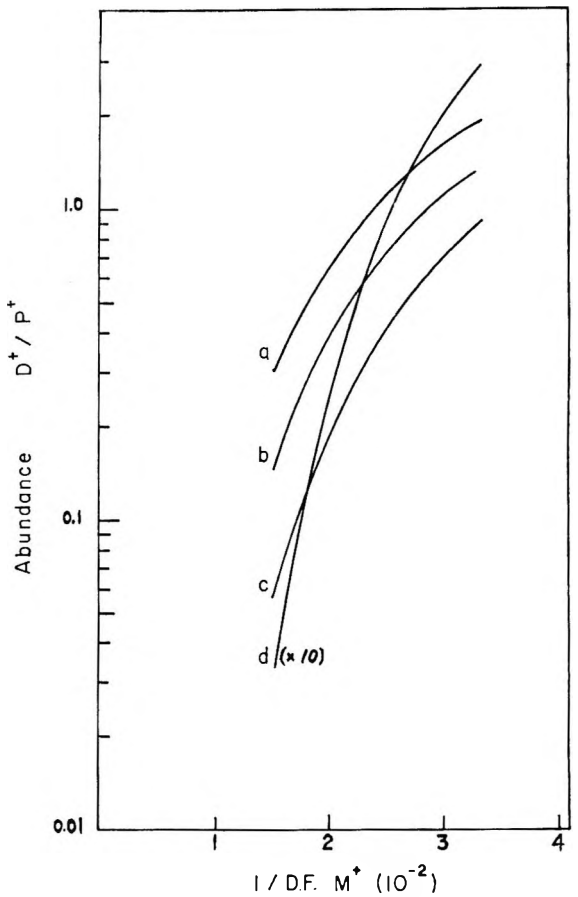

Figure 5. Variation of relative abundance of D^+ *vs.* DF M^+ for cases a, b, c, and d.

The Abundance of the Daughter Ion. A complete mass spectrum for 1-alkanols with 70-eV electrons at 250° was reported by Friedel, Shultz, and Sharkey.[16] By assigning m/e 19 as uniquely from H_3O^+, the ratios of the abundances of m/e 19 to m/e 45 ($C_2H_5O^+$) for 1-alcohols are 0.60, 0.50, 0.36, 0.27, and 0.27 for C_3, C_4, C_5, C_6, and C_7 alcohols, respectively. Cases a and b in our calculation give ratios of D^+/P^+ of the

(16) R. A. Friedel, J. L. Shultz, and A. G. Sharkey, Jr., *J. Anal. Chem.*, **28**, 926 (1956).

correct order of magnitude but larger variation with n in the series (Table III). The log D^+/P^+ *vs.* the reciprocal of the DF in the molecular ion is plotted in Figure 5.

Conclusion

A statistical theoretical model gives a reasonable account of some important metastable phenomena observed in mass spectrometry. The method can also be applied to systems other than the alcohols.

Acknowledgment. This work was supported by the U. S. Air Force Office of Scientific Research (SRC) Contract No. AF49 (638)-1633. We have enjoyed several conversations with Professor F. W. McLafferty.

Appendix

Frequency Assignments

A. ROH and the Rigid Model for M^+ Decomposition. The alcohol frequencies (cm^{-1}) were assigned by combining the frequencies of the n-alkanes[17a] with those of the alcohol function[17b]: six new modes (O–H stretch 3685, C–O–H bend 1390, C–O stretch 1066, C–C–O bend 898, C–C–O bend 470, O–H twist 280) were added to, and three modes (C–H stretch 2965, H–C–H bend 1460 (2)) were removed from the alkane assignment. The reaction coordinate was a C–C stretch at ~1020 cm^{-1}.

The frequencies of $C_2H_5O^+$ combined the six new modes described above with C–H stretch 2966 (2), 2882 (2); C–H bend 1388 (2), 1305 (2); C–C stretch 1046; C–C bend 1279; C–C rock 903; C–C torsion 270.

The alkyl radical frequencies and the transitional modes were those that remained after the $C_2H_5O^+$ frequencies were removed from the original alcohol.

These assignments are very approximate, but are adequate for the present purpose.

B. The Loose Model for M^+ Decomposition. The reductions in frequencies were arbitrary. In the loose model for propanol ion decomposition, three C–H bendings and one C–C bend were reduced to 0.1 of their values, and two torsions were reduced to 0.167. For butanol ion and the rest of the series, two C–C bendings and two C–H bendings were reduced to 0.1 of their values and three torsions were reduced to 0.167 of their original values. One torsional mode in the $C_2H_5O^+$ part of the complex was reduced to 0.167, *i.e.*, $270 \rightarrow 45$ cm^{-1}.

C. $C_2H_5O^+$ Metastable Decomposition. The frequencies of oxirane ion were obtained by adding three frequencies for one extra H^+ to the assignment for ethylene oxide;[18] these three frequencies were estimated from the known frequencies for H_3O^+ *vis à vis* H_2O. The grouped frequencies are 3040 (5), 1450 (4), 1170 (5), 837 (4).

The frequencies of the activated complex depend on the reaction path. The specific rate for the m* = 8.0 process is twice that for m*′ = 18.7.[1b] The frequency factor for the thermal decomposition of ethylene oxide is $10^{14.13}$.[19] From these considerations, the grouped frequencies of the activated complex were taken as follows: (a) m* = 8.0: 3040 (3) 1523 (4) 1170 (3) 837 (4) 582 (2) 363; (b) m* = 18.7: 3040 (3) 1466 (3) 1203 (4) 837 (4) 725 (2) 567.

Calculation of Metastable Abundances

This method of calculating metastable ion abundances is "quick and dirty" and neglects the fact that $k(E^P)$ is a relaxation time and that the lifetime of excited molecules is *not* a δ-function distribution, $\delta_{\tau,k_E^{-1}}$. The correct method of counting the metastable ion events should sum all the contributions for all $k(E^P)$ values. For each $k(E^P)$ value, there is a decay curve obeying the relation $n_t/n_0 = \exp(-k(E^P)t)$. The metastables are observed in a one-microsecond interval taken at $t = (3.3 \times 10^5)^{-1} = 3 \times 10^{-6}$ sec. The fraction of P^+ ions observed as the metastable so obtained is <0.02 for $k(E^P) < 1 \times 10^4$ or $> 1.5 \times 10^6$ sec^{-1}; the largest contribution (0.125) is from $k(E^P) \sim 3 \times 10^5$ sec^{-1}. The energy width ΔE^P for $k(E^P)$ between 1×10^4 and 1.5×10^6 sec^{-1} is 8.5 kcal (0.37 eV); the appropriate weightings for each $k(E^P)$ are given in Figure 2.

A comparison of the absolute metastable ion (m* (8.0)) abundances obtained by both methods is shown for C_3 and C_7 (case b) in Table IV. It is seen that the two methods give nearly the same abundance of m* (8.0) at each value of $E^{\dagger M}$ (the horizontal sums, each suitably weighted, will be an even closer match) and hence the practical method is justified here.

(17) (a) J. H. Schachtschneider and R. G. Snyder, *Spectrochim. Acta*, **19** (1963); (b) E. K. Plyler, *J. Res. Nat. Bur. Stand.*, **48**, 281 (1952).

(18) H. W. Thompson and W. T. Cave, *Trans. Faraday Soc.*, **47**, 946 (1951).

(19) M. Neufeld and A. T. Blades, *Can. J. Chem.*, **41**, 2956 (1963).

Salting Coefficients from Scaled Particle Theory

by W. L. Masterton and Tei Pei Lee

Department of Chemistry, University of Connecticut, Storrs, Connecticut *(Received October 27, 1969)*

Scaled particle theory is used to derive a general expression for the salting coefficient, k_s, which appears in the Setschenow equation. This expression is essentially a sum of two terms, one of which will ordinarily be positive (salting out), while the other will be negative (salting in). Calculated values of k_s are in excellent agreement with experiment for systems in which the molecular and ionic diameters are relatively small. For large molecules, the agreement is poorer, as is true with classical theories of the salt effect. The magnitude of k_s is very sensitive to uncertainties in the diameters of anions and cations.

Introduction

The solubility of a nonelectrolyte in an aqueous salt solution, at low salt concentrations, is given by the Setschenow equation

$$\log S_0/S = k_s c \qquad (1)$$

where S_0 is the solubility in pure water, S is the solubility in a salt solution of concentration c (mol/l.), and k_s is the salting coefficient, which has a characteristic value for a given salt–nonelectrolyte pair. A positive value of k_s corresponds to salting out ($S_0 > S$); if k_s is negative, salting in is observed ($S_0 < S$).

The electrostatic theory of the salt effect, proposed originally by Debye and McAulay,[1] and refined most recently by Conway, Desnoyers, and Smith,[2] relates the sign of k_s to the effect of the nonelectrolyte on the dielectric constant of water. Species which lower the dielectric constant should be salted out by all electrolytes. Electrostatic theory gives values of k_s which are of about the right order of magnitude, but, contrary to observation, vary very little with the nature of the salt. Moreover, this theory cannot explain the general phenomenon of salting in by large ion electrolytes such as the tetraalkylammonium halides.

The McDevit–Long theory of the salt effect[3] attributes the sign of k_s to the influence that the salt has on the water structure. If it "compresses" the water structure, it becomes more difficult to introduce nonelectrolyte molecules and salting out occurs. If, on the other hand, the water structure is "loosened" by the addition of salt, salting in is predicted. In terms of this picture, the McDevit–Long theory offers a plausible explanation of salting in by tetraalkylammonium halides. It also gives relative values of k_s for different salts with the same nonelectrolyte which fall in the correct order (*e.g.*, k_s LiCl $< k_s$ NaCl $> k_s$ KCl $> k_s$ KI). However, the absolute values of k_s calculated from the equation of McDevit and Long are in poor agreement with experiment. For example, it predicts the salting coefficient for the sodium chloride–benzene system to be 0.42; the observed value is 0.198.

Bockris, Bowler-Reed, and Kitchener[4] have modified the electrostatic expression for k_s by including a term whose sign depends upon the relative polarizabilities of nonelectrolyte and water. For most nonelectrolytes, this dispersion term leads to salting in; the overall sign of k_s depends upon the relative magnitudes of the electrostatic (salting out) and dispersion (salting in) terms. The Bockris theory has been quite successful in explaining trends in k_s with the sizes of molecules and ions.[5,6] However, the theory is difficult to apply quantitatively since the parameters required to calculate k_s are not readily available. The other theories of the salt effect suffer from this same weakness, albeit to a lesser extent.

A few years ago, Pierotti[7,8] adapted the scaled particle theory of Reiss, *et al.*,[9,10] to predict the solubilities of nonelectrolytes in water. The equation of Pierotti relates aqueous solubility to the sum of two free energy terms: the work required to create a cavity large enough to accommodate a nonelectrolyte molecule and the energy of interaction between the solute molecule and the surrounding solvent. This model has been reasonably successful in predicting the solubilities and other thermodynamic properties of nonelectrolytes in water solution.

Quite recently, Shoor and Gubbins[11] have extended

(1) P. Debye and J. McAulay, *Phys. Z.*, **26**, 22 (1925).

(2) B. E. Conway, J. E. Desnoyers, and A. C. Smith, *Phil. Trans. Roy. Soc. London*, **A256**, 389 (1964).

(3) W. F. McDevit and F. A. Long, *J. Amer. Chem. Soc.*, **74**, 1773 (1952).

(4) J. O'M. Bockris, J. Bowler-Reed, and J. A. Kitchener, *Trans. Faraday Soc.*, **47**, 184 (1951).

(5) W. L. Masterton and R. N. Schwartz, *J. Phys. Chem.*, **69**, 1546 (1965).

(6) W. L. Masterton, T. P. Lee, and R. L. Boyington, *J. Phys. Chem.*, **73**, 2761 (1969).

(7) R. A. Pierotti, *J. Phys. Chem.*, **69**, 281 (1965).

(8) R. A. Pierotti, *ibid.*, **67**, 1840 (1963).

(9) H. Reiss, H. L. Frisch, E. Helfand, and J. L. Lebowitz, *J. Chem. Phys.*, **32**, 119 (1960).

(10) H. Reiss, H. L. Frisch, and J. L. Lebowitz, *ibid.*, **31**, 369 (1959).

(11) S. K. Shoor and K. E. Gubbins, *J. Phys. Chem.*, **73**, 498 (1969).

Pierotti's scaled particle model to obtain an equation for the solubility of a nonelectrolyte in an aqueous salt solution. They have applied this equation to calculate the solubility of certain nonpolar gases (He, H_2, Ar, O_2, CH_4, SF_6, and $C(CH_3)_4$) in concentrated solutions of potassium hydroxide (10–50 wt % KOH). The agreement with experiment is excellent for Ar, O_2, and CH_4. For the other gases, agreement is not as good, particularly at high electrolyte concentrations. This may reflect the fact that the several approximations which must be made lead to serious errors at high concentrations. Then too, one can hardly consider an alkali hydroxide to be a typical 1:1 electrolyte.

The scaled particle approach to the calculation of salt effects has the great advantage that the required molecular parameters are readily available. For this reason among others, it is of interest to extend the derivations of Shoor and Gubbins to obtain a general expression for the salting coefficient, applicable to any salt–nonelectrolyte pair. By comparing calculated and observed values of k_s, it should be possible to judge the applicability of scaled particle theory to the prediction of salt effects. This paper presents the results of such an analysis.

Expression for the Salting Coefficient

In practice, the Setschenow eq 1 is found to be valid only at low salt concentrations, *i.e.*, as $c \rightarrow 0$. To obtain an expression for k_s, it is convenient to differentiate eq 1 with respect to c

$$k_s = -\left(\frac{\mathrm{d}\ (\log S)}{\mathrm{d}(c)}\right)_{c\rightarrow 0} \tag{2}$$

Shoor and Gubbins[11] derived from scaled particle theory the following expression for $\log S$

$$-\log S = \frac{\bar{g}_1{}^{\mathrm{h}}}{2.3kT} + \frac{\bar{g}_1{}^{\mathrm{s}}}{2.3kT} + \log kT \sum_{j=1}^{4} \rho_j \tag{3}$$

where $\bar{g}_1{}^{\mathrm{h}}$ is the free energy change when a cavity large enough to hold the nonelectrolyte molecule is formed in the solution, $\bar{g}_1{}^{\mathrm{s}}$ is the free energy change when the nonelectrolyte is introduced into the cavity, and ρ_j is the number density (particles/cc) of a solution species. Following Shoor and Gubbins, we use the subscript 1 to represent the nonelectrolyte, 2 the solvent (water), 3 the cation (Na^+, K^+, etc.), and 4 the anion (Cl^-, I^-, etc.).

Combining eq 2 and 3

$$k_s = \left[\frac{\mathrm{d}(\bar{g}_1{}^{\mathrm{h}}/2.3kT)}{\mathrm{d}(c)}\right]_{c\rightarrow 0} + \left[\frac{\mathrm{d}(\bar{g}_1{}^{\mathrm{s}}/2.3kT)}{\mathrm{d}(c)}\right]_{c\rightarrow 0} + \left[\frac{\mathrm{d}\ \log \Sigma\rho_j}{\mathrm{d}(c)}\right]_{c\rightarrow 0} \tag{4}$$

$$= k_\alpha + k_\beta + k_\gamma \tag{5}$$

where k_α, k_β, and k_γ represent the contributions to the salting coefficient of each of the three terms on the right of eq 4. The problem now becomes one of deriving general expressions for k_α, k_β, and k_γ in terms of parameters characteristic of the nonelectrolyte and the ions of the salt. For simplicity, the derivation will be limited to 1:1 salts and slightly soluble nonelectrolytes at 25°; the extension to other systems is an obvious one. We start with the expression for k_γ, since this is the easiest to evaluate.

Expression for k_γ. For slightly soluble nonelectrolytes, ρ_1 can be dropped from the summation[12] and we can write

$$\Sigma\rho_j = \rho_2 + \rho_3 + \rho_4 \tag{6}$$

For a 1:1 electrolyte

$$\rho_3 = \rho_4 = Nc/1000 \tag{7}$$

where N is Avogadro's number. Applying the defining equation for the apparent molal volume, ϕ, to 1 cc of solution, it is readily shown that the variation of the number density of water, ρ_2, with concentration is given by the equation

$$\rho_2 = \frac{Nd_2}{M_2}\left[1 - \frac{c\phi}{1000}\right] \tag{8}$$

where d_2 is the density of pure water (0.997 g/ml at 25°), M_2 is the molecular weight of water, 18.02 g/mol, and ϕ is the apparent molal volume of the salt in solution.

Substituting for ρ_2, ρ_3, and ρ_4 in eq 6, we obtain, after rearranging

$$\Sigma\rho_j = \frac{Nd_2}{M_2}\left[1 + \frac{2cM_2}{1000d_2} - \frac{c\phi}{1000}\right] \tag{9}$$

At low concentrations, *i.e.*, as $c \rightarrow 0$

$$\ln \Sigma\rho_j = \ln \frac{Nd_2}{M_2} + \frac{2cM_2}{1000d_2} - \frac{c\phi}{1000} \tag{10}$$

To obtain k_γ, we neglect the (small) variation of ϕ with c and write

$$k_\gamma = \left[\frac{\mathrm{d}\ \log \Sigma\rho_j}{\mathrm{d}c}\right]_{c\rightarrow 0} = \frac{2M_2}{2300d_2} - \frac{\phi_0}{2300}$$

$$= 0.016 - 4.34 \times 10^{-4}\phi_0 \tag{11}$$

where ϕ_0 is the apparent molal volume of the salt at infinite dilution.

Expression for k_β. Shoor and Gubbins derive the following expression for the interaction energy between

(12) To justify dropping ρ_1, we must show that its concentration dependence is negligibly small compared to that of ρ_2, ρ_3, or ρ_4. The Setschenow equation can be written in the form $\ln \rho_1/\rho_1{}^0 = -2.3k_sc$, or $\rho_1 = \rho_1{}^0 e^{-2.3k_sc}$, where $\rho_1{}^0$ is the number density of the nonelectrolyte in pure water. Expanding the exponential and retaining only the first two terms: $\rho_1 = \rho_1{}^0 - 2.3k_s\rho_1{}^0c$. Realizing that $\rho_1{}^0 = NC_1{}^0/1000$, where $C_1{}^0$ is the molar concentration of nonelectrolyte in pure water, we have $\Delta\rho_1/\Delta c = (-2.3k_sNC_1{}^0)/1000$. From eq 7 $\Delta\rho_3/\Delta c = \Delta\rho_4/\Delta c = N/1000$. For slightly soluble nonelectrolytes, $C_1{}^0$ is very small, k_s is ordinarily less than unity, and $2.3k_sC_1{}^0 \ll 1$. Consequently, $\Delta\rho_1/\Delta c \ll \Delta\rho_3/\Delta c = \Delta\rho_4/\Delta c$.

a nonelectrolyte molecule and the solution species forming the cavity

$$\frac{\bar{g}_1^s}{2.3kT} = \frac{-32\pi}{9(2.3T)} \sum_{j=1}^{4} \frac{\rho_j \epsilon_{1j} \sigma_{1j}^3}{k} - \frac{4\pi\rho_2\mu_2^2\alpha_1}{3(2.3kT)\sigma_{12}^3} \quad (12)$$

where ϵ_{1j} and σ_{1j} are the mixture potential parameters, μ_2 is the dipole moment of water, and α_1 is the polarizability of the nonelectrolyte. As before, we neglect ρ_1 in taking the summation and write

$$\frac{\bar{g}_1^s}{2.3kT} = \frac{-32\pi}{9(2.3T)}\left[\frac{\rho_3\epsilon_{12}\sigma_{12}^3}{k} + \frac{\rho_3\epsilon_{13}\sigma_{13}^3}{k} + \frac{\rho_4\epsilon_{14}\sigma_{14}^3}{k}\right] - \frac{4\pi\rho_2\mu_2^2\alpha_1}{3(2.3kT)\sigma_{12}^3} \quad (13)$$

$$= \frac{-32\pi}{9(2.3T)}\left[\frac{\rho_3\epsilon_{13}\sigma_{13}^3}{k} + \frac{\rho_4\epsilon_{14}\sigma_{14}^3}{k}\right] - \frac{4\pi\rho_2}{3(2.3T)}\left[\frac{8\epsilon_{12}\sigma_{12}^3}{3k} + \frac{\mu_2^2\alpha_1}{k\sigma_{12}^3}\right] \quad (14)$$

Substituting for ρ_2, ρ_3, and ρ_4 from eq 7 and 8

$$\frac{\bar{g}_1^s}{2.3kT} = \frac{-32\pi Nc}{9000(2.3T)}\left[\frac{\epsilon_{13}\sigma_{13}^3}{k} + \frac{\epsilon_{14}\sigma_{14}^3}{k}\right] - \frac{4\pi N d_2}{3(2.3T)M_2}\left[1 - \frac{c\phi}{1000}\right]\left[\frac{8\epsilon_{12}\sigma_{12}^3}{3k} + \frac{\mu_2^2\alpha_1}{k\sigma_{12}^3}\right] \quad (15)$$

Taking the derivative with respect to c as $c \rightarrow 0$, and inserting numbers for the various constants ($\mu_2 = 1.84 \times 10^{-18}$; $T = 298°$K)

$$\left[\frac{d(\bar{g}_1^s/2.3kT)}{dc}\right]_{c\rightarrow 0} = k_\beta = -9.80 \times 10^{18}\left[\frac{\epsilon_{13}\sigma_{13}^3}{k} + \frac{\epsilon_{14}\sigma_{14}^3}{k}\right] + 5.43 \times 10^{17}\frac{\phi_0\epsilon_{12}\sigma_{12}^3}{k} + 5.00 \times 10^{-3}\frac{\phi_0\alpha_1}{\sigma_{12}^3} \quad (16)$$

To assign a numerical value to k_β, the mixture parameters ϵ_{1j} and σ_{1j} must be related to those of the pure species. Following Pierotti, we use the mixing rules

$$\epsilon_{1j} = (\epsilon_1\epsilon_j)^{1/2}; \quad \sigma_{1j} = (\sigma_1 + \sigma_j)/2 \quad (17)$$

The energy parameter, ϵ_2/k, for water is taken to be 35.3.[7] Values of ϵ/k for the cation and anion are evaluated from the Mavroyannis–Stephen theory.[13]

$$\frac{\epsilon_j}{k} = 2.28 \times 10^{-8}\frac{\alpha_j^{1/2}Z_j^{1/2}}{\sigma_j^6} \quad (18)$$

where α_j (*i.e.*, α_3 or α_4) is the polarizability of the ion, Z_j is the total number of electrons in the ion, and σ_j is its diameter.

Making these substitutions in eq 16, we arrive at a final expression for k_β.

$$k_\beta = -1.85 \times 10^{14}\left(\frac{\epsilon_1}{k}\right)^{1/2}\left[\alpha_3^{3/4}Z_3^{1/4}\frac{(\sigma_1 + \sigma_3)^3}{\sigma_3^3} + \alpha_4^{3/4}Z_4^{1/4}\frac{(\sigma_1 + \sigma_4)^3}{\sigma_4^3}\right] + 6.26 \times 10^{17}\phi_0\left(\frac{\epsilon_1}{k}\right)^{1/2}(\sigma_1 + \sigma_2)^3 + 4.00 \times 10^{-2}\frac{\phi_0\alpha_1}{(\sigma_1 + \sigma_2)^3} \quad (19)$$

To evaluate k_β, the diameter of the water molecule, σ_2, is taken to be 2.75×10^{-8} cm (ref 7).

Expression for k_α. The term for the free energy of cavity formation, according to scaled particle theory,[11] can be written in the form[14]

$$\frac{\bar{g}_1^h}{2.3kT} = -\log(1 - \tau_3) + A \quad (20)$$

$$A = \frac{3\tau_2\sigma_1}{2.3(1 - \tau_3)}\left[1 + \frac{\tau_1\sigma_1}{\tau_2} + \frac{3\tau_2\sigma_1}{2(1 - \tau_3)}\right] \quad (21)$$

$$\tau_n = \frac{\pi}{6}\sum_1^4 \rho_j\sigma_j^n \quad (22)$$

Neglecting the terms involving ρ_1, substituting for ρ_2, ρ_3, and ρ_4 from eq 7 and 8, and taking $\sigma_2 = 2.75 \times 10^{-8}$ cm, we arrive at the following expressions for τ_1, τ_2, and τ_3.

$$\tau_1 = \frac{\pi}{6}\left[\frac{Nd_2}{M_2}\left(1 - \frac{c\phi}{1000}\right)\sigma_2 + \frac{Nc}{1000}(\sigma_3 + \sigma_4)\right] = 4.80 \times 10^{14} + c[3.15 \times 10^{20}(\sigma_3 + \sigma_4) - 4.80 \times 10^{11}\phi] \quad (23)$$

$$\tau_2 = \frac{\pi}{6}\left[\frac{Nd_2}{M_2}\left(1 - \frac{c\phi}{1000}\right)\sigma_2^2 + \frac{Nc}{1000}(\sigma_3^2 + \sigma_4^2)\right] = 1.32 \times 10^7 + c[3.15 \times 10^{20}(\sigma_3^2 + \sigma_4^2) - 1.32 \times 10^4\phi] \quad (24)$$

$$\tau_3 = \frac{\pi}{6}\left[\frac{Nd_2}{M_2}\left(1 - \frac{c\phi}{1000}\right)\sigma_2^3 + \frac{Nc}{1000}(\sigma_3^3 + \sigma_4^3)\right] = 0.363 + c[3.15 \times 10^{20}(\sigma_3^3 + \sigma_4^3) - 3.63 \times 10^{-4}\phi] \quad (25)$$

In order to evaluate k_α, it is necessary to have an expression for the quantitity $(1 - \tau_3)$, which appears in eq 20. It is readily shown from eq 25 that

$$1 - \tau_3 = 0.637[1 - c\{4.95 \times 10^{20}(\sigma_3^3 + \sigma_4^3) - 5.69 \times 10^{-4}\phi\}] \quad (26)$$

(13) C. Mavroyannis and M. J. Stephen, *Mol. Phys.*, **5**, 629 (1962).

(14) We take $a_j = \sigma_j$, where a_j is the hard-sphere diameter.[7,8] The term $4\pi P(\sigma_1/2)^3/3kT$, which is negligibly small at atmospheric pressure, is dropped.

As $c \rightarrow 0$

$$\ln (1 - \tau_3) = \ln 0.637 - c[4.95 \times 10^{20}(\sigma_3^3 + \sigma_4^3) - 5.69 \times 10^{-4}\phi_0]$$

$$\log (1 - \tau_3) = \log 0.637 - c[2.15 \times 10^{20}(\sigma_3^3 + \sigma_4^3) - 2.47 \times 10^{-4}\phi_0] \quad (27)$$

To calculate A, it is necessary to obtain expressions for τ_1/τ_2 and $\tau_2/(1 - \tau_3)$. As before, we are interested in the values of these quantities at low concentrations, *i.e.*, as $c \rightarrow 0$. The ratio τ_1/τ_2 can be obtained by dividing eq 23 by eq 24 and retaining only the first two terms in the power series.

$$\tau_1/\tau_2 = 3.64 \times 10^7 + c[2.39 \times 10^{13}(\sigma_3 + \sigma_4) - 8.69 \times 10^{20}(\sigma_3^2 + \sigma_4^2)] \quad (28)$$

The quantity $\tau_2/(1 - \tau_3)$ can be evaluated in a similar manner, using eq 24 and 26

$$\frac{\tau_2}{1 - \tau_3} = 2.07 \times 10^7 + c[4.95 \times 10^{20}(\sigma_3^2 + \sigma_4^2) + 1.03 \times 10^{28}(\sigma_3^3 + \sigma_4^3) - 3.25 \times 10^4\phi_0] \quad (29)$$

Combining terms, we find

$$\left[1 + \frac{\tau_1\sigma_1}{\tau_2} + \frac{3\tau_2\sigma_1}{2(1 - \tau_3)}\right] = 1 + 6.74 \times 10^7\sigma_1 + c\sigma_1[2.39 \times 10^{13}(\sigma_3 + \sigma_4) - 1.27 \times 10^{20}(\sigma_3^2 + \sigma_4^2) + 1.54 \times 10^{28}(\sigma_3^3 + \sigma_4^3) - 4.88 \times 10^4\phi_0] \quad (30)$$

We can now obtain an expression for A by multiplying the terms on the right of eq 30 by the quantity $3\tau_2\sigma_1/2.3(1 - \tau_3)$. Carrying out this multiplication, discarding terms in c^2, we obtain

$$A = 2.70 \times 10^7\sigma_1 + 1.82 \times 10^{15}\sigma_1^2 + c\sigma_1[6.45 \times 10^{20}(\sigma_3^2 + \sigma_4^2) + 1.34 \times 10^{28}(\sigma_3^3 + \sigma_4^3) - 4.23 \times 10^4\phi_0] + c\sigma_1^2[6.45 \times 10^{20}(\sigma_3 + \sigma_4) + 4.01 \times 10^{28}(\sigma_3^2 + \sigma_4^2) + 1.32 \times 10^{36}(\sigma_3^3 + \sigma_4^3) - 4.17 \times 10^{12}\phi_0] \quad (31)$$

Table I: Calculated Values of k_α, k_β, and k_γ for Several Salt–Nonelectrolyte Pairs

	k_α	k_β	k_γ	k_s
H_2–NaCl	+0.126	−0.023	+0.008	+0.111
H_2–KI	+0.115	−0.031	−0.004	+0.080
CH_4–NaCl	+0.203	−0.080	+0.008	+0.131
CH_4–KI	+0.182	−0.102	−0.004	+0.076
SF_6–NaCl	+0.387	−0.194	+0.009	+0.202
SF_6–KI	+0.343	−0.226	−0.004	+0.113

Having obtained expressions for $\log (1 - \tau_3)$ and A, we can now write

$$k_\alpha = \left[\frac{d(\bar{g}_1^h/2.3kT)}{dc}\right]_{c\rightarrow 0} = \left[\frac{-d \log (1 - \tau_3)}{dc} + \frac{dA}{dc}\right]_{c\rightarrow 0} = 2.15 \times 10^{20}(\sigma_3^3 + \sigma_4^3) - 2.47 \times 10^{-4}\phi_0 + \sigma_1[6.45 \times 10^{20}(\sigma_3^2 + \sigma_4^2) + 1.34 \times 10^{28}(\sigma_3^3 + \sigma_4^3) - 4.23 \times 10^4\phi_0] + \sigma_1^2[6.45 \times 10^{20}(\sigma_3 + \sigma_4) + 4.01 \times 10^{28}(\sigma_3^2 + \sigma_4^2) + 1.32 \times 10^{36}(\sigma_3^3 + \sigma_4^3) - 4.17 \times 10^{12}\phi_0] \quad (32)$$

The salting coefficient, k_s, can be calculated by adding k_α (eq 32), k_β (eq 19), and k_γ (eq 11). In order to find k_s for a particular system, it is necessary to know: (1) the apparent molal volume, ϕ_0, of the salt at infinite dilution; (2) the diameters (σ_3, σ_4) and polarizabilities (α_3, α_4) of cation and anion; (3) the diameter, σ_1, energy parameter, ϵ_1/k, and polarizability, α_1, of the nonelectrolyte molecule.

Discussion

Values of k_α, k_β, and k_γ. It is of interest to compare the relative contributions of the three terms k_α, k_β, and k_γ to the salting coefficient, k_s. This comparison is made in Table I for several typical systems. The parameters required to evaluate k_α, k_β, and k_γ are taken from Table II. It will be noted that k_γ is always a small quantity. Indeed, considering the uncertainties in k_α and k_β, one could well neglect the contribution from k_γ unless ϕ_0 is very large.

In all cases, k_α is positive. Physically, this can be interpreted to mean, in terms of eq 4, that the free energy change for cavity formation becomes more positive as the concentration of salt increases. In this sense, it is more difficult to form a cavity in an aqueous solution of an alkali halide than in water itself.

The k_β values are negative, indicating that the last two terms in eq 19 are outweighed by the first term. Physically, one can interpret the negative sign of k_β to mean that, once a cavity is formed in a salt solution, it is easier to introduce a nonelectrolyte molecule than it is in pure water. In other words, the nonelectrolyte experiences a net attractive force when water molecules in the surrounding cavity are replaced by alkali halide ions.

The sign of the salting coefficient, k_s, will, of course, depend upon the relative magnitudes of k_α and k_β. For small molecules such as H_2, where the attractive forces in solution are weak, k_β makes a relatively small contribution and one can confidently expect k_s to be positive (salting out). As the size of the nonelectrolyte molecule increases, as in the sequence $H_2 < CH_4 < SF_6$,

Table II: Parameters for Calculating Salting Coefficients

Molecules[a]			Ions[b]			Salts[c]	
	$10^{24}\alpha_1$	$10^8\sigma_1$	ϵ_1/k		$10^{24}\alpha$	$10^8\sigma$		ϕ_0, cc
He	0.204	2.58	10.2	Li^+	0.075	1.20	LiCl	17.1
Ne	0.393	2.75	35.6	Na^+	0.21	1.90	NaCl	16.6
Ar	1.63	3.47	116	K^+	0.87	2.66	NaBr	23.5
Kr	2.46	3.60	158	Rb^+	1.81	2.96	NaI	35.1
H_2	0.802	2.87	29.2	Cs^+	2.79	3.38	KCl	26.8
O_2	1.57	3.54	88	Cl^-	3.02	3.62	KBr	33.7
N_2	1.74	3.71	95.9	Br^-	4.17	3.90	KI	45.4
CH_4	2.70	3.82	137	I^-	6.28	4.32	RbCl	31.9
C_2H_4	3.70	4.23	205				CsCl	39.2
C_2H_6	4.33	4.42	230				CsI	57.7
SF_6	6.21	5.51	201					

[a] Taken from ref 7, 11, and 15. [b] B. E. Conway, "Electrochemical Data," American Elsevier Publishing Co., New York, N. Y., 1952. Values of σ were calculated by doubling the crystallographic radii. [c] H. S. Harned and B. B. Owen, "Physical Chemistry of Electrolyte Solutions," 3rd ed, Van Nostrand–Reinhold Co., Inc., Princeton, N. J., 1958.

both k_α and k_β increase in absolute magnitude, and it is difficult to predict in advance what will happen to k_s. Depending on the nature of the salt, the calculated value of k_s may increase, as it does with NaCl, or it may decrease, as it does with KI in going from H_2 to CH_4. For large nonelectrolyte molecules with strong intermolecular forces (ϵ_1/k large), the predicted value of k_s may be negative (salting in) as is the case in benzene systems with RbCl, CsCl, and CsI (*cf.* Table V).

It will be noted from Table I that the magnitude of k_α decreases as one goes from NaCl to KI. Both the ion sizes (σ_3, σ_4) and the apparent molal volume, ϕ_0, are greater for KI than for NaCl. Looking at eq 32, it appears that the increase in ϕ_0, which makes a negative contribution to k_α, somewhat outweighs the effect of the increase in σ_3 and σ_4. The quantity k_β becomes more negative as one goes from NaCl to KI. This reflects the effect of the increase in polarizability and number of electrons ($K^+ > Na^+$; $I^- > Cl^-$) on the leading term in eq 19. Combining these two trends, it is clear that scaled particle theory predicts that k_s will become algebraically smaller (less salting out or more salting in) as the sizes and polarizabilities of the cation and anion increase. This general trend is observed experimentally. An exception is LiCl, which ordinarily salts out less than NaCl. Interestingly enough, scaled particle theory predicts that LiCl should be out of line, primarily because its apparent molal volume is abnormally large (*cf* Table II).

In many respects, the expression for k_s derived from scaled particle theory resembles that from the theory of Bockris, *et al.*[4] In both cases, k_s is essentially a sum of two terms, one of which leads to salting out (k_α), the other to salting in (k_β). In the Bockris approach, the first term takes into account electrostatic forces and is always positive; the second term, which is usually negative, arises from dispersion forces, as does k_β. Both theories predict that the second term will become more important as the size and polarizability of the ions increase. The advantage of scaled particle theory is that the parameters necessary to evaluate k_s are more readily available.

Table III: Effect of Uncertainties in Parameters on the Calculated Value of k_s

System	$\Delta\epsilon_1/\epsilon_1$ = 0.05	$\Delta\sigma_1/\sigma_1$ = 0.05	$\Delta\sigma_3/\sigma_3$ = 0.05	$\Delta\sigma_4/\sigma_4$ = 0.05
H_2–NaCl	−0.001	+0.008	+0.005	+0.022
H_2–KI	−0.001	+0.006	+0.011	+0.035
CH_4–NaCl	−0.002	+0.010	+0.010	+0.039
CH_4–KI	−0.003	+0.006	+0.020	+0.062
SF_6–NaCl	−0.005	+0.015	+0.022	+0.078
SF_6–KI	−0.006	+0.009	+0.042	+0.123

Estimated Uncertainties in Calculated Salting Coefficients. Of the several parameters required to evaluate k_s for a particular salt–nonelectrolyte pair, Z_3 and Z_4, the numbers of electrons in the ions, are known exactly. The apparent molal volumes, ϕ_0, of the salts are known quite accurately. The polarizabilities, α_1, α_3, and α_4, are somewhat less certain, but literature values generally agree with each other within a few per cent.

The parameters most subject to error are the energy parameter of the nonelectrolyte, ϵ_1/k, its molecular diameter, σ_1, and the ionic diameters σ_3 and σ_4, probably in that order. Hirschfelder, Bird, and Curtiss[15] list values of ϵ_1/k and σ_1 which, for a given nonelectrolyte, may vary by as much as 10%. The problem of estimating ionic diameters is even more serious. We have chosen to use for σ_3 and σ_4 values calculated by simply doubling the crystallographic radii. Alternatively, one could use hydration radii, calculated by

(15) J. O. Hirschfelder, C. F. Curtiss, and R. B. Bird, "Molecular Theory of Gases and Liquids," John Wiley and Sons, New York, N. Y., 1954.

Table IV: Comparison of Observed and Calculated Salting Coefficients at 25°

	LiCl			NaCl			KCl			KI		
	Obsd	*d*	*e*	Obsd	*d*	*e*	Obsd	*d*	*e*	Obsd	*d*	*e*
He	0.050[a]	**0.081**	0.112	0.081[a]	**0.102**	0.151	0.068[a]	**0.091**	0.123	0.083[a]	**0.076**	0.070
Ne	0.059[a]	0.079	**0.060**	0.097[a]	**0.100**	0.080	...	0.088	0.066	0.080[a]	**0.067**	0.037
Ar	0.096[a]	0.087	**0.098**	0.133[a]	0.117	**0.132**	...	0.100	0.108	0.108[a]	0.067	0.061
Kr	0.116[a]	0.082	**0.119**	0.146[a]	0.114	**0.160**	0.124[a]	0.096	**0.131**	0.120[a]	0.060	0.074
H_2	0.076[b]	**0.088**	0.091	0.114[b]	**0.111**	0.123	0.102[b]	0.099	0.100	0.081[c]	**0.080**	0.057
O_2	0.100[b]	**0.097**	0.108	0.141[b]	0.129	**0.146**	...	0.113	0.119	...	0.082	0.068
N_2	0.095[c]	**0.102**	0.140	0.121[c]	**0.137**	0.188	...	0.119	0.154	0.100[c]	0.085	0.087
CH_4	0.097[c]	**0.095**	0.136	0.127[c]	**0.131**	0.184	...	0.113	0.151	0.097[c]	0.076	**0.086**
C_2H_4	0.089[c]	**0.090**	0.175	0.127[c]	**0.132**	0.236	...	0.111	0.193	0.061[c]	**0.065**	0.109
C_2H_6	0.124[c]	**0.089**	0.192	0.162[c]	**0.134**	0.260	...	0.111	0.212	0.101[c]	0.062	**0.120**
SF_6	0.145[a]	**0.131**	0.266	0.195[a]	**0.202**	0.358	0.165[a]	**0.171**	0.292	0.145[a]	0.113	**0.166**

[a] T. J. Morrison and N. B. B. Johnstone, *J. Chem. Soc.*, 3655 (1955). [b] F. A. Long and W. F. McDevit, *Chem. Rev.*, **51**, 119 (1952). [c] T. J. Morrison and F. Billett, *J. Chem. Soc.*, 3819 (1952). [d] Calculated from scaled particle theory, eq 11, 19, and 32. [e] Calculated from McDevit–Long theory.[3] Molar volumes of nonelectrolytes taken from J. H. Hildebrand and R. L. Scott, "Solubility of Nonelectrolytes," 3rd ed, Van Nostrand–Reinhold Co. Inc., Princeton, N. J., 1950.

various means,[2] which are generally much larger than the crystal radii.

In Table III we have listed the effect upon the calculated value of k_s of increasing ϵ_1/k, σ_1, σ_3, and σ_4 by 5%. Clearly, the most critical parameters are σ_3 and σ_4, precisely the ones that are least accurately known. Shoor and Gubbins[11] suggest evaluating these parameters by empirically fitting salt effect data for nonelectrolytes of low polarizability. The values of σ_3 and σ_4 they obtain for K^+ and OH^- fall within a few per cent of those calculated from crystal radii.

It is clear from Table III that the uncertainties in the various parameters become more critical with large, highly polarizable molecules ($SF_6 > CH_4 > H_2$) or ions ($K^+ > Na^+$; $I^- > Cl^-$). One can expect the k_s values for systems involving such species to show relatively poor agreement with experiment. This conclusion is reinforced by the fact that in deriving the expression for k_s from scaled particle theory, it is assumed that the entropy of interaction between solute and solvent species is negligible and that the molecular distribution is uniform.[11] These assumptions are likely to break down with large molecules and/or ions. They would almost certainly lead to serious errors with polar nonelectrolytes.

Comparison with Experiment. In view of the various approximations implicit in scaled particle theory and the uncertainties in the several parameters required to calculate k_s, the values calculated using eq 11, 19, and 32 and reported in Table IV are in remarkably good agreement with experiment. In about two thirds of the systems, the salting coefficient predicted from scaled particle theory is closer to the observed value than that calculated from the McDevit–Long theory. This effect is most pronounced with the aliphatic hydrocarbons and sulfur hexafluoride, where, for LiCl, NaCl, and KCl, the McDevit–Long theory predicts salting coefficients which are nearly twice as large as those observed.

The poorest agreement with experiment is found with the krypton systems; here the McDevit–Long theory clearly gives better results. Scaled particle theory also gives relatively poor results for systems involving potassium iodide; the calculated values of k_s are almost always significantly smaller than those observed. This suggests that the diameter we have chosen for the iodide ion should be modified; an increase of 0.1 Å in σ_4 would bring most of the salting coefficients for KI to within a few per cent of the experimental values.

The nonelectrolyte for which the greatest amount of salt effect data is available is probably benzene. In Table V, the observed salting coefficients for benzene with various alkali halides are compared to the predictions of scaled particle theory (column *a*), the McDevit–Long theory (column *b*), and the electrostatic theory (column c). Clearly, the agreement is rather poor in all three cases. The scaled particle and McDevit–Long

Table V: Salting Coefficients for Benzene at 25°

	a	*b*	*c*	*d*	Obsd
NaCl	0.105	0.42	0.166	0.188	0.198
KCl	0.077	0.34	0.156	0.162	0.166
NaBr	0.058	0.35	0.163	0.153	0.155
LiCl	0.045	0.31	0.172	0.124	0.141
RbCl	−0.024	0.31	0.153	0.089	0.140
KBr	0.030	0.34	0.153	0.128	0.119
NaI	0.036	0.27	0.158	0.137	0.095
CsCl	−0.032	0.26	0.150	0.085	0.088
CsI	−0.101	0.11	0.141	0.034	−0.006

[a] Calculated from scaled particle theory, using $\alpha_1 = 9.89 \times 10^{-24}$, $\sigma_1 = 5.27 \times 10^{-8}$ cm, $\epsilon_1/k = 440$. [b] Calculated from McDevit–Long theory.[3] [c] Calculated from electrostatic theory.[2] [d] Calculated as in (*a*), but taking $\epsilon_1/k = 214$.

theories predict the correct salt order, but the absolute values of k_s are too small in the former case and too large in the latter. Electrostatic theory gives salting coefficients of the right order of magnitude but does not yield the correct salt order. Indeed, it predicts essentially the same value of k_s for each of the alkali halides, contrary to what is observed.

The salting coefficients for benzene calculated from scaled particle theory using the parameters of ref 7 are uniformly low by about 0.08–0.10 unit. This suggests that we may be overestimating the effect of the interaction between the benzene molecule and the surrounding ions. If the free energy of interaction were smaller, k_β would be less negative and the salting coefficient, k_s, would be larger.

One way to obtain better agreement between scaled particle theory and experiment for benzene would be to adjust the values of ϵ_1/k and σ_1, which determine the magnitude of k_β. In this connection, it is interesting to see what would happen if we were to use Pierotti's value for σ_1 but calculate ϵ_1/k from the Mavroyannis–Stephen theory (eq 18), which was used to obtain ϵ_3/k and ϵ_4/k. The values of k_s obtained in this manner are given in column d of Table V. These numbers are in quite good agreement with the experimentally determined salting coefficients. Only with RbCl and, to a lesser extent, NaI, are there large discrepancies when values of ϵ_1/k calculated from eq 18 are used to evaluate k_β and hence k_s.

Lest it be supposed that this treatment will always give salting coefficients in better agreement with experiment, it should be pointed out that we have tested it with all of the systems listed in Table IV and find little overall improvement. Values of ϵ_1/k calculated from eq 18, assuming the nonelectrolyte diameters given in Table II, give somewhat better agreement for the ethane systems, but poorer results for sulfur hexafluoride. It may well be that the discrepancies found for benzene are of a more fundamental origin related to the approximations which are made in scaled particle theory.

In conclusion, we can say that: (1) For nonpolar solutes of relatively small size, scaled particle theory leads to values of k_s which are in good agreement with experiment. On the whole, it would appear to be an improvement over the McDevit–Long theory in these cases. (2) With large solute molecules, agreement with experiment is relatively poor, as is the case with all present theories of the salt effect. It is possible, however, to select solute parameters which give good agreement with experiment for those salts for which salting coefficients are available. These parameters can then be used to predict quite accurately the salting coefficients for other electrolytes. (3) Values of k_s calculated from scaled particle theory are quite sensitive to ionic size (σ_3, σ_4). This effect is particularly serious with large ions. In order to get good agreement with experiment for systems involving Rb^+, Cs^+, or tetraalkylammonium ions, it may be necessary to use a semiempirical method similar to that employed by Shoor and Gubbins[11] to obtain σ_3. With smaller ions, crystal radii can be used to obtain satisfactory values of σ_3 and σ_4.

Acknowledgment. This work was supported by the National Science Foundation under Grant GP-6163 and by funds provided by the United States Department of the Interior as authorized under the Water Resources Research Act of 1964, Public Law 88-379. Computer time was donated by the University of Connecticut Computer Center under funds provided by the National Science Foundation.

Thermodynamics of Molten Salt–Water Mixtures. I. Solubility of Water Vapor in a Potassium Nitrate–Sodium Nitrite Melt

by H. S. Hull and A. G. Turnbull

Division of Mineral Chemistry, C.S.I.R.O., Port Melbourne, Victoria, Australia *(Received September 22, 1969)*

The solubilities of water vapor at partial pressures of 5 to 24 Torr in a melt containing 55.5 wt % potassium nitrate and 44.5 wt % sodium nitrite have been measured at nine temperatures in the range 143–279°, using nitrogen at atmospheric pressure as a carrier gas. The dependence of the Henry's law constant, K, mole of water (mole of melt)$^{-1}$ Torr^{-1}, on absolute temperature, T°K, is given by the equation $\ln K = 3.4917 \ln T + 6040/T - 31.4638$. The partial molal enthalpy, entropy, and heat capacity of water at infinite dilution in the melt are derived from this equation and interpreted in terms of strong cation–water bonding.

Introduction

The study of solutions of inorganic salts in water is currently being extended to regions of high temperature and high salt concentration.[1,2] In particular, thermodynamic data are urgently required for the hot, strong solutions used in chemical processes such as hydrothermal extraction. Furthermore, it appears that improved theories of the structure and properties of electrolyte solutions may come from a study of the molten salt end of the concentration range.[1,2]

The present work forms part of a study of the complete thermodynamic properties of a model molten salt–water system over the entire concentration range. The salt selected was the 55.5 wt % KNO_3–44.5 wt % $NaNO_2$ mixture which forms a congruently melting solid solution of mp 141°.[3] Experience with this salt as an industrial heat transfer medium showed that it forms stable liquid mixtures with water in all proportions under moderate pressures. In contact with normal atmospheres containing water vapor the melt dissolves up to 0.2 wt % water. This concentration region was chosen for initial study because interactions between water molecules in the melt may be considered negligible compared to ion–water interactions. This is the "infinite dilution" approach which has proved so useful at the other end of the salt–water concentration range.

There have been a number of recent studies of water vapor solubility in melts.[2,4] In all cases Henry's law is obeyed, the solubility being proportional to pressure, and in low-melting salts at least the water appears to retain molecular identity in the melt. However, all work so far reported has been of insufficient precision or covered a temperature range inadequate for the evaluation of reliable thermodynamic properties. The present work aimed to obtain accurate values of enthalpy, entropy, and heat capacity for water at infinite dilution in the 55.5 wt % KNO_3–44.5 wt % $NaNO_2$ melt.

Thermodynamics

The system studied consists of a molten salt containing low concentrations of water and nitrogen in equilibrium with a gas phase containing water and nitrogen. The molten salt has negligible vapor pressure and, although a mixture, may be treated as a single component. On approaching infinite dilution of a solute it is empirically found that the mole fraction in the liquid, x, is proportional to the fugacity, f, in the gas phase

$$x = Kf \tag{1}$$

This is a statement of Henry's law, which applies independently to all solutes present at sufficiently low concentration. For the low partial pressures used here, 5–24 Torr water vapor and 760 Torr nitrogen, the fugacity may be replaced by the partial pressure, P. Also, for the low concentrations used, the mole fraction may be replaced by mole ratio, r, in units of moles of solute per (moles of KNO_3 + moles of $NaNO_2$), giving

$$r = KP \tag{2}$$

This relation has the advantage of applying empirically to higher concentration limits[5] than eq 1 and is more convenient to use with multiple solutes.

Data of sufficient accuracy relating the Henry's law constant, K, and absolute temperature, T, may be fitted by the relation

$$\ln K = a/T + b \ln T + c \tag{3}$$

(1) J. W. Cobble, *Science*, **152**, 1479 (1966).

(2) J. Braunstein, *Inorg. Chim. Acta Rev.*, **2**, 19 (1968).

(3) M. Ya. Kagan and N. J. Kamuischan, *J. Appl. Chem.* (USSR), **5**, 347 (1932).

(4) R. Battino and H. L. Clever, *Chem. Rev.*, **66**, 395 (1966).

(5) T. B. Tripp and J. Braunstein, *J. Phys. Chem.*, **73**, 1984 (1969).

Application of the van't Hoff equation[6] to (3) gives the partial molal enthalpy of solution

$$\overline{\Delta H} = -Ra + RbT \quad (4)$$

where R is the gas constant. Differentiation of (4) with respect to temperature[6] gives the partial molal heat capacity of solution

$$\overline{\Delta C_P} = Rb \quad (5)$$

which is assumed independent of temperature over the experimental range in this treatment. Assuming that Henry's law extends to infinite dilution, the partial molal enthalpy and heat capacity refer to infinite dilution also.

The partial molal entropy of solution is given by

$$\overline{\Delta S} = \overline{\Delta H}/T \quad (6)$$

It is useful to consider also the change in partial molal entropy due to the change in water concentration from gas (P/RT) to solution (KPd/M)

$$\overline{\Delta S_c} = R \ln (M/KRTd) \quad (7)$$

where M is the mean molecular weight of the melt, d the melt density, and R the gas constant in appropriate units. The difference $\overline{\Delta S} - \overline{\Delta S_c}$ then refers to the solution process without concentration change.

The activity coefficient of water in the melt may be defined by

$$\gamma = P/xP_w^0 \quad (8)$$

where P_w^0 is the vapor pressure of pure liquid water at the temperature considered.

Experimental Section

The materials used were Analar reagent grade potassium nitrate and sodium nitrite, air dried at 150°, and mixed in the proportion 55.5:44.5 by weight. The mix was premelted to give a clear pale yellow melt with a freezing point of 141 ± 0.5°. Samples of 40 g were held in a Pyrex saturator containing a sintered glass gas distributor, thermocouple well, and spray trap. Nitrogen bubbled through the melt at 25 cm^3 min^{-1} after passing in series through two water saturators and a spray trap held in a water bath controlled to ±0.01°. A series of water vapor pressures was obtained using analyzed H_2SO_4 solutions in the saturators. The gas was shown to be fully saturated by measuring the weight of water absorbed in drying tubes from a known volume of saturated gas. Saturation of the melt was continued for 16 hr although tests showed no further uptake of water after 5 hr under the conditions used. The pressure of the gas leaving the final saturator and of that leaving the melt were measured to 0.1 Torr with a calibrated capsule gauge.

After saturation, dry nitrogen was passed to strip water from the melt and collect it in two drying tubes containing magnesium perchlorate. Drying was normally completed in 4–5 hr after which a small continuous carryover from the melt was observed, attributed to spray, decomposition, vapor pressure of the melt, and traces of water in the dry nitrogen. Blank runs established a correction of 0.08 mg/hr which was applied to all runs independent of temperature. The drying tubes could be reproducibly weighed to 0.1 mg provided they always contained nitrogen at the same temperature and pressure. The weighing error thus varied from 0.1% at 150° to 1% at 280°. Further blank runs without melt in the saturator enabled the water vapor in the 50 cm^3 gas spaces between melt and drying tubes to be accounted for, giving corrections of 1–2 mg with an accuracy of 0.1 mg, depending on temperature, water vapor pressure, and melt volume. A check on overall operation was made by passing dry nitrogen through the melt at 280° and injecting 10.0 ± 0.05 mg of water into the inlet with a microsyringe through a rubber seal. All the water thus passed through the melt was collected again in the drying tubes within 3 hr.

The saturator was held in a well-lagged furnace, with a proportional controller giving better than ±0.1° constancy over the period of a run. Temperatures were measured at the center of the melt with a Pt—Pt–13% Rh thermocouple which was calibrated *in situ* at the freezing points of tin and lead to give an accuracy of 0.1°. Tests showed that the gas stream caused negligible cooling of the melt and produced good temperature uniformity. The temperatures of the solubility runs were chosen in random order, and the melt showed no detectable change in color or freezing point and negligible alkalinity.

Throughout this paper 1 cal = 4.184 J and 1 Torr = $(101.325/760)KNm^{-2}$.

Table I: Solubility of Water in 55.5 Wt % KNO_3–44.5 Wt % $NaNO_2$ Melt

Temp, °C	Melt, g	Water, mg	Correction, mg	P_w, Torr	$K \times 10^6$, mol of water (mol of melt)$^{-1}$ Torr^{-1}
142.9	44.05	116.4	2.2	19.76	61.0
149.8	44.05	100.2	2.15	19.74	52.4
160.1	44.55	75.2	2.05	19.65	38.1
180.8	44.55	46.5	1.95	19.63	24.2
201.0	44.55	33.3	1.85	19.65	16.7
220.9	44.05	23.1	1.75	19.91	11.3
239.8	44.55	17.0	1.65	19.76	8.12
260.1	44.55	12.7	1.5	19.76	5.92
278.5	44.55	10.1	1.4	19.65	4.62

(6) G. N. Lewis and M. Randall, revised by K. S. Pitzer and L. Brewer, "Thermodynamics," McGraw-Hill Book Co., New York. N. Y., 1961.

Results

In Table I are listed for nine solubility runs the temperature at the end of saturation, the weight of dry melt introduced, and the weight of water collected on stripping, corrected for carryover (see Experimental Section). A further correction is next listed for water vapor in the gas space above the melt. The partial pressure of water vapor, P_w', in the gas leaving the final water saturator was obtained from published data[7] for the relevant temperature and composition of the saturator solution. This was then corrected for expansion through the sintered glass bubbler in the melt and the head of melt. The mean partial pressure of water vapor in contact with the melt was calculated from

$$P_w = (P_A + 0.5H)P_w'/P_B \quad (9)$$

where P_A is the pressure after the melt, P_B the pressure after the final water saturator, and H the static head of melt above the bubbler outlet. It is assumed that there is a slight concentration gradient of water in the melt due to the head in spite of the melt circulation, but this has at most only 0.5% effect on the solubility.

A test of Henry's law was made at several temperatures using water vapor pressures in the range 5–24 Torr. In all cases solubility was proportional to pressure within this range as generally found for water in molten salts.[2] In Table I Henry's law constants are given for temperatures from just above the freezing point to 280°, above which the precision was inadequate due to the small weight of water collected. The plot of log K *vs.* $1/T$ given in Figure 1 has a significant curvature as predicted by eq 3 for a finite change in partial molal heat capacity on solution. The relationship corresponding to eq 3 found by the method of least squares

$$\ln K = 6040/T + 3.4917 \ln T - 31.4638 \quad (10)$$

gives a mean deviation in K of ±1.6%. The enthalpy and entropy of solution, calculated from (4), (6), and (7) for three rounded temperatures within the experimental range, are given in Table II. For this purpose the melt density was obtained by interpolation of published data[8] on KNO_3–$NaNO_2$ mixtures to give

$$d = 2.043 - 6.65 \times 10^{-4}t \quad (11)$$

The solubilities reported here refer to a melt saturated with nitrogen under atmospheric pressure. Provided the water and nitrogen are both at concentration low enough for Henry's law to apply, their solubilities should be independent. The nitrogen concentration may be estimated by an extrapolation of published data for nitrogen in molten sodium nitrate[9]

$$\log K_{N_2}\,(\text{mol cm}^{-3}\,\text{atm}) = 597/T - 6.64 \quad (12)$$

The concentrations calculated from (11) combined with molar volumes of the present melt give nitrogen solubilities of 2.7×10^{-4} mol of N_2 (mol of melt)$^{-1}$ at 140° and 1.2×10^{-4} mol of N_2 (mol of melt)$^{-1}$ at 280°. By comparison with data in Table II these represent 2% at 140° and 12% at 280° of the water contents. Under these conditions the nitrogen should have a negligible effect on the water solubility.

Table II: Partial Molal Enthalpy and Entropy of Solution of Water in 55.5 Wt % KNO_3–44.5 Wt % $NaNO_2$ Melt

Temp, °C	$\overline{\Delta H}$, kcal mol^{-1}	$\overline{\Delta S} - \overline{\Delta S_c}$, cal deg^{-1} mol^{-1}	S_r,[a] cal deg^{-1} mol^{-1}
150	−9.1	−10.0	11.50
200	−8.7	−9.1	11.83
250	−8.4	−8.2	12.13

[a] From ref 19.

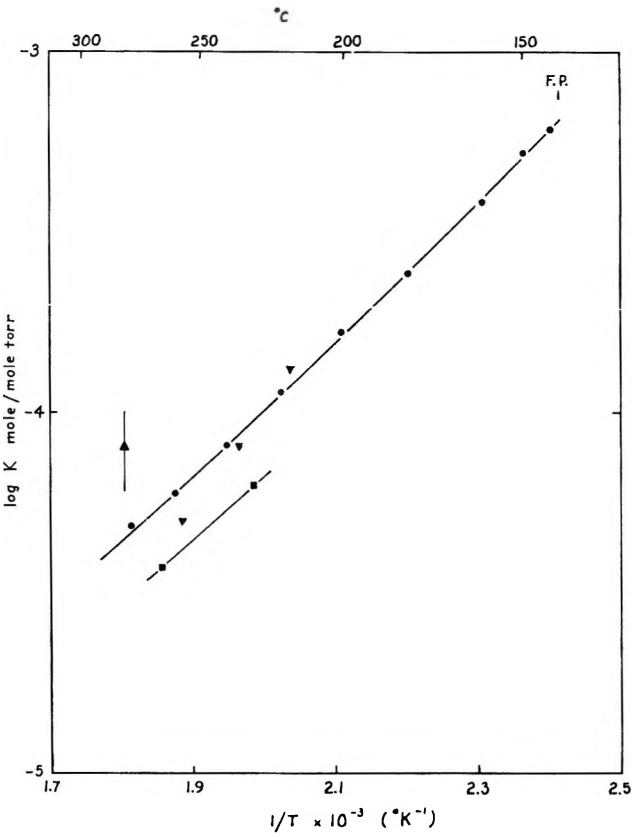

Figure 1. Temperature dependence of solubility of water vapor in various molten salts: ●, present work, 55.5 wt % KNO_3–44.5 wt % $NaNO_2$; ▼, ref 11, 54 wt % KNO_3–39.5 wt % $NaNO_2$–6.3 wt % $NaNO_3$; ▲, ref 12, $NaNO_2$; ■, ref 16, KNO_3.

(7) R. H. Stokes and R. A. Robinson, *Ind. Eng. Chem.*, **41**, 2013 (1949).

(8) V. D. Polyakov and S. I. Berul, *Izv. Sektora Fiz. Khim. Analiza Inst. Obshch. Neorgan. Khim. Akad. Nauk SSSR*, **26**, 164 (1955).

(9) J. L. Copeland and L. Siebles, *J. Phys. Chem.*, **70**, 1811 (1966).

Another factor requiring consideration is the slight hydrolysis of sodium nitrite over long periods, producing sodium hydroxide. Titration of melt samples with acid showed a gradual buildup of alkalinity to a value of 4×10^{-4} equiv/mol (0.02 wt % NaOH) at the end of the solubility runs. This amount would have negligible effect on the solubility of water, and it is known[10] that sodium hydroxide has negligible vapor pressure and decomposition pressure at the temperatures used here. The water injection tests (see Experimental Section) showed that water itself may be reversibly added to and removed from the melt.

In Figure 1 are shown three values of water vapor solubility in a heat transfer melt (54 wt % KNO_3, 39.5 wt % $NaNO_2$, 6.3 wt % $NaNO_3$). These were calculated from the boiling points[11] of this melt containing 0.8, 1.28, and 2.08 wt % water, assuming that Henry's law is obeyed up to these relatively high concentrations. The agreement with the present work is good, but no significance should be attached to the trend with temperature in view of the approximate nature of the measurements and derivation.

The solubility of water vapor in molten sodium nitrite at partial pressures of 7 and 19.5 Torr has been determined cryoscopically.[12] Assuming ideal behavior and a heat of fusion of 2.48 ± 0.07 kcal mol^{-1}, the freezing point depressions gave solubilities of 6×10^{-5} and 1.0×10^{-4} mol (mol of $NaNO_2$)$^{-1}$ $Torr^{-1}$, respectively, at 281°. Similarly, a cryoscopic study[13] of water in potassium nitrate, when reevaluated using the most recent heat of fusion,[14] 2.413 kcal mol^{-1}, gives a solubility of $(2.0 \pm 0.2) \times 10^{-5}$ mol (mol of KNO_3)$^{-1}$ $Torr^{-1}$ at 335°. Other workers[15] used a method of saturation with pure steam and stripping with nitrogen to obtain solubilities of (2.0 ± 0.7) and $(1.5 \pm 0.7) \times 10^{-5}$ mol (mol of KNO_3)$^{-1}$ $Torr^{-1}$ at 335 and 360°, respectively. The agreement of the two sets of data for potassium nitrate at 335° suggests that Henry's law applies up to a pressure of 760 Torr, but this may be fortuitous. Further data for potassium nitrate may be derived from solubilities in potassium nitrate–lithium nitrate mixtures,[16] measured directly with a microbalance at water vapor pressures up to 30 Torr. Data for 25, 50, and 75 mol % mixtures may be extrapolated by a smooth curve to give 6.3 and 3.7×10^{-5} mol (mol of KNO_3)$^{-1}$ $Torr^{-1}$ at 230 and 265°, respectively. As seen in Figure 1, the present data for a 54 mol % sodium nitrite–46 mol % potassium nitrate melt falls roughly midway between the literature data for sodium nitrite and potassium nitrate.

Discussion

The fact that water solubility in the melt considered here is proportional to the partial pressure suggests simple solution without dissociation or association of the molecule. In contrast, water solubility in halides, silicates, and borates at higher temperatures is proportional to the square root of pressure suggesting dissociation,[2] while water solubility in organic solvents above a concentration of about 0.05 *M* deviates from proportionality to partial pressure due to association of water molecules.[17]

The activity coefficients of water in the melt, relative to the liquid water standard state, vary from 0.55 at 150° to 0.45 at 280°. These figures suggest that the water–melt system is relatively ideal. In the water–lithium nitrate system[15] the water activity coefficient is only 0.13 at 265–280°. On the other hand, a value as high as 12 is observed in a water–liquid paraffin (mean molecular weight 345) mixture[18] at 150°. The activity coefficients reflect the free energy of the water–solvent interactions relative to those in pure water and thus depend on both enthalpy and entropy of bonding of water to the solvent species.

The solution of water in the 55.5 wt % KNO_3–44.5 wt % $NaNO_2$ melt is strongly exothermic (Table II). The partial molal enthalpy of solution of −8.4 kcal mol^{-1} at 250° compares quite well with values of −8.1 kcal $mole^{-1}$ for potassium nitrate and −9.9 kcal mol^{-1} for sodium nitrate at 230–265°, obtained by extrapolation of water vapor solubilities[16] in mixtures of these salts with lithium nitrate. The partial molal enthalpy of solution is almost equal to the enthalpy of condensation to liquid water at the same temperature. Thus the nearly ideal behavior results mainly from the similar enthalpy of ion–water interactions in the melt and water–water interactions in liquid water. In such solutions the ion–water interactions[2] include cation–permanent dipole and cation–induced dipole forces as well as anion–water hydrogen bonding. By comparison, the enthalpy of solution of nitrogen in molten sodium nitrate[9] is −2.7 kcal mol^{-1} over the range 355–454°. A small endothermic enthalpy is expected for both solutions due to expansion of the solvent to accommodate the solute, but for nitrogen the strong ion–permanent dipole forces are missing, leading to a less exothermic solution. For the water–paraffin mixture an even lower enthalpy of solution of −1.8 kcal mol^{-1} at 150° is observed,[18] since here there are

(10) E. Kay and N. W. Gregory, *J. Amer. Chem. Soc.*, **80**, 5648 (1958).

(11) C. A. Angell, J. A. Corbett, and R. C. Gifkins, *J. Aust. Inst. Metals*, **10**, 332 (1965).

(12) T. Kozlowski and R. F. Bartholomew, *J. Electrochem. Soc.*, **114**, 937 (1967).

(13) J. P. Frame, E. Rhodes, and A. R. Obbelohde, *Trans. Faraday Soc.*, **57**, 1075 (1961).

(14) O. J. Kleppa and F. G. McCarty, *J. Chem. Eng. Data*, **8**, 331 (1963).

(15) H. Haug and L. F. Albright, *Ind. Eng. Chem., Process Des. Develop.*, **4**, 241 (1965).

(16) G. Bertozzi, *Z. Naturforsch.*, **22a**, 1748 (1967).

(17) S. D. Christian and H. E. Aufsprung, *U. S. Office Saline Water, Saline Water Res. Develop. Progr. Rept.*, 301 (1968).

(18) S. Peter and M. Weinert, *Z. Phys. Chem.* (Frankfurt am Main), **5**, 114 (1955).

only the weak dispersion forces acting between non-charged molecules and possibly weak hydrogen bonding.

There is also a large negative change in the partial molal entropy of water on solution in the melt (Table II). Since correction has been made for the entropy due to the change in concentration from gas to melt, $\overline{\Delta S_c}$, this reduction of entropy must be attributed to changes in the translational or rotational motions of the molecule, the vibrational motions making negligible contribution to the entropy. The rotational entropy, S_r, of the free water molecule, calculated by statistical mechanical methods,[19] is given in Table II. This term alone is of sufficient magnitude to account for the observed entropy of solution. The tight bonding of water molecule to cations suggested by the enthalpy of solution could lead to a loss of most of the rotational entropy of the gas molecule. At more elevated temperatures the increasing thermal energy would then cause increased libration about the lowest energy orientation so that less of the rotational entropy would be lost. The decrease in the ratio $(\overline{\Delta S} - \overline{\Delta S_c})/S_r$ with rise in temperature supports this theory.

The change in the partial molal heat capacity of water from vapor to solution is 6.9 cal deg^{-1} mol^{-1}. Although $\overline{\Delta C_p}$ probably varies with temperature, the solubility data are not of sufficient accuracy to reveal this. Since the heat capacity of water vapor[19] is 8.0 cal deg^{-1} mol^{-1}, almost independent of temperature within the range considered, the partial molar heat capacity of water at infinite dilution in the melt is 14.9 cal deg^{-1} mol^{-1}. This is significantly less than the heat capacity of liquid water[20] in the same temperature range, 18.6–22.0 cal deg^{-1} mol^{-1}. The difference may be attributed to the contribution of the hydrogen bond network to heat capacity in water as well as to a restriction of the rotational heat capacity of water bonded to cations in the melt.

(19) K. K. Kelley and E. G. King, U. S. Bureau of Mines Bulletin 592, U. S. Government Printing Office, Washington, D. C., 1961, p 49.

(20) N. S. Osborne, M. F. Stimson, and E. F. Fiock, *Trans. Amer. Soc. Mech. Engrs.*, **52**, 191 (1930).

The Palladium-Catalyzed Carbon Monoxide Oxidation. Catalyst "Break-in" Phenomenon

by Raymond F. Baddour, Michael Modell, and Robert L. Goldsmith

Department of Chemical Engineering, Massachusetts Institute of Technology, Cambridge, Massachusetts 02139
(Received August 21, 1969)

The break-in period for CO oxidation over pressed-disk catalysts of silica-supported palladium was investigated. Kinetic parameters and infrared spectra of adsorbed CO were monitored during this period. At various stages of break-in, the reaction was interrupted and spectra of chemisorbed CO at 35° were determined in the absence of oxygen. Break-in did not commence until the catalyst was exposed to O_2. For a stabilized catalyst, the apparent activation energy was 15 kcal/mol lower and the apparent preexponential a factor of 10^7 lower than the values observed prior to break-in. Apparent discrepancies in literature values of peak frequencies were correlated with the state of the catalyst with respect to break-in. The break-in phenomenon was interpreted as arising from a redistribution of surface structures resulting from surface diffusion of palladium.

Introduction

The activity of a freshly prepared catalyst almost invariably changes with time in use. Three regimes can usually be identified: a break-in period during which the change (increase or decrease) in activity is relatively rapid and sometimes erratic; a steady-state period during which the activity is relatively constant with time; and a deactivation period. The third regime is sometimes associated with catalyst poisoning and/or aging and is well documented in the literature for many systems.

Break-in is so commonly exhibited by catalysts that it is rarely reported in the literature. However, very few quantitative studies have been made of break-in and, hence, the phenomenon is not clearly understood. It may be the result of removal of a contaminant or

foreign species introduced during preparation of the catalyst, or it may be the result of some modification of the true catalyst induced by the presence of the reactants and products and/or the occurrence of the reaction itself.

The importance of understanding changes which occur during break-in has not been stressed adequately. Many catalytic and chemisorption studies are made with systems for which the history of the catalyst with respect to break-in is uncertain. For example, many studies of chemisorption are made without measurement of catalyst activity and, in general, are conducted in the absence of some reactants and products. Such results are commonly used in the interpretation of steady-state kinetics and mechanisms. Such interpretation may be very misleading if, for example, break-in occurs by modification of the catalyst as a result of the catalyzed reaction.

In a previous investigation in this laboratory of the oxidation of carbon monoxide over palladium wire catalysts, a relatively slow break-in period was observed.[1] Over a period of five days, the apparent activation energy decreased from 45 to 28 kcal/mol. The activity was stable after this period, and the initial activation energy could not be regained by retreatment with hydrogen. Schwab and Gössner also reported a period of changing activity preceding a steady state for the same reaction over palladium foils.[2] The present study was undertaken to determine if a similar break-in pattern could be observed for supported palladium catalysts suitable for study by infrared transmission spectroscopy. Changes occurring during break-in were followed by monitoring catalyst activity and the infrared spectrum of adsorbed carbon monoxide.

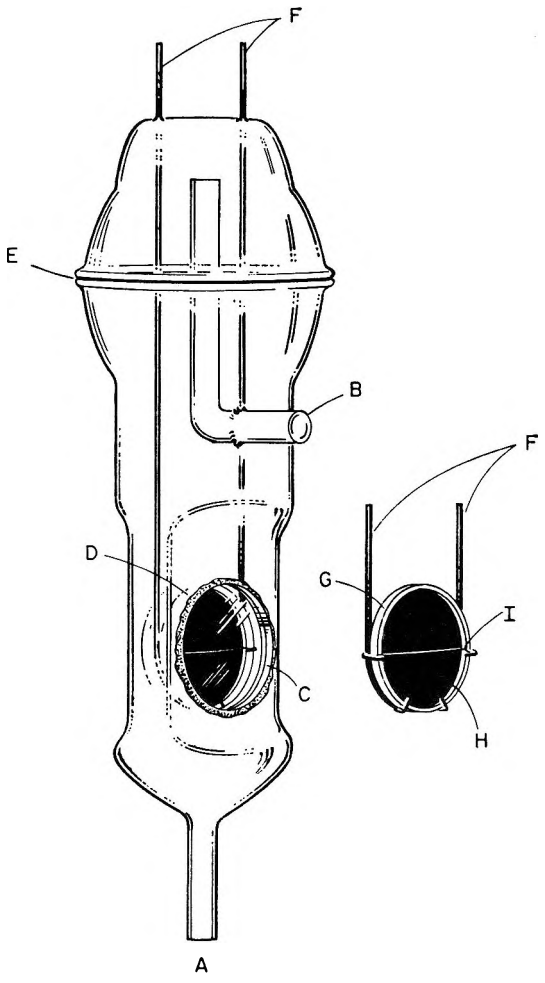

Figure 1. Reactor and catalyst mount: A, gas inlet; B, gas outlet; C, CaF_2 window; D, epoxy cement; E, Viton O ring; F, palladium rods; G, quartz ring; H, catalyst disk; I, palladium wire.

Experimental Section

Gas Mixtures. During adsorption experiments, catalysts were exposed to pure CO (Matheson CP, 99.5% minimum purity) or mixtures of CO and He (99.99% minimum purity). Oxygen-free mixtures of CO and He were prepared by passing mixed gases through a heated bed of copper. During kinetic experiments, mixtures of He, CO, and O_2 (Matheson CP, 99.5% minimum purity) were used. The gases were metered separately, mixed, and passed over beds of Drierite and Ascarite. The total reactor pressure was maintained at approximately 1 atm.

Reactor. Gas mixtures were contacted with a catalyst sample in a single pass using the reactor shown in Figure 1. Two calcium fluoride windows (30-mm diameter) were sealed onto the sides of the reactor with an epoxy–silicone rubber potting compound (Emerson and Cuming, Eccosil 4712). The catalyst disk was supported in the cell, facing the calcium fluoride windows, on two $^3/_{32}$-in. palladium rods, which were passed through glass-to-Kovar feed-throughs at the top of the cell. The palladium rods were silver soldered to the Kovar feed-throughs to provide a vacuum-tight seal. The catalyst was replaced by removing the cell top, which was connected to the lower portion by an O-ring joint.

The catalyst disk and cell were heated by irradiation from two 250-W heating lamps facing the cell windows. The voltage to the lamps was controlled by a potentiometer and, in this manner, the reaction temperature was varied. The disk temperature was controllable to within 0.5° with this arrangement.

Catalyst Preparation and Characterization. A nonporous silica powder with a mean particle size of 80 Å, Cab-O-Sil HS5 (Cabot Corp.), was slurried in a 5% $PdCl_2$ solution (Fisher Chemical Co.). The resulting paste was mixed in predetermined proportions to yield a final catalyst of 10 wt % Pd on silica. The paste was dried at 70° and ground to a fine powder. One catalyst

(1) M. Modell, Sc.D. Thesis, Department of Chemical Engineering, M.I.T., Cambridge, Mass., 1964.

(2) G. M. Schwab and K. Gössner, *Z. Phys. Chem.* (Frankfurt am Main), **16**, 39 (1958).

batch was used for the preparation of all catalyst samples described in this paper. For the preparation of a catalyst disk, about 0.15 g of this powder was pressed at 3000 psig into a thin self-supporting disk enclosed in a quartz ring. The resulting disk had a diameter of 22 mm and a thickness of 0.2–0.3 mm.

The catalyst temperature was followed by monitoring the resistance of a 2 mil in diameter palladium wire (99.9% purity, Engelhard Industries), which was embedded in the disk by placing it in the powder prior to compression. The ends of the wire, which extended beyond the quartz ring, were spot-welded to the palladium rods supporting the catalyst disk (see Figure 1). The resistance of the wire in the disk was much greater than that of the support rods, so that the total resistance could be related to a mean disk temperature. The area of the palladium wire and rods was negligible when compared to the area of the silica-supported metal.

Pretreatment of catalyst disks began with a 12-hr evacuation at 25° and 5×10^{-6} Torr, followed by a 6-hr evacuation at 275° and 10^{-5} Torr. During this period the disks turned from brown to black probably as a result of a reaction of $PdCl_2$ with residual water to form palladium oxide. After a 4-hr reduction in 20 torr of flowing H_2 at 150°, the disks were evacuated at 275° and 10^{-5} Torr for 24 hr. Samples which were reduced with hydrogen directly from $PdCl_2$ at about 100° exhibited behavior similar to those reduced from palladium oxide.

Recording of Spectral Data. A Perkin-Elmer Model 12 C spectrometer, described in detail previously,[3] was used. The instrument was modified with a continuous slit width drive in order to obtain greater accuracy over the spectral range studied. The region from 2200 to 1800 cm^{-1} was investigated. The background spectra of the catalyst disks were always measured for reduced samples in a vacuum or in helium, at room and reaction temperatures, prior to admitting CO or O_2. The spectra of the reduced samples in a vacuum and in helium were identical. Little change was observed in background spectra over the temperature range 25–200°.

Since only the carbonyl frequency region was scanned, the spectra represent infrared absorption of chemisorbed carbonyl compounds. Very little gaseous CO infrared absorption was observed because the path length of the cell was small (0.5 cm). Spectral data are reported as fractional infrared radiation transmitted (I/I_0) *vs.* wave number, where I and I_0 are, respectively, the transmission of the catalyst disk with and without CO adsorbed.

Recording of Kinetic Data. Product gas samples were analyzed with an on-line Fisher-Hamilton gas partitioner (Fisher Scientific Co., Model 29). The instrument was frequently calibrated with known composition mixtures of CO, CO_2, and O_2 in helium. The accuracy of the analysis was about 1% above partial pressures of 0.02 Torr.

Under the conditions studied here, it was shown previously that the rate of reaction is directly proportional to O_2 partial pressure and inversely proportional to CO partial pressure for the infrared-transmitting silica-supported palladium catalyst.[4] Conversion of both reactants was maintained below 5%, and since the reaction was not product inhibited, the reactor was treated kinetically as a differential reactor. The reaction rate and rate constant were calculated from

$$R = FX_{CO_2} = \frac{kP_{O_2}}{P_{CO}} \quad (1)$$

where R is the reaction rate (mol of CO_2/sec); F is the total flow rate (mol/sec); X_{CO_2} is the mole fraction of CO_2 in the product gas mixture; k is the reaction rate constant (mol of CO_2/sec); and P_{O_2} and P_{CO} are the partial pressures (Torr). The reaction temperature was varied from 75 to 175°. Since the reaction mixture always contained more than 95% helium and since conversion of the reactants was maintained below 5%, the change in the flow rate due to reaction was neglected. On the basis of calculation of effectiveness factors[3,4] it was concluded that bulk and pore diffusion limitations were unimportant.

Results

Variation of Rate. A freshly reduced catalyst sample (disk I) was exposed to a gas stream of constant composition (12 Torr of O_2, 17 Torr of CO) at 150° for 42 hr. The gas composition and infrared spectrum were recorded periodically. The calculated results are given in Figures 2 and 3. The spectra in Figure 3 were recorded at the times indicated for the corresponding data points in Figure 2. During the break-in period, the concentrations of the CO surface species increased with time, as indicated by the decreasing infrared transmission.

Variation of Kinetic Parameters and Spectra. The variation of apparent activation energy during the break-in period was observed for a second catalyst sample (disk II). The results, given in Figure 4, were obtained after disk II was exposed for prolonged periods to an oxygen-free mixture of CO and He. Points A1 through A15 were recorded in the order as numbered. Line I, drawn through points A1 to A5, was traced through data recorded during the 6-hr period following the introduction of O_2 to the CO–He mixture. The data for line II, points A8 to A12, were obtained at the end of the first day of the break-in period. Points A13, A14, and A15 were recorded on the fifth day of the break-in period. Data points B1 through B8 were recorded at a later time after the catalyst disk had undergone other studies. Immediately before record-

(3) R. F. Baddour, M. Modell, and U. K. Heusser, *J. Phys. Chem.*, 72, 3621 (1968).

(4) R. L. Goldsmith, Ph.D. Thesis, Department of Chemical Engineering, M.I.T., Cambridge, Mass., 1966.

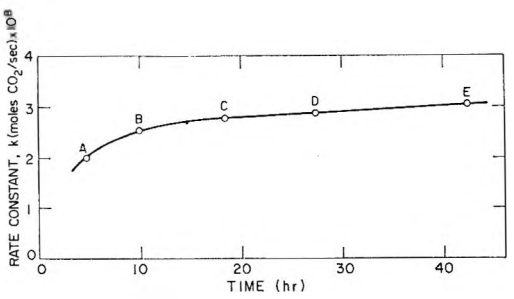

Figure 2. Variation of rate constant during break-in. Disk I, initially exposed to reactants at time zero. Conditions invariant at 12 Torr of O_2, 17 Torr of CO, and 150°.

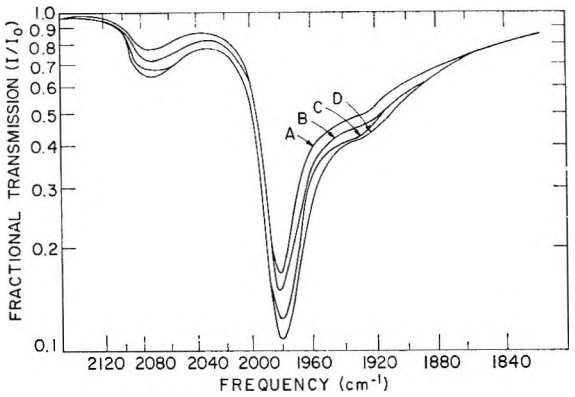

Figure 3. Variation of spectrum during break-in. Data recorded at times corresponding to A, B, C, and D in Figure 2.

ing the data in the B series, disk II was retreated with 1 atm of hydrogen in a manner otherwise identical with the initial hydrogen reduction pretreatment.

The apparent preexponential factors, k_0, corresponding to lines I, II, and III in Figure 4 are 1.9×10^{15}, 1.6×10^{10}, and 2.2×10^{8} mol of CO_2/sec, respectively.

Infrared spectra corresponding to several of the data points given in Figure 4 were recorded. The spectra above 2000 cm^{-1} are given for A1–4 and A10–12 in Figures 5a and b, respectively. The transmission of disk II in the region below 2000 cm^{-1} could not be measured quantitatively because this catalyst sample was relatively thick. The data in Figures 5a and b each cover the temperature range of 140–180°. The results are in general agreement with those for disk I (Figure 3) in that the band intensity in the region above 2000 cm^{-1} increased during the break-in period. The increase in intensity occurred preferentially on the high-frequency side of the asymmetric band.

Variation of Spectra of Chemisorbed CO. Most of the previous work on infrared spectra of CO adsorbed on palladium was conducted in the range of 25–35° under an oxygen-free gas phase.[5-7] To determine the effect of break-in on the low-temperature spectrum of chemisorbed CO, a fresh catalyst (disk III) was prepared and CO chemisorption studies were conducted at various stages of break-in.

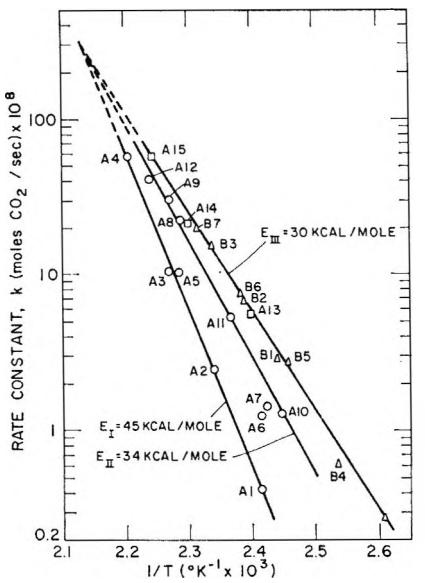

Figure 4. Variation of apparent activation energy during break-in.

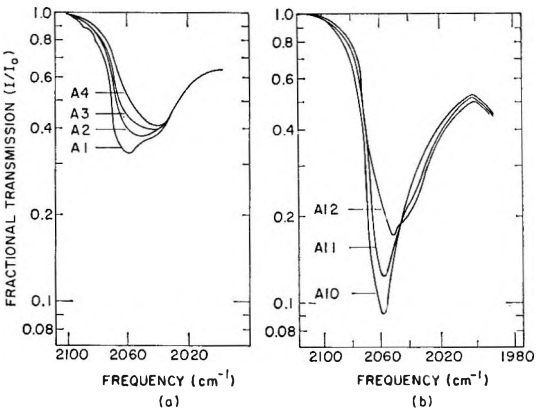

Figure 5. Variation of spectrum above 2000 cm^{-1} during break-in. Data points correspond to those given in Figure 4. Partial pressures invariant at 14 Torr of O_2 and 19 Torr of CO.

Immediately after the normal *in situ* pretreatment, spectra were recorded for disk III in the absence of oxygen as a function of CO partial pressure at a constant temperature of 35°. The results are illustrated in Figure 6. In the region below 2000 cm^{-1}, bands appeared first at 1920, 1885, and 1865 cm^{-1} (spectrum A). With increasing coverage, two additional bands appeared at 1942 and 1967 cm^{-1} (spectrum B). The most intense bands at high coverage were at 1965 and 1985 cm^{-1}. In the region above 2000 cm^{-1}, there first appeared a broad shallow band with its center at about 2035 cm^{-1} (spectrum A). At pressures above

(5) R. P. Eischens, S. A. Francis, and W. A. Pliskin, *J. Phys. Chem.*, **60**, 194 (1956).

(6) N. N. Kavtaradze, E. G. Boreskova, and V. J. Lygin, *Kinet. Catal.*, **2**, 349 (1961).

(7) C. W. Garland, R. C. Lord, and P. F. Troiano, *J. Phys. Chem.*, **69**, 1188 (1965).

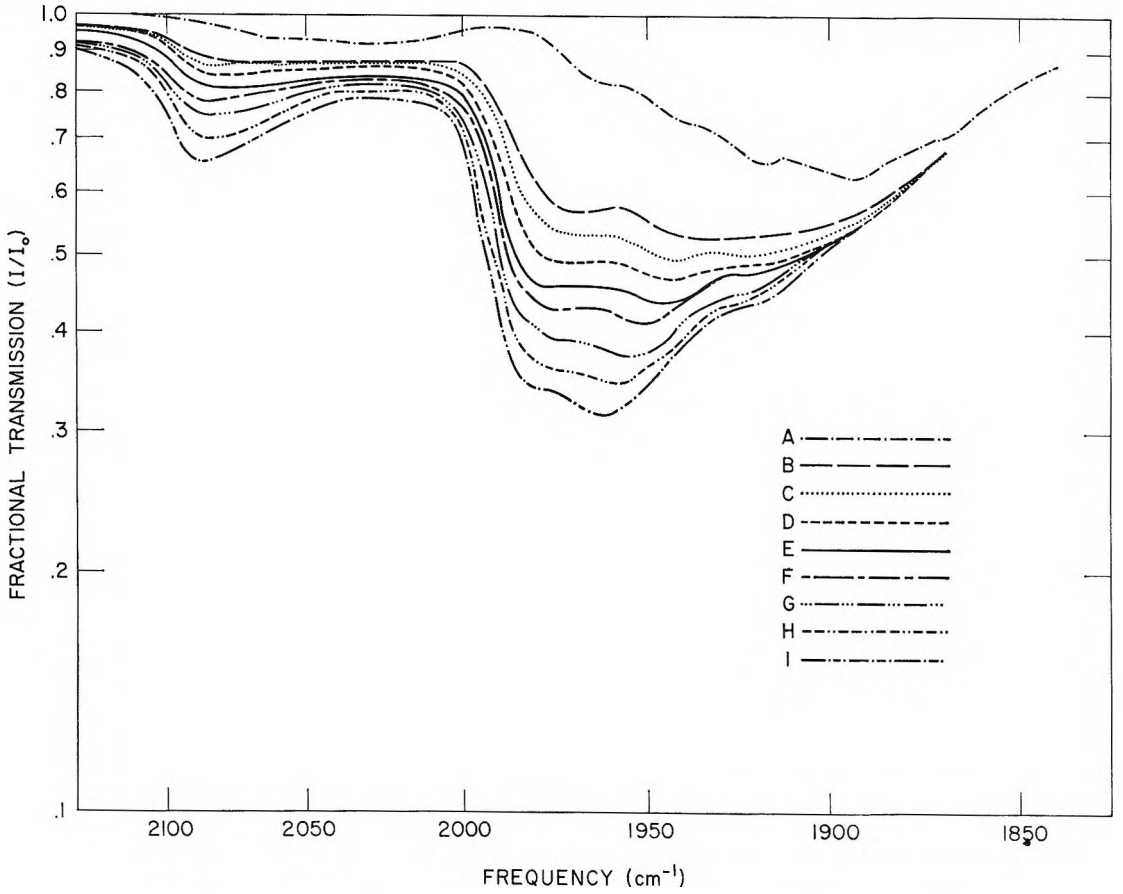

Figure 6. Spectra of CO chemisorbed on Pd prior to break-in. Temperature constant at 35° (disk III). CO partial pressures (Torr): A, 0.005; B, 0.068; C, 0.146; D, 0.34; E, 0.67; F, 1.81; G, 5.3; H, 15.7; I, 30.0.

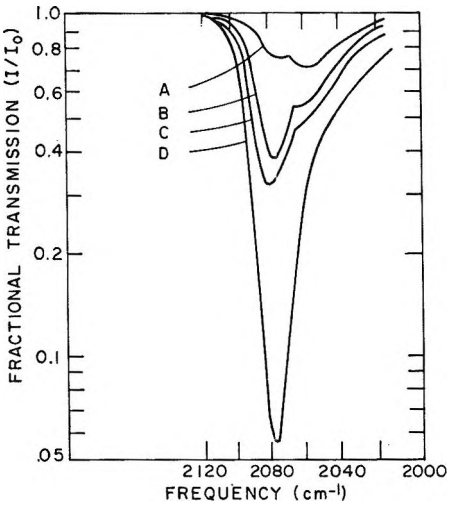

Figure 7. Spectra of linear species for CO chemisorbed on Pd prior to break-in. Temperature constant at 3° (disk IV). CO partial pressures (Torr: A, 0.001; B, 0.03; C, 0.6; D, 8.2.

10^{-2} Torr, a band appeared at 2078 cm^{-1} and became the dominant band in this region at higher pressures. These observations are somewhat more discernible in the spectra shown in Figure 7, which were obtained for a somewhat thicker sample (disk IV).

The spectra of Figures 6 and 7 were invariant with time provided that the gas phase was maintained free of oxygen.

The catalyst was then alternately exposed at room temperature to oxygen and carbon monoxide for three times. After a fourth oxidation, the sample was reduced again with H_2, evacuated, and the spectra of oxygen-free carbon monoxide were recorded again at 35° (see Figure 8). In the region below 2000 cm^{-1}, bands appeared again at 1920, 1885, and 1865 cm^{-1} at low coverage (spectrum A), and were followed by bands appearing at 1942 and 1967 cm^{-1} at moderate coverage (spectrum B) and at 1965 and 1865 cm^{-1} at high coverage. In the region above 2000 cm^{-1}, there first appeared a broad shallow band centered at about 2060 cm^{-1}, and at higher coverage a band at 2087 cm^{-1} predominated. These spectra differ from those in Figures 6 and 7 in that the dominant band above 2000 cm^{-1} is sharper and shifted slightly to higher frequency, and the 1985-cm^{-1} and is now somewhat more intense than the 1965-cm^{-1} band at high coverage.

After contacting the sample with a reacting mixture of CO and O_2 at about 200° for 12 hr, the spectra of Figure 9 were recorded for carbon monoxide (oxygen-free) at 35°. The bands above 2000 cm^{-1} exhibited similar behavior to those of Figure 8. Below 2000

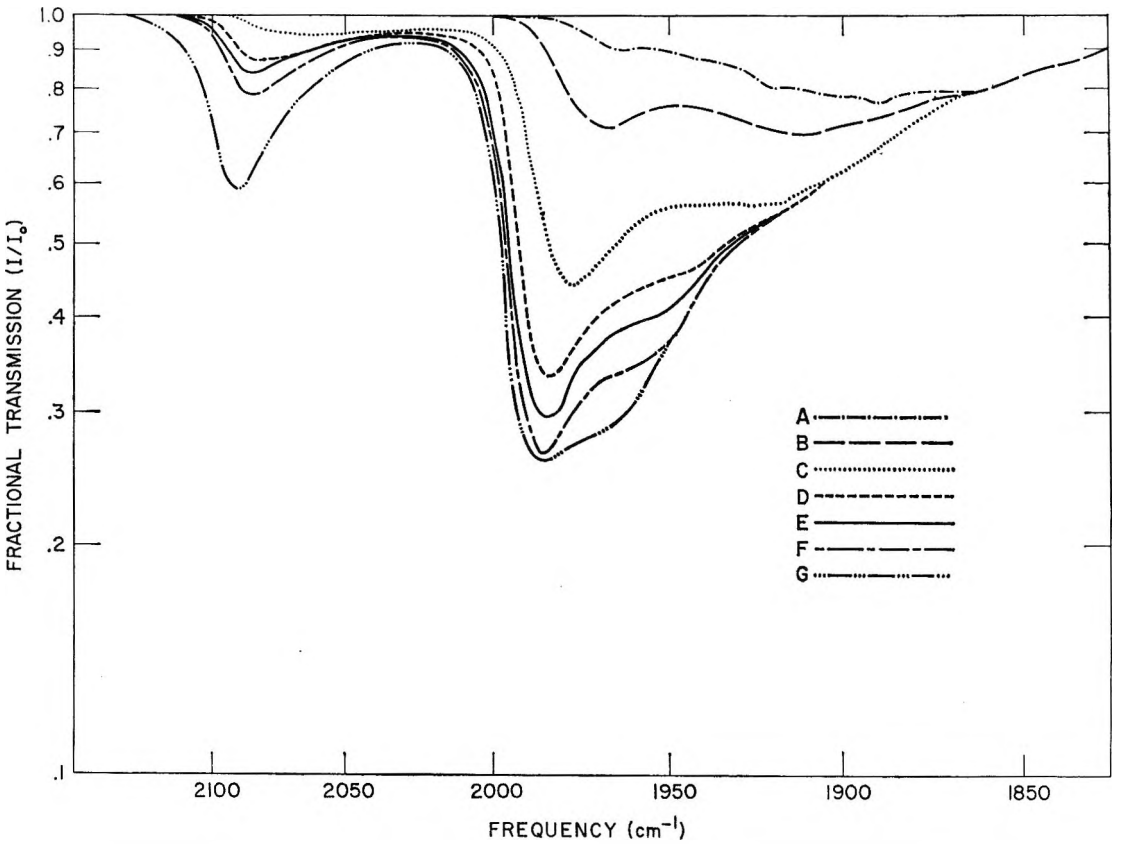

Figure 8. Spectra of CO chemisorbed on Pd after partial break-in. Temperature constant at 35° (disk III). CO partial pressures (Torr): A, 0.019; B, 0.035; C, 0.051; D, 0.23; E, 0.71; F, 3.5; G, 110.0.

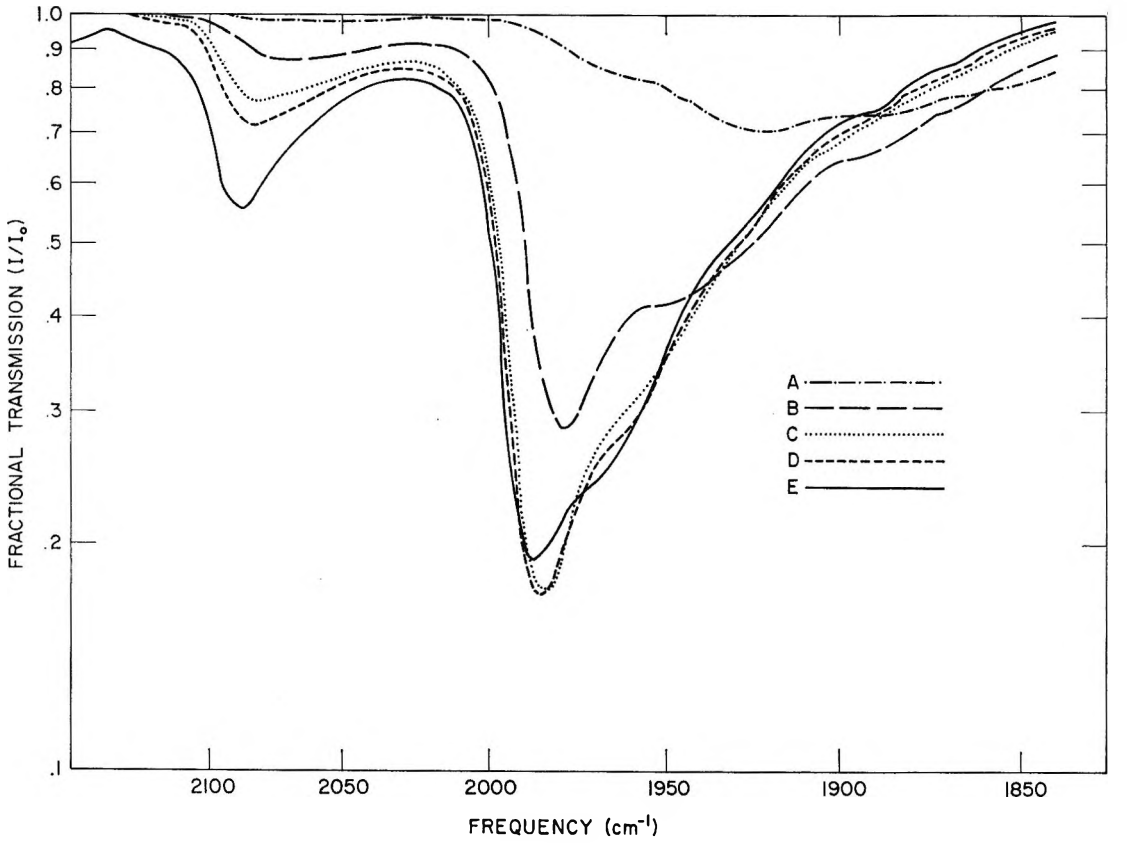

Figure 9. Spectra of CO chemisorbed on Pd after complete break-in. Temperature constant at 35° (disk III). CO partial pressures (Torr): A, 0.008; B, 0.109; C, 0.30; D, 1.91; E, 110.0.

Table I: Summary of Reported Spectra of CO Chemisorbed on Palladium

Pretreatment	Conditions
Silica-supported; H_2 redn, purged at 25° (ref 5)	25°; 10^{-4}–10^{-1} Torr of CO
Silica-supported; H_2 redn, evacuated at 500° and 10^{-5} Torr for 5 hr (ref 6)	25°; 10^{-4}–1.5 Torr of CO, with and without 8 Torr of O_2
Vapor deposited under 5–20 Torr CO (ref 7)	25°; 5–20 Torr of CO
Silica-supported; H_2 redn, evacuated at 200–280° and 10^{-5} Torr for 16 hr (ref 3)	20.5°; 0.04 Torr of CO, 0.2 Torr of O_2, and 780 Torr of He
Same as above (this work)	35°; 10^{-3}–1.0 Torr of CO, prior to break-in
	35°; 1.0–30 Torr of CO, prior to break-in; 0.1–110 Torr of CO, after break-in
Gaseous CO	

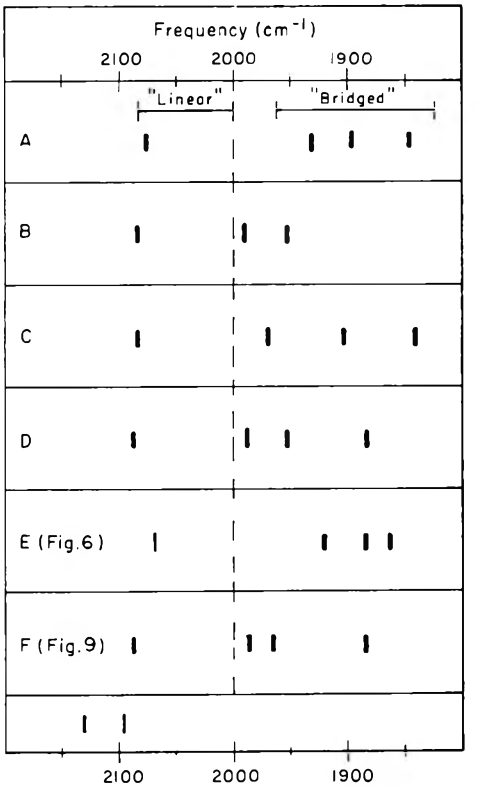

cm^{-1}, weak bands at low coverage were observed at 1920 and 1885 cm^{-1} (spectrum A). Bands at 1985 and 1965 cm^{-1} were again present, showing the same shift with coverage previously observed. However, the 1965-cm^{-1} band appeared as a very weak shoulder on the much stronger 1985-cm^{-1} band (spectra C through G). In addition, the intensity of the 1985-cm^{-1} band decreased noticeably from 1.9 to 110 Torr of CO (spectra D to E), while the linear band continued to increase. Additional spectra, obtained at 5.7 and 13.1 Torr fall between spectra D and E. These data were omitted from Figure 9 so as to illustrate more clearly the changes observed.

The amount of CO adsorbed at high coverage was determined volumetrically for disk III at each of the three stages of break-in. No large variations were observed: all three values were within ±15% of 6×10^{-6} mol.

Thermal Desorption of CO. The peak absorption intensities were monitored during thermal desorption of CO in the following manner. Disk I, after the end of the break-in period, was exposed to a flowing mixture of 20 Torr CO in He at 87°. After equilibration, the flow was switched to a stream of pure He. In Figure 10, the results are given in terms of the transmission at 2087 and 1985 cm^{-1} as a function of time following the switching to pure He. The transmission at 2087 cm^{-1} increased monotonically with time, but the transmission at 1985 cm^{-1} passed through a minimum.

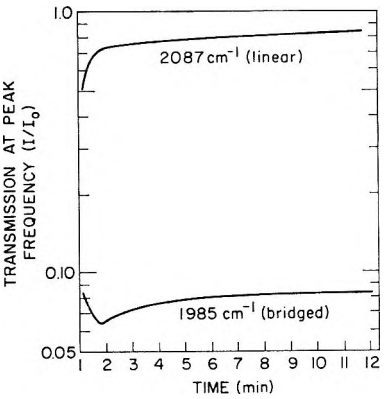

Figure 10. Peak frequency transmission during thermal desorption at 87° (disk I after break-in).

Discussion

Interpretation of Spectra of CO Adsorbed on Palladium. Spectra of chemisorbed CO on palladium have been obtained by several groups.[3,5–9] As previously noted,[3] there are marked differences between groups in the

(8) J. K. A. Clarke, G. Farren, and H. G. Rubalcava, *J. Phys. Chem.*, 71, 2376 (1967).

(9) C. P. Nash and R. P. DeSieno, *ibid.*, 69, 2139 (1965).

reported frequencies of the peak maxima. A summary of the reported values for those groups presenting quantitative information is given in Table I.

The band positions reported by Eischens, *et al.* (row A), are very close to those observed in this study for a catalyst prior to break in (row E). Furthermore, the shapes of the spectra in these two cases are similar in that the two bands between 1800 and 1930 cm^{-1} are of about equal intensity. The preparation and pretreatment procedures reported by Eischens, *et al.*, are also consistent with the interpretation that their catalyst was not broken-in; there is no report of the catalyst having been exposed to oxygen.

The band positions reported by Kavtaradze, *et al.* (row B), are similar to those for the post break-in period (row F). They observed no effect of oxygen on the spectra of chemisorbed CO. This observation is consistent with results obtained in this laboratory for catalysts which had undergone break-in.[3,4] In one experiment reported by Kavtaradze, *et al.*, the catalyst was exposed to 8 Torr of oxygen at 200° for 5 min. It is conceivable that the catalyst was exposed to oxygen for much longer periods prior to recording the reported spectra and, hence, that their catalyst had already been broken-in.

The results of Garland, *et al.* (row C), obtained with vapor-deposited palladium under 5 to 20 Torr CO, are similar to those of Eischens, *et al.* (row A), except for a weak band which appeared at 1970 cm^{-1}. Due to the radically different preparation procedure, a direct comparison with results for silica-supported palladium is not feasible.

The results of Baddour, *et al.* (row D), are very similar to those reported here for catalysts which had undergone break-in. The catalyst studied by Baddour, *et al.*, was exposed to mixtures of carbon monoxide and oxygen at relatively high temperature prior to recording the reported spectra.

It is clear from the above discussion that the apparent discrepancies among different groups for the reported band positions can be correlated in terms of the history of the catalyst with regard to break-in. Thus, it is essential to clearly relate the history of a catalyst when reporting infrared spectra of surface species.

Some differences of opinion exist regarding the structures of carbon monoxide surface species corresponding to the infrared active bands. Eischens, *et al.*,[10] originally assigned the bands above 2000 cm^{-1} to "linear" CO species in which the carbon atom is bonded to a single metal atom, while the bands below 2000 cm^{-1} were attributed to species in which the carbon is "bridged" between two adjacent metal atoms. These assignments were made by comparison with spectra of bulk metal carbonyls. Such a comparison is by no means conclusive and, in fact, the existence of the bridged species has been seriously questioned.[11] On the other hand, the assignment of the bands in the 2090-cm^{-1} region to a linear species is well accepted since this represents a relatively small displacement from the gaseous CO doublet.

Additional evidence for the existence of bridged species can be obtained from the spectra of Figure 9. The decrease in intensity of the 1985-cm^{-1} band with increasing pressure (D to E) is difficult to explain on the basis of single-site adsorption. However, the explanation is straightforward if the 1985-cm^{-1} band is interpreted as due to multisite adsorption. Upon increasing pressure, one would predict from Le Chatelier's principle that the following reaction should shift in favor of the linear species

$$CO_B(a) + CO(g) \rightleftharpoons 2CO_L(a)$$

where (a) and (g) refer to adsorbed and gaseous species, respectively, and B and L refer to bridged and linear forms, respectively. Thus, the linear species would eventually increase in concentration at the expense of bridged species. As observed in Figure 9, at high surface coverages all of the bridged species, except that corresponding to the 1965-cm^{-1} band, decreased in concentration with increasing pressure. This reaction should be important only at high coverage because the bridged form is preferred over the linear form when vacant neighboring sites are available.[3] If the rate of conversion of bridged to linear species is a slow process, one would observe a slow chemisorption in the high-pressure region. Such observations (*i.e.*, slow residual chemisorption) in which days or weeks have been required to reach equilibrium have been reported previously in many chemisorption studies. Since the spectra shown in Figure 9 were recorded at approximately 1-hr intervals, it is conceivable that equilibrium was not attained.

The assignment of the 1985-cm^{-1} band to a bridged species is consistent with the thermal desorption results given in Figure 10. The linear species desorbs faster than the bridged species because it is less tightly bound to the surface. As vacant sites are created by desorption of linear species, some of the remaining linear species are converted to bridged species by the reaction: $CO_L(a) + * \rightarrow CO_B(a)$. Thus, the concentration of bridged species reaches a maximum at an early stage in the desorption process.

Effect of Break-in on Kinetics. It has been shown previously[3] that the observed rate expression

$$R = \frac{kP_{O_2}}{P_{CO}} \qquad (2)$$

is consistent with either of the following mechanisms: (a) adsorption of molecular oxygen rate-limiting, or (b) surface reaction between chemisorbed carbon mon-

(10) R. P. Eischens, W. A. Pliskin, and S. A. Francis, *J. Chem. Phys.*, 22, 1786 (1954).

(11) G. Blyholder, *J. Phys. Chem.*, 68, 2772 (1964).

oxide and chemisorbed molecular oxygen rate-limiting. In either case, it is assumed that oxygen coverage is much smaller than carbon monoxide coverage. For cases (a) and (b), respectively, the derived rate expressions are given in eq 3 and 4

$$R_a = \frac{k_a P_{O_2}}{K_{CO} P_{CO}} \quad (3)$$

$$R_b = \frac{k_b K_{O_2} P_{O_2}}{K_{CO} P_{CO}} \quad (4)$$

where k_a and k_b are the rate constants for the rate-limiting steps, and K_{CO} and K_{O_2} are adsorption equilibrium constants. Activation energies corresponding to these two rate equations may be expressed as

$$(E_A)_a = E_a - q_{CO} \quad (5)$$

$$(E_A)_b = E_b + q_{O_2} - q_{CO} \quad (6)$$

where E_a and E_b are activation energies for the rate constants R_a and R_b, and q_{CO} and q_{O_2} are the heats of adsorption for CO and O_2, respectively. On the basis of present data, it is not possible to determine what changes in these energy terms are responsible for the observed decrease in the apparent activation energy during break-in.

Interpretation of the Break-in Phenomenon. The break-in pattern observed here was very similar to that observed with palladium wire catalysts.[1] Since these catalysts were prepared under very different conditions, it is unlikely that break-in was the result of removal of a contaminant or foreign species.

The initially high apparent activation energy (45 kcal/mol) could not be reproduced by H_2 retreatment of the catalyst (B series data in Figure 4). Therefore, the break-in period could not result from gradual removal of hydrogen remaining after the initial catalyst reduction. The observed break-in period was not a purely thermal process since the catalyst samples were heat-treated for several hours at a temperature of 50° higher than the highest reaction temperature studied. It is also unlikely that break-in was associated with a significant change in total palladium surface area since the total amount of adsorbed CO at high coverage did not vary significantly.

It is proposed that the break-in phenomenon results from a structural rearrangement of the palladium catalyst. This rearrangement occurs only in the presence of oxygen or O_2–CO mixtures, since the spectrum of CO adsorbed on a freshly prepared catalyst from an oxygen-free gas phase is invariant with time. This interpretation is supported by the results of Manly and Rice[12] which indicated that crystal growth of palladium can occur well below the Tamman temperature (460°) and that oxygen is an accelerator for this process.

The structural rearrangement is most likely associated with a redistribution of exposed crystallographic planes

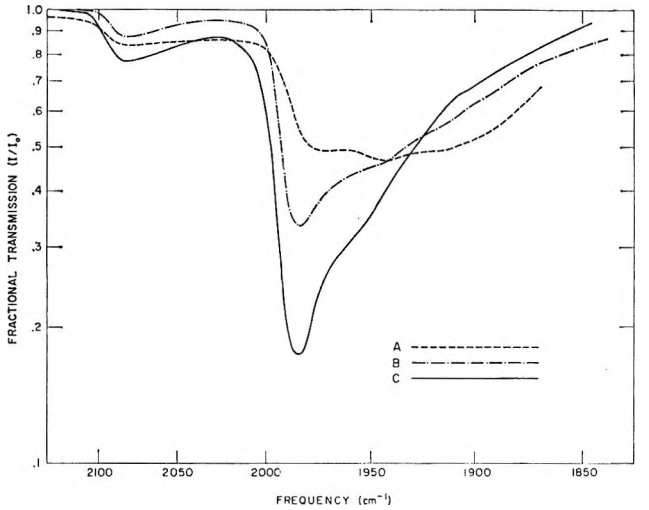

Figure 11. Spectral changes during break-in: A, prior to break-in at 0.34 Torr of CO; B, partial break-in at 0.23 Torr of CO; C, after break-in at 0.30 Torr of CO.

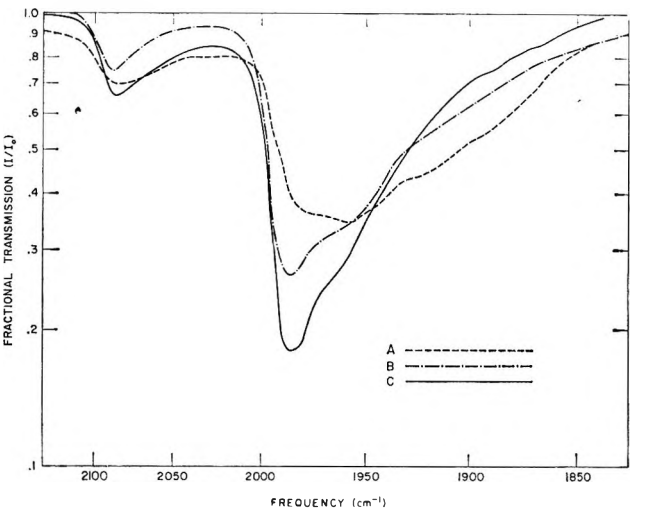

Figure 12. Spectral changes during break-in: A, prior to break-in at 15.7 Torr of CO; B, partial break-in at 11.2 Torr of CO; C, after break-in at 13.1 Torr of CO.

resulting from surface diffusion of palladium atoms or palladium–oxygen complexes. The process most likely involves transformations from structures which bind CO tightly to those of lower binding energy. This result can be seen more clearly in Figures 11 and 12, in which spectra from Figures 6, 8, and 9 are cross-plotted for two different regions of pressure. The overall result of break-in is a shift of absorption from low to high frequency. In each of Figures 6, 8, and 9 upon increasing pressure the bridged bands appeared in order of increasing frequency. Eischens, *et al.*,[5] reported similar results and furthermore found that the bands were removed in reverse order of appearance upon evacuation. Since increasing frequency is characteristic of a stronger carbon–oxygen bond, which in turn

(12) D. G. Manly and F. J. Rice, Jr., *J. Phys. Chem.*, 68, 4201 (1964).

is probably associated with weaker metal–carbon bonds, it was concluded that the lower frequency bridged species are more tightly bound to the palladium.

The type of structural rearrangement proposed here has been observed on palladium and other transition metal single crystals by low-energy electron diffraction.[13–15] On the (100) face of palladium, several ordered surface structures were found, each of which was stable in well-defined temperature ranges.[14] Transitions from one structure to another were accomplished by temperature manipulation under high-vacuum conditions. Thus, it is conceivable that phenomena similar to break-in could be initiated by controlled heating of the catalysts in the absence of oxygen. It would be extremely interesting to see how the low-energy electron diffraction patterns change when a crystal is exposed to the conditions which have resulted in break-in.

Acknowledgment. This work was supported in part by the National Science Foundation (Grant GP-607). The authors are grateful to the Atlantic Refining Co. for the use of the spectrometer. The authors are indebted to Drs. R. P. Eischens, C. W. Garland, and R. C. Lord for discussions and advice during the course of the investigation.

(13) C. W. Tucker, Jr., *J. Appl. Phys.*, **35**, 1897 (1964).

(14) A. M. Mattera, R. M. Goodman, and G. A. Somorjai, *Surface Sci.*, **7**, 26 (1967).

(15) H. B. Lyon and G. A. Somorjai, *J. Chem. Phys.*, **46**, 2539 (1967).

Damping of Capillary Waves on Water by Monomolecular Films of Linear Polyorganosiloxanes

by W. D. Garrett and W. A. Zisman

Naval Research Laboratory, Washington, D. C. 20390 *(Received September 26, 1969)*

We have investigated the wave damping effects caused by adsorbed insoluble monolayers of a variety of organic compounds with emphasis on the behavior of polyfunctional molecules, especially surface-active linear polymers. We report here the results obtained with various polyorganosiloxanes, some of which were of exceptional purity and freedom from homologs. Graphs are given of the wave damping coefficient (k) *vs.* the area per adsorbed molecule (A) and of the film pressure (F) *vs.* A. The k *vs.* A graphs were both reproducible and reversible. Our results reveal the importance of measuring the wave damping behavior of each polymer over the entire film pressure range, because with some polymers as many as four maxima and three minima were found in the k *vs.* A plot. We also found conditions where k had nearly the same value as that for water free of organic film for several values of F distributed over the film pressure range between the gaseous film state and that of complete film collapse. The results of this investigation teach also that the k *vs.* A graph of an insoluble monomolecular film can be used as a sensitive surface-chemical tool having particular value for following and identifying changes in molecular configuration through intermolecular or intramolecular rearrangements.

Introduction

Waves on a large body of water having wavelengths of less than 1.7 cm are known as "capillary waves,"[1] and these are sometimes damped with remarkable effectiveness by an adsorbed film of surface-active material. Interesting early reviews of the history of sea slicks and wave calming oils have been given by Banting[2] and Davies[3] and Davies and Rideal.[4] Reynolds[5] theorized that an elastic surface film dissipated wave energy due to an alternating tangential drag on the water as the surface film was expanded and contracted by the passing crests and troughs. This concept was later expressed mathematically by Lamb,[6] who essentially ignored any other properties of the adsorbed surface film.

(1) Sir William Thomson, *Phil. Mag.*, **42**, 368 (1871).

(2) J. D. Banting, "The Influence of Oil on Water," Report, 3rd International Lifeboat Conference, Rotterdam, Holland, June 1932, pp 155–173.

(3) J. T. Davies, *Chem. Ind.* (London), 906 (1962).

(4) J. T. Davies and E. K. Rideal, "Interfacial Phenomena," Academic Press, New York, N. Y., 1961, pp 266–274.

(5) O. Reynolds, *Brit. Assoc. Advan. Sci. Rep.*, paper i409 (1880).

(6) H. Lamb, "Hydrodynamics," 6th ed, Cambridge University Press, London, 1932.

Agnes Pockels[7] gave the first demonstration that capillary waves in a clean water trough could be damped by spreading on it various surface-active compounds. Dorrestein's[8] theoretical treatment of capillary waves and wave damping was a major advance which influenced all later investigators. Of particular interest here is that he related the wave damping coefficient to the surface viscosity, to the compressional modulus of the surface film, and to a hysteresis of the surface tension. Vines'[9] experiments on the damping of water capillary waves by cetyl alcohol films demonstrated that the damping effect exceeded that predicted by existing theories. Garrett and Bultman[10] reported a maximum in the graph of the wave damping coefficient (k) *vs.* the film pressure (F) on water at values of F of only 1 dyn/cm (or less) for a number of pure, insoluble, conventional, surface-active compounds, as well as the enzyme, crystalline ovomucoid. The same was true of their graphs of k *vs.* the area per adsorbed molecule or of k *vs.* the modulus of surface compressibility of the film. Similar maxima were obtained with a number of other insoluble surface-active agents by Avetisyan and Trapeznikov.[11] A more extensive investigation of wave damping by soluble and insoluble surface-active agents was made by Davies and Vose,[12] who concluded that their results were in excellent agreement with Dorrestein's theory.

Since 1961 a rapid succession of theoretical papers have been published concerning the damping of capillary waves by soluble and/or insoluble adsorbed monolayers on water. These include the work of Goodrich,[13] Hansen and Mann,[14,15] van den Tempel, Lucassen, and Lucassen-Reynders,[16] van den Tempel and van de Riet,[17] Lucassen and Hansen,[18,19] Bendure and Hansen,[20] and Lucassen.[21] Besides using various theoretical approaches and approximations in the solution of the hydrodynamical equations involved, these papers have in one way or another emphasized or elaborated on various aspects of the interaction of the monolayer with the wave energy at the liquid–air interface including surface viscoelasticity, the Gibbs elasticity relating the excess surface tension in the extended region to the relative increment of the surface area, the existence of a term concerned with the fluctuations in surface tensions resulting from periodic contraction and expansion of the liquid surface, and the existence and influence of longitudinal waves which are stated to be normally superimposed on capillary waves but are usually damped out much more rapidly.

Some Theoretical Aspects

Sir William Thomson[1] derived the following classic relation for the velocity (V) of a surface wave on a liquid free of adsorbed surface film in a large deep basin

$$V^2 = g\lambda/2\pi + 2\gamma/\rho\lambda \qquad (1)$$

where λ is the wavelength, γ is the surface tension of the liquid, ρ is its density, and g is the acceleration of gravity. For values of λ of 0.5 cm or less, the first term on the right-hand side of eq 1, which is known commonly as the "gravity wave" term, becomes negligible as compared to the second, or "capillary wave" term. Equation 1 simplifies for capillary waves to

$$V^2 = 2\pi\gamma/\rho\lambda \qquad (2)$$

Hence, V^2 decreases linearly with γ on a film-free liquid in a deep and large basin. If the basin is not deep, a corrective term derived by Rayleigh[22] must be inserted in eq 2.

From eq 1 it has been shown by Lamb[6] that the amplitude "a" of a train of plane waves originating from an infinitely long linear source decays exponentially with the distance x from the source, *i.e.*

$$a = a_0 e^{-kx} \qquad (3)$$

where a is the amplitude at a distance x from the source, a_0 is the amplitude at $x = 0$, and k is the damping coefficient of the liquid free of adsorbed film. According to Lamb,[6] the value of k for a clean water surface can be calculated when $\lambda \leq 0.5$ cm by the following relation

$$k = a\pi^2\nu/\rho U^2 \qquad (4)$$

where U is the group velocity of the waves, and ν is the kinetic viscosity of the bulk liquid. As is well known,[6] U and V are related as follows

$$U = V - \lambda dV/d\lambda \qquad (5)$$

For slightly damped, sinusoidal waves on a film-free water surface and with $\lambda \leq 0.5$ cm, Goodrich[13] showed that k can be calculated to a good approximation from the ripple frequency (f) by the following simpler expression than eq 4

(7) A. Pockels, *Nature*, **43**, 437 (1891).

(8) R. Dorrestein, *Proc. Acad. Sci.* (Amsterdam), **B54**, 260, 350 (1951).

(9) R. G. Vines, *Aust. J. Phys.*, **13**, 43 (1960).

(10) W. D. Garrett and J. D. Bultman, *J. Colloid Interface Sci.*, **18**, 798 (1963).

(11) R. A. Avetisyan and A. A. Trapeznikov, *Russ. J. Phys. Chem.*, **38**, 1660 (1964).

(12) J. T. Davies and R. W. Vose, *Proc. Roy. Soc.*, **A286**, 218 (1965).

(13) F. C. Goodrich, *ibid.*, **A260**, 481, 490, 503 (1961).

(14) J. A. Mann and R. S. Hansen, *J. Colloid Sci.*, **18**, 751 (1963).

(15) R. S. Hansen and J. A. Mann, *J. Appl. Phys.*, **35**, 152 (1964).

(16) M. van den Tempel, J. Lucassen, and E. H. Lucassen-Reynders, *J. Phys. Chem.*, **69**, 1798 (1965).

(17) M. van den Tempel and R. P. van de Riet, *J. Chem. Phys.*, **42**, 2769 (1965).

(18) J. Lucassen and R. S. Hansen, *J. Colloid Interface Sci.*, **22**, 32 (1966).

(19) J. Lucassen and R. S. Hansen, *ibid.*, **23**, 319 (1967).

(20) R. L. Bendure and R. S. Hansen, *J. Phys. Chem.*, **71**, 2889 (1967).

(21) J. Lucassen, *Trans. Faraday Soc.*, **64**, 2221 (1968).

(22) Lord Rayleigh, *Phil. Mag.*, **30**, 386 (1890).

$$k = 8\pi\nu f/3\gamma \quad (6)$$

When the water is covered with an adsorbed surface film, eq 3 will be used to calculate k from a_0, a, and x. We will try to relate the resulting k to the energy-dissipating properties of the adsorbed insoluble film including its drag interaction with the water substrate. That the latter interaction must exist to a depth of at least 0.03 mm if the film contains hydrophilic groups is an inevitable consequence of the early and convincing experiments by Bressler and Talmund[23] and Schulman and Teorell.[24]

Compounds whose wave damping effects on water have been investigated included some well-defined soluble or insoluble fatty alcohols, acids, and salts, as well as a variety of esters. Except for Garrett and Bultman[10] and Davies and Vose,[12] no other polyfunctional surface-active compounds, nor any polymer, had been used until this investigation.

It is the purpose of this paper to report our results presented orally earlier[25] on the wave damping behavior on water of various pure, insoluble, surface-active polymers belonging to the family of linear polyorganosiloxanes.

Some Essentials about Polyorganosiloxane Monolayers on Water. In selecting polyorganosiloxanes for this investigation, we were guided by certain adsorptive characteristics of monolayers on water of the open-chain polydimethylsiloxanes and their phenylated substituents which had been investigated fully by Fox, Taylor, and Zisman.[26] These results were, in the main, confirmed later by Newing[27] and Noll, Steinbach, and Sucker.[28,29] Another invesitgation by Fox, Solomon, and Zisman[30] also had established the influence of varying the pH of the water on the rate of hydrolysis of the adsorbed polydimethylsiloxanes; their results established that at 20° above pH 3 and below pH 11, the rate of hydrolysis of the polysiloxane chain was insignificant. Furthermore, in reference 26 it was demonstrated that the open-chain polydimethylsiloxane molecules are extremely flexible because the large diameter of the silicon atom creates ample spacing between neighboring monomers of the polysiloxane main chain so that the methyl side chains are not sterically hindered from freely rotating about the carbon–silicon bonds. Roth,[31] by an X-ray analysis of a crystalline polydimethylsiloxane, showed also that there was freedom of rotation of methyl groups about the carbon–silicon bonds. Of particular importance here, Fox, Taylor and Zisman[26] proved that: (a) the open-chain polydimethylsiloxanes adsorbed at low film pressures with the hydrophilic polysiloxane chain in direct contact with the surface of the water with every methyl side chain projecting upwards at the air–water interface; (b) when in such an adsorbed configuration, the polymer had great flexibility; and (c) in that configuration the polymer had an essential structural characteristic of a surface-active agent in that it exhibited a hydrophilic, as well as a hydrophobic, aspect at opposite regions (or portions) of the molecule. For these reasons the polyorganosiloxanes are admirably suited for studies of the effects of the adsorptive properties and molecular configuration on wave damping properties at various stages of film compression.

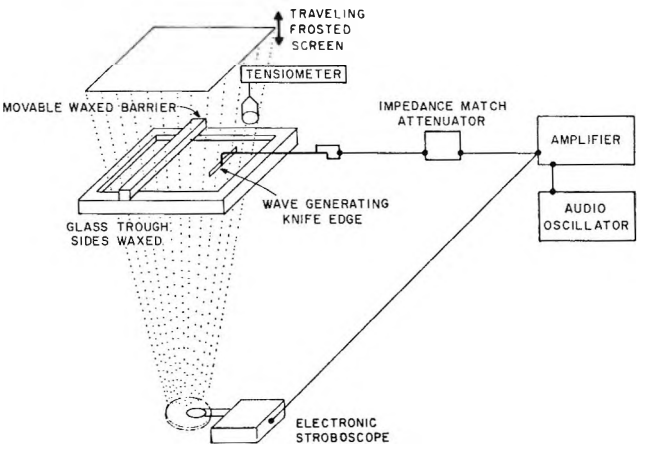

Figure 1. Schematic diagram of harmonic wave generator and amplitude-measuring system.

Experimental Apparatus and Methods

A convenient and precise experimental system was constructed for this investigation which (a) generates plane, transverse surface waves, in a large hydrophil trough, (b) measures their amplitudes accurately, (c) provides means for varying the state of condensation of the insoluble compound adsorbed on the water surface, and (d) allows the film pressure to be measured. The equipment assembly, which is shown schematically in Figure 1, was patterned after a device developed earlier by Schooley.[32] A signal generated by an audio frequency oscillator was amplified and fed into an electromechanical transducer which vibrated a linear knife edge contacting the surface of the water substrate contained in the glass ripple tank. Linear waves were gen-

(23) S. E. Bressler and D. C. Talmund, *Physik. Z. Sowjetunion*, **4**, 864 (1933).

(24) J. H. Schulman and T. Teorell, *Trans. Faraday Soc.*, **34**, 1337 (1938).

(25) W. D. Garrett and W. A. Zisman, Abstract 54, Preprint of the Division of Colloid and Surface Chemistry, 150th National Meeting of the American Chemical Society, Atlantic City, N. J., Sept 13–17, 1965.

(26) H. W. Fox, P. Taylor, and W. A. Zisman, *Ind. Eng. Chem.*, **39**, 1401 (1947).

(27) M. J. Newing, *Trans. Faraday Soc.*, **46**, 766 (1950).

(28) W. Noll, H. Steinbach, and C. Sucker, *Ber. Bunsenges. Phys. Chem.*, **67**, 407 (1963).

(29) W. Noll, H. Steinbach, and C. Sucker, *Kolloid-Z.*, **204**, 94 (1965).

(30) H. W. Fox, E. Solomon, and W. A. Zisman, *J. Phys. Colloid Chem.*, **54**, 723 (1950).

(31) W. R. Roth, *J. Amer. Chem. Soc.*, **69**, 474 (1947).

(32) A. H. Schooley, NRL Report 3559, "The Ripple Tank as an Aid to Phase Front Visualization," Oct 15, 1949, Washington, D. C.

erated by using a carefully machined knife-edge dipper having a 45° edge angle and a length of 20 cm. It was constructed from a hydrophobic plastic, such as polymethylmethacrylate or polytetrafluoroethylene. The power generated by the oscillator was passed through an impedance-matching device and an attenuator before going to the transducer and vibrator; with this arrangement the wave amplitude could be controlled or varied conveniently.

The same oscillator was used to trigger an electronic stroboscope (General Radio 1531A) so that light flashes were produced at the same frequency as that of the water waves generated in the ripple trough. This interrupted beam of light was passed upward through the glass-bottomed trough where it was converged by the cylindrical lens action of the wave crests, and the resulting optical standing wave pattern was projected onto a horizontal translucent plastic screen placed above the ripple trough. The travelling plastic screen followed metal guides attached to the tank sides. Spring tension was used to hold the screen at a particular height above the trough liquid level until a reading of the screen height was completed. A millimeter rule attached to one of the guides indicated screen height, and a spirit level mounted on the screen height was used to be sure that the screen was parallel to the water surface.

The surface tension of the water in the trough was measured with a Cenco du Nouy ring tensiometer fitted with a 6-cm diameter platinum ring which could be dipped in the trough when desired. A stop screw attached to the tensiometer supporting stand was adjusted so that the ring could not quite break through the film-coated surface at the time when the surface tension was being measured. This arrangement prevented contaminating the platinum ring with an adsorbed silicone film, and yet it allowed one to obtain an accurate measurement of the surface tension. Such an arrangement has been used often for a series of measurements when it was necessary to maintain the platinum ring hydrophilic. The film pressure (F) was obtained as usual from the difference in the surface tensions of unrippled water when uncoated and then coated by the adsorbed insoluble film.

The 50 × 50 cm glass ripple trough was 1 cm deep with the ground parallel edges of its thick vertical wall coated with clean, white, high-melting paraffin wax, which allowed the tank to be slightly overfilled in the usual way so that the water surface could be swept clean of surface contaminants with a pair of wax-coated glass sliding barriers; the latter also could be used to compress the monolayer to the desired degree during the investigation. The trough depth of 1 cm was selected to conserve the doubly distilled water used, and it also reduced the time required for soluble impurities to reach the surface where they could be removed (as is usual) by sweeping the water surface with paraffin-coated barrier bars. Lord Rayleigh[22] had calculated the wave damping corrections to be applied to plane wave measurements made in shallow water basins. The correction proved to be negligible in our trough for the 0.5-cm wavelength and small amplitude (0.1 mm) generally used in these experiments. Unless otherwise indicated, the dipper frequency (f) was 60 cps.

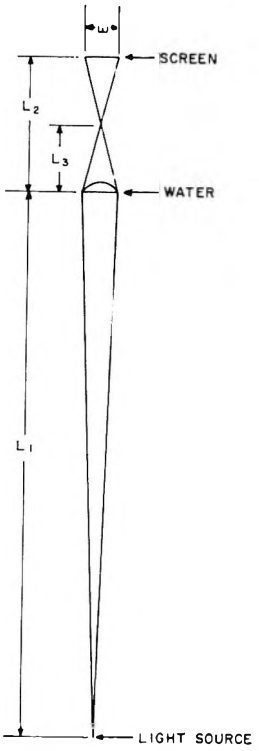

Figure 2. Geometry of light ray path in ripple focusing.

Schooley[32] had derived equations for calculating "h," the crest-to-wave trough height (or twice the wave amplitude "a") from the light path geometry shown in Figure 2. In this derivation, each wave crest was treated (as is customary) as a cylindrical lens. Light passing through a wave crest is refracted and focused at a point above the water surface. The greater the wave height, the shorter the focal length of the transmitted ray. When the translucent plastic screen was placed near the water surface below the focal point, a diffuse light pattern was seen. When placed at the focal point, a sharp light pattern resulted, and as the screen was raised above the focal point, the image widened but remained rather sharp. The following expression for the wave height "h" results from the geometry of Figure 2

$$h = 0.15\lambda^2(1/L_1 + 1/L_2 + 3w/\lambda L_3) \qquad (7)$$

where λ is the wavelength of the transverse wave train on the water, L_1, L_2, and L_3 are the distances from the water surface to the light source, the screen, and the focal point, respectively, and w is the width of the bright image. The above expression holds when the screen is above the focal point. In this investigation the position of the screen above the water surface was

adjusted so that it was located at the focal point for each wave measured. Hence $w = 0$, and the wave height eq 7 simply becomes

$$h \equiv 2a = 0.15\lambda^2(1/L_1 + 1/L_2) \qquad (8)$$

Since L_1 is fixed, the amplitudes are an inverse function of the height of the screen above the water surface at which a wave pattern just becomes sharp and bright. The wavelength was measured by placing the screen at the surface and measuring the space between the wave generator and a modest number of wave crests. Since the wavelength decrease with distance was small for the wavelengths studied, little error was introduced into the method of measuring the wave amplitude.

In the experimental procedure, the glass trough was thoroughly cleaned with chromic acid, followed by a thorough soaking in distilled water; then it was dried and waxed. Next, while the trough was horizontal, the trough was filled with distilled water at pH 5.7–6.0 until the water level was above that of the waxed edge. After that, 1 hr wait was allowed for any soluble or diffusible surface-active impurities from water or trough to reach the water surface and adsorb there. During this time the trough was kept covered with a plastic shield to eliminate contamination of the surface by airborne dust and other contaminants. The water surface was then swept clean several times with the barriers after which the surface tension of the clean water was measured.

All the experiments reported here were performed with the water and surrounding air at 25°. The amplitude of the linear wave generator was maintained at approximately 0.1 mm. The wave damping coefficient (k) for distilled water after it had been carefully scraped with the barriers was calculated from the slope of the log a *vs.* x graph using eq 3. The resulting experimental value of k agreed within the accuracy of measurements with that calculated from eq 6. From $f = 35$ to $f = 180$ cps, a graph of k *vs.* f was a straight line which when extrapolated passed through the origin.

Once the cleanliness of the water surface had been established, the polyorganosiloxane was added to the surface dropwise using a dilute stock solution in pure chloroform by means of a Starrett microsyringe fitted with a clean glass tip. The uncertainty in the drop volume was ±0.001 ml. A series of wave amplitudes and the corresponding surface tensions were measured as the surface concentration of adsorbed film was increased by the slow dropwise addition of the stock solution. In each instance, after solvent evaporation and after the desired surface concentration of the silicone compound was obtained, the amplitudes of a number of successive waves were determined; usually 8–10 wave amplitudes were measured to establish the value of k. In no case was the uncertainty in k from ten independent repeat runs greater than ±1.6% for distilled water

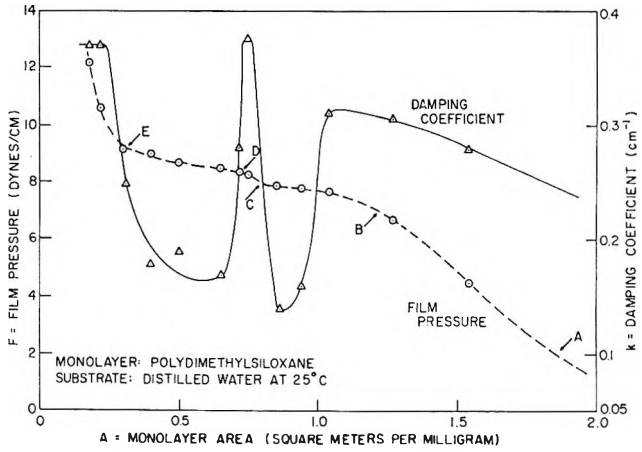

Figure 3. Wave damping behavior of polydimethylsiloxanes (DC 200) at 60 cps.

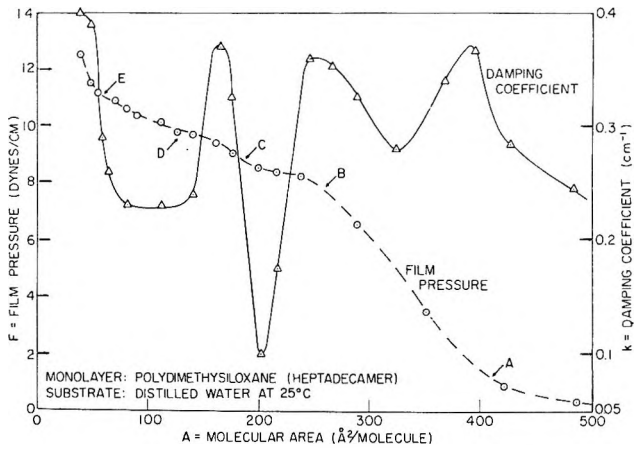

Figure 4. Wave damping behavior of polydimethylsiloxane heptadecamer at 60 cps.

or greater than ±4.8% for water covered by a silicone monolayer.

Materials Investigated. The liquid polyorganosiloxanes investigated were obtained years ago from the Dow Corning Corp. for two earlier NRL investigations.[26,30] Even though every liquid had been stored in the dark in a refrigerator for some years, before again using each was purified (as in ref 26) by a slow percolation through a long, narrow, adsorption column packed with a layer of Fluorosil and a layer of 80–200 mesh adsorption grade activated alumina. The chemical constitution and physical properties of the polyorganosiloxanes investigated here were all described in ref 26; they included (a) a commercial mixture labeled DC-200 having a viscosity of 50 centistokes at 25°, (b) a pure trimethylsilyl end-blocked dodecamer of the same family of polyorganosiloxanes, (c) a pure homologous heptadecamer having the same terminal groups, (d) a mixture of polymethylphenylsiloxanes having a viscosity at 25° of 50 centistokes and a phenyl-to-methyl ratio of 0.05, (e) still another mixture of polymethyl-

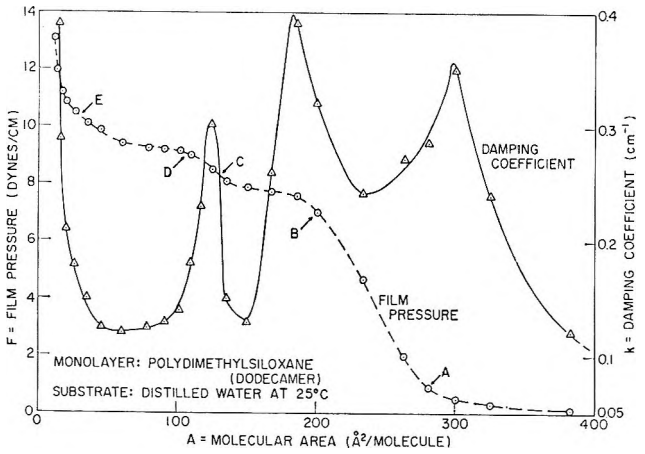

Figure 5. Wave damping behavior of polydimethylsiloxane dodecamer at 60 cps.

phenylsiloxanes having a viscosity at 25° of 500 centistokes and a phenyl-to-methyl ratio of 1.0, and (f) a mixture of polydiethylsiloxanes having a viscosity at 25° of 2320 centistokes.

Results Obtained

The first wave damping experiments were performed with the mixed, open-chain polydimethylsiloxane liquid listed above as item (a). A plot of the 60 cps damping coefficient (k) *vs.* the area (A) expressed in square meters per milligram of the spread monolayer and another of the film pressure (F) *vs.* (A) are both given in Figure 3. This F *vs.* A graph agreed well with that reported years ago by Fox, Taylor, and Zisman.[26] In Figures 4 and 5 are plots of k *vs.* A with the latter expressed in square angstroms per molecule. In the same figures are plotted the film pressure (F) *vs.* the area per molecule (A) obtained in our experiments which also agreed with the F *vs.* A data of reference 26. In all cases the F *vs.* A graphs were reversible and reproducible within the experimental uncertainty of F of ± 0.2 dyn/cm. It is remarkable that the k *vs.* A graphs of Figures 4 and 5 exhibit four well-defined maxima and three minima, and certainly these are the most complex wave damping curves ever reported. Nevertheless, these k *vs.* A graphs and all the others reported in later figures were reproducible and reversible. For example, when k was 0.30 cm^{-1}, values of ΔK of ± 0.01 cm^{-1} could be detected; hence, the uncertainty in K was about 3.0%. Of especial interest is the relatively undamped condition at film pressures of 8.4 and 10.1 dyn/cm in Figure 4 and 8 and 9.3 dyn/cm in Figure 5. The corresponding values of k of 0.10 and 0.12, respectively, are close to that of 0.05 for clean water at the same wave frequency. Such major decreases in the damping coefficient are new and remarkable, and the causes will be discussed later in this report in molecular structural terms.

The F *vs.* A plots of Figures 4 and 5 need a brief summary in terms of Fox, Taylor, and Zisman's[26] analysis of the state of the monolayer in regions A, B, C, D, and E of each graph along with the relation of the peculiar changes in slope to the corresponding changes in the molecular configuration. In region A the molecular area of the monolayer corresponds to close packing of horizontally oriented molecules with every silicon and oxygen atom adsorbed on the water surface. In region B the monolayer becomes highly compressible, and it was concluded that the molecule was in a zigzag configuration such that every other silicon or oxygen atom was adsorbed at the air–water interface. Between regions A and B the monolayer is collapsing by buckling, and it was postulated that each polymer molecule was in the process of coiling into a horizontally oriented helix containing six monomer units per turn. In region C a small change in the slope of the F *vs.* A curve develops at a molecular area which corresponds closely to the monolayer thickness expected of such a helical arrangement with the axis of the helix horizontal. In region E the area per molecule is beginning to approach the cross-sectional area of the uncoiled or extended polydimethylsiloxane taken at right angles to its long axis. Between regions D and E, therefore, the principal axis of each molecule was becoming uncoiled and was beginning to be forced toward a more upright and axially adlineated arrangement with its neighbors.

Note that k in Figures 4 and 5 increases rapidly with decreasing area per molecule in advancing from region A to reach a first maximum of 0.37 cm^{-1}. Then k decreases rapidly to a first minimum of from 0.26 to 0.25 cm^{-1}, respectively, before reaching stage B. A second maximum of 0.35 cm^{-1} and 0.37 cm^{-1}, respectively, is reached close to region B. Then at B when the film becomes very compressible, k decreases steeply to a second minimum of 0.10 cm^{-1} and 0.14 cm^{-1}, respectively. This dramatic effect on the damping was easily observed on the moveable screen on which the optically standing wave patterns were projected because the rapid decrease in k was evident from a brightening projection of the pattern in going from weak diffuse lines to bright lines across the entire width of the screen. This low minimum between regions B and C occurs where Fox, Taylor, and Zisman[26] stated the monolayer became most compressible because the horizontally oriented helical coils were being compressed together. Between regions C and D, there is slight shoulder in the F *vs.* A curve and k increases abruptly to attain a third maximum of about 0.37 cm^{-1} for the heptadecamer and 0.30 for the dodecamer. Next k decreased again to its third minimum of about 0.24 cm^{-1} for the heptadecamer and 0.14/cm for the dodecamer when the second ridge of high compressibility was reached. In the F *vs.* A curve of Figures 4 and 5 there will be noted between stages C and D another very slight shoulder, and with this there is a rise in the compressibility and the third mimimum is therefore made rather broad. In Figure 4 in region E, k increases for the fourth time and appears to be ap-

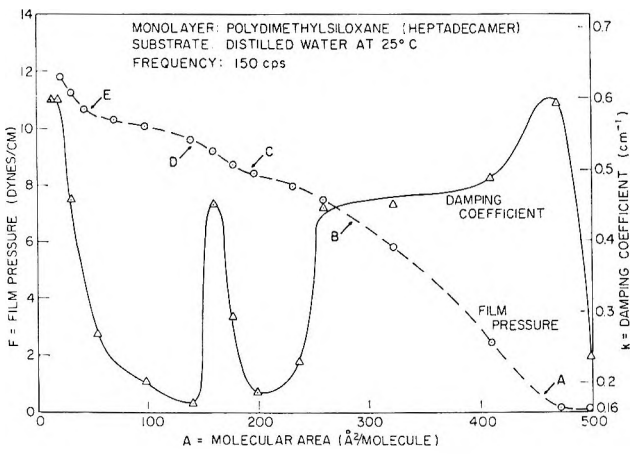

Figure 6. Wave damping behavior of polydimethylsiloxane heptadecamer at 150 cps.

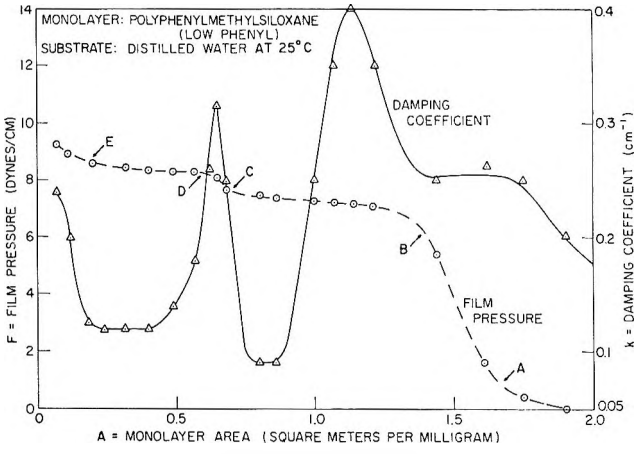

Figure 7. Wave damping behavior of polymethylphenylsiloxanes at 60 cps (phenyl:methyl ratio of 0.05).

proaching a maximum value somewhat above 0.4 cm^{-1} for the heptadecamer. In Figure 5 for the dodecamer, the k *vs.* A curve is rising rapidly as if to approach a high maximum which is not reached in the figure.

Hence, the experimental results plotted in Figures 4 and 5 for the polydimethylsiloxane heptadecamer and dodecamer, respectively, lead to the same molecular interpretation of the relation between the k *vs.* A and F *vs.* A graphs for each compound. Transition regions of the F *vs.* A curve, namely regions B, C, and D in Figure 3 occur in our new data on Figures 4 and 5 at about A = 250, 175, and 50 Å²/molecule, respectively. These values are close to those reported by Fox, Taylor, and Zisman.[26] Apparently, dk/dA changes its sign abruptly in the regions A, B, C, and D of each F *vs.* A curve, and it is evident that each major change in the monolayer configuration was more clearly revealed by the k *vs.* A than by the F *vs.* A graph.

Wave damping characteristics of the heptadecamer were also investigated using a wave frequency (f) of 150 cps instead of 60 cps. The results obtained (see Figure 6) are in many ways quite like those in the 60 cps experiments of Figure 4. The changes in slope of the F *vs.* A curve and the corresponding reversals in sign of the slope of the k *vs.* A curve occurred at approximately the same values of the area per molecule at both frequencies. The maximum values of k were always much larger at the higher frequency. However, there were some other differences between Figures 4 and 6 in the maxima and minima in various regions of the k *vs.* A plots. Between regions A and B there is again a first maximum in k *vs.* A, but there is no first minimum; instead, there is a shoulder. This behavior suggests that at 150 cps there is too little time allowed for thermal and adsorption equilibrium to be attained so the film buckling and coiling into helices are both delayed and restricted. Between regions B and C during the monolayer coiling process, k has a minimum value very close to that for clean water, but the curve minimum is wider than in the 150 cps than in the 60 cps curve. Between regions C and D, k decreased to a value only twice that for clean water at 150 cps (0.16/cm^{-1}). Furthermore, the value of A of 460 Å², where k reached its first maximum at 150 cps, is to be compared with A = 390 at 60 cps. The second maximum shown in Figure 4 had become more like a shoulder at the same value of A of about 250 Å² at both 150 and 60 cps. However, the third maximum and the second and third minima occurred at about the same values of A at 60 and 150 cps.

The effect of partial replacement of methyl by phenyl groups attached to the polyorganosiloxane chain was first investigated by measuring at 60 cps the damping characteristics of the polymethylphenylsiloxanes containing about 1 phenyl group to every 20 silicon atoms, or a phenyl to methyl ratio of 0.05. Our results in Figure 7 show many similarities to those in Figure 3 for the polymethylsiloxanes of the same viscosity at 25°. Although the F *vs.* A graphs are very similar, that is not true of the entire course of the k *vs.* A curves. Since the molecular weight of this polymethylphenylsiloxane was not known, as in Figure 3 the area ordinate A had to be expressed in square meters per milligram. In Figure 7 at values of F ranging between 0 and 0.5 dyn/cm, there was a rectilinear increase in the slope of the k *vs.* A curve. But from F = 0.5 to F = 5.5 dyn/cm, the k *vs.* A graphs became a horizontal shoulder corresponding to a constant k = 0.26 cm^{-1}. Thus there is a difference in going between regions A and B, because no shoulder is evident in Figure 3. In going from region B to C, there is a maximum in k which is higher and more sharply defined in Figure 7, but it occurs at nearly the same value of F = 8 dyn/cm in both Figures 3 and 7. In going from region C to D of Figure 7 a lower maximum occurs than in Figure 4; although this second peak appears at about the same value of F, it occurs at a lower value of A. In going from region D to E of Figure 7, a broad minimum in k occurs; and in approaching region E, there is evidence that a third peak

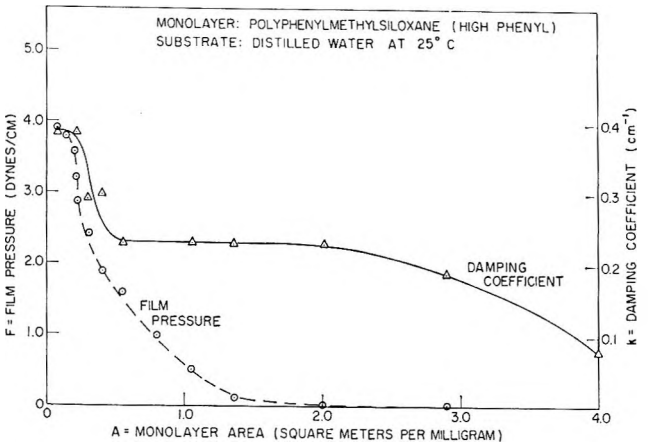

Figure 8. Wave damping behavior of polymethylphenylsiloxanes at 60 cps (phenyl:methyl ratio of 1.0).

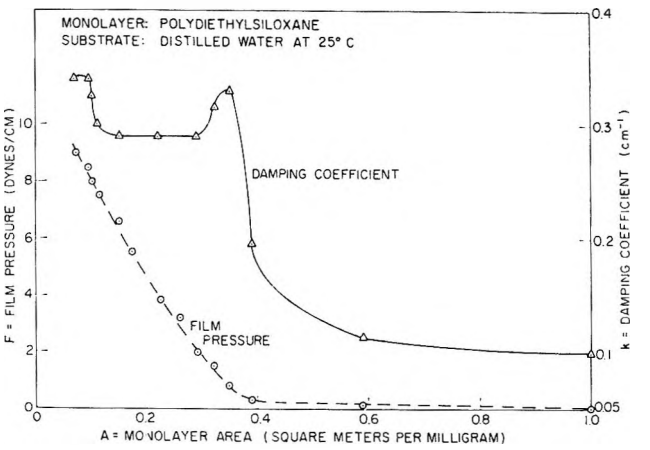

Figure 9 Wave damping behavior of polydiethylsiloxanes at 60 cps.

is forming at $A = 0.25$ m²/mg. This effect may be caused by steric interference created by the phenyl side chains on the main polysiloxane chain, which would prevent the close packing of molecular chains needed to allow molecular adlineation as was true of the polydimethylsiloxanes of Figure 4. In Figure 7, k attains a maximum of 0.22 cm^{-1} at $F = 7.5$ dyn/cm, whereas in Figure 4 there is a well-defined maximum of $k = 0.37$ cm^{-1} at $F = 10.2$ dyn/cm. These differences show the significant influence of one phenyl substituent per 20 methyl groups in the wave damping properties, and clearer differentiation of the effects of such a difference in polyorganosiloxane structure are seen in the k *vs.* A than in the F *vs.* A graphs.

In Figure 8 are the results obtained when the phenyl:methyl ratio is 1.0. Note that there is a gradual collapse of the monolayer at film pressures of from 1 to 2 dyn/cm. Presumably, there is a steady film collapse—probably without regular helical coiling and more like an early onset of random buckling of the film as the monomers are successively ejected out of the water surface. The k *vs.* A plot shows a plateau is attained at $k = 0.2$ cm^{-1} which is about four times greater than the damping coefficient for clean water at 60 cps. At a film pressure of about 2.3 dyn/cm, major film collapse starts to occur and is completed at $F = 3.8$ dyn/cm. At the same time k increases rapidly to a maximum value of 0.38/cm^{-1}. The general film behavior is that which one would expect of any linear polymer so hindered from adsorbing all of its Si–O groups that there is low adhesion to the water surface and a gradual film collapse at low pressures.

The polydiethylsiloxane curves of F *vs.* A and k *vs.* A which are plotted in Figure 9 are in some ways similar to those of Figure 8. At low film pressures k is about twice the value for clean water; it remains constant until F reaches about 0.7 dyn/cm after which k increases rapidly to a maximum of about 0.33 dyn/cm at $F = 1.2$ dyn/cm. Then k drops to level off at a value of 0.30 cm^{-1} until at $F = 8$ dyn/cm it rises to $k = 0.34$ cm^{-1} as F increases to 9 dyn/cm. Thus a second slight maximum appears to have occurred at the highest film pressures attained. Until the first maximum is reached, the F *vs.* A graph is typical of the results observed with many other polymers lacking chain flexibility. The fact that F first rises rapidly from $A = 0.4$ m²/mg and that k rises sharply with F is presumed to mean that the first maximum in k *vs.* A is caused by the rapidly increasing amount of work which must be done to complete lifting essentially all of the surface film from its early adsorbed state on the water. We do not have any explanation yet of the very shallow minimum evident between $A = 0.38$ and $A = 0.16$ m²/mg. It is possible that some sort of large-order chain coiling rather than simply general random buckling and film collapse occurs with this hindered polymer. The advent of the second maximum may be the result of complete film collapse to form bulk-phase silicone droplets in equilibrium with a very condensed surrounding film.

Discussion

The results plotted in Figures 3 through 9 show that the wave damping coefficient k is not always a direct function of film pressure because k can be very small between regions B and D on the F *vs.* A graphs of the linear polyorganosiloxane monolayers, even though F in this region is around 8 dyn/cm. Low values of k are encountered in the region of low compressibility of the monolayer, and high damping rates occur in regions where large changes in slope occur in the F *vs.* A curve (or wherever the film compressibility, $1/A\ (-dA/dF)$, has fallen below some critical value). These results are consistent with the qualitative conclusions of Dorrestein[8] and the later experimental results of Garrett and Bultman[10] who found that a large increase in k occurred whenever the modulus of surface compressibility, $A\ (-dE/dA)$, was from 0.5 to 2.0 dyn/cm for a number of water insoluble monolayers.

Dorrestein[8] based the development of his theory on the periodic extensions and contractions of the water surface caused by the spreading of the rectilinear system of capillary waves and the consequent increase and decrease in the surface area available to each adsorbed organic molecule. By this reasoning he was able to predict that liquid-expanded, and even gaseous, monolayers could affect the attenuation rate of capillary waves. However, the success of Dorrestein's analysis in explaining the observed wave damping behavior of organic surface films did not explain or identify the molecular mechanisms responsible for the striking capillary wave damping caused by monomolecular films, nor could it predict the complex k *vs.* A behavior reported here.

Our results prove that wave energy absorption by the surface film on water may be caused by changes in intermolecular or intramolecular arrangement as well as by changes in the "drag" or hydrogen-bonding interaction between the film and water surface. There will always be a water substrate transport with lateral movements of the adsorbed monolayer because a thin film of hydrogen-bonded substrate water must be also moved.[23,24] However, wave energy must also be dissipated by the adsorbed organic film as a result of the development of molecular rearrangements, or changes in the adhesion of the organic film to the water accompanying any change in molecular packing or arising through intermolecular or intramolecular rearrangements. Which of these factors is the more dominant at any film pressure in consuming wave energy depends upon the molecular structure and configuration of the particular type of organic molecules when adsorbed on the water surface under the existing conditions of surface film pressure, temperature, and wave frequency.

Certainly the remarkable changes with film pressure of the damping effect of any polymethylsiloxane on water cannot be caused by corresponding changes in the surface viscosity of the adsorbed monolayer because Jarvis,[33] using the reliable canal viscometer, has shown that the surface viscosity of each of a homologous series of trimethylsilyl end-blocked polymethylsiloxanes has a constant and low value up to a film pressure of 10 dyn/cm at 20°, even when there were 44 dimethylsiloxane monomers per molecule. Especially important here is that he found[34] that the surface viscosities on water of these silicone compounds were about one 1000th those of typical fatty alcohols, acids, and amides at the same film pressures and film flow rates. The remarking different wave damping behavior (Figure 8) of the polymethylphenylsiloxanes having a phenyl:methyl ratio of 1.0 and also that of the polyethylsiloxanes (Figure 9) may well have a contribution to the wave damping from the presumably much higher surface viscosities of such films when highly compressed than Jarvis found in the film of the polymethylsiloxanes. Unfortunately, we do not have available any reliable data on the surface viscosities of these two classes of polyorganosiloxanes.

We believe the importance of molecular configuration in the adsorbed organic film on the value of k has now been demonstrated by our description and comparisons of the various factors which relate k to the molecular configuration of the various types of adsorbed polydimethylsiloxane monolayers. With near approach of the molecules (between regions A and B of the F *vs.* A curve of Figure 4) where the molecules were forced into a zigzag configuration corresponding to early chain buckling, some of the hydrophilic polysiloxane chain of atoms were pushed out of the water surface, external work had to be done, and therefore k rose to its first maximum. The remaining hydrophilic groups were still hydrogen bonded to associated chains of water molecules immediately beneath the surface, and viscous drag still resulted when the molecules of the monolayer were forced to follow the surface film through small surface expansions and compressions caused by passage of the transverse waves of water. Between regions A and B, the molecule was forced into more buckling and eventually into helical chain-coiling, as the result of which according to Stuart–Briegleb molecular models, almost all of the silicon and oxygen atoms were removed from contact with the bulk water surface, and more external work was done in the process. As this work was done by adsorbing wave energy, k rose to a second peak. In going from B to C a screen of methyl groups began to shield many of the Si and O atoms in the helical coils from direct water interaction. Thus, there was a much decreased monolayer-substrate interaction and consequently a decreased viscous drag on the water substrate; hence, the k *vs.* A curve decreased to its first minimum (in some cases to a value little more than the k characteristic of clean water). As shown by the F *vs.* A curves, there was a corresponding and expected increase in monolayer compressibility during the helical chain-coiling process.

The sudden rise in k in region C to a third maximum was more difficult to explain. There appeared to be an energy barrier to be overcome, or a need for external work on the polymer molecules which had to be done before the most closely coiled molecular helices could form. The wave energy consumed at this stage may have been that required to desorb some hydrogen-bonded water from the siloxane coils as they became more compressed. Once this process had finished, k again rose to its third peak between regions C and D and the monolayer could be compressed further. Next, the helices began to buckle; once the resulting disorganizing and lifting stage had approached completion, methyl terminal groups (in the main) were left adsorbed on the water. This explained why k decreased to attain its

(33) N. L. Jarvis, *J. Phys. Chem.*, **70**, 3027 (1966).
(34) N. L. Jarvis, *ibid.*, **69**, 1789 (1965).

third minimum. Finally, the molecules were forced at higher film pressures into an increasingly more upright and more adlineated, condensed structure, the resulting film became coherent (and probably more viscous); hence k rose to attain its final maximum, or else it simply continued to rise if there were too many monomers per molecule to allow vertical orientation of the long chains.

Although Fox, Taylor, and Zisman[26] interpreted the minimum in the k *vs.* A graph in the region between C and D of the F *vs.* A curves to indicate the lifting and uncoiling of the polymer molecule, they concluded that going from region D to E the molecules were being stacked as more or less close-packed rods oriented vertically with their chain terminal groups in contact with the water surface. A different interpretation was later given to this portion of the curve by Noll, Steinbach, and Sucker[28] who contended that in region D to E the film was merely collapsing as the molecules were slipping over one another as the film was being compressed. They did not find reproducible changes in slope in going from region C to D and from D to E, and they concluded the graphical changes reported by Fox, Taylor, and Zisman[26] was an artifact of their apparatus. However, Noll, *et al.*,[28] continuously recorded their F *vs.* A data, and the rapidity of their recording system could have prevented their film from attaining thermal equilibrium with the water substrate. It is a well-known problem in F *vs.* A measurements as in those reported here that one must wait at least several minutes to obtain a steady value of F after each change in A.

Jarvis[33] has reported a more recent and reliable determination of the F *vs.* A curve for the same type of polymer containing 6, 10, 15, and 43 monomers per molecule, respectively. His F *vs.* A graphs showed clearly all of the peculiarities and changes of slope in the F *vs.* A graphs reported both here and by Fox, Taylor, and Zisman.[26] It is to be noted that in this present report the graphs in Figures 4 and 5 of the k *vs.* A data for the heptadecamer and the dodecamer showed sharp increases in k in going from region D to E, thereby revealing clearly a change of compressibility which probably corresponded to the close packing of the adlineated uncoiling chains originally proposed by Fox, Taylor, and Zisman.[26] Jarvis,[33] using the hexamer, decamer, and pentadecamer, came to the same conclusions. However, his graphical data on the pure polymethylsiloxane containing 43 monomer units did not show a well-defined rise in the F *vs.* A graph in going from region D to E. It may well be that polymers of such high molecular weights could not stand end up under high film pressures, so that in going from region D to E the long-chain compounds may have collapsed by the sliding of one adsorbed molecule over another as proposed by Noll, Steinbach, and Sucker.[28] The data presented in Figures 4, 5, and 6 are therefore consistent with the proposition that the molecules of the chain length investigated were uncoiling in going from regions C to D. As k became constant about $A = 25$ Å^2 for the heptadecamer, it appears that in going from D to E the film became more nearly a plastic solid of lower compressibility once the polymer molecules had begun to orient into upright, more closely packed, weakly cohering chains.

A plot of k *vs.* A obtained from wave damping measurements can be used with the F *vs.* A plot to confirm its molecular interpretation; also, the k *vs.* A plot always contributes valuable information regarding the molecular configuration and changes in intermolecular or intramolecular forces affecting the adsorbed film and its interaction with the liquid substrate. Precisely this situation was encountered in the investigation reported here because several types among the linear polyorganosiloxanes were capable of coiling into highly compressible monomolecular films having monolayer–substrate interactions which varied substantially with configuration. The damping coefficient (k) increased and decreased abruptly with the modulus of compressibility and also with any change of film state or configuration change in the adsorbed molecules. In conclusion, we believe it should be possible to use the same approach as a remarkably sensitive tool for studying the properties of monolayers of many other types of linear polymeric molecules.

The Vaporization Thermodynamics of Europium Dibromide

by John M. Haschke[1a] and Harry A. Eick[1b]

Department of Chemistry, Michigan State University, East Lansing, Michigan 48823 *(Received November 21, 1969)*

The congruent vaporization of condensed europium dibromide to the gaseous molecule has been studied over the temperature range 1185–1568°K by a target collection Knudsen effusion technique. For the reaction at 1377, $\Delta H°_T = 58.27 \pm 0.76$ kcal/gfw and $\Delta S°_T = 23.03 \pm 0.56$ eu. Calculations employing estimated heat capacities yield $\Delta H°_{298} = 71.4 \pm 2.7$ kcal/gfw, $\Delta S°_{298} = 36.8 \pm 2.8$ eu, and for $EuBr_2(s)$ $S°_{298} = 39.4 \pm 3.0$ eu. Enthalpies and free energies of formation calculated for condensed and gaseous dibromide are presented and discussed.

Introduction

The preparative and thermodynamic properties of the lanthanide bromides are poorly characterized. Novikov and Polyachenok reported in their review[2] that experimental thermodynamic data are unavailable for either the lanthanide di- or tribromides. Only estimated values are available for heat capacities, thermodynamics of fusion, vaporization, and dissociation.[3-6] Since these estimated values follow general trends established by certain physical properties of the elements, they are probably internally consistent sets, and experimental confirmation of the data for only one of the lanthanide phases should establish the accuracy of an entire set. Because of this dearth of experimental thermochemical data, and as a check on the estimated values, the vaporization behavior of europium dibromide was examined.

Experimental Section

Samples of single crystal europium dibromide ($EuBr_{2.000\pm0.017}$) were prepared and characterized as described previously.[7]

The vaporization reaction of the dibromide from graphite effusion cells was investigated by a combination of X-ray diffraction and mass spectrometric procedures. The solid residues which remained after partial vaporization were examined with a Haegg-type Guinier X-ray diffraction camera, and the vapor species in equilibrium with the condensed phase in the temperature range 900–1350° were analyzed with a Bendix Model 12–107 time-of-flight mass spectrometer (10–70 eV ionizing electrons). Appearance potentials were obtained by a linear extrapolation technique using mercury as a reference.

Target collection Knudsen effusion measurements were made as described previously.[8] The condensed effusates were analyzed for both europium and bromine by X-ray fluorescence. Symmetrical graphite cells (knife-edged orifice areas of 8.6×10^{-4} and 59.0×10^{-4} cm^2), which were employed in the temperature range 912–1295°, were charged with 0.1–0.2 g of $EuBr_2$ in an inert atmosphere glove box.[7] To prevent hydrolysis of the samples, orifices were closed with paraffin oil before the cells were removed to the collection apparatus where the oil was pumped off under vacuum.

The sticking coefficient of the dibromide on copper was determined by a bouncing experiment in which a 0.2 mm thick copper sheet with a 6.4 mm diameter hole mounted 2 mm from the face of a copper collection target was exposed *via* the hole to dibromide effusate (1193°). The exposure time was lengthened so that the quantity of effusate normally collected (5–7 μg $EuBr_2$) could strike the target through the hole. Both the target face and the back of the copper sheet were analyzed for dibromide by X-ray fluorescence.

Results

Europium dibromide was found to vaporize congruently according to reaction 1. X-Ray diffraction

$$EuBr_2(l) \longrightarrow EuBr_2(g) \qquad (1)$$

analysis of the vaporization residues indicated only the tetragonal dibromide ($a = 11.574 \pm 0.006$ Å, $c = 7.098 \pm 0.005$ Å) and were invariant even after 50% weight loss. Mass spectrometric analysis of the vapor indicated only the monomeric dibromide, which gave the fragmentation pattern $EuBr^+:Eu^+:EuBr_2^+$ in the relative intensity ratio 100:50:15. Both the fragmentation pattern and the appearance potential of

(1) (a) Abstracted in part from the Ph.D. thesis of J. M. Haschke submitted to the Graduate College, Michigan State University; (b) to whom correspondence should be addressed.

(2) G. I. Novikov and O. G. Polyachenok, *Usp. Khim.*, **33**, 732 (1964); *Russ. Chem. Rev.*, **33**, 342 (1964).

(3) L. Brewer, "Chemistry and Metallurgy of Miscellaneous Materials: Thermodynamics," L. L. Quill, Ed., McGraw-Hill Publications, New York, N. Y., 1950, paper 7.

(4) L. Brewer, L. A. Bromley, P. W. Gilles, and N. L. Lofgren, *ibid.*, paper 6.

(5) R. C. Feber, U. S. Atomic Energy Commission Report LA-3164, Los Alamos, N. M., 1965.

(6) C. E. Wickes and F. E. Block, "Thermodynamic Properties of 65 Elements—Their Oxides, Halides, Carbides, and Nitrides," Bureau of Mines Bulletin 605, U. S. Government Printing Office, Washington, D. C., 1963.

(7) J. M. Haschke and H. A. Eick, *J. Inorg. Nucl. Chem.*, in press.

(8) J. M. Haschke and H. A. Eick, *J. Phys. Chem.*, **73**, 374 (1969).

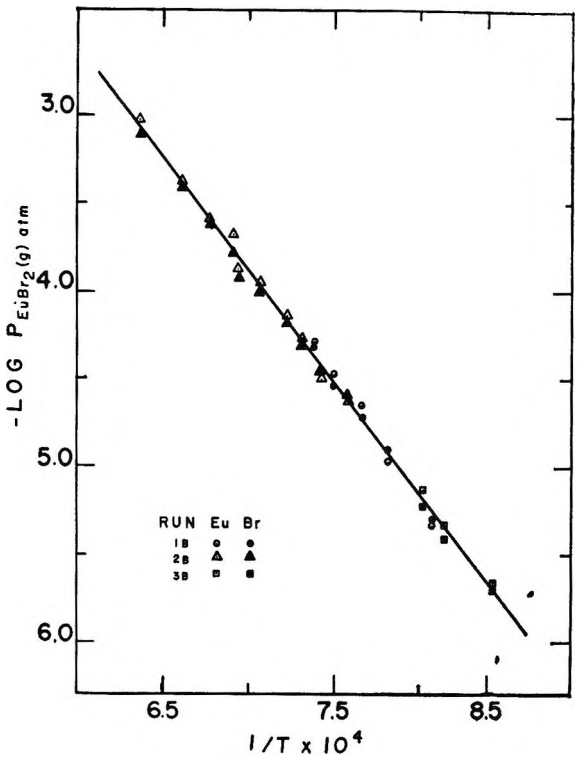

Figure 1. The pressure of $EuBr_2(g)$ in equilibrium with $EuBr_2(l)$.

$EuBr^+$ (10.4 eV) are consistent with those observed for gaseous $EuCl_2$[9] ($EuCl^+$:Eu^+:$EuCl_2^+$; 100:46:12; A.P. of $EuCl^+$, 10.3 eV). In addition, fluorescence analysis of the collected condensates for the elements showed that the equilibrium vapor contained an Eu:Br ratio of 1:2.

The bouncing experiment indicated that, within detectable limits, the sticking coefficient of gaseous europium dibromide on liquid nitrogen-cooled copper is ≥ 0.95. Since the effusion cell orifices were essentially knife-edged (45° taper from center line) and the collection angles were small (θ from perpendicular to target face <4°), no correction for orifice channeling was applied to the measured pressures.

The log P *vs.* $1/T$ results obtained for the vaporization reaction are presented in Figure 1, and the linear least-squares fit pressure equation for these data in the temperature range $1185 \leq T \leq 1568$°K follows

$$\log P_{EuBr_2}(\text{atm}) = -(1.27_3 \pm 0.01_7) \times 10^4/T + 5.0_3 \pm 0.1_2$$

At the median temperature (1377°K), $\Delta H°_{1377}$ = 58.27 ± 0.76 kcal/gfw and $\Delta S°_{1377}$ = 23.03 ± 0.56 eu. These second-law results have been corrected to 298°K using enthalpy and entropy functions, estimated by Brewer, *et al.*,[4] and those based on an estimated heat capacity for the gaseous phase. The heat capacities of gaseous linear ($D_{\infty h}$) $TiBr_2$ and $HgBr_2$ differ by only 0.06 eu (0.025%) at 298°K and converge at higher temperatures; those of bent (C_{2v}) $PbBr_2$ (Br–Pb–Br angle = 95°) and $ZrBr_2$ (Br–Zr–Br angle = 120°) exhibit a similar behavior (0.875% difference).[10] However, the values for the two sets (linear *vs.* bent) differ by 1.5 eu (>10%). These observations indicate that the high-temperature heat capacities of gaseous dihalides are primarily dependent on molecular symmetry, with little contribution from molecular weight or magnitude of molecular bend. In molecular beam deflection experiments on gaseous dihalides of the alkaline earths, Buechler, *et al.*,[11] found both bent (CaF_2 and $SrCl_2$) and linear ($CaCl_2$) molecules. Since the symmetry is apparently related to the cation–anion radius ratio, europium, which has a divalent radius almost identical with that of strontium, should form a linear dibromide. Therefore, the data for gaseous mercuric dibromide[10] have been utilized for the europium species.

For the vaporization of $EuBr_2(s)$, $\Delta H°_{298}$ = 71.4 ± 2.7 kcal/gfw and $\Delta S°_{298}$ = 36.8 ± 2.8 eu. The estimated error in these values was obtained by assuming a ± 20% error in the reduction to 298°K.

The third-law enthalpy of vaporization has been calculated using free energy functions based on the estimated heat capacities and entropies of the solid and gaseous phases. The estimated $S°_{298}$ for $EuBr_2(s)$ (40.1 eu) was obtained using the scheme of Latimer[12] plus the magnetic contribution of Eu(II) proposed by Westrum.[13] The entropy of $EuBr_2(g)$ was estimated by graphically interpolating the $S°_{298}$ values for MBr_2 phases[14] (M = Zn, Cd, Hg) as a function of molecular weight and including a magnetic contribution for Eu(II). Since the $S°_{298}$ so obtained (77 eu) was essentially identical with that of $HgBr_2(g)$ (76.3 eu),[10] the fef values of the mercuric phase were employed again. Combination of these values with the experimental pressures yielded $\Delta H°_{298}$ = 69.54 ± 0.40 kcal/gfw with no observable temperature trend in the results.

The second-law enthalpy of vaporization, the enthalpies of formation of Eu(g)[15] and Br(g),[10] and the dissociation energy estimated for $EuBr_2(g)$[5] have been combined to give $\Delta H°_{f,298}$ of $EuBr_2(s)$ = −178.0 ± 3.0 kcal/gfw, and $\Delta H°_{f,298}$ of $EuBr_2(g)$ = −106.6

(9) J. W. Hastie, P. Ficalora, and J. L. Margrave, *J. Less-Common Metals*, **14**, 83 (1968).

(10) D. R. Stull, Project Director, "JANAF Interim Thermochemical Tables," Dow Chemical Co., Midland, Mich., 1960, and Supplements.

(11) A. Buechler, J. Stauffer, and W. Klemperer, *J. Chem. Phys.*, **40**, 3471 (1964).

(12) W. M. Latimer, "Oxidation Potentials," 2nd Ed., Prentice-Hall, Englewood Cliffs, N. J., 1952, Appendix III.

(13) E. F. Westrum, Jr., Advances in Chemistry Series, No. 71, American Chemical Society, Washington, D. C., 1967, pp 25–50.

(14) L. Brewer, G. R. Somayajulu, and E. Brackett, *Chem. Rev.*, **63**, 111 (1963).

(15) R. Hultgren, "Supplement to Selected Values of Thermodynamic Properties of Metals and Alloys," private communication.

± 3.0 kcal/gfw. From the entropy of vaporization and the estimated entropy of $EuBr_2(g)$, $S°_{298}[EuBr_2(s)] = 39.5 \pm 3.0$ eu was calculated. Combination of this value with the entropies of Eu(s)[15] and $Br_2(l)$[9] yielded for $EuBr_2(s)$ $\Delta S°_{f,298} = -16.2 \pm 3.0$ eu, from which $\Delta G°_{f,298}[EuBr_2(s)] = -173.2 \pm 3.0$ kcal/gfw. From this value and the free energy of vaporization, $\Delta G°_{f,298}$ of $EuBr_2(g) = -112.8 \pm 3.0$ kcal/gfw was obtained.

Extrapolation of the pressure equation to one atmosphere indicated that the normal boiling point of $EuBr_2(l)$ is 2530 ± 35°K. The $(H_T - H_{298})$ data for $EuBr_2(l)$ were extrapolated beyond 1500°K by utilization of the trend with temperature established by $BBr_3(l)$,[6] and the resulting data were combined with $\Delta H°_{1377}$ to give $\Delta H°_v$ of $EuBr_2(l) = 52.0 \pm 3.0$ kcal/gfw. From $\Delta H°_v/T_b$, $\Delta S°_v = 20.6 \pm 1.9$ eu.

Discussion

In the vaporization experiments europium dibromide behaved as anticipated, but experimental difficulties were evident. Graphite, which has been used successfully as a crucible material for the vaporization of strontium dichloride,[16] appeared to be both inert and impervious to the dibromide. However, dibromide samples were either partially or completely transported to the crucible lids during the course of the vaporization experiments. This transport probably resulted from the presence of a temperature gradient within the effusion cells even though external surface gradients could not be detected, and comparisons of sample and optical cavity temperatures never indicated a temperature difference of greater than ±5°. The Monte Carlo calculations done by Ward[17] have shown that the cosine law of effusate distribution is obeyed in the forward direction only when the sample is on the surface directly opposite the orifice. Because of the low vapor pressure of the dibromide in the temperature range of the measurements, complete transport of the sample could not have occurred during the exposure time of the first target, or even during that of the first few targets. An examination of the pressure data with order of exposure revealed no anomalies or trends and suggested that the cosine law is obeyed completely by this dibromide. The linearity of the data also suggests that $EuBr_2(g)$ exhibits free molecular flow over the entire experimental range.

With a gaseous dibromide molecular diameter of 6.1 Å obtained from the metal–halide separation in the strontium analog,[14] the ratio of the mean free path to orifice diameter calculated at the highest temperature and pressure measured with the smallest orifice (1568°K and 8×10^{-4} atm, $\lambda/d = 0.5$) is within the limits accepted for molecular flow.[18]

The thermodynamic approximations made for data reduction seem valid. The estimated heat capacities of the liquid and gaseous dibromide give a ΔC_p of −10 cal/deg gfw, a value which is identical with that recommended by Brewer[3] for vaporization of a liquid dihalide to the monomeric gas. The approximated entropy of $EuBr_2(s)$ (40.1 eu) is in close agreement with the value calculated independently from the second-law results (39.5 eu). A further check on the internal consistency of the estimated heat capacity and entropy values is the good agreement of the second- and third-law enthalpies of vaporization (71.4 and 69.5 kcal/gfw, respectively).

The various estimated thermodynamic values are in agreement with these observed results. The equilibrium pressure equation is well within the limits estimated by Brewer;[3] however the observed vapor pressure is lower and boiling point higher than the estimated values. The experimental $\Delta H°_v$ (52.0 kcal/gfw) agrees with the approximated value (50 kcal/gfw),[3] and the entropy of vaporization at the boiling point (20.6 eu) is consistent with Trouton's rule. Since these latter results and the boiling temperature were calculated by assuming linearity of the vapor pressure equation over a 1000° interval, they should be used with caution. The enthalpy of vaporization estimate of Feber,[5] 72 kcal/gfw at 298°K, agrees well with the observed value (71.4 kcal/gfw). Nevertheless, these results and the enthalpies and entropies of formation for solid and gaseous europium dibromide should be reevaluated when additional experimental data become available.

Acknowledgment. The support of the U. S. Atomic Energy Commission AT(11-1)-716 and a National Science Foundation Fellowship to J. M. H. are gratefully acknowledged.

(16) R. E. Toehman, R. A. Kent, and J. L. Margrave, *J. Chem. Eng. Data*, 10, 296 (1965).

(17) J. W. Ward, U. S. Atomic Energy Commission Report LA-3509, Los Alamos, N. M., 1966.

(18) D. A. Schulz and A. W. Searcy, *J. Phys. Chem.*, 67, 103 (1963).

NOTES

Paramagnetic Relaxation of Hexacoordinated Chromium(III) Complexes with Anionic Ligands in Aqueous Solutions[1a]

by L. Burlamacchi, G. Martini, and E. Tiezzi

Institute of Physical Chemistry, University of Florence, Florence, Italy *(Received August 15, 1969)*

The analysis of the factors which affect the line width of an esr spectrum often provides useful kinetic and chemical information. Little work has been done as yet on the electron spin relaxation of Cr(III) in water solution in the presence of anionic ligands. The electron spin resonance absorption of chromic ion consists of a single line, about 150 G wide at points of maximum slope, with no hyperfine structure.[1b] The spectrum may be interpreted in terms of the general hamiltonian for a quartet spin state

$$\mathcal{H} = g\beta \mathrm{Hs} + D[S_z^2 - {}^1/_3 S(S+1)] + E[S_x^2 - S_y^2] \quad (1)$$

in which the last two terms determine the relaxation.

In a perfectly cubic field, such would arise from a hexaaquo chromic complex $[Cr(H_2O)_6]^{3+}$, D and E should be zero and no relaxation should be induced. However, modulation of the quadratic zero field splitting parameter by changes in orientation or by collision with solvent particles may result in a mixing of different electronic spin states. The dominant mechanism of relaxation is indeed believed to be the modulation of the quadratic crystalline field splitting term $SD_{(t)}S$, where $D^2 = {}^2/_3 D^2 + 2E^2$ is the trace of the square of the zero-field splitting (zfs) hamiltonian. This mechanism was treated by McGarvey[2] and Bloembergen and Morgan[3] and more recently by Carrington and Luckhurst.[4] Using the Redfield density matrix formalism, they found that for a d^3 configuration the spectrum consists of three lorentzian curves: one for the $m_s + {}^1/_2 \rightleftharpoons -{}^1/_2$ transition and two equivalent for the $m_s + {}^3/_2 \rightleftharpoons +{}^1/_2$ and for $-{}^1/_2 \rightleftharpoons -{}^3/_2$ transitions. In the limit of fast motion, when the correlation time τ_c for the time dependence of the zfs modulation is much shorter than the reciprocal of the Larmor frequency ω_0, the three lorentzians are exactly superimposed and have the same relaxation time

$$T_2^{-1} = ({}^6/_5)\langle D^2 \rangle 2\tau_c \quad (2)$$

At room temperature this condition is generally realized.

In addition to the fluctuating distortion, when anionic ligands are coordinated around the transition metal ion in solution, complexes of lower symmetry are formed and a static electric field distortion may arise. This induces larger zfs, and line broadening over that of the aquo ion is observed. Dealing with ionic association, two main possibilities must be examined: (a) the ligand enters an outer coordination sphere and only a slight distortion is induced, and (b) the ligand displaces one of the solvent molecules from the first coordination sphere. In the latter case, an inner complex is formed, with large crystalline field distortion. Paramagnetic resonance has seldom been observed in these complexes because line width is usually so large as to escape detection. Sancier[5] has studied the association of aqueous Cr(III) with several inorganic anions and cations at relatively high concentrations. He developed his theory in terms of relaxation induced by electric field anisotropy and by restricted rotation of the complex due to cations which enter a third coordination sphere. However, this study is confined to outer-sphere coordination.

We wish to show that esr absorption intensity and line width variations as a function of ligand concentration are closely related to the inner- and outer-sphere equilibrium constants. We shall use the method previously outlined for Mn(II).[6] Briefly, this method may be described as follows: the stepwise equilibrium reaction may be expressed as

$$Cr_{aq}^{3+} + L^{-n} \underset{k_{ba}}{\overset{k_{ab}}{\rightleftharpoons}} Cr(aq)L^{(3-n)+} \underset{k_{cb}}{\overset{k_{bc}}{\rightleftharpoons}} CrL^{(3-n)+} \quad (3)$$

where the subscript aq means the hexaaquo coordination. Each species has a different line width which we define as ΔH_{ion}, ΔH_{out}, and ΔH_{in}, respectively. Under rapid exchange conditions, that is $\tau_{ab} = 1/k_{ab}[L^{-n}] \ll T_{2ion}$ and $\tau_{ba} = 1/k_{ba} \ll T_{2out}$, the observed line width is given by the well-known relation

(1) (a) This research was supported by the Italian National Council of Research (CNR); (b) R. G. Hayes, Lawrence Radiation Laboratory, Report UCRL 9873, University of California, Berkeley, 1961.

(2) B. R. McGarvey, *J. Phys. Chem.*, **61**, 1232 (1957).

(3) N. Bloembergen and L. O. Morgan, *J. Chem. Phys.*, **34**, 842 (1961).

(4) A. Carrington and G. R. Luckhurst, *Mol. Phys.*, **8**, 125 (1964).

(5) K. M. Sancier, *J. Phys. Chem.*, **72**, 1317 (1968).

(6) L. Burlamacchi and E. Tiezzi, *J. Mol. Struct.*, **2**, 261 (1968).

$$\Delta H_{obsd} = (1 - x)\Delta H_{ion} + x\Delta H_{out} \qquad (4)$$

where x is the mole fraction of the ion-pair species. The observed line width should be, therefore, a linear function of x between ΔH_{ion} and ΔH_{out}. Rapid exchange conditions are certainly not verified in the inner-sphere complex formation, according to the known inertness of the chromium complexes. The expected broad spectrum from the inner-sphere complex species is not detected under normal experimental conditions, in which other species are detected. Inner-sphere formation thus results in signal intensity decrease. For each Cr^{3+}–ligand system at a given temperature, a set of two values of K_{out} and K_{in} and one value of ΔH_{out} may be chosen for which the concentration of the various species in solution account for the observed line width and signal intensity at any ligand concentration. Determination of the equilibrium constants from the experimental points is then a problem of fitting which can be solved with the aid of a computer program.

The interconversion rate between the free ion and the ion-pair is very likely a diffusion-controlled reaction, characterized by high rate constants ($k \simeq 10^{11}$ sec^{-1}). Since the spin relaxation times, derived from experimental line widths, are $\simeq 5 \times 10^{-10}$ sec, conditions of rapid exchange described above could appear very critical, particularly at low ligand concentration. However, a number of observations indicates that eq 4 holds. Under slow interconversion conditions, the coincidence of equilibrium constants derived from signal intensity and line width, would be fortuitous, which seems quite improbable. Furthermore, if $\tau_{ab} \simeq T_{2ion}$, at room temperature, the passage from slow to rapid exchange could be merely achieved by changing temperature. Some additional experiments made at 10 and 40° showed that the excess line width over the free Cr^{3+} ion, due to addition of ligand, is almost independent of temperature. Finally, comparison with a number of analogous cases with Mn^{2+} ion,[7,8] which undergoes the same relaxation mechanism, although with relaxation time longer by a factor $\simeq 7$, make us feel quite confident of the correctness of the model.

Experimental Section

Solutions of 10^{-2} M $Cr(ClO_4)_3$ were analyzed in the presence of added KF, NaCl, Na_2SO_4, and $Na_2C_2O_4$. Esr spectra were registered with a Varian V-4502 X-band, 100-Kc field modulation spectrometer with a dual sample cavity, using Fremy salt as a reference standard. The probe temperature was controlled by means of a copper–constantan thermocouple with an accuracy of ±1°. Assuming lorentzian line shape, the absorption intensity was evaluated by the known relation $(\Delta H)^2 h$, where h is the peak-to-peak height of the first derivative spectrum. Chromium perchlorate was obtained by the method of Phipps and Plane.[9] In order to avoid the presence of dinuclear species, the pH of the solutions

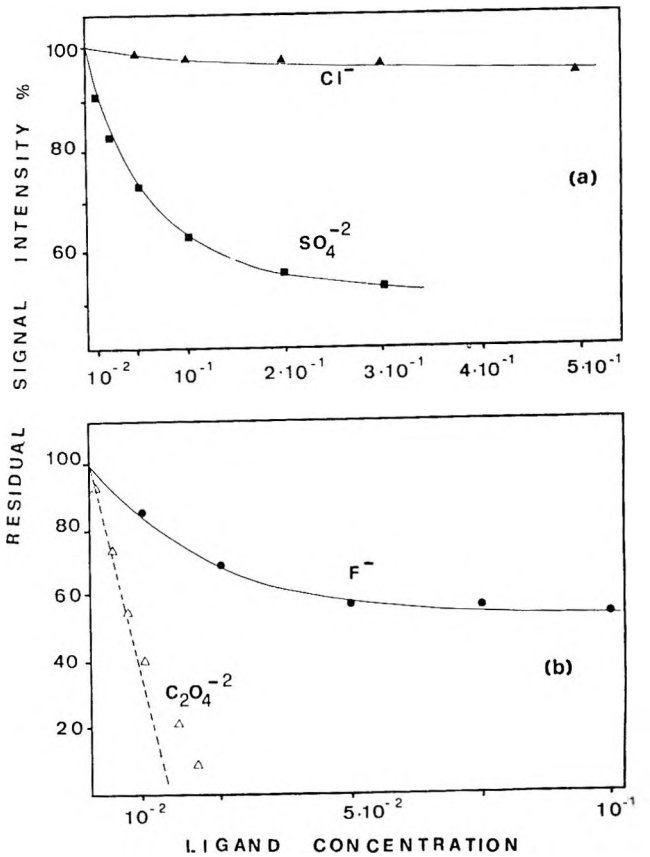

Figure 1. Esr residual signal intensity per cent of 0.01 M Cr^{3+} aqueous solutions *vs.* ligand concentration. The full lines represent values calculated with equilibrium constants given in the text.

was kept between 3 and 4. Ionic strength was controlled by adding $NaClO_4$ at $\mu = 1$. Only the F^- solutions were made without ionic strength control at pH 4 to prevent precipitation and HF association. All solutions were stored at 26° for 6 weeks and then analyzed at the same temperature. Samples analyzed after longer periods of time gave the same results within the limit of experimental error.

Results and Discussion

Figures 1 and 2 show the Cr^{3+} esr absorption intensity ($I\%$) and the observed line width as a function of ligand concentration. As expected, complexation increases in the order $Cl^- \ll SO_4^{-2} < F^- \ll C_2O_4^{-2}$. The latter ion is known to have a high stability constant even for $[Cr(C_2O_4)_3]^{-3}$ ($K_3 > 10^5$).[10] From the initial slope of the intensity per cent curve, an overall equilibrium constant for the monooxalate complex may be evaluated to be 3×10^2. Outer-sphere coordination should be consequently very low, as shown by the negligible line

(7) L. Burlamacchi and E. Tiezzi, *J. Phys. Chem.*, **73**, 1588 (1969).
(8) L. Burlamacchi, G. Martini, and E. Tiezzi, to be published.
(9) A. L. Phipps and R. A. Plane, *J. Amer. Chem. Soc.*, **79**, 2458 (1957).
(10) N. K. Dutt and B. Sur, *Z. Anorg. Chem.*, **293**, 195 (1957).

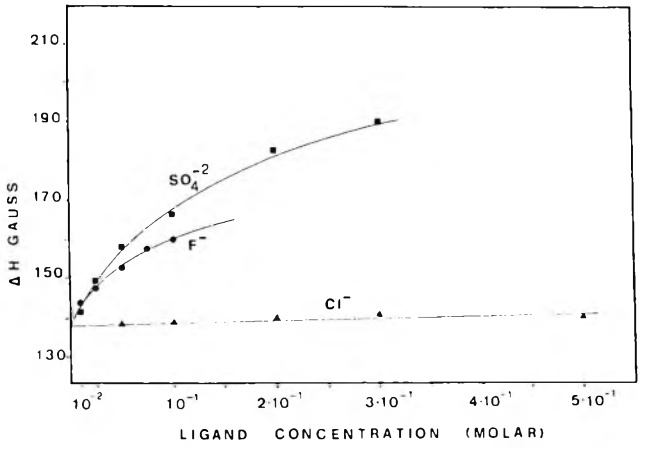

Figure 2. Esr line width of 0.01 M $Cr(ClO_4)_3$ solution *vs.* ligand concentration. Full lines represent values calculated with equilibrium constants given in the text.

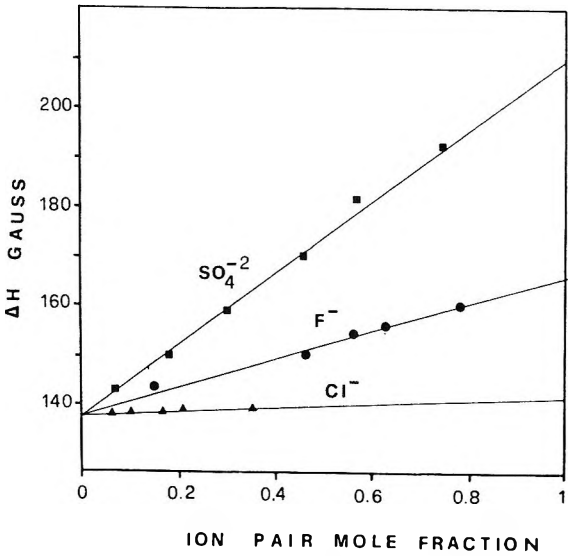

Figure 3. Experimental esr line width of 0.01 M Cr^{3+} *vs.* mole fraction of ion pair.

width increase even at the highest $C_2O_4^{-2}$ concentrations. More significant results are obtained with SO_4^{2-} ion. Experimental points, both for signal intensity and line width, fit very well with values of $K_{out} = 9.5 \pm 0.5$ l. mol^{-1} and $K_{in} = 1.3 \pm 0.1$. These values may be compared with the data given by Fogel, *et al.*,[11] at the same ionic strength, $K_{out} = 12 \pm 3$ l. mol^{-1} (not temperature dependent) and $K_{overall} \simeq 13$ l. mol^{-1} extrapolated at 26°. Complexation with Cl^- is very weak and experimental points allow only a rough evaluation of the equilibrium constants. Comparison with data from literature appear therefore very useful. The outer-sphere equilibrium constant has been evaluated by Connick and Tsao,[12] who found $K_{out} = 1.5$ l. mol^{-1} at 25 ° and $\mu = 1$. Unfortunately, no values of equilibrium constant for inner coordination are reported under the same conditions. Gates and King[13] give an overall $K \simeq 0.22$ l. mol^{-1}—extrapolated at 26°—in 5 M $HClO_4$. Assuming $K = 0.2$ l. mol^{-1} we obtain $K_{in} = 0.13$. Using these constants the calculated values of intensity per cent and line widths agree very well with the experimental points (Figures 1 and 2). Fluoride complexes fit with values of K_{out} and $K_{in} = 30 \pm 3$ l. mol^{-1} and 1.2 ± 0.1, respectively. To our knowledge no data of outer-sphere complexation are available. However, these results appear quite plausible in relation to the greater complexation activity of F^- ions in comparison with Cl^- and SO_4^{-2} anions.

Data of ΔH_{obsd} plotted as a function of the mole fraction of the outer-sphere complex are reported in Figure 3. According to eq 4, the experimental points fit a straight line very well. From the intercept with the ΔH axis at $x = 1$, $\Delta H_{out} = 142$, 167, and 210 G may be derived for chloride, fluoride, and sulfate complexes. Assuming $\tau_c = 2.10^{-12}$ the ΔH_{out} values give $D = 0.112$ cm^{-1}, 0.122 cm^{-1}, and 0.138 cm^{-1}, respectively. D factor calculated for the free ion is 0.107 cm^{-1}. The difference of zfs for the different ions is not precisely understandable as charge density, size, polarization, and the relative position of the ion in the spectrochemical series may contribute to the crystalline field distortion.

We believe that the dependence of the line broadening and the signal intensity upon the inner- and outer-sphere equilibria in solution might be quite general for those ions in which modulation of the zero field splitting parameter is the dominant relaxation mechanism. In spin $^1/_2$ ions relaxation is induced by tumbling averaging of the anisotropic parameters, which also depends on electric field symmetry. However, the presence of other relaxation mechanisms, such as spin rotation and the Orbach process, makes the above consideration inconsistent. Detectable spectra of transition metal ions with $S > {}^1/_2$ in solution are almost exclusively given by d^3 and d^5 configurations. In the d^3 system, in addition to Cr(III), the V(II) spectrum has been observed in aqueous solution at room temperature, due probably to $[V(H_2O)_6]^{+2}$.[14] This spectrum is broad with unresolved hyperfine structure, but the relaxation mechanism should be the same as for Cr(III) complexes and in principle the above considerations should apply.

Relaxation of Mn(II) and Fe(III) complexes (d^5) in octahedral field has been recognized to be dominated by motional modulation of the zfs parameter, with negligible contribution from modulation of the anisotropic A and g tensors and from spin rotation. The hexacoordinated Mn^{2+} ion has been extensively studied in various

(11) N. Fogel, J. M. J. Tai, and J. Yarborough, *J. Amer. Chem. Soc.*, **84**, 1145 (1962).

(12) R. E. Connick and M. S. Tsao, Abstract, 123rd National Meeting of the American Chemical Society, March 1953, No. 9.

(13) H. S. Gates and E. L. King, *J. Amer. Chem. Soc.*, **80**, 5011 (1958).

(14) W. B. Lewis and L. O. Morgan, "Transition Metal Chemistry," Vol. 4, Marcel Dekker Inc, New York, N. Y., 1968, p 101.

solvents,[15-17] and the outer-inner sphere equilibrium has been checked quantitatively.[6] Some complications arise at high temperature, where a sharp line broadening is observed in the presence of various ligands, which cannot be explained in terms of outer-sphere complexation. However, if the temperature dependence of ΔH_{out} and equilibrium constants are taken into account, the ligand dependent line broadening can be handled in the same way.[7,8]

Complexation of Fe^{3+} by Cl^- and SCN^- ions has been recently investigated by Levanon, *et al.*[18] The curves of esr absorption intensities as a function of ligand concentration are quite similar to those observed for Cr^{3+}–F^- and Cr^{3+}–SO_4^{2-} systems, thus suggesting the presence of ion-pair species. The hexaaquo ion itself displays a relatively short relaxation time which results in a broad spectrum about 1100 G wide, almost independent of ligand concentration. This suggests that the line broadening mechanism in Fe^{3+} complexes is much more sensitive to random distortion of the cubic field from collision with neighboring particles rather than from static distortion due to outer-sphere coordinated ligands. However, too little work has been done on this subject to derive quantitative conclusions.

(15) R. G. Hayes and R. J. Myers, *J. Chem. Phys.*, **40**, 877 (1964).
(16) B. B. Garrett and L. O. Morgan, *ibid.*, **44**, 890 (1966).
(17) H. Levanon and Z. Luz, *ibid.*, **49**, 2031 (1968).
(18) H. Levanon, Z. Luz, and G. Stein, in press.

Evaluation of the Basic Ionization Constants of Water and Alcohols from Their Ionization Potentials

by L. S. Levitt and Barbara W. Levitt

Chemistry Department, School of Science, University of Texas at El Paso, El Paso, Texas
(*Received September 10, 1969*)

The presence of electron-releasing alkyl substituents on the oxygen of an alcohol molecule obviously increases the electron density at the oxygen atom and this results in a corresponding decrease in the magnitude of the ionization energy for removal of an electron from the oxygen lone pair.

$$R\ddot{O}H \xrightarrow{E_I} R\ddot{O}^+H + e^-$$

The ionization potential, E_I, of course, corresponds approximately to the energy of the highest occupied molecular orbital. It is apparent that the increase in electron density should result also in a concomitant increase in the basicity at the oxygen atom

$$R\ddot{O}H + H^+ \rightleftharpoons R\ddot{O}^+H_2$$

The pK_{BH^+} values of various *N*-heterocycles have already been correlated with the ionization potentials calculated theoretically by a self-consistent molecular field method.[1]

With respect to the aliphatic alcohols, Ballinger and Long[2] have determined the *acid* ionization constants by a conductivity procedure in aqueous solution for the reaction $ROH + H_2O \rightleftharpoons RO^- + H_3O^+$. The *basicity* constants pK_{BH^+} for the alcohols are defined for the reaction $ROH + H_3O^+ \rightleftharpoons ROH_2^+ + H_2O$, and are, of course, identical with the hydrolysis constants of the conjugate acids (ROH_2^+) of the alcohols. Until recently, the pK_{BH^+} values for the alcohols were known only to an approximate order of magnitude. The pK_{BH^+} values were believed by Arnett[3] to fall within the range -2 to -4. A more recent study[4] of CH_3OH in aqueous H_2SO_4 using Raman spectroscopy yielded a value of -2.2 for the pK_{BH^+} of $CH_3OH_2^+$, but the method was judged unreliable for EtOH, *i*-PrOH, and *t*-BuOH by the experimenters.[4] Subsequently, two investigations of the basicity of alcohols, determined by solvent extraction[5] and by their solubilities[6] in varying concentrations of aqueous H_2SO_4, were carried out. The following pK_{BH^+} values were arrived at: MeOH[6] (-2.5); *n*-BuOH[5,6] (-2.3); *sec*-BuOH[5,6] (-2.2); and *t*-BuOH[5,6] (-2.6). It was concluded by Arnett and Anderson[5] that the effect of a change in structure of the R group on the basicity of the alcohol is probably too small to be resolved by these experimental methods.

Water, as pointed out by Arnett,[3] is the most important solvent in chemistry, and yet surprisingly little is known about its behavior as a base, particularly insofar as definitive quantitative data are concerned. For example, the pK_{BH^+} of H_3O^+ has been estimated variously as -1.8,[7] -2.35,[8] -3.43,[9] -5.9,[10] and -6.66.[11]

A careful and detailed study of the base strengths of aliphatic alcohols was carried out by Gerrard and Macklen,[12] who measured the solubility of gaseous HCl in

(1) K. Nakajima and B. Pullman, *J. Chim. Phys. Physicochim. Biol.*, **55**, 793 (1958).
(2) P. Ballinger and F. A. Long, *J. Amer. Chem. Soc.*, **82**, 795 (1960).
(3) E. M. Arnett, *Progr. Phys. Org. Chem.*, **1**, 223 (1963).
(4) N. C. Deno and M. J. Wisotsky, *J. Amer. Chem. Soc.*, **85**, 1735 (1963).
(5) E. M. Arnett and J. N. Anderson, *ibid.*, **85**, 1542 (1963).
(6) N. C. Deno and J. O. Turner, *J. Org. Chem.*, **31**, 1969 (1966).
(7) J. N. Brønsted and W. F. K. Wynne-Jones, *Trans. Faraday Soc.*, **25**, 59 (1929).
(8) H. Lemaire and H. J. Lucas, *J. Amer. Chem. Soc.*, **73**, 5198 (1951); T. L. Smith and J. H. Elliott, *ibid.*, **75**, 3566 (1953).
(9) L. P. Hammett and A. J. Deyrup, *ibid.*, **54**, 4239 (1932).
(10) W. Smith, Jr., Thesis, Harvard University, 1960.
(11) N. C. Deno and R. W. Taft, Jr., *J. Amer. Chem. Soc.*, **76**, 244 (1954).
(12) W. Gerrard and E. D. Macklen, *J. Appl. Chem.*, **9**, 85 (1959); **9**, 89 (1959); *Chem. Rev.*, **59**, 1105 (1959).

the various pure alcohol solvents. The question, however, may legitimately be raised (and indeed has been) whether the solubility of HCl in the alcohol at a fixed temperature really represents the base strength of the alcohol, or rather does it represent a combination, in varying proportions, of the base strength, the dipole–dipole interactions between solute and solvent molecules, hydrogen-bonding interactions between solute and solvent molecules, polarizability effects, and extraneous ionic field effects.[13] Conductance studies[14] on these systems have shown that the interaction is predominantly one of proton transfer since the solutions of HCl in the alcohols produce considerable conductivity, the Λ_0 in the case of HCl in methanol approaching that of HCl in water.

In their studies of the basicity of various aliphatic and alicyclic alcohols, Gerrard and Macklen[12] found, in general, that the alcohols with electron-releasing R groups absorb larger quantities of gaseous HCl than those which have electron-attracting R groups. This behavior was interpreted, qualitatively, in terms of the relative electron densities at the oxygen atom. For example, the magnitude of the solubility of HCl at 10°, (in moles of HCl/mole of ROH), was found to be in the following order: $(CH_3)_3COH \gg CH_3OH \gg Cl_3CCH_3OH$.

It would appear, therefore, that the HCl solubility data *are* actually representative of the basicity of alcohols, and might well be related to the magnitude of the E_I's of the alcohol. Such, indeed, we find to be the case. Table I gives the solubility data[12] (S) and the ionization energies[15] (E_I) for the corresponding alcohol or water. In order to interpolate water into the series of alcohols, we have calculated the solubility of gaseous HCl in H_2O at 10° from data in the literature.[16] Also included in Table I are the "relative basicity parameters," β, referred to water as the standard, where

$$\beta = \left(\frac{S_{ROH}}{S_{HOH}}\right) - 1 \qquad (1)$$

The data are presented graphically in Figure 1 where the "relative basicity parameters," β, are plotted as a function of E_I. It is seen that an excellent correlation exists between the β values and E_I. Note that water has been included as a special case of the simplest alcohol, and it is interesting to observe that it fits right into the correlation.

The ionization energies are actually free energy changes,[17] which are therefore proportional to log K_{ion}.

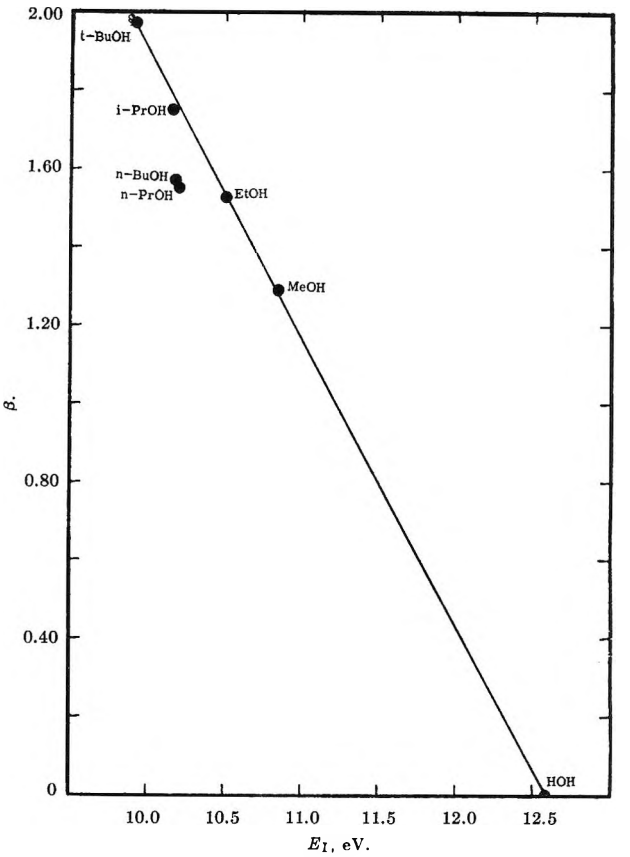

Figure 1. A plot of the "relative basicity parameters", β, of the alcohols *vs.* their ionization potentials, E_I.

Table I: Solubility of Anhydrous Hydrogen Chloride in Various Alcohols and the Ionization Potentials of the Alcohols

ROH	S, HCl soly at 10°, (mol of HCl/ mol of ROH)	β, relative basicity parameter	E_I, ionization potential, eV
HOH	0.380[a]	0	12.59
MeOH	0.857	1.26	10.85
EtOH	0.950	1.50	10.50
n-PrOH	0.956	1.52	10.20
n-BuOH	0.964	1.53	10.17[b]
i-PrOH	1.030	1.71	10.16
t-BuOH	1.115	1.93	9.92[c]
c-$C_6H_{11}OH$	1.030	1.71	...[d]
$C_6H_5CH_2OH$	0.812	1.11	...[d]
$ClCH_2CH_2OH$	0.550	0.45	...[d]
Cl_3CCH_2OH	0.087	−0.77	...[d]
F_3CCH_2OH	0.060	−0.84	...[d]

[a] Calculated from solubility data in ref 16. [b] Average of values given in ref 15 and in W. Reed, "Ion Production by Electron Impact," 1962; see C. Noller, "Chemistry of Organic Compounds," W. B. Saunders Co., Philadelphia, Pa., 1965, p 995. [c] Value not given in ref 15. See W. Reed and C. Noller.[b] [d] E_I values not available.

(13) F. Franks and D. J. G. Ives, *Quart. Rev.*, **20**, 1 (1966).

(14) G. J. Janz and S. S. Danyluk, *Chem. Rev.*, **60**, 209 (1969); T. Shedlovsky and R. L. Kay, *J. Phys. Chem.* **60**, 151 (1956); A. M. El-Aggan, D. C. Bradley, and W. Wardlaw, *J. Chem. Soc.*, 2092 (1958).

(15) K. Watanabe, *J. Chem. Phys.*, **26**, 542 (1957); Dept. of the Army, Report No. 5B-99-01-004, ORD TB2-0001-00R-1624 (1959).

(16) N. A. Lange, Ed., "Handbook of Chemistry," Handbook Publishers, Sandusky, Ohio, 1944, p 1246.

(17) P. R. Wells, *Chem. Rev.*, **63**, 171 (1963).

The linear relationship of Figure 1 makes it apparent that the β values are proportional to E_I, and therefore, we must have

$$\beta = \log\left[\frac{K_{BH^+(H_2O)}}{K_{BH^+(ROH)}}\right] \quad (2)$$

If, then, we have an absolute value for any one of the K's of the alcohols or water, we are in a position to establish a quantitative scale of K's for the entire series of compounds. As indicated above, the values for the alcohols are not known with any reasonable degree of certainty, and the values for water are widely disparate. We are prompted, therefore, to select arbitrarily one of the values for H_3O^+ upon which to construct the scale. The value decided upon is that of Hammett and Deyrup,[9] -3.43 for pK_{BH^+} of H_3O^+, since this was obtained by what appears to be a valid experimental procedure and it is, incidentally, the median (and nearly the mean) value of the five quoted above.

From eq 2 it is seen that the pK_{BH^+} of the alcohol can be calculated from

$$pK_{BH^+(ROH)} = pK_{BH^+(HOH)} + \beta = -3.43 + \beta \quad (3)$$

Table II gives the new values for pK_{BH^+} for various alcohols as calculated from eq 3.

Table II: Calculated pK_{BH^+} Values for Various Alcohols

Alcohol	pK_{BH^+}, eq 3	pK_{BH^+}, eq 5
HOH	-3.43[a]	-3.44
MeOH	-2.17	-2.17
EtOH	-1.93	-1.92
n-PrOH	-1.91	-1.70
n-BuOH	-1.90	-1.68
i-PrOH	-1.72	-1.67
t-BuOH	-1.49	-1.49
c-$C_6H_{11}OH$	-1.72	...
$C_6H_5CH_2OH$	-2.32	...
$ClCH_2CH_2OH$	-2.98	...
Cl_3CCH_2OH	-4.20	...
F_3CCH_2OH	-4.27	...

[a] Standard.

In Figure 2 the new pK_{BH^+} values for the alcohols are plotted *vs.* the corresponding E_I values from Table I. The excellent correlation would appear to justify the assumptions and the procedures adopted in this analysis. It is interesting to note that our pK_{BH^+} value for $CH_3OH_2^+$, -2.17 is in close agreement with the Raman experimental[4] value, -2.2, but it does not agree well with the solubility value[5,6] of -2.5. The equation for the straight line of Figure 2 relating the pK_{BH^+} of ROH_2^+ to the ionization potential (in eV) is given by

$$pK_{BH^+} = +5.73 + aE_I \quad (4)$$

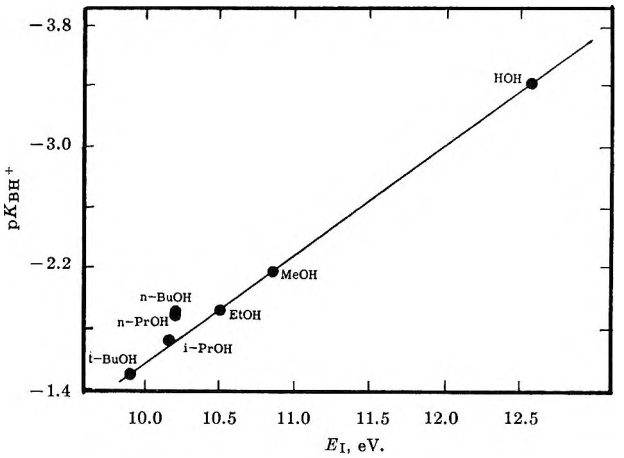

Figure 2. A plot of the calculated pK_{BH^+} values for various alcohols *vs.* the ionization potentials, E_I, of the alcohols.

The slope of the line, a, is found to be -0.727[18] and therefore

$$pK_{BH^+} = +5.73 - 0.727E_I \quad (5)$$

The pK_{BH^+} values calculated from eq 5 are also included in Table II.

Calculated values are not shown for the last five alcohols listed because their corresponding ionization potentials either have not been experimentally determined or they do not represent removal of an electron from an oxygen lone pair (*e.g.*, $C_6H_5CH_2OH$). Using eq 5 we can, however, calculate the ionization energy from the pK_{BH^+}. The values obtained are as follows: *c*-$C_6H_{11}OH$, 10.2 eV; $C_6H_5CH_2OH$, 11.1 eV; $ClCH_2CH_2OH$, 12.0 eV; Cl_3CCH_2OH, 13.6 eV; F_3CCH_2OH, 13.8 eV.

In the future, should a different and better value for the pK_{BH^+} of H_3O^+ be obtained, this relationship is still valid and the only change would be a shift in the line of Figure 2 up or down, correspondingly.

(18) Actually, a least-squares treatment gives the slope as -0.691 with a correlation coefficient of 0.990. However, chemical intuition requires, in this case, placing greater emphasis on the series H, Me, Et, *i*-Pr, *t*-Bu and lesser weight on *n*-Pr and *n*-Bu.

Pure Nuclear Quadrupole Resonance in Hexachlorostannates of Hydrated Divalent Cations

by Jack D. Graybeal,[1] Ruth J. McKown,[2] and Shen D. Ing[1a]

Department of Chemistry, West Virginia University, Morgantown, West Virginia 26506, and the Department of Chemistry, Virginia Polytechnic Institute, Blacksburg, Virginia 24061
(Received September 22, 1969)

The pure nqr frequencies of K_2SnCl_6, $(NH_4)_2SnCl_6$ and $RbSnCl_6$ at 23° have been reported to be at 15.065

15.474, and 15.60 MHz, respectively.[3] The crystal structures of these compounds are cubic with the cations occupying the corner, face-centered, edge-centered, and body-centered positions and the $SnCl_6^{2-}$ anions occupying alternate octant center positions.[4] If $M(H_2O)_6^{2+}$ cations were substituted for the univalent cations in this structure and if the electric field gradient (EFG) tensor components at the chlorine nuclei possessed an appreciable contribution from the cation charges, then there should be a noticeable difference between the nqr frequencies of these two type compounds. If the primary contribution to the chlorine EFG tensor is, however, from the electrons in the Sn–Cl bond then such a substitution should produce little change in the nqr frequencies.

Of the compounds studied, only the detailed crystal structure of $Ni(H_2O)_6SnCl_6$ has been determined.[5] It has a rhombohedral structure with $\alpha = 96° 45'$. Except for the slight skewing of the angles, the cation surroundings of the $SnCl_6^{2-}$ anion is very similar to that in the cubic structure of the M_2SnCl_6 compounds with a $M(H_2O)_6^{2+}$ replacing the corner M^+ ions. Unit cell dimensions for the compounds of Mg^{2+}, Mn^{2+}, and Ni^{2+} have been reported.[6] All three were found to be hexagonal with slightly different a and c dimensions. This presents a slight conflict regarding the determined structure of $Ni(H_2O)_6SnCl_6$). The Sn–Cl bond lengths determined for the M_2SnCl_6 compounds[4] and for $Ni(H_2O)_6SnCl_6$[5] all lie between 2.41 and 2.45 Å, indicating little effect on this bond by the cation.

Bonding of the $d\pi$–$p\pi$ type between tin and chlorine atoms has been suggested by many authors. The low values of the nqr frequencies of chlorine in the group IVa tetrachlorides have been cited as evidence for this type of bonding.[7,8] A determination of the chlorine nqr asymmetry parameters in the group IVa tetrahalides[9] strongly suggests the presence of such type bonding. The structure of the $SnCl_6^{2-}$ anion has O_h symmetry and is geometrically more suited for π-bond formation between the tin atom and the surrounding chlorine atoms than is the structure of $SnCl_4$ where one has the less symmetrical T_d group. If this were the only factor to be considered then the nqr frequencies of the $SnCl_6^{2-}$ chlorine atoms should be less than those in $SnCl_4$.

The longer Sn–Cl bond length in the $SnCl_6^{2-}$ anion as compared to that in $SnCl_4$ (2.33) indicates that the Sn–Cl bond in the former is probably more ionic and perhaps also possesses less π-bond character. Although there is this indication of less π-bond character in the $SnCl_6^{2-}$ anion, it certainly does not suggest the absence of π-bond character. The lower value for the resonance frequency in $SnCl_6^{2-}$, as compared to $SnCl_4$, could be due to more ionic character, more π-bond character, or some compensating combination of these. It is not possible from an experiment of the type reported to unambiguously characterize the amounts of both ionic character and π bonding.

Haas and Marram[10] have suggested that a molecule, in which π bonding of a chlorine atom to another atom occurs, should show a decrease in π bonding with increased bending vibration activity, *i.e.*, an increase in temperature. This in turn should result in an increase of the nqr frequency with increasing temperature. The normal behavior of nqr frequencies was first discussed by Bayer[11] and consists of a decrease with increasing temperature. Measurement of the temperature coefficients of the nqr frequencies can provide further evidence regarding the nature of the bonding. Using the results of Haas and Marram,[10] the temperature coefficient due to vibrational activity is estimated to be about $+1.5$ kHz deg^{-1}. The normal Bayer coefficient is of the order of -2 kHz deg^{-1}.

Experimental Section

All of the compounds studied were prepared using a published method for preparation of hexabromostannates.[12] The preparation of all compounds, except $Ni(H_2O)_6SnCl_6$, consisted of adding 0.2 mol of reagent grade metal chloride in 100 ml of 2 *N* HCl to 0.2 mol of $SnCl_4$ in 50 ml of 2 *N* HCl, evaporation of the resulting solution on a hot plate until crystal formation began, cooling of the solution to room temperature, and recovery of the product by filtration. For the preparation of $Ni(H_2O)_6SnCl_6$ a 2–3 molar excess of $SnCl_4$ was found to be necessary to produce the product in good yield. All compounds were dried in a vacuum desiccator over $CaCl_2$. All of the compounds are very hygroscopic and are easily hydrolyzed. The composition of all compounds was ascertained by elemental analysis for tin and chlorine.

All nqr frequencies were measured using a noise-controlled super regenerative spectrometer.[13] The method used for frequency measurement has been

(1) (a) Department of Chemistry, Virginia Polytechnic Institute, Blacksburg, Va. 24061. (b) To whom correspondence should be addressed.

(2) Department of Chemistry, West Virginia University, Morgantown, W. Va. 26506.

(3) D. Nakamura, *Bull. Chem. Soc. Jap.*, **18**, 183 (1963).

(4) G. Engel, *Z. Kristallogr.*, **A90**, 341 (1935).

(5) L. Pauling, *ibid.*, 72, 482 (1930).

(6) M. Giglio, E. Novales, and A. Arias, *Naturwissenschaften*, **52**, 182 (1965).

(7) R. Livingston, *J. Phys. Chem.*, **57**, 496 (1953).

(8) M. A. Whitehead and J. H. Jaffe, *Theor. Chim. Acta*, **1**, 209 (1963).

(9) J. D. Graybeal and P. J. Green, *J. Phys. Chem.*, **73**, 2948 (1969).

(10) T. E. Haas and E. D. Marram, *J Chem. Phys.*, **43**, 3985 (1963).

(11) H. Bayer, *Z. Phys.*, **130**, 227 (1951).

(12) M. Gatierrez De Celis and J. A. Quinos, *Acta. Salmanticensia, Ser. Cienc.*, **1**, 14 (1955).

(13) J. D. Graybeal and R. P. Croston, *Rev. Sci. Instrum.*, **38**, 122 (1967).

described elsewhere.[14] All frequency measurements are accurate to ±0.005 MHz. The observed nqr frequencies at 300°K are given in Table I.

Table I: Nqr Frequencies of Hexachlorostannates of Divalent Cations

Compd	^{35}Cl Resonance, MHz	S/N
$Mg(H_2O)_6SnCl_6$	15.836	100
$Ca(H_2O)_6SnCl_6$	15.904	50
$Mn(H_2O)_6SnCl_6$	15.770	20
$Zn(H_2O)_6SnCl_6$	15.720	5
	15.763	5
$Cd(H_2O)_2SnCl_6$	15.907	10
$Ni(H_2O)_6SnCl_6$	15.716	10
	15.719	10

The temperature dependence of the nqr frequencies of $Mg(H_2O)_6SnCl_6$ and $Ca(H_2O)_6SnCl_6$ were studied from 77 to 300°K by use of constant temperature slushes. The samples were placed in a finger dewar with the sample immersed in the slush and the oscillator coil external to the finger. The results of these studies are given in Table II.

Table II: Temperature Dependence of the Nqr Frequencies for $Mg(H_2O)_6SnCl_6$ and $Ca(H_2O)_6SnCl_6$

Temp, °K	$Mg(H_2O)_6SnCl_6$ freq, MHz	$Ca(H_2O)_6SnCl_6$ freq, MHz
300	15.836	15.904
278	15.835	15.903
240	15.823	15.894
188	15.819	15.896
147	15.822	15.902
113	15.827	15.909
	15.801	
77	15.838	15.928
	15.804	15.900

Results and Discussion

A comparison of the nqr frequencies of the $M(H_2O)_n$-$SnCl_6$ compounds studied with those of the univalent cation compounds shows that the latter are only slightly lower than the former. Comparing the structures of the two types of compounds and making an estimate of the ratio of the EFG tensor at a chlorine nucleus due to the nearest-neighbor cations one finds that the contribution of the cation charges to the EFG tensor is about 4 times as large for the M_2SnCl_6 type as for the $M(H_2O)_6$-$SnCl_6$. This is due to the fact that although the charge of the cation is larger in the latter type of compounds the interatomic distances between the cations and the chlorine atom are increased. If the EFG tensor has any appreciable contribution from the cation charges then it should result in lower coupling constants for the divalent cation compounds. The fact that there is little difference in the nqr frequencies of the two series indicates that the EFG tensor is determined predominantly by the bonding electrons. The average temperature coefficients for $Mg(H_2O)_6SnCl_6$ and $Ca(H_2O)SnCl_6$ are given in Table III.

Table III: Temperature Coefficients for Nqr Frequencies of $Mg(H_2O)_6SnCl_6$ and $Ca(H_2O)_6SnCl_6$

Temp range, °K	Temp coeff KHz deg^{-1} $Mg(H_2O)_6SnCl_6$	Temp coeff KHz deg^{-1} $Ca(H_2O)_6SnCl_6$
300–188	0.15	
300–240		0.17
188–113	−0.11	
240–77		−0.21

It is apparent from the magnitude and sign of the coefficients that the normal inverse temperature behavior is not followed. The near zero magnitudes and the sign inversion suggest that the normal Bayer effect is being opposed by an effect of comparable magnitude and opposite signs. It was pointed out earlier that the presence of π bonding would provide just such a contribution. The presence of appreciable π character in the Sn–Cl bond is thus concluded from this study.

The presence of multiple room temperature resonances for the Zn and Ni compounds indicates the occurrence of two different crystallographic environments of the chlorine atoms. This would be expected for compounds having the rhombohedral structure. The closeness of the members of the frequency pairs is further evidence that the cations contribute little to the chlorine EFG tensor. The observation of two nqr frequencies of the Mg and Ca compounds at lower temperatures indicates that either there has been a phase change or else the resonances due to the two inequivalent crystallographic positions are so similar as to be unresolvable at higher temperatures.

In summary it can be said that the bonding in the $SnCl_6^{2-}$ anion for compounds with hydrated divalent cations is comparable to that in compounds with univalent cations that is it is little effected by the nature of the cation. Furthermore, the nature of the temperature coefficients indicates that there is appreciable π character in the Sn–Cl bond of $SnCl_6^{2-}$.

Acknowledgments. The authors wish to thank the National Science Foundation for a grant which supported this work.

(14) J. D. Graybeal and R. J. McKnown, *J. Phys. Chem.*, **73**, 3156 (1969).

Micelle Size of Barium Dinonylnaphthalenesulfonate in Low Polarity Solvents by Vapor Pressure Osmometry

by R. C. Little

Surface Chemistry Branch, Chemistry Division, Naval Research Laboratory, Washington, D. C. 20390
(Received October 30, 1969)

The solubility behavior of the alkali metal sulfonates has been thoroughly studied in a wide variety of polar and nonpolar solvents.[1] The observed trends in the solubility and micellar behavior of these sulfonates have been successfully described through the application of Hildebrand's solubility parameter theory.[2] The solubility parameter concept has also been a useful index to soap–solvent behavior for phase change phenomena in a number of carboxylate soap–solvent systems.[3] In addition, the solubility parameter concept has been shown to be of some utility in practical applications for the prediction of lithium grease dropping points.[4] The solubility parameter concept, however, was found to be inapplicable to soap solutions in strongly polar solvents, particularly those which bring about extensive dissociation of the soap molecule into its constituent ions.[5] While earlier work treated the effect of solvent on the micelle size of the monovalent alkali salts of dinonylnaphthalenesulfonic acid, no work has yet been reported on divalent salts. Barium dinonylnaphthalenesulfonate in particular was selected as a candidate divalent salt toward this purpose since its benzene and toluene solutions have been studied by several other techniques.[6–8]

Experimental Section

The dinonylnaphthalenesulfonic acid used (HDNNS) was a specially prepared research grade supplied by King Organic Chemicals Inc. The preparation of this acid has been previously described.[7]

Barium dinonylnaphthalenesulfonate, $Ba(DNNS)_2$, was prepared by neutralizing a 2-propanol–water solution of the acid with an excess of solid barium hydroxide and back titrating to the neutralization end point. The soap was then extracted with petroleum ether and flash evaporated. Benzene solutions of this barium sulfonate were subsequently flash evaporated to remove the bulk amounts of alcohol and petroleum ether. After three flash evaporations with dry benzene the soaps were again taken up in dry benzene and freeze-dried under vacuum. The barium soap was a nearly white powder. The barium soap structure—as a result of steric and group-directing effects in the alkylation and sulfonation steps—is considered to consist of two highly branched nonyl groups in the 1,4 positions with the sulfonate group in either the 6 or 7 position of the naphthalene ring.

The solvents used were ACS grade or better except for the polymethylsiloxane dimer, which was a commercial sample from the Dow Corning Corp. All solvents were passed through molecular sieve materials and Florisil to remove water and polar contaminants and were used as soon as possible after percolation.

Benzil, used for calibrating the osmometer, was twice crystallized from anhydrous ethanol, dried at 50°, and stored in a desiccator over P_2O_5 until use.

Vapor pressure lowering data were obtained by means of a commercial thermoelectric device, the Mechrolab Model 301A osmometer. In all cases a drying agent, Linde molecular sieves, was added to the solvent cup to maintain a water-free solvent atmosphere in the vapor chamber.

Results and Discussion

Figure 1 presents number average aggregation numbers for barium sulfonate micelles in low polarity solvents as a function of concentration. As was found in earlier work[1,7] the aggregation number (monomers per micelle) is again independent of concentration. This invariance of aggregation number for a specific soap in a specific nonpolar solvent appears to be a definite characteristic of the metal dinonylnaphthalenesulfonates regardless of the cation or the nonpolar solvent chosen [except for those solvents which possess functional groups capable of interacting with a specific cation and provided studies are not made in the region of the critical micelle concentration.][7]

The invariance of micelle size in a given solvent as the soap concentration is varied is a necessary condition for the application of a theory recently proposed which accounts for the effect of solvent on micelle size.[1] The relation between micelle size and solvent solubility parameter may be expressed as follows $N = 1/K\ (\delta_2 - \delta_1) + 1$ where N = the aggregation number; δ_2 = the solubility parameter of the soap monomer; δ_1 = the solubility parameter of the solvent; K = a constant (considered to be a shielding factor). This equation should be of general applicability provided that the

(1) R. C. Little and C. R. Singleterry, *J. Phys. Chem.*, **68**, 3453 (1964).

(2) J. H. Hildebrand and R. L. Scott, "The Solubility of Nonelectrolytes," 3rd ed, Van Nostrand-Reinhold Co., Inc., Princeton, N. J., 1950.

(3) R. C. Little, *J. Colloid Interfac. Sci.*, **21**, 266 (1966).

(4) R. N. Bolster and R. C. Little, *Ind. Eng. Chem. Prod. Res. Develop.*, **5**, 198 (1966).

(5) R. C. Little and C. R. Singleterry, *J. Phys. Chem.*, **68**, 2709 (1964).

(6) T. F. Ford, S. Kaufman, and O. Nichols, *ibid.*, **70**, 3726 (1966).

(7) S. Kaufman and C. R. Singleterry, *J. Colloid Sci.*, **10**, 139 (1955).

(8) A. Fryar and S. Kaufman, *J. Colloid Interfac. Sci.*, **29**, 444 (1969).

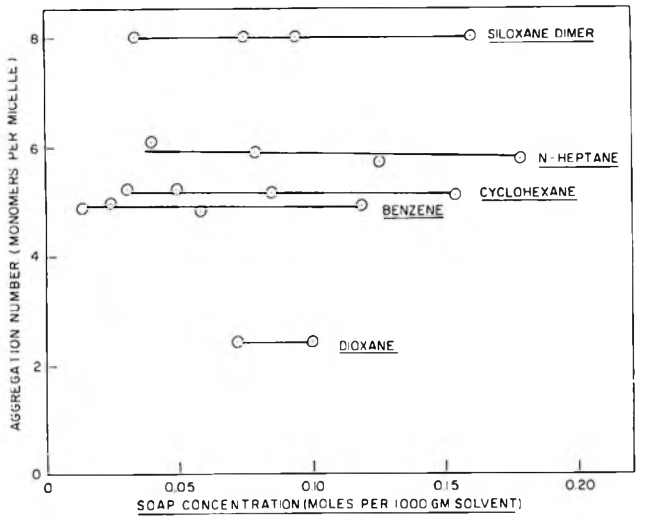

Figure 1. Barium sulfonate aggregation numbers *vs.* concentration in low polarity solvents.

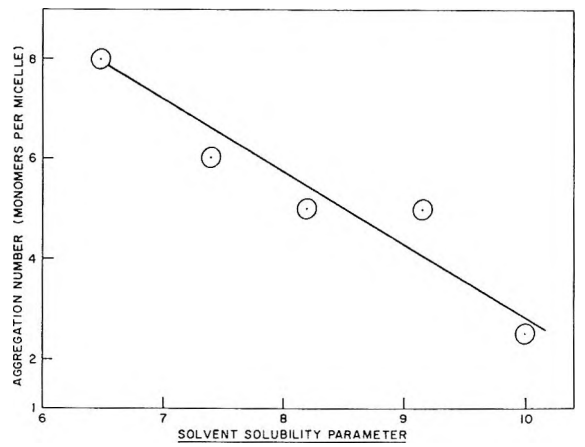

Figure 2. Dependence of barium sulfonate aggregation number on solvent solubility parameter.

following conditions are met: (1) that the micelles be essentially monodisperse in the given solvent; (2) that the micelles be spherical in structure and contain a polar core; (3) that the condensed micellar phase have an amorphous or liquid-like character; and (4) that the micellar concentration be at least an order of magnitude greater than the monomer concentration.

Figure 2 summarizes the experimentally observed effect of solvent on barium sulfonate micelle size. Aggregation number in terms of monomers per micelle is plotted against the solubility parameter of the solvent. The values of $\delta_2 = 11.3$ and $K = 0.690$ for the barium soap obtained from the plot compare with $\delta_2 = 10.5$ and $K = 0.295$ for the alkali sulfonates. The greater solubility parameter value for the barium soap monomer reflects the increased polarity of its ionic head while the greater K value is primarily a result of the larger degree of shielding per monomer unit by the hydrocarbon residues in the bivalent soap.

An aggregation number containing 18 acid residues appears to be the ultimate micelle size reached in low polarity solvents for both the bivalent and monovalent soaps since the micellar phase begins to separate as a liquid-like phase below a solvent solubility parameter of 6.0.[1] An ultimate aggregation number of 18 residues appears to be consistent with the most probable spatial geometry of the dinonylnaphthalenesulfonates. Rotation of representative molecular models in space indicate that an average solid angle of 26° is generated by tangents between the polar head group and the bulkiest section of the hydrocarbon residue. As an exercise, one can construct spheres from cones of various solid angles and thus count the number of cone units which make up the sphere. From simple geometry, however, one may also easily arrive at a relation between the number of cones in a sphere and the solid angle that they subtend without the use of models. Such a general relation derived from formulas involving the area of a sphere, the area of the curved surface of a right circular cone, and a correction for those areas of the sphere not covered by conical curved surfaces is as follows

$$N = \frac{16}{1.0512\theta\sqrt{\theta^2 + 4}} + 0.487$$

Substituting $\theta = 26°$ (0.436 radian) into the formula yields $N = 18$ acid residues for the fully packed micelle—in good keeping with the experimental results obtained in the polymethylsiloxane dimer ($\delta = 6.5$) in which 8 monomer units or 16 acid residues are counted. In addition, extension of the aggregation number *vs.* solubility parameter plot of Figure 2 to $\delta = 6.0$—close to the unmixing point—strongly suggests an ultimate size of approximately 18 acid residue units.

On the Liquid Film Remaining in a Draining Circular Cylindrical Vessel

by Paul Concus

Lawrence Radiation Laboratory, University of California, Berkeley, California 94720 *(Received October 23, 1969)*

It is of interest to have a theoretical estimate for the thickness of the film that remains on the wall of a right circular cylindrical vessel as it is being drained of a wetting liquid. Such an estimate, which includes the effects of surface tension and viscosity, has been given by Levich[1] for the case where the contact angle is zero and the static meniscus away from the wall becomes essentially a horizontal plane. In this note we

(1) V. G. Levich, "Physicochemical Hydrodynamics," Prentice-Hall, Englewood Cliffs, N. J., 1962, p 681, eq 133.26.

describe how, with the aid of recently published graphs,[2] Levich's technique can be extended to obtain estimates for the cases where the static meniscus away from the wall may be curved, such as in a vessel of small radius or in a reduced gravitational field.

The analysis presented for the flat plate film behavior on p 678, 679, and the top half of p 680 of ref 1 carries over unchanged for our problem. (The assumption that the film thickness be small compared with the radius of the vessel is, of course, needed.) The resulting expression for the constant asymptotic film thickness, h_0, for a withdrawal velocity that is not too large can be written as

$$h_0 = 1.34(\mu v_0/\sigma)^{2/3}/\kappa \qquad (1)$$

where μ is the liquid viscosity, v_0 is the bulk velocity of the fluid, σ is the surface tension, and κ is the curvature at the wall of a meridian of the static meniscus. (The coefficient 1.34 in eq 1 was calculated using a computed value of 0.643 for α, the asymptotic dimensionless film curvature, rather than the less accurate value of 0.63 given in eq 133.24 of ref 1.)

The appropriate value of κ to insert into eq 1 for any cylinder radius and gravitational field can be found from ref 2. From eq 1 of ref 2 one obtains that for a perfectly wetting liquid (0° contact angle)

$$\kappa = \frac{1}{a}(Bf_w + \lambda - 1)$$

where a is the radius of the vessel and $B = \rho g a^2/\sigma$ is the bond number (a dimensionless parameter) where ρ is the liquid density and g is the gravitational acceleration; the values of f_w, the dimensionless meniscus height at the wall ($r = 1$) and λ, twice the dimensionless mean curvature at the meniscus center ($r = 0$), can be read directly as a function of B from the graphs for zero contact angle in Figures 2 and 5 of ref 2, (see Figure 1).

Limiting values for κ and h_0 for very large B (essentially horizontal meniscus away from the wall) and very small B (essentially hemispherical meniscus) can be obtained using the asymptotic expressions for f_w and λ given in ref 2. For very large B, eq 15a, 18, and 23 of ref 2 yield $\kappa \approx (1/a)\sqrt{2B}$, so that

$$h_0 \approx 0.95 \frac{(\mu v_0)^{2/3}}{(\rho g)^{1/2}\sigma^{1/6}}$$

which is the same as the expression given by eq 133.26 of ref 1 (after the value of α is corrected). For very small B, eq 9 of ref 2 yields $\kappa \approx 1/a$, so that

$$h_0 \approx 1.34a(\mu v_0/\sigma)^{2/3}$$

for this case. Note that for large B the film thickness is independent of the vessel radius and, as noted on p 681 of ref 1, is only weakly dependent on the surface tension. For small B, on the other hand, h_0 is proportional to the vessel radius and depends more strongly on the surface tension.

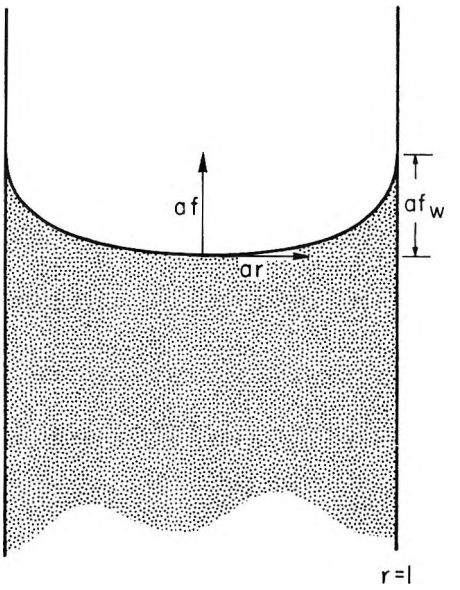

Figure 1. Static meniscus meridian. The variables r and f, which are the ones used in ref 2, are dimensionless. The radius of the cylinder is a. The quantity κ denotes the meridian's curvature at $r = 1$, and $\lambda/2a$ its curvature at $r = 0$.

Acknowledgment. This note is an outgrowth of a discussion with G. D. Bizzell, G. E. Crane, and H. M. Satterlee in which the author was made aware of the problem and the pertinent contents of ref 1. The work was performed in part under Contract NAS 3-11526 of Lockheed Research Laboratory with NASA-Lewis Research Center and in part under the auspices of the U. S. Atomic Energy Commission.

(2) P. Concus, *J. Fluid Mech.*, **34**, 481 (1968).

The Absolute Reactivity of the Oxide Radical Ion with Methanol and Ethanol in Water[1]

by R. Wander, Bonnie L. Gall, and Leon M. Dorfman

Department of Chemistry, The Ohio State University, Columbus, Ohio 43210 *(Received November 24, 1969)*

The reactivity of the basic form of the hydroxyl radical, O^-, formed in the radiolysis of water by the ionic dissociation[2,3] of OH

$$OH \rightleftharpoons O^- + H^+ \qquad (1)$$

(1) This work was supported by the U. S. Atomic Energy Commission.

(2) J. Rabani and M. S. Matheson, *J. Phys. Chem.*, **70**, 761 (1966).

(3) J. L. Weeks and J. Rabani, *ibid.*, **70**, 2100 (1966).

has been determined recently on a relative basis[4] for the reactions with methanol and ethanol

$$O^- + CH_3OH = \cdot CH_2OH + OH^- \quad (2)$$

$$O^- + C_2H_5OH = \cdot C_2H_4OH + OH^- \quad (3)$$

This has been done by competition kinetics using as reference reaction

$$O^- + O_2 = O_3^- \quad (4)$$

and observing O_3^- at 430 nm, the maximum[5-8] of the uv absorption band, in the absence and presence of the alcohol. The values[4] reported, $k_2 = 5.2 \times 10^8\ M^{-1}$ sec^{-1} and $k_3 = 8.4 \times 10^8\ M^{-1}\ sec^{-1}$ at 25° are thus related to the rate constant[7,9] $k_4 = 2.5 \times 10^9\ M^{-1}\ sec^{-1}$, and were obtained from a complex function of k_4, k_2, or k_3, k_{OH+CH_3OH} or $k_{OH+C_2H_5OH}$, K_{OH} and K_w (the dissociation constants for the hydroxyl radical and for water), the alcohol concentration, and the oxygen concentration.

It would be desirable to determine k_2 and k_3, as well as the analogous reactions of OH, absolutely by direct observation in pulse radiolysis, of the formation curves (in reactions 2 and 3) of the alcohol radicals which absorb[10] in the far-uv. However, the absorption of $\cdot C_2H_4OH$ is very weak, the extinction coefficient[10,11] being about 250 $M^{-1}\ cm^{-1}$ at 290 nm, and the absorption overlapping that of the OH radical[12] in this region, so that this experiment, for the reactivity of OH, is very difficult. However, at sufficiently high pH, k_2 and k_3 may be determined directly since the alcohol radicals undergo an ionic dissociation[13,14]

$$\cdot CH_2OH \rightleftharpoons \cdot CH_2O^- + H^+ \quad (5)$$

$$\cdot C_2H_4OH \rightleftharpoons \cdot C_2H_4O^- + H^+ \quad (6)$$

to form anion radicals for which the molar extinction coefficients at 290 nm are slightly less than $10^3\ M^{-1}$ cm^{-1}, the pK's being, respectively, 10.7 and 11.6. We report here the direct determination of absolute values for k_2 and k_3 by this method.

Experimental Section

The detailed pulse-radiolysis technique used in this laboratory, with a Varian V-7715A electron linear accelerator as pulse source, has been described.[8,4] Electrons of 3.5 to 4.0-MeV energy with a pulse duration of 50 to 400 nsec and a pulse current of 300 to 325 mA were used. The dose per pulse at maximum current with a 0.1-μsec pulse was approximately 6×10^{16} eV/g.

The formation of the radical anion was observed spectrophotometrically at 360 nm using an RCA 1P28 photomultiplier. Quartz reaction cells[8] were used with the analyzing light making a double pass through 20 mm of cell width. The absorption was measured through a 1.5-mm exit slit of the monochromator with a B & L No. 33-86-07 grating, so that the band pass of the analyzing light was 11.0 nm.

Triply distilled water was used in the preparation of all solutions. Concentrated sodium hydroxide, 19.4 M, was prepared from Baker Analyzed Reagent. Sodium carbonate is insoluble in this solution and can be filtered out. The reaction of O^- with carbonate ion is, in any case, not of serious concern since the rate constant is reported[3] to be less than $10^7\ M^{-1}\ sec^{-1}$. The solution was diluted to the desired pH which was determined by titrating with a standardized acid to a phenolphthalein end point. All runs were done at pH >13.3 so that the concentration of OH formed would be negligible compared with O^-, the pK[2,3] being 11.9.

Methanol was Baker Analyzed Reagent which was refluxed with added sulfuric acid and 2,4-dinitrophenyl hydrazine and distilled. U. S. I. Chemical Co. ethanol was used without further purification. The alcoholic solutions for individual runs were prepared with the use of a bulb technique as described,[15] which permitted the concentration of reactant to be varied in a sealed cell system while maintaining the same initial starting solution. This procedure was advantageous as it maintained a constant natural decay of O^-, which varies slightly from one solution to another, over each concentration series. As many as five concentrations of alcohol could be handled in the same cell. Methanol was varied over the concentration range from 0.45 $\times 10^{-3}$ to 4.5 $\times 10^{-3}\ M$, and ethanol from 0.22 $\times 10^{-3}$ to 2.2 $\times 10^{-3}\ M$.

All solutions were saturated with N_2O at slightly less than 1 atm (which gives approximately $2 \times 10^{-2}\ M$) to convert the hydrated electron to O^-

$$e_{aq}^- + N_2O = N_2 + O^- \quad (7)$$

The N_2O was USP anhydrous, with an assay of 98.5%, and was used without further purification.

Results and Discussion

Because of the occurrence of reaction 7, the system

(4) B. L. Gall and L. M. Dorfman, *J. Amer. Chem. Soc.*, **91**, 2199 (1969).

(5) G. Czapski and L. M. Dorfman, *J. Phys. Chem.*, **68**, 1169 (1964).

(6) J. W. Boag and G. E. Adams, 18th Annual Symposium on Cellular Radiation Biology, Houston, Texas, published by Williams and Wilkins Co., Baltimore, Md., 1965.

(7) G. E. Adams, J. W. Boag, and B. D. Michaels, *Proc. Roy. Soc.*, **A289**, 321 (1966).

(8) W. D. Felix, B. L. Gall, and L. M. Dorfman, *J. Phys. Chem.*, **71**, 384 (1967).

(9) G. E. Adams, J. W. Boag, and B. D. Michaels, *Nature*, **205**, 898 (1965).

(10) I. A. Taub and L. M. Dorfman, *J. Amer. Chem. Soc.*, **84**, 4053 (1962).

(11) L. M. Dorfman and I. A. Taub, *ibid.*, **85**, 2370 (1963).

(12) J. K. Thomas, J. Rabani, M. S. Matheson, E. J. Hart, and S. Gordon, *J. Phys. Chem.*, **70**, 2409 (1966).

(13) K. D. Asmus, A. Henglein, A. Wigger, and G. Beck, *Ber. Bunsenges. Physik. Chem.*, **70**, 756 (1966).

(14) M. Simic, P. Neta, and E. Hayon, *J. Phys. Chem.* **73**, 3794 (1969).

(15) J. L. Dye, M. DeBacker, and L. M. Dorfman, *J. Chem. Phys.* in press.

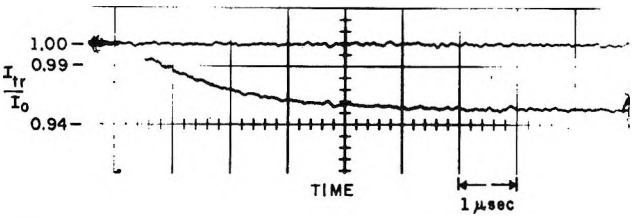

Figure 1. Rate curve for the formation of $\cdot C_2H_4O^-$ observed at 360 nm following a 300-nsec electron pulse in an aqueous solution at pH 13.92 containing 4.3×10^{-4} M ethanol.

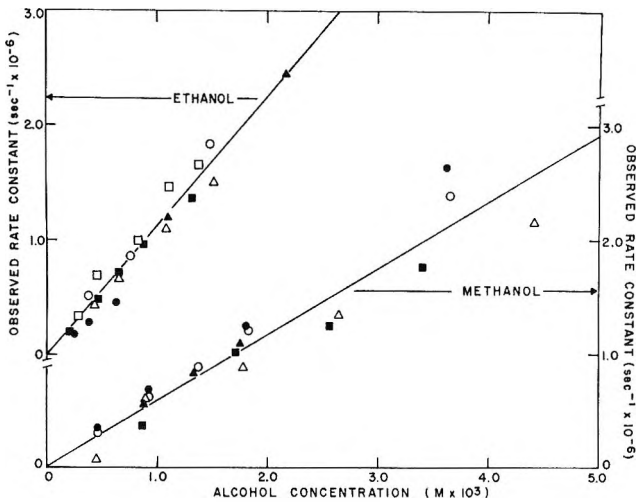

Figure 2. Plot of the observed first-order rate constant from formation curves (as in Figure 1) *vs.* alcohol concentration. The individual points represent the following experimental conditions. Ethanol: ▲, pH 13.80; ○, pH 13.78; ■ △, pH 13.92; ●, pH 13.90 with 50-nsec pulse, □, pH 13.89 with 50-nsec pulse (the pulse width for all other conditions ranged from 200 to 400 nsec). Methanol: ▲, pH 13.63; ●, pH 13.76; ○, pH 13.83; ■, pH 13.33; △, pH 13.46. The data for each set have been normalized to zero intercept.

consists exclusively of O^- as the reactive species, with the slight exception of H-atom, formed to the extent of 10%. At the high pH used, however, this is converted rapidly to e_{aq}^-

$$H + OH^- = e_{aq}^- + H_2O \qquad (8)$$

and hence also to O^-.

A typical rate curve for the formation of $\cdot C_2H_4O^-$ is shown in Figure 1. It is clear that, at the low pulse intensities used, a well-defined plateau is formed, the rate of the radical anion association reaction being sufficiently slow. These formation rate curves were found to fit closely to a first-order rate law. The observed first-order rate constants, obtained from the slope of such linear first order plots, show a linear dependence upon alcohol concentration with a positive intercept which varies slightly from one solution to another. All the data for both methanol and ethanol are presented in Figure 2 which shows a plot of the observed rate constant, normalized to zero intercept, against alcohol concentration. Each set of points represents a single solution with three to five different alcohol concentrations, and with different pH and different pulse length in some cases. Five such sets were done for methanol and six for ethanol. There is no significant depletion of the alcohol with succeeding pulses at the low pulse intensity used. The values for k_2 and k_3 may be obtained from the slopes of the straight lines in Figure 2. The individual sets show no increase in the rate constant with decreasing pH, indicating that OH (which reacts more rapidly than O^- with the alcohols[16]) plays no significant role. The values obtained are $k_2 = (5.8 \pm 0.8) \times 10^8$ and $k_3 = (11.3 \pm 1.7) \times 10^8$ M^{-1} sec^{-1} at 25°, both slightly higher than the values from competition kinetics,[4] but within agreement according to the indicated experimental uncertainty. It is clear from the data that reactions 2 and 3, rather than 5 and 6, are rate determining. From the data, considering the highest ethanol concentration used, we may conclude that the rate constant for reaction 6, which should be written in the form

$$\cdot C_2H_4OH + OH^- = \cdot C_2H_4O^- + H_2O \qquad (9)$$

is $k_6 > 3 \times 10^7$ M^{-1} sec^{-1}, but may of course be much higher.

Acknowledgment. We are indebted to Mr. John Richter for his invaluable help in maintaining and improving the electronic detection system and for operating the linac. It is a pleasure to acknowledge helpful discussions with Mr. Norman Shank and Professor J. L. Dye.

(16) P. Neta and L. M. Dorfman, "Radiation Chemistry I," Advances in Chemistry Series, No. 81, American Chemical Society, Washington, D. C., 1968, p 222.

Conductance of Dilute Aqueous Solutions of Hexafluorophosphoric Acid at 25°

by E. Baumgartner,[1] Margarita Busch, and R. Fernández-Prini[1]

Cátedra de Fisicoquímica, Ftd. Química y Farmacia, Universidad de Chile, Santiago, Chile
(Received December 1, 1969)

In the course of research on the behavior in dipolar aprotic solvents of simple inorganic acids which are strong in aqueous solutions, we became interested in studying hexafluorophosphoric acid. The reasons for this were that (a) PF_6^- is a very symmetric ion having a rather large crystallographic radius (2.95 Å);[2] (b) the scanty references to HPF_6 in literature[3] indicate that it is a strong monobasic acid in aqueous solutions; (c)

(1) Department of Chemistry, University of Maryland, College Park, Md. 20740, where correspondence should be addressed.

(2) H. Bode and G. Teufer, *Acta Cryst.*, **8**, 611 (1955); H. Bode and H. Clausen, *Z. Anorg. Chem.*, **265**, 229 (1951).

Randles[4] has shown that PF_6^- is adsorbed on the solution–air interface more strongly than halide ions and even more than SCN^-, probably indicating PF_6^- to be an easily polarized anion.

All this evidence makes it interesting to study how the dissociation of HPF_6 is modified in dipolar aprotic solvents, which are known as differentiating solvents,[5] when compared to its behavior in water, a leveling solvent. An apparent drawback in the choice of HPF_6 is that it has been reported to decompose[3] in dilute aqueous solutions. We report here the behavior of HPF_6 in dilute aqueous solutions as shown by the study of their conductances. The measurements indicate that HPF_6 is a strong acid in water and can be studied reasonably well without significant decomposition.

Experimental Section

Preparation of HPF_6 Solutions. The starting material was practical HPF_6 65% aqueous solution (Matheson Coleman and Bell) which was neutralized with 0.5 *M* KOH until the solution was slightly alkaline. The solution was digested for 2 hr and the solid filtered off.[6] The remaining solution was evaporated until KPF_6 crystallized; the salt was recrystallized three times from conductivity water and the KPF_6 thus obtained was dried over H_2SO_4. Polyethylene vessels were used throughout. The potassium salt was analyzed for its content of phosphate, free fluoride, and PF_6^-, the latter using nitron.[3a,7] The analysis showed the salt to be 99.9% KPF_6. The potassium salt was used to prepare the solutions of HPF_6 used for density and conductance measurements. The salt was converted to the acid by passage through a column containing 100 ml of strong cation exchange resin in the H^+ form. The content of K^+ and free F^- in the acid solution was checked by flame spectrophotometry and with the zirconium–alizarin test, respectively.

At first, HPF_6 solutions were prepared at a concentration of about 0.1 *M*. However, these decomposed partially yielding free fluoride and increasing the H^+ concentration by about 1% in 3 hr, and reaching a value 3% higher after 2 days. If NaF was added to the HPF_6 solution after it had decomposed, it attained the original H^+ concentration within 5 hr. These facts suggest that the decomposition of HPF_6 may be very similar to that recently proposed for the decomposition of $HAsF_6$,[8] *i.e.*, a slow rate-determining reaction which finally reaches equilibrium, preceded by the fast association of H^+ and AsF_6^- ions. However, it was found possible to prepare HPF_6 under such conditions that its decomposition was slow enough to be undetectable within at least 10 hr from the time when KPF_6 was converted to the acid. These conditions are: 50 ml of KPF_6 solution having a concentration of about 0.08–0.1 *M* was converted into the acid in 25 min. The acid coming out of the resin column was received in a polyethylene vessel containing enough conductivity water to make the final HPF_6 solution not more than 0.02 *M*. In this way no appreciable decomposition occurs during the time necessary to measure the conductance of 4 or 5 solutions prepared by dilution of the stock HPF_6 solution. In each run the content of free F^- was checked and was always smaller than 0.1%.

The concentration of acid in the stock solution was determined by weight titration with freshly prepared 0.04 *M* KOH using thymol blue as indicator. Near the end point the titration was carried out with 0.006 *M* KOH, thus increasing the precision of the determination. Dilution of the stock solution was accomplished by weighing the appropriate amount of HPF_6 stock and adding it to a vessel already containing the necessary quantity of conductance water.

Conductance Measurements. The conductance apparatus consisted of a variable frequency signal generator (Advanced Electronics J-2); a calibrated Tinsley Type 4896 electrolytic conductance bridge with external capacitance added in parallel to the Wagner earth capacitance of the bridge; a Tinsley Frequency Selector Detector Amplifier Type 5710 for bridge output amplification; and an oscilloscope for a detector. The precision of resistance measurements was better than 0.01%, while the accuracy was better than 0.1%.

The conductance cells used were of the type recommended by Marsh and Stokes,[9] thus avoiding "shaking"[10] and Soret[11] effects. The electrodes were lightly platinized; the solution resistances showed no measurable frequency dependence in the range 500–5000 cps. The cell constant was determined by measurement of the resistances of several KCl solutions whose conductances are known as a function of concentration.[12]

The specific conductance of the water used to make up the solutions was (1–3) 10^{-7} ohm^{-1} cm^{-1} and was assumed to be due to CO_2; hence no correction was applied to the measured values of the specific conductance of HPF_6 solutions.

All manipulations were carried out under a nitrogen atmosphere saturated with water vapor. Before measuring the resistance of a solution, the conductance cell was rinsed several times with the solution.

The density of HPF_6 solutions was found to vary linearly with concentration according to eq 1

(3) (a) R. E. Kirk and D. F. Othmer, "Encyclopedia of Chemical Technology," Interscience Publishers, New York, N. Y., 1951, Vol. 6, p 715. (b) "Gmelins Handbuch der Anorganischen Chemie," Vol. 16, Phosphorus, Verlag Chemie, Weinheim, 1965, part c, p 409.

(4) J. E. B. Randles, *Discuss. Faraday Soc.*, **24**, 194 (1957).

(5) A. J. Parker, *Quart. Rev.*, **16**, 163 (1962).

(6) M. M. Woyski, "Inorganic Synthesis," Vol. II, L. Audrieth, Ed., McGraw-Hill Publications, New York, N. Y., 1950, p 111.

(7) W. Lange and E. Müller, *Chem. Ber.*, **63B**, 1058 (1930).

(8) W. L. Lockhart, M. M. Jones, and D. O. Johnston, *Inorg. Nucl. Chem.*, **31**, 407 (1969).

(9) K. N. Marsh and R. H. Stokes, *Aust. J. Chem.*, **17**, 740 (1964).

(10) J. E. Prue, *J. Phys. Chem.*, **67**, 1152 (1963).

(11) R. H. Stokes, *ibid.*, **65**, 1277 (1961).

(12) J-C. Justice, *J. Chim. Phys.*, **65**, 353 (1968).

Table I

Run	10^4c	Λ/ohms^{-1} cm^2 mol^{-1}
a	91.967	395.275
	31.946	400.429
	16.458	402.765
	7.4792	404.922
	5.4289	405.544
b	97.136	394.755
	35.046	399.760
	22.339	401.518
	14.821	402.842
	6.6046	404.823
c	152.37	391.474
	56.458	397.305
	47.059	398.202
	5.0031	405.169

$$\rho = \rho_0 + 0.0856(\pm 0.0011)m \qquad (1)$$

where m is the molality of the acid solutions.

Conductance cells were thermostated in an oil bath at 25.00° (±0.002°). The largest uncertainty in the determination of conductance is due to the titration of the acid solution (repeatability 0.06%). The overall accuracy of measurements was better than 0.1%.

Results and Discussion

Table I gives the conductance of HPF_6 solutions at different concentration; they correspond to three stock solutions of HPF_6 prepared independently.

The data in Table I were fitted by a least-squares technique using an IBM/360 computer to the equation

$$\Lambda = \Lambda_0 - S\sqrt{c} + Ec \ln c + J_1 c - J_2 c^{3/2} \qquad (2)$$

which corresponds to a dissociated electrolyte. In this way values of Λ_0 and the distance of closest approach of ions, a, were obtained. The expressions for the coefficient J_1 and J_2 which involve the a parameter depend on the theory used to derive eq 2; we have analyzed the data using the expressions resulting from the Pitts[13,14] and the Fuoss and Hsia[15] theories.[16] Since the largest experimental error lies in the determination of the stock solution concentration, it seems adequate to analyze each run separately. The uncertainty in the stock solution concentration will only affect the value of Λ_0, the concentration dependence of Λ remaining almost unaltered. Thus, from the individual runs we obtain the value of a, and the three runs together yield the value of Λ_0.

Table II reports the values of Λ_0, a, and σ_Λ the standard deviation. It may be observed that the Fuoss and Hsia (F-H) expressions for the J coefficients fit the data somewhat better than the Pitts (P) expressions. This is contrary to the behavior observed for HCl in water.[15] The present data, however, are not accurate enough to allow a severe test of the theories. Table II shows that HPF_6 may be considered a strong acid in aqueous solutions with a distance of closest approach of 3.90 ± 0.05 Å (from F-H theory). Thus the behavior of HPF_6 is very similar to that found for $HAsF_6$,[17] which is a strong acid having a = 3.80 Å, and may also be compared with a = 3.90 Å for HCl.[15]

Table II

Run	Theory	Λ_0/ohms^{-1} cm^2 mol^{-1}	a, Å	σ_Λ
a	P	409.02	3.58	0.101
	F-H	409.07	3.88	0.079
b	P	408.69	3.73	0.075
	F-H	408.76	3.95	0.055
c	P	408.23	3.86	0.185
	F-H	408.49	3.85	0.091
a, b, c	P	408.79	3.47	0.239
	F-H	408.93	3.67	0.223

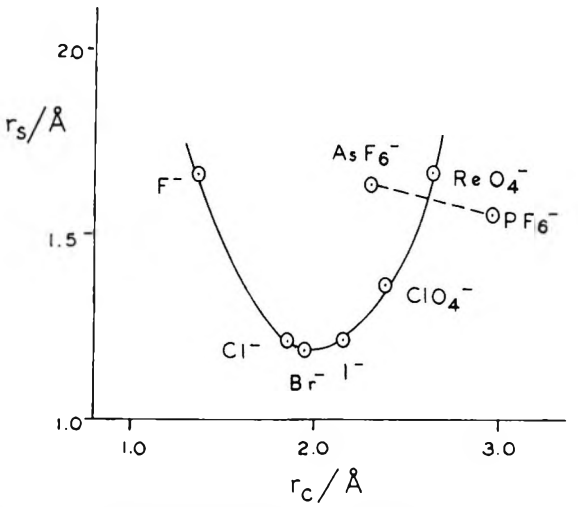

Figure 1. Plot of the Stokes radii, r_s, against the crystallographic radii, r_c, for some symmetric univalent anions.

Properties at Infinite Dilution. From Table II, Λ_0 = 408.93 ±0 .22 ohms^{-1} cm^2 mol^{-1} for HPF_6 which, subtracting $\lambda^0_{H^+}$ = 349.81,[18] gives 59.12 ± 0.22 ohms^{-1} cm^2 mol^{-1} for the limiting conductance of the PF_6^- ion, in good agreement with the value 59.28 found for $\lambda^0_{PF_6^-}$ in a study of the conductance of KPF_6.[19]

A very good agreement was also found for the partial molal volume of PF_6^- anion. From eq 1 the partial molal volume of the acid at infinite dilution is found to be 60.4 ± 0.8 ml mol^{-1}. When the contribution of H^+ is subtracted ($V^0_{H^+}$ = −7.2 ml mol^{-1}),[20] the value for

(13) R. Fernández-Prini and J. E. Prue, *Z. Physik. Chem.* (Leipzig), 228, 373 (1965).

(14) Pitts' expression[13] for J_2 has been slightly modified according to Pitts, Tabor, and Daly.[16] In ref 13 the numerical constant in σ_4 becomes 0.52772.

(15) R. Fernández-Prini, *Trans. Faraday Soc.*, 65, 3311 (1969).

(16) E. Pitts, B. E. Tabor, and J. Daly, *ibid.*, 65, 849 (1969).

(17) G. Atkinson and C. Hallada, *J. Phys. Chem.*, 64, 1487 (1960).

(18) R. A. Robinson and R. H. Stokes, "Electrolyte Solutions," Butterworth and Co., Ltd., London, 1959, p 453.

(19) R. A. Robinson, J. M. Stokes, and R. H. Stokes, *J. Phys. Chem.*, 65, 542 (1961).

$V^0_{PF_6^-}$ becomes 67.6 ± 0.8 which coincides within experimental error with $V^0_{PF_6^-}$ = 67.2 ml mol^{-1} found in KPF_6 solutions.[19]

The Stokes' radii of AsF_6^-, PF_6^-, halide ions, ClO_4^-, and ReO_4^- have been plotted in Figure 1 against their crystallographic radii. All the anions are almost spherically symmetric; however, the points for both fluorinated anions fall off the smooth curve which represents the behavior of all the other anions. This implies that a different kind of solvent–anion interaction takes place in the fluoro ions, probably due to the presence of fluorine atoms on the surface of these octahedral anions.

Acknowledgment. The authors are grateful to the Comisión Nacional de Investigaciones Científicas y Tecnológicas (Chile) for financial support.

(20) R. H. Stokes and R. A. Robinson, *Trans. Faraday Soc.*, **53**, 301 (1957).

COMMUNICATIONS TO THE EDITOR

Permittivity Measurements in the Time Domain

Sir: Fellner-Feldegg[1] has recently described a method of measuring the static permittivity κ_0, the high-frequency permittivity κ_∞, and the relaxation spectrum of a dielectric, by examination of the leading edge of a step function reflected from a sample of the dielectric terminating a coaxial transmission line.

The value of κ_0 he presents for the alkyl alcohols are in good agreement with the literature[2] but his calculated values of κ_∞ and the single relaxation time τ are not.

It is the purpose of this letter to consider why this is so. Equation 3 in the above paper is fundamental to the method of determining the relaxation spectrum. The equation relates the voltage reflection coefficient ρ from the plane interface of the air and dielectric filled sections of the coaxial line to the permittivity κ of the dielectric and is presented as

$$\rho = \frac{1 - \sqrt{\kappa}}{1 + \sqrt{\kappa}} \qquad (1)$$

Whenever dispersion is considered, κ should properly be replaced by $\kappa^*(\omega) = \kappa'(\omega) - j\kappa''(\omega)$, and ρ should be represented as a corresponding complex number $\rho^*(\omega)$. Both $\kappa^*(\omega)$ and $\rho^*(\omega)$ can only be defined for a given frequency ω, and eq 1 can only be applied to a continuous wave of that frequency.

The time variation of the reflected voltage resulting from a step function reaching the dielectric interface could be described by a reflection coefficient $r(t)$, and the instantaneous polarization $P(t)$ of the dielectric could be used to define an "instantaneous static permittivity $\kappa(t)$"

$$\kappa(t) = 4\pi \frac{P(t)}{E(t)} + 1 \qquad (2)$$

where $E(t)$ is the applied field. However, since $r(t)$ and "$\kappa(t)$" are defined as transient effects it is quite impermissible to substitute them into eq 1.

The substitution is possible for the times $t = 0$ and $t = \infty$ as the response at these times corresponds to the reflection coefficients at infinite and zero frequency (which, being outside the dispersion region, are real numbers). Thus eq 1 is valid for determining κ_0 and κ_∞. As substitution of $r(t)$ for ρ into (1) for any other value of t gives a solution for κ which is physically meaningless, it follows that the relaxation times calculated by Fellner-Feldegg on this basis are not the true relaxation times of the dielectrics.

Although Fellner-Feldegg's procedure for determining dispersion data from the reflected step pulse is invalid, the experimental concept presented in the paper must be considered as a very important development in dielectric technique. Point by point permittivity measurements in the frequency domain can be very accurate but invariably demand expensive equipment and are very time consuming.

The development of a time domain method would have revolutionary benefits, in terms of speed, measurement ease, and information content, for dielectric work.

Comparison of reflected and incident pulse shapes by Fourier transforms would automatically compensate for both irregularly shaped pulses and the frequency response of the detecting system, and would give complete dispersion data at all frequencies up to the limit imposed by signal to noise considerations. The Laplace transform approach advocated by Fellner-Feldegg does not recover the permittivity values of the dielectric inside the dispersion region, and relies rather heavily on the least accurately known parameter of all: ρ_∞.

Acknowledgment. The author is indebted to the British Empire Cancer Campaign for financial support.

(1) H. Fellner-Feldegg, *J. Phys. Chem.*, **73**, 3 (1969).
(2) E. H. Grant, *Proc. Phys. Soc.*, **70**, 937 (1957).

DEPARTMENT OF MEDICAL PHYSICS T. A. WHITTINGHAM
UNIVERSITY OF ABERDEEN
FORSTERHILL, ABERDEEN, SCOTLAND

RECEIVED AUGUST 15, 1969